Cranfield University

LT. COL. RODRIGO I CARO

HYDROXY-TERMINATED POLYETHER BINDERS FOR COMPOSITE ROCKET PROPELLANTS

Defence College of Management and Technology
Department of Environmental and Ordnance Systems

PhD THESIS

Cranfield University
Defence College of Management and Technology
Department of Environmental and Ordnance Systems

PhD THESIS

Academic Year 2004-2006

LT. COL. RODRIGO I CARO

HYDROXY-TERMINATED POLYETHER BINDERS FOR COMPOSITE ROCKET PROPELLANTS

SUPERVISOR: Dr John Bellerby

December 2006

ABSTRACT

Propellants based on cross-linked Hydroxy Terminated PolyEther (HTPE) binders are being used as alternatives to Hydroxy Terminated PolyButadiene (HTPB) compositions. HTPE propellants have similar mechanical properties to HTPB propellants but they give a less severe response in 'slow cook-off' tests for IM compliance. A literature review is presented on the development and properties of HTPE propellants in an attempt to place them in relation to recent trends in Insensitive Munitions. To gain a better understanding of the behaviour of HTPE propellants an HTPE pre-polymer and a range of binder network samples with different NCO/OH equivalence ratios, with and without plasticizer, have been synthesised and characterised by a range of techniques. The thermal decomposition of the HTPE binder network and propellant samples were also studied. Desmodur N-3200 was used as a curing agent and n-BuNENA as an energetic plasticizer. Similar analyses were performed on analogous HTPB pre-polymer and binder network samples and the results were compared with those obtained for the corresponding HTPE samples. Two kinds of HTPE propellant were manufactured containing HTPE pre-polymer, n-BuNENA, 2NDPA and either AP or AP+PSAN as oxidiser. Also HTPB propellant was prepared. Small cook-off test vehicles (SCTV) were filled with HTPE and HTPB propellants and slow cook-off tests were performed. In contrast to HTPB binders, which become harder during slow heating, it was found that the HTPE binders soften under the same conditions. This behaviour is possibly due to chain scission of the soft and hard segments of the HTPE polymer matrix. Thermo-oxidative processes and reactions of the energetic plasticizer decomposition products are believed to be the responsible for the scission of the polymeric matrix. From the binder characterisation and slow cook-off results it is concluded that there is a relation between the degree of polymeric matrix scission during slow heating and the violence of the response at the point of self ignition. This underlies the main difference between HTPB and HTPE propellants in slow cook-off. While HTPB compositions become harder and more brittle, HTPE propellants become softer and have a lower surface area at the self ignition point.

ACKNOWLEDGEMENTS

First of all, thanks to the Chilean Government for giving me the opportunity to study for a PhD at Cranfield University, Defence College of Management and Technology, through the scholarship called ”Beca Presidente de la Republica de Chile” and also thanks to the Chilean Army for supporting me.

I would like to say thanks to my supervisor Dr. John Bellerby for his directions and permanent support, positiveness and fantastic sense of humour through these three years of challenges. Special thanks to Dr Essam Kronfli for his advice, time and expertise during the synthesis of the hydroxy terminated copolyether. I also want to give special thanks to Dr Alistair MacCuish for the synthesis of the energetic plasticizer n-BuNENA and for his productive discussions related to this research. I want also to say thanks to Dr Mike Cartwright for the useful discussions about slow cook-off, to Dr Tony Bellamy for the NMR analysis, to Dr Phil Gill for his advice and assistance in SEC and GC-MS analysis, to Mr Anjum Agha for his help with HPLC analysis, Mrs Jenny Lovell for her help and advice in DSC/TGA analysis and to all the people from the Department of Environmental and Ordnance Systems who have helped me during these three years.

I want to highlight my thanks to Mr Dave Catton from Roxel UK, for his help to prepare and manufacture the first hand made HTPE propellant and for his practical advice on cross linking preparation. Also special thanks to Dr Doug Wagstaff for his help to manufacture the HTPE propellant on a bigger scale in Roxel facilities using a one litre IKA mixer. It is also time to thank Roxel (UK Rocket Motors) Ltd. for helpful discussions, for providing HTPB samples, material and the facilities for the HTPE propellant manufacture.

Finally, but not of least importance, thanks to my wife Susan and my daughters Fernanda, Valentina, Camila and Florencia because once again the time I spent on this project belonged to them.

TABLE OF CONTENTS

LIST OF TABLES

LIST OF FIGURES

LIST OF ACRONYMS

ADN	Ammonium Dinitramide
ALM	Air Launched short range attack Missile
AN	Ammonium Nitrate
AP	Ammonium Perchlorate
ARC	Atlantic Research Corporation
ATK	Alliant Techsystems Inc
BHEGA	Bishydroxyethyl glycolamide
BHT	Phenol, 2,6-bis(1,1-dimethylethyl)-4-methyl
BTTN	Butanetriol Trinitrate
n-BuNENA	n-Butyl-2-nitratoethylnitramine
B-2000	Poly(1,2-oxybutylene)diol
CL-20	Hexanitrohexaazaisowurtztane
COSY	Correlation spectroscopy sequence
DBTDL	Dibutyltin dilaurate
DCMT	Defence College of Management and Technology
DEGDN	Diethyleneglycol Dinitrate
DEOS	Department of Environmental and Ordnance Systems
DDI	Dimeryl Diisocyanate
DOS	Dioctyl Sebacate
DOA	Dioctyl Adipate
DSC	Differential Scanning Calorimetry
ESSM	Evolved Sea Sparrow Missile
ESD	Electrostatic Discharge
EO	Ethylene Oxide
EM	Energetic Materials
EthylNENA	Ethyl-2-nitratoethylnitramine
EFP	Emission Flame Photometry
FTIR	Fourier Transform Infra Red
GC	Gas Chromatography
GC-MS	Gas Chromatography Mass Spectrometry

GLM	Ground Launched short range ballistic Missile
GPC	Gel Permeation Chromatography
HDI	Hexamethylene Diisocyanate
HTCE	Hydroxy Terminated Caprolactone Ether
HTPB	Hydroxy Terminated PolyButadiene
HTPE	Hydroxy Terminated PolyEther
IM	Insensitive Munition
IPDI	Isophorone Diisocyanate
LD-124	Poly(1,4-oxybutylene)diol,
MS	Mass Spectrometer
MNA	N-Methyl-p-nitroaniline
NATO	North Atlantic Treaty Organisation
NDPA	2-Nitrodiphenylamine
NEPE	Nitrate ester plasticized polyether
NENA	Nitratoethylnitramine
NG	Nitroglycerine
NIMIC	NATO Insensitive Munition Information Center
NMR	Nuclear Magnetic Resonance
NPSAN	Non phase stabilised ammonium nitrate
OHEB	Ordnance Hazards Evaluation Board
PDSC	Pressure Differential Scanning Calorimetry techniques
PEG	Polyethylene Glycol
PPG	Poly(1,2-oxypropylene)diol
PSAN	Phase stabilised ammonium nitrate
PTHF	Polytetrahydrofuran
RDX	Cyclotrimethylenetrinitramine
RID	Refractive Index Detector
SB	Space booster ground
S_N2	Nucleophilic substitution
SCTV	Small Cook-off Test Vehicle
SEC	Size Exclusion Chromatography
THF	Tetrahydrofuran

T-30	Poly(1,4-oxybutylene)diol
TEGDN	Triethylene Glycol Dinitrate
TGA	Thermogravimetric analysis
THM	Tetramethylsilane
TMETN	Trimethylolethane Trinitrate
TPB	TriPhenyl Bismuth
TPEG	Block copolymer of poly THF and polyethylene glycol

LIST OF SYMBOLS

Ea	Activation Energy, kJ mol^{-1}
Eo	Young's modulus, MPa
f_n	Average functionality
Is	Specific impulse, N s kg^{-1}
$(Is)_M$	maximum specific impulse, N s kg^{-1}
(Is)m	medium specific impulse, N s kg^{-1}
Mn	Number average molecular weight, g mol^{-1}
M.p.	Melting point, ^oC
Mw	Weight average molecular weight, g mol^{-1}
n	Burning rate pressure exponent
rb,	burning rate**,** mm s^{-1}
Tc	Critical Temperature, ^oC
Tg ,	Glass Transition Temperature, ^oC
Δ*Hf*	Heat of formation, J g^{-1}
ρ	Density**,** kg m^{-3}
σ_m	Stress, MPa
ϵ	Strain, %
ϵ_m	Strain at maximum Stress, %
ϵ_b	Strain at break, %

LIST OF APPENDICES

I. INTRODUCTION AND LITERATURE REVIEW

1.1 Introduction

During the history of energetic materials, many catastrophic incidents have occurred because of the sensitiveness of munitions to thermal and mechanical shock/impact and these has led to the development of "Insensitive Munitions" (IM). IM, also called by the French "Munitions à Risques Atténués, MURAT", have been defined as munitions that reliably fulfil their performance, readiness, and operational requirements on demand, but will minimize the violence of a reaction and subsequent collateral damage when subjected to unplanned stimuli [Victor, 1996]. STANAG 4439 [1998], is a standardisation agreement which gives a policy for the introduction, assessment and testing of IM (MURAT) by defining a series of criteria which should be met. Particularly in rocket propellants, IM will reduce the threat to personnel and minimize the effect of adverse rocket motor response on operational capabilities. Some of these criteria, e.g. fast and slow cook-off, are related to the thermal threat.

Focussing on thermal threats, in a rocket motor, heat causes degradation, decomposition, and finally ignition and reaction of the propellant. The level of violence has been classified according to a scale recommended by the NATO [2002]. According to Victor [1996], a munition's response to fast cook-off is controlled largely by the design and material of the case and its attachments and by the case/propellant interface. In this way acceptable reaction levels are reached for fast cook-off tests when the case is designed to fail structurally prior to propellant ignition. Slow cook-off tests are defined in STANAG 4382 [1996], "Slow heating tests for munitions". The test consists of subjecting the item to a gradually increasing temperature, i.e. 3.3°C h^{-1}, until a reaction occurs [STANAG 4382, 1996]. Thus, although the overall process needs a systemic approach [NIMIC, 2002], the phenomenon is mainly a function of the energetic material (EM) characteristics, which make it more complex than fast cook-off [Victor 1996].

Many rocket motors for tactical applications are composed of a metal case loaded with propellant based on an oxidiser, normally ammonium perchlorate, aluminium fuel, and a

non-energetic rubbery matrix, the most common being polybutadiene binders, e.g. hydroxy terminated polybutadiene (HTPB). These kinds of propellant have been optimized over the past 30 years in terms of improving energy density, mechanical properties, processing and signal characteristics according to the needs of tactical missiles [Hartman, 2000]. An ideal solid propellants should, according to Davenas [1993] and Stacer [1991], have the following characteristics:

1. High specific impulse
2. Good mechanical properties over a wide temperature range
3. Good compatibility between ingredients
4. Good thermal and ageing stability
5. Good processability properties
6. Low toxicity and high level of safety during manufacture
7. Low cost

Therefore an ideal binder needs to meet the following requirements [Stacer, 1991]:

1. Low or non existent glass transition temperature Tg, and low temperature limit between glass transition and rubbery region.
2. Ability to accept high solid loading
3. Low viscosity in high solid loading mixture
4. Molecular weight around 3000 (g mol^{-1}) to avoid increasing viscosity above usable limits and increasing cross-link density of the cured propellant.
5. Chemical compatibility with the oxidiser and plasticizer
6. Narrow molecular weight distribution
7. Two or more functional groups in order to complete the curing reaction
8. Curing through polyaddition (avoiding the production of volatile products), and an athermic reaction.
9. Solubility parameter above 18 $[MJ\ m^{-3}]^{1/2}$, in order to accommodate nitrated ester plasticizers.

From operational conditions for ground, space and air-to-air rockets, Stacer [1991] has identified general structural/rheological properties for an all-application solid propellant (Table 1).

Table 1 General Structural/Rheological Properties of an All-Application Solid Propellant, [Stacer, 1991]

Parameter	Value
Density, (g cm^{-3})	> 1.66
Maximum operating temperature, Tmax, (˚C)	43 to 74
Minimum operating temperature, Tmin, (˚C)	-54 to -18
End of mix viscosity, (kPa s)	< 1.5
Solid loading, (wt %)	> 84
Maximum stress, σm, at Tmax, (kPa)	> 700
Young's modulus, Eo, at 25 ˚C, (MPa)	2 to 6
Strain at maximum stress, Єm at 25 ˚C, (%)	> 45
Єm at Tmin, at 25 ˚C, 5cm/min, (%)	> 20
Єm at Tmin, at 50 m/min at 6.9 MPa, (%)	>15

Together with the characteristics stated in Table 1, a rocket propellant formulation must meet the requirement stated in the STANAG 4439 [1998], related to Insensitive Munitions (IM), as shown in Table 2.

Table 2. Insensitive Munitions Requirements and Tests from STANAG 4439, [1998]

Potential Threat	Test and Test Specification	IM Requirements
Magazine, store, aircraft or vehicle fuel fire	Liquid fuel fire test for munitions (fast heating) STANAG 4240	No response more severe than burning reaction.
Fire in adjacent magazine, store or vehicle	Slow Heating STANAG 4382 3.3 ˚C/h heating rate	No response more severe than explosion reaction.
Small arms attack	Bullet attack test for munitions STANAG 4241	No response more severe than burning reaction.
Fragmenting munition attack	Mil-Std-2105B (US) IT 9282-4 ED1989 (FR)	No response more severe than burning reaction.
Shaped charge weapon attack	Mil-Std-2105B (US)	No response more severe than explosion reaction.
Behind armour debris from armour attack	Mil-Std- 2105B (US)	No sustained burning reaction
Detonation in magazine/store/aircraft or vehicle	Sympathetic Reaction, Munition test procedure STANAG 4396	No response more severe than type III (explosion) of acceptor munitions.

Although Davenas [1993] and Stacer [1991] stated the main ideal characteristics for a rocket propellant and binder, they did it only from a mechanical, rheological, performance and chemical compatibility point of view. Nothing is said about the ideal

material properties to achieve IM requirements, especially taking into account that most rocket motors do not fulfil all IM requirements, particularly in the slow cook-off test [Hartman, 2000].

According to Davenas [2003], despite the fact that the rocket propellant is only one component of a complete system, there are specific characteristics that are contributing factors in reducing the sensitiveness of a propellant. These can be summarised as: 1) modify the reaction of propellants to slow cook-off, 2) increase their toughness, 3) develop less sensitive ingredients, and 4) suitable energy management partitioning between the binder and the fillers.

Today a new family of propellants that would fulfil IM requirements has emerged. They are based on cross-linked Hydroxy-Terminated Polyether (HTPE) binders and are being used in certain composite rocket propellant formulations as alternatives to Hydroxy-Terminated Polybutadiene binders. It is claimed that one advantage of HTPE propellants is that they give a less severe response than HTPB propellants in 'slow cook-off' tests for IM compliance.

The work described in this thesis seeks to gain an understanding of the behaviour of HTPE propellants, particularly in slow cook-off, by investigating the properties of the pre-polymers and the cross-linked binders and their interactions with propellant ingredients such as plasticizers and oxidisers.

1.1.1 General objective

The general objective of the work is to understand the behaviour of HTPE propellants, particularly in slow cook-off tests.

1.1.2 Specific objectives

- To investigate the properties of the pre-polymers and the cross linked binders, and the interaction with propellant ingredients such as fillers and plasticizers.
- To compare properties of HTPE and HTPB propellants.

- To characterise HTPE pre-polymer, HTPE binder and HTPE propellant, by using different chemical, mechanical and ballistic techniques.
- To investigate and compare polymer cross-linking in HTPE and HTPB binders.
- To assess HTPE and HTPB propellants; to study and compare their behaviour under slow cook-off tests.

1.1.3 Research project flow-sheet

The objectives stated previously are presented in a general flow sheet presented in Figure 1 and Figure 2. A literature survey and review was undertaken on hydroxy terminated polyether pre-polymer, binder and propellant and is presented in Chapter I "Introduction and Literature Review". The project was planned to start with the HTPE pre-polymer, as suggested after box 1 in Figure 1. However it was not possible to obtain this copolymer from commercial suppliers or from Roxel UK. Therefore a synthesis process was developed and a copolymer from tetrahydrofuran (THF) and ethylene oxide (EO) was produced and characterised as explained in Chapter II, "HTPE Pre-polymer Synthesis and Characterisation".

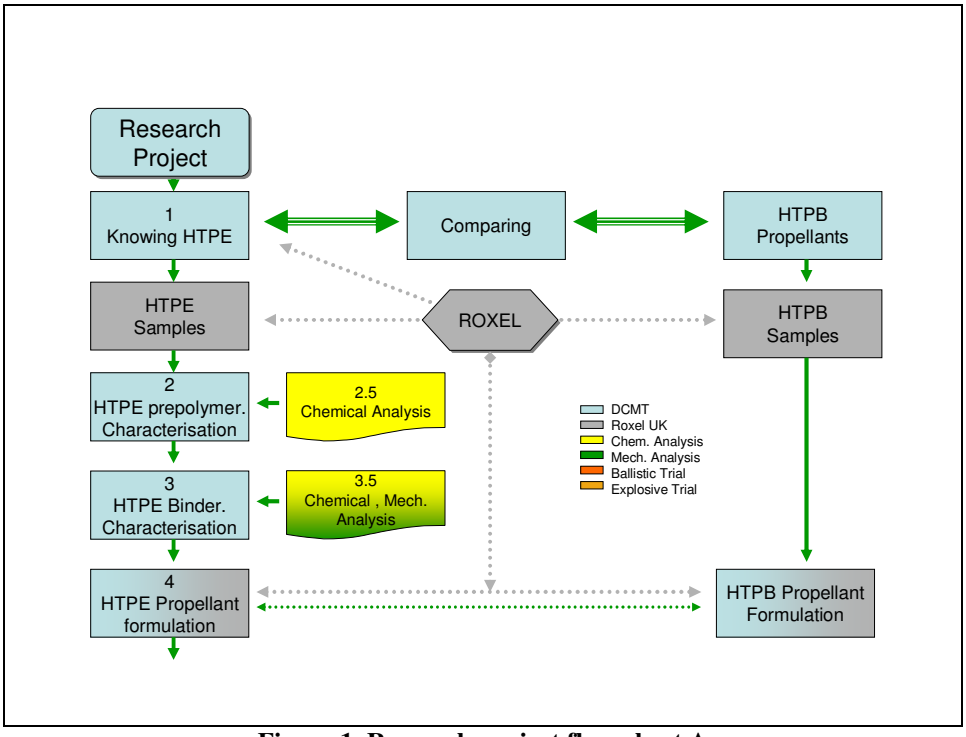

Figure 1. Research project flow-sheet A

In order to try to understand HTPE binder behaviour in terms of thermal threat, HTPE binder network, either plasticized with n-BuNENA or not, was manufactured and characterised. The results are presented in Chapter III, "HTPE Binder Network and Gumstock Manufacture and Characterisation".

The HTPE propellant manufacture, its preparation, curing, characterisation and its use in small cook-off test vehicles for slow cook-off trials are presented in Chapter IV "HTPE Propellant Manufacture and Characterisation" and in Chapter V "Slow Cook-off Tests". Finally the research conclusions and recommendations for future work are presented in Chapter VI "Conclusions and Recommendations".

From Figure 2, box 5 and 6, it can be seen that the propellant manufacture was carried out in Roxel UK facilities. This was because the special equipment needed to make a suitable composite rocket propellant.

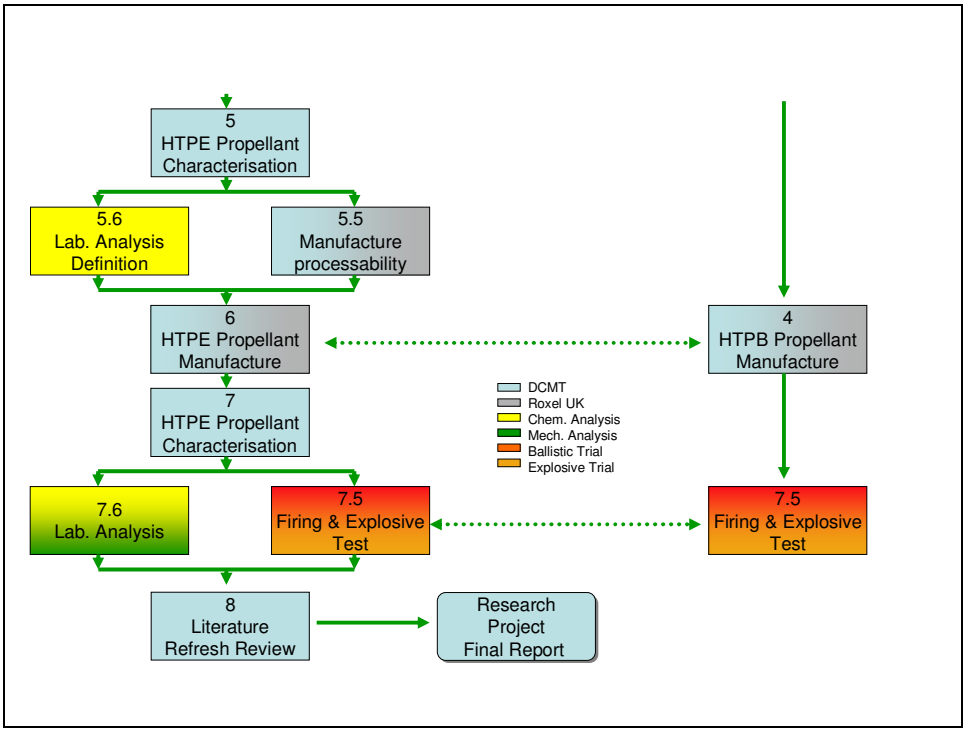

Figure 2. Research project flow-sheet B

1.2 Literature Review

According to Klager [1984], Hydroxy Terminated PolyEther (HTPE) propellants belong to the polyurethane group of rocket propellants and were originally developed in the mid-1950s, before the development of Hydroxy Terminated PolyButadiene (HTPB) propellants. Polyurethane binders are formed by the reaction of hydroxy groups in a molecule with isocyanates, giving a rubbery matrix, as shown in the following general chemical equation (R = general organic group, R'= pre-polymer):

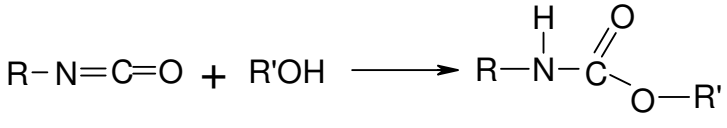

(1.1)

The matrix keeps oxidiser, fuel and other solid or liquid components dispersed. The matrix may or may not contain nitrated ester plasticizers.

Although HTPE is claimed by Alliant Techsystems Inc (ATK), to be a new kind of binder [ATK, 2004], the concept of a polyether binder belongs to an established family of propellants. Initially they were called just polyether propellants and are mentioned by Klager [1984], as a member of the first generation of polyurethane propellants. Later their combination with a nitrated ester plasticizer gave them the name of Nitrate Ester Plasticized Polyether (NEPE) propellants [Zhao, 1999]. They are also called HTPE propellants, developed as less sensitive replacements for HTPB/AP propellants currently used in several tactical missile rocket motors [NIMIC, 2003].

1.2.1 Early polyether binder based propellant

According to Oberth [1969], at the end of the 1960s three kinds of polyether diols were used for propellant applications, all of them using a homopolymeric chain. Two pre-polymers were terminated with secondary hydroxyl groups, poly(1,2-oxypropylene)diol, called PPG, and poly(1,2-oxybutylene)diol, called B-2000. A third polymer was terminated with a primary hydroxyl group called poly(1,4-oxybutylene)diol, designated LD-124, a considerably more reactive component than the first two pre-polymers. Some

of their properties, like molecular weight (Mw), glass transition temperature (Tg), mechanical properties and their applications, together with those of other polyether binders, are shown in Table 3. Oberth [1969] did not present figures for Tg and mechanical properties and did not clarify the concepts "Moderate and High", which are used to describe the mechanical properties. It can be assumed that high means good mechanical properties.

Table 3. Properties of Early HTPE Binders, [Oberth, 1969]

Compound	Name	Made by	Mw, g mol^{-1}	Tg	Mechanical properties	Main application
poly(1,2-oxypropylene)diol	PPG	Dow Chem.	2000*	low	Moderate	propellant
poly(1,2-oxybutylene)diol	B-2000	Dow Chem.	2000	low	Moderate	propellant
poly(1,4-oxybutylene)diol	LD124	Dupont	1000	high	High	liner
poly(1,4-oxybutylene)diol	T30	Dupont	3000	high	High	liner

*The most widely used at that time

Oberth [1969] reported that at low temperature B-2000 does not suffer from moisture embrittlement like LD124 and T30. Some pre-polymers, essentially those containing propylene oxide moieties, are capable of dissolving large quantities of NH_4ClO_4 in the presence of water, thus affecting their low temperature strain capabilities. Polyoxybutylenes are less polar than PPG propellants and hence absorb less water, making them less susceptible to moisture embrittlement.

Oberth [1969] also reported that in comparison with other propellants, those using polyether binders had intermediate specific impulse (***Is***) between polybutadiene and polyester propellants, but had the advantage of greater ageing stability than the other two. One disadvantage of this kind of polyether polymer is that it absorbs oxygen forming peroxides, which at elevated temperatures decompose causing chain cleavage. This problem was controlled by adding aromatic amine antioxidants.

Other polyethers like poly-ethylene oxide are mentioned by Oberth [1969] and also by Arendale [1969], but they are reported to have limited applications as propellant binders.

Table 4 shows mechanical properties reported by Oberth [1969] for the early HTPE propellants, considering different ratios of the two polymers. There is no information about percentages of each pre-polymer. It can be appreciated that in order to produce propellants with good strain (Є) capabilities, binders with low Young's modulus (Eo) at low temperatures are required.

Table 4. Mechanical Properties of HTPE Binder and Propellant Composition, [Oberth, 1969]

Ingredients	Binder		Propellant	
	Eo, psig, (MPa)	**Є, %**	**Eo, psig, (MPa)**	**Є, %**
poly(1,2-oxybutylene)diol + poly(1,4-oxybutylene)diol (*)	2800 (19.30)	>700	54000 (372.3)	4
	620 (4.774)		20000 (137.8)	17
	101 (0.696)		11100 (76.53)	43
	32 (0.220)		7300 (50.33)	57
	20 (0.137)		5500 (37.92)	72

* Strain rate: 0.74 min^{-1}, Temperature: -61˚C

Some ballistic properties of aluminized HTPE and polybutadiene propellants, e.g. maximum specific impulse (***Is***) and density (***ρ***), have been reported by Oberth [1969]. They are summarized in Table 5, where ***Is*** for HTPE propellant is reached using 14% of poly(1,2-oxypropylene)diol binder.

Table 5. Ballistic Properties for Early HTPE Propellant Compositions, [Oberth, 1969]

Binder	***Is*** **(N s kg^{-1})**	***ρ*** **(kg m^{-3})**
poly(1,2-oxypropylene)diol	2423	1.0
Polybutadiene	2442	0.9

Binder density is mentioned due to its influence on ***Is***. In fact, at lower solid loading the higher density of the polyether becomes an advantage because it allows the use of nitro plasticizers, which shift the ***Is*** and maintain propellant density.

A polyether polyurethane propellant composition was reported by Klager [1984], as shown in Table 6. It was called a typical first generation composition and was used in an American project for case bondable propellant called "The Genie Program". It is not specified in the paper which kind of polyether pre-polymer was used.

Table 6. Early HTPE Propellant Composition, [Klager, 1984]

Ingredients	Weight %
Ammonium perchlorate, AP	69.7
Potassium perchlorate	12.3
Burning rate catalyst	0.5
Polyurethane binder	17.5

1.2.2 Nitrate ester plasticized polyether (NEPE) propellants

Attempts at increasing the performance of tactical rocket motors in the middle of the 1970s led to the addition of an energetic plasticizer, i.e. nitrate esters, to polyether binders giving a new family of polyether propellants more often called NEPE propellants [Sparks 1999 and Davenas 2003]. They were developed from a higher molecular weight polyether (4500) and had relatively high elongation, greater than 200% [AGARD, 1990]. Tatcher [1991], reported that NEPE propellants were developed and introduced by Hercules in some missiles like Peacekeeper, Small ICBM and Trident II.

According to Chan [2000], one of the polymers used as a binder for NEPE propellants was based on polyethylene glycol (PEG), and was called PEG propellant. In her work looking for more energetic compositions containing minimum signature propellants, different kinds of plasticizer and oxidant were used, and a comparison with other kinds of binder was included. A summary of the specific impulses for different formulations using PEG is given in Table 7. However, there is no information about ingredient percentages in the propellant formulation and about PEG pre-polymer characteristics.

Table 7. *Is* of PEG Propellant for Different Compositions, [Chan 2000]

Is **s, (N s kg^{-1})**	**Plasticizer**	**Oxidiser**	**Additive**	**Fuel**	**Observations**
270 (2649)	NG[b]	AP	HMX	Al	-
271 (2658)	N.S[a]	ADN[d]	-.-	Al	45% weight of oxidiser
274 (2688)	NG[b]	-.-	HMX	Al	-
277 (2717)	BTTN[c]	ADN	-.-	Al	-
291 (2855)	BTTN	ADN	-.-	AlH3	-

[a]Not Specified, [b]Nitroglycerine, [c]Butanetriol trinitrate, [d]Ammonium dinitramide

Although Chan [2000] was analysing the potential use of PEG in high energy propellants, Huimin Tan [2000] says that it is known that polyethyleneglycol pre-

polymers used in NEPE propellants at low temperatures tend to form crystals. These crystals are mainly spherulites, and he found they still exist in the NEPE propellant binder, although the crystallisation tendency is suppressed by the addition of large amounts of nitrate ester plasticizers. Propellants with a tendency to crystallise have low strain capabilities, especially at low temperature. According to Chan [2000], elongation in NEPE propellant is around 20% at -40°C. This is relatively low when compared with 30% HTPB elongation at -42°C reported by Hartman [2000], but within the limits according to the ideal rheological properties proposed by Stacer [1991] in Table 1.

Zimmerman [1982], attempted to eliminate the loss in strain capabilities of NEPE propellants on storage at low temperature. This work was done with propellants based on PEG binder containing different energetic plasticizers, such as butanetriol trinitrate (BTTN), triethylene glycol dinitrate (TEGDN), trimethylolethane trinitrate (TMETN), diethylene glycol dinitrate (DEGDN), NG and their mixtures. Mechanical properties were measured after long storage periods at low temperatures i.e. 4 weeks at -40°C, and tests were carried at -54°C. They found that the primary cause of poor mechanical properties at low temperature was the plasticizer crystallization, which is not necessarily related to plasticizer freezing point, and that crosslink and propellant composition have a secondary effect.

Table 8. Mechanical Properties from Embrittlement Testing. PEG Binder Propellant with BTTN Plasticizer, [Zimmerman, 1982]

Cycles -12 to -40 (°C)	Maximum stress, σ_m (MPa)	Strain at maximum Stress, ϵ_m (%)	Strain at break ϵ_b, (%)	Young's modulus, Eo, (MPa)
0	5.57	13	68	193
2	5.22	13	71	179
4	5.62	11	83	230
8	4.68	13	76	179
14	5.27	13	75	217
28	5.74	10	74	191
42	5.80	12	60	219
84	5.51	11	73	218

As a result of their experiment, Zimmerman [1982] showed that BTTN eliminates embrittlement of nitrate ester plasticized propellants, and they reported that other investigators have found that mixtures with NG containing at least 50% of BTTN are suitable to eliminate that problem. Apparently its strong resistance to crystallization

gives BTTN this characteristic. Table 8 shows the results of mechanical tests at -54°C, after submitting propellant to temperature cycling for up to 84 days.

Good mechanical properties over a wide temperature range, i.e. -40 to 70°C, is one of the important properties that a rocket propellant must have. A comprehensive study of mechanical properties, i.e. tensile strength, strain, modulus and structural assessment for rocket propellant, has been published [AGARD, 1997].

According to Huimin Tan [2000], good mechanical properties in a polymer binder are influenced by chain symmetry and regularity. In other words, flexible chains consisting of symmetrical structural units and/or highly regular sequence arrangements, show a tendency to crystallise below the melting point due to the decrease of free energy and system entropy. Thus, decreasing a binder chain's stereoregularity by introducing a suitable proportion of another structural unit into the polymer chain will contribute to reduce the crystallization tendency, thus improving mechanical properties, especially at lower temperatures. Consequently, a random copolymer based on 50% of ethylene oxide (EO) and 50% of tetrahydrofuran (THF), having the extent of alternation of the structural units close to 50%, was mentioned by Huimin Tan [2000] as a good copolymer for NEPE propellant binders.

Results showed by Huimin Tan [2000] in terms of having a EO/THF random copolyether are in accordance with the data presented by Zhang [1994]. In fact by using 1D ^{1}H and ^{13}C Nuclear Magnetic Resonance (NMR) techniques, Zhang [1994] found an average alternate degree of 50% and an average functionality (f_n) of 2, when a volume ratio of 50% of EO and 50% of THF is used for copolymer manufacture. An average molecular weight of 3385 was found. Zhang [1994] also reported some peak overlaps in the ^{13}C spectra of the copolymer which produced difficulties in assignments.

According to Huimin Tan [2000], the copolyether was synthesized by bulk polymerisation using BF_3 as a complex catalyst. The exact molecular weight of this copolymer it is not mentioned, but it is claimed to be between 2000 and 6000. Figure 3

shows the equation for the reaction between EO and THF presented by Huimin Tan [2000].

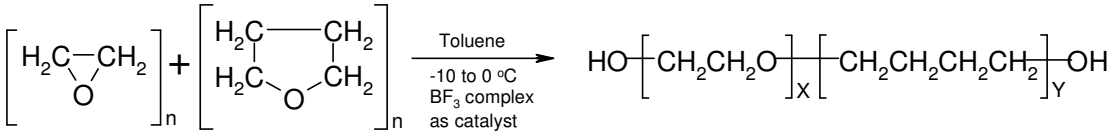

Figure 3. General chemical equation for EO/THF copolymer formation

Ingredients and mechanical properties of a propellant based on an EO/THF copolymer binder proposed by Huimin Tan [2000], are shown in Table 9 and Table 10 respectively.

Table 9. Ingredients of a Propellant Based on a THF/EO Copolymer Binder, [Huimin Tan, 2000]

Ingredients	Content	Function
THF/EO alternation extent, %	50	Copolymer
NG/BTTN, ratio 1:1	n.s.	Plasticizer
Ammonium perchlorate (AP)*	n.s	Oxidiser
Aluminium (Al)*	n.s	Fuel
HMX*	n.s	Solid filler
Isocyanate N-100	n.s	Curing and cross link agent

* Total solid content 75 %; Weight ratio between copolymer and plasticizer (Wpl/Wpo): 2.80; n.s. not specified

Table 10. Mechanical Properties of THF/EO Propellant, [Huimin Tan, 2000]

Temperature (^oC)	Max. stress, σ_m (MPa)	Max. strain, ϵ_m (%)
70	0.642	62
20	0.945	67
-40	1.860	107

Despite good mechanical properties of the THF/EO propellant reported by Huimin Tan [2000], Zhao [1999] affirms that there are limited applications for this sort of composition due to their high pressure exponent (***n***), e.g. 0.7 at 5 MPa. In order to understand the high pressure exponent of this kind of propellant, Zhao [1999] carried out thermal decomposition studies of NEPE propellants containing HMX and AP oxidiser, using Pressure Differential Scanning Calorimetry techniques (PDSC). He found that in comparison with pure HMX decomposition, when HMX is mixed with an energetic plasticizer, i.e. NG/BTTN and AP, its decomposition temperature decreases by around 50^{o}C. Also by the use of a catalyst, i.e. lead salt, AP decomposition can be promoted in order to release heat at a lower temperature, thereby increasing the burning rate and leading to a lower pressure sensitivity. Composition and burning rate

information on a NEPE propellant used by Zhao [1999] are shown in Table 11 and Table 12 respectively.

Table 11. Composition of NEPE Propellants, [Zhao, 1999]

Ingredients	Content	Obs
NEPE and NG/BTTN	25 %	-.-
AP* and HMX	73 %	Ratio 20/7
Lead Salt	2%	Burning catalyst

*Particle size: 80-120 μm

Table 12. Burning Rates (r_b) and Pressure Exponent (n) of NEPE Propellant at Different Pressures, [Zhao, 1999]

Formulation	r_b (mm s^{-1})				n		
	4 (MPa)	5 (MPa)	6 (MPa)	7 (MPa)	4-5 (MPa)	5-6 (MPa)	6-7 (MPa)
without lead Salt	7.49	8.68	9.86	11.16	0.66	0.70	0.75
with Lead Salt	8.53	9.67	10.46	11.82	0.57	0.56	0.65

Luo [1999], using Fourier Transform Infrared (FTIR) and NMR techniques, studied the effect of energetic plasticizers, i.e. NG and BTTN, on the degradation of EO/THF NEPE propellants. After 500 h of thermooxidative degradation, the presence of carbamates was detected. They proposed that carbamates were produced by the reaction between alcohols and isocyanates. Alcohols were generated by the hydrolysis of nitrate esters through the degradation process.

1.2.3 Present hydroxy terminated polyether propellant concept

According to NIMIC [2003], a new family of propellants based also on a binder system containing hydroxy terminated polyether (HTPE) has been developed by the company Alliant Techsystems (ATK). It is claimed these propellants were developed by ATK under contract to the Naval Air Warfare Center Weapons Division, China Lake, USA, as a less sensitive replacement for HTPB/AP used in many tactical rocket motors, i.e. to fulfil IM requirement stated in STANAG 4439 [STANAG, 1998].

The chemical structure of the ATK HTPE copolymer has been presented by Comfort [2004] and consists in a block copolymer of poly-1,4-butanediol and polyethyleneglycol in a ratio of 1 to 1 approximately. Davenas [2003] and NIMIC [2004 a] agree that the

development of this type of propellant was to reduce solid loading by using an energetic plasticizer compatible with HTPE binder i.e. n-BuNENA, maintaining in this way the specific impulse at or above of a comparable HTPB, and also reducing sensitivity by replacing a percentage of AP by AN.

1.2.3.1 HTPE propellant formulations

In 1994 Goleniewski [1994] from Hercules Incorporated patented a solid propellant based on a polyether binder with an inert plasticizer. They claimed this material had improved characteristics in comparison with HTPB propellants, in particular:

- Higher electrical conductivity, which reduces the possibility of having accidents due to electrostatic discharges, like the aluminized HTPB propellant incidents reported by Davenas [2002]. Because polyethers are more polar than HTPB, they can be mixed with polar plasticizers. The higher polarity allows this kind of binder to dissipate the static electricity much more rapidly.
- Lower depressurization rates to extinguishment is what make them safer, as shown in Table 25. Higher levels of inorganic oxidiser are associated with high depressurization rates, however due to the oxygen content of the polymer and plasticizer the oxygen to fuel ratio is increased and less inorganic oxidiser is required.
- Higher solid loadings, which increase the density and improves the overall performance of the propellant.
- Lower response to IM tests. Reduction of solid load, i.e. AP, is related to reduced propellant sensitiveness.

It is also reported by Goleniewski [1994] that binders made from poly-tetrahydrofuran (PTHF) crystallize and have reduced strain capabilities at low temperatures. The polyether used by Goleniewski [1994], includes random copolymers of EO and THF with a Mw between 1000 and 3000 g mol^{-1}. It has an EO content from 15 to 40% and was supplied by E.I. duPont de Nemour Inc., under the name of Teracol TE 2000 (Mw

2000 g mol^{-1}, EO 38% and THF 62%), and by BASF Corporation under the name of ER-1250/25 (Mw 1250 g mol^{-1}, EO 25% and THF 75%).

Due to their polarity, polyethers have a wider spectrum of potential plasticizers than HTPB. The latter is plasticized only by dioctyl sebacate (DOS), and dioctyl adipate (DOA). A summary by Goleniewski [1994] of propellant compositions containing different ingredients is presented in Table 13. Goleniewski [1994] presented three kinds of rocket propellant formulations: space booster, ground launched short range ballistic missile and air launched short range attack missile, as seen in Table 14.

Table 13. Ingredients for HTPE/Inert Plasticizer, [Goleniewski, 1994]

Ingredients	Alternative ingredients	Range	Function
Polyether non crystalline	Teracol TE 2000 ER-1250/25	3-10 %	Binder
Inert Plasticizer	Triacetin, Acetyl tri-n-butyl citrate, Acetyl triethyl citrate, Triethylene glycol bis-2 ethylbutyrate, Tetraethylene glycol bis-2-ethylexoate	3-10 %	Plasticizer
Bis hydroxyethyl glycolamide (BHEGA)	Epoxy-Amine (0.06% bisphenol-A epoxy resin and 0.04% triethylenetetramine	0-0.3 %	Bonding agent
Isocyanates	Isophorone diisocyanate (IPDI, Hexamethylene diisocyanate (HDI), Dimeryl diisocyanate (DDI), Desmodur N-100	0.5-2.0 %	Cross link agent
AP	 AN, Hydrazinium nitrate, Lithium nitrate, Sodium nitrate (scavenger), HMX or RDX	0-70% 0-70 % 0-70 % 5-56 % 0-60 % 0-50 %	Oxidiser
Aluminium	Magnesium, Zirconium and combinations	16-25 %	Fuel
Triphenyl bismuth	Maleic anhydride	0-0.1 %	Cure catalyst
Iron oxide	2-Nitrodiphenylamine (NDPA)	0-1.0 %	Burning rate catalyst

In 1998, Goleniewski [1998] patented a solid HTPE propellant having an energetic plasticizer in its formulation. They used the same binder as in their previous patent, and reported similar characteristics but improved specific impulse compared to HTPB propellants due to the use of an energetic plasticizer, and also improved mechanical properties. Propellant compositions containing different ingredients are presented in Table 15 and formulations for several rocket motor applications are presented in Table 16.

Table 14. Propellant Formulation for Different Applications, [Goleniewski, 1994]

Alternative ingredients	Space Booster (SB), Weight %	Ground launched missile (GLM), Weight %	Air Launched Missile (ALM), Weight %
ER-1250/25	4.85	6.93	5.05
Acetyl tri-n-butyl citrate,	6.50	8.50	6.50
Epoxy-Amine*	0.10	0.10	0.10
IPDI	-.-	1.046	0.72
DDI	1.31	-.-	
Desmodur N-100	0.14	0.324	0.63
AP	63.50	54.00	53.00
HMX	-.-	10.00	12.00
Aluminium	23.50	19.00	22.00
Triphenyl bismuth	0.05	0.05	0.02
Maleic anhydride	0.05	0.05	0.02

*0.06% bisphenol-A epoxy resin and 0.04% triethylenetetramine

Table 15. Ingredients for HTPE/Energetic Plasticizer, [Goleniewski, 1998]

Alternative	Range	Function
Teracol TE 2000, ER-1250/25	3-12 %	Polyether non crystalline binder
n-butyl-2-nitratoethylnitramine (n-BuNENA), ethyl-2-nitratoethylnitramine (EthylNENA) TEGDN, DEGDN, NG	1-12 %	Plasticizer
BHEGA Epoxy-Amine (0.06% bisphenol-A epoxy resin and 0.04% triethylenetetramine)	0-0.3 %	Bonding agent
Isophorone diisocyanate (IPDI, Hexamethylenediisocyanate (HDI), Dimeryl diisocyanate (DDI), Desmodur N-100	0.5-2.0 %	Cross link agent
AN, AP, Sodium nitrate (scavenger), Hydrazine nitrate, Lithium nitrate,	0-60%	Oxidiser
HMX or RDX	0-20	Oxidiser
Al, Mg, Zr and combinations	2-24 %	Fuel
Maleic anhydride	0-0.1 %	Cure catalyst
N-methyl-p-nitroaniline (MNA) 2-nitrodiphenylamine (2-NDPA)	0-0.1%	Nitrate ester stabilizer
Fe_2O_3, Al_2O_3, Cr_2O_3	0-4.0 %	Burning rate catalyst

Table 16. Propellant Formulation for Different Applications, [Goleniewski, 1998]

Alternative ingredients	Space booster (SB), Weight %	Ground launched missile (GLM), Weight %	Air launched missile (ALM), Weight %
ER-1250/25	6.649	-.-	-.-
TERACOL TE 2000	-.-	6.042	5.946
n-BuNENA	8.5	8.5	6.5
MNA	0.1	0.4	0.4
BHEGA	0.1	-.-	-.-
IPDI	1.24	-.-	-.-
Desmodur N-100	0.311	0.589	0.348
Triphenyl bismuth	0.05	0.05	0.05
Maleic anhydride	0.05	0.05	0.05
AP	35.1	51.5	60.0
Sodium Nitrate	25.4	-.-	-.-
Aluminium	22.5	21.5	23.0
Epoxy-Amine*	-.-	0.10	0.10
DDI	-.-	2.112	-.-
RDX	-.-	10.0	-.-

*0.06% bisphenol, an epoxy resin and 0.04% triethylenetetramine

Although Goleniewski [1998] presented n-BuNENA and EthylNENA plasticizers for use in HTPE propellant formulations, Provatas [2000] has reported a potential incompatibility between NENA plasticizers and ammonium perchlorate. Provatas [2000] also reported that on long-term ageing NENA plasticizers can migrate, although this behaviour has not been seen when they are used in polyNIMMO and poly GLYN binders. However, those problems were not reported by Goleniewski [1998]. Although Goleniewski [1998] claimed this kind of propellant can be used for IM formulations, they did not report any results related to this issue.

Based on the work of Goleniewski [1994, 1998] Comfort [2000 a] patented a propellant composition using bismuth oxide as oxidant together with AP, an HTPE like binder and n-BuNENA from the family of NENA plasticizers. This formulation had an increased impulse-density of around 10% compared with propellants using just AP as oxidiser. In this patent, the binder is described as a group of various copolymers of ethylene oxide and THF and claims that the most suitable for propellant application is the one derived from THF and polyethylene glycol (PEG), called TPEG. However, there is no detailed definition of the copolymer composition. Different ingredients and propellant compositions are mentioned, as shown in Table 17.

Table 17. Ingredients for HTPE Propellants, [Comfort, 2000 a]

Ingredients	Alternative ingredients	Range	Function
TPEG	Hydroxy terminated polyether having with average MW of 1000 to 9000	3-12 %	Binder
n-BuNENA	TMETN, TEGDN, BTTN and mixtures	5-15 %	Plasticizer
Bi_2O_3	-.-	10-40 %	Oxidiser
AP	-.-	25-60 %	Oxidiser
Ammonium nitrate (AN)	-.-	0-10 %	Oxidiser
Aluminium	Magnesium, Zirconium and combinations	15-25 %	Fuel
Isocyanates	Isophorone diisocyanate (IPDI, Hexamethylene diisocyanate (HDI), Dimeryl diisocyanate (DDI), Desmodur N-100	0.5-2.0 %	Cross link agent
N-methyl-p-nitroaniline (MNA)	2-Nitrodiphenylamine (NDPA)	0.2-1.0 %	Stabilizer

Comfort [2000 a] also presented as a baseline an HTPE propellant formulation both with and without Bi_2O_3, as shown in Table 18. This information is complemented with the formulation presented by Smith [2000] when testing two samples of Alliant Techsystems HTPE propellants. Smith [2000] says nothing about the plasticizer,

however it can be read across that the 19% of binder in the formulation includes the plasticizer content. Comfort [2000 a] does not report any incompatibilities between AP and the energetic plasticizer n-BuNENA, or its migration. It is also reported by him that these kinds of polyether were available from E.I. duPont de Nemours, Inc. of Welmington, Del, USA and from Alliant Techsystems ABL of Rocket Center, W. Va, USA.

Table 18. Ingredients for HTPE Propellants with and without Bi_2O_3, [Comfort 2000a, Smith 2000]

Ingredients	Base line 1 HTPE (%)	Base line 2 HTPE (%)	Base line HTPE (%)	HTPE with Bi_2O_3 (%)
HTPE	19	19	-.-	-.-
TPEG	-.-	-.-	6.6	5.5
n-BuNENA	-.-	-.-	10.4	8.2
Bi_2O_3	-.-	-.-	-.-	21
AP	51	69.5	51	44
AN	10	10	10	0
AL	20	-	20	20
Isocyanates	-.-	-.-	1.3	0.8
MNA, NDPA	-.-	-.-	0.7	0.5
Other	-.-	1.05	-.-	-.-
Volumetric impulse, Lb s in^{-3} (Kg s cm^{-3})	-.-	-.-	16.98 (0.4700)	18.60 (0.5148)

Particle size for the AP oxidiser has been proposed by Chan [2002] to be between 200 to 80 μm and between 10 to 15 μm, as it is normally used in bimodal mixtures. On the other hand Chan [2002] proposed to used AN of particle size between 40 to 60 μm.

More information was provided later by Comfort [2004] in relation to the kind of HTPE pre-polymer used by ATK. According to Comfort [2004] the HTPE pre-polymer was designated as TPEG. TPEG is a block copolymer synthesized by the reaction between poly-1,4-butanediol (poly THF) and polyethylene glycol (PEG). The synthesis process was reported to be performed with 25% of sulphuric acid (as a catalyst) at a reaction temperature of approximately 130°C. The depolymerisation and copolymerisation was reported to be complete after 12 to 14 h. After that period the reacting mix was quenched by water, neutralized by using lime, separated by decantation, dried, filtered, mixed with BHT antioxidant and stored. No details were given relating to the cocatalyst or to the process itself. A summary of the main TPEG characteristics, described by Comfort [2004] for the first lot of TPEG pre-polymer, are presented in Table 19.

Table 19. HTPE TPEG Pre-polymer Main Characteristics, [Comfort 2004]

Ingredients	PEG (%)	Poly THF (%)	Mn (%)	OH equiv. weight (%)	Viscosity at 120°F (49°C) (p)	BHT %)	Water (%)
Max. specification	55	55	3400	1700	15	0.2	0.05
Min. specification	45	45	2700	1300	-.-	0.05	-.-
Average	47	53	2903	1535	12	0.07	0.03

No details about HTPE TPEG propellant manufacture were presented. Propellant was plasticized with n-BuNENA and mechanical properties at -40°F (-40°C) were presented as: Stress 331 psi (2.2 MPa), failure strain 57% and modulus 1077 psi (7.4 MPa). However later on Fletcher [2006], gave more information regarding the TPEG HTPE based propellants of Comfort [2004]. It was reported by Fletcher [2006] that the propellant was stabilised with MNA and 2NDPA, around 0.37 and 0.24% respectively for a reduced smoke HTPE propellant. Mechanical properties at ambient temperature were presented as: Stress 152 psi (1.048 MPa), failure strain 36% and modulus 757 psi (5.22 MPa).

Tzeng [1998], introduced another kind of HTPE pre-polymer called hydroxy terminated caprolactone ether (HTCE). The pre-polymer was a block copolymer of tetramethylene ether and caprolactone. Tzeng [1998] stated that the HTPE block copolymer of tetramethylene ether and ethylene ether can dissolve the AP because of the poly-ethylene blocks, increasing the propellant sensitivity to mechanical shock stimuli. Tzeng [1998] stated that AP solubility in poly ethylene ether is around 10% while in HTCE is less than 1.5%. However no mechanical data or insensitive munition test results were supplied and no further paper from the author was found. Also AN was not reported as an oxidiser in the formulations. Isophorone diisocyanate (IPDI), dimeryl diisocyanate (DDI), Desmodur-W-di-functional Isocyanate Desmodur N-100 and Desmodur N-3200 were used as curing agents. Tetrafunctional caprolactone was used as cross-linker, except with Desmodur N-100 and N-3200. As plasticizer n-BuNENA was used.

Chan [2005] based her research on the Tzeng [1998] HTCE binder and was looking for a new high performance booster propellant (to be operating at chamber pressures between 27 and 35 MPa). She proposed the use of a HTCE binder for HTPE propellant, based on polycaprolactone and polytetrahydrofuran in a ratio 1 to 2. According to Chan [2005] the pre-polymer has an equivalent weight of 1000 eq g^{-1} and was produced by

Solvay Interox Inc. in the USA. The propellant used n-BuNENA as plasticizer and several oxidiser or energetic fillers such as CL-20, RDX or AP were used with or without Al as fuel. There is no information about the kind of curing agent, although it is likely to be similar to that suggested by Tzeng [1998]. However, Chan [2005] incorporated different bonding agents, such as HX-72 and HX-878 (Tepanol) in order to improve mechanical properties. Chan [2005] found that in propellants containing only AP as oxidiser, mechanical properties were not considered acceptable compared to when using CL-20 or RDX as fillers.

1.2.3.2 HTPE propellant performance

Performance comparisons of HTPE against HTPB propellants containing 88% solids loading was presented by Goleniewski [1994] for three kinds of rocket motor propellant formulations: space booster (SB), ground launched short range ballistic missile (GLM) and air launched short range attack missile (ALM). SB and ALM rocket motor propellant performances are shown in Table 20.

Table 20. Performance Comparison for SB and ALM Applications versus Standard HTPB Propellant, [Goleniewski, 1994].

Parameter	Comparison SB		Comparison ALM	
	HTPB 88% solids	**HTPE 87% solids**	**HTPB 87% solids**	**HTPE 87% solids**
Theoretical *Is*[a], Lbf s lbm^{-1}, (N s kg^{-1})	263.6 (2585.9)	260.8 (2558.4)	263.6 (2585.9)	262.9 (2579.0)
Density, lb in^{-3}, (kg m^3)	0.065 (1799.19)	0.067 (1854.55)	0.065 (1799.19)	0.067 (1854.55)
Oxygen-fuel ratio*	1.26	1.26	1.221	1.156
σm, psi (2 ipm @ 77 ˚F), (MPa)	116 (0.799)	150 (1.034)	-.-	-.-
Єm, %	35	69	-.-	-.-
Eo, psi (MPa)	552 (3.805)	550 (3.792)	-.-	-.-
Volume resistivity at 20 Volts (ohm-cm)	$1*10^{13}$	$8.4*10^{9}$	-.-	-.-
Dielectric constant at 1000 Hertz	8.0	13.1	-.-	-.-
Volumetric impulse, $Lbsin^{-3}$, Kg s cm^{-3}	17.13 (0.4742)	17.47 (0.4836)	17.13 (0.4742)	17.61 (0.4874)

*moles O_2 · (moles C + 1.5 moles Al)$^{-1}$, [a]at sea level

According to Goleniewski [1994] (Table 20), the HTPE propellant formulation for Space Booster application is more electrically conductive than HTPB propellant. Its volume resistivity is lower by around three or four orders of magnitude, which is also reflected in the higher dielectric constant. The lower the volume resistivity, the lower the probability of having electrostatic discharge accidents [Davenas, 2002]. These values agree with the volumetric resistivity data for binders reported by Davenas

[2002]. In fact, for HTPB and HTPE binders, volume resistivity is reported to be around $2x10^{12}$ ohm-cm and $6x10^{8}$ ohm-cm respectively. There is no information from Davenas [2002] about what kind of HTPE was used as the binder in their measurements.

Goleniewski [1998] presented a performance comparison between a HTPE propellant having an energetic plasticizer in its formulation and a standard HTPB propellant, as shown in Table 21.

Table 21. Performance Comparison for SB and GLM Applications versus Standard HTPB Propellant, [Goleniewski, 1998]

Parameter	Comparison SB		Comparison GLM		Comparison ALM	
	HTPB 88% solids	**HTPE 83% solids**	**HTPB 89% solids**	**HTPE 83% solids**	**HTPB 89% solids**	**HTPE 83% solids**
Theoretical *Is*[a], Lbf s lbm^{-1} (N s kg^{-1})	243 (2384)	247 (2423)	265.8 (2607.5)	266.2 (2611.4)	263.5 (2584.9)	264.4 (2593.8)
Density, lb in^{-3} (kg m^{-3})	0.067 (1854.5)	0.068 (1882.2)	0.065 (1799.1)	0.065 (1799.1)	0.066 (1826.8)	0.066 (1826.8)
Oxygen-fuel ratio*	1.26	1.25	1.17	1.16	1.23	1.20
σm, psi (2 ipm @ 77˚F), (MPa)	116 (0.799)	134 (0.924)	109 (0.751)	85 (0.586)	85 (0.586)	145 (0.999)
Єm, %, (2 ipm @ 77 ˚F (25˚C))	31	34	29	27	35	45
Eo, psi (2 ipm @ 77 ˚F (25˚C)), (MPa)	534 (3.681)	519 (3.578)	668 (4.605)	646 (4.454)	419 (2.888)	431 (2.971)
Єm, % (100 ipm @ 40 ˚F (4.4˚C), 1000 psi),	40	73	-.-	-.-	-.-	-.-
σm, psi (2 ipm @ -25˚F, (-31.6˚C), (MPa)	-.-	-.-	219 (1.509)	200 (1.378)	-.-	-.-
Єm, %, (2 ipm @ -25 ˚F), (MPa)		-.-	30	55	-.-	-.-
Eo, psi (MPa), (2 ipm @ -25 ˚F (-31.6 ˚C)), (MPa)	-.-	-.-	1699 (11.71)	1140 (7.860)	-.-	-.-
Єm, % (100 ipm @ -25 ˚F (-31.6 ˚C), 1000 psi),	-.-	-.-	40	62	49	58
Єm, % (100 ipm @ -45 ˚F (-42.7˚C), 1000 psi),	-.-	-.-	-.-	-.-	37	40
Єm, % (100 ipm @ -65 ˚F (-53.8˚C), 1000 psi),	-.-	-.-	-.-	-.-	16	18
Volume resistivity at 20 Volts (ohm cm)	1 10^{13}	1 10^{8}	1 10^{13}	1 10^{8}	1 10^{13}	1 10^{8}

*moles O_2 · (moles C + 1.5 moles Al)$^{-1}$

[a]at sea level

According to Goleniewski [1998], the HTPB propellants presented in Table 21 had similar formulations to the corresponding HTPE propellants. It can be seen that all HTPE formulations have better electrical conductivity characteristics than HTPB propellants and are also better than HTPE with inert plasticizers (Table 20). Specific Impulse is also higher than in HTPB formulations. A similar situation occurs with mechanical properties, especially at low temperatures and high strain rate.

In 1994 Comfort [1994] presented an HTPE propellant formulated with polymers obtained from BASF and DuPont, cured by using isocyanates and a cure catalyst and having AP as oxidant. A similar study was presented in 1996 by Comfort [1996] with slight differences from the previous paper. There are no details about quantities or quality of the formulation. Hartman [2000] and Comfort [1994, 1996 and 2000 b] compared ballistic and physical properties of HTPE and HTPB propellants. Also Coleno [2003] presented a comparison between HTPB and an HTPE propellant called "Oxargol". The oxargol formulation was: AP 80%, Al 4% and n-BuNENA like energetic plasticizer and a commercial polyether which was not detailed. The results are presented in Table 22.

Table 22. Ballistic and Physical Properties Comparison of HTPE and HTPB Propellants

Properties	HTPB			HTPE		
	Reference			Reference		
	Comfort 1994 and 1996	Hartman 2000	Comfort 2000 b	Comfort 1996, Coleno, 2003	Hartman 2000	Comfort 2000b
Ballistics						
Is ρ, Lbf s in^{-3}, (kgf s cm^{-3})	≥ 15 (0.42)	≥ 15 (0.42)	-.-	≥ 15 (0.42)	≥ 15 (0.42)	-.-
*Is*ρ, metallized Lbf s in^{-3}, (kgf s cm^{-3})	-.-	≥ 17 (0.47)	-.-	-.-	≥ 17 (0.47)	-.-
Burning rate at 1000 psi, rb_{1000}, ins^{-1}, (mm s^{-1})	0.40 (10.16)	(7.6-30)	-.-	0.40 (10.16)	(7.6-20)	-.-
Burning rate at 7 MPa, at 20 ˚C, mm s^{-1}	-.-	-.-	39.6	-.-	-.-	14.5
Burning rate at 20 MPa, at 20 ˚C, mm s^{-1}	-.-	-.-	56.8	-.-	-.-	23.4
Pressure exponent	0.45	0.5	0.34	0.50	0.5	0.45
Temperature sensitivity π_p, K^{-1}	0.10	0.18	0.3	0.10	0.18	0.17
Mechanical						
Stress at 77 ˚F (25˚C), MPa	120	-.-	-.-	150	-.-	-.-
Strain at 77 ˚F (25˚C), %	55	-.-	-.-	45	-.-	-.-
Young's modulus at 77 ˚F (25˚C), psi, (MPa)	600 (4.137)	-.-	-.-	500 (3.447)	-.-	-.-
Young's modulus at 25˚C, MPa	-.-	4.2	-.-	-.-	3.5	-.-
Stress at 25 ˚C, MPa	-.-	0.84	-.-	-.-	1.0	-.-
Strain at 25 ˚C, %	-.-	40	-.-	-.-	50	-.-
Ignition strain at -54 ˚C, %,	-.-	15	-.-	-.-	20	-.-
Thermal Strain at -65 ˚F (-53˚C), %	30	30	-.-	40	40	-.-
Viscosity, kp	4	4	-.-	2	2	-.-
Others						
Pot life, h	10	-.-	-.-	20	-.-	-.-
Shock sensitivity	Zero Card	-.-	-.-	Zero Card	-.-	-.-
Service life, years	>10	-.-	-.-	>10	-.-	-.-
signature	Reduced smoke	-.-	-.-	Reduced smoke	-.-	-.-

From Table 22, it can be seen that results show better mechanical and processing properties for HTPE propellants rather than HTPB propellants, but in terms of ballistic properties HTPE propellants have larger pressure exponents than HTPB propellants.

Smith [2000] reported the temperature sensitivity (π_p) behaviour, for both of the propellant formulations presented in Table 18 (Baseline 1 and 2). The burning rate was

measured at 24˚C and 64˚C using an ultrasonic rate measurement technique, and then temperature sensitivity was calculated. They found that in the aluminised propellant the trend is for π_p to decrease when pressure is increased, i.e.; π_p at 500 psi (3.4 MPa), 1000 psi (6.9 MPa) and 3000 psi (20.7 MPa), was found to be 0.0015, 0.001 and 0.0005 K^{-1} respectively, while in non-aluminised formulations it was the other way round, i.e.; π_p at 500 psi (3.4 MPa), 1000 psi (6.9 MPa) and 2000 psi (13.8 MPa) was found to be 0.0, 0.001 and 0.0015 K^{-1}. On the other hand, values of π_p found by Smith [2000] are considerably lower than the ones presented by Hartman [2000], Comfort [1994, 1996 and 2000 b] and Coleno [2003], as can be seen from Table 22.

Although Comfort [1994, 1996 and 2000 b] did a comparison with HTPB using different criteria, they did not specify the Mw of the polymers. However, they presented in the same paper the mechanical properties corresponding to two kinds of molecular weight polymers (as seen in Table 23). The polymer having Mn of 3018 looks like the one used for the comparison against HTPB in Table 21.

Table 23. Mechanical Properties of Two HTPE Propellants, [Comfort, 1994, 1996 and 2000 b]

Properties	HTPE	HTPE
Molecular Weight, g mol^{-1}	2730	3018
Stress at 77 ˚F (25˚C), psi (MPa)	141 (0.97)	150 (1.03)
Strain at 77 ˚F (25˚C), %,	40	45
Young's modulus at 77 ˚F (25˚C), psi, (MPa)	585 (4.033)	500 (3.447)
Thermal expansion coefficient, in in^{-1} $°F^{-1}$	$0.38*10^{-4}$	$0.38*10^{-4}$

In 2000, Comfort [2000 b] presented complementary information to that presented before [Comfort, 2000 a], in relation to the performance of HTPE propellant containing bismuth oxide. By adding AN to the composition they obtained specific impulse, propellant density, burning velocity and pressure exponent for two kinds of HTPE propellant, as shown in Table 24.

Comfort [2000 b] presented data for seven years ambient ageing of HTPE propellant (unspecified composition). They found the stabilizer loss was around 0.01%, the tensile strength remained almost unchanged at about 150 psi and the strain % showed a gradual increase from 35% to around 40%.

Table 24. Performances for HTPE Propellants with and without Bi_2O_3, [Comfort, 2000 b]

Propellant	HTPE with Bi_2O_3	Aluminised HTPE
Density, Lb in^{-3}(kg m^{-3})	0.079, (2186)	0.064, (1771)
Specific impulse, Lbf lbm^{-1} s^{-1}, (N s kg^{-1})	235, (2305)	264, (2590)
Pressure exponent	0.44	0.44
Burning rate at 1000 psi, mm s^{-1}	7.6-20	7.6-20

1.2.3.3 IM performance of HTPE propellants

Comfort [1994, 1996] presented HTPE as a new class of propellant to be used in IM, based on tests done to a generic motor of five or ten inch diameter with a composite case which was submitted to slow and fast cook-off, fragment and bullet impact tests. Insensitive Munitions results presented by Comfort [1994, 1996] are related to trials carried out on ten inch diameter graphite composite case motors following the requirements stated in the MIL-STD-2105B. The HTPE used for these trials was called GHE HTPE and was referred to as an "optimised pre-polymer" but no further details were presented.

Also Goleniewski [1998] reported that HTPE propellant made for a ground launched missile passed different IM tests such as: bullet impact, slow cook-off, fast cook-off and sympathetic detonation. IM test results for HTPE and HTPB propellants found in several papers are presented in Table 25.

As can be seen from Table 25, according to Comfort [1994, 1996], HTPE propellants presented better behaviour that HTPB propellants in IM tests, passing all the tests. It can be noticed that ignition temperature for slow cook-off is considerably lower for HTPE propellants than for HTPB based propellants. The same six-inch Card Gap test was reported by Comfort [1994, 1996] and by Hartman [2000]. They found that the shock wave velocity decreased along the tube from 6000 to 2180 meters per second when a steel pipe of 6 inch (15.24 cm) diameter and 24 inch (60.96 cm) length, loaded with 42 lbs (19.05 kg) of HTPE propellant was initiated to detonation with an explosive booster. No details were given about the characteristics of the booster.

Table 25. IM Behaviour Comparison between HTPE and HTPB Propellants

Test	HTPB		HTPE	
	Reference		Reference	
	Comfort [1994, 1996] Hartman [2000]	Goleniewsky [1998]	Goleniewsky [1998]	Comfort [1994, 1996] Hartman [2000]
Kind of motor	10 inch diameter	GLM	GLM	10 inch diameter
Case	Graphite	Graphite	Graphite	Graphite
Solid content, %	-.-	88	83	-.-
Slow cook-off, ignition temperature, ˚F, (˚C)	Explosion 414 (212)	-.-	-.-	Pass 273 (134)
Fast cook-off	Pass	-.-	-.-	Pass
Bullet impact	Deflagration	Ignited and burned	Did not ignite	Pass
Fragment impact.	Explosion	-.-	-.-	Pass
Over pressure, psi, (MPa)	78 (0.537)	-.-	-.-	0
Electrostatic Discharge (ESD), dissipation	-.-	2	0.002	-.-
ESD Breakdown Voltage, (kV)	-.-	6	30	-.-
Depressurisation rate for extinguishment, psi s^{-1} (MPa s^{-1})	-.-	158000 (1089.3)	15000 (103.45)	-.-

According to personal communications with Dr Duncan Watt [NIMIC, 2004 a], in 1998 eight Evolved Sea Sparrow Missile (ESSM), each containing 119 kg of HTPE propellant, were submitted to IM testing in accordance with MIL-STD-210B (two rocket motors for each test). The motor cases were made from steel, having an external diameter of 25.4 cm and a length of 167.6 cm. Table 26 summarises the results obtained from that trial. The reaction was classified according the judgement of an Ordnance Hazards Evaluation Board (OHEB), following the NATO AOP-39 "Guidance on the Development, Assessment and Testing of Insensitive Munition (MURAT)". Details from the slow cook-off trial can be seen in Table 27.

Table 26. ESSM IM Results, [NIMIC, 2004 b]

IM Test	Reaction Type
Bullet Impact	Burning (V)
Fragment Impact	Deflagration (IV)
Slow Cook-off	Explosion (III)
Fast Cook-off	Explosion (III)

From Table 26 it can be seen that the ESSM failed the slow and fast cook-off test. From Table 27 it can be seen that the reaction temperatures for both motors are different but there is no explanation for these differences. If the case temperature is taken as the critical temperature (Tc), a rough estimate of the cook-off ignition temperature is between 130 and 140˚C. These data are consistent with those presented by DeMay [1996]. In fact, DeMay [1996] found that at a temperature of 132.8˚C a seven inch

diameter dual-pulse motor using HTPE propellant reacted to give an explosion when it was submitted to the slow cook-off test of MIL-STD-210B.

Table 27. ESSM Slow Cook-off Test Details, [NIMIC, 2004 b]

Motor N°	Reaction at Oven Temperature (°C)	Reaction at Motor Case Temperature (°C)	ΔT (°C)	Overpressure at 10 meters, mbar (kPa)
1	146	140	6	80-90 (8-9)
2	141	131	10	100-160 (10-16)

Although the rocket motor for the ESSM did not meet all IM requirements, according to Watt [NIMIC, 2004 b] the HTPE propellant was chosen because it was reported to give better overall IM behaviour than the HTPB rocket motors tested previously (no comparison figures for HTPB propellants are presented). Despite the failure in the slow and fast cook-off tests, the reaction was less violent than with HTPB based propellants.

DeMay [1996 and 1997] also presented a summary of IM tests done on several motor configurations using the same HTPE propellant, as shown in Table 28.

Table 28. IM Tests for Different Rocket Motor Configurations, [Demay, 1996 and 1997]

Motor Configuration	Reaction Classification for			
	Fast Cook-off	Slow Cook-off	Bullet Impact	Fragment Impact
7 inch, dual-pulse motor, steel case	Deflagration	Explosion	Burn	Explosion
5 inch, composite case motor	Burn	Explosion	Burn	Burn
5 inch, composite cylinder	Burn	Burn	Burn	Burn
8 inch, steel case motor	Burn	Deflagration	Burn	Explosion
10 inch, composite case motor	Burn/Deflg	Deflagration	Burn	Deflagration
10 inch, composite cylinder	Burn	Burn	Burn	Explosion

As can be seen from Table 28 the slow cook-off IM requirement, i.e. no reaction greater than burning (type IV), is not met in all motor configurations.

Comfort [2000 b] reported that a 5 inch rocket motor having a graphite case and containing propellant based on HTPE and 21% bismuth oxide, passed bullet attack and fragment impact but failed the slow cook–off IM test. However when 2% of AN was added to the same formulation, a mild burning response was obtained.

Atwood [2005] reported the results of a slow cook-off comparison between two AP/Al propellants. One was manufactured with HTPE, plasticized with n-BuNENA and

contained AN as cooxidiser (it was not stated which kind of AN, if PSAN or NPSAN), and the other with HTPB (no information was supplied about the plasticizer). The slow cook-off test was performed at a heating rate of 0.05^{o}C min^{-1} and the events occurred at a temperature of 133 and 238^{o}C for the HTPE and HTPB propellants respectively. The cook-off results, despite the difference in the temperature of ignition, were similar for both kinds of propellants, resulting in a burning reaction.

On the other hand, the HTPE propellant chosen by Atwood [2005], was selected because shock sensitivity results showed it to be more reactive and the reactivity increased as the diameter of the sample increased. Although Atwood concluded, among other things, that there is not a correlation between shock and thermal stimuli, she did not take into account what was proposed by Tzeng [1998] in relation to sensitivity and the solubility of the AP in polyethylene blocks of HTPE block copolymers, based on poly THF and polyethylene glycol.

Rice [2005] reported that when comparing two similar 11 inch (27.9cm) analog rocket motors made from HTPE and HTPB propellant, HTPE shows a slightly better performance than HTPB in fragment impact test, but a more energetic reaction in cook-off tests. No further information was presented by Rice [2005] in relation to the HTPE propellant formulation. Only AP, AN, n-BuNENA and MNA are mentioned without details.

1.2.3.4 Theories of HTPE propellant thermal decomposition

In order to try to understand the mechanisms of slow cook-off violence moderation when ammonium nitrate (AN) and an energetic plasticizer such as n-BuNENA is incorporated into HTPE propellant formulation, Parr [1999] studied the flame structure of propellants made from AP/HTPE and AP + AN/HTPE and their thermal properties. Although Parr [1999] did not state clearly which kind of HTPE binder and propellant formulation was used, three kinds of samples are mentioned and they are summarised in Table 29.

Table 29. HTPE Propellants Formulation Used in Studies by Parr, [Parr, 1999]

Sample	AP (%)	AN (%)	Plasticizer	Binder	Observations
1	70	10	n-BuNENA	HTPE	Coarse AN
2	70	10	n-BuNENA	HTPE	Fine AN
3	80	-	n-BuNENA	HTPE	-

From the thermal diffusivity, heat capacity and decomposition behaviour analyses, they found that there are no significant differences in dependant thermal properties between the samples. However, they observed that in the condensed phase thermal profiles and in the rheology of the decomposing samples, remarkable difference can be noticed. In fact, the difference in the condensed phase, between propellants with and without AN, found by Parr [1999], is based on significant differences in thermal diffusivities. The propellant containing AN has values almost 50% lower than the one containing only AP in its formulation. Surface temperatures were also measured and they are shown in Table 30. From the rheological point of view they found that samples containing only AP as oxidant (sample 3), decompose at higher temperatures and become hard, brittle and crumbly. On the other hand, the ones containing AN (samples 1 and 2), become pliable and soft even at temperatures below the AN melting point and evolve liquid upon heating. From flame analyses they found that, for all the samples, the flame temperature was around 2869 K. Also flame distance to the condensed phase was measured and they found that flames in samples containing AN are less close to the surface than those from only AP samples. In fact, the stand off for the sample containing only AP was 80 μm against 170 μm for samples containing AN; a difference of more than 112%. Although they explain this behaviour in terms of the slower reaction rates of nitrates and nitramines, they do not discuss whether it can affect condensed phase properties.

Parr [1999] proposed that possibly, propellants that do not contain AN in their formulation become hard and brittle on decomposition, fracturing and then creating a big surface area which after self-ignition can lead to an explosion in a slow cook-off scenario. This behaviour would not be present in propellants containing AN, since they will have less propensity to fracture and form a larger surface area. However, no comments were made or trials done on slow cook-off tests for samples with and without

AN. Also they did not do any comparison against AP+AN/HTPB samples in order to compare the influence of AN in that case.

Kudva [2000] studied the effect of laser and pressure driven thrust response of HTPE propellants containing AP and AP+AN. Although Kudva [2000] did not detail the propellant composition, it looks very similar to that used by Parr [1999]. The goal of the work by Kudva [2000] was to study the dynamic response of a flame perturbation during propellant combustion. They measured the surface temperature of the propellant samples and found similar results to Parr [1999], as shown in Table 30.

Table 30. HTPE Surface Temperatures Ts, According Kudva [2000] and Parr [1999]

Sample	AP (%)	AN (%)	Kudva [2000] Ts, (K)	Parr [1999] Ts, (K)
1	70	10, coarse	900	812
2	70	10, fine	1000	1050
3	80	-	1025	1100

In contrast to Parr [1999], Kudva [2000] compared the results against similar experiments done with HTPB/AP propellants and found that all HTPE propellant samples had higher surface temperatures than HTPB propellants, that for the latter being around 750 K. They suggested that this behaviour could be due to exothermic reactions in the condensed phase. Also they found from the laser driven response amplitudes for HTPE propellants that this response is opposite to the response observed for other AP composite propellants with inert binders. In fact while in HTPE propellants laser driven response amplitudes increase with the increase in laser flux, in HTPB propellants they decrease with an increase in laser flux. From this behaviour they suggest that the presence of the HTPE binder appears to have altered the propellant response to mean heat flux. However, although Kudva [2000] included the presence of HTPE as a factor affecting the exothermic reactions at condensed phase, they did not comment or take into account the presence of the energetic plasticizer, or the combination of those two compounds.

1.2.3.5 HTPE propellant ageing characteristics

Several reports have been written related to the characteristics of HTPE propellants

during ageing, focussing on the residual stabiliser percentage as well as the mechanical properties. However, there is no agreement about HTPE propellant ageing behaviour.

Comfort [2004] reported that HTPE propellants made from TPEG pre-polymer have stable mechanical properties during a period of ten years of ageing, i.e. tensile strength and modulus, when samples were storage at 25^{o}C. In fact according to his report tensile strength and modulus have not changed after ten years. On the other hand, Comfort [2004] reported that strain has been slightly increased during the same period of time and that the same was observed when strain was measured at -40^{o}C. Stabiliser depletion from MNA was reported to be less than 0.1% per year and under accelerating ageing conditions at 68^{o}C was reported to be depleted from 0.4% to around 0.2% after 100 days.

However, Rice [2005] reported different behaviour when HTPE propellants are aged. In fact, Rice [2005] reported that because several publications have been presenting results that are inconsistent and also reporting possible incompatibilities between components present in propellants based on HTPE/AP/AN and n-BuNENA, an accelerated ageing program was developed by the USA Army. According to Rice [2005], four samples made from HTPE, containing AP, AN, n-BuNENA, MNA stabilizer and differing between them mainly in the kind of bonding agent, were submitted to ageing at 24, 54, 60 and 71^{o}C. It was not specified what kind of curing agent or bonding agent were used. During these trials Rice [2005] stated that the MNA depletion was similar to that stated by Comfort [2004]. However, they found during tensile tests on the aged samples that mechanical properties were strongly affected and that the propellant begun to soften when stored at the high temperatures. This is not in agreement with results presented by Comfort [2004]. Rice [2005] suggested that possibly some acid-base reaction is producing a chain scission of the binder network during ageing.

Fletcher [2006] stated that HTPE propellants are very stable and they are designed to support a ten year life programme. Because the inconsistency in HTPE behaviour during ageing presented by Rice [2005], Fletcher [2006] presented the HTPE (produced by ATK) tensile test data, for samples submitted to a similar ageing programme as that

of Rice [2005] and included information for samples aged during three years at 49°C and samples aged during thirteen years at 25°C. The HTPE samples were aged at 25, 49 and 68°C. In all the cases the mechanical properties, i.e. tensile strength, strain and modulus are relatively stable; almost without change in samples aged at 25°C, a slight decrease in samples aged at 49°C and strain slightly increased during ageing.

Although Fletcher [2006] did not present details about the HTPE ingredients, except MNA and 2NDPA as stabilisers, he suggested that the ageing behaviour, especially mechanical properties, will depend on the compatibility of the different HTPE ingredients. In fact, it was suggested that nitrate esters such as n-BuNENA can be incompatible with some phase stabilisers for the AN or with some anticaking agents or some other impurities. Therefore, compatibility tests should be done on all raw materials before incorporating them into the formulations. Although 2NDPA is part of the stabiliser included in HTPE formulation, Fletcher [2006] did not present any information about 2NDPA depletion. However, Mullay [1994] in a thermal study about NENA and AP mixtures stated that when using 2NDPA as stabiliser in mixtures of n-BuNENA and AP, no influence or a lack of effectiveness of the stabiliser was observed. Mullay [1994] suggested that stabilizing species rely on acid base interaction. Thus the presence of acid species on the molecule and also steric effect reduces the stabilisation effects.

1.2.4 Literature review conclusions

As can be seen from the literature review, hydroxy terminated polyether propellant has been present for many years (mid-1950's). However, the degree of development reached has been low, possibly due to the fast development of the HTPB propellants. Although HTPB propellant are very reliable and have been intensively studied and improved upon over the years, the lower polarity, the incompatibility with energetic plasticizers, and the poor performance under thermal threat have made the scientific community look again at other binder systems such as the polyethers. Several kinds of polyether pre-polymers plasticized with different energetic plasticizers can be found in the literature. The newest of these used in propellants is HTPE. This is actually used in

some missile systems, being a combination of a copolymer based on THF and EO, plasticized with n-BuNENA and having AP as main oxidiser and PSAN as a co-oxidiser. Although some researchers claim they have good ageing properties and that they accomplish all IM requirements, in particular slow and fast cook-off, some others disagree. Therefore, there is inconsistency in the limited amount of information presented in the open literature on HTPE binders and propellants, especially regarding the behaviour under thermal threat, i.e. slow cook-off and accelerated ageing.

II. HTPE COPOLYMER SYNTHESIS AND CHARACTERISATION

2.1 Introduction

Copolymers of ethylene oxide (EO) and tetrahydrofuran (THF) are usually synthesized by using either bulk or solution polymerisation. According to Zhiping [1999], bulk polymerisation is suitable for obtaining polymer molecular weights up to 10,000 g mol^{-1} and has the advantage of a high reaction velocity and high purity products. On the other hand, solution polymerisation has a lower viscosity and a lower reaction velocity and needs a suitable solvent, making the process more complex and the products more difficult to purify and therefore more expensive.

Cationic bulk copolymerisation of EO with THF in the presence of low molecular weight diols and a catalyst, is a suitable method to produce telechelic random copolymers with hydroxyl terminal groups, i.e. hydroxyl terminated polyethers [Bednarek, 1999a]. A comprehensive study of the mechanism of formation and kinetics of the process and of copolymer composition in the presence of diols has been conducted by Bednarek [1998, 1999a, 1999b]. In order to have a random copolymer structure, the selection of the catalyst is very important. In fact, as stated by Zhiping [1999], the catalyst should not catalyse the homo polymerisation of THF or EO. In that sense, Lewis and protonic acids are most suitable [Zhiping 1999, Bednarek 1999a]. Equations 2.1 to 2.3 show the chemical reactions between the protonic acid i.e. tetrafluoroboric acid, and low molecular diol i.e. ethylene glycol (Eq. 2.1), THF (Eq. 2.2), and EO (Eq. 2.3).

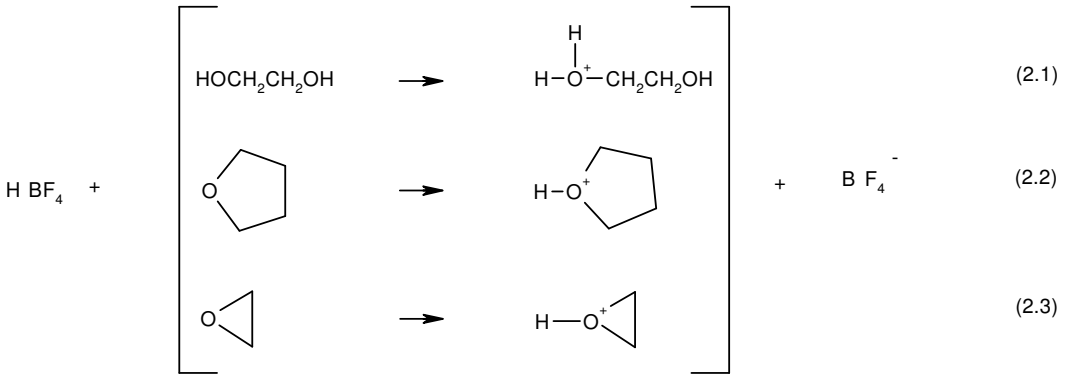

Bednarek [1999a], showed that the first step in the synthesis of a hydroxyl terminated copolyether is the formation of a secondary oxonium ion from EO (Eq. 2.3). Only protonated EO can initiate the copolymerization reaction, where the low molecular weight diol acts as proton reservoir. It was also shown that alkylated THF is about two orders of magnitude less reactive towards THF and HO- groups than secondary oxonium ion of EO. They proposed the following reaction sequence to obtain an EO-THF random copolymer, (Equations 2.4 to 2.7).

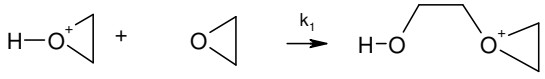
(2.4a)

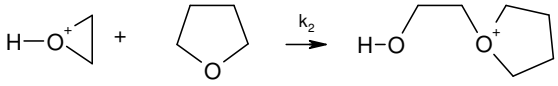
(2.4b)

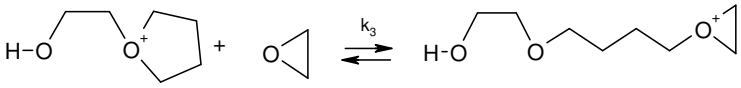
(2.5)

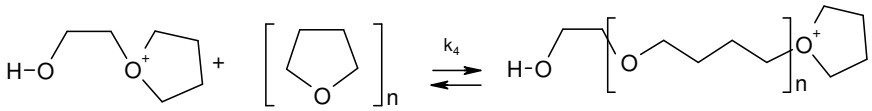
(2.6)

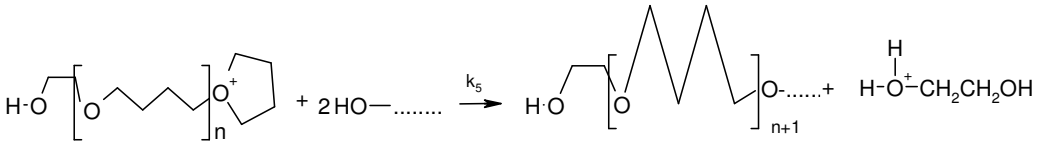
(2.7)

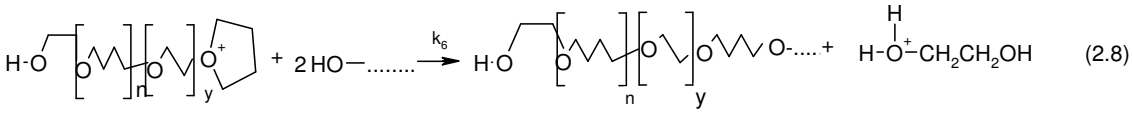
(2.8)

It can be seen from Equations 2.4a,b and 2.5 that EO is incorporated into the copolymer by reaction of a secondary and tertiary oxonium ion through nucleophilic substitution (S_N2) while THF is incorporated by the reaction of a tertiary oxonium ion and S_N2. Also, according to Bednarek [1999b] the opening reaction of a THF ring is reversible (Equations 2.5 and 2.6), while in the case of EO ring opening is essentially irreversible. Thus, by changing the concentration of ethylene oxide and the temperature, the structure of the copolymer can be modified. In fact, in the experiment carried out by Bednarek [1999b], it was found that a structure having a $\{[EO]\text{-}[THF]_n\}_m$ composition, can be obtained by adding very small amounts of EO during the copolymerisation reaction, as

stated by Equation 2.7. Thus, in order to synthesise a copolymer with different "n" values; i.e. different [EO]/[THF] ratios, the feeding mass flow of EO should be modified to give a random copolymer as shown by Equation 2.8.

The reaction sequences presented above should lead to a copolymer structure shown in Figure 4.

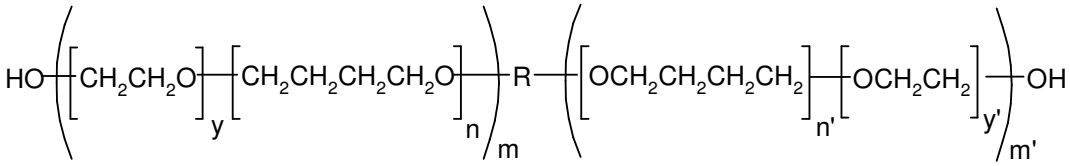

Figure 4. EO/THF copolymer structure

Where ***R*** corresponds to an ethylene oxide unit when ethylene glycol is used as initiator, and ***y***, ***n*** and ***m*** will be functions of temperature, concentration of THF and HO- groups present in the system, instantaneous concentration of EO and catalyst concentration [Zhiping 1999, Bednarek 1999a].

Bednarek [1999a], showed that the copolyether molecular weight (Mn) can be predicted accurately up to a value of 2500 according to Equation 2.9, where $[THF]_0$ is the initial concentration of THF, $[THF]_t$ is the concentration of THF at the end of the reaction, [EO] is the overall concentration of EO introduced to the reaction mixture and $[EG]_0$ is the initial concentration of EG. The concentrations are multiplied by their respective Mn values.

$$Mn = \frac{72.11\{[THF]_0 - [THF]_t\} + 44.05[EO] + 62.07[EG]_0}{[EG]_0} \qquad (2.9)$$

It can be seen from Equation 2.9 that the final molecular weight will depend not only on the concentration of THF and EO but also on the selected diol concentration. Bednarek [1999a] found that at a higher Mn range the equation becomes inaccurate, with calculated values lower than the measured values. There is no full understanding of the reason for such behaviour. However, one of the reasons could be that Equation 2.9 does not take into account the acid concentration, which also has an influence on Mn, as

stated by Zhiping [1999]. In fact according to Zhiping [1999], the Mn is inversely proportional to the quantity of catalyst used in the reaction.

Copolymerisation of EO and THF can also produce by-products. These must be avoided because of their effect on reducing copolymer functionality and molecular weight and because they could in future affect the properties of the binder due to their tendency to volatilise [Zhiping, 1999]. These by-products are normally non-functional and low molecular weight cyclic ether oligomers e.g. mixtures of cyclic dimers, trimers, tetramers, and pentamers [Bednarek, 1998]. Their mass fraction can reach up to 15 or 20% according to Zhiping [1999]. However Bednarek [1999c] reported that by reducing the temperature and conducting the polymerisation in the presence of diols through an activated monomer mechanism, the cyclization products can be limited to 3%.

A different synthesis process to produce a block HTPE copolymer was described later on by Comfort [2004]. They reported that the HTPE synthesis was performed at 130^{o}C by bulk copolymerisation of poly-tetrahydrofuran, i.e. Poly-1,4-butanediol (Terathane) and polyethylene glycol and by using sulphuric acid as catalyst. The authors gave no information about the polymers molecular weight, or any other technical information related to the copolymerisation process.

2.2 Materials and Methods

2.2.1. Introduction

It was decided to take as a reference the experimental procedure presented by Bednarek [1999a]. This procedure was also complemented by direct communications with Dr Melania Bednarek from the Centre of Molecular and Macromolecular Studies at the Polish Academy of Sciences, and by the study of other papers [Bayer 1960, Pruckmayr 1979, Stewart 1994 and Bednarek 1999c]. The synthesis process to obtain the copolymer of ethylene oxide and tetrahydrofuran was carried out through bulk polymerisation using EO, THF, EG as a diol and tetrafluoroboric acid diethyl ether complex. Quantities of each reagent were modified in each experiment in order to obtain a copolymer with different EO/THF ratios and different molecular weights, and

thus different chemical, physical and mechanical properties. In Appendix A the experimental protocol used for each synthesis can be seen. Table 31 shows the molar percentage range of each reagent related to THF used in the different experiments.

Table 31. Percentage of Reagents Used in EO/THF Copolymer Synthesis

Name	Molar percentage related to THF
Ethylene oxide	5% to 30% per h
Ethylene glycol	3% to 9.4%.
Fluoroboric acid diethylether complex	0.1% to 3.34%.

In order to study the behaviour of the reaction, to obtain a higher Mn copolymer and to reduce the by-product content, the experiments were performed under sub-zero temperature conditions, i.e. between -42 to -20˚C. Polymerisation was initiated by passing EO gas through a stainless steel needle immersed in the reaction solution. Different EO mass flow rates and catalyst percentages were used.

2.2.2 Copolymerisation equipment and reagents

Copolymerisation of ethylene oxide and tetrahydrofuran was carried out in a fume cupboard using the equipment configuration shown in Figure 5 and Figure 6.

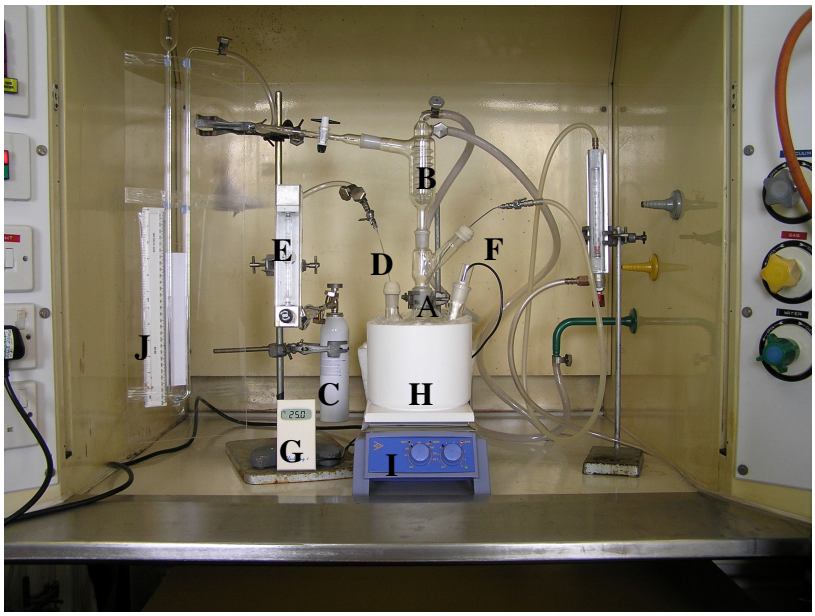

Figure 5. Chemical reactor for copolymerisation of THF and EO

A:1 litre flask, B: Condenser, C: EO container with regulator, D: EO feeding needle, E: EO flow meter (graduated between 5 and 45 cc/min), F: Probe for bulk temperature measurement, G: thermometer, H: Cooling bath, I: Stirring plate, J: Mercury manometer

Figure 6. General view of the chemical reactor for copolymerisation of THF and EO
A: Nitrogen flow meter, B: Nitrogen cylinder

For experiments 1-6 a mixture of dry ice-chlorobenzene was used for the low temperature bath. For experiments 7-27 an electrical cooler using industrial methylated spirit as cooling fluid was used as shown in Figure 7. The reagents used for the copolymerisation synthesis and their role are shown in Table 32.

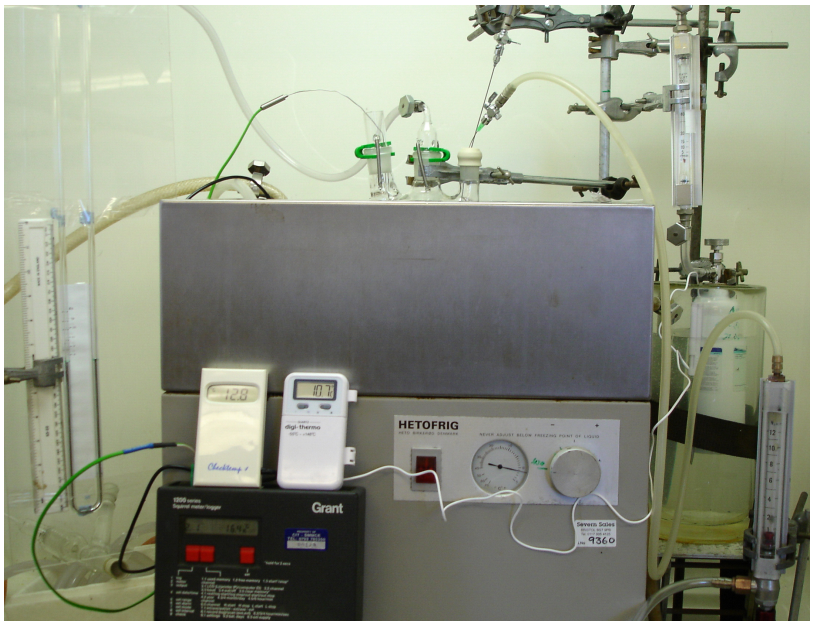

Figure 7. General view of the cooler equipment and configuration

Table 32. Reagents Used in EO/THF Copolymer Synthesis

No	Reagent	Name	Supplier	Characteristics	Molecular weight
1	Monomer	Tetrahydrofuran, THF, C_4H_8O	Sigma-Aldrich Company Ltd.	Purity 99.9 %, HPLC grade, inhibitor free. 2.5 litres bottle	72.11
2	Monomer	Ethylene oxide, EO, C_2H_40	Sigma-Aldrich Company Ltd.	Pressure container with 250 ml	44.05
3	Initiator	Ethylene glycol, EG, $C_2H_6O_2$	Sigma-Aldrich Company Ltd.	Anhydrous, 99.8% 1litre bottle,	62.07
4	Catalyst	Fluoroboric acid diethylether complex, $HBF_4{\cdot}Et_2O$	Fluka Chemica supplied by Sigma-Aldrich Company Ltd.	Purum 51-57% HBF_4, 100 ml,	HBF_4; 87.81
5	Neutralising agent	Sodium bicarbonate, $NaHCO_3$	BDH	Grade Analar	83.969
6	Washer	Deionised water	Main Lab	-.-	18.00
7	Drying agent	Calcium chloride, $CaCl_2$ Sodium sulphate Na_2SO_4 Molecular Sieves 4Å	BDH Sigma-Aldrich Company Ltd	Mesh 12-24, purity 99.8 % Beads particle size, 4-8 mesh	110.99

The synthesis process can be divided into the following steps: raw materials and reactor preparation, synthesis and synthesis termination, neutralisation and purification process. Experimental conditions for each experiment are shown in Table 33.

2.2.3 Raw materials and reactor preparation

Tetrahydrofuran, ethylene oxide, ethylene glycol and tetrafluoroboric acid diethyl ether complex were used as supplied. Their main characteristics are shown in Table 32. An empty round-bottom flask containing a small magnetic stirrer was weighed. THF was added first into the flask and then ethylene glycol. The solution was stirred using a magnetic stirrer for 3 min and then tetrafluoroboric acid diethyl ether complex was added. The flask containing the mixture was placed in a low temperature bath at -42˚C. Nitrogen was slowly added through a stainless steel needle over the course of 1 h to take out traces of oxygen in the solution, which can inhibit the polymerisation process. At the same time a cold water flow was maintained through the condenser throughout the copolymerisation process. While this process was carried out the ethylene oxide container was weighed.

2.2.4 Synthesis

After 1 h of cool stirring, the nitrogen supply was stopped and the stainless steel needle was taken out of the solution but kept in the flask. Ethylene oxide was introduced

slowly into the bulk through a stainless steel needle. EO flow was regulated by adjusting the regulator valve on the EO container (Figure 8). Due to the flow meter not being calibrated for use with ethylene oxide, the first experiment established the correlation between the flow meter reading and the real mass of EO per minute that was being introduced into the bulk. This information was used in further experiments to adjust the valve in order to introduce the desired amount of monomer.

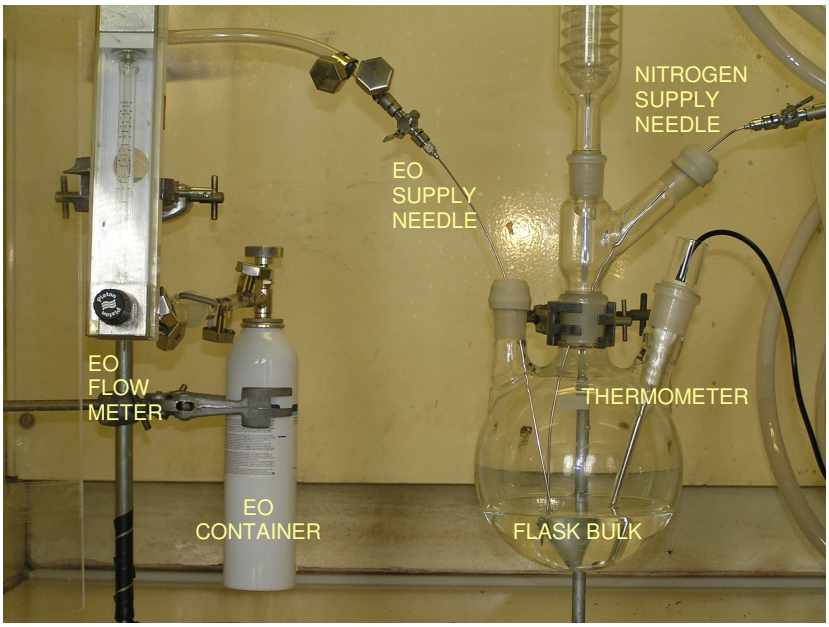

Figure 8. Specific view of the chemical reactor for copolymerisation of THF and EO

As soon as EO was introduced into the bulk the copolymerisation reaction started, as could be noticed by the temperature increase. During EO addition the pressure in the flask increased, as shown by the mercury manometer. Pressure rose normally up to 29 Hg mm in 2 h and was released when this figure was reached. Initially the system was sealed using PTFE sleeves in all the joints but after experiment N^{o} 7 these seals were replaced by high vacuum silicon grease to prevent leaking in some of the joints.

For experiments 1-6, the temperature was maintained at around -42˚C during the polymerisation reaction by using a mixture of solid carbon dioxide (dry ice) and chlorobenzene in the cooling bath. Because the process is exothermic it was necessary to be continually adding the cooling mixture to the cooling bath in order to maintain an average temperature of -42˚C.

From experiment 7 onwards, a Hetofrig cooled bath model CB4-502 (electrical cooler equipment) using industrial methylated spirit as cooling fluid was used. This equipment enabled a constant temperature to be maintained throughout the synthesis. The temperature was measured from a digital thermometer placed in the bulk. For experiments 7-20, the temperature was maintained at around -42˚C and for experiments 21-27 at around -20˚C.

Once the required quantity of EO had been added to the solution i.e. after a fixed period of time at a particular mass flow rate, the EO valve was completely closed and the container was weighed. If the quantity of EO was less than calculated, then more EO was added to the bulk. After this last action, the final weight of EO added to the sample was recorded and the mass flow calculated. After EO feeding was stopped, the stirring and low temperature were maintained for several minutes, or hours, depending on the experimental requirements, to ensure that all EO was incorporated into the copolymer. The experimental conditions used for the different samples are shown in Table 33.

Table 33. Experimental Conditions for EO-THF Copolymer Synthesis

Exp Nº	Temp. (˚C)	THF (g)	EG (g)	Catalyst (g)	EO Mass flow (g h^{-1})	EO Feeding time (min)	EO Total mass (g)	Stirring time (min)
1	-42	100	8.00	7.5	18.2	358	108.3	0
2	-42	100	4.00	7.5	15.6	210	54.5	69
3	-42	100	4.00	7.5	9.49	320	50.7	60
4	-42	100	4.00	7.5	18.7	200	62.3	146
5	-42	100	4.00	7.5	7.61	370	46.9	65
6	-42	100	4.00	7.5	3.54	360	21.3	60
7	-37	100	3.00	7.50	8.19	345	47.1	0
8	-37	100	3.00	7.50	10.95	155	28.31	945
9	-37	100	4.00	7.50	12.01	198	39.64	948
10	-37	100	8.00	7.50	2.07	240	8.30	1190
11	-38	100	4.00	7.50	8.58	327	46.77	854
12	-38	100	4.00	7.50	11.65	330	64.06	1020
13	-39	100	4.00	7.50	11.53	320	61.47	1040
14	-37	66	2.70	4.90	9.83	215	35.21	1160
15	-38	8.5	0.34	0.60	3.19	120	6.38	1380
16	-38	5.07	0.20	0.38	3.16	60	3.16	1245
17	-38	5.13	0.20	0.37	5.20	30	2.60	1288
18	-38	5.07	0.15	0.37	4.52	30	2.26	1443
19	-38	100	3.00	7.50	10.04	320	53.58	1054
20	-37	100	3.00	4.51	7.99	583	77.72	1167
21	-20	66	1.97	4.97	10.71	95	16.96	-.-
22	-20	66	1.97	2.90	5.62	278	26.06	-.-
23	-20	66	1.97	0.74	10.39	228	39.47	1063
24	-30	66	1.97	1.48	12.68	227	47.98	1473
25	-20	66	1.97	1.48	9.52	228	36.16	1280
26	-20	180	5.40	3.03	19.04	327	103.82	1285
27	-20	348	10.7	5.84	39.19	320	209.00	1160

2.2.5 Neutralisation and purification process

Once the stirring process had finished and in order to neutralise the copolymer, the sample was transferred to a separating funnel. Sodium bicarbonate was mixed with deionised water and this solution was added to the bulk and shaken for several minutes. Subsequently, the aqueous phase was separated from the organic phase by using chloroform or dichloromethane (liquid-liquid extraction process). The sample was washed three times with deionised water. An excess of 10% of $NaHCO_3$ was used in the neutralisation process, a ratio 1:1 between chloroform ($CHCl_3$) and the sample, and 2:1 between deionised water and the sample.

Figure 9 shows the liquid-liquid extraction process where the aqueous phase which is the transparent top part of the separating flask and the organic phase containing the copolymer, the opaque bottom part of the separating flask. Acidity was determined by using litmus paper.

Figure 9. Neutralisation process for THF-EO copolymer

After neutralisation, the sample containing the copolymer, extraction solvent traces and (sometimes) THF, was dried to remove traces of water. Sodium sulphate was used as the drying agent. The sample was stirred while sodium sulphate was added. The overall mixture was stirred for several hours until it was completely transparent. The sample was then filtered under vacuum by using a 0.45 μm nylon Whatman membrane filter

and a Buchner flask. Subsequently, the sample was poured into a flask containing beads of molecular sieve 4Å, particle size 4 to 8 mesh, and stored for a period of 48 h. This method was used for all the samples. The water content was measured using a Karl Fischer Titrator.

After drying, the sample was filtered again and solvents such as chloroform and THF were removed by means of heat and vacuum using a rotary evaporator. The sample was maintained for between 2 to 6 h under a vacuum of 13.3 kPa and a temperature of 68˚C. Once this process was complete the sample was labelled and stored under nitrogen. Figure 10 shows HTPE copolymer samples from experiments 1 and 2.

Figure 10. Samples from experiments 1C and 2B

2.3. Analysis and Results

2.3.1 Introduction

In order to characterise the product obtained from the copolymerisation of ethylene oxide and tetrahydrofuran, several analyses were carried out. Initially, molecular weight, molecular structure, glass transition temperature (Tg), melting point (M.p.), thermal decomposition characteristics and by-products or impurities were determined by using Size Exclusion Chromatography (SEC), Nuclear Magnetic Resonance (NMR) spectroscopy, Infra Red (IR) spectroscopy, and Gas Chromatography-Mass Spectrometry (GC-MS). Differential Scanning Calorimetry (DSC) and

Thermogravimetric analysis (TGA), together with density and viscosity measurements, were also carried out on a sample of HTPB supplied by ROXEL UK. Similar analyses were performed on a sample of Aldrich THF-EO copolymer. No technical information was available from the manufacturer on this copolymer.

2.3.2 SEC analysis and results

In order to determine molecular weight and impurities, size exclusion chromatography (SEC) analysis were performed using a Visotek SEC pump, model VE 1121, with a Waters 2410 Refractive Index Detector (RID) equipped with a set of two 5µm PLgel Mixed-C 300x7.5 columns and a 5µm PLgel 100Å 300x7.5 mm column. The SEC was controlled via a PC running Walters Millennium software. THF stabilised with BHT (250 ppm) was used as an eluent and polyethylene glycol standards were used for calibration. In order to prepare the analysis one drop of copolymer sample was diluted in 10ml of THF, then the diluted sample was transferred into a SEC vial to start the analysis. Figure 11 shows a chromatogram for the HTPE copolymer obtained in experiment 13, where Mn is equal to 2680. HTPE copolymer broad band SEC results are presented in Table 34, where Mw is the weight-average molecular weight, Mn the number average molecular weight, MP the main peak average molecular weight and the polydispersity is the ratio between Mw and Mn.

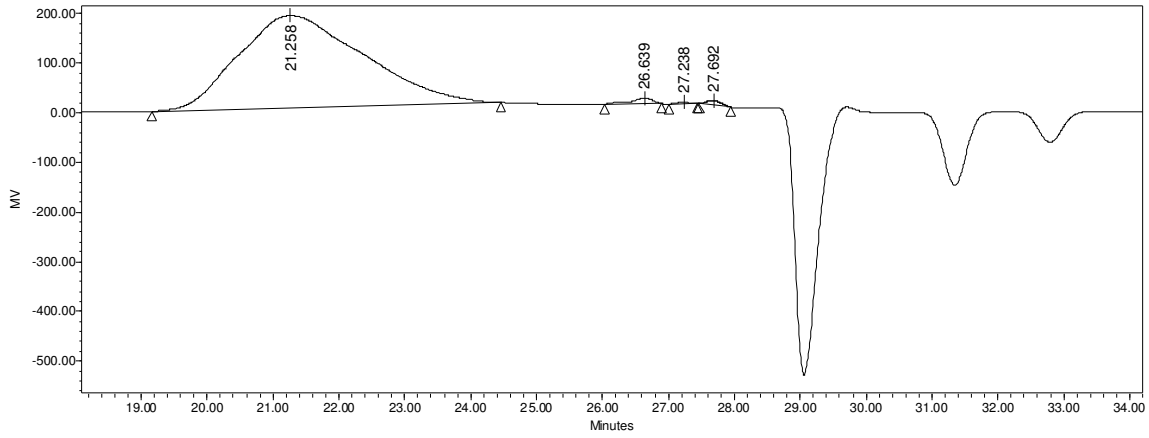

Figure 11. SEC chromatogram for experiment N° 13

Table 34. HTPE Copolymer SEC Results

Exp. No	Mw	Mn	MP	Polydispersity	Retention time. min
1	1369	989	1234	1.39	23.01
2	2555	1611	2246	1.58	16.17
3	2624	1385	2477	1.91	22.31
4A	1569	1106	1478	1.42	22.26
4B	1765	1248	1677	1.41	22.04
4C	1842	1268	1715	1.45	22.01
4D	1918	1312	1776	1.46	21.95
5A	1418	1124	1329	1.26	22.32
5B	1436	1127	1320	1.27	22.34
5C	1547	1206	1419	1.28	22.2
6A	777	566	760	1.37	23.90
6B	692	510	620	1.36	24.32
7A	3252	2495	3087	1.29	21.75
7B	3252	2345	3011	1.39	21.78
7C	2939	1909	3042	1.53	21.78
7D	3031	1984	2999	1.51	21.80
8A	2945	1934	2914	1.52	21.70
8B	3377	2314	3276	1.45	21.54
8B2	4005	2667	3509	1.50	21.46
8B1A	3749	2553	3534	1.46	21.46
8B2A	4959	2993	4052	1.65	21.28
9A	2227	1451	2255	1.53	22.41
9B	3099	1988	2932	1.55	22.05
10A	961	755	260	1.27	23.98
10B	1016	816	914	1.24	24.01
11A	3957	2581	3567	1.53	21.34
11B	3428	2206	3176	1.55	21.48
12A	3092	2021	3043	1.52	21.54
12B	4681	2853	4140	1.64	21.15
13	4123	2680	3838	1.53	21.26
14	3769	2498	3467	1.51	21.29
15	2181	1481	1981	1.47	22.10
16	2310	1684	2213	1.37	21.93
17	2205	1477	2338	1.49	21.76
18	2480	1615	2628	1.53	21.59
19	6028	4050	4622	1.48	21.03
20	3024	2097	3015	1.47	21.57
21	4434	2732	3861	1.63	20.92
22	5472	3239	4264	1.69	20.81
23	8644	4318	9730	2.00	20.63
24	9754	4789	10380	2.04	20.57
25A	8272	4249	9456	1.95	20.65
26E3	7826	4076	5189	1.92	21.21
27B	8460	4340	9711	1.95	20.63
Aldrich THF-EO	2036	1281	1192	1.59	22.55

Percentage areas of all peaks and their corresponding molecular weights for some of the experiments, are presented in Table 35. The corresponding SEC reports for each experiment are presented in Appendix B.

Table 35. HTPE Copolymer SEC Results

Exp. No	Mw	Mn	% Area	Retention time, min
11B	3428	2206	98.88	21.48
	208	205	0.48	26.40
	129	129	0.23	27.34
	92	91	0.39	27.80
12B	4681	2853	98.78	21.15
	192	191	0.24	26.72
	138	138	0.18	27.27
	97	96	0.61	27.73
13	4123	2680	98.17	21.26
	202	201	1.05	26.64
	145	144	0.18	27.23
	104 (MP)	-.-	0.59	27.69
15	2181	1481	97.16	22.10
	136	132	1.81	26.48
	71	70	0.14	27.07
	40	39	0.89	27.52
16	2310	1684	97.31	21.93
	119	117	1.58	26.58
	64	63	0.14	27.17
	34	33	0.97	27.62

2.3.3 NMR analysis and results

In order to determine molecular structure, proton and carbon-13 nuclear magnetic resonance spectroscopy was performed using a Bruker DPX 250 spectrometer. 16 pulses for ^{1}H and 1024 pulses for ^{13}C were used for the NMR analysis. Deuterated chloroform ($CDCl_3$) was used as solvent and tetramethylsilane (TMS) as reference. Figure 12 A and B show typical ^{13}C and ^{1}H NMR spectra respectively, obtained for the different samples. The spectra for all samples for each experiment are presented in Appendix C.

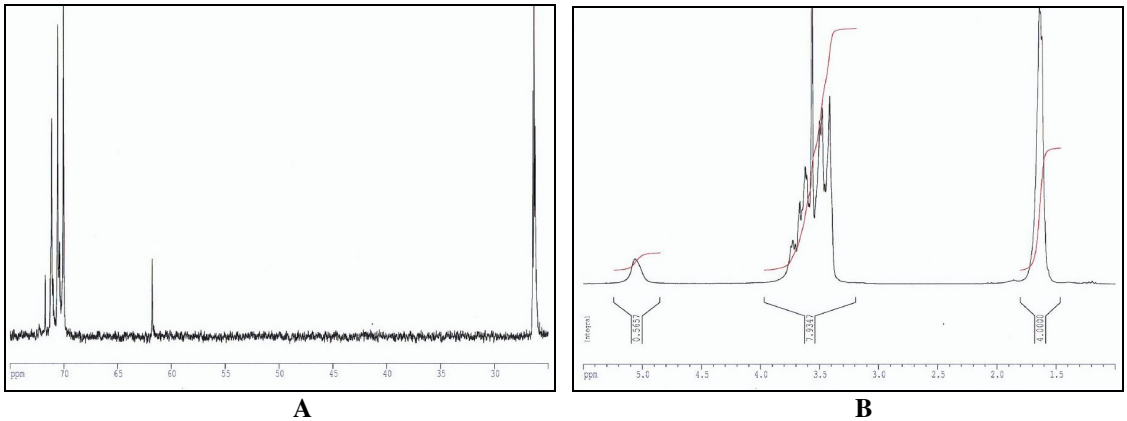

A **B**

Figure 12. (A) ^{13}C NMR spectrum for sample 2B and (B) ^{1}H NMR spectrum for sample 2B

The ratio "**n**" between THF and EO groups presents in the HTPE copolymer chain obtained from ^{1}H NMR results are presented in Table 36. "n" was obtained from the

ratio of the peak areas corresponding to the protons of the -$OCH_2\mathbf{CH_2CH_2}CH_2O$- groups in THF and those of the –$O\mathbf{CH_2}$- groups present in both EO and THF.

Table 36. HTPE Copolymer Results from ^{1}H' NMR Spectrum

Experiment N°	n [THF]/[EO]	THF groups in main chain, (%)	EO groups in main chain, (%)
1	0.6	37.70	62.30
2	1.02	50.40	49.60
3	0.83	45.21	54.79
4D	1.01	50.29	49.71
5C	1.29	56.20	43.80
6C	1.937	66.00	34.00
7D	0.98	49.5	50.50
8B1A	1.53	60.81	39.19
8B2A	1.55	51.92	48.08
9B	1.08	51.90	48.10
10B	1.44	58.90	41.10
11B	1.01	50.20	49.80
12B	0.9	47.50	52.50
13	0.84	45.63	54.37
14	0.86	46.3	53.70
15	1.14	53.23	46.77
16	0.99	49.69	50.31
17	1.19	54.31	45.69
18	1.17	53.90	46.10
19	1.06	51.51	48.49
20	1.21	54.85	45.15
21	1.65	62.26	37.74
22	1.33	56.62	43.38
23	0.89	47.09	52.91
24	0.79	44.00	56.00
25	1.025	50.51	49.49
26	0.9861	49.65	50.35
27	0.9788	50.54	49.46
Aldrich THF-EO	1.91	66.00	34.00

2.3.4 DSC and TGA analysis and results

In order to determine glass transition temperature (Tg) and melting point (M.p.), differential scanning calorimetry analysis was performed using a Mettler TA4000 thermal analyser equipped with a TA processor TC-11 and a DSC 30 measuring cell. Sample weights were around 8-18 mg. Samples were heated at a rate of 2˚C per min from –100 - +100˚C. The copolymer thermal decomposition characteristics were studied by using DSC and Thermogravimetric analysis (TGA). TGA was performed using a Mettler thermo balance model TG 50, using the same analyser as DSC. Sample masses were around 14 - 18 mg and they were heated at a rate of 10˚C per min from 30 - +600˚C under a nitrogen atmosphere. In Table 37 are presented glass transition

temperatures, melting points and melting heat results obtained from the different HTPE samples and also for the HTPB sample. Further DSC results are presented in Appendix D. Thermogravimetric results are presented in Appendix E.

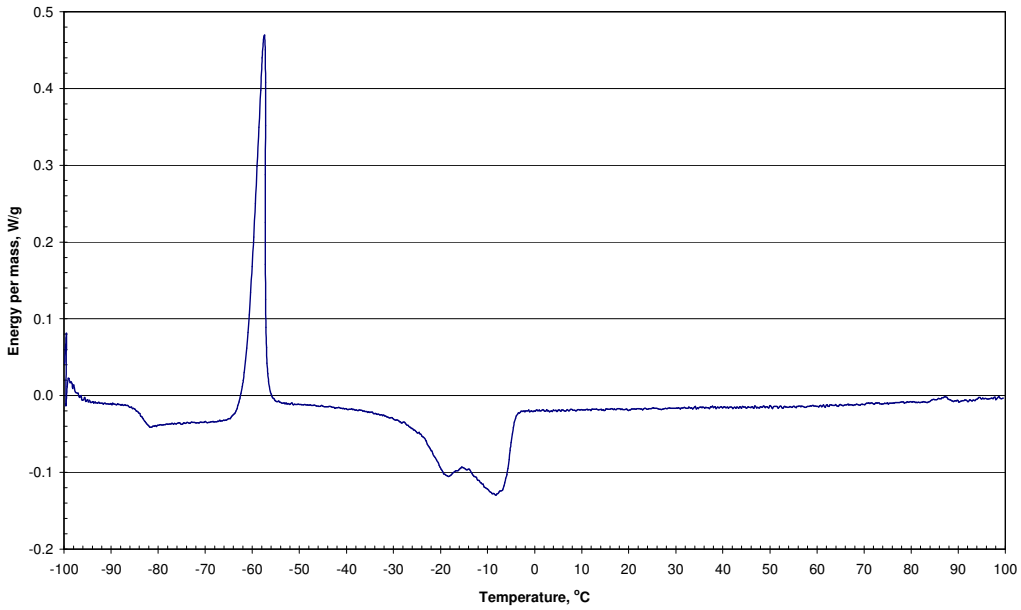

Figure 13. DSC thermogram of HTPE copolymer, experiment 9B

Figure 13 shows a DSC thermogram for the HTPE copolymer obtained in experiment 9B, in the temperature range -100 - 100˚C. Figure 14 shows the corresponding thermogram for a sample of HTPB polymer.

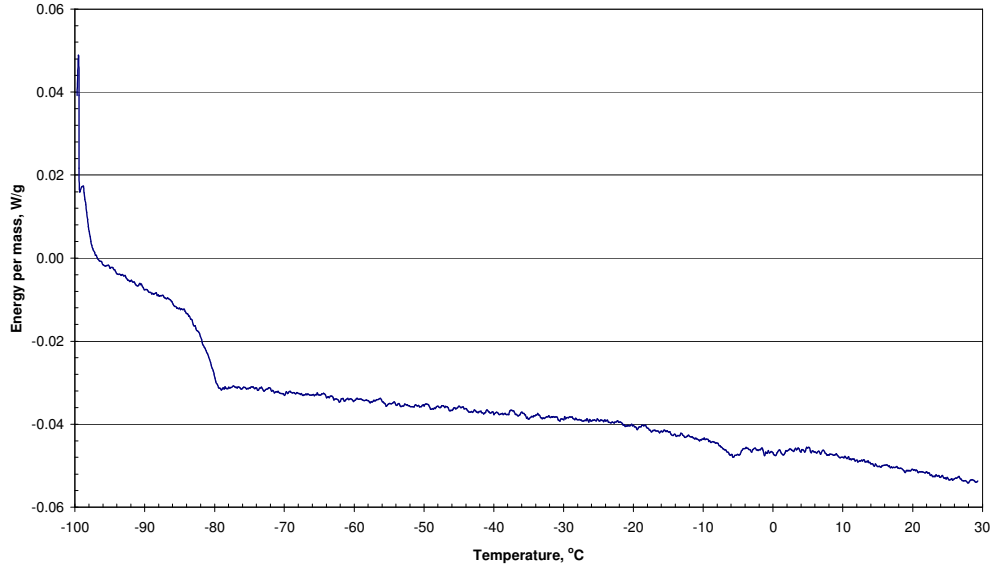

Figure 14. DSC thermogram of HTPB pre-polymer

The DSC thermograms for the HTPE and HTPB pre-polymers in the temperature range 30 - 600˚C are shown in Figure 15 and Figure 16 respectively.

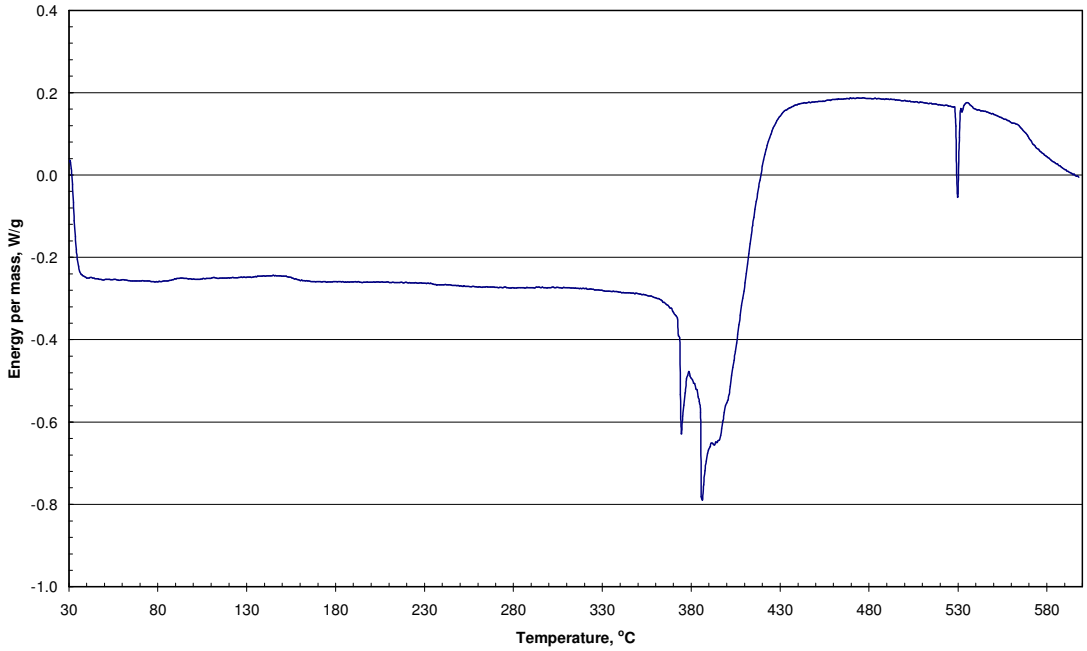

Figure 15. DSC thermogram of HTPE copolymer

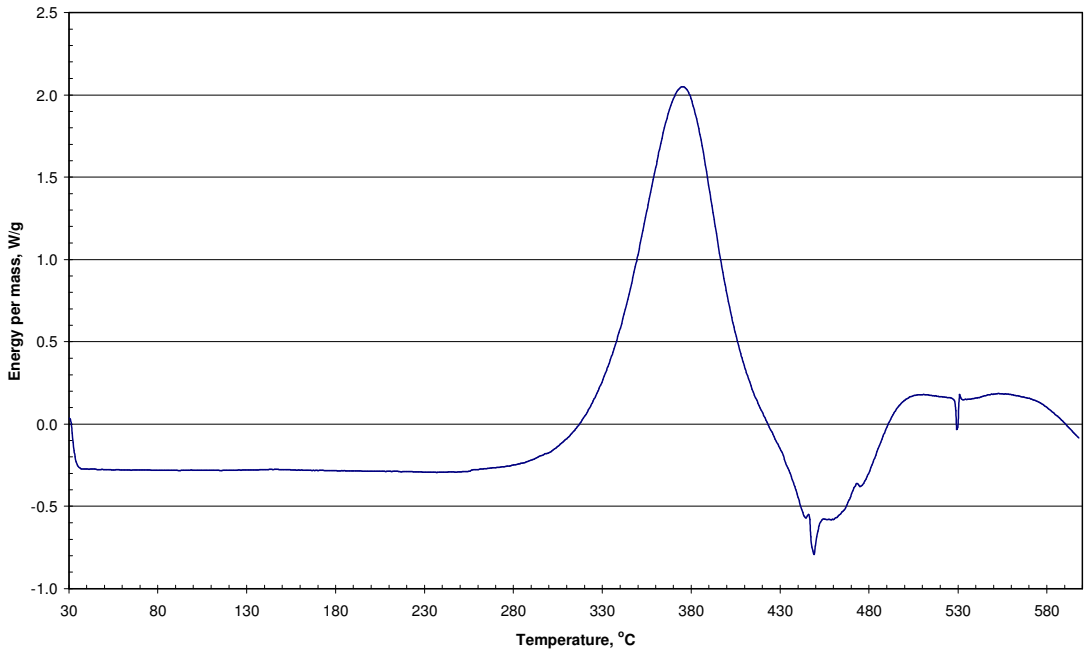

Figure 16. DSC thermogram of HTPB pre-polymer

Thermogravimetric analysis results for HTPE and HTPB pre-polymers are shown in Figure 17 and Figure 18 respectively.

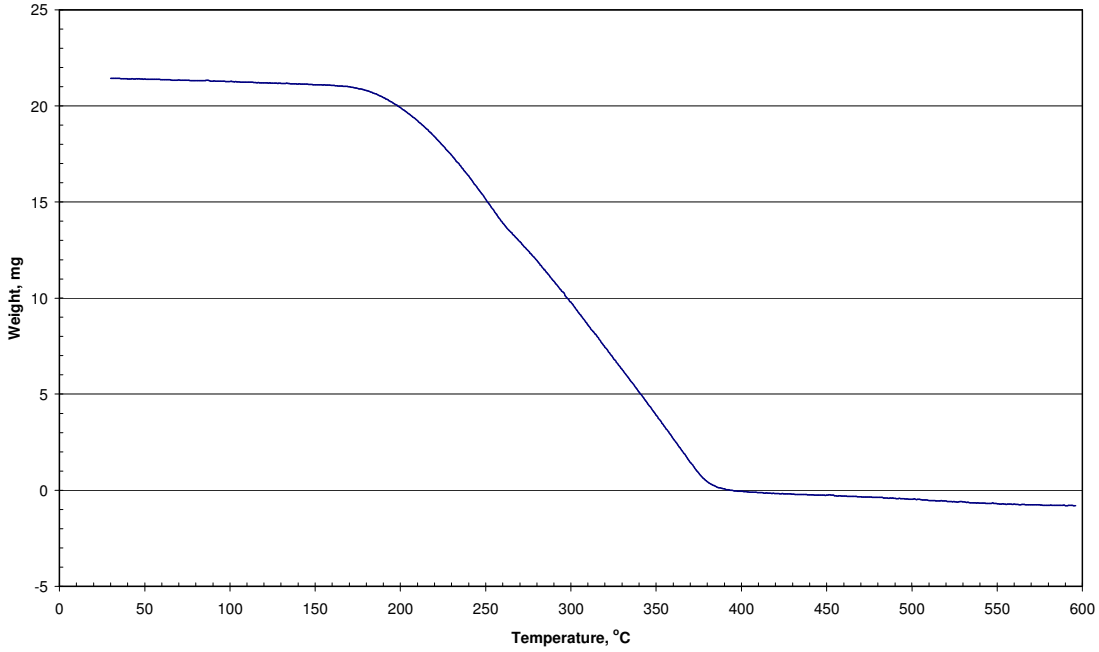

Figure 17. TGA thermogram of HTPE copolymer

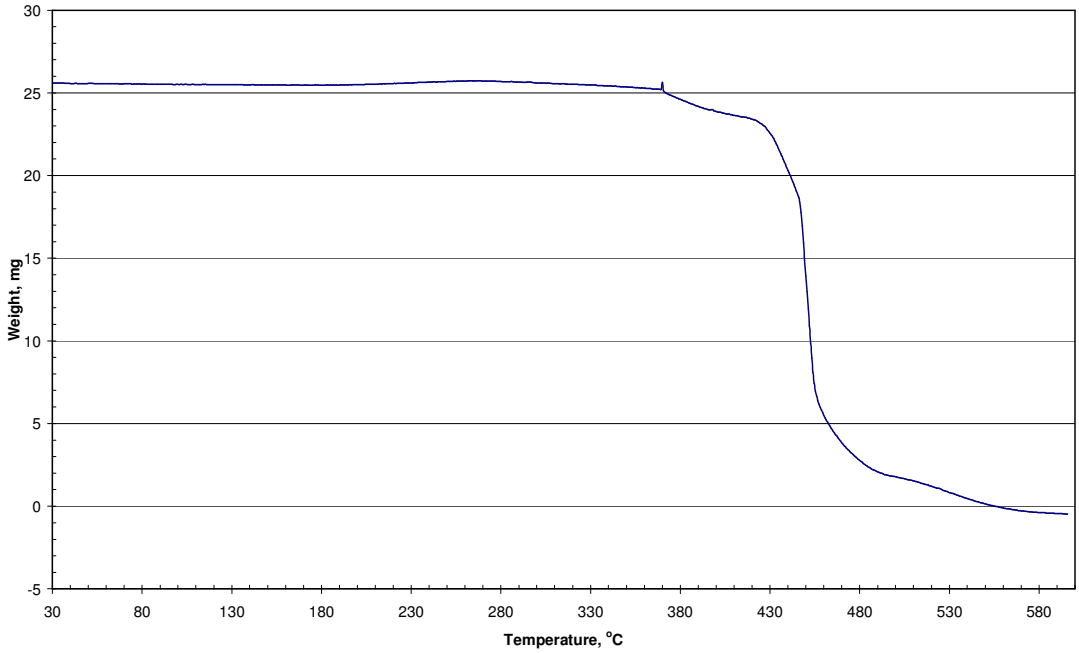

Figure 18. TGA thermogram of HTPB pre-polymer

Table 37. HTPE Copolymer Results from DSC and TGA Analysis

Experiment N°	Tg	Melting		Microcrystallisation	
		Temperature	Heat	Temperature	Heat
	(˚C)	(˚C)	(J g^{-1})	(˚C)	(J g^{-1})
1	-84.20	-24.00	26.4	-.-	-.-
2	-79.80	-10.57	40.8	-.-	-.-
3	-79.40	-16.07	35.9	-.-	-.-
4D	-79.00	-12.80	4.4	-.-	-.-
5C	-80.70	-4.56	45.6	-.-	-.-
6C	-90.00	-20.00	25.1	-.-	-.-
7D	-83.90	-16.51	36.2	-17	39.7
8B1A	-84.60	-1.83	56.9	-.-	-.-
8B2A	-84.30	-2.20	52.6	-.-	-.-
9B	-83.40	-7.77	44.6	-8.4	47.6
10B	-88.80	-10.00	-.-	-.-	-.-
11B	-82.50	-8.40	44.4	-8.4	44.4
12B	-82.12	-10.00	41.3	-10.0	41.3
13	-82.50	-11.00	44.2	-21.2	44.2
14	-83.40	-15.00	38.1	-15.0	38.1
15	-84.30	-9.90	48.4	-9.9	48.4
17	-85.30	-7.10	53.7	-7.1	53.7
18	-84.70	-6.40	51.8	-6.4	51.8
19	-83.50	-11.90	36.0	-11.9	41.6
20	-86.10	-10.79	39.0	-12.3	39.0
23	-81.6	-11.0	37.4	-56.1	30.6
24	-80.8	-14.1	32.3	-55.3	27.1
25	-82.4	-3.9	37.5	-56.4	23.8
26	-82.4	-8.5	37.2	-54.6	30.8
27	-81.6	-7.0	38.3	-56.4	29.4
Aldrich THF-EO	-84.90	-1.00	-.-	-.-	-.-
HTPB R45M File 33	-81.3	-.-	-.-	-.-	-.-
HTPB R45M File 50	-81.5	-5.3	0.2	-.-	-.-

2.3.5 FTIR analysis and results

Fourier Transform Infrared spectroscopy was performed using a Bruker FTIR spectrometer, model Vector 22, with Optic User Software (OPUS) version 3.1. A thin layer of sample was placed between two plates of sodium chloride. Figure 19 shows a typical infra red spectrum for the HTPE copolymer and Table 38 gives a summary of the main peaks. Further results are presented in Appendix F.

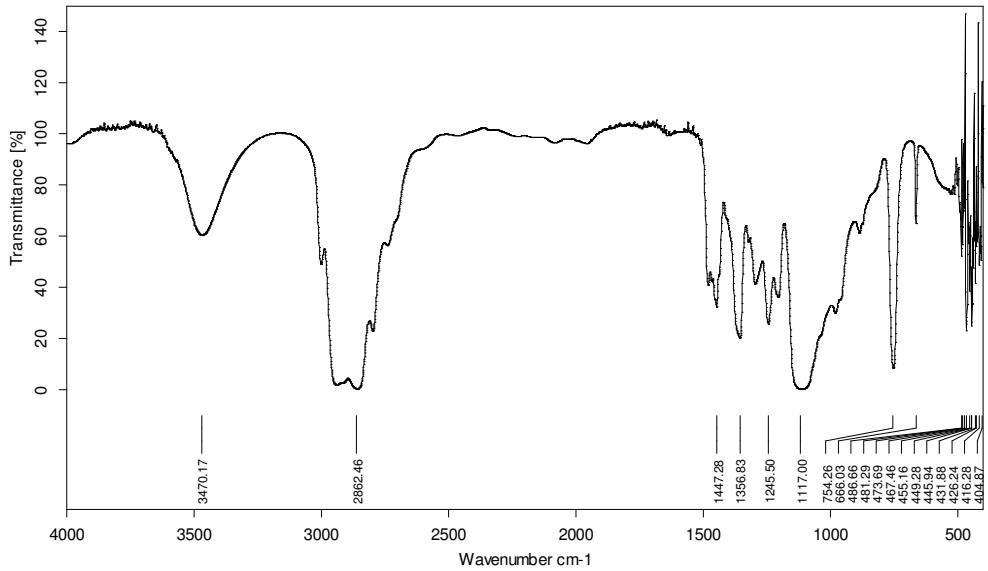

Figure 19. HTPE FTIR spectrum

Table 38. FTIR Main Characteristic Infrared Peaks, [Nakanishi 1964, Bellamy 1980]

Wave Number, cm^{-1}	Assignment	
3470	Primary alcohol	$-CH_2OH$
2862	Alkane group	CH_2CH_2
1447	Primary alcohol	CH_2OH
1356	Primary alcohol	CH_2OH
1245	Alcohol; group in plane bend; vinyl ether	-OH;
1117	Aliphatic ether	CH_2-O-CH_2
754	Alkane group; halogen	$-CH_2CH_2CH_2CH_2-$; C-Cl
666	Halogen	C-Cl

2.3.6 GC-MS analysis and results

In order to determine impurities and byproducts, gas chromatography mass spectrometry was performed using a ThermoQuest Trace gas chromatograph (GC) interfaced to a Fisons MD800 mass spectrometer (MS). The GC and MS were controlled via a PC running Xcalibur software. A Chrompak DB5 column of 15 metres length, 0.25 mm internal diameter and 0.25 μm film thickness was used. A small quantity of the sample was diluted in 10 cm^3 of acetone and then placed in a headspace vial. The loaded vial was placed in the headspace analyser and maintained at 100˚C for

2 min before being sampled. A characteristic Total Ion Chromatogram (TIC), of volatile components in an HTPE sample from experiment 7D is presented in Figure 20. The TIC ignoring peaks with retention times less than 1.00 min is presented in Figure 21. Further results are presented in Appendix G.

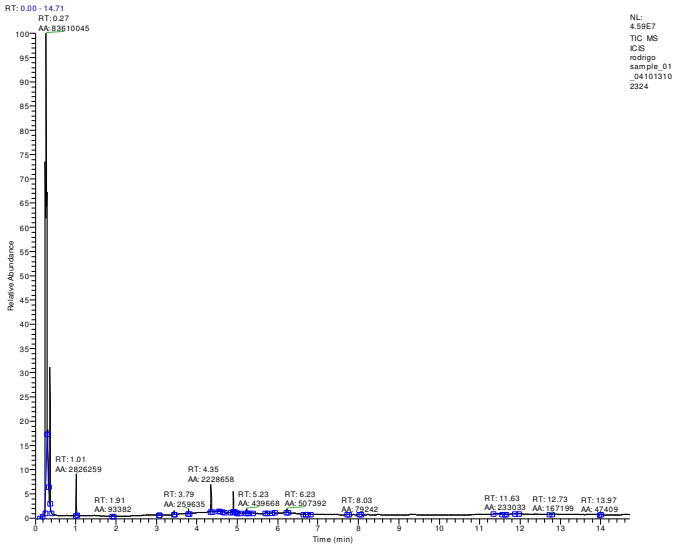

Figure 20. Total ion chromatogram (TIC) of volatile components in HTPE copolymer, experiment 7D.

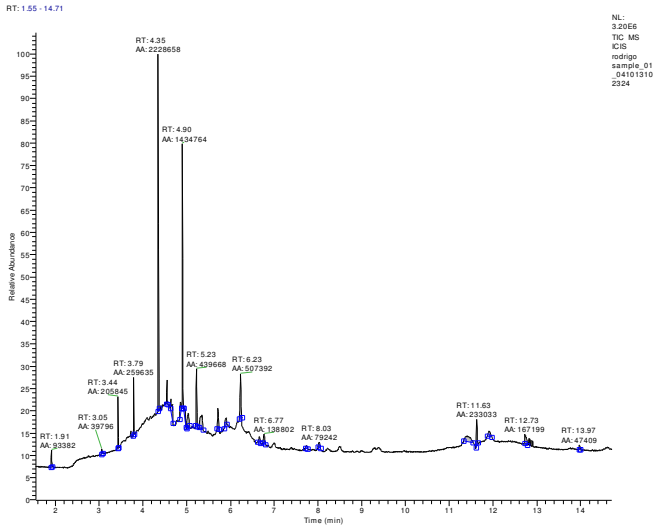

Figure 21. Total ion chromatogram (retention time > 1 min) of volatile components in HTPE copolymer, experiment 7D.

Table 39 and Table 40 show a summary of the peak retention times and component identification in the HTPE samples from the different experiments and in the Aldrich THF-EO **c**opolymer. Component identification was based on a NIST Spectral Library

Search. **SI** is a direct matching factor for the unknown and the library spectrum based on peak positions and intensities. **RSI** is a reverse search matching factor, ignoring any peaks in the unknown that are not in the library spectrum. Finally, the probability is a probability factor based on the differences between adjacent compound hits in an SI ordered list. Chromatograms are presented in Appendix G.

Table 39. Identification of Volatile Components in HTPE Copolymer from NIST Spectral Library Searches

Peaks in HTPE sample (Retention time, min)	Assignment	SI	RSI	Probability	Hit List Position
0.27	Acetone	896	891	85.84	1
0.37	Chloroform	756	774	23.80	1
1.01	2-Pentanone,4-hydroxy-4-methyl	893	893	87.29	1
1.1	Acetone	754	789	46.29	1
1.44-1.46	2-Hexanone, 4-methyl	737	784	18.26	1
1.68	Tetrahydrofuran	902	912	79.55	1
2.05	2-Pentanone,4-hydroxy	679	704	29.13	1
2.90-2.91	2-Pentanone,4-hydroxy	794	840	76.53	1
3.79-3.80	15-Crown-5	727	743	20.37	1
3.90	1,3-Dioxolane, 2,2-dimethyl	920	921	93.28	1
4.36	Butane,1,1'-oxybis[3-methyl]	679	756	15.25	1
4.90-4.91	1-Butanol,4(hexyloxy)	684	8.01	16.00	1
5.22-5.24	Cis-2,3-epoxyoctane	720	771	24.27	1
6.23-6.25	Butane,1,1'-oxybis[3-methyl]	635	730	13.32	1
7.61	2-Pentanone, 4-hydroxy-4-methyl	875	906	91.80	1
8.03-8.05	1,Penten-3ol,3methyl	724	736	25.11	1
12.6, 13.6	2.3-Dichloro-methylenbicyclo[2.2.1]heptane	631	642	71.21	1
13.6	Hexadecane,1-chloro	702	878	39.95	1
14.62	Heptadecane, 2,6-dimethyl	766	870	6.669	1
14.79	1-Butanol,4(hexyloxy)	664	807	24.4	1
15.37	Arsenous acid,tris(trimethylsilyl)ester	753	786	89.51	1
15.69	Arsenous acid,tris(trimethylsilyl)ester	772	824	93.74	1
15.95	Butanal,4-[(tetrahydro-2H-pyran-2-yl)oxy]	632	701	11.74	1

Table 40. Identification of Volatile Components in Aldrich THF-EO Copolymer from NIST Spectral Library Searches

Peaks in HTPE sample (Retention time, min)	Assignment	SI	RSI	Probability	Hit List Position
0.27	Acetone	764	820	34.31	1
0.37	THF	787	820	34.31	1
1.01	2-Pentanone,4-hydroxy-4-methyl	893	893	87.29	1
4.90-4.91	Isophytol	724	758	7.55	1
9.56	11-Heptadecenal	553	553	35.25	1
11.91	Phthalic acid, diisooctyl ester	790	790	74.72	1

2.3.7 Density measurements

Density determinations at 25^{o}C were performed using an AccuPyc 1330 Pycnometer for 1cm^3 samples from Micromeritics. The pycnometer can determine density and volume by measuring the pressure change of helium in a calibrated volume. The pressures observed upon filling the sample chamber and then discharging it into a second empty

chamber allow computation of the sample solid phase volume. Gas molecules rapidly fill the tiniest pores of the sample; only the truly solid phase of the sample displaces the gas. A sample chamber of 1 cm^3, was selected. The instrument automatically purges water and volatiles from the sample and then repeats the analysis until successive measurements converge upon a consistent result. A sample of the liquid copolymer weighing between 0.2 and 0.3 g was introduced into the calibrated volume container and then placed into the instrument. Five measurements were taken and the average density calculated and reported by the instrument together with the standard deviation. The test was carried out at a helium gas pressure of 20 psi (0.137 MPa). HTPB pre-polymer density was not measured and the figure was taken from the technical data sheet [Elf Atochem, 1996]. Table 41 shows the measured density for different HTPE pre-polymers. Also samples of n-BuNENA and Aldrich THF/EO samples where analysed.

Table 41. HTPE Pre-polymer Results from Density Measurements

Sample	Average density (g cm^{-3})	Sample weight (g)	Average volume (cm^3)	Volume standard deviation (cm^3)	Density standard deviation, (g cm^{-3})
1	1.0658	0.5453	0.5117	0.0003	0.0007
7D	1.0430	0.8913	0.8546	0.0001	0.0001
8B1A	1.0206	0.5734	0.5618	0.0001	0.0002
8B2A	1.0171	0.8559	0.8415	0.0001	0.0001
9B	1.0296	0.8130	0.7896	0.0000	0.0000
11B	1.0303	0.8818	0.8559	0.0001	0.0001
12B	1.0376	0.8285	0.7985	0.0000	0.0000
22	1.0217	0.5621	0.5501	0.0001	0.0002
23	1.0334	0.5904	0.5713	0.0001	0.0002
24	1.0524	0.4427	0.4207	0.0019	0.0048
25	1.0283	0.6505	0.6326	0.0001	0.0001
26E	1.0524	0.7987	0.7590	0.0002	0.0002
27B	1.0305	0.8219	0.7976	0.0000	0.0000
Aldrich THF-EO	1.0119	0.7611	0.7521	0.0001	0.0001
n-BuNENA	1.2195	0.6300	0.5166	0.0009	0.0021

2.3.8 Viscosity measurements

Viscosity values for different samples of HTPE and HTPB were obtained using a Brookfield Viscometer model RVDVE-230, connected to a small sample adapter of 8 cm^3 volume capacity, model SC4-21/13R/RP, as can be seen in Figure 22.

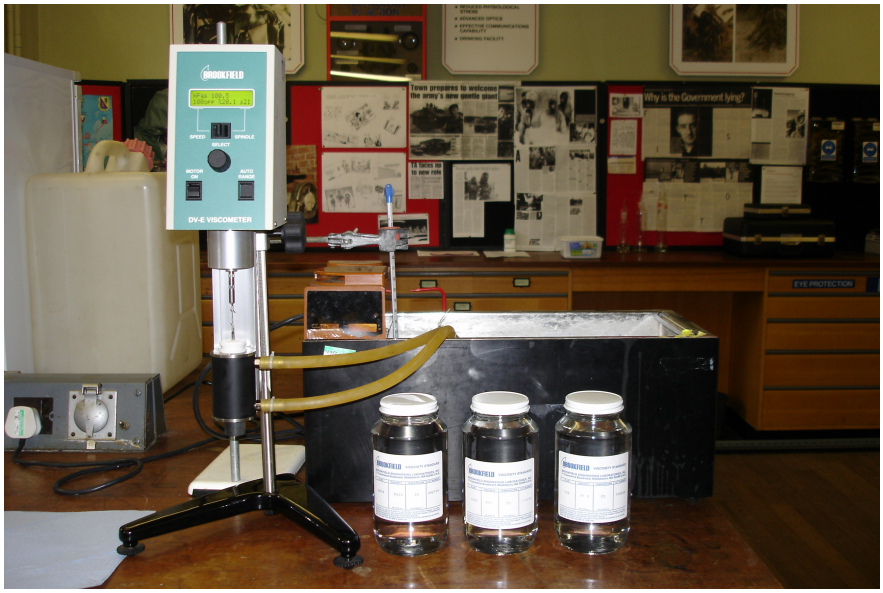

Figure 22 Brookfield viscometer and viscosity standards

Measurements were carried out at different temperatures, i.e. 25, 35, 45, 50 and 60˚C. In order to calibrate the viscometer, three Brookfield viscosity standards were used, with viscosities of 97, 990 and 5060 mPa s (cP). Standards, HTPB and HTPE samples were conditioned for 30 min at the desired temperature before the measurement was made. After that, the viscometer was turned on and the spindle revolutions per min (rpm) were settled according the sample requirement.

Table 42. Viscosity Values for Standard and HTPE Samples

Sample	Theoretical viscosity mPa s (cP)	Measured viscosity mPa s (cP)	r.p.m.	%	Temperature, ˚C
Standard 100	97	100	100	20.0	25
Standard 1000	990	998	30	59.9	25
Standard 5000	5060	5083	6.0	61.0	25
7D	-.-	508	60	60.9	25
13	-.-	1043	30	62.6	25
19	-.-	1825	20	73.0	25
9	-.-	807	50	80.7	25
11B	-.-	947	30	56.6	25
12B	-.-	1338	20	53.5	25
8B2A	-.-	1485	20	559.4	25
14	-.-	703	60	84.4	25
21	-.-	978	30	58.8	25
22	-.-	785	60	94.2	25
23	-.-	933	30	56.0	25
24	-.-	3785	10	75.7	25
25	-.-	2938	12	70.5	25
26	-.-	2350	20	94.0	25
27	-.-	2796	12	67.1	25

The viscosity reading was not made until the viscosity values shown on the equipment screen were constant. Table 42 shows the viscosity values obtained for the standards and different HTPE samples at 25˚C, while Table 43 and Table 44 shows the viscosity for HTPE samples 24 and 27 and for HTPB and Aldrich THF-EO samples respectively at different temperatures.

Table 43. Values for HTPE Samples at Temperatures Different from 25˚C

Sample	Theoretical viscosity mPa s (cP)	Measured viscosity mPa s (cP)	r.p.m.	%	Temperature, ˚C
24	-.-	1485	30	89.0	45
24	-.-	1228	30	73.7	49
24	-.-	835	50	83.4	60
27B	-.-	1703	20	68.1	35
27B	-.-	621.7	60	74.5	49
27B	-.-	925	50	92.5	60

Table 44. Viscosity Values for HTPB and Aldrich THF-EO Samples at Different Temperatures

Sample	Theoretical viscosity mPa s (cP)	Measured viscosity mPa s (cP)	r.p.m.	%	Temperature, ˚C
HTPB R45M	< 7000	6475	6.0	77.7	25
HTPB R45M L2		6375	6.0	76.5	25
HTPB R45M L2		3735	10	74.7	35
HTPB R45M L2		2075	20	83.2	45
HTPB R45M L2		1047	30	62.8	60
Aldrich THF-EO		610	60	73.2	25
Aldrich THF-EO		391	100	78.1	34
Aldrich THF-EO		243	100	48.6	45
Aldrich THF-EO		138	100	27.5	60

2.3.9 Flame test and EFP analysis and results

After experiment 6, it was noticed that some of the samples were cloudy and behaved like a gel. Because of that it was thought that samples were contaminated with sodium or calcium compounds, used in neutralisation and drying respectively. In order to establish if the samples from experiment 1 to 6 were contaminated with calcium or sodium compounds, a flame test was carried out. A platinum wire was immersed in each sample and then inserted into a Bunsen burner flame. A characteristic colour was observed i.e. orange light for calcium and yellow light for sodium compounds, as can be seen in Figure 23. In order to quantify each compound flame photometry analysis was carried out.

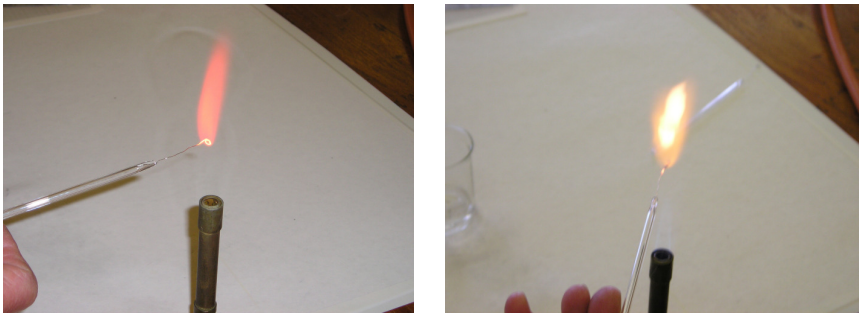

A **B**

Figure 23. Flame test for samples for experiments 1C1 (A) and 6B1 (B)

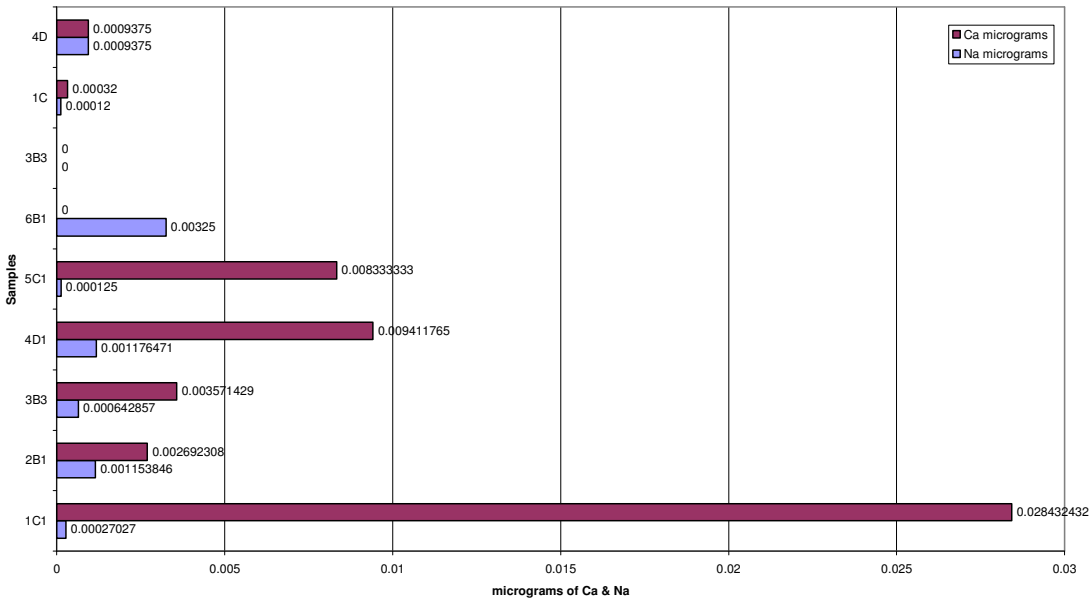

Figure 24. Emission flame photometry results

Emission Flame Photometry (EFP) analyses were performed using a Jemway Flame Photometer model PFP 7. Standards of 60, 40, 20, 10 and 5 ppm were use for the sodium calibration curve and standards of 100, 80, 40, 20 and 10 ppm for calcium. Results are presented in Figure 24.

2.3.10 Hydroxyl content determination

Hydroxyl content (meq g^{-1}) determinations were carried out by titration and performed by following the procedure stated in the ROXEL [2000] specification. In general terms, a test portion was refluxed in a solution of acetic anhydride in pyridine to acetylate the

hydroxyl groups presents. The excess reagent was hydrolysed with water and the resulting acetic acid was titrated with standardized sodium hydroxide solution. The hydroxyl content was calculated according to Equation 2.10 from the difference in titration of the test portion and a blank solution and corrected by the acid value of the sample. Data from the titration and the hydroxyl content are presented in Table 45.

$$\textbf{Hydroxyl Content } [\text{meq g}^{-1}] = \frac{A + \frac{B * C}{D} - E}{B} * N \qquad (2.10)$$

Table 45. Hydroxyl Content Results for Experiments 7D, 23, 24, 25A, 26E3 and 27B

Sample	N NaOH normality (meq cm^{-3})	A NaOH Volume for blank, (cm^3)	B Sample weight, (g)	C NaOH Volume for acid value, (cm^3)	D Sample weight for acid value (g)	E NaOH Volume for sample, (cm^3)	Hydroxyl content. (meq g^{-1})
E7d	0.259	16.40	1.010	0.100	1.000	13.100	0.872
E23	0.260	14.16	1.003	0.101	1.002	11.950	0.600
E24	0.260	14.16	1.002	0.100	1.002	12.200	0.535
E25A	0.260	12.35	1.000	0.100	1.002	10.050	0.625
E26E3	0.260	12.35	1.003	0.100	1.003	9.940	0.651
E27B	0.260	12.40	1.004	0.090	1.001	10.120	0.615

2.4 Discussion of Results

2.4.1 Experimental

2.4.1.1 Synthesis

During the synthesis process two events (apparently related), took place after adding the reagents and possibly at the end of the copolymerisation propagation step. Both affected the control of the chemical reaction. These events were characterised by a temperature increase, producing a change in the colour of the sample and in its molecular weight.

One of the events took place in experiments 1, 3, 4 and 5. All these experiments showed a temperature increase of approximately 70˚C following removal of the reaction flask from the cooling bath. Stirring time for these reactions was less than 2 h after completion of EO addition. Although it was thought that the reaction was finished, it was subsequently apparent that the propagation step was still going on because not all the EO was copolymerised. Since the copolymerisation reaction is exothermic, when the

flask was taken out of the low temperature bath the copolymerisation reaction started going faster as the temperature was increasing. When the temperature reached 20˚C it started going up more quickly and from 30˚C (after the start of the boiling) it increased up to 70˚C in approximately 30 seconds. After that it stopped boiling and the temperature fell. During this process the colour of the sample changed from transparent to dark brown. The colour change in the reaction mixture is mentioned by Zhiping [1999] as a problem which happens when the temperature rise is too high. No figures are quoted by Zhiping [1999] to describe this phenomenon.

After the Hethofrig electrical low temperature bath was installed, as explained in Section 2.3, samples were left stirring overnight before taking them out of the cool bath. This ensured that all the EO had reacted. Figure 25 shows the HTPE copolymer from experiment 8 when it was taken out of the low temperature bath (photograph A) and after melting (photograph B). It can be seen that in A it is white and almost completely frozen, i.e. melting point equal to -8˚C. This was an indication that almost all the reaction was complete and that if there was any EO remaining its reaction was not exothermic enough to prevent the copolymer from freezing.

A **B**

Figure 25. HTPE copolymer from experiment 8

However although samples were now stirred for a longer period, a similar situation happened in experiments 11, 12, 13, 14 and 19. As can be seen from Figure 26, after a period of more than 15 h stirring some samples were still dark brown in colour.

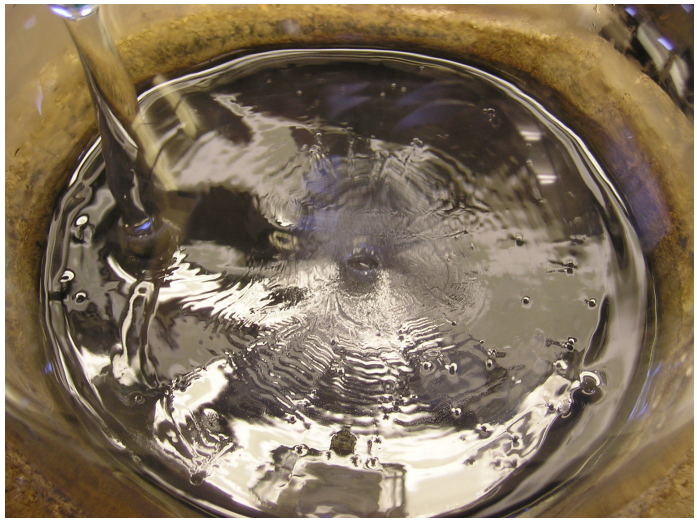

Figure 26. HTPE copolymer from experiment 14

Although the temperature never rose to that reached during the event discussed previously, a temperature increase of 35˚C was detected during the reaction. This was measured by a thermo couple connected to a Grant Squirrel data logger. As can be seen from Figure 27, some hours after finishing the EO addition in experiment 19, the temperature started going up and suddenly an exponential increased occurred. After that, no further temperature rise was detected and this was taken as an indication that the polymerisation reaction was finished.

It is believed that a catalysed THF-EO polymerisation reaction is taking place. It can be seen from the ^{1}H and ^{13}C NMR results in Appendix C and from results presented in Table 36, that the product obtained has the same molecular structure as the one produced in the absence of this phenomenon. Despite that, the ratio "n" of all of them is close to 1. All of this is an indication that, despite the temperature increase, the same product is obtained but there is a loss of control over the molecular weight.

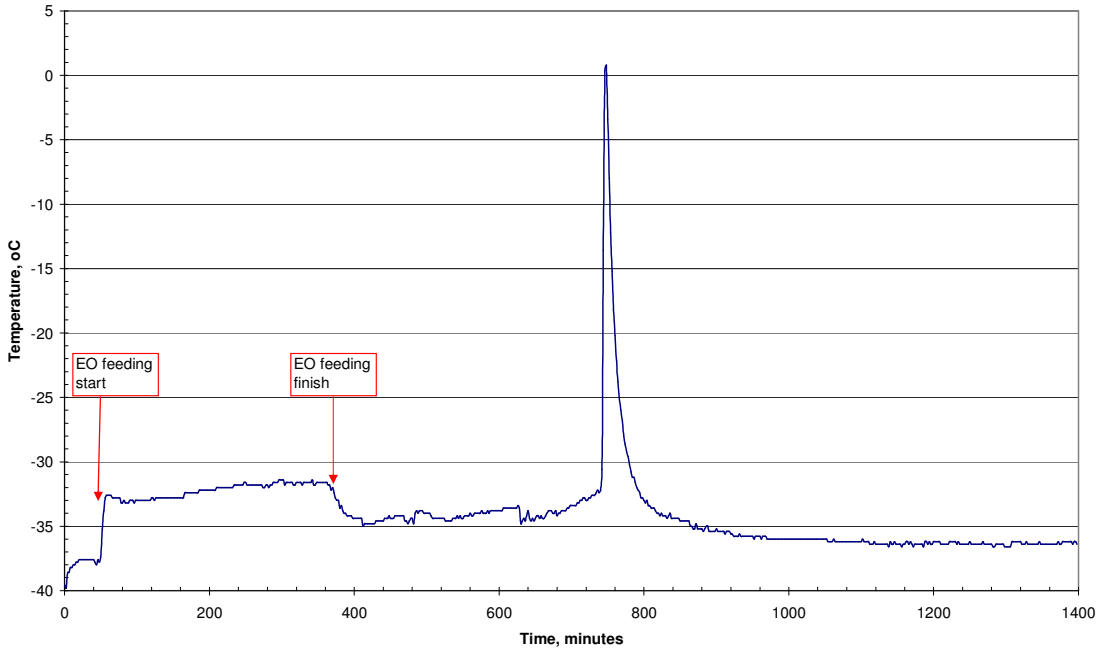

Figure 27. Temperature behaviour of experiment 19

One possible polymerisation catalyst is hydrofluoric acid (HF) generated by the reaction between HBF_4 and traces of H_2O present in the flask or in the reagents. The influence of water in the reagents is mentioned by Zhiping [1999] and Bednarek [1998, 1999a] as a killer of the reaction, which can finish the copolymerisation before reaching the desirable molecular weight. However, although BF_4^- is quite stable to hydrolysis, it can hydrolyse slowly to generate hydrofluoric acid (HF) [Kirk-Othmer, 1994], as shown in Equation 2.11.

$$BF_4^- + H_2O \rightarrow BF_3OH^- + HF \qquad (2.11)$$

It was noticed that the catalytic reaction only happened in the presence of EO oxonium ions. No further reaction was observed when H_2O was added to a sample containing THF, HBF_4 and EG which was left to react for a couple of days. Also samples containing higher concentrations of EO were affected by this reaction. It is therefore believed that due to the low reaction temperature i.e. -40˚C, the rate of the reaction is low, which allows a high concentration of EO oxonium ion to build up in the bulk. Because the EO addition is continuous, its concentration is increasing over time and maybe, when there is enough HF and EO, the reaction is triggered.

Actions were taken in an attempt to avoid this undesirable reaction: the rate of the EO/THF reaction was increased by increasing the reaction temperature by 10˚C, the instantaneous concentration of EO was reduced by reducing the mass flow during feeding and the content of HBF_4 in relation to the reagents was reduced.

A reduction in the EO mass flow and in the concentration of HBF_4 were carried out in experiment 20. The temperature was kept at -40^{o}C. The catalytic reaction was not observed after finishing the experiment. However, it was noticed that the reaction was not completed almost 20 h after the end of the EO additions. The sample was not frozen and when agitated the pressure increased, being an indication of the presence of THF and or EO in the bulk. The Mn obtained was 2097 g mol^{-1} and the ratio THF/EO was 1.21 despite an excess of EO. Therefore it was believed that an increase in the temperature is the best means to improve the process.

The process temperature for experiments 21 to 27 was increased to -20^{o}C and the percentage of HBF_4 was decreased to between 3.35 to 0.5 mole %. As expected the increase in the temperature of the process increases the system reactivity. However, in experiment 21 and 22, having a HBF_4 concentration of 3.35 and 1.95 mole % respectively, the high reactivity raised the viscosity in such a way that made impossible to keep the sample under stirring. Because of that, the EO supply was stopped and the copolymerisation reaction finished. The same temperature condition but a reduced percentage of catalyst was used in experiments 23 to 27. In these experiments the percentage of HBF_4 was between 0.5 and 0.75 mole %. As a result of this change a suitable molecular weight was reached and a copolymer with a ratio of THF/EO around 1 was obtained. Because the best observed copolymerisation process was in experiment 26, having 0.75 mole % HBF_4, it was decided to use that percentage for the synthesis of the biggest batch in experiment 27. The copolymerisation process shows good reproducibility and allowed us to have similar copolymers in terms of Mn and THF/EO ratio when the batch size was increased, as can be seen in Table 34 and Table 36 respectively.

2.4.1.2 Neutralisation

Initially, as suggested by Bednarek [1999a], calcium oxide was added to neutralise the acid after finishing the polymerisation. However, when the acidity level was measured after the neutralisation process in experiments 1 to 6, it was noticed that the copolymer was still acid. Several portions of calcium oxide were added to the samples to be neutralised, however no further reaction was observed. It was decided not to mix calcium oxide with water because the resultant strong base would have a negative effect on the copolymer. A moderated base solution was chosen. As explained in Section 2.2.5, an excess of 10% $NaHCO_3$ in relation to the acid, diluted in deionised water, was used in the neutralisation process. Afterwards the sample was washed with water three times in order to remove traces of sodium bicarbonate.

2.4.1.3 Drying

After the neutralisation process samples were initially dried using anhydrous sodium sulphate. However it was noticed that after separating the solvent from the copolymer in the rotary evaporator, samples were cloudy and behaved like a gel. Because of that it was thought that samples were contaminated with sodium or calcium compounds, used in neutralisation and drying procedures respectively. As explained in Section 2.3.9, a flame test and emission flame photometry analysis were carried out, indicating the presence of calcium in the samples, as can be seen in Figure 23. According to Panaitov [1980], alkaline earth metal cations can create complexes with high molecular weight polyethers and according to Yanagida [1978] hydroxyl terminal groups play an important role in the complexation process. Because of that and the low presence of sodium compounds after the neutralisation process, it was decided to use anhydrous sodium sulphate instead of calcium chloride after neutralisation in the drying process.

2.4.2 Molecular structure

^{13}C NMR spectra obtained from copolymer samples were compared against the spectra presented by Bednarek [1999a] and Zhang Jianguo [1994], and ^{1}H NMR spectra were

compared against those of Zhiping [1999] and Bednarek [1999a]. From the comparison it was established that the copolymer obtained from THF and EO presented above is a hydroxy terminated copolyether.

Figure 28 and Figure 29 show ^{13}C and ^{1}H NMR spectra which correspond to the product from experiment 2. All other NMR spectra corresponding to each experiment follow a similar pattern, as can be seen from Appendix C. As stated by Bednarek [1999a], the peaks at 61.7 and 71.7 ppm in Figure 28 ("B" and "D"), correspond to CH_2 groups in the alpha and beta positions relative to HO- terminal groups in an EO segment i.e. HO-**CH_2CH_2**-O-. The peaks designated as "A" at 25 ppm corresponds to the CH_2 groups in the beta and gamma positions in a THF segment, i.e. –OCH_2**CH_2CH_2**CH_2-, and the triplets in "C" correspond to the CH_2 groups in the alpha position in both EO and THF segments, i.e. –O**CH_2**CH_2-.

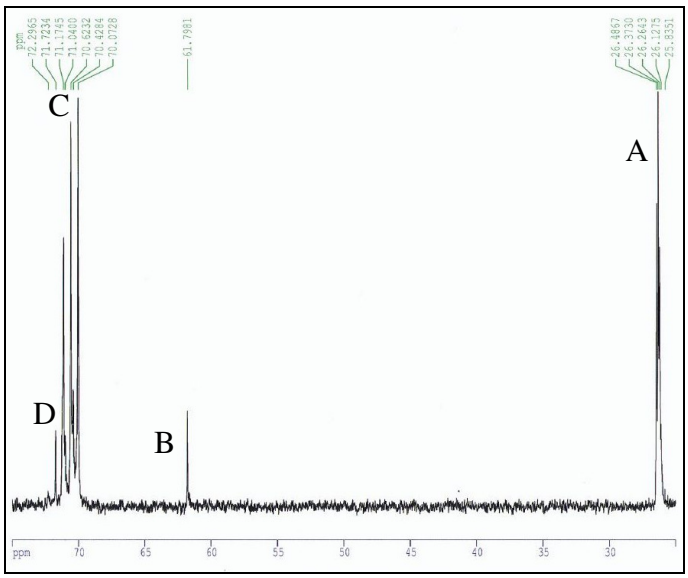

Figure 28. ^{13}C NMR spectrum for sample 2B

Quantitative analysis to determine the ratio of [THF]/[EO] was based on the ^{1}H NMR spectra. Protons of the -OCH_2**CH_2CH_2**CH_2O- groups of THF gave a separate signal at 1.6- 1.7 ppm (Figure 29 letter "F"), while –O**CH_2-** groups present in both EO and THF give a mixed signal pattern at 3.40 – 3.75 ppm (Figure 29 letter "A to E"). Thus the overall composition of the copolymer was determined from the integration of both groups of signals.

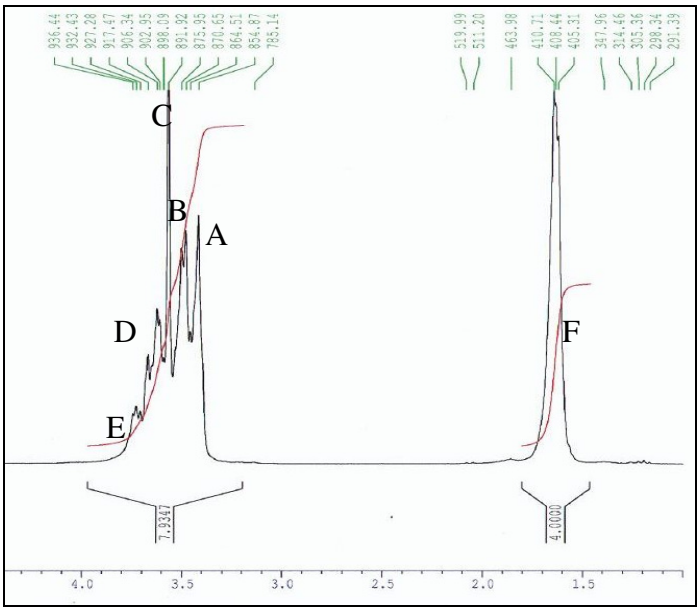

Figure 29. ^{1}H NMR spectrum for sample 2B

According to Bednarek [1999a], the peak at 3.73 ppm in Figure 29 "E" (an expanded view can be seen in Figure 30) corresponds to CH_2 groups in the alpha positions relative to HO- terminal groups in an EO segment, i.e. HO-**CH_2**CH_2-O-.

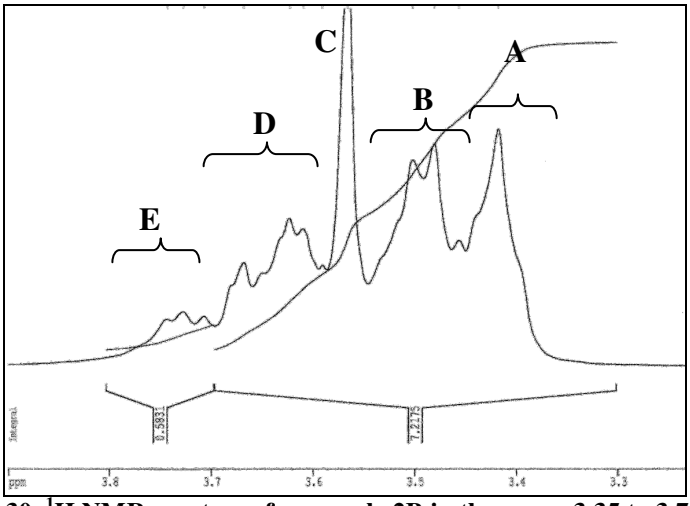

Figure 30. ^{1}H NMR spectrum for sample 2B in the range 3.35 to 3.75 ppm.

The peak designated as "D" corresponds to the CH_2 groups in the alpha positions in an EO-EO segment, i.e. -OCH_2**CH_2**-O-**CH_2**CH_2O-. The peak designated as "C" corresponds to the CH_2 groups in the alpha positions in an EO-THF segment, i.e. -OCH_2**CH_2**-O-CH_2CH_2**-**CH_2CH_2O-. The peak designated as "B" corresponds to the CH_2 groups in the alpha positions in a THF-EO segment, i.e. -OCH_2CH_2**-**CH_2**CH_2**-O-

CH_2CH_2O-, and the peak designated as "A" corresponds to the CH_2 groups in the alpha positions in a THF-THF segment, i.e. -OCH_2CH_2-CH_2**CH_2**-O-**CH_2**$CH_2CH_2CH_2$.

2.4.3 Influence of EG on Mn

In order to estimate the Mn that will be obtained after the copolymerisation reaction, Equation 2.9 was used and the theoretically calculated values compared against Mn values obtained by SEC techniques. The results are presented in Table 46. Initially it was assumed that all THF and EO was copolymerised during the reaction, which is not a correct assumption for all the samples. As stated before, not all reactions finished completely when they were stopped, which means that THF and EO were present although not quantified at this stage. However, a comparison between predicted and experimental Mn values allows trends to be observed.

Table 46. Theoretical Mn versus Measured Mn for EO/THF Copolymer

Experiment Nº	EG Weight related THF (%)	HBF_4 Weight related THF (%)	Theoretical Mn	Measured Mn	Difference (%)
1	8	7.5	1559.8	989	36.6
2	4	7.5	2465.0	1611	34.6
3	4	7.5	2423.2	1385	42.8
4	4	7.5	2550.9	1312	48.6
5	4	7.5	2381.3	1206	49.4
6	4	7.5	2099.4	510	75.7
7	3	7.5	3157.3	1984	37.2
8B1A	3	7.5	2881.4	2553	11.4
8B2A	3	7.5	2888.4	2993	-3.9
9	4	7.5	2301.4	1451	37.0
10	8	7.5	1009.1	816	19.1
11	4	7.5	2379.9	2206	7.3
12	4	7.5	2570.3	2021	21.4
13	4	7.5	2541.8	2680	-5.4
14	4	7.4	2399.2	2498	-4.1
15	4	7.1	2691.4	1481	45.0
16	4	7.5	2586.0	1684	34.9
17	4	7.2	2484.3	1477	40.5
18	3	7.3	3163.1	1615	48.9
19	3	7.5	3252.5	4050	-24.5
20	3	4.5	3606.9	2097	41.9
23	3	1.1	3360.5	4318	-28.5
24	3	2.2	3550.8	4789	-34.9
25	3	2.2	3286.5	4249	-29.3
26	3	1.7	3312.6	4076	-23.0
27	3	1.7	3267.7	4340	-32.8

Data from Table 33 were used to calculate Mn from Equation 2.9, and appear in Table 46 as theoretical Mn. These values are compared with the measured Mn obtained from the SEC analysis.

The general trend, as can be seen in Table 46, is that the higher the percentage of ethylene glycol, the lower the molecular weight predicted and obtained. The highest Mn is the one obtained when 3 weight % EG was used. Also it can be seen that some of the experiments which had an unexpected catalysed reaction (8, 13, 14, and 19) have an Mn between 4% and 25% higher than that predicted. There is then a possibility that the high molecular weight obtained in the previously mentioned experiments might be due to a complete EO polymerisation plus a polycondensation of the copolymer. In fact, the copolymer from experiment 8B1A was made from the same batch as 8B2A but was separated from the bulk just before the catalysed reaction started. As can be seen, the Mn from 8B2A is about 17 % higher than that from 8B1A and their THF/EO ratios are 1.55 and 1.53 respectively. Bednarek [1999a] said that for Mn over 2500 the predicted values are higher than those obtained experimentally, but in our case the measured Mn for samples synthesised at -20^{o}C were higher than the predicted. As stated previously, one of the reasons could be that Equation 2.9 does not take into account the protic acid concentration, which also has an influence on Mn, as can be seen from Table 46, which is in agreement with that reported by Zhiping [1999]. In fact, according to Zhiping [1999], the Mn is inversely proportional to the quantity of catalyst used in the reaction, and then, because of that the observed Mn was higher than that predicted by Equation 2.9. On the other hand, the difference in Mn values for experiments where the expected Mn should have been less than 2500 suggests that the reaction was finished before the propagation step was completed.

2.4.4 Influence of EO mass flow on THF/EO ratio

Figure 31 shows the relation between the THF/EO ratio and EO mass flow rate. Data have been presented with highlighting in red to show the experiments where no catalytic reaction was observed and in blue where it was affected by the catalytic reaction. It can be seen that there is no real influence of the different mass flow conditions on the polymerisation reaction and the ratio between THF and EO groups in the copolymer chain. Experiments shown in blue are closer to a THF/EO ratio equal to one than experiments shown in red. This suggests that in these cases there is complete reaction of EO despite a stoichiometric excess of THF in most of the experiments i.e. in 3, 5, 7,

8B2A, 11, 14, 19, the trend is to give a copolymer closer to **n** = 1. On the other hand, experiments labelled in red show an **n** value greater than one in most cases. This means there is a major presence of THF groups in the copolymer chain.

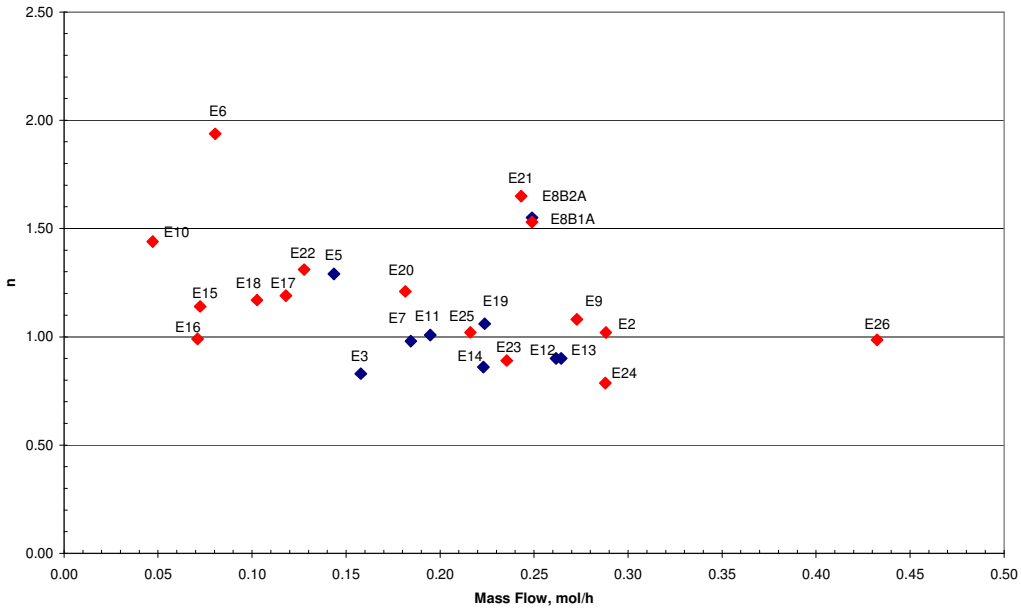

Figure 31. THF/EO ratio "n" versus mass flow, for experiments with catalysed reaction (blue label) and without catalysed reaction (red label)

2.4.5 Mn and EO incorporation in the copolymer

During the copolymerisation reaction in experiment 4, different samples were taken at different times, as can be seen in Figure 32. After 6 h of reaction in a cold bath at a temperature of -40˚C, the Mn increased to 1312, 2547 being the maximum theoretical Mn estimated by Equation 2.9 for an ethylene glycol weight percentage of 4% (compared to THF). A trend line was determined and the theoretical time to reach the maximum Mn value was calculated to be around 21 h (Figure 32).

No further measurements during the copolymerisation process were done for other experiments but from this analysis it was estimated that using a lower amount of EG in order to obtain a higher molecular weight, at least a similar reaction time will be necessary to reach the required Mn and complete the reaction. From experiment 7 onwards, and with the use of the "Hetofrig" electrical cooler, samples were maintained

with stirring at a temperature of -40 and -20˚C during periods longer than 15 h in all the cases, as can be seen from Table 33.

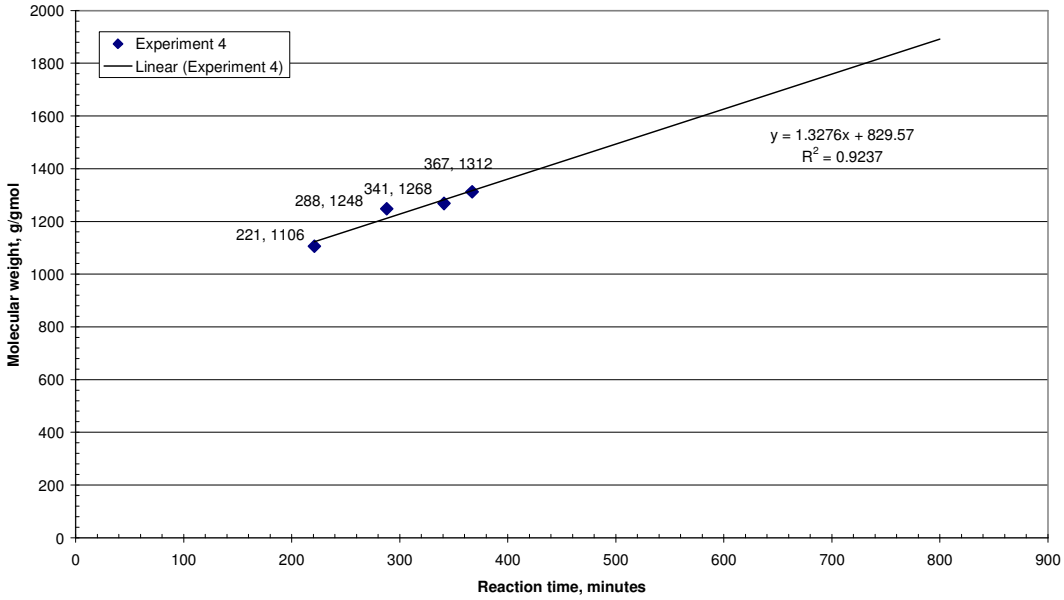

Figure 32. Mn versus process time, for different EO flow mass, EG and stirring time

2.4.6 FTIR and GC-MS determination of impurities and by-products

As stated in Section 2.3.5, FTIR analyses were performed on different HTPE samples in order to characterise the copolymer and some impurities. The characteristic spectrum presented in Figure 19 together with data from Table 38, show that the bands from 1170 up to 3470 cm^{-1}, are in good agreement with those in the infra red spectrum presented by Zhiping [1997] and with the spectrum of the Aldrich THF-EO copolymer presented in Appendix F, indicating that the spectrum corresponds to a hydroxy terminated copolymer of THF and EO. However some of the samples show two peaks at 745 and at 666 cm^{-1}, which correspond to contamination with chloroform. In order to confirm the source of contamination, sample 8B1A was intentionally contaminated with chloroform and its FTIR spectrum compared against the original sample. It was observed that the two peaks at 745 and at 666 cm^{-1} increased their intensity, as can be seen from Figure 33, becoming similar to the spectrum presented in Figure 19.

According to FTIR analysis, samples 3 and 20 were the most contaminated with chloroform, and samples 8B1A, 8B2A, 11, 12, 14, 15, 16, 17, and 19 had lower levels. At this stage chloroform was not quantified and either the solvent extraction process should be modified or the solvent changed.

The identification of components from GC-MS results is related to three factors that describe the match between a library spectrum and that of an unknown; the **SI, RSI,** and the **Probability**. As a general guide an SI of 900 or greater is an excellent match, 800-900 a good match, 700-800 a fair match. A matching factor less than 600 is considered a poor match. From Table 39 it can be seen that the peak with retention time 0.27 min, has a good match to acetone. The impurities presents in the acetone have retention times 1.01, 2.90 and 7.61 presenting good and fair matches. They should not be taken into account as copolymer impurities

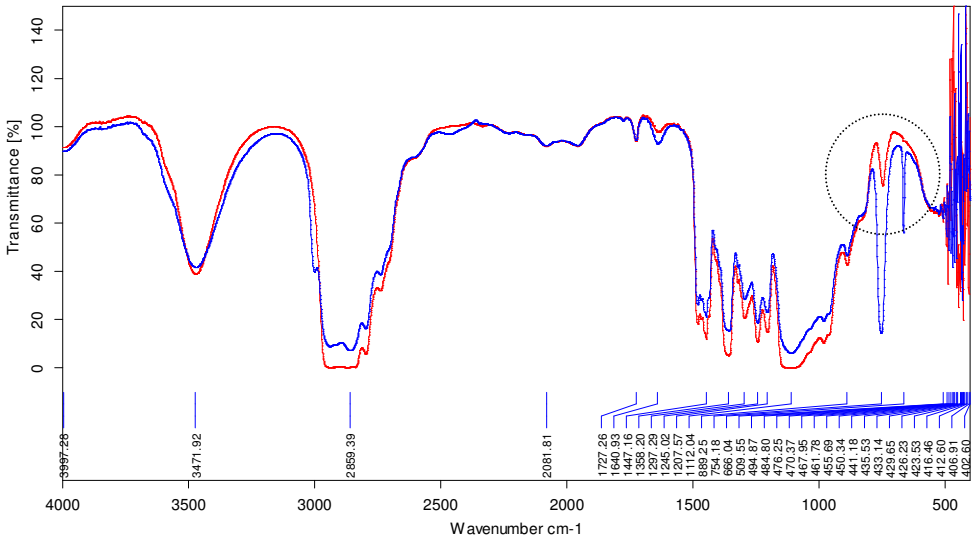

Figure 33. Chloroform contamination in sample E8B1A (red: before adding chloroform, blue after adding chloroform)

Because of the kind of stationary phase column used for GC-MS analysis (Chrompack CP-Sil 8 CB), chloroform and the THF main peak were detected at the same retention time of 0.37 min. In fact, because the stationary phase has not a high polarity, retention times for solvents like THF and chloroform are overlapped and presented at the same time scale. This peak was found in almost all the samples. Then, an analysis of the mass

spectrum of each peak at this retention time was necessary in order to identify the assignment of each compound.

Most of the peaks at retention times 3.79, 4.36, 4.90, 5.22, 6.23, 8.03, 14.62, 14.79 and 15.95 min have an SI factor close to 700, but with a very low probability. When comparing their mass spectra it is apparent that they are similar, possibly indicating they arise from the same polymer chain, i.e. the HTPE copolymer. This is probably due to the copolymer chain breaking at high temperature.

The match at retention time 3.90 min can be considered excellent, and it is present only in samples 3 and 6. According to the NIST library it can be a cyclic compound as stated in Table 39. Possibly it is a cyclic oligomer: THF_1-EO_1.

The presence of other products from the copolymerisation of THF and EO can be seen from the SEC Figure 11. In addition to the main peak that corresponds to the linear copolymer, small peaks in the low molecular weight region are observed and their presence as a percentage of the total peak area is presented in Table 35. According to Bednarek [1999c] they mainly correspond to cyclic oligomers. As can be seen from Table 47, the total presence in all the cases is less than 3.3%. Assuming an error percentage in SEC Mn, components can be ordered according to similar molecular weights and retention times. Then, a structure considering THF and EO units can be assigned, as presented in Table 47.

Table 47. Identification of Cyclic Components in HTPE Copolymers

Peaks in HTPE sample [Retention time, min]	Mn from SEC	Average content (%)	Assignment	
			Number of units in the ring	Mn
26.4, 26.64, 26.72	205, 201, 191	0.59	THF_1-EO_3	204
27.23, 27.27, 26.48, 27.34	144, 138,132, 129	0.60	EO_3	132
26.58	117	1.58	THF_1-EO_1	116
27.8, 27.73	91, 96	0.50	EO_2	88

The small amount of cyclic oligomers present in the copolymer is an indication that the applied conditions of EO rate of addition and temperature give a product with only a small percentage of undesirable components.

2.4.7 Relation between Mn, ratio of THF/EO, Tg and M.p.

The relation between the Tg and Mn behaviour is presented in Figure 34. Data from experiments 1, 6, 10, 17 and 20 have not been taken into account since they are contaminated with THF or chloroform. Also, HTPB information has been included.

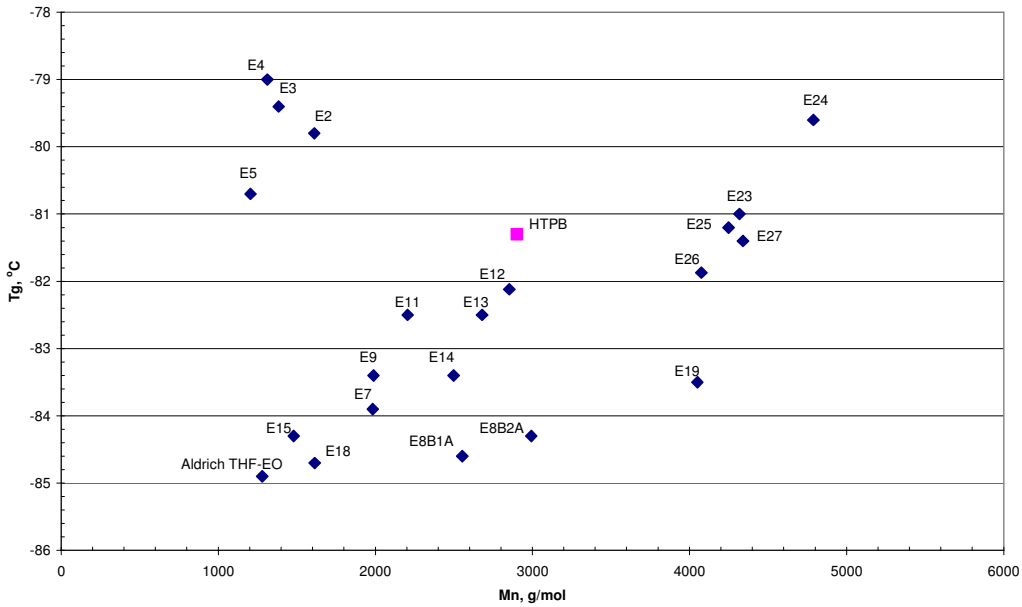

Figure 34. Tg versus Mn

Three different groups can be identified from Figure 34. One is composed of experiments 2, 3, 4 and 5, the other by experiments 7 upwards and the last one by HTPB alone. From Figure 34 it can be seen that HTPB shows a higher Tg than HTPE copolymer with similar and even higher Mn. In general terms, the first group has a slight trend to decrease Tg while Mn is increased. However, it can be seen that in some cases copolymers having similar molecular weight have different Tg e.g. E8B2A in comparison to E12. This difference can be explained by the difference in copolymer chain structure as can be seen in Figure 35. These two groups were synthesized under different experimental conditions in terms of the cooling system.

As was mentioned before, there is a Tg dependence on "n". In fact as "n" increases i.e. the presence of THF groups in the polymer chain is higher than the EO groups, Tg decreases. These results are consistent with the data presented by Bednarek [1999a], about the Tg relation between Poly THF and Poly EG, which is -82.5˚C for a 2000 Mn and -58.3˚C for a 1000 Mn respectively.

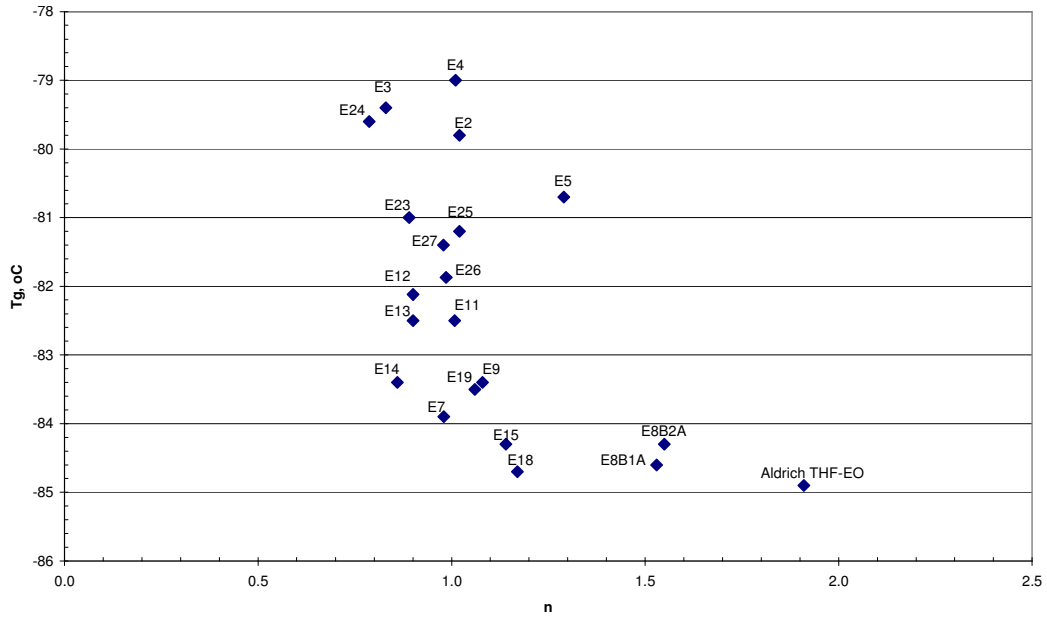

Figure 35. Tg versus ratio "n" of THF/EO segments present in the polymeric chain

On the other hand, melting point (M.p.) changes the other way round with respect "n" in comparison with Tg, as can be appreciated from Figure 36. The higher the content of THF groups in the copolymer chain, the higher the melting point. Also in general, for a similar "n", the higher the molecular weight the higher the melting point, i.e. E11: Mn 2206, and E4: Mn 1312.

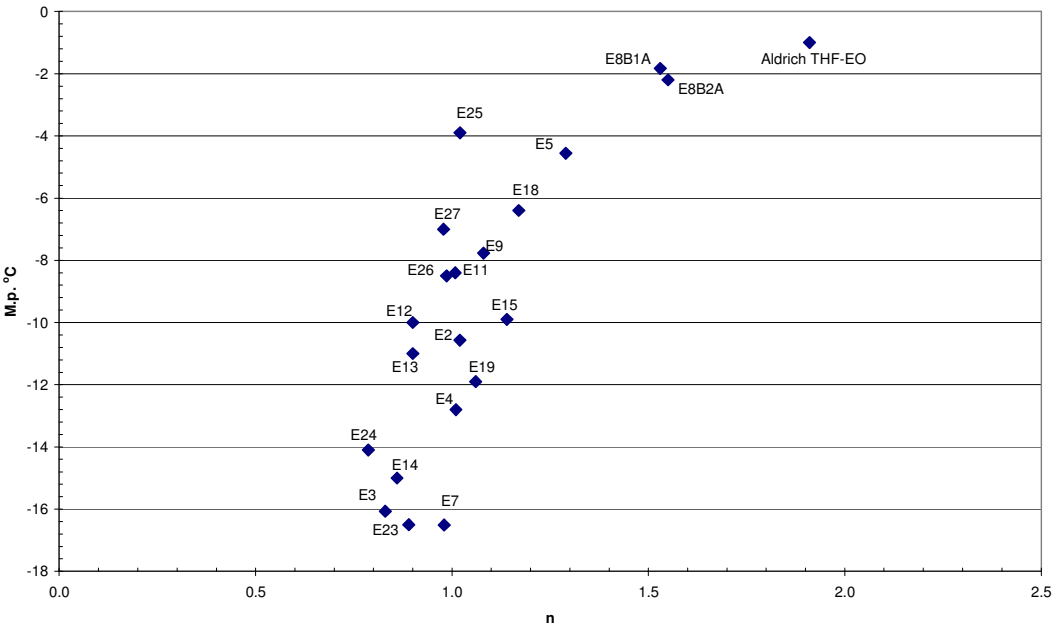

Figure 36. M.p. versus ratio "n" of THF/EO segments in the polymeric chain

2.4.8 Density, molecular weight and ratio of THF/EO analysis

Density figures presented in Table 41 correspond to HTPE pre-polymers having different molecular weights and also different ratios of ethylene oxide (EO) and tetrahydrofuran (THF) segments in the main chain. A correlation was found when plotting density versus THF/EO ratio (n), as can be seen in Figure 37.

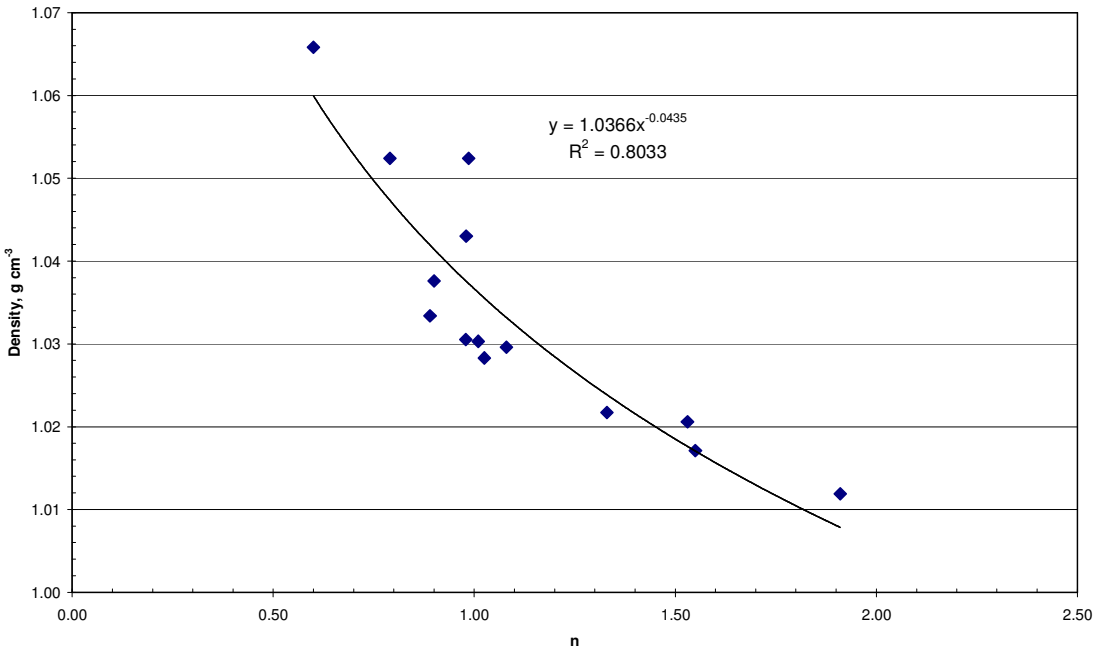

Figure 37. Pre-polymer density versus THF/EO for different Mn

As can be seen from Figure 37, there is a relationship between density and the ratio THF/EO in the copolymer chain, for samples having different Mn. In general terms, the density decreases as the percentage of ethylene oxide groups in the copolymer chain decreases, i.e. HTPE sample E1 has n = 0.6 and density = 1.066 g cm^{-3} while HTPE sample 27B has n = 0.98 and density = 1.031 g cm^{-3} and the Aldrich sample has n = 1.91 and density = 1.012 g cm^{-3}. However, from the relationship between copolymer structure, molecular weight and density, it appears that for similar THF/EO ratios, the trend is for the density to decrease as the molecular weight increases, i.e. HTPE sample 26E has Mn = 4076 g mol^{-1} and density = 1.052g cm^{-3} while HTPE sample 27B has Mn = 4340 g mol^{-1} and density 1.031 g cm^{-3}. This is in agreement with results presented by Bednarek [1998].

2.4.9 Viscosity, molecular weight and THF/EO ratio analysis

The relation between viscosity and temperature for four samples is presented in Figure 38 together with information presented by Bednarek [1998] and by Comfort [2004].

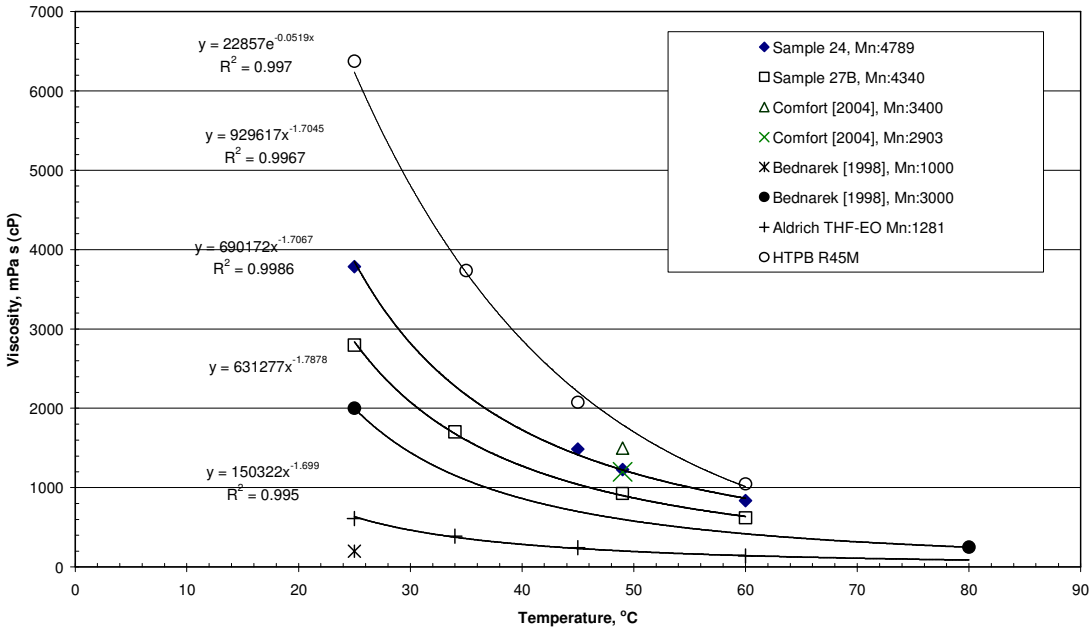

Figure 38. Viscosity versus temperature for different samples of EO/THF copolymer and HTPB

It can be seen that the trend is for viscosity to decrease when temperature increases with a similar pattern for all molecular weight samples. Also it can be observed that the viscosity value for each sample, independently of its molecular weight, tends to be very close to each other at temperatures above 60°C.

Although there is not much viscosity data from other researchers, the result presented by Bednarek [1998] follows the same trend of the HTPE samples. However, the information presented by Comfort [2004] shows a difference in Mn for the same viscosity (Mn = 3400 and 2903). Both Comfort samples have a higher viscosity and a lower Mn value than sample 24 (Mn = 4789).

The relation between viscosity and number average molecular weight, Mn is presented in Figure 39. It can be seen that as the molecular weight increases, the viscosity increases, following an exponential trend. This indicates that viscosity is mainly a function of molecular weight.

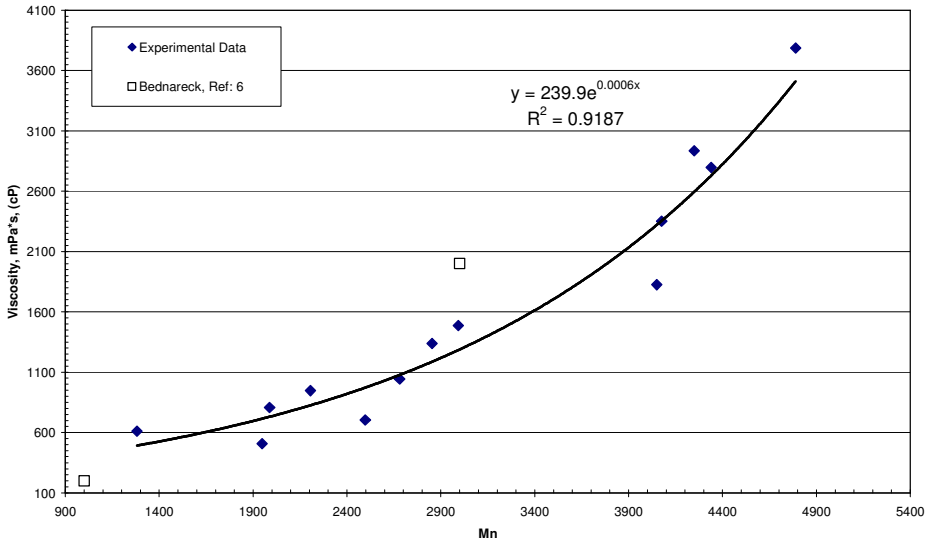

Figure 39. Viscosity at 25°C versus Mn for different samples of EO/THF copolymer

2.4.10 Hydroxyl content analysis

From the hydroxyl content presented in Table 45, the hydroxyl number was calculated. According to the British Standard [2001], the hydroxyl number is the number of milligrams of potassium hydroxide equivalent to the hydroxyl content of 1g of a test portion. Also, functionality "***f***" was obtained as the product of the number average molecular weight Mn, obtained by size exclusion chromatography and presented in Table 34, and the hydroxyl content presented in Table 45. Equivalent weight is the reciprocal of the hydroxyl content but in grams per equivalent. These results are presented in Table 48.

Table 48. Hydroxyl Properties for Experiments 7D, 23, 24, 25A, 26E3 and 27B

Sample	Hydroxyl content (meq g^{-1})	Hydroxyl number (mgKOH g^{-1})	*f*	Equivalent weight (g eq^{-1})
HTPB R45M*	0.720	40.392	2.088	1388
E7d	0.872	48.927	1.730	1146
E23	0.600	33.648	2.590	1667
E24	0.535	30.022	2.563	1868
E25A	0.625	35.044	2.654	1600
E26E3	0.651	36.543	2.562	1535
E27B	0.615	34.475	2.667	1627

*Data from Elf Atochem [1996]

As can be seen from Table 48 the different HTPE pre-polymers have a functionality of around 2.5 with the exception of sample 7D. When comparing HTPE with HTPB it can be seen that the functionality of HTPB is lower than that of the HTPE pre-polymer.

2.4.11 Thermal decomposition analysis

DSC and TGA analysis were performed on two samples of HTPE copolymer and one of HTPB. HTPE samples were from Experiments 9 and 13, having a Mn of 1988 and 2680 and a THF/EO ratio of 1.08 and 0.84 respectively. Figure 40 and Figure 41 show the integrated thermograms for each sample.

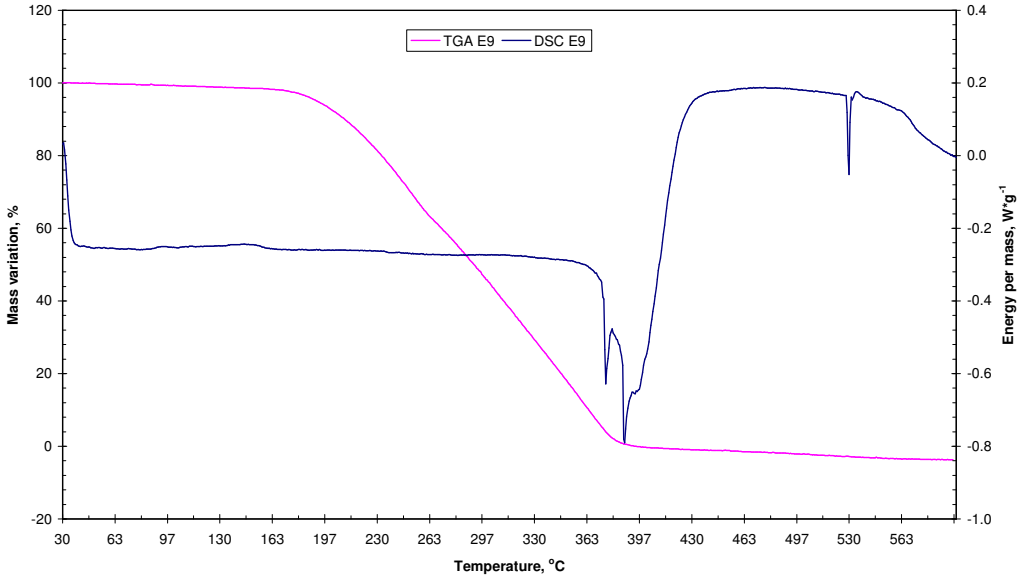

Figure 40. DSC and TGA results for HTPE copolymer from E9

From the DSC thermogram, it can be seen that before the onset of decomposition no exothermic or endothermic reactions occur. However when the remaining mass is around 17% for E9 and 29% for E13, an endothermic peak can be seen. According to Tingfa [1989], who performed thermal analysis on HTPB samples, this endothermic peak corresponds to the decomposition of the residual polymer. The endothermicity was calculated by extending the baseline just before the DSC onset commenced and was for both cases similar, i.e. 66.7Jg^{-1}. Two relevant endothermic peaks appeared at this stage, the first one at 4.7 and 15% and the second peak at 0.4 and 5% of the remaining mass

for E9 and E13 respectively. The shapes and intensities of these peaks are different in both cases. They are possibly related to the structure of the copolymer, as they can also be observed at the melting point. However since no further analysis has been done no firm conclusions can be drawn.

The TGA traces indicate, in both cases, a constant rate of weight loss, with an onset around 169˚C for E9 and at 174˚C for E13. This is an indication of copolymer decomposition, possibly a depolymerisation. The temperature gradient for E13 is slightly lower than for E9. The offset temperatures are around 410˚C and 393˚C and the ΔT values are 236 and 224˚C respectively.

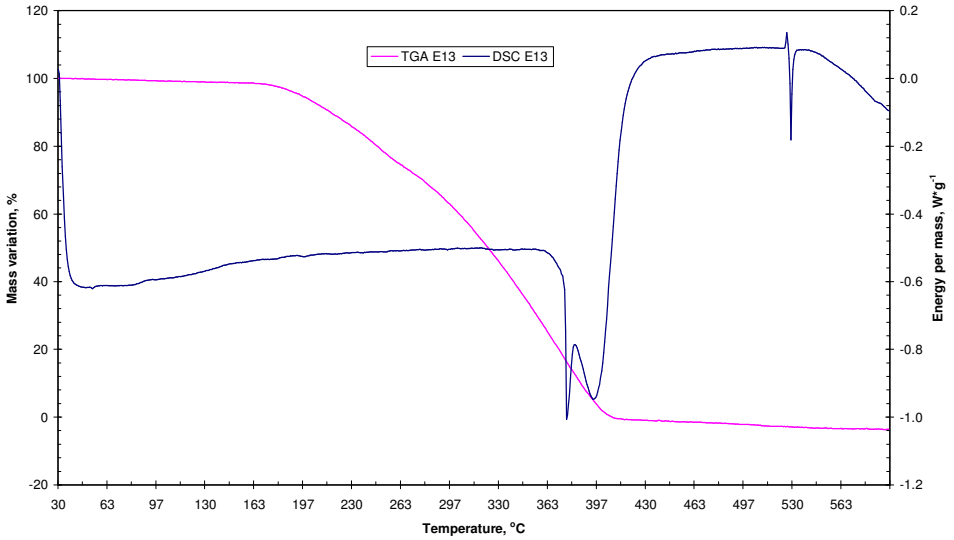

Figure 41. DSC and TGA results for HTPE copolymer from E13

When the thermal behaviour of HTPE copolymers is compared with that of HTPB, two relevant differences can be appreciated from TGA analysis: the onset decomposition temperature and the curve gradient, as can be seen from Figure 42. First, the onset decomposition temperature is considerably lower for HTPE copolymers than for HTPB, there being a ΔT between onsets of around 146˚C. Secondly, the curve gradient for HTPB shows a different rate of weight loss, which is consistent with that stated by Tingfa [1989]. In fact while three stages around 377, 423 and 446˚C can be observed in the HTPB TGA thermogram, HTPE samples shows only one relatively smooth rate of weight loss.

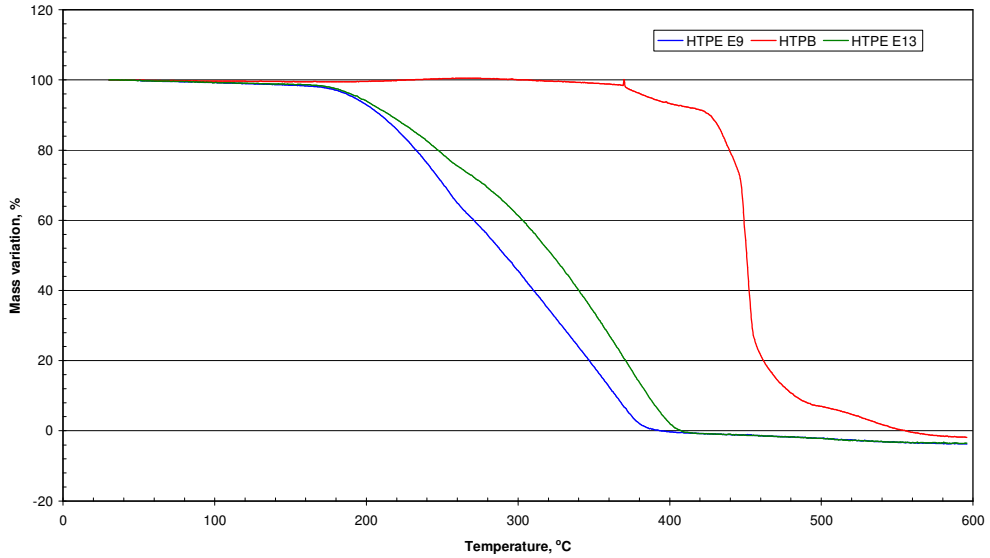

Figure 42. TGA results for HTPE copolymers and HTPB

From the DSC thermogram in Figure 43 it can be seen that, despite the difference in the decomposition peak temperatures, the main difference in behaviour is the exothermic peak present in the HTPB polymer at 377˚C. In fact according to Tingfa [1989] and Gupta [1989], this first stage in the decomposition of HTPB corresponds to the exothermic reaction due to primarily depolymerisation, new bond generation by cyclization and crosslinking of material that has not undergone depolymerisation. The endothermic peak observed in all cases at around 530˚C is thought be to due to the DSC equipment.

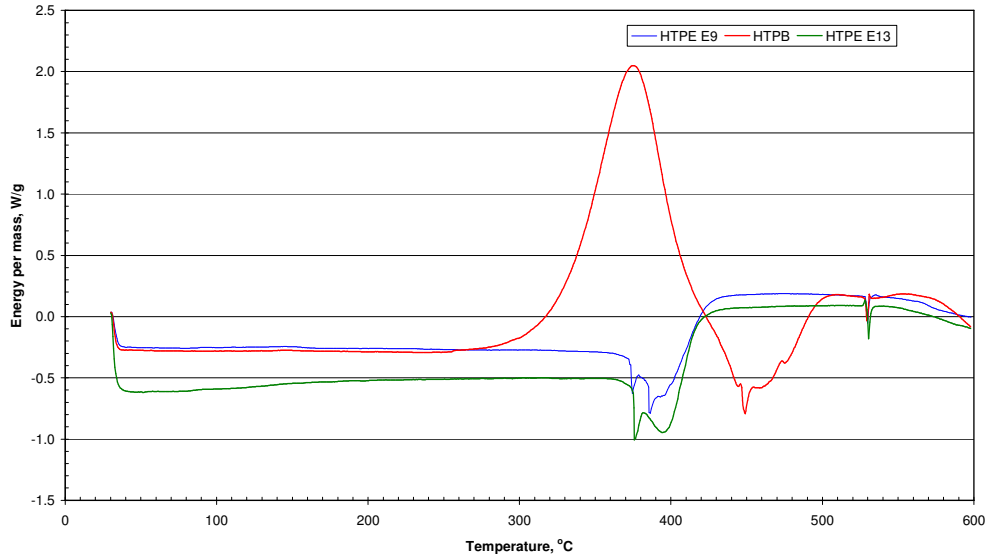

Figure 43. DSC results from HTPE copolymers and HTPB

The exothermicity of HTPB was calculated in the same way i.e. by extending the baseline just before the DSC onset commenced. A value of 68.2 J $g^{-1}$was found, which is similar though slightly higher than that of the HTPE samples, which gave 66.7 J g^{-1}.

2.5 Conclusions

Since it was not possible to obtain HTPE copolymer samples from the chemical industry, a synthesis method to produce the material was designed and implemented. Several samples having different molecular weights and THF/EO ratios were produced and characterised. The small amount of cyclic oligomers found in the HTPE copolymer is an indication that the applied experimental procedure has enabled a product with only a small percentage of undesirable components to be obtained. It is believed that the generation of hydrofluoric acid was catalysing the copolymerisation reaction between THF and EO when the concentration of EO oxonium ion in the solution is high. It was found that by increasing the process temperature and reducing the proportion of protic acid, that undesirable reaction could be controlled.

It was observed that the lower the percentage of ethylene glycol used in the reaction, the higher the molecular weight in the final copolymer. It was observed that a 3 weight % of EG related to THF is a suitable proportion to obtain a copolymer molecular weight between 3000 to 4000 g mol^{-1} when a synthesis temperature of -20^{o}C was used. The characterisation of the HTPE copolymers was carried out using a range of techniques in order to identify the properties and characteristics of different pre-polymer materials. A comparison was then made between the various HTPE copolymers. The comparisons suggest that there are slight differences in thermal decomposition behaviour. However, further differences in the thermal properties such as glass transition temperature and melting point as a function of the molecular weight and microstructure were observed.

A comparison between the synthesised HTPE copolymer and a sample of HTPB R45M pre-polymer supplied by Roxel was also carried out. The comparisons suggest that there are differences in thermal decomposition behaviour and thermal properties.

III. HTPE BINDER NETWORK AND GUMSTOCK MANUFACTURE AND CHARACTERISATION

3.1 Introduction

It was stated in Chapter I, that Hydroxy Terminated PolyEther (HTPE) propellants belong to the polyurethane group of rocket propellants. Polyurethane binders are formed by the reaction of hydroxyl groups in a molecule with isocyanates, a chemical reaction known as crosslinking giving a rubbery matrix, as shown in Equation 1.1

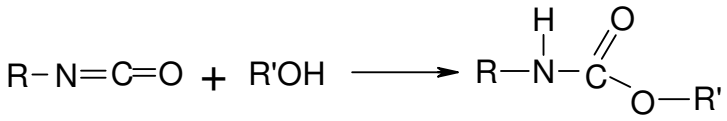

(1.1)

The matrix keeps oxidizer, fuel and other solid or liquid component dispersed and may or may not contain nitrated ester plasticizers. The resulting product of only curing agent and binder is known as the network or binder network. In polyurethanes, the network is composed of two distinct phases, normally called hard and soft segments. The curing agent defines the hard segment and it is characterized by a relative high melting point. On the other hand, the pre-polymer fixes the soft segment, which influences the elasticity, the mechanical properties (especially at low temperatures) and the chemical behaviour of the final product, [Groll, 1991].

Davenas [1993] reported that the molecular structure of the isocyanate will have an influence on the polymerisation kinetics. He reported that more reactive isocyanates, such as an aromatic based isocyanate, i.e. DDI or TDI, are the most suitable to react with polymers containing secondary hydroxyl groups. On the other hand, aliphatic or cycloaliphatic isocyanates, i.e. IPDI, are preferable to react with polymers containing primary hydroxyl groups because these isocyanates are less reactive. Steyn [1998], highlight that polyfunctional isocyanates such as Desmodur N-100, that are trifunctional, do not need a cross linking agent to form a suitable network, as is the case for IPDI or DDI. Also Steyn [1998] suggested that because of the molecular structure, IPDI is more rigid than DDI and polyfunctional isocyanates.

The crosslink density of a binder as well as the molecular mass between two links, are essential characteristics of the binder network to establish its mechanical properties [Davenas, 1993]. The number of isocyanate compared to hydroxyl groups, known as the NCO/OH ratio, determines the crosslink density and this in turn determines the mechanical properties such as strength, strain, modulus and hardness [Serkan, 1997]. In fact, according to Gupta [2003], an optimised hard segment concentration is required to get maximum tensile strength. However, according to Luo [2003], not only crosslink density affects the mechanical properties; they suggest that different network structures have different mechanical properties. NCO/OH ratio figures for rocket propellants are frequently between 0.7 and 1.3. It was reported by Davenas [1993] that beyond a ratio of 0.94, maximum strain and stress increase, which is general behaviour in this kind of mixtures.

Meulenbrugge [1998] stated that when an excess of isocyanate is used a side reaction can create allophanates, affecting the crosslinking between chains. Also impurities such as water and/or acids, can easily react with isocyanates and affect the calculated crosslinking ratio.

According to the literature [Chan 2000, Comfort 2000, Davenas 1993, Desai 2000, Desilets 2000, Eroglu 1998, Gupta 2003, Jain 1993, Serkan 1993 and Steyn 1998], some of the following curing agents are the most used in propellant manufacture, either alone or in a mix: Isophorone diisocyanate (IPDI), Dimeryl diisocyanate (DDI), Hexamethylene diisocyanate (HMDI), 2,4-Toluene diisocyanate (TDI) and poly hexamethylene-1,6-diisocyanate an aliphatic biuret polyisocyanate of trade name Desmodur N-100.

Despite the Roxel [Sloan 2004] recommendation to use pluriyisocyanate Desmodur N-100 as a curing agent, two other curing agents were initially chosen to study their interaction with HTPE pre-polymer samples. One would then be selected to be used during network and propellant manufacture. These two additional curing agents were pluriyisocyanate Desmodur N-3200 and Isophorone Diisocyanate (IPDI).

Desmodur N-100 and N-3200 are biuret polyisocyanates and they were supplied by Bayer. According to Mohring [1978], due to the synthesis process, biuret polyisocyanates are a mixture of mono, bis, tris and tetra-biuret. Therefore, apparently Desmodur N-100 and N-3200 differ only in the percentage of the ingredient. However, the ideal molecular structure for these curing agents (assuming a tri functional structure) and of IPDI is presented in Figure 44 and Figure 45 and their main characteristics are presented in Table 49.

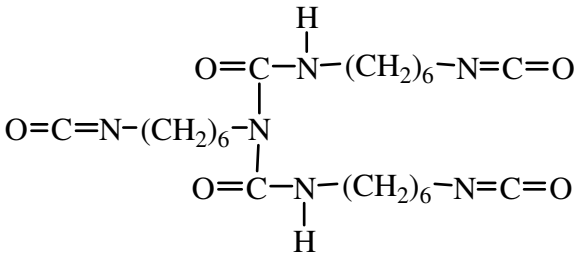

Figure 44. Ideal molecular structure of Desmodur N-100 and Desmodur N-3200, [Steyn, 1998]

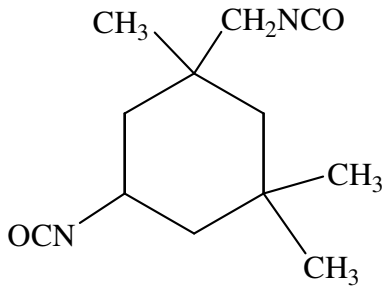

Figure 45. Molecular structure of IPDI

Table 49. Curing Agent Main Characteristics

Characteristic	Units	N-100*	IPDI	N-3200**
Viscosity at 25 ^{o}C	mPa s	8000	15 (at 23^{o}C)	2100
Equivalent weight	g mol^{-1}	191.0	111.1	183.0
Density at 20 ^{o}C	g cm^{3}	1.14	1.06	1.13
Flash Point	^{o}C	181	155	170
NCO content	%	22.0±0.3	37.8	23.0±0.5

*Bayer [2004], **Bayer [2001]

3.2 Manufacture of Binder Network and Gumstock

Hydroxy terminated copolyether (HTPE) binder networks were manufactured by polycondensation of HTPE pre-polymer and a curing agent. The reaction was carried

out at a temperature between 55 and 65°C, in a closed round-bottom flask and under a vacuum environment to avoid the presence of air and moisture that can produce bubbles in the binder network. Once the mixing of the components was finished, the flask contents were poured into a PTFE mould and the mould was placed into an oven for six days at a temperature of 65°C, to allow it to cure.

When samples were made only from the mixture of a pre-polymer and the curing agent, with or without a catalyst, they were called binder network, or gumstock when a plasticizer, either energetic or inert, was added to the formulation. For the purposes of nomenclature they were indicated in order of manufacture and with the name of the HTPE pre-polymer sample used for the manufacture. A letter N or G was used if they were called binder network or gumstock respectively, i.e. 1N27B or 1G27B.

3.2.1 Equipment and reagents

HTPE binder network and gumstock samples preparations were carried out in a fume cupboard using the equipment configuration shown in Figure 46. Once the mixture between the HTPE sample and the curing agent was homogeneous, it was poured into the mould shown in Figure 47 and then placed into a curing oven and cured at 60°C for seven days.

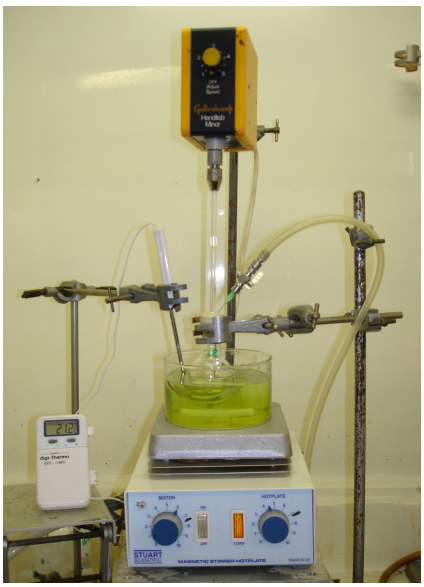

Figure 46. Chemical reactor for HTPE binder network and gumstock manufacture

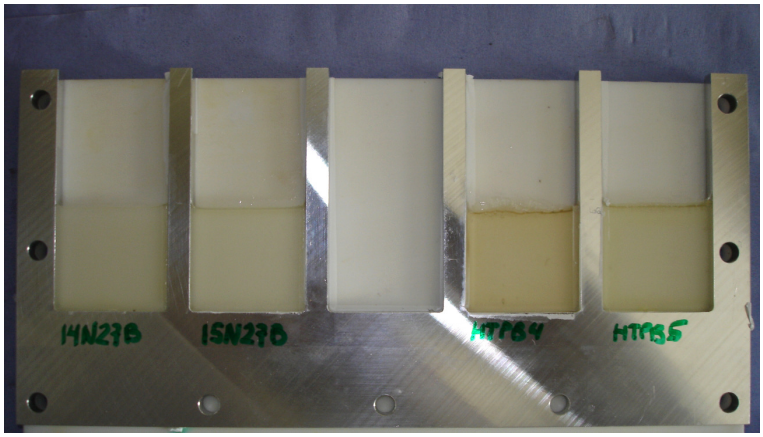

Figure 47. Curing mould for HTPE network manufacture

The HTPE pre-polymers and curing agents used for the network manufacture and their main characteristics are shown in Table 50.

Table 50. Reagents Used in HTPE and HTPB Binder Network and Gumstock Manufacture

Reagent	Name	Company	Characteristics	Equivalent weight g eq^{-1}	Molecular Weight g mol^{-1}
HTPE	E23	Synthesized in this work	Pre-polymer	1667	4318
HTPE	E24	Synthesized in this work	Pre-polymer	1868	4789
HTPE	E25	Synthesized in this work	Pre-polymer	1600	4249
HTPE	E26E3	Synthesized in this work	Pre-polymer	1535	4076
HTPE	E27B	Synthesized in this work	Pre-polymer	1627	4340
HTPB	R45M	Supplied by Roxel UK	Pre-polymer	3497	2900
Curing agent	Desmodur N-100	Bayer	Polyisocyanate	191	-.-
Curing agent	Isophorone Diisocyanate	Supplied by Roxel UK	Diisocyanate	111	222.11
Curing Agent	Desmodur N-3200	Bayer	Polyisocyanate	183	-.-
Catalyst	Dibutylil Dilaurate (DBTDL)	Sigma Aldrich	Slightly yellow liquid	-.-	631.56
Catalyst	Triphenyl Bismuth (TPB)	Roxel	White powder	-.-	440.29
Stabilizer	Nitro Diphenyl Amine (2-NDPA)	Aldrich	Orange crystal	-.-	214.22
Energetic Plasticizer	n-butyl-2-nitratoethylnitramine (n-BuNENA)	Synthesized in this work	Slightly yellow liquid	-.-	207.18
Inert Plasticizer	Diisooctyl sebacate (DOS)	Supplied by Roxel UK	Transparent liquid	-.-	426.67

3.2.2 Curing agent calculation

Different isocyanates, as stated before, were chosen as curing agents for manufacturing the binder network and gumstock. As the mechanical properties of the propellant are a function of the cross-linking level [Eroglu, 1998], different theoretical NCO/OH

reactive group ratios were initially chosen to be: 1.0, 0.9, 0.8 and 0.7 for sample preparation. However, because of the small size of the samples that were prepared, as can be seen from Table 51 and Table 52, the NCO/OH ratio was recalculated according to the real mass of the added isocyanate.

In order to have a theoretical NCO/OH reactive group ratio, i.e. 1.0, 0.9, 0.8 or 0.7, the pre-polymer sample percentage related to the isocyanate was calculated by using the equivalent weight of the pre-polymer sample ($OH_{eqweight}$) and curing agent ($NCO_{eqweight}$) according to the following expression [Catton, 2005]:

$$\text{HTPE Sample } \% = \frac{OH_{eqweight}}{\left(OH_{eqweight} + NCO_{eqweight} * \left(\frac{NCO}{OH} \right)_{ratio} \right)} \qquad (3.1)$$

Where the equivalent weight corresponds to the reciprocal OH content number in equivalents per gram. The equivalent weight [g eq^{-1}] is the amount in grams of product needed to have one equivalent of reactive groups.

3.2.3 Binder network manufacture

In order to prepare the binder network specimens, HTPE samples were weighed into a round-bottom 50 cm^3 flask or into a 20 cm^3 vial. Either the vial or the flask were evacuated by using a 100 cm^3 syringe and then placed into an oven and preheated for 1 h at a temperature of 65°C. After preheating the round-bottom flask or the vial containing the HTPE sample, the curing agent was added and the flask was placed into a heated oil bath and stirred manually using a spatula for 15 min until a homogeneous mixture was reached. For samples 16N27B onwards the manufacture method was improved in order to produce all the samples from a similar manufacture method. In order to do that, samples were stirred mechanically for a period of 10 min at a temperature of 65°C using a glass blade coupled to an electrical stirrer as shown in Figure 46. After 10 min the mixture was degassed and placed into the oven. After no bubbles were seen in the bulk, the samples were poured into a previously heated mould.

Different kinds of mould were used, some of them were just small vials, others formed a flat film having a thickness of 6.00mm (Figure 47) or 0.86mm. The moulds were placed again into the oven at 65°C for 7 days to allow the curing process.

Table 51 presents the formulation matrix for the preparation of several samples of binder network, prepared by using HTPE and HTPB pre-polymers.

Table 51. HTPE and HTPB Binder Network Formulation Matrix

Binder network sample	NCO/OH ratio	HTPE sample 24 (g)	HTPE sample 25 (g)	HTPE sample 27 (g)	HTPB (g)	N-100 (g)	IPDI (g)	N-3200 (g)	TPB mg (%w)	DBTDL mg, (%w)
1N24	1.031	18.15	-.-	-.-	-.-	1.91	-.-	-.-	-.-	-.-
2N24	0.790	18.67	-.-	-.-	-.-	1.50	-.-	-.-	-.-	-.-
3N24	1.606	6.71	-.-	-.-	-.-	1.10	-.-	-.-	-.-	One drop
4N24	1.117	7.08	-.-	-.-	-.-	-.-	0.47	-.-	-.-	-.-
5N24	1.141	7.08	-.-	-.-	-.-	-.-	0.48	-.-	-.-	One drop
6N25A	1.050	-.-	4.47	-.-	-.-	0.53	-.-	-.-	-.-	14 (0.278)
7N25A	1.013	-.-	4.49	-.-	-.-	-.-	-.-	0.51	-.-	15.5 (0.308)
8N25A	1.600	-.-	4.5	-.-	-.-	-.-	0.5	-.-	-.-	11.8 (0.235)
9N25A	1.100	-.-	4.58	-.-	-.-	0.18	0.24	-.-	-.-	11.1 (0.222)
10N25A	1.000	-.-	4.49	-.-	-.-	-.-	-.-	0.51	-.-	-.-
11N25A	0.800	-.-	4.61	-.-	-.-	0.44	-.-	-.-	-.-	2.13
12N25A	1.000	-.-	4.47	-.-	-.-	0.53	-.-	-.-	1.5 (0.03)	-.-
13N25A	1.000	-.-	4.49	-.-	-.-	-.-	-.-	0.51	1.5 (0.03)	-.-
14N27B	1.037	-.-	-.-	8.95	-.-	1.09	-.-	-.-	3 (0.03)	-.-
15N27B	1.013	-.-	-.-	8.99	-.-	-.-	-.-	1.03	3 (0.03)	-.-
16N27B	1.002	-.-	-.-	17.977	-.-	-.-	-.-	2.027	6 (0.03)	-.-
17N27B	0.900	-.-	-.-	18.161	-.-	-.-	-.-	1.840	8 (0.03)	-.-
18N27B	0.803	-.-	-.-	18.348	-.-	-.-	-.-	1.658	7 (0.03)	-.-
19N27B	0.702	-.-	-.-	18.536	-.-	-.-	-.-	1.465	6 (0.03)	-.-
20N27B	0.744	-.-	-.-	18.540	-.-	-.-	-.-	1.552	6 (0.03)	-.-
Aldrich THF/EO 1	1.000	-.-	17.15	-.-	-.-	2.85	-.-	-.-	-.-	10.8 (0.054)
Aldrich THF/EO 2	1.000	-.-	51.44	-.-	-.-	8.56	-.-	-.-	-.-	14.4 (0.024)
1NHTPB	1.013	-.-	-.-	-.-	21.98	3.06	-.-	-.-	-.-	-.-
2NHTPB	0.740	-.-	-.-	-.-	22.81	2.32	-.-	-.-	-.-	-.-
3NHTPB	1.000	-.-	-.-	-.-	13.25	-.-	-.-	1.76	-.-	One drop
4NHTPB	0.996	-.-	-.-	-.-	8.84	-.-	-.-	1.16	3 (0.03)	-.-
5NHTPB	1.005	-.-	-.-	-.-	8.79	1.21	-.-		3 (0.03)	-.-
6NHTPB	0.865	-.-	-.-	-.-	10.801	-.-	-.-	1.231	-.-	-.-

3.2.4 Gumstock manufacture method

The manufacture method was similar to the one referred to at the end Section 3.2.3, but was modified by the fact that new components were incorporated into the formulation: n-BuNENA and 2-NDPA. Initially the energetic plasticizer n-BuNENA was weighed into the flask, then 2-NDPA was added. To dissolve the stabiliser crystals the sample was heated for 20 min at 60°C. After that, when all the 2-NDPA was dissolved, the HTPE pre-polymer and the catalyst TPB were incorporated into the flask and then

stirred manually until all the TPB was dissolved. After that, the flask was degassed and heated for 20 min at a temperature of 60°C. When no more bubbles were observed the curing agent was added and the samples were stirred mechanically for a period of 10 min at a temperature of 65°C. As for the binder network samples preparation, a glass blade coupled to an electrical stirrer was used. After that the samples were degassed again for a period of 20 to 50 min in the oven, then poured into the moulds and cured for seven days in a vacuum oven at 65°C. Vacuum was maintained for the first 4 h in order to avoid the presence of bubbles in the cured samples. After 4 h, the pressure was increased up to ambient by injecting nitrogen.

Table 52 presents the formulation matrix for the preparation of several samples of gumstock, prepared by using HTPE and HTPB pre-polymers.

Table 52. HTPE and HTPB Gumstock Formulation Matrix

Gumstock sample	NCO/OH ratio	HTPE sample 26 g	HTPE sample 27 g	HTPB R45M g	IPDI g	N-3200 g	n-BuNENA g	2-NDPA g	DOS g	TPB mg (%w)
1G26E	0.850	10.378	-.-	-.-	-.-	1.036	8.007	0.498	-.-	0.049
2G26E	1.270	10.019	-.-	-.-	-.-	1.520	8.004	0.297	-.-	0.050
3G27B	1.000	-.-	10.502	-.-	-.-	1.180	8.017	0.300	-.-	0.050
4G27B	1.001	-.-	10.500	-.-	-.-	1.185	8.025	0.300	-.-	0.050
5G27B	0.877	-.-	10.833	-.-	-.-	1.069	8.053	0.081	-.-	0.030
1GHTPB	0.850	-.-	-.-	11.512	0.780	-.-	-.-	-.-	3.530	-.-
3GHTPB	0.856	-.-	-.-	10.801	-.-	1.218	-.-	-.-	3.497	-.-

3.2.5 HTPE binder network manufacture, discussion of results

3.2.5.1 Binder network samples: HTPE 1N and 2N and HTPB 1N and 2N

Figure 48 shows HTPB and HTPE samples prepared using Desmodur N-100 as curing agent. A curing catalyst was not used in these samples. The samples were placed in the oven and cured during seven days. However, although sample 1NHTPB (A) was completely cured after seven days, samples 2NHTPB (B), HTPE 1N24A (C) and 2N24A (D) required twelve days. From Figure 48 it can be seen that there are regions of light yellow colour in almost all the samples and they are located at the top, at one lateral wall and at the bottom of the mould. This effect is more noticeable in HTPB rather in HTPE samples. In samples B, C and D, the top surface of the samples was still like gel and very sticky, especially sample D, which looks more like liquid than gel. On

the other hand, samples C and D had some thin and long lines at the interface between network and mould where the sample was not solid, being an indication that the HTPE was not cured at that stage. Samples B, C and D were relatively homogeneous, however the bottom part of those samples looks harder than the rest, possibly because of the curing agent migration. In fact, the colour of the Desmodur N-100 is light yellow.

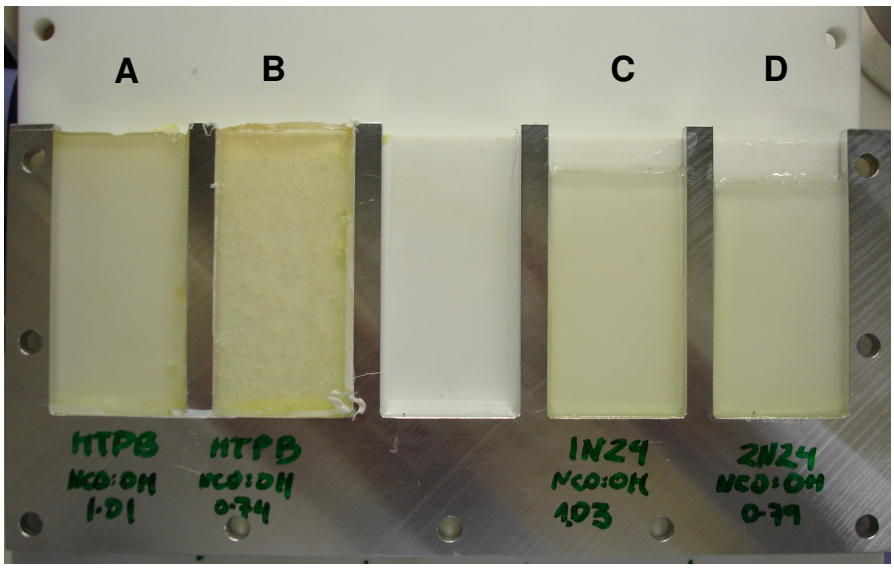

Figure 48. Cured network samples, (A) 1NHTPB NCO/OH 1.013, (B) 2BHTPB NCO/OH 0.74, (C) HTPE 1N24A and (D) HTPE 2N24A

A different behaviour in terms of colour was noticed when curing the samples either with Desmodur N-100, N-3200 or with IPDI. When Desmodur N-100 and N-3200 were added to the pre-polymer, i.e. HTPE or HTPB, the colour turned to white and remained in that way during the whole process. However, when IPDI was added to the HTPE sample, there was no change in colour and the sample remained completely transparent yellow during the whole curing process.

3.2.5.2 Binder network samples: HTPE 3N to 9N

In order to improve the curing process, it was decided to add a curing catalyst. Dibutyltin dilaurate (DBTDL) was used as catalyst together with the curing agents Desmodur N-100, N-3200 or IPDI.

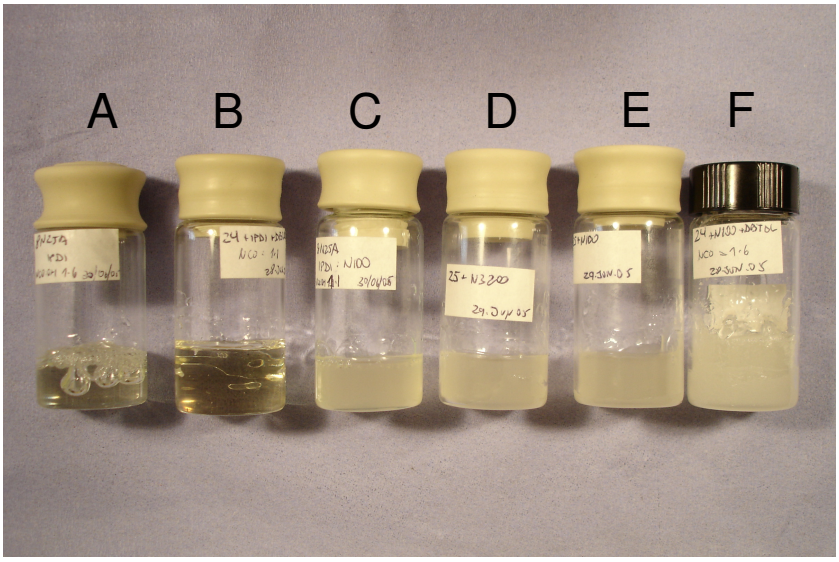

Figure 49. Cured network samples, A: 8N25A; B: 5N24; C: 9N25A; D: 7N25A; E: 6N25A; F: 3N24

Figure 49 shows HTPE samples cured with different curing agents and using DBTDL. When DBTDL was added to sample 3N24 (F), containing N-100 and having a NCO/OH ratio of 1.6, the binder network was hard before reaching 20 min. The same happened with sample 6N25A (E) containing N-100 and with sample 7N25A (D) containing N-3200, with an NCO/OH ratio of 1.050 and 1.013 respectively. Due to the slightly higher number of bubbles trapped in the binder network containing N-3200, it is possible that it is more reactive than the one containing N-100, when DBTDL is used as catalyst. On the other hand when DBTDL was added to sample 5N24A (B) containing IPDI in a NCO/OH ratio of 1.14, it took several hours before becoming solid and cured. Although as expected, it was softer than samples prepared from Desmodur N-100, presumably due to IPDI being a diisocyanate from which only linear chains of hard and soft segments are created instead of a net.

The three samples 4N25A, 5N25A and 8N25A containing IPDI as curing agent were transparent after mixing and curing. On the other hand, sample 9N25A (Figure 49 C), containing a curing agent mix of IPDI and N-100, had a white transparent colour as in all samples containing any kind of Desmodur. However, this sample was more transparent than the others. After the curing agent addition in samples 8N25A and

9N25A, the samples were evacuated and placed in the oven at a temperature of 65°C for 30 min. After this period of time they were without bubbles and one drop of DBTDL was added to each sample. After mixing, the reaction vial was sealed and the sample evacuated and placed in the oven again. 20 min later, sample 9N25A was solid with several bubbles in the surface, as can be see from Figure 49 A. It can be seen that bubbles were not able to leave the bulk before curing occurred. Due the NCO/OH ratio being lower in sample 8N25A it took longer to be cured i.e. over 40 min, and also because of that only a small amount of bubbles can be seen from Figure 49 C. All samples were very much more reactive in the presence of DBTDL.

3.2.5.3 Binder network samples: Aldrich THF/EO 1 and 2 and HTPE 10N25A and 11N25A

In order to try to increase the pot life of the binder network, a sample of Aldrich THF/EO was cured with N-100 and a reduced amount of catalyst of around 0.05%, as suggested by Chan [2002] and by Goleniewsky [1998], was used. The sample was called Aldrich THF/EO 1. To do that, the size of the sample was increased to 17.15g and the amount of curing agent N-100 to produce a NCO/OH ratio of 1.0 was 2.85g. The amount of DBTDL catalyst was equivalent to 0.054% of the pre-polymer weight. The ingredients were mixed as previously stated and 25 min (at ambient temperature) after the catalyst was added the sample surface was relatively dry and non-sticky but still very soft, being an indication that the pot-life was finished. After that the sample was placed in the oven and left there for 24 h to complete the curing cycle.

Because the pot life was not increased substantially, a new sample: Aldrich THF/EO 2 was cured with Desmodur N-100 and the amount of catalyst reduced to around 0.023%. To have a better control of the small amount of catalyst that should be added to the bulk, the pre-polymer amount was increased to 51.44g and the amount of curing agent Desmodur N-100 to 8.56g to produce a NCO/OH ratio of 1.0. The ingredients were mixed as previously stated and after 20 min the catalyst was added and the bulk stirred for 10 min until it was homogeneous. After that the sample was poured into four vials labelled A, B, C and D. After 4 h the samples were solid and with some bubbles in the binder network bulk.

Because it was observed that Desmodur N-3200 is more reactive than Desmodur N-100 when DBTDL is added to the sample, it was decided to test Desmodur N-3200 with HTPE pre-polymers but with a smaller proportion of DBTDL. This sample was called 10N25A. Because a 2μL syringe was used to try to introduce a smaller amount of catalyst into the bulk, and due to the density of the DBTDL it was not possible to add such a volume, there was no control over the amount of DBTDL added. However sample 10N25A was solid after 72 h.

Sample 11N25N; NCO/OH 0.8, was cured with Desmodur N-100 as for sample 6N25A; NCO/OH 1.0, but using a smaller amount of DBTDL. Despite the reduction in the amount of DBTDL the pot life was not increased and after 30 min the sample was relatively solid and sticky.

3.2.5.4 Binder network samples: 3NHTPB

Because Desmodur N-3200 was apparently more reactive than Desmodur N-100 when DBTDL was added to the sample, it was decided to test Desmodur N-3200 with HTPB pre-polymers. The sample was called 3NHTPB and was solid after 24 h, presenting a slightly yellow colour at the top of the mould. HTPB pre-polymers are apparently more reactive to Desmodur N-3200 or N-100 in the curing process than HTPE pre-polymers.

3.2.5.5 Binder network samples: HTPE 12N and 13N

Because of the short pot-life and lack of curing control seen for the binder networks when DBTDL is used, it was decided to use a different curing catalyst as suggested by Chan [2005], Triphenyl Bismuth (TPB). Because TPB is a white crystalline solid it allows a better control on the amount to be added to the curing sample, especially when handling small samples. The TPB sample was supplied by Roxel UK. HTPE samples 12N25A and 13N25A were cured using Desmodur N-100 and Desmodur N-3200 respectively. They were maintained for 1 h at ambient temperature (25^{o}C), and later placed in the curing oven at a temperature of 65^{o}C. At the end of the ambient period

both samples were liquid. After 4 h the samples were still liquid, although very viscous. Sample 12N25A was apparently more viscous than sample 13N25A. After 24 h both samples were completely solid. The effect of the TPB on curing time was considered acceptable because the pot life was increased considerably in comparison to when DBTDL was used. A longer pot life allows gases to leave the binder before it is fully cured, avoiding the formation of bubbles.

3.2.5.6 Binder network samples: HTPE 14N to 15N

Because of the better pot life obtained when using TPB, it was decided to use it as curing catalyst for HTPE samples. Samples 14N27B and 15N27B were manufactured using Desmodur N-100 and N-3200 as curing agents and TBP as a catalyst respectively. The specimens produced would be tested for mechanical properties and the information used to choose one curing agent to go ahead with further research. Both formulations were prepared in the same way as before. The samples were cured for 7 days in a vacuum oven at 65^{o}C. Vacuum was mantained during the first 4 h in order to avoid the presence of bubbles in the cured samples. After 4 h the pressure was increased to ambient by injecting nitrogen.

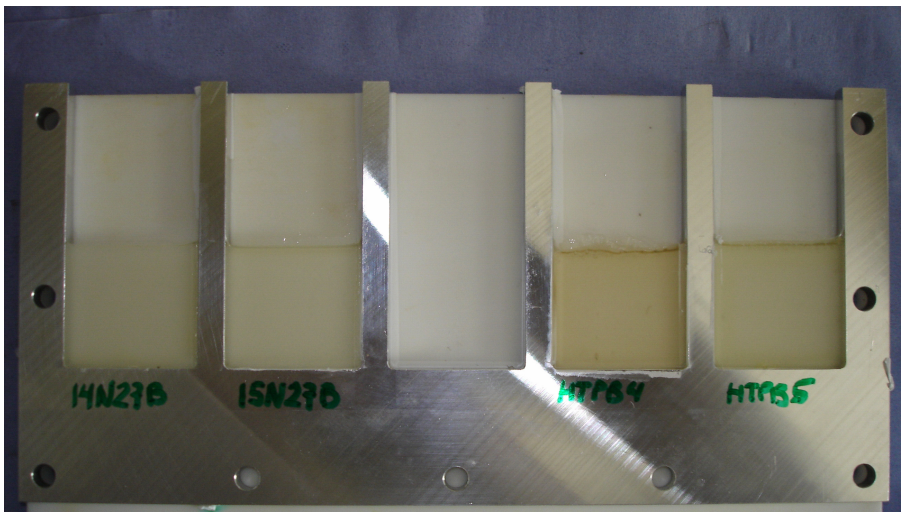

Figure 50. Cured network samples, 14N27B, 15N27B, 4NHTPB and 5NHTPB

Together with HTPE samples, two HTPB samples were processed following the same procedure i.e. 4NHTPB cured with N-3200 and 5NHTPB cured with N-100. The binder

networks obtained were all homogeneous solids, as can be seeing from Figure 50. However, the surface of sample 14N27B, which was cured with N-100, was covered with a thin liquid layer. HTPE samples were without bubbles while some small bubbles can be seen in the propellant made from HTPB, this being an indication that the TPB catalyst works faster in HTPB than in HTPE.

3.2.5.7 Binder network samples: HTPE 16N to 20N and 6NTHPB

Samples 16N27B to 20N27B were manufactured using only Desmodur N-3200 as curing agent and TPB as catalyst. This time the manufacture method was improved and standardised. In order to do that, after all the ingredients, except the curing agent, were added in the flask, the samples were stirred mechanically for a period of 10 min at a temperature of 65^{o}C as before. After the curing agent was added the samples were stirred for a further 5 min. After that, the samples were poured into the moulds and cured for 7 days in a vacuum oven at 65^{o}C. The vacuum was maintained for the first 4 h in order to avoid the presence of bubbles in the cured samples. After 4 h, the pressure was increased to ambient by injecting nitrogen.

Figure 51 shows the HTPE binder network samples 16N27B to 20N27B after seven days in the curing oven in a 6mm thick mould. It can be seen that they look homogeneous and without bubbles, except for one small one in sample 18N27B. However, the binder network samples that were poured into a 0.8mm thick mould produced some bubbles, as can be seen from Figure 52.

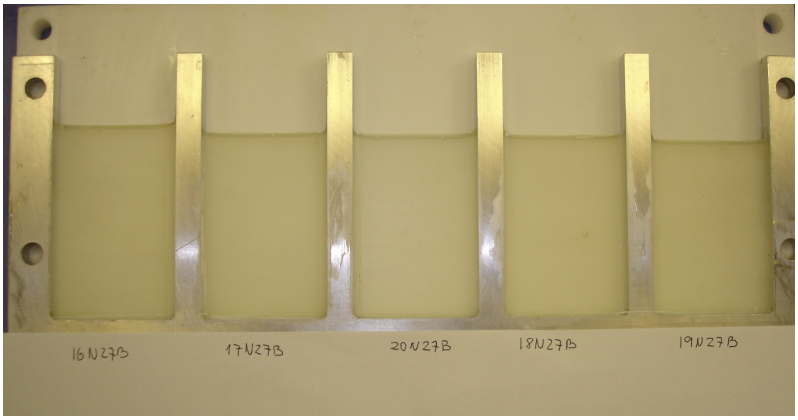

Figure 51. Binder network samples, 16N27B to 20N27B cured in an 8mm thick mould

Sample 6NHTPB was prepared from HTPB R45M and Desmodur N-3200. TPB was not used in order to allow a longer period of time before cross linking. The sample was stirred manually, the ingredients mixed, degassed, poured in moulds and cured in the oven at 65°C. After 6 h in the curing oven the sample was still liquid. However, after 21 h the sample was solid and homogeneous and without bubbles.

Samples HTPE 16N27 to 20N27 were used to characterise and compare binder network samples prepared either using N-100 or N-3200 and samples with the same curing agent but different NCO/OH ratio, as well as to compare the HTPE and HTPB binder network characteristics.

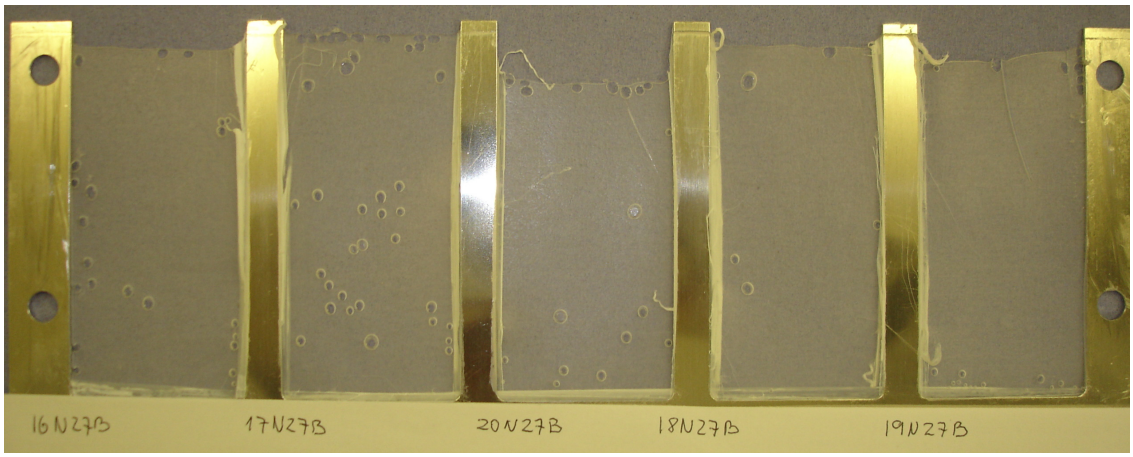

Figure 52. Binder network samples, 16N27B to 20N27B cured in a 0.8mm thick mould

3.2.6 HTPE gumstock, manufacture and discussion of results

Hydroxy terminated copolyether (HTPE) gumstock samples were manufactured in a similar way to the binder network samples. However, two new ingredients were incorporated into the formulation; the energetic plasticizer n-butyl-2-nitratoethylnitramine (n-BuNENA) and the stabilizer 2-Nitrodiphenylamine (2-NDPA). Similarly for HTPB an inert plasticizer, Diisooctyl sebacate (DOS), was incorporated into the formulation. Gumstock manufacture was carried out at a temperature of 65°C, in a closed round-bottom flask and under a nitrogen atmosphere to avoid the presence of air and moisture that can produce bubbles in the binder network. For HTPE gumstock samples, the energetic plasticizer was introduced first into the flask and then the stabiliser 2-NDPA and the flask placed into the hot oil bath. Once all the 2-NDPA

crystal were dissolved in the n-BuNENA the HTPE pre-polymer was added and after that the curing catalyst TPB. The bulk was stirred for 5 min until the sample was homogeneous. Once the mix of the gumstock ingredients was finished, the curing agent Desmodur N-3200 was added to the bulk, stirred for 10 min and then the flask contents were poured into a PTFE mould. The mould was then placed in an oven for 6 days at a temperature of 65^{o}C, to allow curing. Because it was not possible to obtain n-BuNENA commercially, this energetic plasticizer was synthesized in the Department by Dr. A. MacCuish. The n-BuNENA synthesis and characterisation are presented in Appendix H.

3.2.6.1 Gumstock samples: HTPE 1G26E, 2G26E, 3G27B and 4G27B

Sample 1GN26E was manufactured using a NCO/OH ratio of 0.85 and was done mainly to observe the processability differences in comparison with the binder network samples that did not incorporate n-BuNENA and 2-NDPA. The main difference was that the 2-NDPA crystals had to be dissolved by applying heat and stirring. That process took a couple of minutes until all 2-NDPA crystals were completely dissolved. In terms of pot life, gumstock sample 1G26E was still liquid 6 h after the mould was placed in the oven but after 24 h the sample was solid. After the curing process, when samples were taken out of the oven, some bubbles were observed in the gumstock bulk.

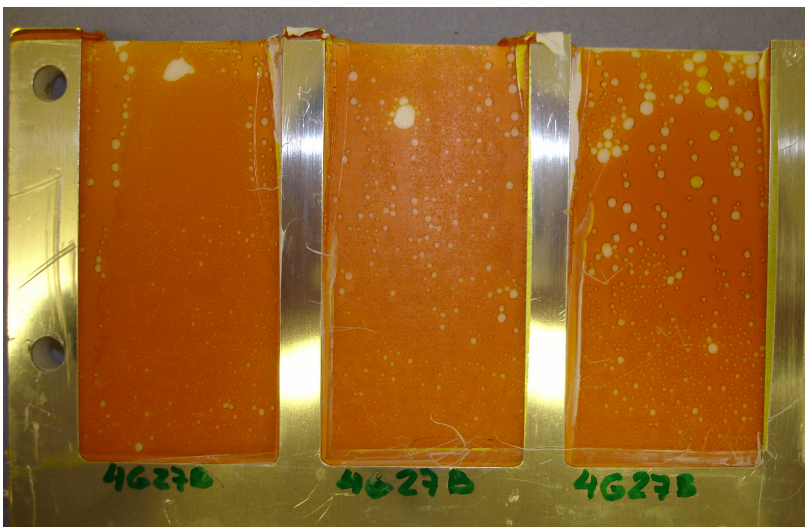

Figure 53. Cured gumstock sample 4G27B

Because the sample was injected into a thin mould by a syringe, it was thought that air was introduced by this process and was trapped there, not having enough time to be extracted before the sample was cured. Samples 2GN6E, 3G27B and 4G27B were manufactured using a higher NCO/OH ratio than gumstock sample 1G26E, i.e. 1.27, 1.0 and 1.0 respectively, and involved applying vacuum after mixing the ingredients, before pouring the gumstock into the mould and during the curing process in the oven. The samples were still liquid 6 h after the mould was placed in the oven but after 24 h the sample was solid. However, despite this the cured gumstock at the end of curing showed a considerably number of bubbles when the thin mould was used, as can be seen from Figure 53. Because of the gas generation and its effect on the gumstock, combinations of ingredients were tested separately to try to isolate the source of the bubbles.

3.2.6.2 Gumstock samples and gas generation during curing process

As stated in the previous sections, during the mixing and curing process bubbles appeared in some binder network samples and in all gumstock samples. This behaviour was seen in samples made from HTPE and cured with N-3200 when a 0.8mm thick mould was used. As can be seen from Figure 52, the number of bubbles in each sample appears to be related to the amount of NCO/OH equivalence ratio present in the samples. In fact, samples 16N27B, 17N27B, 18N27B, 19N27B and 20N27B have equivalence ratios of: 1.0, 0.9, 0.8, 0.7, and 0.744 respectively and the number of bubbles per sample appears to increase as the NCO/OH ratio increases.

However the number of bubbles increased dramatically when n-BuNENA and 2-NDPA were incorporated into the formulation as can be seen when comparing gumstock sample 4G27B (NCO/OH 1.0) in Figure 53, with binder network samples presented in Figure 52, especially with samples 16N27B and 17N27B (NCO/OH 1.0 and 0.9 respectively). This suggests the possibility of a parallel reaction between the curing agent and moisture present in the polymer or with the new ingredients. Sample 1G26E3, having an NCO/OH equivalence ratio of 0.85, did not show many bubbles, however sample 2G26E3 and 3G27B, having an NCO/OH equivalence ratio of 1.0, showed a larger number of bubbles.

A matrix with different ingredients combination was drawn up, as presented in Table 53. The ingredients were mixed and observed at different stages during the mixing and curing process.

Table 53. Ingredients Combination Formulation Matrix

Sample	HTPE 27B	n-BuNENA	N-3200	2-NDPA	TPB
1a	1.040	-.-	0.190	-.-	0.004
2b	1.040	0.800	0.184	0.030	0.004
3c	1.016	0.804	0.202	0.008	0.004
4d	1.040	-.-	0.784	0.030	0.004
5e	1.011	0.808	0.202	-.-	0.004

Table 54 shows the observed behaviour of the ingredients during the initial stages of mixing.

Table 54. Ingredients Mixing Reaction Matrix

Ingredients	HTPE	n-BuNENA	N-3200	2-NDPA	IPDI
HTPE	-.-	No bubbles are generated	-.-	bubbles are generated	No bubbles are generated
n-BuNENA	No bubbles are generated	-.-	No bubbles are generated	No bubbles are generated	-.-
N-3200	-.-	No bubbles are generated	-.-	bubbles are generated	-.-
2-NDPA	bubbles are generated	No bubbles are generated	bubbles are generated	-.-	No bubbles are generated
IPDI	-.-	-.-	-.-	No bubbles are generated	-.-

After the ingredients were added to the flask, mixed and then preheated in an oven for 20 min, their reaction was observed and the results presented in Figure 54 to Figure 57.

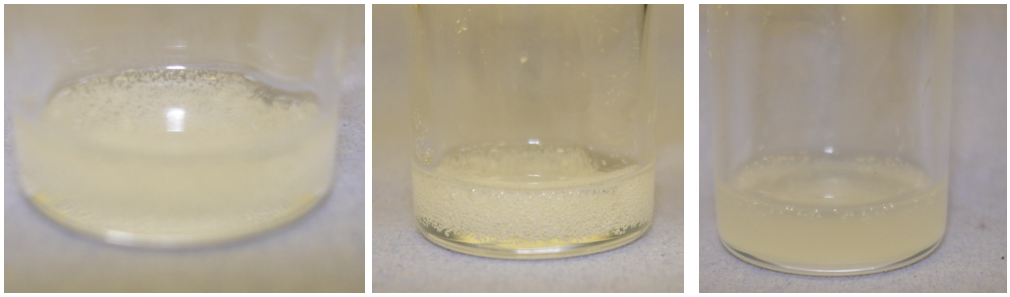

A **B** **C**

Figure 54. HTPE pre-polymer sample 27B: (A, B) stirred alone, (C) after N-3200 addition

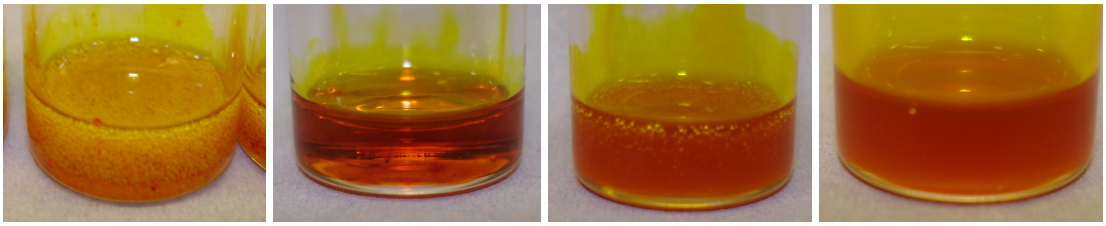

A **B** **C** **D**

Figure 55. HTPE pre-polymer sample 27B+2-NDPA: (A) just stirred, (B) after 5 min, (C) after N-3200 addition, (D) 10 min after N-3200 addition

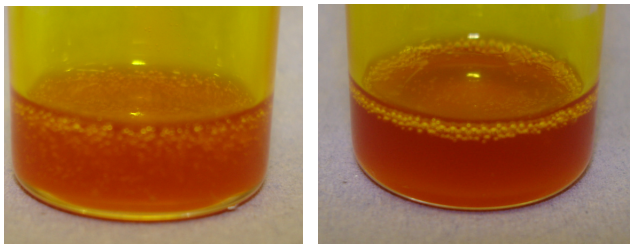

A **B**

Figure 56. HTPE pre-polymer sample 27B+2-NDPA+ N-3200: (A) just after TPB addition, (B) 5 min after addition

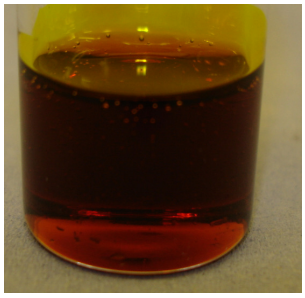

Figure 57. HTPE pre-polymer sample 27B + 2-NDPA and IPDI

As can be seen in Figure 54 to Figure 57, with the exception of the IPDI sample, the higher viscosity of N-3200, in comparison with IPDI, is helping to trap air during stirring. However, after applying heat and vacuum to the samples for some minutes, the bubbles disappear and the samples look like those in Figure 54 C and Figure 55 D.

2-NDPA was mixed with IPDI first and then with HTPE and no bubble generation was observed at either stage. IPDI has a lower viscosity than Desmodur N-3200, which helps to avoid trapping air during mixing. When 2-NDPA was mixed first with N-3200 and then with HTPE, the behaviour was similar to that observed when mixing first with HTPE and then the rest of the ingredients, with bubbles disappearing after some minutes.

When using the 0.8mm thick mould, as presented in Figure 53, it was observed that during the curing process the uncured liquid gumstock was getting out of the mould even when no vacuum was applied to the curing oven, suggesting that some reaction due to the curing process was generating gases that later became trapped in the cured gumstock, as shown in Figure 53. To catalyse the curing reaction in samples 1a to 5e, TPB was added. The samples were mixed, degassed and placed in sealed head space vials in the oven and the observations over time are stated in Table 55.

Table 55. Ingredient Mix Curing information

Date	**10/11/05,**	**11/11/05,**	**12/11/05**	**16/11/05**	**17/11/05**	**18/11/05**	**21/11/05**
Time	**17:00**	**10:00**	**09:00**	**10:00**	**16:00**	**10:00**	**17:30**
Sample 1a				Liquid transparent	Solid transparent, 1 bubble	Solid yellow transparent	Solid yellow transparent
Sample 2b	Liquid, orange transparent colour	Liquid, orange transparent colour	Solid, orange transparent colour				
Sample 3c	Liquid, orange transparent colour	Liquid, orange transparent colour	Solid, orange transparent colour				
Sample 4d	Liquid not really transparent	Liquid not really transparent	Solid not transparent, no bubbles observed	Solid not transparent, no bubbles observed			
Sample 5e				Liquid, orange transparent colour	Solid orange transparent colour 1 bubble	Solid orange transparent colour 1 bubble	Solid orange transparent colour 1 bubble

Few bubbles were created by using a headspace vial as a mould, possibly because the distance that a bubble has to travel before reaching the free space in the vial is much smaller than when a 0.8mm thick mould is used. In order to determine if any gases were generated during the curing process, gas chromatography-mass spectrometry (GC-MS) was performed on samples 1a, 2b, 3c and 4d. Table 56 shows the results of the GC-MS analysis. The percentage of gas generated was normalised taking into account the presence of Ar gas as reference. The analyses were performed as explained in Section 2.3.6.

As can be seen from Table 56, all samples are generating carbon monoxide and carbon dioxide. Certainly CO is not present in the blank. The highest amount of CO_2 was generated by sample 3c which is the one with highest percentage of curing agent. On the other hand, sample 4d, having the lowest amount of curing agent, is the one with least

CO and CO_2 generation. Because there is no n-BuNENA in sample 4d it is not possibly to do a direct one to one comparison. According to Arendale [1969] CO_2 generation can be an indication of water present in the samples, because the reaction between water and isocyanates generates CO_2. Water could come from the pre-polymer and/or from the n-BuNENA.

Table 56. GC-MS Head Space Analysis

Sample	N_2 (%)	O_2 (%)	CO (%)	CO_2 (%)	N_2O (%)	H_2O (%)	CH_3CHO (%)	CH_3CH -$CHCH_3$ (%)	CH_3CH_2 -$CHCH_2$ (%)	$CHCl_3$ (%)	THF (%)
Blank	29.30	13.79	0.00	0.47	0.00	72.17	0.00	0.00	0.00	0.00	0.00
1a	34.05	9.99	0.13	19.1	0.00	85.99	0.28	0.00	0.00	5.96	0.31
2b	42.45	12.36	0.11	18.5	1.02	120.9	0.00	0.00	0.00	4.81	0.00
3c	42.19	11.54	0.16	32.4	0.75	115.3	0.00	1.68	0.51	7.99	0.00
4d	33.81	14.65	0.06	14.53	0.00	87.74	0.09	0.00	0.00	6.11	0.00

Only samples containing n-BuNENA produced nitrous oxide, 2-butene and 1-butene, although the last two compounds were not seen in sample 2b. Also samples containing n-BuNENA (2b, 3c) produced or already had more water than the others (1a, 4d). Possibly some sort of decomposition is affecting the n-BuNENA and leading to the formation of N_2O and Butenes.

Karl Fischer analyses were carried out on HTPE and n-BuNENA samples and they were found to contain 0.046 and 0.004 wt % water respectively. According to Comfort [2004], the water content should be no greater than 0.05%, which means the HTPE pre-polymer 27B is theoretically under the specification. For HTPB the specification allows a greater water content i.e. 0.1% [Royal Ordnance, 2000]. On the other hand, according to technical data for n-BuNENA [ICI, RXL 647], its water content should be less than 0.75%.

Although the water content obtained by Karl Fischer is below specification limits for the HTPE pre-polymer, it is possible that some molecules of water can be trapped in the pre-polymer chain. As suggested by Takaya [1999, 2002], up to 5% by weight of water can be held in hydroxyl terminated polyethers in two ways. First, water molecules can be coordinated directly to OH groups and secondly they can be interacting with the oxygen atoms of the main chain by hydrogen bonds. This can be creating distortions in

the real amount of water present in the pre-polymer and in that detected by the Karl Fischer analysis. Some of the isocyanate groups could be reacting with water molecules trapped in the main chain and with those coordinated to the OH groups, producing carbon dioxide and amines.

Possibly there are two reactions happening in parallel or one as a consequence of the other. First, water present in both pre-polymer and plasticizer is generating CO_2 and CO in a reaction with isocyanates, and secondly either this reaction is promoting the n-BuNENA decomposition or the decomposition is due to the instability of n-BuNENA during thermal binder curing.

One of the possible reactions produces CO_2 and an amine from the isocyanate and water. According to Carey [1993], amines can react with nitrate esters and this reaction is known as aminolysis of esters. Possibly this reaction can be generating gaseous products from the n-BuNENA decomposition, including N_2O and butenes as presented in Table 56.

It was decided to take two actions in an attempt to reduce bubble generation; firstly to dry the pre-polymer and plasticizer and secondly, to reduce the curing temperature to allow more time in the liquid phase before the pre-polymer becomes cured i.e. solid. In order to reduce Takaya's water effect, it was decided to dilute the pre-polymer in a hydrophilic solvent to release water molecules either trapped or coordinated in the polymer. Because the pre-polymer is soluble in THF, this was the solvent chosen.

In order to dry the HTPE pre-polymer and the n-BuNENA, 50 cm^3 of HTPE sample 27B were diluted in 300 cm^3 of THF. As stated previously the HTPE water content was 0.046% and the sample was diluted in THF until all the pre-polymer was dissolved. Then 108 g of molecular sieve 4Å were added to the solution. After 24 h, 79 g of molecular sieve 4Å were added to the solution and it was left for 5 days. After that period of time the water content of the HTPE sample was 0.019%. Similarly, 45 g of a new batch of n-BuNENA were diluted in 111 cm^3 of THF and 44 g of molecular sieve 4Å were added to dry the mixture to a final water content of 0.036%.

A new batch of gumstock was prepared with the dried HTPE pre-polymer 27B and n-BuNENA. A gumstock sample called 5G27B was cured with N-3200 at an NCO/OH equivalence ratio of 0.877. After 25 h in the curing oven the sample still was liquid and after 40 h of curing at 55°C the sample was solid and no bubbles were observed during all the curing process. Samples were poured into a 0.8 mm thick mould and also between two Teflon sheets in order to produce a very thin film of gumstock to be able to create extreme conditions for the curing process. Figure 58 B shows gumstock sample 4G27B that contains bubbles and Figure 58 A sample 5G27B without bubbles.

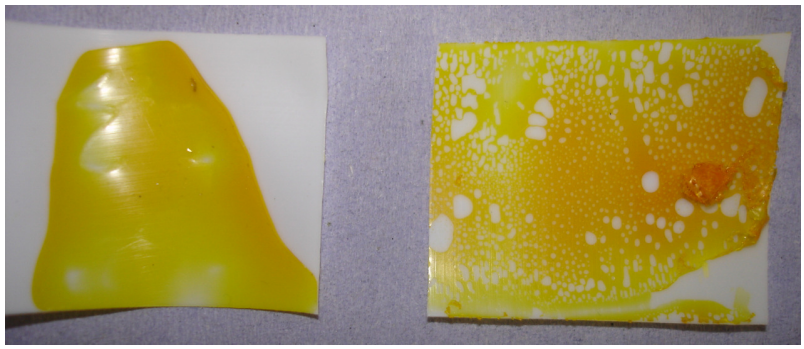

A **B**

Figure 58. Cured gumstock samples, A:5G27B and B:4G27B

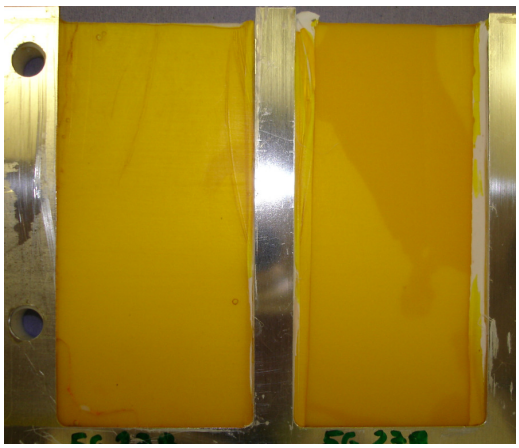

Figure 59. Cured network samples, 5G27B

The same can be seen in Figure 59 for the 5G27B gumstock sample cured into the 0.8mm thick mould. These results are an indication that possibly bubble generation was controlled by drying the pre-polymer with molecular sieve in a hydrophilic solvent and that they were generated from the water molecules present in the pre-polymer chain and its reaction with isocyanates. Also, by reducing the curing temperature from 65 to 55°C

the curing process is delayed, allowing any generated gases to be evacuated before the bulk becomes solid

3.2.7 HTPE FTIR curing process analysis and results

In order to understand the curing process when the isocyanate groups from the curing agent, Desmodur N-3200, react with the pre-polymer hydroxyl groups, Fourier Transform Infrared spectroscopy was performed using a Bruker FTIR spectrometer. As explained in Section 2.3.5, a thin layer of curing sample was placed between two plates of sodium chloride and placed in an oven at 60°C. The sample was taken out from the oven periodically and IR spectra were obtained during the curing process.

3.2.7.1 FTIR binder network curing analysis

Figure 60 shows the IR spectrum for the HTPE pre-polymer, sample 27B, before the curing agent addition and Figure 61 shows the IR spectrum of curing agent Desmodur N-3200.

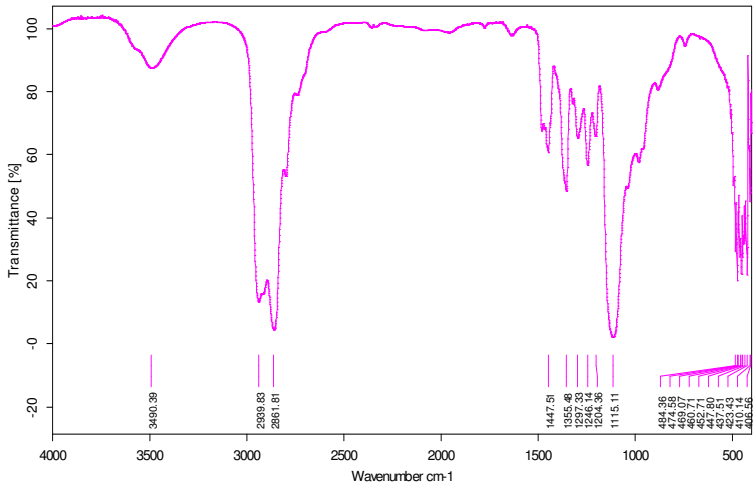

Figure 60. HTPE FTIR spectrum

The course of the curing reaction as followed by FTIR analysis is presented in Figure 62 to Figure 65. The spectra were obtained immediately after mixing the pre-polymer with the curing agent and also after 4, 7 and 23 h.

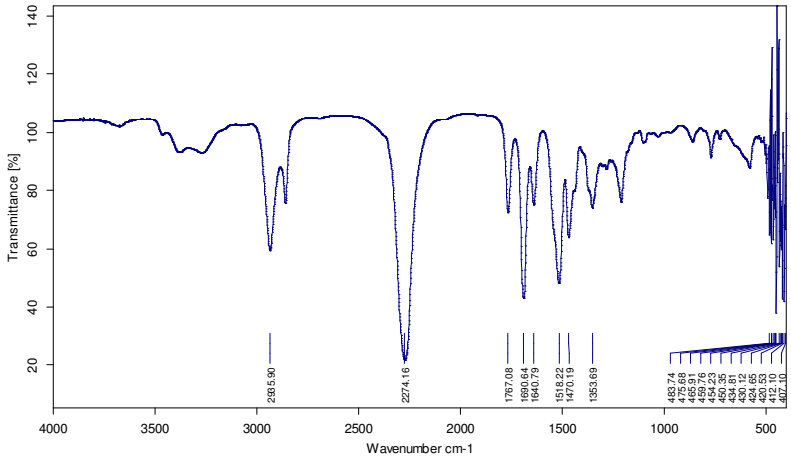

Figure 61. Curing agent Desmodur N-3200 FTIR spectrum

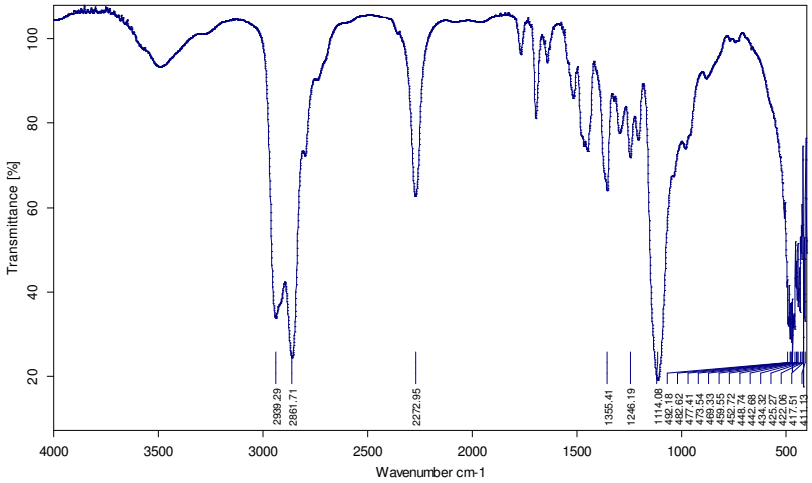

Figure 62. HTPE curing process FTIR spectrum after 5 min of curing

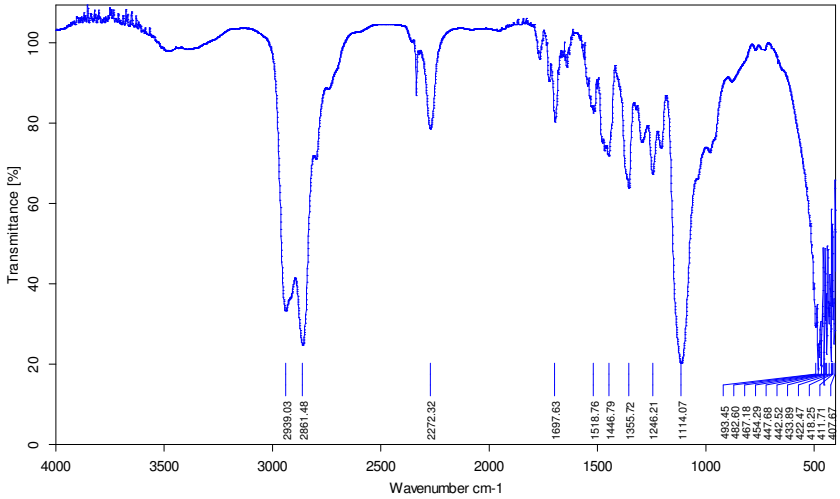

Figure 63. HTPE curing process FTIR spectrum after 4 h of curing

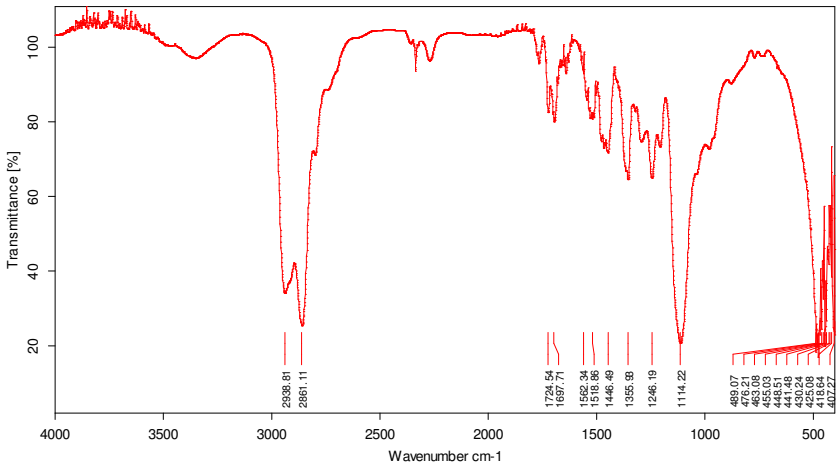

Figure 64. HTPE curing process FTIR spectrum after 7 h of curing

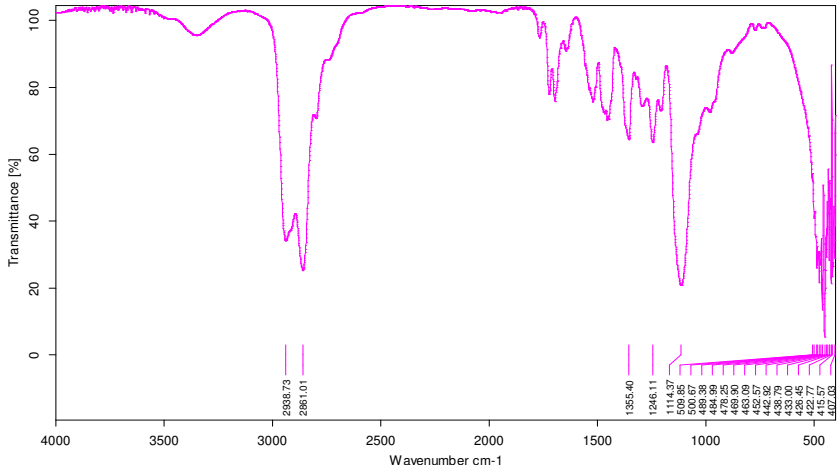

Figure 65. HTPE curing process FTIR spectrum after 23 h of curing

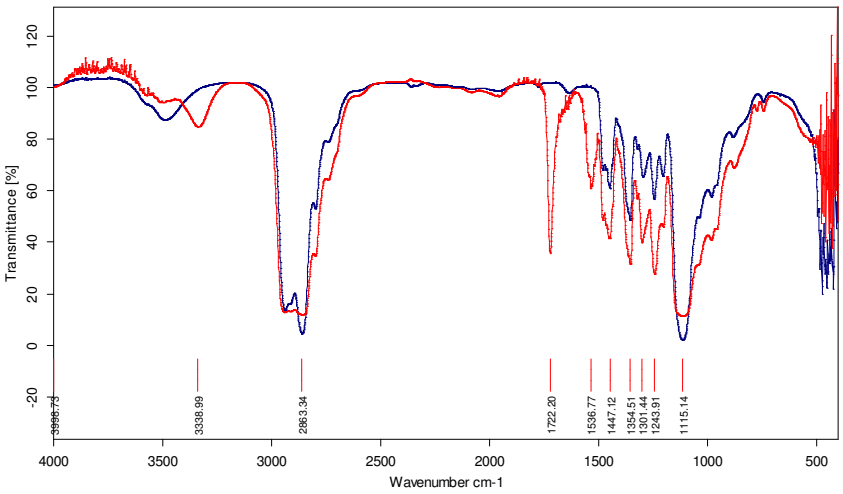

Figure 66. HTPE pre-polymer sample 24N (blue) and same sample cured with IPDI (red)

Table 57 gives a summary of the main peaks and their suggested assignments. Figure 66 shows the IR spectrum for the HTPE pre-polymer, sample 24 and the same sample cured with IPDI.

Table 57. Main Characteristic FTIR Peaks
[Bellamy 1980]] and [Nakanishi, 1964]

Wave Number, cm^{-1}	Assignment	
3490	Primary alcohol, OH stretching	$-CH_2OH$
3350	Mono subst. Amide, NH stretching	-CO-NH-R
2935	Alkane groups, CH stretching	$-CH_2CH_2-$
2272	Isocyanate groups, stretching	-N=C=O
1722	Urethane groups, CO stretching	-NH-CO-OR-
1690	Biuret, CO stretching	-HN-CONH-CO-NH-
1640	Urea, CO stretching; Di substituted amide, CO stretching	N-CO-N, $-CO-NR_2-$
1518	Mono subst. Amide, NH bend	-CO-NH-R-
1355	Alkane, CH bending	$-CH_2CH_2-$
1117	Aliphatic ether, CO stretching	$-CH_2-O-CH_2-$

3.2.7.2 Binder network curing: discussion of IR results

The HTPE/Desmodur N-3200 curing process was followed by FTIR, taking IR spectra during the curing reaction. In order to better appreciate the initial IR spectra of both compounds, Figure 60 and Figure 62 are overlayed in Figure 67. Also, the curing process FTIR spectra presented in Figure 62 to Figure 65 have been overlayed in Figure 68 .

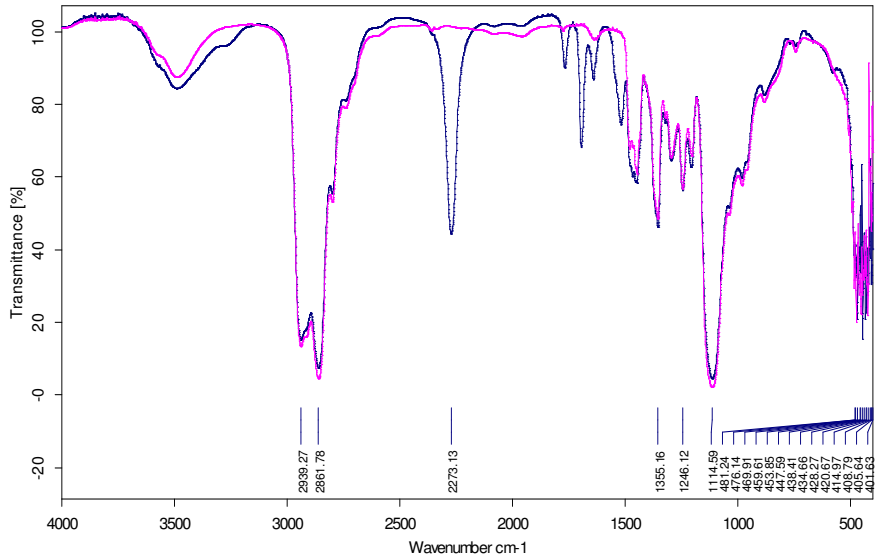

Figure 67. HTPE pre-polymer (red) and HTPE pre-polymer mixed with Desmodur N-3200 (blue) at the beginning of the reaction, FTIR spectrum

As can be seen from Figure 67, between 1618 and 2272 cm^{-1} the HTPE IR spectrum shows new peaks coming from the curing agent. In fact, the sharp and intense peak at 2272 cm^{-1} can be assigned to the anti symmetric stretch of the isocyanate NCO group (Figure 61), as suggested in Table 57. This peak can be seen more clearly in the IR spectrum of HTPE sample 24 cured with IPDI in Figure 66. The peak at 1696 cm^{-1} can be assigned to the carbonyl group present in the biuret group of the curing agent and the peak at 1519 cm^{-1} to the NH stretch of a mono-substitutited amide group. The peak at 1642 cm^{-1} can possibly assigned to the carbonyl group in the urea segment of the curing agent. As stated by Mohring [1978], the biuret polyisocyanates such as Desmodur N-3200 have different percentages of mono, bis, tris and tetra-biuret groups in their molecular structure, together with a small percentage of 1,6-diisocyanatohexane and some unidentified constituents. Therefore the IR spectra can be very complex.

To have a better understanding of the changes that are happening during the curing process i.e. the disappearance and formation of new groups, the infra red spectra presented in Figure 62 to Figure 65 are overlayed in Figure 68 and a expansion between 2272 and 1400 cm^{-1} is presented in Figure 69. As expected, the isocyanate group peak at 2272 cm^{-1} decreased in intensity during the curing process until it disappeared completely; the absorption at 1722 cm^{-1} showed a concomitant increase in intensity. As the reaction between isocyanate and hydroxyl groups was going on, the new peak can be assigned to the carbonyl group stretch. This is an indication of secondary alkyl polyurethane formation.

As can be appreciated from Figure 68, the peak corresponding to the hydroxyl group of a primary alcohol at 3490 cm^{-1} is decreasing in intensity during the curing reaction while a peak at 3350 cm^{-1} is growing. This peak can possibly be assigned to an absorption band of the –NH from the urethane groups. This was more apparent from the reaction between HTPE sample 24N and IPDI. As can be seen from the HTPE sample 24N cured with IPDI in Figure 66, the peak at 3339 cm^{-1} is in the region that can be assigned to the NH stretch. In the molecular structure of IPDI there are no NH groups and therefore they appeared due to the urethane formation, suggesting that the peak at 3339 cm^{-1} can be assigned to the NH stretch of the urethane groups. Although similar

cure process monitoring was performed by Burakl [1997] and by Tokui [1991], on a HTPB sample cured with IPDI, they did not report the NH stretching peak as they found no changes around 3400 cm^{-1} in the OH absorption band region after the curing process. Possibly this was because the OH absorption band in HTPB is weaker and broader than in HTPE, and the NH stretching band was superimposed on the OH band, despite the fact some of the hydroxyl groups were disappearing during the curing reaction.

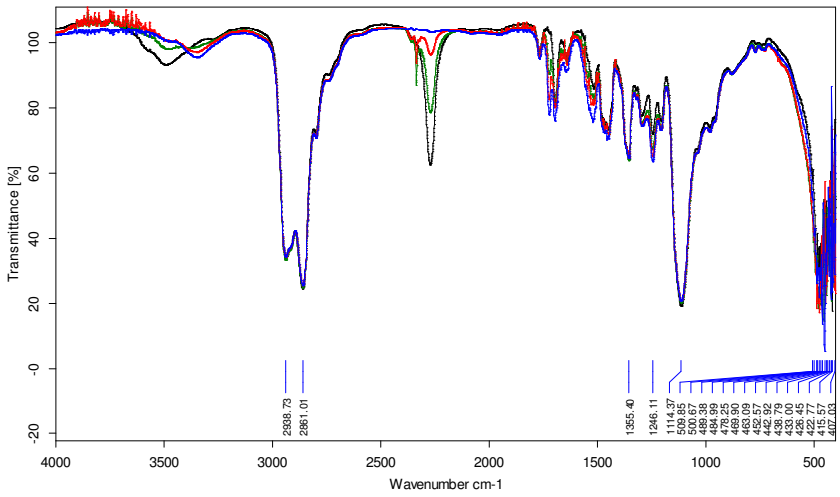

Figure 68. HTPE curing process FTIR spectrum, from the initial reaction (black), after 4 h (green), 7 h (red) and 23 h (blue).

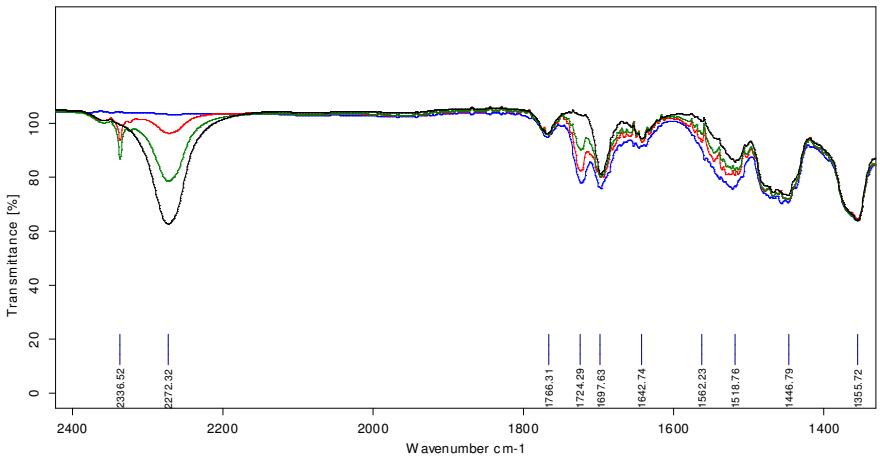

Figure 69. Expansion of the HTPE curing process FTIR spectrum, from the initial reaction (black), after 4 h (green), 7 h (red) and 23 h (blue).

The increase in the intensity of the peak at 1518 cm^{-1}, that can be assigned to the NH bending, is probably due the effect of the new N-H bond from the urethane formation plus the NH from the curing agent. As expected, no changes were observed in the bands at 2935 and 1355 cm^{-1} that are assigned to alkane group C-H stretching and C-H

bending respectively. From Figure 66, and as also found by Tokui [1991], the peaks at 1722 and at 1537 cm^{-1}, can be assigned respectively to the CO stretching and to the NH bending from the urethane groups due to the reaction between the IPDI isocyanate groups and OH groups from the copolyether.

3.3 Binder Network and Gumstock Characterisation

3.3.1 Mechanical analyses

In order to compare curing agents and choose one to be used in the manufacture and characterisation of HTPE binder networks, gumstocks and propellants, tensile strength and other mechanical test were performed. The tests were performed using a "Zwick material prufung", model 1445 tensile tester machine (Figure 70). The influence of the degree of cross-linking on the mechanical properties of the HTPE binder network was also studied.

Figure 70. Mechanical tensile test for a binder network sample

The tests were developed at ambient temperature (21°C), at a crosshead speed of 5 mm min^{-1} following Eroglu's [1988] method and the data were analyzed using a "TESTEXPERT version 1.1" software. Young's module ($\mathbf{E_t}$) was calculated from the stress/strain curve according to Equation 3.2 [Osswald, 2003].

$$E_t = \frac{d\sigma}{d\varepsilon} \tag{3.2}$$

where **σ** (MPa) represents the tensile stress and **ϵ** (%) the strain.

HTPE binder network and gumstock specimens for mechanical tests were obtained initially by cutting rectangular binder network slides from the samples cured in the 6 mm thick moulds as presented in Section 3.2.5.6 Figure 50. Later on during the programme, mechanical test specimens were obtained by cutting a thin binder network slice made from a 0.8mm thick mould as presented in Section 3.2.6.2 Figure 59. This time a dumbell shaped cutter was used. Figure 71 shows binder network specimens made by using the dumbell shaped cutter.

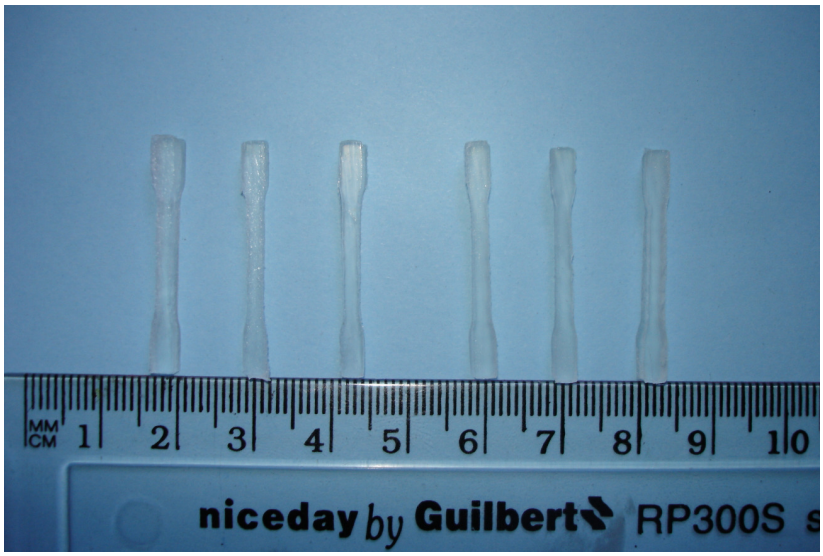

Figure 71. Dumbell specimen shapes

3.3.1.1 Tensile test for HTPE samples cured with N-100 and N-3200

HTPE binder network samples made by using curing agent Desmodur N-100 (sample 14N27B) and N-3200 (sample 15N27B) were tested in a tensile test machine to compare their mechanical properties. Also, samples prepared from HTPB samples 5NHTPB and 4NHTPB and cured with Desmodur N-100 and N-3200 respectively were prepared and tested. A NCO/OH equivalence ratio equal to 1.0 was chosen for all the samples.

The binder network specimens were made from rectangular samples having an average cross sectional area of 11.6 mm^2. Force and strain at break were obtained from the best measurements for each kind of sample and Young's modulus was calculated as stated above. The results are plotted in Figure 72 for HTPE and in Figure 73 for HTPB binder networks respectively. Table 58 shows the tensile test average results for six trials for each specimen.

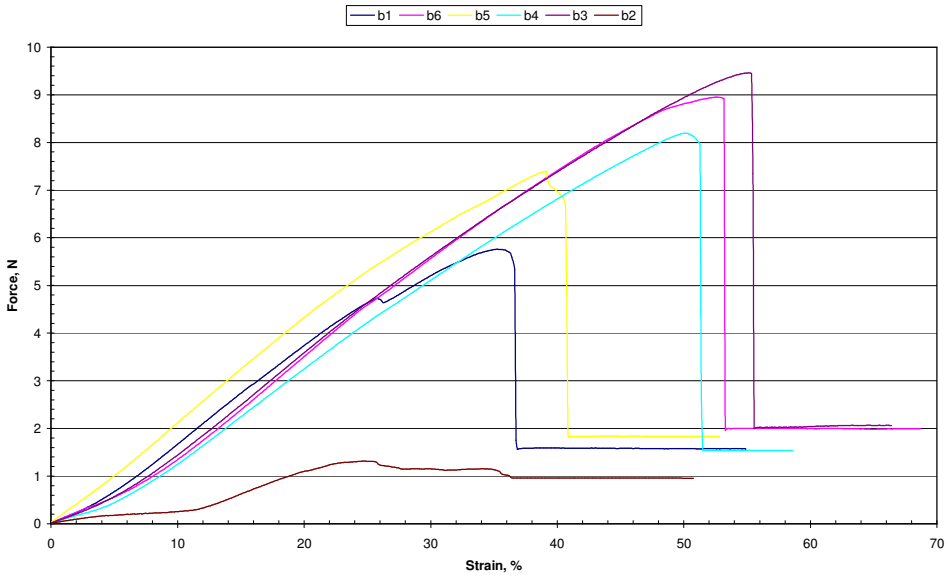

A

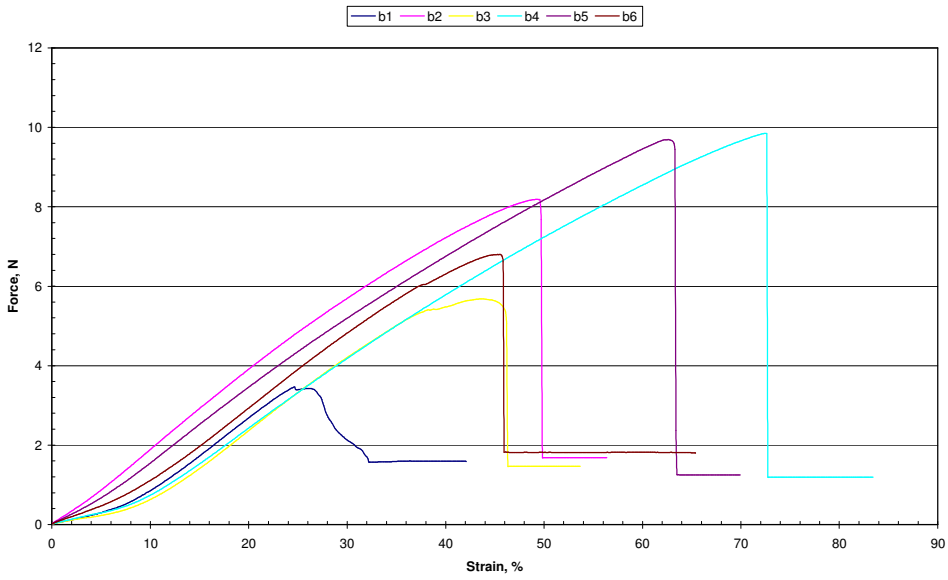

B

Figure 72. Mechanical tensile test for HTPE samples (A) 14N27B and (B) 15N27B

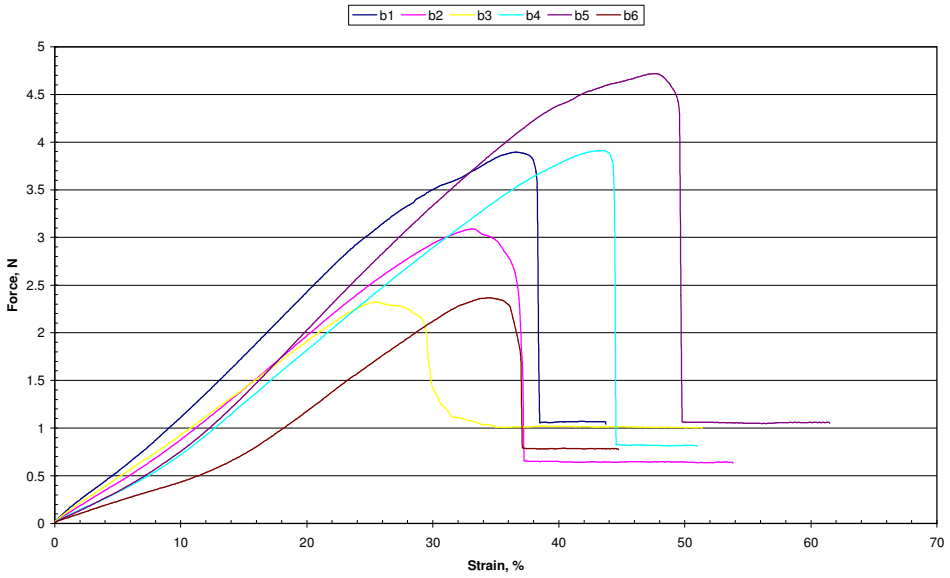

A

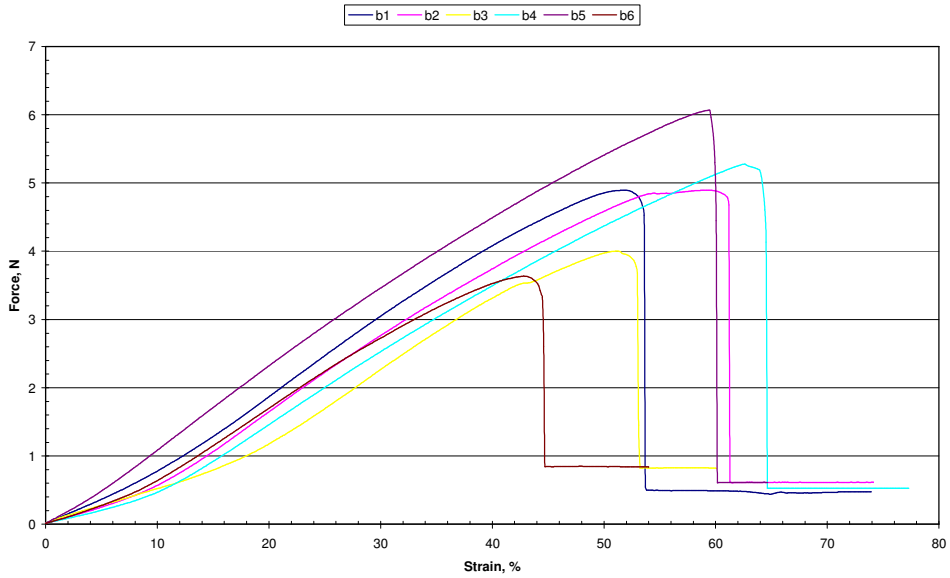

B

Figure 73. Mechanical tensile test for samples (A) 4NHTPB and (B) 5NHTPB

Because of measurement problems during the tensile tests arising from the irregular shape of the specimens and the system to clamp them, as can be seen from Figure 72 and Figure 73, only the three best curves for each sample were taken into account to obtain the force and strain at break average figure, as presented in Table 58.

Comparatively speaking, as it can be seen from Table 58, HTPE samples cured with Desmodur N-3200 show slightly better mechanical properties than those cured with

Desmodur N-100 i.e. higher tensile strength and strain and lower modulus [Stacer, 1991]. In fact, for samples cured with N-3200 the tensile strength at break was 3.8% higher than for samples cured with N-100.

Table 58. Mechanical Test Results for HTPE Samples 14N27B, 15N27B, 4NHTPB and 5NHTPB

Sample	Strength at Break, MPa				Strain at Break, %				Young's Modulus Eo, MPa			
	14N27B	15N27B	4NHTPB	5NHTPB	14N27B	15N27B	4NHTPB	5NHTPB	14N27B	15N27B	4NHTPB	5NHTPB
A	0.451	0.235	0.248	0.369	35.250	24.656	36.546	51.600	1.656	1.174	0.797	0.868
B	0.105	0.543	0.215	0.381	24.729	49.258	33.195	59.480	0.824	1.366	0.618	0.908
C	0.677	0.380	0.144	0.255	55.144	43.650	25.413	51.158	1.770	1.258	0.547	0.707
D	0.609	0.729	0.302	0.411	50.184	72.515	43.446	62.627	1.431	1.315	0.855	0.847
E	0.501	0.714	0.316	0.436	39.112	62.646	47.619	59.360	1.511	1.411	0.902	0.889
F	0.627	0.451	0.178	0.259	52.604	45.529	34.371	42.788	1.553	1.261	0.710	0.766
Ave.	**0.638***	**0.662****	**0.288+**	**0.399++**	**52.644**	**61.473**	**42.537**	**58.267**	**1.585**	**1.364**	**0.851**	**0.878**

*Average from specimens: C, D, F; **Average from specimens: B, D, E; +Average from specimens A, D, E; ++Average from specimens A, B, D, E.

Strain at break shows bigger differences than strength, the samples cured with Desmodur N-3200 being 16.8% higher than the samples cured with Desmodur N-100. On the other hand the estimated Young's modulus was 13.9% lower in samples cured with Desmodur N-3200. Taking into account the tensile test results and the easier processability compared to Desmodur N-100 due to its lower viscosity, it was decided to use Desmodur N-3200 as the curing agent for the preparation and characterisation of the binder network and gumstock samples and also for propellant formulation and manufacture.

As stated above, HTPB samples to be tested mechanically were cured with the same curing agents as HTPE. However, they showed the opposite behaviour to that of the HTPE binder network. As can be seen from Table 58, HTPB samples cured with Desmodur N-3200 have poorer mechanical properties than those cured with Desmodur N-100. In fact, for samples cured with N-3200 the tensile strength at break is 27.8% lower than for samples cured with N-100. Strain at break show similar differences to strength; the samples cured with Desmodur N-3200 were 27.0% lower than those cured with Desmodur N-100. On the other hand the Young's modulus is better for the samples cured with Desmodur N-3200, being 3.1% lower than in samples cured with Desmodur N-100.

3.3.1.2 Tensile test for HTPE samples cured with N3200 at different NCO/OH ratios

In order to study the influence of the degree of cross linking on the mechanical properties of the HTPE binder network, several samples prepared from HTPE pre-polymer batch 27B were cured with Desmodur N-3200. Different NCO/OH equivalence ratios were used i.e. 1.0, 0.9, 0.8 and 07. This time a dumbell shaped binder network specimen was used.

Table 59 shows the results obtained from the mechanical tensile tests. Tensile strength and strain at break were obtained from five measurements for each kind of sample and the average was plotted against the NCO/OH equivalence ratio, as shown in Figure 74.

Table 59. Mechanical Tensile Test for Samples 16N27B to 19N27B

Sample	Strength at Break, MPa				Strain at Break, %			
	16N27B (NCO/OH 1.0)	**17 N27B (NCO/OH 0.9)**	**18 N27B (NCO/OH 0.8)**	**19 N27B (NCO/OH 0.7)**	**16 N27B (NCO/OH 1.0)**	**17 N27B (NCO/OH 0.9)**	**18 N27B (NCO/OH 0.8)**	**19 N27B (NCO/OH 0.7)**
A	0.70	0.89	0.62	0.41	77.32	145.28	209.48	374.23
B	0.86	0.85	0.76	0.4	76.71	118.12	263.42	334.56
C	1.02	0.90	0.85	0.45	87.74	110.46	256.31	400.36
D	1.10	1.05	0.72	0.46	88.89	122.74	186.14	393.53
E	1.08	0.92	0.69	0.42	66.51	100.64	166.45	346.48
F	1.14	0.97	0.84	0.27	68.86	116.18	224.65	499.01
Average	**0.98**	**0.93**	**0.75**	**0.40**	**77.67**	**118.90**	**217.74**	**391.36**

As can be seen from Figure 74 and from the data presented in Table 59, the mechanical behaviour of the HTPE sample cured with Desmodur N-3200 at different NCO/OH equivalence ratios follows the expected trend. In fact, in a similar way to the information presented by Eroglu [1998] when characterizing the network structure of HTPB cured with different isocyanates such as Desmodur N-100, IPDI and HMDI, as the NCO/OH equivalence ratio decreases the strength at break decreases and the strain increases.

The maximum strength of 0.98 MPa was obtained at an NCO/OH of 1.0 while the maximum strain of 391% was obtained at a 0.7 equivalence ratio. This behaviour is in agreement with that expected. The balance in the change of strength and strain was found at an equivalence ratio of approximately 0.79. At this ratio the strength is 0.70 MPa and the strain 250%.

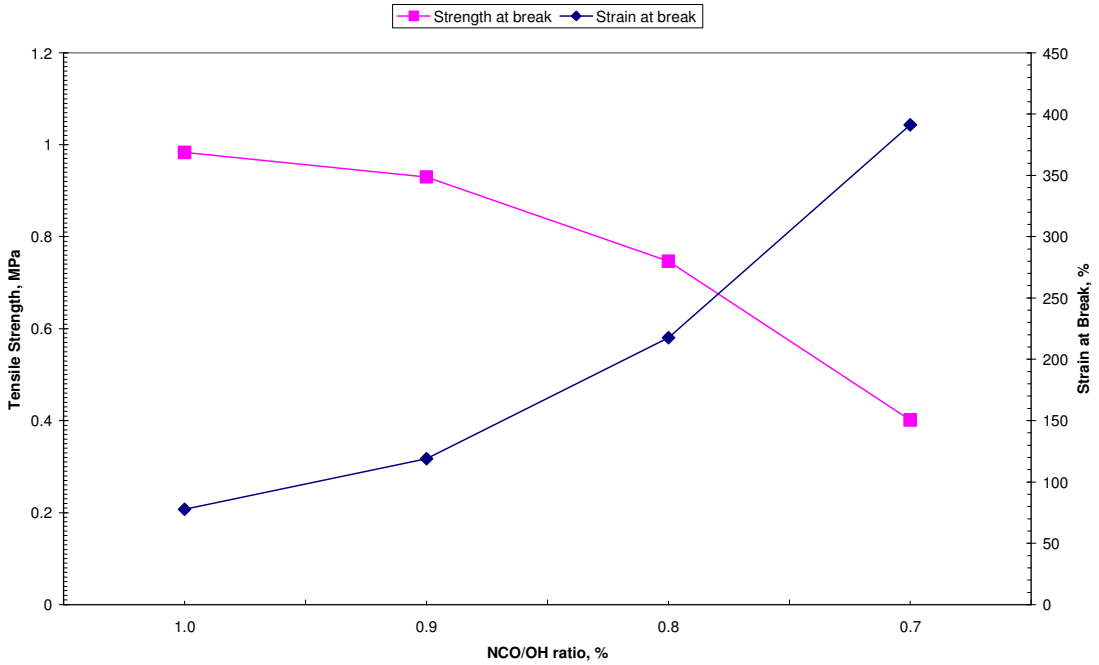

Figure 74. Strength and strain at break for different NCO/OH ratios in samples 16N27B to 19N27B

3.3.1.3 Tensile test for gumstock HTPE sample 1G26E

Mechanical tests were performed on gumstock sample 1G26E in order to observe the effects on mechanical properties when a HTPE pre-polymer, cured with N-3200 at a NCO/OH ratio equivalence of 0.85, is plasticized with n-BuNENA. Strength and strain at break data obtained from the tensile tests are presented in Table 60. It was not possible to obtain the modulus Eo, due to software problems at the end of the trials.

Table 60. Tensile Test Data for Sample 1G26E

Test N°	Strength at Break, (MPa)	Strain at Break, (%)
A	0.22	235
B	0.22	218
C	0.24	246
D	0.29	324
E	0.23	252
Average	**0.24**	**255**

To quantify the effect of the plasticizer on the binder i.e. to compare binder network and gumstock mechanical properties, a theoretical strength and strain at break was calculated for the NCO/OH equivalence ratio used in gumstock sample 1G26E. From

the data plotted in Figure 74 and by interpolation, the expected value for strength and strain in a binder network sample without any plasticizer and with NCO/OH ratio of 0.85, was estimated as 0.84 MPa and 168.32% respectively. As can be seen from Table 60, the measured strength and strain at break for sample 1G26E were 0.24 MPa and 255% respectively. The difference in strength and strain obtained from the previous figures means that mechanical properties are affected when the plasticizer n-BuNENA is introduced into the binder network formulation. In fact, in this case strength was decreased by 71.4% and strain was increased by 51.5% in comparison with a binder network sample having the same NCO/OH equivalence ratio.

3.3.1.4 Tensile test conclusions

Slightly better mechanical properties were found in HTPE binder network samples cured with Desmodur N-3200 than in those cured with N-100. Because of that and improved processability, Desmodur N-3200 was chosen to be part of the HTPE gumstock and propellant formulation. It was also noticed that for HTPE and HTPB binder network samples, cured with the same curing agents and similar NCO/OH equivalence ratio, HTPE binder network samples show a higher strength and strain at break but also higher modulus. When n-BuNENA was introduced into the binder network formulation, it was observed that strength at break decreased by 71% but strain increased by 51%.

3.3.2 Density measurements

Density determinations at 25^{o}C were performed on binder network and gumstock samples made from HTPE pre-polymer and on equivalent samples made from HTPB. In order to do this an AccuPyc 1330 Pycnometer for 1 cm^3 samples from Micromeritics was used, as explained in Section 2.3.7. A sample weighing between 0.2 and 0.3 g was introduced into the calibrated volume container and then placed in the instrument. Five measurements were taken and the average density was calculated and reported together with the standard deviation. The test was performed at a helium gas pressure of 20 psi (0.137 MPa).

3.3.2.1 HTPE and HTPB density results

HTPE Binder network density results for samples 16N27B to 20N27B are presented in Table 61 and those for HTPE gumstock samples 1G26E, 4G27B and 5G27B are presented in Table 62. Results for HTPB binder network sample 1NHTPB and gumstock sample 5GHTPB are presented in Table 63 and Table 64 respectively.

Table 61. HTPE Binder Network Density Measurements

Sample	Average density (g cm^{-3})	Sample weight (g)	Average volume (cm^3)	Volume standard deviation (cm^3)	Density standard deviation (g cm^{-3})
16N27B	1.0623	0.2680	0.2523	0.0001	0.0005
17N27B	1.0630	0.2542	0.2391	0.0001	0.0006
18N27B	1.0583	0.2676	0.2529	0.0001	0.0003
19N27B	1.0605	0.2256	0.2127	0.0001	0.0006
20N27B	1.0615	0.2730	0.2572	0.0004	0.0015

Table 62. HTPE Gumstock Density Measurements

Sample	Average density (g cm^{-3})	Sample weight (g)	Average volume (cm^3)	Volume standard deviation (cm^3)	Density standard deviation (g cm^{-3})
1G26E3	1.1254	0.1963	0.1744	0.0001	0.0009
4G27B	1.1245	0.3524	0.3134	0.0002	0.0007
5G27B	1.1631	0.1407	0.1210	0.0001	0.0008

Table 63. HTPB Binder Network Density Measurements

Sample	Average density (g cm^{-3})	Sample weight (g)	Average volume (cm^3)	Volume standard deviation (cm^3)	Density standard deviation (g cm^{-3})
1NHTPB	0.9342	0.2661	0.2848	0.0003	0.0009

Table 64. HTPB Gumstock Density Measurements

Sample	Average density (g cm^{-3})	Sample weight (g)	Average volume (cm^3)	Volume standard deviation (cm^3)	Density standard deviation (g cm^{-3})
3GHTPB	0.9401	0.2129	0.2265	0.0003	0.0013

3.3.2.2 HTPE and HTPB density measurement, discussion of results

As can be seen from Table 61, the binder network average density for samples prepared from HTPE pre-polymer is 1.061 g cm^{-3}. This value as expected, was slightly higher than for the pre-polymer i.e. 1.036 g cm^{-3}, and this difference is possibly due to the

density of the curing agent, Desmodur N-3200, which is 1.130 g cm^{-3} [Bayer, 2001]. On the other hand, the density figures look similar for all the binder network samples, independent of their NCO/OH equivalence ratio. Those with lower NCO/OH equivalence ratios have slightly lower density.

HTPE gumstock density results are similar for samples 1G26E3 and 4G27B, being slightly higher than for sample 1G26E i.e. 1.125 and 1.125 g cm^{-3} respectively. HTPE pre-polymer 26E3 has a higher density than pre-polymer 27B i.e. 1.052 and 1.031g cm^{-3} respectively. However, the density for both samples was higher than that obtained for the binder network samples. This is due to the influence of n-BuNENA which has a density of 1.221 g cm^{-3}. The density of the n-BuNENA was obtained by the same method used for the pre-polymer as stated previously. The result was exactly the same as that reported by ICI [RXL 647].

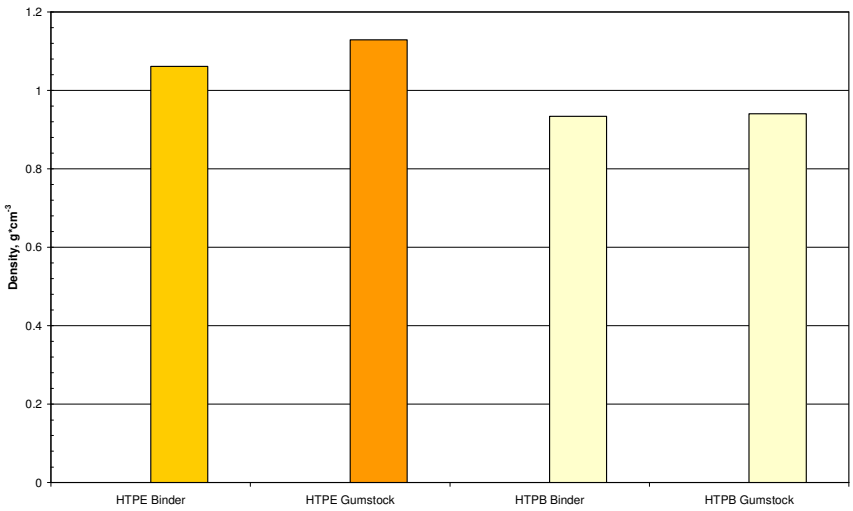

Figure 75. HTPE and HTPB density comparison

As shown in Figure 75, samples prepared with HTPE, either binder network or gumstock, had a higher density than HTPB samples. The HTPE binder network density presented in Figure 75 was obtained from the average of the density figures presented in Table 61 and was 1.061 g cm^{-3} and HTPB density was 0.934 g cm^{-3}. As for the binder, HTPE and HTPB gumstock samples were prepared using the same curing agent Desmodur N-3200 but a different plasticizer. Gumstock samples made from HTPE were

prepared using 42.64 % n-BuNENA (density 1.221 g cm^{-3}) relative to the pre-polymer, while HTPB samples were prepared using 24.46 % DOS plasticizer (density 0.910 g cm^{-3} [DOS, 1994]), relative to the pre-polymer. Therefore, the presence of the plasticizer in HTPB, density 0.906 g cm^{-3}, does not appear to be affecting the density figures.

3.3.2.3 HTPE and HTPB density measurement, conclusions

HTPE binder network and gumstock samples have a higher density than the similar samples made from HTPB pre-polymer. The higher density is mainly due to the higher HTPE pre-polymer density and also to the higher density of the energetic plasticizer n-BuNENA used in HTPE formulations.

3.3.3 DSC analyses

In order to determine thermal properties of binder network and gumstock samples made from the pre-polymer HTPE 27B and cured with Desmodur N-3200 at different NCO/OH ratio, glass transition temperature (Tg) measurements and thermal decomposition analyses were performed in a similar way to that described in Section 2.3.4 for the pre-polymer. The software "STARe, version 8.1x for Windows® 2000 and Windows® XP from METTLER TOLEDO", was use to analyze the data. Sample weights were 6 to 9 mg. Samples were placed in an aluminium crucible closed with a pinhole lid and heated at a rate of 2˚C per min from –100 to + 30˚C for Tg and at a rate of 10˚C per min from 30 to + 550˚C for thermal decomposition. An inert environment was created by adding nitrogen gas during all the analyses at a flow rate of 25 cm^3 per min.

3.3.3.1 Binder network Tg analysis and results

Figure 76A and B and Figure 77A and B shows the DSC thermograms for binder network samples 16N27B to 19N27B having a NCO/OH ratio of 1.0, 0.9, 0.8 and 0.7 respectively.

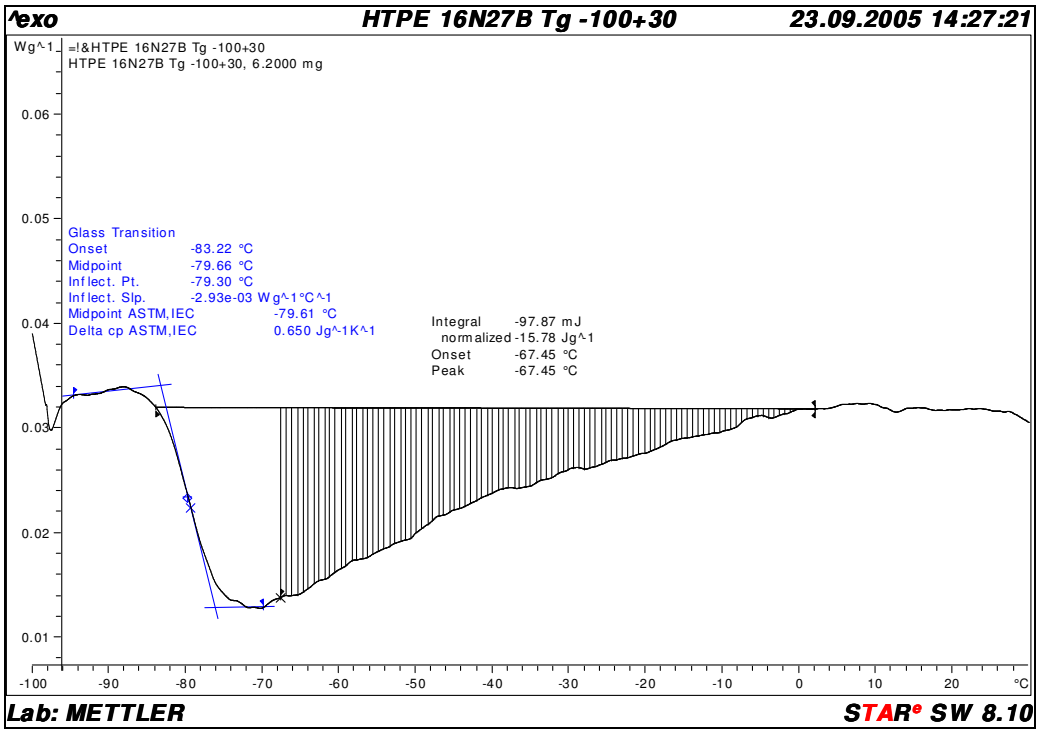

A

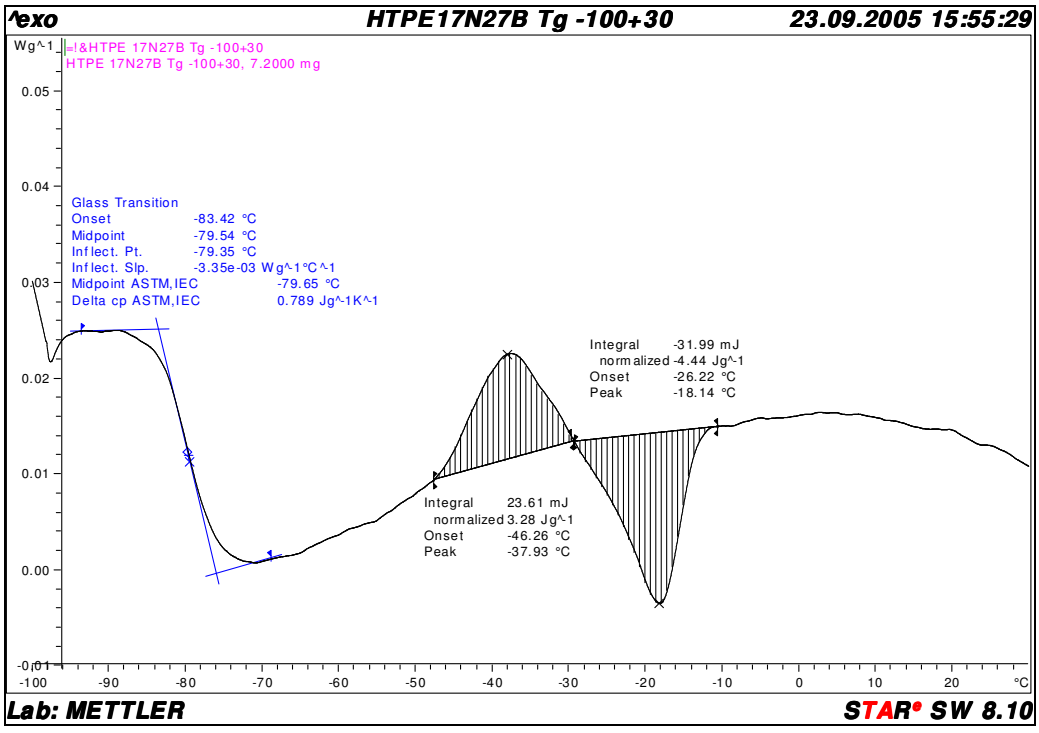

B

Figure 76. DSC Thermogram of HTPE network, sample 16N27B (A) and sample 17N27B (B)

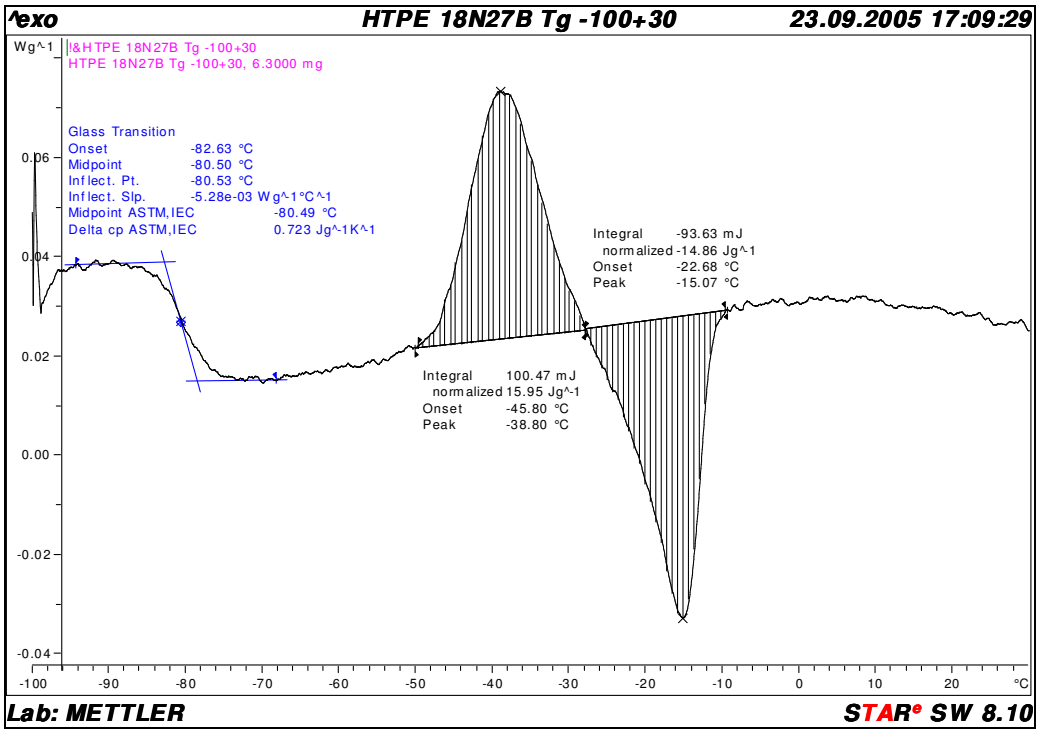

A

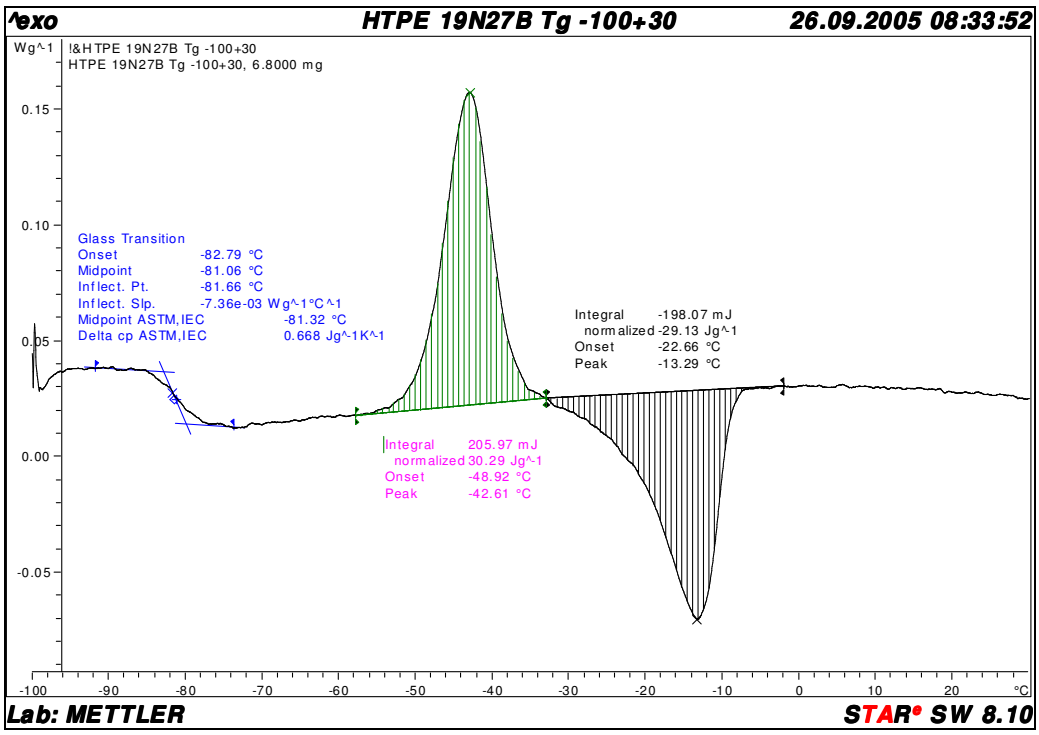

B

Figure 77. DSC thermogram of HTPE network, sample 18N27B (A) sample 19N27B (B)

Table 65 shows the summary of the DSC Tg thermograms data presented in Figure 76 and Figure 77.

Table 65. HTPE Binder Network Results from DSC Tg Analysis

Exp. No	NCO/OH ratio	Tg (˚C)	MCP (˚C)	Melting Heat (J g^{-1})	Melting Point (˚C)	Melting Heat (J g^{-1})
27B	-.-	-81.60	-56.00	29	-7.00	38
16N27B	1.0	-79.30	0.00	0	0.00	0
17N27B	0.9	-79.35	-37.50	3.3	-18.14	4.4
18N27B	0.8	-80.53	-38.8	16	-15.07	15
19N27B	0.7	-81.66	-42.61	30	-13.29	29

As can be seen from Figure 76 and Figure 77, from the overlayed Tg curves in Figure 78 and from the data presented in Table 65, binder network Tg shows almost the same behaviour as in the HTPE pre-polymer, suggesting that urethane links, produced by the reaction between the isocyanate groups from the Desmodur N-3200 and the OH groups from the pre-polymer, do not affect this thermal property. While the Tg of the pre-polymer is -81.6°C, in the binder network cured with N-3200 at equivalence ratios of 1.0, 0.9, 0.8 and 0.7, the Tg is in the range of -79.3 to -81.6°C, increasing slightly with increasing NCO/OH equivalence ratio.

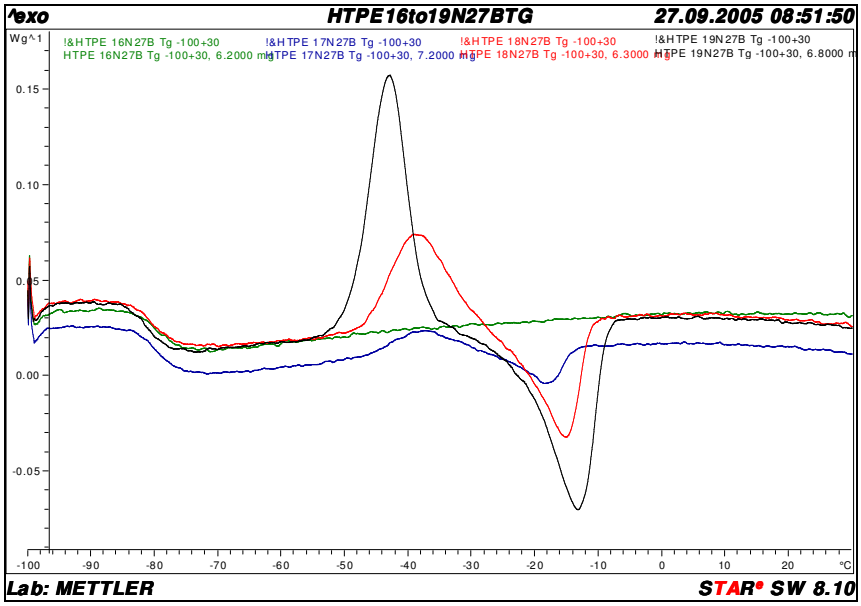

Figure 78. Tg for samples 16N27B (green), 17N27B (blue), 18N27B (red) and 19N27B (black)

On the other hand, for sample 16N27B, which has the highest NCO/OH equivalence ratio, the micro crystallisation peak present in the DSC thermogram of the pre-polymer does not appear in the thermogram, suggesting that almost all the hydroxyl groups have reacted with the isocyanates when the NCO/OH equivalence ratio is 1. However, as the equivalence ratio decreases in the binder network the thermal behaviour of the network

samples becomes more similar to that of the pre-polymer. As can be seen in Figure 78, the microcrystallisation peak appeared in the thermogram of the sample with a NCO/OH equivalence ratio of 0.9 and increases in intensity as the NCO/OH equivalence ratio decreases. The opposite behaviour occurs with the melting point, which increases with decreasing equivalence ratio. This information allows us to state that the presence of the non reacted or partially reacted HTPE pre-polymer, does not affect significantly the glass transition temperature of the binder network but does affect the microcrystallisation and melting point.

3.3.3.2 Gumstock Tg analysis and discussion of results

Figure 79 shows the DSC Tg gumstock thermogram for 4.9 mg of sample 5G27B (A) and for 8.9 mg of sample HTPB 3G (B), having NCO/OH equivalence ratios of 0.88 and 0.87 respectively. Table 66 shows a summary of the DSC Tg thermogram data presented in Figure 79. In addition, the pre-polymer and binder network data are also presented.

As can be seen from Figure 79 and Table 66, the glass transition temperature for gumstock sample 5G27B (NCO/OH equivalence ratio: 0.877) was around -77^{o}C, slightly lower than that of the binder network samples 17N27B and 18N27B (NCO/OH equivalence ratio: 0.9 and 0.8 respectively), where the Tg was -79.3 and -80.5^{o}C respectively.

Despite the fact that the NCO/OH equivalence ratio for sample 5G27B is similar to that for binder network sample 17N27B, the micro crystallisation peak at -37^{o}C and the endothermic peak at -18^{o}C are not present in the gumstock. Therefore, it is suggested that the energetic plasticizer affects the gumstock by slightly increasing the glass transition temperature but at the same time eliminating the micro crystallization effect. On the other hand, at around -25.8^{o}C there is a small change in the energy per unit mass of the gumstock and this can be assigned to the influence of the n-BuNENA.

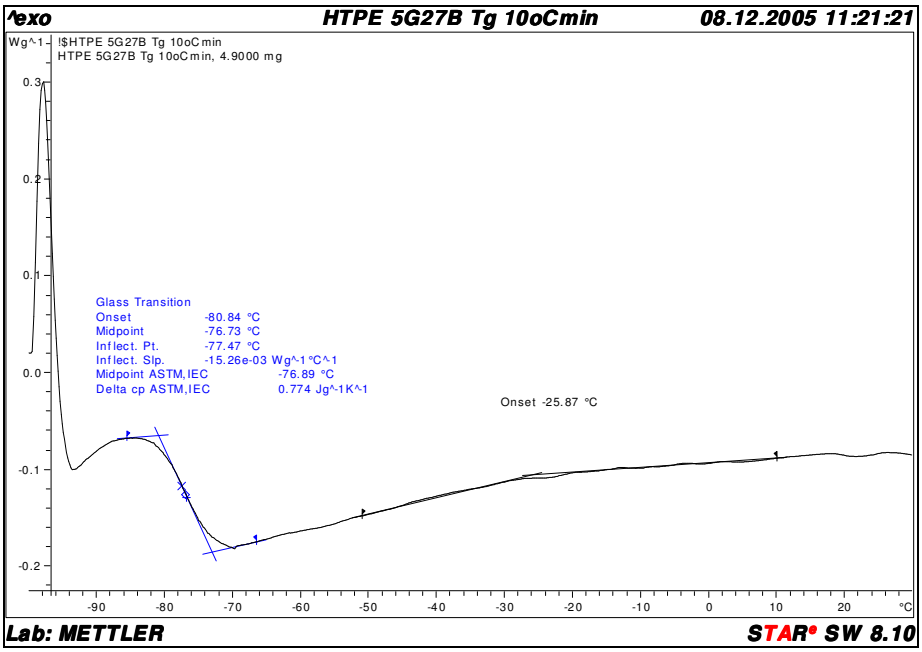

A

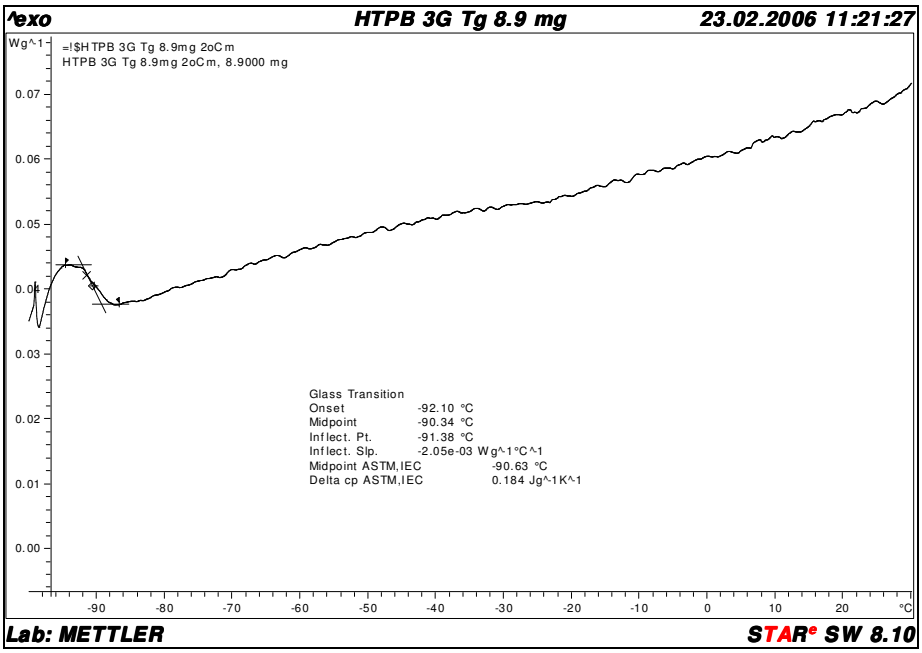

B

Figure 79. DSC Tg thermogram of HTPE gumstock, sample 5G27B.

Table 66. HTPE Gumstock Results from DSC Tg Analysis

Exp. No	NCO/OH ratio (%)	Tg (°C)	Microcrystallisation point (°C)	Microcrystallisation Heat ($J\ g^{-1}$)	Melting Point (°C)	Melting Heat, ($J\ g^{-1}$)
27B	-.-	-81.60	-56.00	29	-7.00	38
17N27B	0.90	-79.35	-37.50	3.3	-18.14	4.4
18N27B	0.80	-80.53	-38.80	15	-15.07	14
5G27B	0.88	-77.47	-.-	-.-	-.-	-.-
HTPB 3G	0.87	-91.38	-.-	-.-	-.-	-.-

When comparing the Tg of HTPE and HTPB gumstock samples it can be seen that HTPB plasticized with DOS has a lower Tg than HTPE. In fact the ΔT was 13.91°C and this can be attributed to the effect of the DOS plasticizer. The Tg of HTPB polymer itself was -81.3°C as stated in Section 2.3.4, Table 37. No further information was available from other authors with which to compare the Tg of the HTPE binder or gumstock manufactured in this work.

3.3.3.3 Binder network thermal decomposition analysis, discussion of results

The DSC thermograms for the binder network samples 16N27B and 19N27B in the temperature range 30 to 600˚C are shown in Figure 80 and Figure 81 respectively. Figure 82 shows the DSC thermograms for HTPB binder network sample 1NHTPB. Table 67 shows the summary of DSC thermal decomposition information from the thermograms presented in Figure 80 and Figure 81 and for the HTPB binder sample thermogram presented in Figure 82.

DSC thermal decomposition traces in Figure 80A and Figure 80B show similar behaviour for samples 16N27B and 19N27B. In fact, in almost all HTPE samples there is a clear endothermic peak between 205 and 270˚C. This endothermic peak was not present during pre-polymer thermal decomposition, as can be seen in the HTPE pre-polymer traces in Chapter II, Section 2.4.11. Also, if the energy associated with the binder network decomposition peak is correlated with the percentage of curing agent in the different samples, a relation can be found. Sample 16N27B with NCO/OH of 1.0 and sample 19N27B with NCO/OH of 0.7 are in a proportion of 59 and 41% and the ratio between the energy of the endothermic peaks is 68 to 32%, following a trend that is related to the amount of curing agent in the formulation. Therefore, the evidence suggests that the endothermic peak between 210 and 260˚C from the binder network samples is due to some sort of bond breaking in the molecular structure of the curing agent segment. In the HTPB binder network, according to Tingfa [1989] the event, as can be seen in Figure 82, is an exothermic one and is possibly due to reaction of the newly formed groups with the polybutadiene double bonds. FTIR spectroscopy was

performed in an attempt to understand this potential bond breaking and results and conclusions are presented in Section 3.5.1.

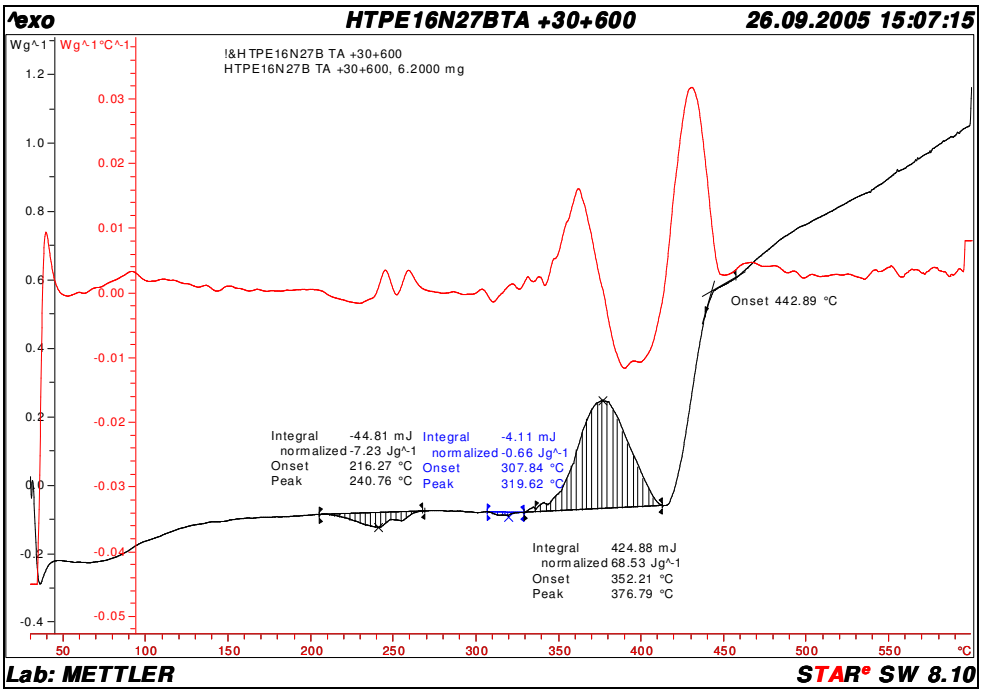

A

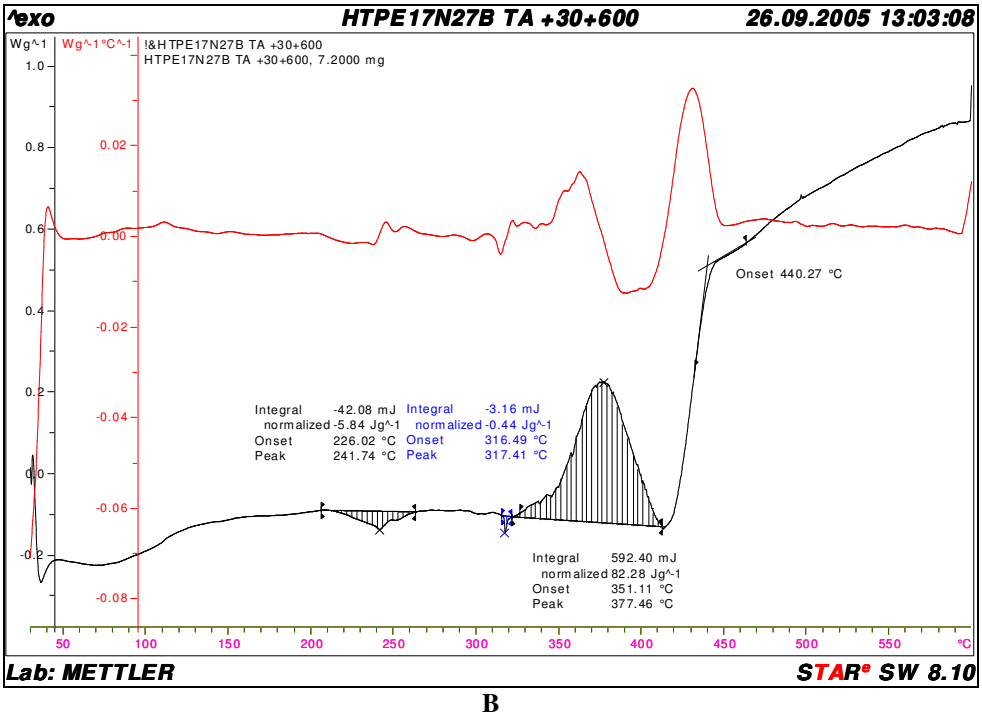

B

Figure 80. DSC thermogram of HTPE network, sample 16N27B (A) and sample 17N27B (B)

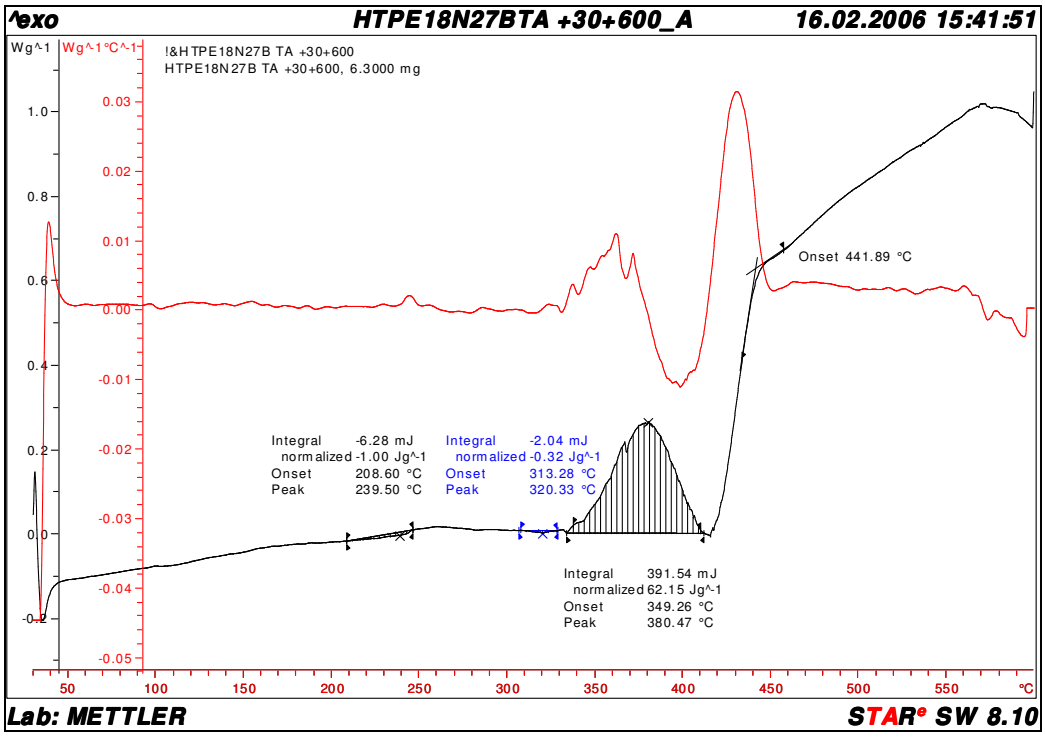

A

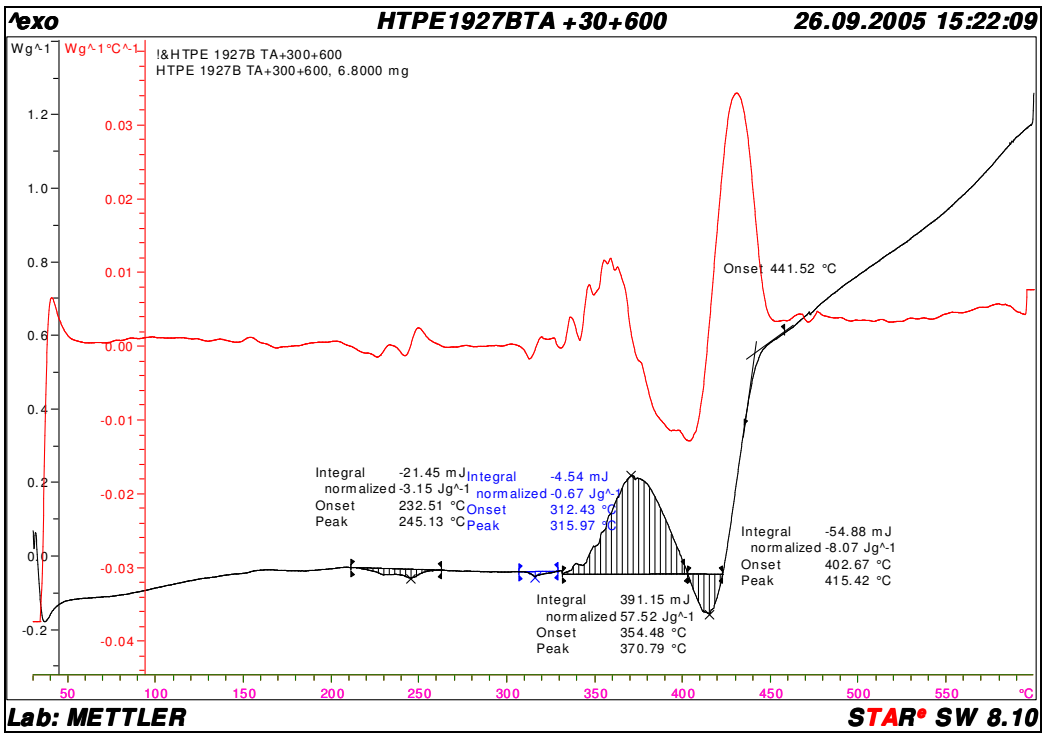

B

Figure 81. DSC thermogram of HTPE network, sample 18N27B (A) and sample 19N27B (B)

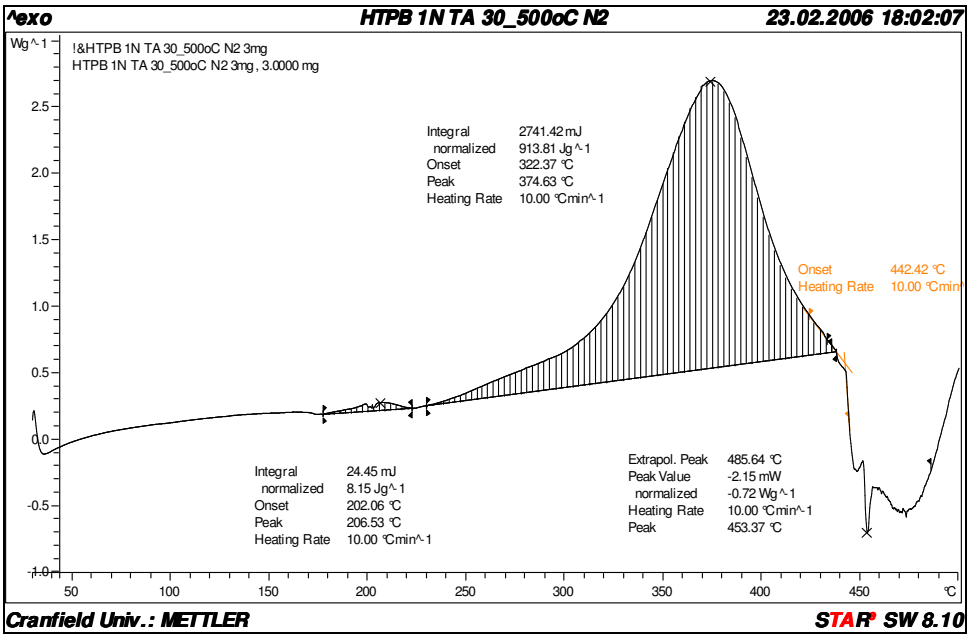

Figure 82. DSC thermogram of binder network sample 1NHTPB

Table 67. HTPE and HTPB Binder Network Results from DSC Analysis

Exp. No	NCO/OH ratio	1st Endothermic peak, (°C)	1st Exothermic peak, (°C)	Endothermicity of 1st peak, (J g^{-1})	Exothermicity of 1st peak, (J g^{-1})
16N27B	1.00	240.76	376.79	-7.2	69
17N27B	0.90	241.75	377.46	-5.8	82
18N27B	0.80	239.50	380.47	-1.0	62
19N27B	0.70	245.13/415.42	370.79	-3.2/-8.1	58
1NHTPB	0.87	456.95	201.72/375.24	-.-	2.30/803

An exothermic peak was observed in all the HTPE samples between the temperatures of 317 and 412˚C, the peak maximum being between 377 and 380˚C. Samples 19N27B and 18N27B also showed an endothermic peak just after the end of the exothermic peak; this was not very strong for the last sample. Possibly several events are taking place at the same time. During the curing agent thermal decomposition, between 340 and 416˚C, a sharp endothermic peak was observed and also, as can be seen in Figure 83, an endothermic peak was observed between 370 and 420˚C. Possibly the decomposition products of both curing agent and pre-polymer are reacting and new decomposition products are generating the exothermic peak that is observed in the same temperature range.

On the other hand, an exothermic peak at around 377°C can also be seen in the DSC of the HTPB binder network sample. In fact, as can be seen in Chapter II, Section 2.3.4

Figure 15 and Figure 16, the thermal behaviour of both uncured pre-polymers is completely different at around 377°C. While the HTPE pre-polymer shows an endothermic peak, the HTPB pre-polymer shows an exothermic peak which, according to Tingfa [1989], is primarily due to depolymerisation and new bond generation by cyclization and crosslinking reactions. The exothermicity was calculated by extending the baseline just before the DSC onset, is considerably lower in HTPE samples, 82 J g^{-1}, than in HTPB sample, 802 J g^{-1}. This is possibly due to the heat contribution from the reaction of the double bonds in HTPB.

Figure 83 shows the DSC thermogram for a sample of the curing agent Desmodur N-3200.

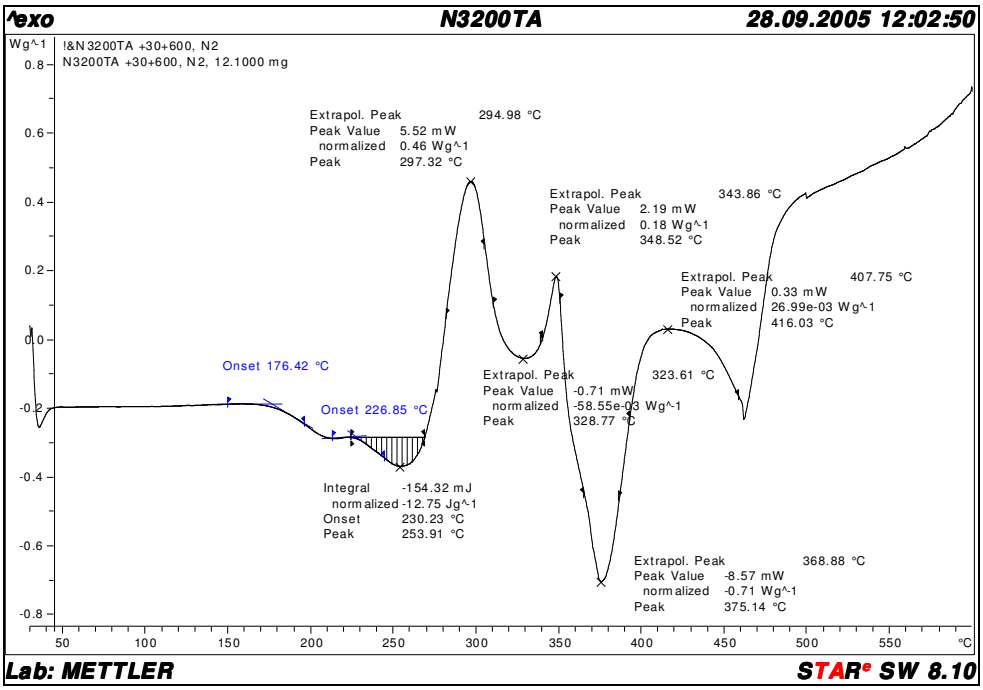

Figure 83. DSC thermogram of Desmodur N-3200

3.3.3.4 Gumstock thermal decomposition analysis and discussion of results

The DSC thermogram for HTPE and HTPB gumstock samples 5G27B and 3GHTPB are presented in Figure 84 and Figure 86 respectively. Table 68 shows the summary of DSC thermal decomposition data from the thermograms presented in Figure 84 and Figure 86.

Table 68. HTPE and HTPB Gumstock DSC Thermal Decomposition Data

Exp. N°	NCO/OH ratio	Endothermic Peak at, (˚C)	Exothermic Peak at, (˚C)	Endothermic Heat, (J g^{-1})	Exothermic Heat, (J g^{-1})
5G27B	0.88	-.-	202 / 277	-.-	1100 / 150
n-BuNENA	-.-	-.-	117/210	-.-	59/1110
3GHTPB	0.87	463	208 / 378	-21	10/ 760

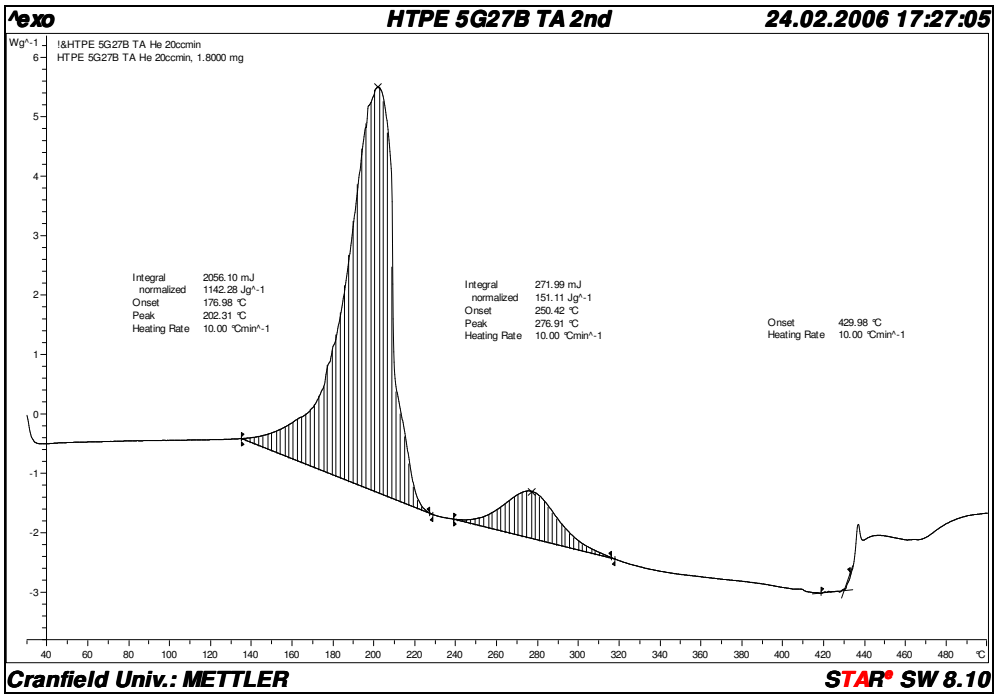

Figure 84. DSC thermogram of HTPE gumstock sample 5G27B

When a plasticizer, either energetic i.e. n-BuNENA, or inert i.e. DOS, was added to the binder network formulations the thermal behaviour changed. This is true particularly for HTPE samples. In HTPE gumstock sample 5GE27, as can be seen from Figure 84, a first exothermic peak can be seen at 202°C. In comparison with the binder network samples, the onset of the thermal decomposition was greatly affected by the presence of the energetic plasticizer.

In the HTPE gumstock the onset of the exothermic reaction occurred at around 139°C, whereas in the binder network sample, as presented in the previous section, no thermal events occur before the endothermic peak at around 202°C; the first exothermic reaction onset is at around 352°C. This first exothermic peak can be assigned to the thermal decomposition of the energetic plasticizer n-BuNENA. In fact, as can be seen from the

pure n-BuNENA thermogram in Figure 85, its decomposition peak is present at 210°C, having the onset of the reaction at around 160°C. Therefore, the interaction between the binder and the plasticizer is also leading to n-BuNENA decomposition at a lower temperature.

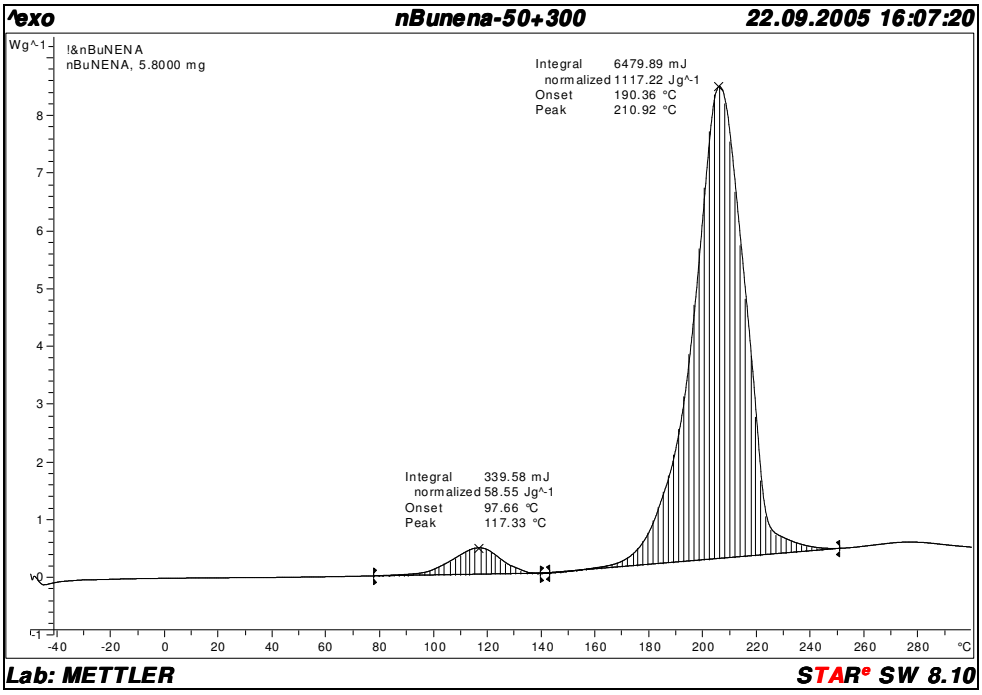

Figure 85. n-BuNENA DSC thermogram

A second exothermic peak is apparent at 276.9°C in the HTPE gumstock thermogram. In the HTPE binder network samples, exothermic reactions were not observed around 276°C but at 373°C. Therefore, it is possible that the decomposition products of the energetic plasticizer, which will probably include nitrogen oxides, may be reacting with the urea or biuret groups present in the hard segment and catalysing the thermal decomposition.

HTPB gumstock thermal decomposition is similar to that of the binder network. However in the gumstock the first and second exothermic peaks are delayed by approximately 4°C as can see in Figure 86. This suggests that the DOS plasticizer in the HTPB gumstock is delaying the onset of the exothermic reaction in contrast with n-BuNENA, which is catalysing an early decomposition process.

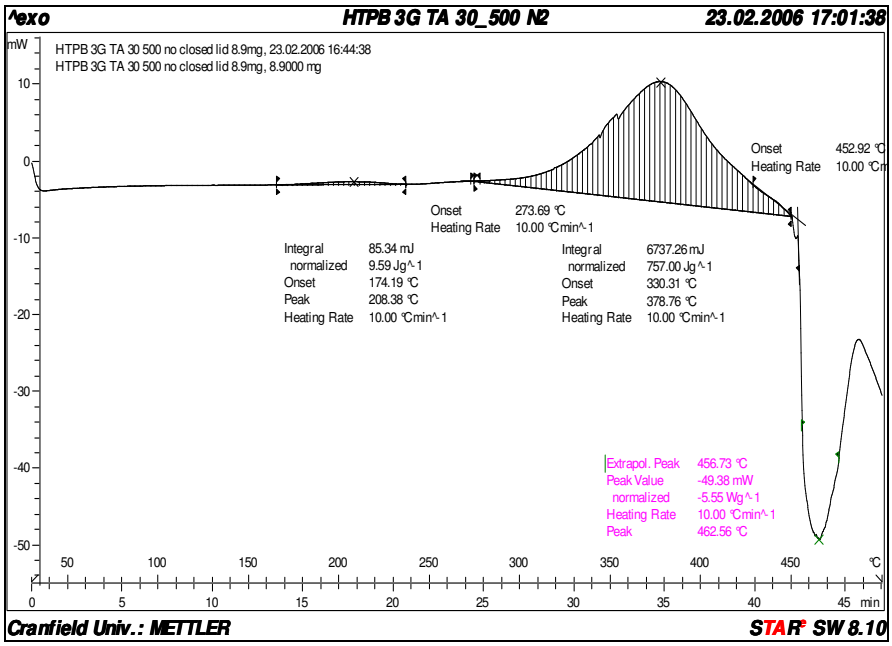

Figure 86. DSC thermogram of gumstock sample 3GHTPB

3.3.3.5 DSC Analysis: conclusions

Samples of HTPE binder network cured with Desmodur N-3200 at different NCO/OH equivalence ratios behave in a similar way in terms of Tg. However, peaks for the microcrystallisation process and melting point disappear when the NCO/OH equivalence ratio is equal to one. On the other hand, the addition of the energetic plasticizer, n-BuNENA, appears to affect the gumstock by increasing slightly the glass transition temperature but at the same time eliminating the micro crystallization effect. It was also found that the Tg of HTPB is lower than that of the HTPE gumstock. Apparently, during thermal decomposition of either the HTPE or HTPB binder network cured by Desmodur N-3200, the first decomposition process is due to the curing agent. However, when the energetic plasticizer is added to the HTPE composition the overall thermal decomposition is apparently controlled by the n-BuNENA.

3.3.4 TGA analyses

Thermogravimetric analyses were performed on binder network and gumstock samples made from the pre-polymer HTPE27B cured with Desmodur N-3200. TGA analyses

were performed in a similar way to that described in Section 2.3.4 for the pre-polymer. "STARe, version 8.1x for Windows® 2000 and Windows® XP from METTLER TOLEDO", was use to analyze the data. Sample weights were 6 to 9 mg. Samples were placed in a ceramic crucible closed with a pinhole lid and heated at a rate of 10˚C per min from 40 to + 600˚C. An inert environment was created by adding nitrogen gas during all the analyses at a flow rate of 10 cm^3 per min.

3.3.4.1 Binder network TGA analysis and results

Thermogravimetric analysis for binder network samples 16N27B and 19N27B are shown in Figure 87 and Figure 88 respectively. The TGA traces indicate that two rates of constant weight loss can be seen in HTPE binder networks. This can be better appreciated in 16N27B, the sample that has the highest curing agent content; in Figure 87 A, the first derivative curve shows two rates of weight loss. In fact, for the first weight loss, the onset is around 200˚C and the highest rate is reached at around 300˚C. The second rate of weight loss onsets at around 310˚C and the highest rate is reached at around 395˚C. Both rates of weight loss can be related to the endothermic and exothermic peaks observed during the thermal decomposition analysis at around 240 and 370˚C. The two step weight losses are easily seen from the first derivative. The step associated with weight loss was determined in each sample by defining a step from the first derivative curve and then projecting it onto the thermogravimetric curve. The weight loss at that temperature was read from the Y axis of the TGA thermogram. The temperature and the percentage weight loss are stated in Table 69.

Table 69. Thermal Gravimetric Analysis, Weight Loss vs. Temperature

Sample name	Initial Temp. (°C)	Onset Temp. (°C)	Temp. at slope Change (°C)	Weight loss (%)	End set Temp. (°C)	Weight loss at end set (%)
HTPE 27B	100	178	-.-	-.-	382	99.7
16N27B	40	171	312	13.18	416	91.35
17N27B	40	194	300	14.84	419	97.15
18N27B	40	156	295	10.71	425	97.37
19N27B	40	200	293	16.58	420	99.35
1NHTPB	40	222	426	15.79	486	100.00

As can be seen, the slope changes according to the amount of hard segment present in the binder network. In fact the higher the curing agent content, the higher the

temperature for the weight loss slope change. These results are in agreement with those of Gupta [2003], from studies of the thermal degradation of HTPB cured with TDI. They suggested that, possibly due to the polyurethane matrix, a higher temperature is required to release the volatile fragments of the decomposed pre-polymer.

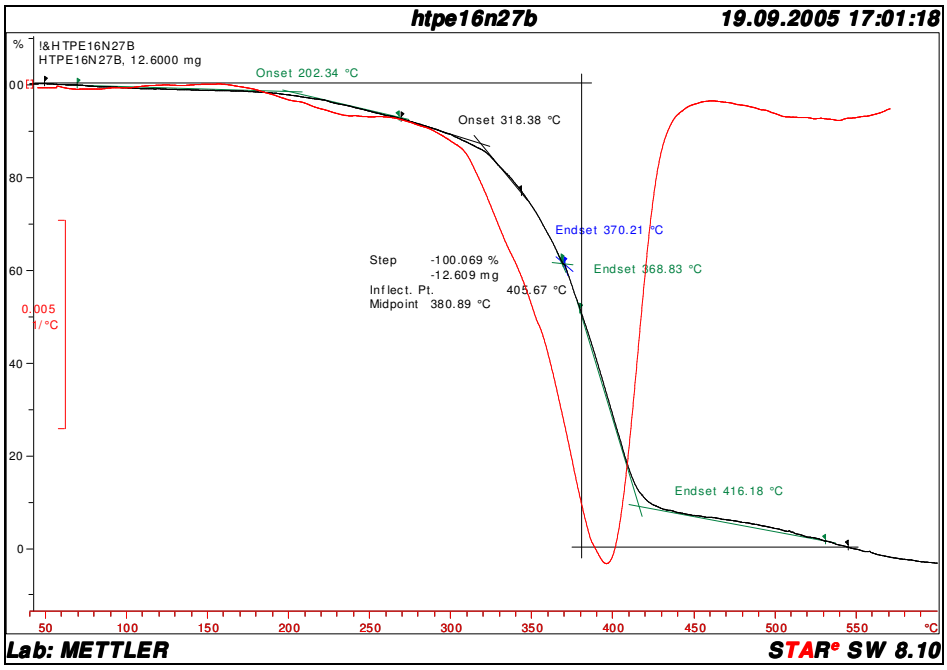

A

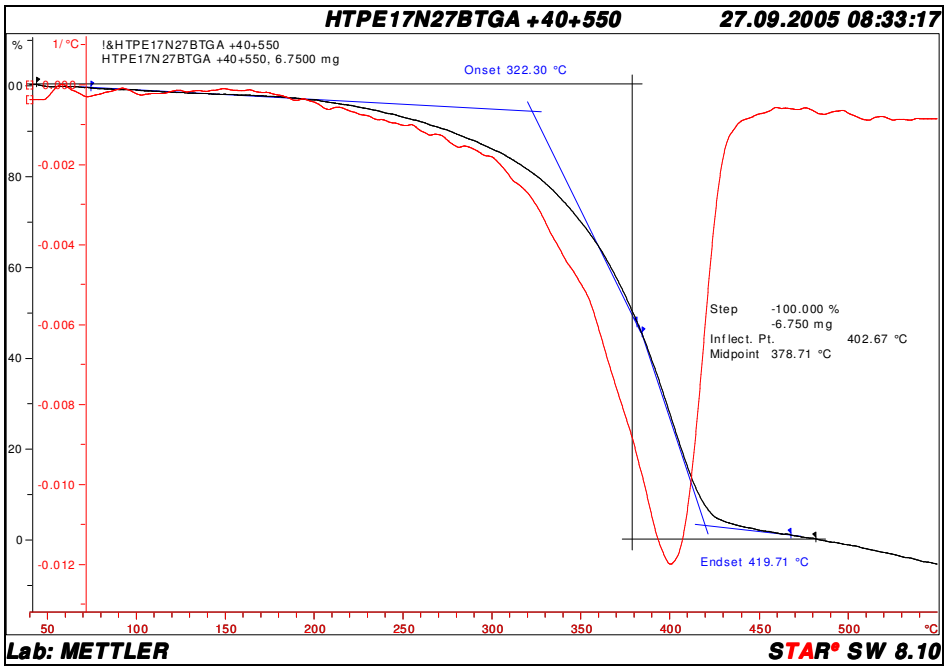

B

Figure 87. TGA thermograms of HTPE binder network sample 16N27B (A) and sample 17N27B (B)

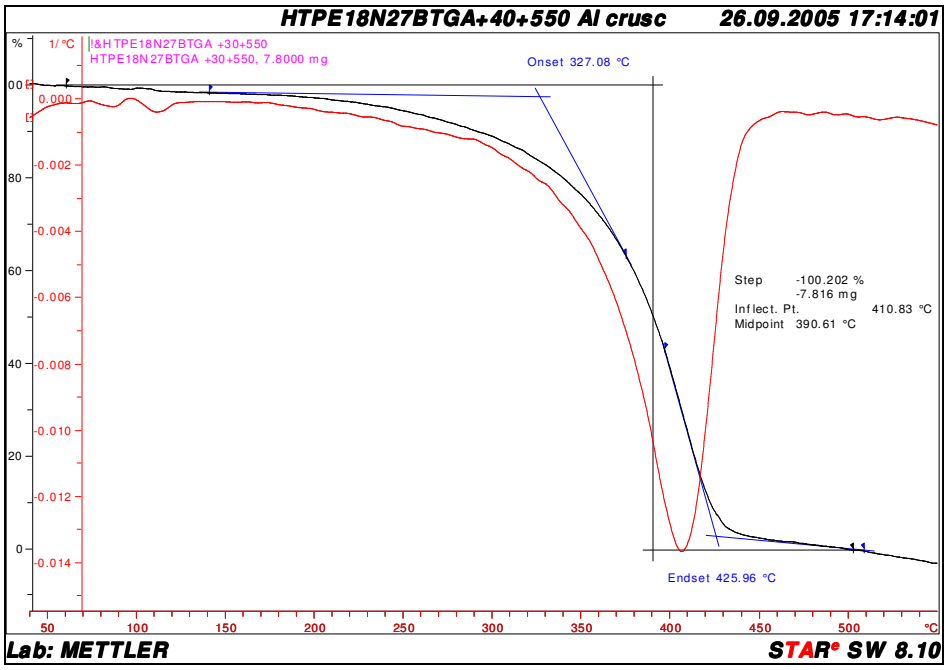

A

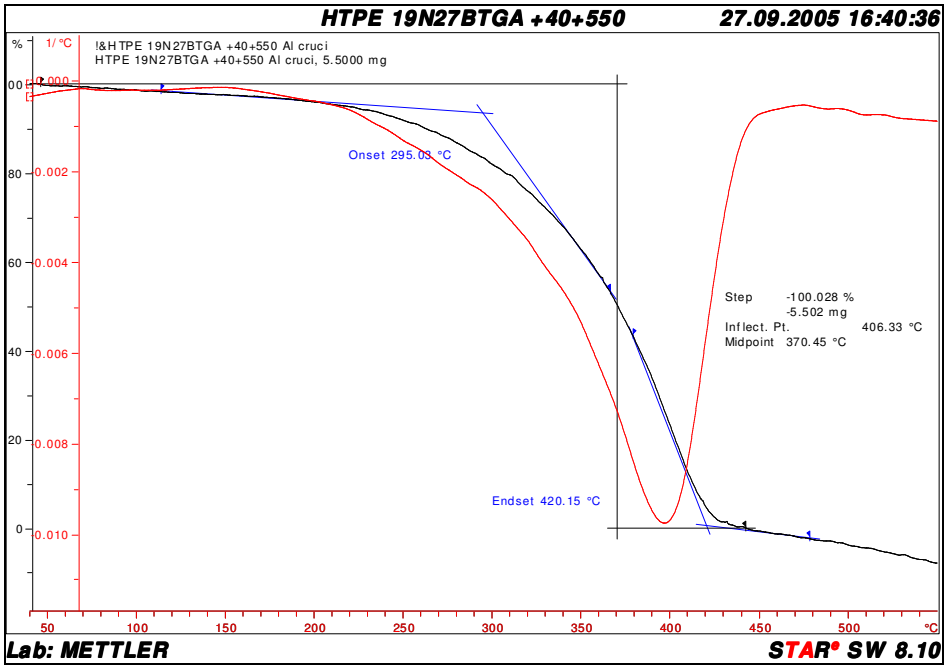

B

Figure 88. TGA thermograms of HTPE binder network sample 18N27B (A) and sample 19N27B (B)

When comparing binder network samples with the pre-polymer itself, the effect of the curing agent and the cross links can be observed. In fact, for the HTPE pre-polymer, the onset temperature is higher than in sample 16N27B and 18N27B. There is not a second slope and the end set temperature is almost 30°C lower than for the binder network samples. It can be suggested that the weight loss is inversely proportional to the hard

segment content; in other words, the lower the hard segment content the higher the weight loss at the first stage. This is also reflected in the weight loss percentage at the end set. The end set was estimated by projecting both TGA lines and taking the intercept as the end set. As can be seen from Table 69, the amount of residual weight at the end set is proportional to the curing agent content for very similar end set temperatures.

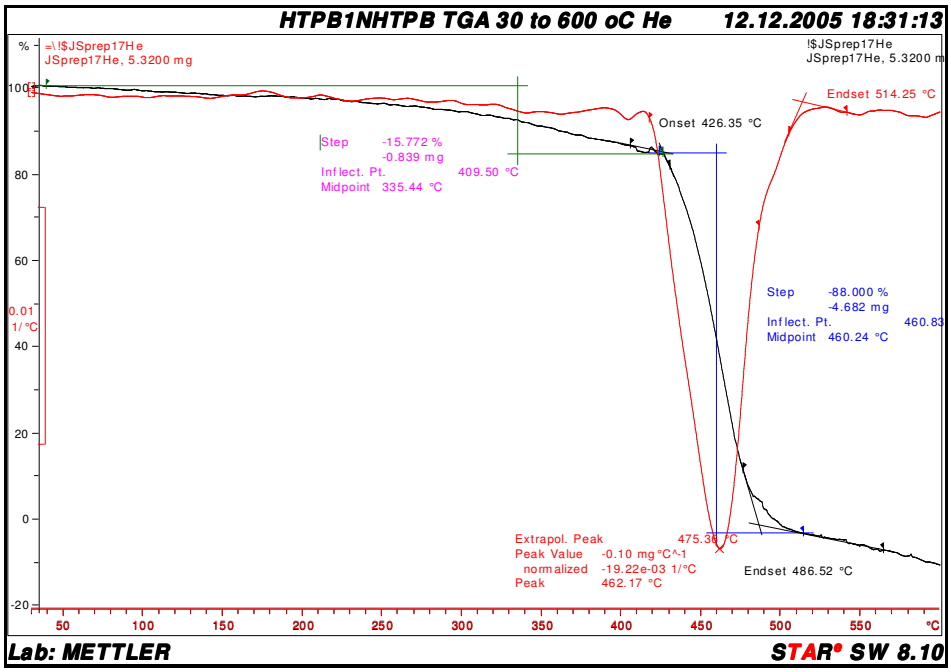

Figure 89. TGA thermogram of sample 1N HTPB

When the thermogravimetric behaviour of the HTPE binder network is compared with that of HTPB, two differences (as in the pre-polymers) can be observed: the onset decomposition temperature and the curve gradient, as can be seen from Figure 90.

First, the onset weight loss temperature is considerably lower for the HTPE binder network than for HTPB, there being a ΔT between onsets of around 126˚C for the main step and around 28˚C for the first step. Secondly, the curve gradient for HTPB shows a more marked difference between the various weight loss rates, which is consistent with that found by Gupta [2003]. In fact, while three stages around 222, 280 and 426˚C can be observed in the HTPB TGA thermogram, HTPE samples shows two relatively smooth rates of weight loss at around 194 and 300˚C.

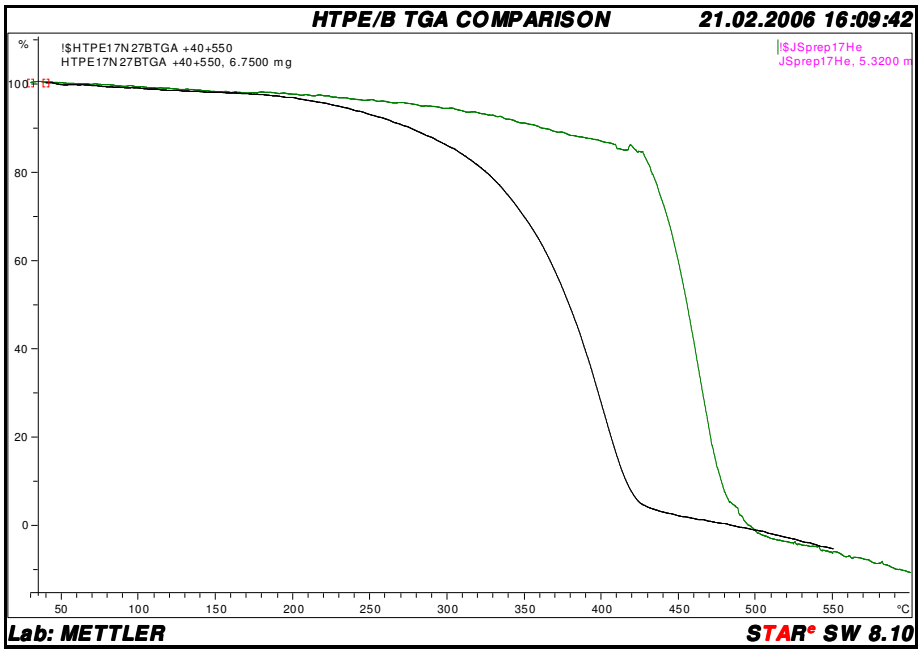

Figure 90. TGA results for HTPE 17N27B (black) and 1N HTPB (green)

3.3.4.2 Gumstock TGA analysis and discussion of results

Thermo gravimetric analysis for gumstock samples HTPE 5G27B (7.1mg) and HTPB 3G (5.09mg), are presented in Figure 91 and Figure 92 respectively.

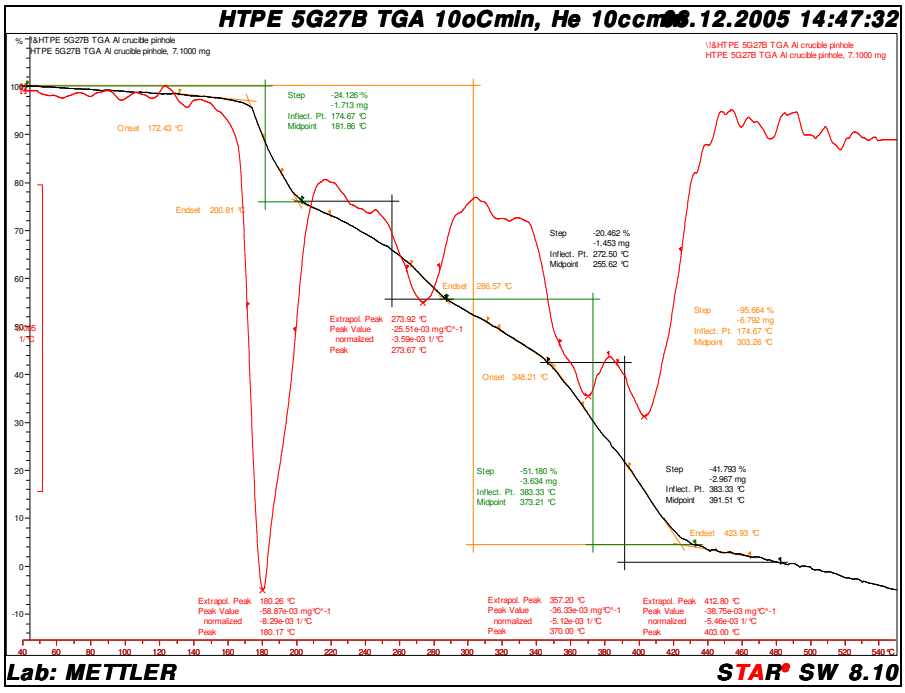

Figure 91. TGA thermogram of HTPE gumstock, sample 5G27B

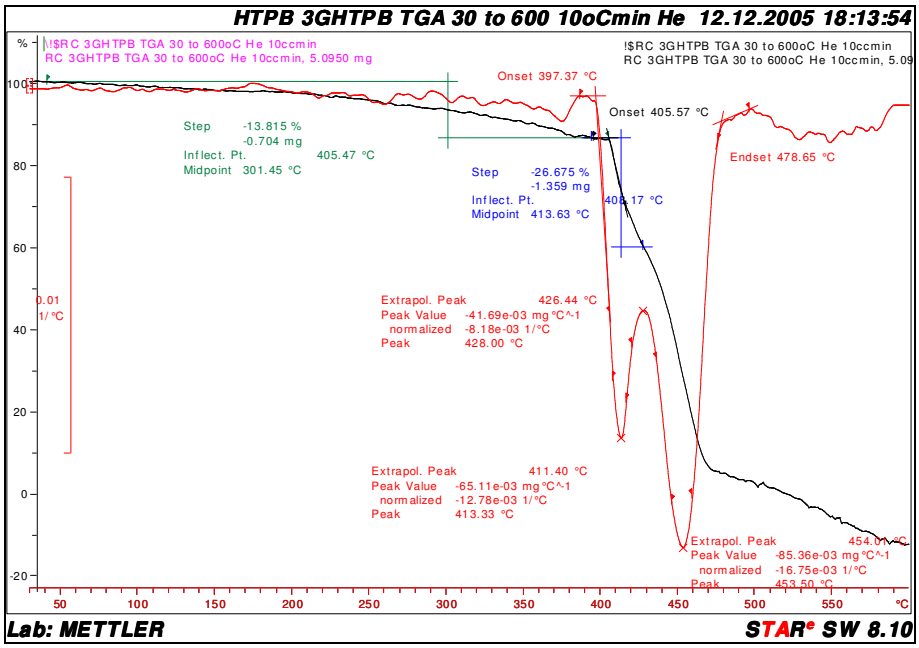

Figure 92. TGA thermogram of HTPB gumstock, sample 3G.

Table 70 shows the summary of DSC TGA data from the thermograms presented in Figure 91 and Figure 92.

Table 70. HTPE and HTPB Gumstock DSC Thermal Gravimetric Data

Sample name	Initial Temp. °C	On Set Temp. °C	Temp. at Slope Change, °C	Weight lost %	End Set Temp. °C	Weight lost at End Set %
HTPE 27B	100	178	-.-	-.-	382	99.7
17N27B	40	194	300	14.84	419	97.2
5G27B	40	172	200.8/ 286.6	24.1/ 44.6	423.9	95.7
1NHTPB	40	222	426.4	15.8	486	99.5
3GHTPB	40	224	405.5/ 436.8	13.8/ 47.2	467.9	94.6

As can be seen from Figure 91, the HTPE gumstock TGA traces show a non-constant rate of weight loss in comparison with the pre-polymer or the binder network, as can be appreciated from Figure 93. The onset temperature is similar to that of the pre-polymer sample being around 172°C. However, above that temperature the different ingredients in the gumstock appear to be affecting the pattern of the weight loss.

In fact, this can be seen from the first derivative curve in the thermo gravimetric analysis trace shown in Figure 91. The first stage of weight loss is between 160 and 215°C, having the maximum rate of weight loss at 180°C, with 24% weight loss. The second stage is between 215 and 290°C, having the maximum rate of weight loss at

274°C, with 20% weight loss. Finally the last stage of weight loss is between 290 and 450°C, where two steps can be appreciated; the maximum rate of weight loss was at 370 and 403°C and there was a total of 51% weight loss.

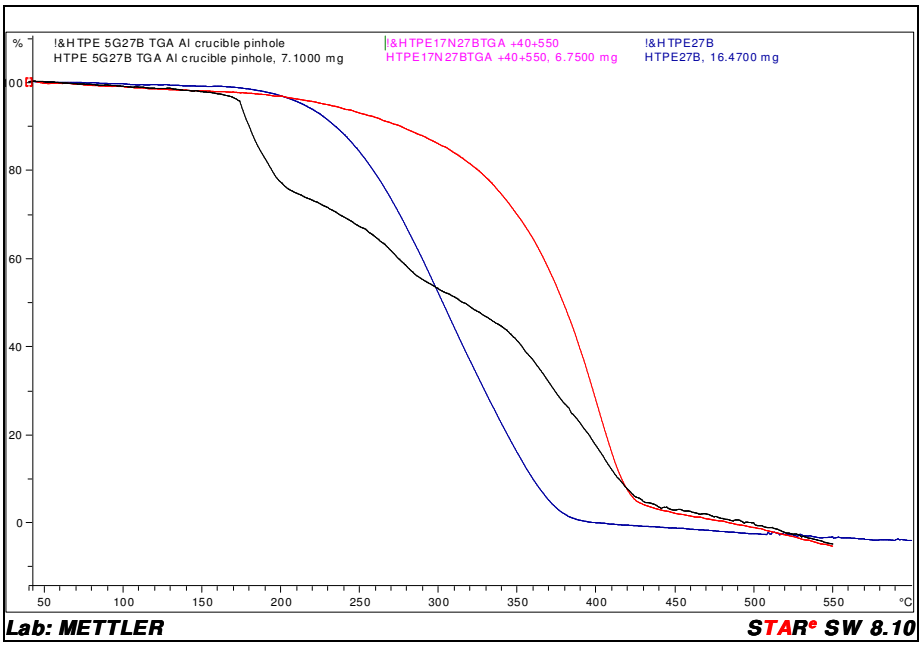

Figure 93. TGA thermogram of HTPE gumstock (black), binder network (red) and pre-polymer (blue).

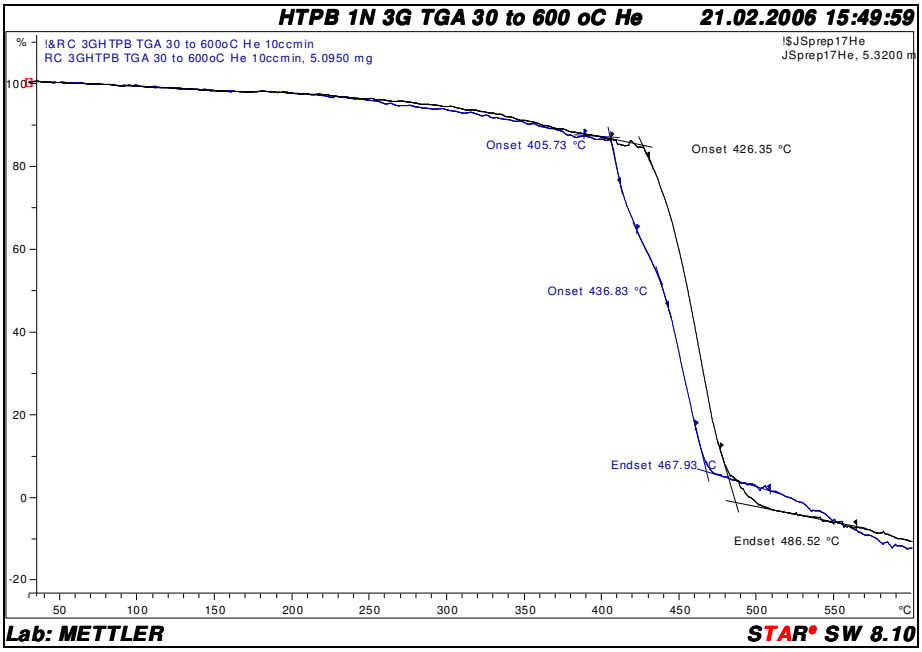

Figure 94. TGA thermogram of HTPB gumstock, (blue), binder network (black).

The first stage of weight loss is strongly affected by the energetic plasticizer thermal decomposition. In fact, as can be seen from the derivative TGA curve in Figure 91, the onset and end set of the weight loss have a good match with the gumstock DSC thermal decomposition curve in Figure 80 A, where there is a strong exothermic peak at 202^{o}C with an onset at around 150^{o}C. This exothermic peak is also present in the n-BuNENA DSC analysis. On the other hand, there is no sign of thermal decomposition at this temperature for the binder network, as can be seen in Figure 93. The second stage of weight loss is apparently affected by the hard segment decomposition, but also by the effect of the energetic plasticizer thermal decomposition products. In fact, as can be seen from the TA curve in Figure 80 A, the onset and end set of the second exothermic peak have a good match with the gumstock weight loss in TGA analysis, where there is a strong exothermic peak at 202^{o}C with an onset at around 150^{o}C. The third stage of weight loss appears to be affected mainly by the thermal decomposition of the soft and hard segments formed by the pre-polymer and the curing agent. In fact, as can be seen from Figure 80 B, in relation to binder network thermal decomposition for sample 17N27B, there is a strong exothermic peak at 377^{o}C, the onset and end set being at around 320 and 425^{o}C. There is therefore a good match with the first derivative weight loss peaks at 370 and 403^{o}C in Figure 91.

When the behaviour of HTPE gumstock is compared with that of HTPB, two differences, as in the pre-polymer and binder network condition, can be appreciated from TGA analysis: the onset decomposition temperature and the curve gradient, as shown in Figure 91 and Figure 92 and in the overlayed TGA curves in Figure 94. Firstly, the onset weight loss temperature is considerably lower for HTPE gumstock than for HTPB, there being a ΔT between onsets of around 233˚C for the main step and around 50˚C for the first step. Because of the effect of the DOS in HTPB gumstock the weight loss main step decreased by 20^{o}C in comparison with the HTPB binder network. Secondly, because of the effect of the energetic plasticizer in HTPE gumstock, the curve shape is different. The first derivative curve for HTPE, shows a smoother but irregular weight loss behaviour than HTPB. Despite that, still the weight loss over a given temperature range is much higher for HTPB samples. They lost almost 95% of their

weight in a ΔT of 62°C, in comparison with a 97% loss in a ΔT of 251°C for the HTPE samples.

3.3.4.3 TGA analysis: conclusions

TGA analysis suggests that there is similarity between binder network and gumstock weight loss processes. However, the energetic plasticizer is playing an important role in the thermal decomposition. From the DTA it can be suggested that a first weight loss stage in the HTPE gumstock is due to the presence of n-BuNENA decomposition products. A second stage of weight loss was observed and, as in the binder network, it is suggested that this is due to the hard segment decomposition. Finally a third and last stage of weight loss would correspond to the soft segment decomposition together with that of the remaining hard segment, possibly interacting also with the decomposition products of the hard segment. When HTPE binder network and gumstock TGA behaviour is compared with that of HTPB two relevant differences were found: the weight loss in HTPE binder and gumstock begins at a much lower temperature than in HTPB i.e. 172 and 405°C respectively, and the weight loss gradient is higher in HTPB than in HTPE; the former losing almost all its mass in a quarter of the HTPE ΔT gradient.

3.3.5 Activation energy, Ea, determinations

In order to calculate the activation energy for decomposition of the different gumstock and binder network samples Ozawa's method [Ozawa, 1970] as used by Matei [2002] was adopted. The methodology consists of obtaining the Ea by plotting the logarithm of the heating rate versus the reciprocal peak temperature, according to the Arrhenius Equation in 3.3.

$$k = Ae^{\frac{-Ea}{RT}} \tag{3.3}$$

From the Arrhenius equation, Ea is the activation energy for decomposition, ***T*** the peak temperature in K, ***R*** the gas constant [J K^{-1} mol^{-1}] and ***A*** the pre-exponential factor. According to Ozawa [1970] the logarithm of the heating rate is linearly related the reciprocal peak temperature, thus Ea can be obtained from the slope of the resultant curve. In order to determine the activation energy of the HTPE gumstock and binder network samples, DSC analysis at different heating rates was performed using DSC equipment as explained in Section 2.3.4. A lid with a pinhole was used and nitrogen gas was introduced in order to have an inert environment. Ea determinations were made from heating rates of 5, 10, 20, 30 and 40^{o}C per min over a temperature range of 25 to +330^{o}C for HTPE gumstock and from 25 to +450^{o}C for HTPE binder network sample. In all cases the decomposition peaks were made to fall within the temperature range.

3.3.5.1 HTPE binder network Ea analysis and results

Figure 95 shows the overlayed DSC thermograms for binder network sample HTPE 17N27B, at a heating rate of: 5 (black), 10 (blue), 20 (red), 30 (green) and 40^{o}C min^{-1} (purple).

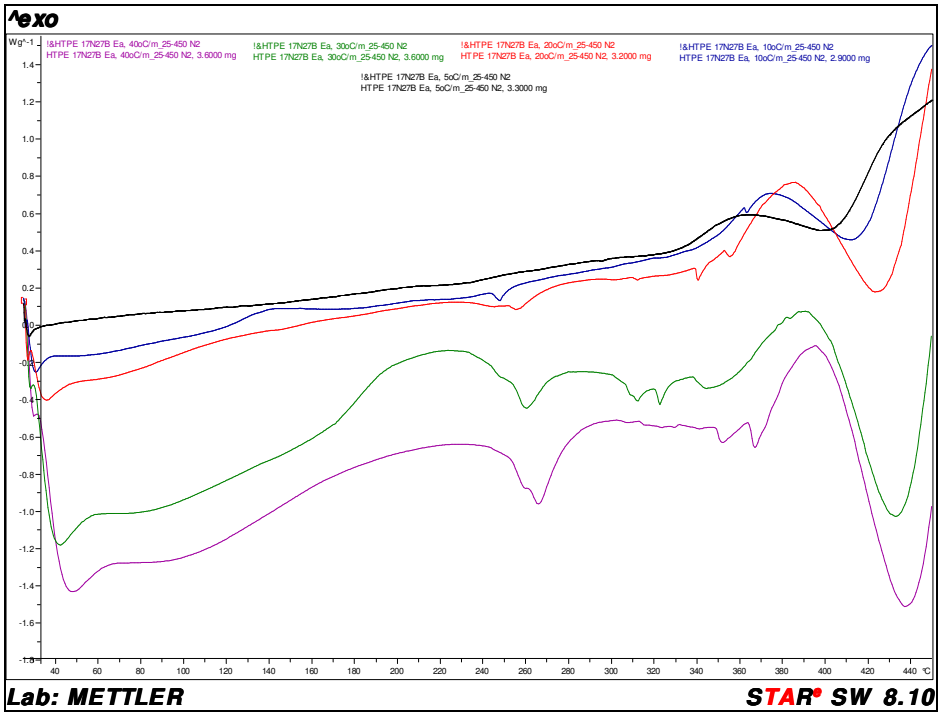

Figure 95. DSC thermograms of HTPE binder network sample 17N27B.

Table 71 shows the summary of DSC thermogram data obtained from Figure 95 for the 1st endothermic peak and the 1st exothermic peak and the parameters used to plot the logarithm of the heating rate versus the reciprocal peak temperature. This information was used to obtain the slope Ea/R and the pre exponential factor A, as presented in Figure 96.

Table 71. HTPE Binder Network DSC Ea Analysis

Heating rate, β (˚C min^{-1})	Sample weight, (mg)	1st Endo. peak , Tp_1 (˚C)	1st Exot. peak , Tp_2 (˚C)	Ln(β), (˚C min^{-1})	$1/Tp_1$, (K)	$1/Tp_2$, (K)
5	3.3	225	-.-	1.60943	0.002008	0.00366
10	2.9	248	375	2.30258	0.001919	0.00154
20	3.2	255	386	2.99573	0.001893	0.00152
30	3.6	260	391	3.40119	0.001876	0.00151
40	3.6	265	396	3.68887	0.001857	0.00149

In order to calculate the activation energy Ea_1 for the first endothermic peak, assuming a first order reaction, the slope of the curve in Figure 96 is determined as Ea/R= 22624 K Thus taking into account the gas constant R as 8.3143 J K^{-1} mol^{-1}, Ea_1 is equal to 188.10 kJ mol^{-1}, and from Ln*A* the pre-exponential factor *A* will be 1.3x10^{18} s^{-1}. Similarly for the first exothermic peak Ea_2 is 239.28 kJ mol^{-1} and the pre-exponential factor *A* is 3.2x10^{18}s^{-1}.

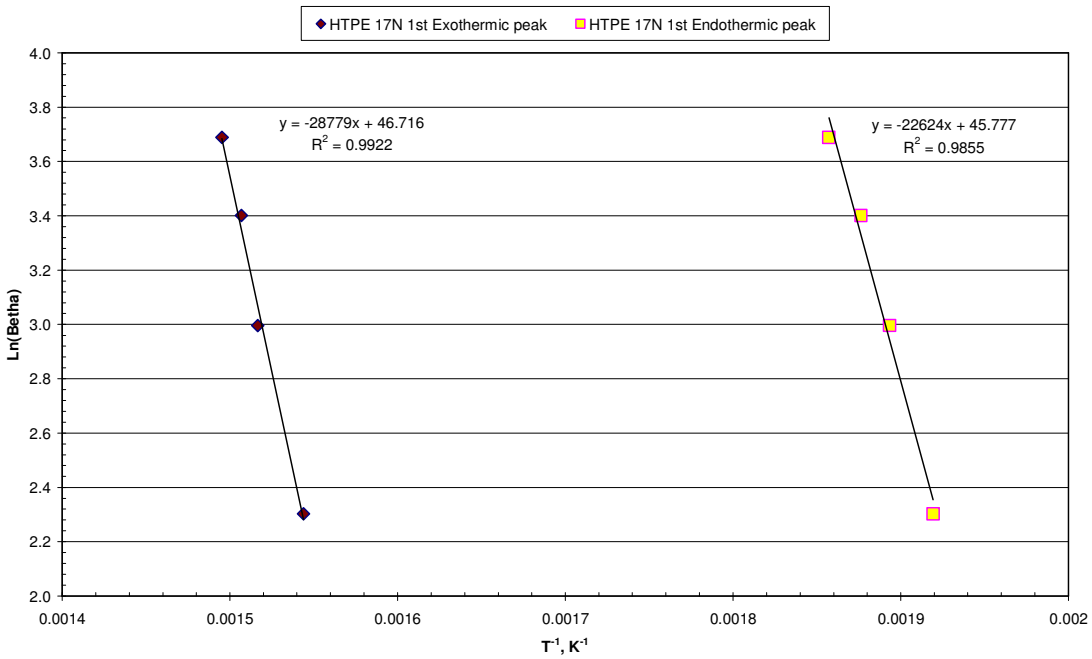

Figure 96. Arrhenius plot of Ln(β) versus $1/Tp_1$ and $1/Tp_2$ for HTPE binder network 17N27B.

3.3.5.2 HTPE gumstock Ea analysis and results

Figure 97 shows the overlayed DSC thermograms for gumstock sample HTPE 5G27B at a heating rate of: 5 (orange), 10 (brown), 20 (purple), 30 (blue) and 40°C min^{-1} (black). Table 72 shows the summary of DSC thermogram data obtained from Figure 97 for the 1st and 2nd exothermic peak and the parameters used to plot the logarithm of the heating rate versus the reciprocal peak temperature in order to obtain the slope Ea/R and the pre-exponential factor A, as presented in Figure 98 .

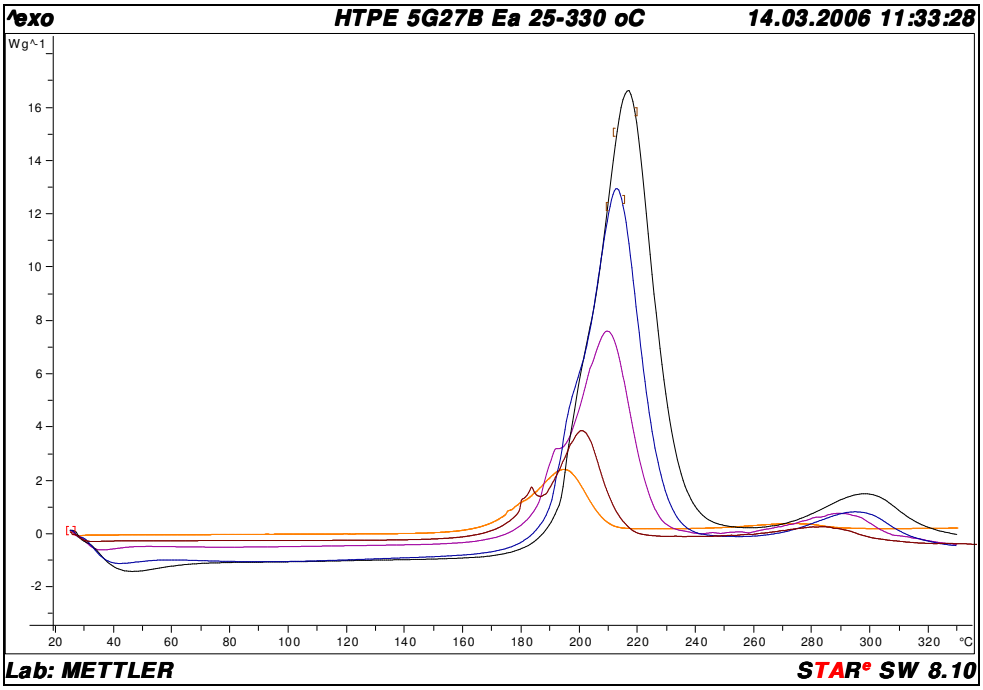

Figure 97. DSC thermograms of HTPE gumstock, sample 5G27B.

Table 72. HTPE Gumstock Results from DSC Ea Analysis

Heating rate, β (°C min^{-1})	Sample weight, (mg)	1st Exot. peak , Tp_2 (°C)	2nd Exot. peak , Tp_3 (°C)	Ln(β), (°C min^{-1})	$1/Tp_2$, (K)	$1/Tp_3$, (K)
5	6.6	194	273	1.609	0.00214	0.00183
10	12.7	203	285	2.302	0.00210	0.00179
20	6.0	210	289	2.995	0.00207	0.00178
30	5.7	213	296	3.401	0.00206	0.00176
40	4.6	217	298	3.688	0.00204	0.00175

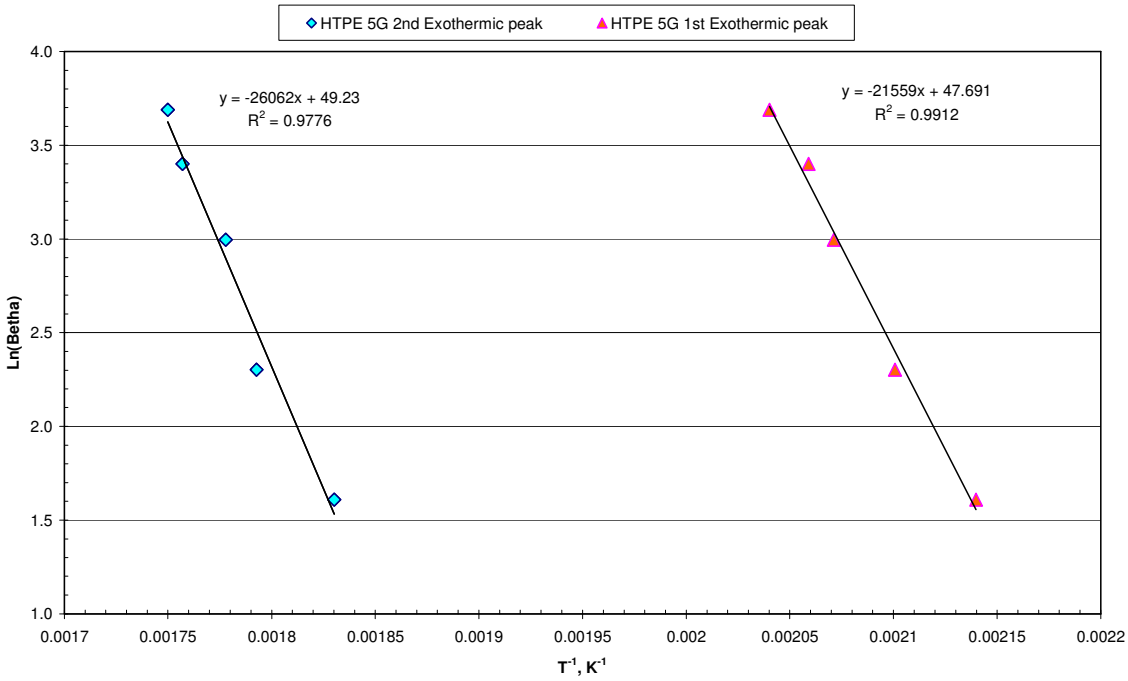

Figure 98. Arrhenius plot of Ln(β) versus $1/Tp_1$ and $1/Tp_2$ for HTPE gumstock 5G27B.

In order to calculate the activation energy Ea_2 for the first exothermic peak, the slope of the curve in Figure 98 is determined as Ea/R= 21559 K. Thus, taking into account the gases constant R as 8.3143 J K^{-1} mol^{-1}, Ea_2 is equal to 179.25 kJ mol^{-1}, and from Ln*A* the pre exponential factor *A* will be $8.6x10^{18}s^{-1}$. Similarly for the second exothermic peak Ea_3 is 216.69 kJ mol^{-1} and the pre exponential factor *A* is $4.0x10^{19}s^{-1}$.

3.3.5.3 HTPB binder network Ea analysis and results

Figure 99 shows the overlayed DSC curves for binder network sample HTPB 1N, at a heating rate of: 20 (green), 30 (blue), 40 (red) and 50°C min^{-1} (black). At a lower heating rate than 20°C min^{-1} it was not possible to distinguish clearly the first endothermic peak.

Table 73 shows the summary of DSC thermogram data obtained from Figure 99 for the 1st endothermic peak and the 1st exothermic peak and the parameters used to plot the logarithm of the heating rate versus the reciprocal peak temperature in order to obtain the slope Ea/R and the pre-exponential factor A, as presented in Figure 100.

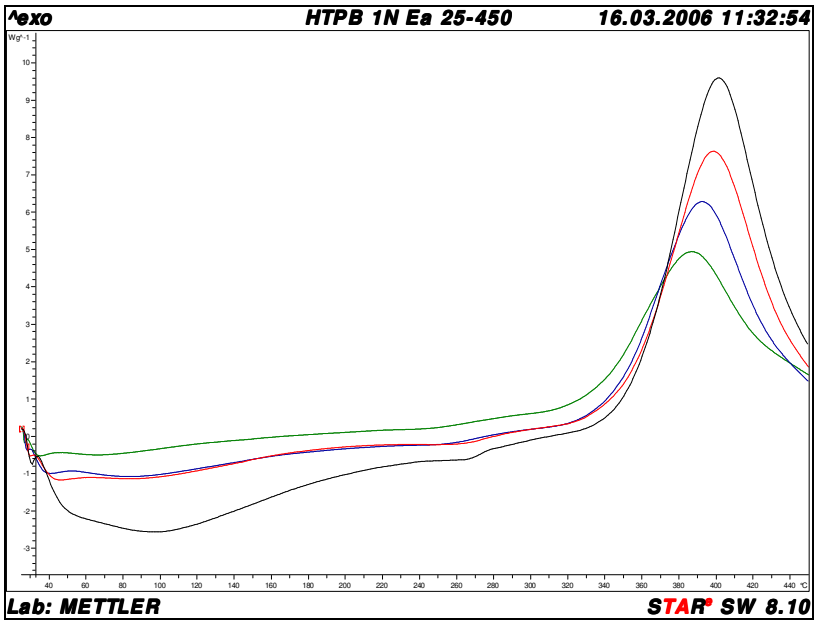

Figure 99. DSC thermograms of HTPB binder network sample 1N.

Table 73. HTPB Binder Network DSC Ea Analysis

Heating rate, β (˚C min^{-1})	Sample weight, (mg)	1st Endo. peak , Tp_1 (˚C)	1st Exot. peak , Tp_2 (˚C)	Ln(β), (˚C min^{-1})	$1/Tp_1$, (K)	$1/Tp_2$, (K)
20	2.1	248	388	2.99573	0.00192	0.001513
30	2.6	254	394	3.40119	0.00189	0.001499
40	2.7	262	401	3.68887	0.00187	0.001484
50	2.8	264	404	3.91202	0.00186	0.001477

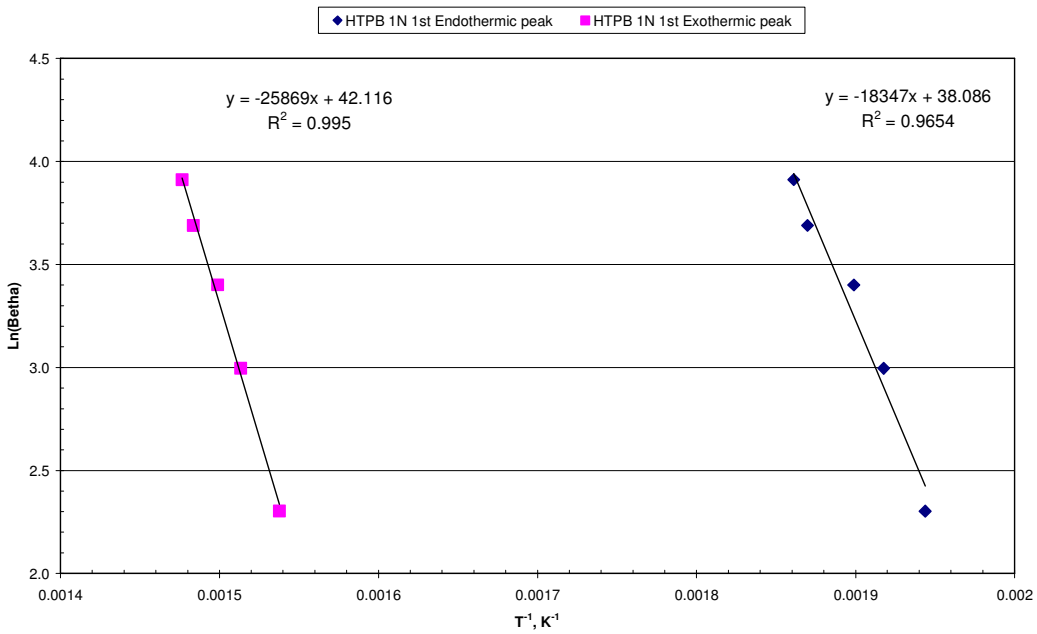

Figure 100. Arrhenius plot of Ln(β) versus $1/Tp_1$ and $1/Tp_2$ for HTPB binder network 1N.

In order to calculate the HTPB gumstock activation energy Ea_1 for the first endothermic peak, the slope of the curve in Figure 100 is determined as Ea/R= 18347 K. Thus taking into account the gas constant R as 8.3143 J K^{-1} mol^{-1}, Ea_1 is equal to 152.5 kJ mol^{-1}, and from Ln*A* the pre-exponential factor *A* will be $5.8x10^{14}s^{-1}$. Similarly, for the first exothermic peak Ea_2 is 215.08 kJ mol^{-1}, and the pre exponential factor *A* is $3.3x10^{16}s^{-1}$.

3.3.5.4 HTPB gumstock Ea analysis and results

Figure 101 shows the overlayed DSC curves for gumstock sample HTPB 3G, at a heating rate of: 20 (blue), 30 (red), 40 (black) and 50°C min^{-1} (green). At a lower heating rate than 20°C min^{-1} it was not possible to distinguish clearly the first endothermic peak.

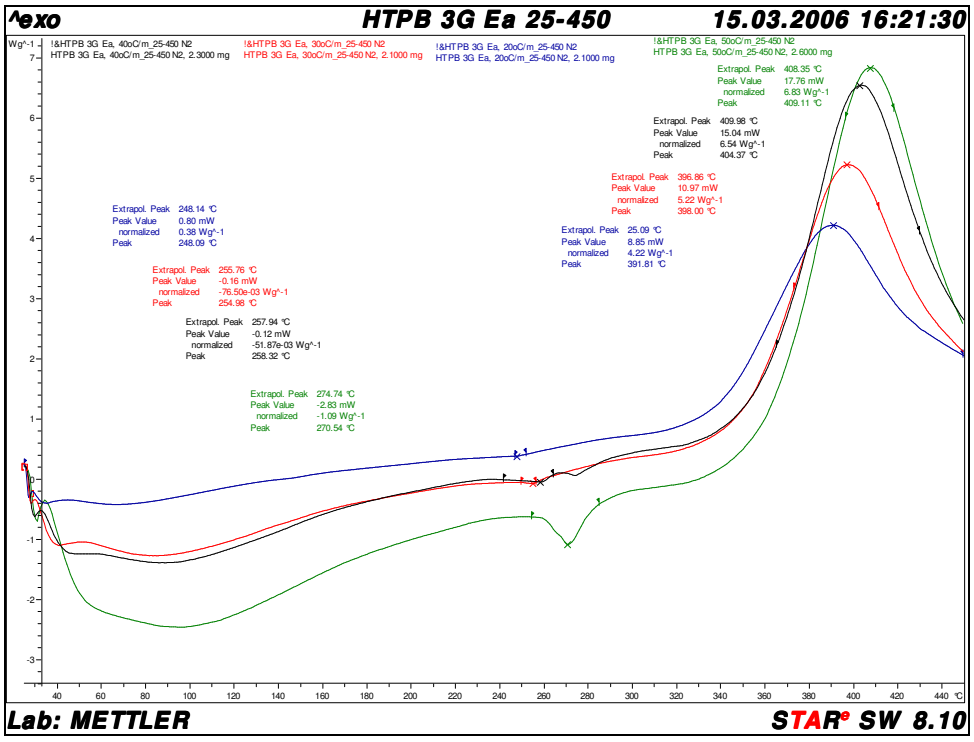

Figure 101. DSC thermograms of HTPB gumstock sample 3G.

Table 74 shows the summary of DSC thermogram data obtained from Figure 101 for the 1st endothermic peak and the 1st exothermic peak and the parameters used to plot the logarithm of the heating rate versus the reciprocal peak temperature in order to obtain the slope Ea/R and the pre-exponential factor A, as presented in Figure 102.

Table 74. HTPB Gumstock DSC Ea Analysis

Heating rate, β (˚C min^{-1})	Sample weight, (mg)	1st Endo. peak , Tp_1 (˚C)	1st Exot. peak , Tp_2 (˚C)	Ln(β), (˚C min^{-1})	$1/Tp_1$, (K)	$1/Tp_2$, (K)
20	2.1	248.00	391.00	2.99573	0.001919	0.00150
30	2.1	254.00	398.00	3.40119	0.001893	0.00149
40	2.3	258.00	404.00	3.68887	0.001882	0.00148
50	2.6	270.00	409.00	3.91202	0.001839	0.00147

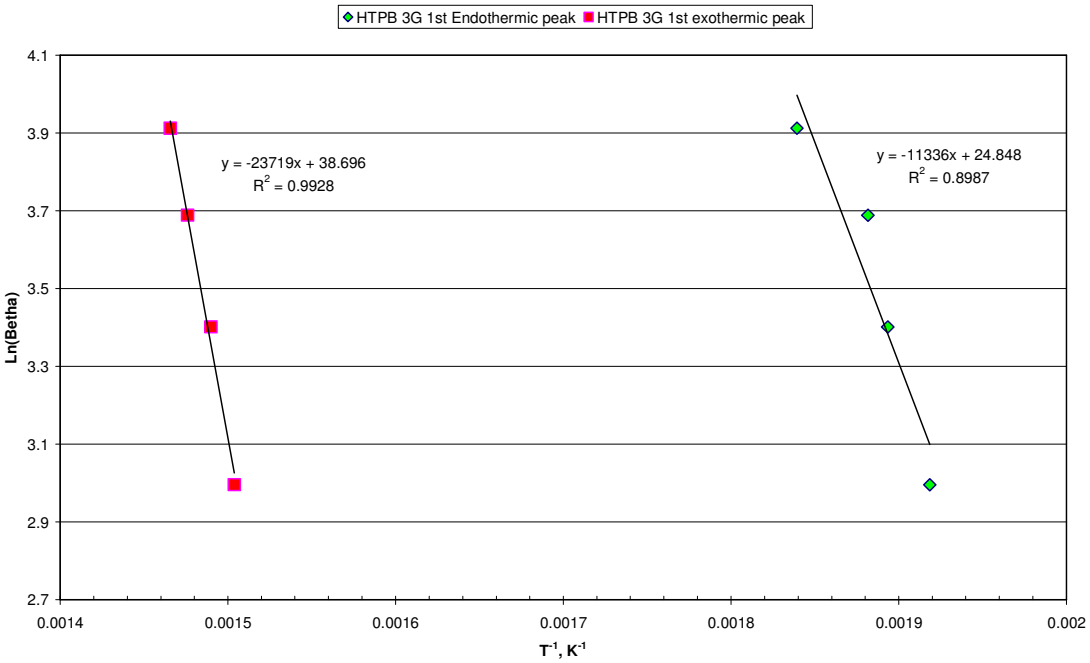

Figure 102. Arrhenius plot of Ln(β) versus $1/Tp_1$ and $1/Tp_2$ for HTPB gumstock 3G.

In order to calculate the HTPB gumstock activation energy Ea_1 for the first endothermic peak, the slope of the curve in Figure 102 is determined as Ea/R= 11336 K. Thus, taking into account the gas constant R as 8.3143 J K^{-1} mol^{-1}, Ea_1 is equal to 94.25 kJ mol^{-1}, and from Ln*A* the pre-exponential factor *A* will be 1.0x10^{9}s^{-1}. Similarly, for the first exothermic peak Ea_2 is 197.21 kJ mol^{-1}, and the pre exponential factor *A* is 1.1x10^{15}s^{-1}.

3.3.5.5 Gumstock Ea discussion of results

As stated previously, Ozawa's method was used for estimating the activation energy, **E**a, and the pre exponential factor, **A**, as kinetic parameters of the propellant thermal decomposition. The method is based on the linear relation between peak temperature and heating rate and also is called the isoconversional method [Rocco, 2004]. Although

several temperature peaks versus rate of heating from the HTPE and HTPB binder network and gumstock were plotted in order to compare the activation energies, only the first exothermic reaction i.e. first exothermic peaks, were taken into account to compare the HTPE propellant decomposition and that of HTPB.

A summary of the activation energy data obtained from the plots presented in Figure 96, Figure 98, Figure 100 and Figure 102 is shown in Table 75. Figure 103 shows the Arrhenius overplot of Ln(β) versus $1/Tp_1$ and $1/Tp_2$ for the different DSC peaks for the HTPE and HTPB binder network and gumstock samples.

Table 75. HTPE and HTPB Ea Summary

Ea for sample	1st Endot. peak Ea_1 (kJ mol^{-1})	1st Exot. peak Ea_2 (kJ mol^{-1})	2nd Exot. peak Ea_3 (kJ mol^{-1})
HTPE 17N27B	188	239	-.-
HTPE 5G27B	-.-	179	217
HTPB 1N	153	215	-.-
HTPB 3G	94	197	-.-

When comparing the Ea values from either binder network or gumstock HTPE samples, only the first exothermic peak is taken into account because it is considered to be representative of the overall thermal decomposition reaction. Therefore, from Table 75 it can be seen that the HTPE propellant gumstock, which contains n-BuNENA as energetic plasticizer, has a lower activation energy, Ea_2 than the HTPE binder network sample, which does not contain any plasticizer i.e. 179 and 239 kJ mol^{-1} respectively. Therefore, it can be stated that the energetic plasticizer, when incorporated into an HTPE binder, reduces the decomposition activation energy by around 25%. Similar behaviour can be seen in HTPB samples when an inert plasticizer is incorporated. In fact in this case Ea decreases by around 8%, which is lower than the effect of n-BuNENA on the HTPE. When comparing Ea_2 between HTPE and HTPB binder network and gumstock samples, from Table 75 it can be seen that the HTPE binder network has a higher Ea_2 than the HTPB binder network sample by around 10%. However, the HTPE gumstock sample 5G27B has a lower Ea_2 than the HTPB 3G by around 10%. Again, the presence of the energetic plasticizer n-BuNENA is thought to be driving the overall kinetics and causing the difference in decomposition behaviour between HTPB and HTPE gumstocks.

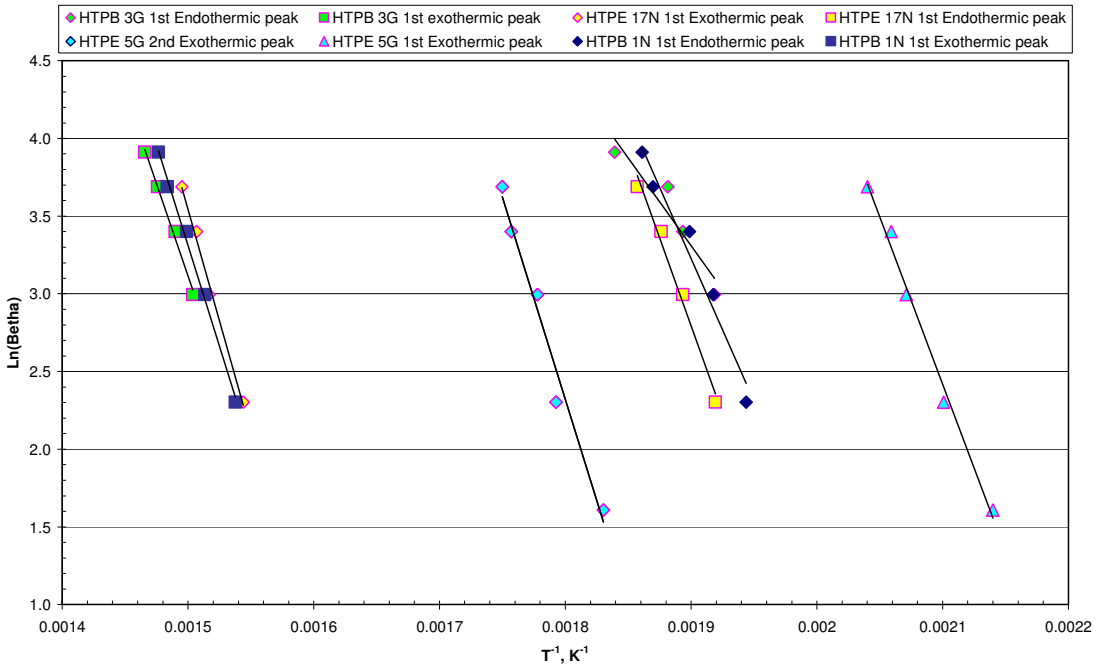

Figure 103. Arrhenius plot of Ln(β) versus $1/Tp_1$ and $1/Tp_2$ for HTPE and HTPB samples.

As discussed in Section 3.3.3, during HTPE binder network thermal decomposition the endothermic peak observed at around 240°C was assigned to the presence of the curing agent and polymer urethane link, possibly a hard segment decomposition. Therefore, as can be seen from Table 75 the activation energy of the first endothermic peak, Ea_1, corresponds possibly to the hard segment debond or scissioning. It was not possible to compare the Ea of the HTPE binder network and HTPE gumstock because the first endothermic peak is in the same temperature range as the first exothermic peak in the gumstock sample. However, a lower Ea_1 can be seen for the HTPB binder and an even lower value for the gumstock, in comparison with the HTPE binder network. In fact Ea_1 is around 19 and 50% lower in the HTPB binder network and gumstock respectively than in the HTPE binder network. Possibly in the HTPB gumstock sample the plasticizer DOS and its interaction with the hard segment i.e. Desmodur N-3200, are responsible for that behaviour.

3.3.5.6 Gumstock Ea conclusions

It was noticed that plasticizer, either energetic or non energetic, reduces the decomposition activation energy of both HTPE and HTPB gumstock samples.

However, the energetic plasticizer n-BuNENA has a bigger influence on the HTPE gumstock Ea, lowering it by 25% compared to the HTPE binder network. In comparison the Ea of the HTPB gumstock, which is plasticized with DOS is only 8% lower than that of the HTPB binder network. On the other hand, HTPE gumstock has a lower Ea than HTPB gumstock, this behaviour being affected mainly because of the energetic plasticizer n-BuNENA.

3.4 Behaviour of Binder Network and Gumstock Under Slow Heating

3.4.1 Introduction

In order to understand the behaviour of binder network and gumstock specimens under slow heating, different samples made from pre-polymer HTPE 27B and polymer HTPB R45M, both cured with Desmodur N-3200, were prepared. Samples were poured into a mould and, after curing, small flake shaped samples were cut from the centre of the specimen, as can be seen from Figure 104 A and B. The samples were then placed in head space vials previously flushed with nitrogen gas in order to have an inert environment during the slow heating process. Taking into account the HTPE and HTPB propellant cook-off ignition temperatures of 133 and 233°C respectively, reported by Atwood [2005] and Chan [2005], samples were placed in a controlled oven and the temperature increased from ambient up to 295°C at a rate of 0.1°C per min (6°C per h). The samples were removed from the oven at 100, 150, 240, 280 and 295°C. Surface profile and SEM analysis were performed.

A **B**

Figure 104. (A) Samples cured in mould and (B) prepared for the slow heating test.

3.4.2 Slow heating test development

A first set of slow heating tests was performed on samples made from pre-polymer HTPE 27B with different NCO/OH equivalence ratios; i.e. 1.0, 0.9, 0.8 and 0.7, which correspond to samples 16N27B, 17N27B, 18N27B and 19N27B. Table 76 shows the time and temperatures at which samples were taken out of the oven. Letters A to E indicate the chronological order in which the samples were taken out of the oven

Table 76. Thermal Conditions for Samples 16N27B, 17N27B, 18N27B and 19N27B

Sample name	Initial Temp. (°C)	Length time in oven (h)	Temperature (°C)
Initial conditions	21	0.00	21
16A, 17A, 18A, 19A	-	13.23	100
16B, 17B, 18B, 19B	-	21.50	150
16C, 17C, 18C, 19C	-	36.50	240
16D, 17D, 18D, 19D	-	43.17	280
16E, 17E, 18E, 19E	-	45.67	295

A second set of slow heating tests was performed on samples made from pre-polymer HTPE 27B and plasticized with n-BuNENA, polymer HTPB R45M plasticized with DOS and HTPB without plasticizer. NCO/OH equivalence ratios were: 0.88, 0.86 and 0.87 respectively. Table 77 shows the time and temperatures at which samples were taken out of the oven and Figure 105 to Figure 107 show specimens from samples 5G27B, 3GHTPB and 1NHTPB before slow heating.

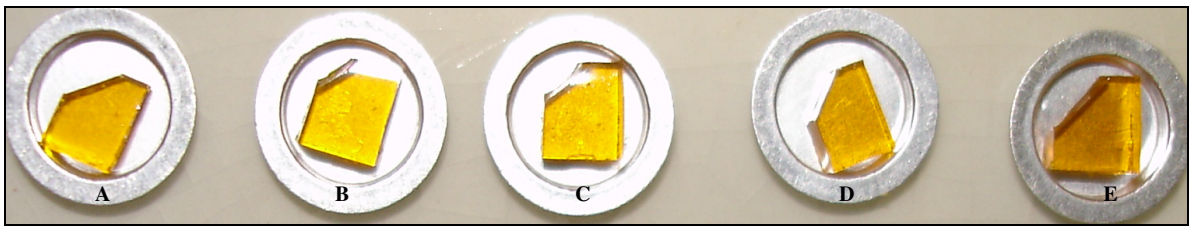

Figure 105. Gumstock samples HTPE 5G27B before slow heating test.

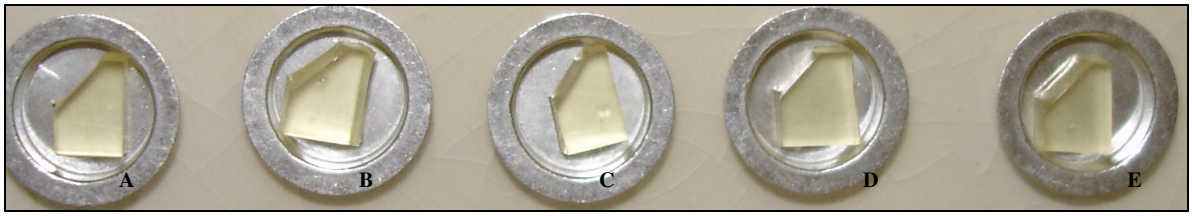

Figure 106. Gumstock samples 3GHTPB before slow heating test.

Figure 107. Binder network samples 1NHTPB before slow heating test.

Table 77. Thermal Conditions for Samples 5G27B, 3GHTPB and 1NHTPB

Sample name	Initial Temp. (°C)	Length time in oven (h)	Temperature (°C)
Initial conditions	17	0.00	17
5G27B1, 3GHTPB1, 1NHTPB1	-	14.80	100
5G27B2, 5G27B5, 3GHTPB2, 1NHTPB2	-	23.38	150
5G27B3, 3GHTPB3, 1NHTPB3	-	30.50	200
5G27B4, 3GHTPB4, 1NHTPB4	-	37.17	240
3GHTPB5, 1NHTPB5	-	46.33	295

3.4.2.1 Samples after slow heating test

To have a better idea of the surface condition after the slow heating test, digital photographs were taken of the first set of samples using a Watec digital camera WAT 202D with a zoom lens 7000 Navitar TV, controlled via PC running JASC Paintshop Pro software. Figure 108 to Figure 111 show the condition of the samples 16N27B to 19N27B after the heating period. The notation "x magnification number" added to the sample name means the magnification that was used for the sample, i.e. 16Ax10 means that photograph from sample 16A was magnified 10 times.

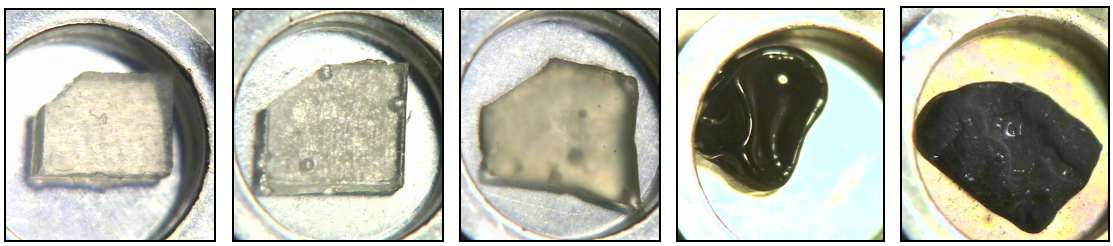

A **B** **C** **D** **E**

Figure 108. Surface photograph of samples 16N27B: (A) 16Ax10 at 100°C, (B) 16Bx20 at 150°C, (C) 16Cx20 at 240°C, (D) 16Dx10 at 280°C and (E) 16Ex20 at 295°C.

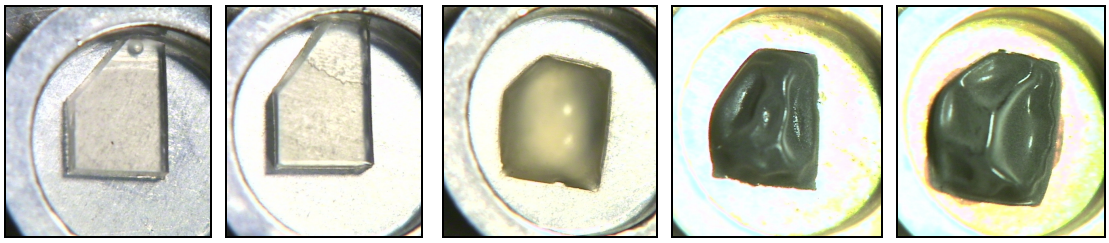

A **B** **C** **D** **E**

Figure 109. Surface photograph of samples 17N27B: (A) 17Ax20 at 100°C, (B) 17Bx20 at 150°C, (C) 17Cx20 at 240°C, (D) 17Dx10 at 280°C and (E) 17Ex20 at 295°C.

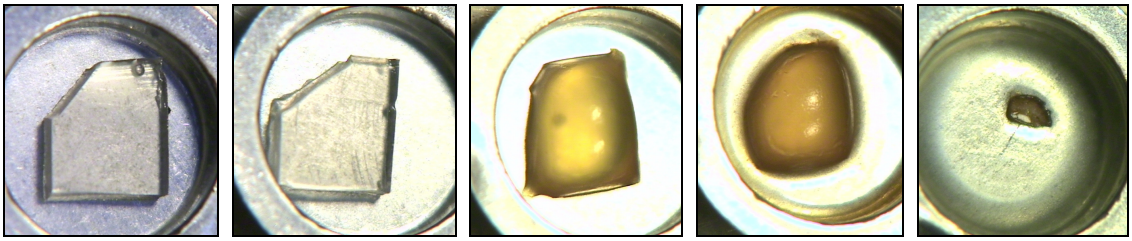

A **B** **C** **D** **E**

Figure 110. Surface photograph of samples 18N27B: (A) 18Ax20 at 100°C, (B) 18Bx20 at 150°C, (C) 18Cx20 at 240°C, (D) 18Dx10 at 280°C and (E) 18Ex20 at 295°C.

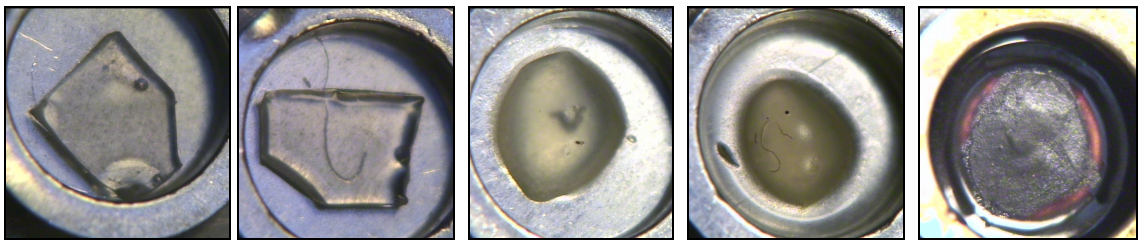

A **B** **C** **D** **E**

Figure 111. Surface photograph of samples 19N27B: (A)19Ax20 at 100°C, (B) 19Bx20 at 150°C, (C) 19Cx20 at 240°C, (D) 19Dx10 at 280°C and (E) 19Ex20 at 295°C.

For samples 5G27B, 3GHTPB and 1NHTPB photographs were taken using a Sony cyber-shot camera. Figure 112 to Figure 114 show the conditions of the samples 5G27B, 3GHTPB and 1NHTPB after the heating period.

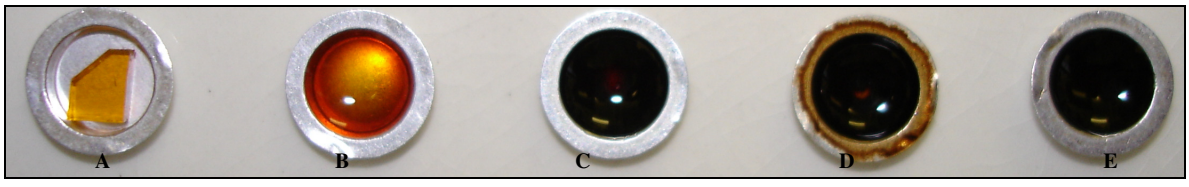

Figure 112. Samples HTPE 5G27B after slow heating trial up to: (A) 100°C, (B) 150°C, (C) 200°C, (D) 240°C and (E) 240°C.

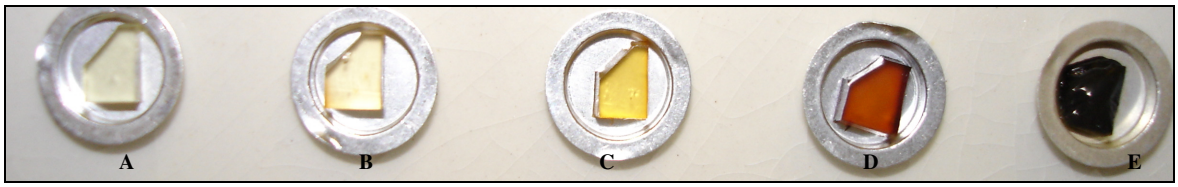

Figure 113. Samples 3GHTPB after slow heating trial up to: (A) 100°C, (B) 150°C, (C) 200°C, (D) 240°C and (E) 295°C.

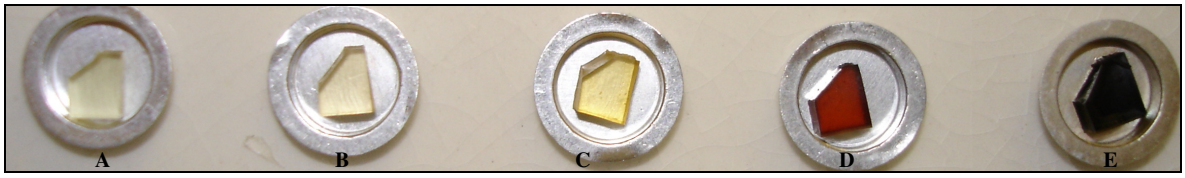

Figure 114. Samples 1NHTPB after slow heating trial up to: (A) 100°C, (B) 150°C, (C) 200°C, (D) 240°C and (E) 295°C.

3.4.2.2 Slow heating discussion of results

HTPE binder network samples

From Figure 108 to Figure 111 it can be seen that as the oven temperature was increased most of the samples follow a similar trend in terms of colour changes. In fact, samples turned from white or transparent to yellow, brown and black colour. In terms of shape all the samples having the same NCO/OH ratio show similar behaviour when they are slowly heated. At 100°C samples are little affected by the heating and maintain their original appearance. As the temperature increases the sample edges start disappearing and become smoother. At 150 and 240°C the samples have lost their original shape and start adopting a semi-spherical shape (reducing surface tension), indicating liquid rather than solid phase behaviour. Also it is evident that between these temperatures the same reaction is affecting the physical structure of the binder network. In fact, at these temperatures the samples are not any longer hard, but are soft like jelly or a viscous liquid. As the temperature increases up to 280 and 295°C the samples become black, indicating apparent carbonisation. All samples are carbonised when they reach 295°C, with the exception of sample 18E in Figure 110E, where only a little portion of it is carbonised and surrounded by a thin film of liquid phase. When samples are compared taking into account NCO/OH ratio and temperature, it is apparent that the higher the isocyanate content in the formulation the better it is able to maintain its morphology. In fact when comparing samples from Figure 108 C to Figure 111 C, which have a

NCO/OH ratio of 1.0, 0.9, .08 and 0.7 respectively, it can be seen that they are loosing their shape at 240°C in relation to the amount of curing agent. The same can be seen at 150°C but it is harder to notice. On the other hand, as can be seen from Figure 108D to Figure 111D, samples having the higher percentage of curing agent are becoming black in colour earlier. This is an indication that they are carbonised before the samples with lower NCO/OH equivalence ratios. It is apparent that, for the samples heated up to 100 and 150°C there is not a great difference in surface shape.

HTPE gumstock samples

HTPE gumstock samples show a different behaviour in comparison with HTPE binder network samples. In fact, as for binder network samples, shape is maintained at 150°C and starts changing at 240°C. In gumstock samples at 150°C the specimens become liquid and then the shape changes completely. It is evident that the energetic plasticizer, n-BuNENA, is playing a role in this behaviour. Apparently at 100°C the sample, as can be seen when comparing Figure 105 A with Figure 112 A, changes little in either colour or in shape. However, a colour change can be observed when the sample is slowly heated from 100 to 240°C, going from light orange to dark orange and finally black. There is not a noticeable visual difference between the sample heated to 240°C and that heated to 200°C. However the borders of the crucible, as can be seen in Figure 112 D, show sample residues, possibly from some bubbling effect. In an attempt to understand the source of these changes, FTIR analyses were performed on the binder network and gumstock samples submitted to slow heating. The results are presented in Section 3.5.1.

HTPB binder network and gumstock samples and comparison with HTPE

From Figure 114 A to D, it can be seen that as the temperature is increased, the HTPB samples turned from white or transparent to yellow, brown and then black. In terms of shape all the samples show similar behaviour, keeping almost the same shape during the slow heating trial. Up to 150°C the samples are little affected by the heat, maintaining their physical structure, colour and shape. As the temperature increases, the colour changes and the samples become harder, possibly due to some carbonisation, as can be noticed on the edge of the sample heated up to 240°C shown in Figure 114 D. This sample is apparently harder than those heated up to a lower temperature, however at

295°C the sample is black and loses its original shape, suggesting carbonisation and embrittlement. HTPB gumstock samples show a similar behaviour to the HTPB binder network samples. From Figure 113 A to E, it can be seen that, as the temperature is increased, the samples turned from white or transparent to yellow, brown and then black. However, in terms of shape there is a remarkable difference at 295°C. In fact, while the binder network samples keeps its rectangular shape at 295°C, the gumstock sample loses its shape at that temperature and although it looks carbonised because of the black colour, its surface is more reflective, possibly because of the effect of plasticizer migration.

3.4.2.3 Slow heating behaviour conclusions

Despite the fact that HTPE and HTPB were cured with the same curing agent, the slow heating behaviour in terms of shape was completely different. In fact, while both HTPB samples retained their shape throughout the heating process, the HTPE gumstock samples lost their shape and became liquid at around 150°C and the HTPE binder network samples became soft at around 240°C. The softening process is possibly a result of the breaking of the hard segment links or of the HTPE pre-polymer chains. A similar softening behaviour in HTPE propellants aged at 71°C, was reported by Rice [2005], however the curing agent he used was not specified. In contrast, HTPB samples become harder and more brittle during slow heating which, according to Ahlblad [1999], is due to the formation of a secondary network produced by oxidative crosslinking. Therefore, if any softening due to hard segment scission occurs in HTPB it is possibly in competition with the hardening due to formation of the secondary network.

3.4.3 Surface profile analysis

3.4.3.1 Introduction

In order to study the surface behaviour of the HTPE binder network samples before and after slow heating, interferometric 3-D surface profile analysis was performed using a

MicroXam surface mapping microscope, with a lens of 1.25mm. The microscope was controlled via a PC running MapVue EX version 6.51 surface mapping software. Scan lengths of 15 μm to 70 μm and a magnification of 25.3 were used. The surface topography was described by the statistical descriptor "surface roughness, **Ra**". This parameter gives the average behaviour of the sample surface height. The interferometric technique used was a non-contact measurement method. It is based on coherent (laser) light illuminating a rough surface. When this happens the diffracted waves from each point of the surface mutually interfere to form a pattern which appears as a grain pattern of bright and dark regions. The spatial statistical properties of this speckle image are related to surface characteristics. The degree of correlation of two speckle patterns produced from the same surface by two different illumination beams can be used as a roughness parameter.

HTPE and HTPB binder network and gumstock samples from the "Slow Heating Test" were analyzed. As an initial reference, surface profile analyses were performed before placing the samples in the oven. After this the samples were placed in an aluminium crucible and put into a head space vial under an inert environment containing nitrogen gas. The head space vials containing the samples were heated in a programmable oven at a rate of temperature increase of 0.1^{o}C per min (6^{o}C per h). Samples were taken out of the oven at different temperatures and their surfaces were analysed. For each of the samples nine measurements on a surface area of 20 μm x 20 μm were taken and the surface roughness parameter **Ra** measured and averaged.

3.4.3.2 HTPE binder network samples having different NCO/OH equivalence ratio

Figure 115 shows the hybrid map of the surface profile of HTPE binder networks 16A to 16D made from HTPE sample 27B and N-3200 before (25^{o}C) and after slow heating at temperatures of 100, 150 and 240. Figure 116 shows the hybrid map for the surface profile of HTPE binder networks 19A to 19D, made from HTPE sample 27B and N-3200 before (25^{o}C) and after slow heating at temperatures of 100, 150 and 240^{o}C.

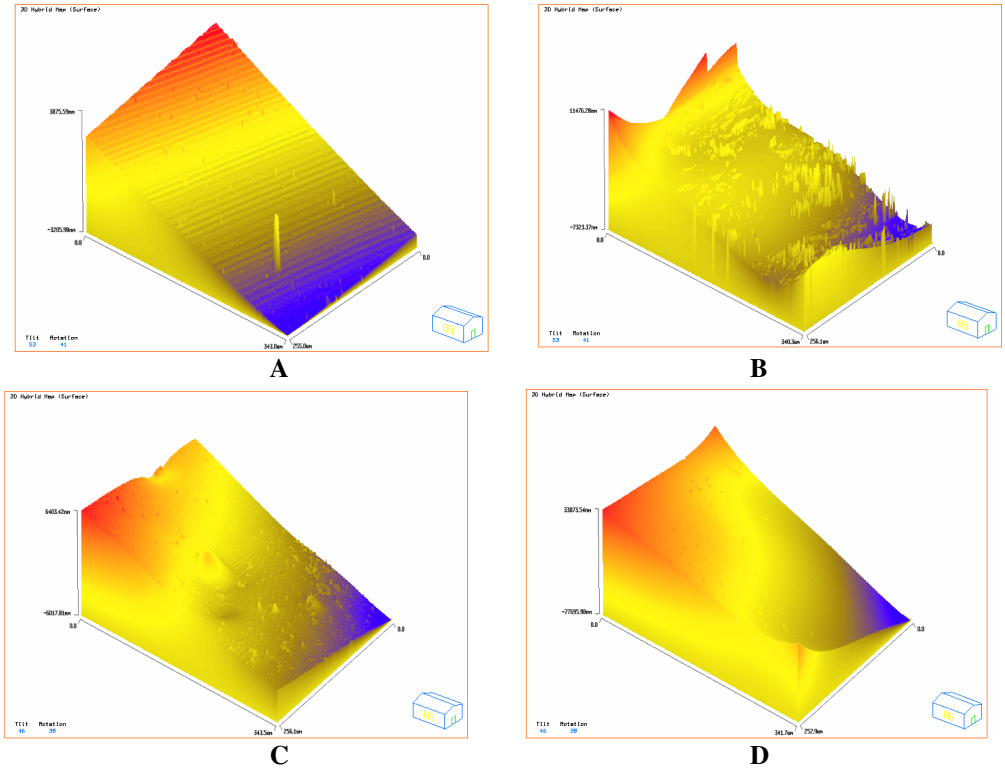

Figure 115. Surface hybrid map of sample (A) 16A at 25°C, (B) 16A at 100°C, (C) 16B at 150°C and (D) 16C at 240°C

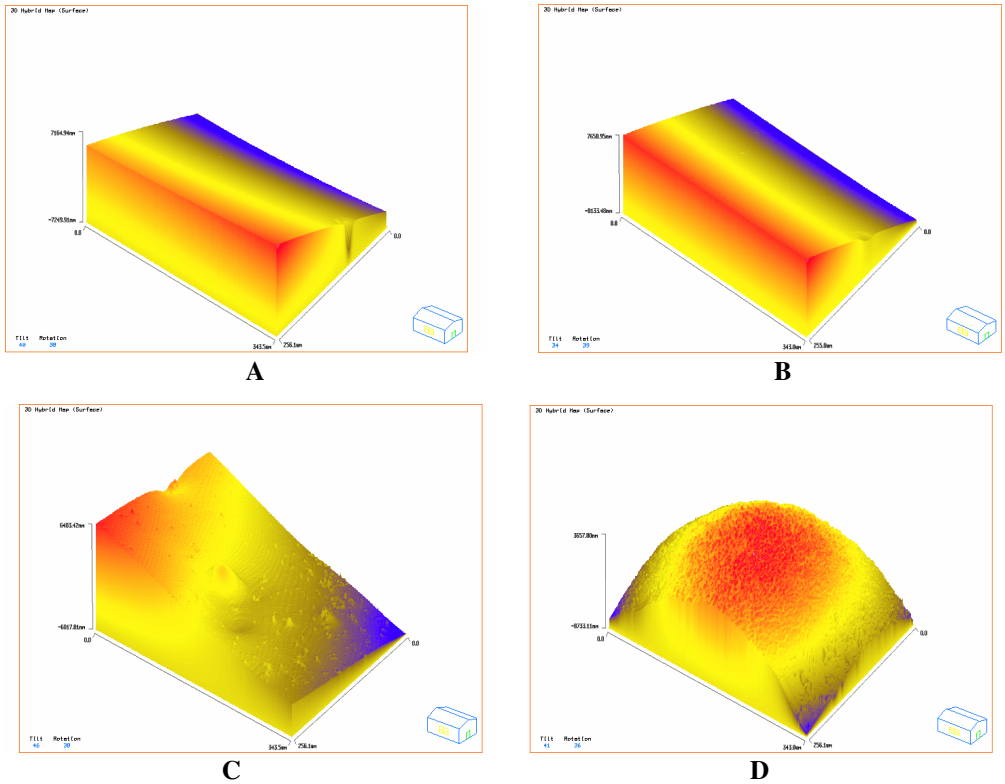

Figure 116. Surface hybrid map of sample (A) 19A at 25°C, (B) 19A at 100°C, (C) 19B at 150°C and 19C at 240°C.

Table 78 to Table 81 gives a summary of the surface roughness parameter **Ra** for binder network samples 16A to 19A respectively.

Table 78. Sample 16A, Surface Profile Statistics

Sample Nº	Heating Temp. (ºC)	Ra									Average Ra	Total Ra Change (%)
		1	2	3	4	5	6	7	8	9		
16A	25	98	94	96	99	96	92	97	92	96	96	**91**
16A	100	222	188	121	205	218	198	118	204	172	183	
16B	25	152	147	139	137	136	136	146	136	153	142	**17**
16B	150	147	160	187	135	203	179	170	162	154	166	
16C	25	199	215	219	201	211	202	223	214	208	210	**529**
16C	240	1507	1221	1206	1398	1154	1254	1800	1185	1169	1322	
16D	25	68	75	67	67	69	69	66	74	69	69	**1066**
16D	100	882	941	903	820	737	764	738	869	627	809	

Table 79. Sample 17A, Surface Profile Statistics

Sample Nº	Heating Temp. (ºC)	Ra									Average Ra	Total Ra Change (%)
		1	2	3	4	5	6	7	8	9		
17A	25	108	93	91	95	97	92	116	120	103	102	**65**
17A	100	164	171	163	162	158	161	178	177	171	167	
17B	25	99	80	79	89	92	89	80	85	90	87	**70**
17B	150	154	153	135	147	144	145	153	144	152	148	
17C	25	95	100	97	95	92	96	100	99	95	97	**941**
17C	240	1061	952	1045	1024	1012	956	1003	1028	965	1005	

Table 80. Sample 18A, Surface Profile Statistics

Sample Nº	Heating Temp. (ºC)	Ra									Average Ra	Total Ra Change (%)
		1	2	3	4	5	6	7	8	9		
18A	25	223	232	202	244	236	206	231	190	209	219	**36**
18A	100	308	298	293	289	301	297	297	303	295	298	
18B	25	41	29	14	22	48	39	48	23	30	33	**372**
18B	150	165	152	168	180	150	139	138	150	147	154	
18C	25	60	69	63	53	56	65	62	66	70	63	**485**
18C	240	302	455	253	277	430	366	425	377	413	366	

Table 81. Sample 19A, Surface Profile Statistics

Sample Nº	Heating Temp. (ºC)	Ra									Average Ra	Total Ra Change (%)
		1	2	3	4	5	6	7	8	9		
19A	25	238	242	233	246	245	242	231	247	245	241	**26**
19A	100	300	305	296	313	310	298	295	304	304	303	
19B	25	59	72	84	84	92	96	100	107	75	86	**99**
19B	150	184	182	146	209	172	154	145	172	170	170	
19C	25	141	146	145	150	142	145	149	144	140	145	**158**
19C	240	342	323	315	310	504	301	402	365	492	373	

3.4.3.3 HTPE gumstock surface profile analysis

Figure 117 shows the hybrid map for the HTPE gumstock 5G27B before (25°C) and after slow heating at a temperature of 100°C. Above 100°C the samples melted and consequently surface profile analyses were not developed.

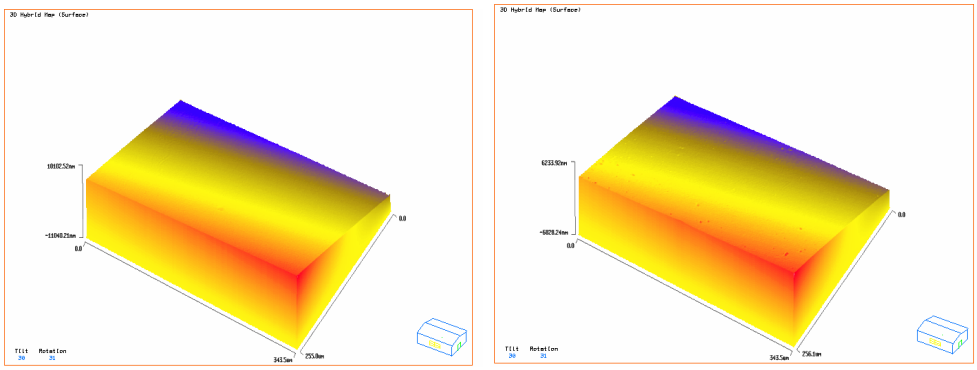

A **B**

Figure 117. Surface hybrid map of sample HTPE 5G27: (A) B1 at 25°C, (B) B2 at 100°C.

Figure 118 shows a hybrid map for the surface of sample 5G27B after being analysed by the scanning electron microscope. A discussion about this phenomenon is presented in the SEM analysis in Section 3.4.4.3.

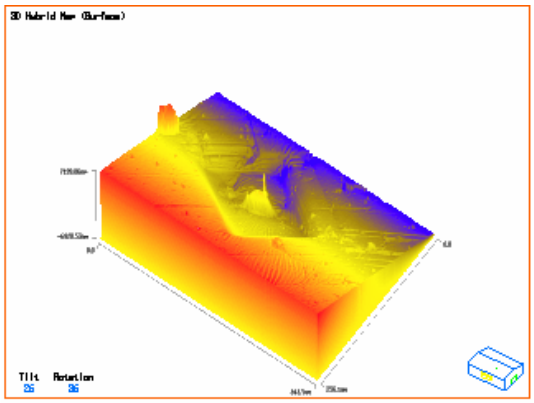

Figure 118. Surface hybrid map of sample HTPE 5G27 B2 at 100°C after SEM analysis.

Table 82 gives a summary of the surface roughness parameter **Ra** for the different HTPE gumstock samples before (25°C) and after the slow heating treatment up to a temperature of 100°C. Samples heated above 100°C were destroyed and therefore no surface profile analyses were done.

Table 82. Surface Profile Statistics HTPE Gumstock Sample; NCO/OH Equivalence Ratio of 0.88

Sample N°	Heating Temp. (°C)	Ra									Average Ra	Total Ra Change (%)
		1	2	3	4	5	6	7	8	9		
5G27B1	25	189	191	188	183	185	192	189	184	185	188	**3**
5G27B1	100	197	201	187	197	183	185	201	188	196	193	

3.4.3.4 HTPB binder network surface profile analysis

Figure 119 shows the relief mapping for the HTPB binder network samples 1N1 after slow heating at the temperatures of 100, 150, 200, 240 and 295°C.

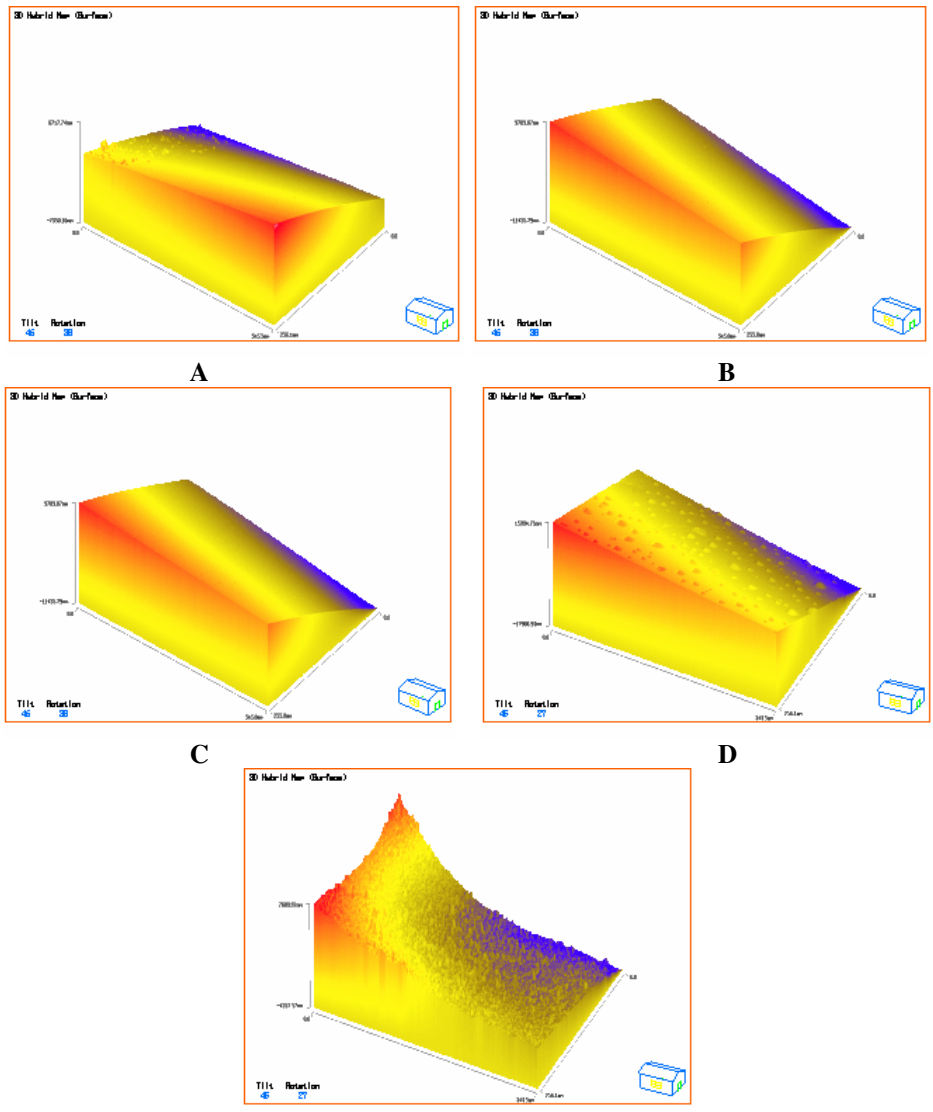

A **B**

C **D**

E

Figure 119. Surface hybrid map of binder network sample HTPB 1N1: (A) B1 at 100°C, (B) B2 at 150°C, (C) B3 at 200°C, (D) B5 at 240°C and (E) B5 at 295°C.

Table 83 gives a summary of the surface roughness parameter **Ra** for the different HTPB binder network surface samples before (25°C) and after slow heating up to a temperature of 295°C.

Table 83. Surface Profile Statistics HTPB Binder Network Sample; NCO/OH Equivalence Ratio of 0.87

Sample Nº	Heating Temp. (°C)	Ra									Average Ra	Total Ra Change (%)
		1	2	3	4	5	6	7	8	9		
1NHTPB1	25	186	206	194	210	195	185	205	185	181	194	**2**
1NHTPB1	100	183	200	193	203	201	185	215	181	220	198	
1NHTPB2	25	107	77	106	101	94	89	94	87	98	95	**12**
1NHTPB2	150	123	12	114	119	113	118	111	126	120	106	
1NHTPB3	25	362	340	365	357	362	359	357	347	347	355	**-11**
1NHTPB3	200	318	320	317	326	313	308	312	317	311	316	
1NHTPB4	25	139	143	153	161	171	181	183	171	176	164	**157**
1NHTPB4	240	424	404	495	476	463	433	434	445	479	421	
1NHTPB5	25	161	148	168	147	159	143	150	147	158	153	**37**
1NHTPB5	297	233	192	208	211	179	191	109	319	250	210	

3.4.3.5 HTPB gumstock surface profile analysis

Figure 120 and Figure 121 shows the surface hybrid map for the HTPB binder network samples 3G after slow heating at the temperatures of 100, 150, 200 and 240°C. At 295°C the sample shape was completely irregular as can be seen in slow heating test, Figure 114 E, and therefore it was not possible to obtain the surface profile.

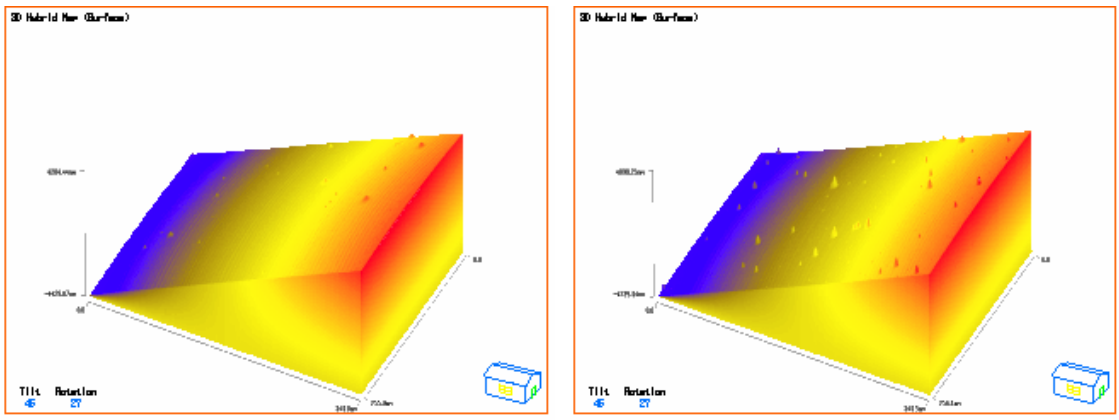

A **B**

Figure 120. Surface hybrid map of gumstock sample HTPB 3G: (A) 1 at 100°C and (B) 2 at 150°C.

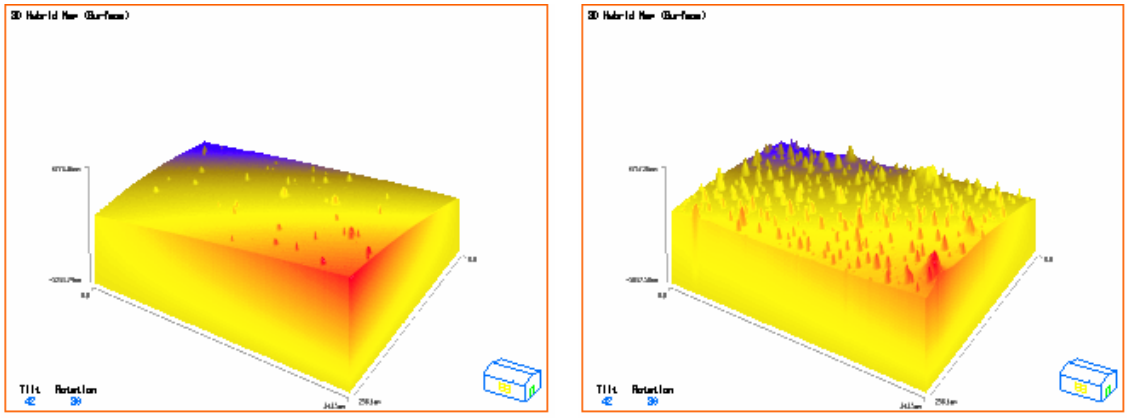

C **D**

Figure 121. Surface hybrid map of gumstock sample HTPB 3G: (C) 3 at 200°C and (D) 4 at 240°C.

Table 84 gives a summary of the surface roughness parameter **Ra** for the different HTPB gumstock samples before (25°C) and after slow heating up to a temperature of 240°C.

Table 84. Surface Profile Statistics HTPE Gumstock Sample; NCO/OH Equivalence Ratio of 0.86

Sample N°	Heating Temp. (°C)	Ra									Average Ra	Total Ra Change (%)
		1	2	3	4	5	6	7	8	9		
3GHTPB1	25	219	212	216	226	226	226	235	217	216	222	**-45**
3GHTPB1	100	122	121	122	120	123	120	121	122	121	121	
3GHTPB2	25	243	245	253	254	254	255	254	248	247	250	**-46**
3GHTPB2	150	132	139	133	134	135	135	135	136	135	135	
3GHTPB3	25	200	199	203	209	212	220	214	199	207	207	**-45**
3GHTPB3	200	111	125	108	119	99	99	125	116	118	113	
3GHTPB4	25	177	177	184	189	198	211	199	189	188	190	**-39**
3GHTPB4	240	104	121	103	118	141	123	115	100	114	115	

3.4.3.6 HTPE binder network samples having different NCO/OH equivalence ratio

As can be seen from Figure 115 and Figure 116, the hybrid map gives a general idea about the total surface area which was affected by the slow heating. Because of that, nine measurements on the surface area of 20 µm x20 µm were taken and the surface roughness parameter **Ra** measured along almost the same profile, avoiding in that way the surface roughness increase due to any surface increase. A better physical understanding of the effect of temperature on change in shape and roughness can be appreciated from the surface of the hybrid maps where the combination of solid shape

and colour change in height allowed us to see the formation of irregularities on the surface produced either by porous, domes or emergent droplets.

To quantify the change in roughness when a binder network sample is slowly heated, the information presented in Table 78 to Table 81 was plotted in Figure 122.

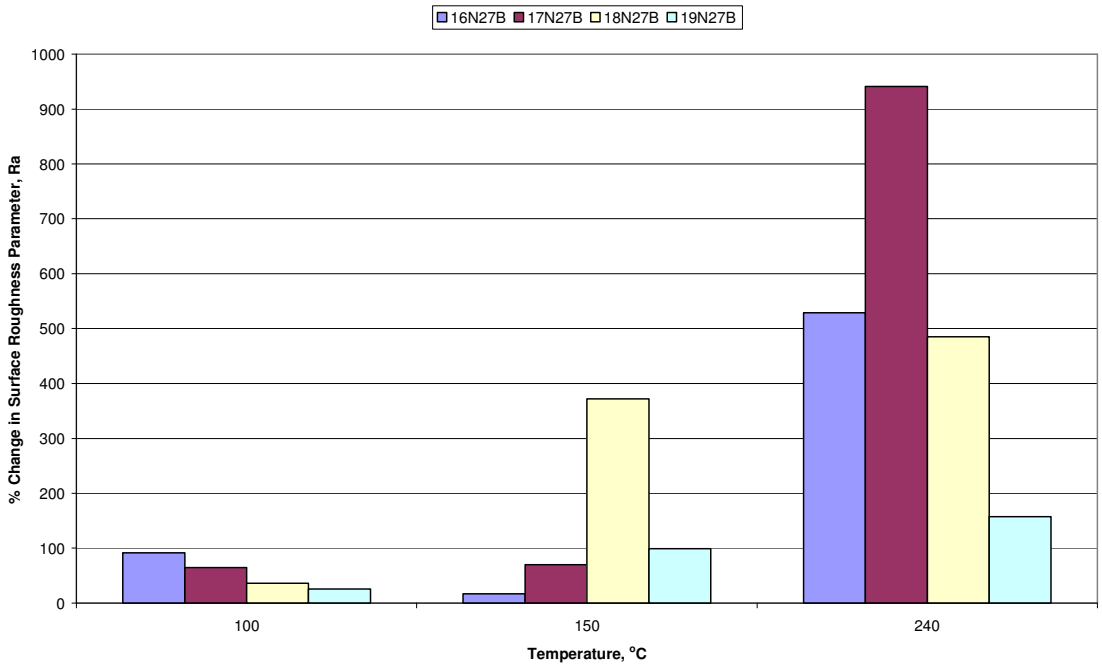

Figure 122. Ra change versus temperature for samples 16N27B to 19N27B

As can be seen, up to 100°C all the samples increase in roughness following a pattern directly proportional to the amount of curing agent in the formulation. In fact sample 16N27B, having the highest NCO/OH equivalence ratio, has the highest change in roughness. On the other hand, sample 19N27B shows the lowest roughness change, although all the samples show a moderate change in roughness. The opposite behaviour can be noticed in the temperature range 100 to 150°C; here the biggest changes in roughness are inversely proportional to the amount of curing agent. However, the change for the samples with the highest amount of curing agent is almost zero while for samples 18N27B and 19N27B it is significant. From the temperature range between 150 to 240°C the roughness for almost all the samples increases even more, however a clear trend cannot be seen. If the information obtained from DSC thermal analysis presented

in Section 3.3.3 is taken into account there is no evidence of chemical reactions or decomposition in the binder network before 200°C. The roughness changes in the temperature range 21 to 150°C can therefore be assigned to the physical interaction between the non-cured pre-polymers and the binder network. In fact, the equivalence ratio NCO/OH is an indication of the degree of polymerization of the initial hydroxy terminated copolyether with the curing agent. As can be seen from the Tg analyses presented in Section 3.3.3, when the binder network has less cross-linking, behaves thermally like the uncured pre-polymer, indicating the influence of free pre-polymer in the binder network. Therefore, possibly the increase in the roughness of the binder network in the temperature range 21 to 100°C is due to thermal damage on the surface and/or to decomposition of the surface uncured pre-polymer, leading to the formation of hills and valleys. The increase in roughness can initially be proportional to the degree of cross-linking due to the influence of the latter on the binder mechanical properties i.e. lower strain and higher strength as in samples 16N27B and 17N27B. This effect would help the migration of the pre-polymer through the binder network as the temperature increases. The change in the behaviour found between 100 and 150°C can possibly be explained by the proportion of free pre-polymer in the samples. In fact because samples 18N27B and 19N27B have less cross-linking and a lower degree of polymerization, when the temperature increases more pre-polymer molecules than in samples 16N27B and 17N27B are proportionally migrating to the surface in the shape of nano or micro droplets, as described in scanning electron microscopy (SEM) analysis in Section 3.4.4.

In the temperature range 150 to 240°C a number of reactions are happening and, as seen in the slow heating test Figure 108, the samples lost their initial shape. In fact, as presented in the thermal decomposition analysis in Section 3.3.3, between 200 and 260°C a first decomposition reaction is taking place on the hard segment and a carbonisation effect can be seen for samples having the highest NCO/OH equivalence ratio. This effect was not seen in samples with a lower NCO/OH equivalence ratio (18N27B and 19N27B) and they present a lower increase of surface roughness, possibly due to the presence of more liquid phase.

3.4.3.7 HTPE gumstock

HTPE gumstock samples were only able to be analyzed up to the temperature of 100 °C. Above that temperature the samples became soft like a gel. This behaviour is possibly due to the chain scissioning as discussed in the slow heating test Section 3.4.2.2. As can be seen from Table 82, there is only a slight increase in surface roughness of almost 3% in comparison with the initial sample surface. This change is proportionally lower than the change observed in samples containing similar amounts of curing agent but no plasticizer, as in the case of samples 18N27B and 17N27B. Possibly the presence of the plasticizer or its migration to the surface is helping to reduce the surface roughness increase at 100 °C.

3.4.3.8 HTPB binder network

HTPB binder network samples show similar behaviour to those of HTPE with similar NCO/OH equivalence ratio such as 17N27B. This is shown in Figure 123. In fact, up to 150°C the surface roughness increases only slightly for the HTPB sample and at 200°C it decreases before increasing again at 240°C.

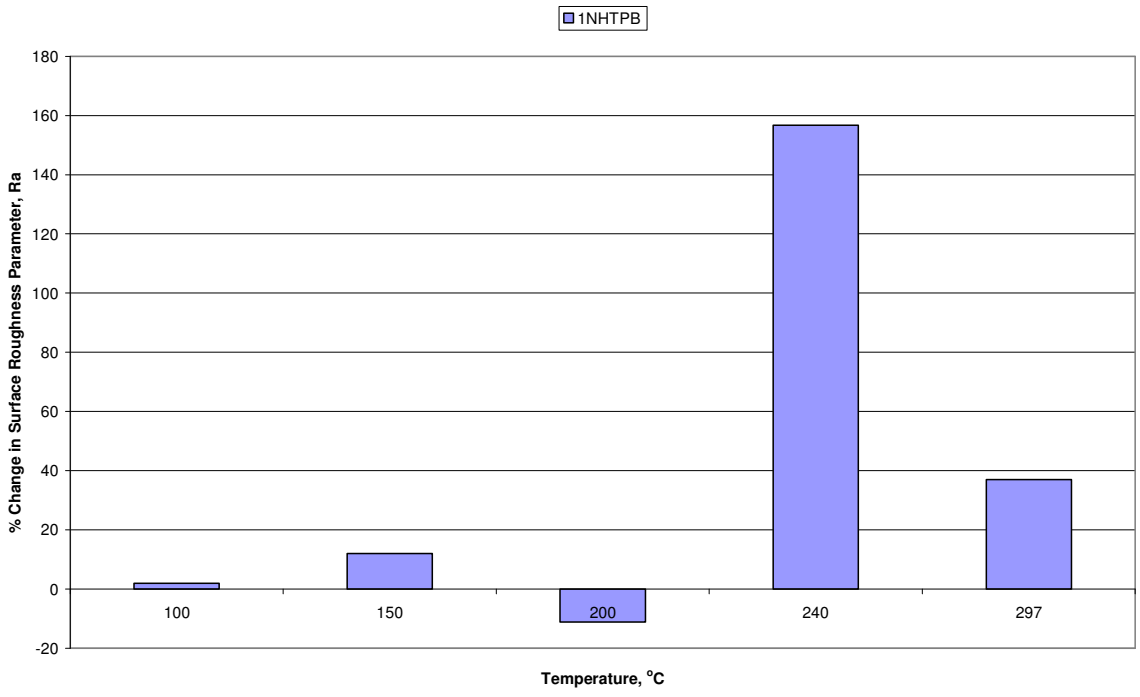

Figure 123. Ra change versus temperature for samples 1N1HTPB

As explained before, the reduction in surface roughness is thought to be due to the migration of the polymer to the surface. In fact as it can be seen from Figure 119A to E, the surface is covered with more and more little domes as the temperature increases. This is an indication of non-cured HTPB pre-polymer migrating to the surface, leading to part of the surface being smoother than at the beginning of the slow heating test. This trend starts changing completely at 240°C and the surface roughness increases radically. As can be appreciated in the SEM photograph in Figure 135 the domes have some sharp little domes in them and some small black spots can also be seen on the surface. This is possibly an indication that at this temperature some thermal decomposition or carbonisation process has started. In fact, as presented in Figure 114 E, in the slow heating test at that temperature the specimen edges become black in colour. At 295°C, from Figure 119E and from the SEM photograph in Figure 136, it can be seen that the surface is completely irregular, although proportionally there is a lower roughness increase in comparison with the sample at 240°C.

3.4.3.9 HTPB gumstock

The addition of plasticizer to the HTPB samples produced different behaviour compared to the HTPB binder network, as can be seen from Figure 124.

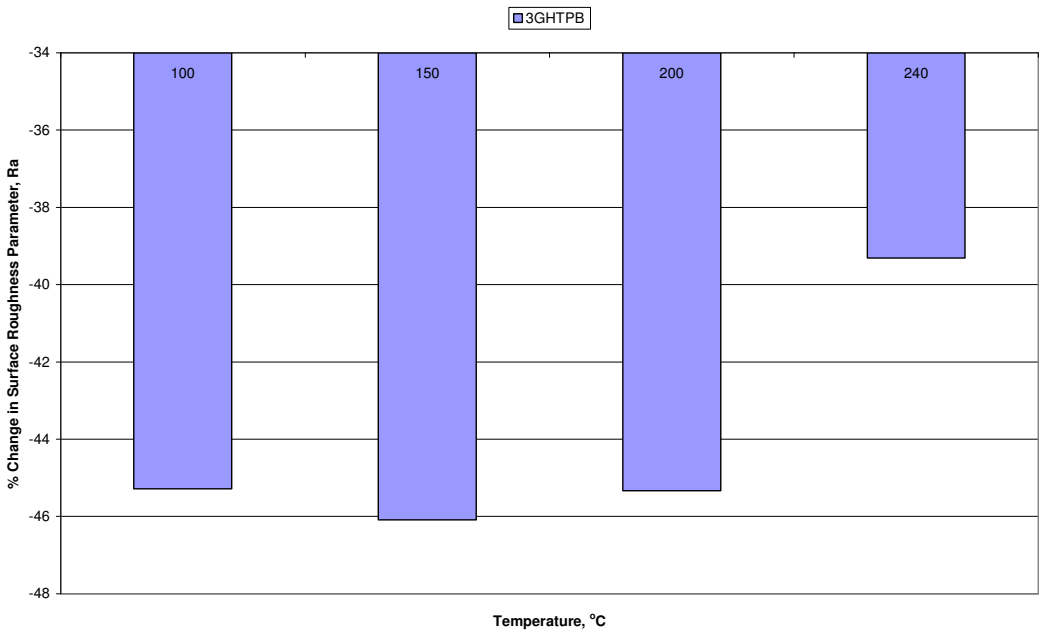

Figure 124. Ra change versus temperature for samples 3GHTPB

In this case the surface roughness was not increased but reduced considerably until 240°C where a small increase can be noticed. As can be seen from Figure 120 and Figure 121, as the temperature increases more domes, in comparison with the HTPB binder network samples, appear on the sample surface during heating.

As explained before a migration process is thought to be taking place. The addition of the plasticizer is triggering a faster migration process either of the plasticizer or the un-cured pre-polymer and plasticizer. In comparison with the HTPE gumstock, a faster migration process is happening with the HTPB gumstock samples. As in the HTPB binder network, at 240°C a change in surface behaviour has started and, like in the HTPB binder network, the edge of the specimen starts becoming black in colour. In this case the surface roughness was increased, although the surface is still smoother than before the heating test, suggesting that possibly at this temperature some thermal decomposition or carbonisation process is starting. In fact, as can be seen in the slow heating test Figure 113 E, at 295°C the sample looks carbonized and oily, giving the impression that the remaining plasticizer was on the surface of the carbonized specimen.

3.4.3.10 Surface profile conclusions

Initially, all binder network samples, either from HTPE or HTPB pre-polymers, showed an increase in roughness proportional to the temperature. However, HTPE gumstock samples behave in a similar way to HTPE binder network samples heated up to 100°C in terms of surface roughness. However, above that temperature the gumstock samples lose their physical characteristics and become liquid. On the other hand, HTPB gumstock behaves in a completely different way to HTPE. The large decrease in the surface roughness of the HTPB samples from that at the initial temperature suggests that a migration process is accelerated by the plasticizer. This migration process appears to be more significant than in HTPE gumstock. The migration process in HTPB polymers suggests that either a non-cured pre-polymer and a plasticizer or a combination of both plus fragmented pre-polymer or pre-polymer itself are migrating from the sample bulk to the surface. If that is happening it means that some nano or micro cavities are being

left during the migration process in the sample bulk. These microcavities potentially can influence the slow cook off performance when the propellant is ignited.

3.4.4 Scanning electron microscope analysis

3.4.4.1 Introduction

In order to study the surface morphology of the HTPE and HTPB samples i.e. binder network and gumstock, that were thermally affected by the slow heating test discussed in Section 3.4.2.2, scanning electron microscopy analyses were performed. A LEO scanning electron microscope model 435 VP was used. HTPE and HTPB samples were coated with a thin layer of gold. An accelerating potential between 3.4 and 25 kV was used for the analysis. A magnification of 400x and 4000x was used in most of the electron micrographs but greater magnification was used in some cases. Several electron micrographs were taken of the HTPE and HTPB binder network and gumstock samples and were analysed by using LEICA Qwin image processor software, version 4.1.

3.4.4.2 HTPE binder network SEM photographs, analysis and discussion of results

Figure 125 to Figure 130 shown SEM photographs from the specimens heated up to 100, 150 and 240^{o}C at a temperature increase rate of 6^{o}C per h, corresponding to samples 16N27B and 19N27B having a NCO/OH equivalence ratio of 1.0 and 0.7 respectively.

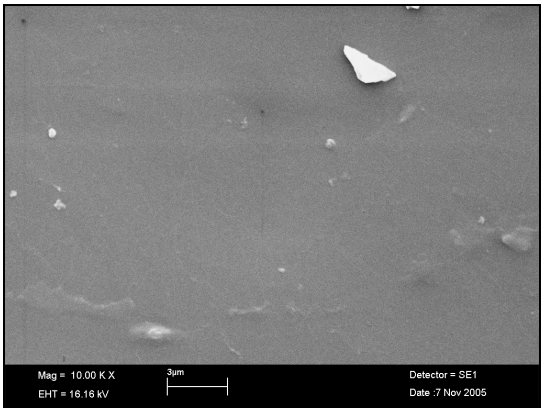

Figure 125. SEM photograph of sample 16AN27B heated up to 100^{o}C.

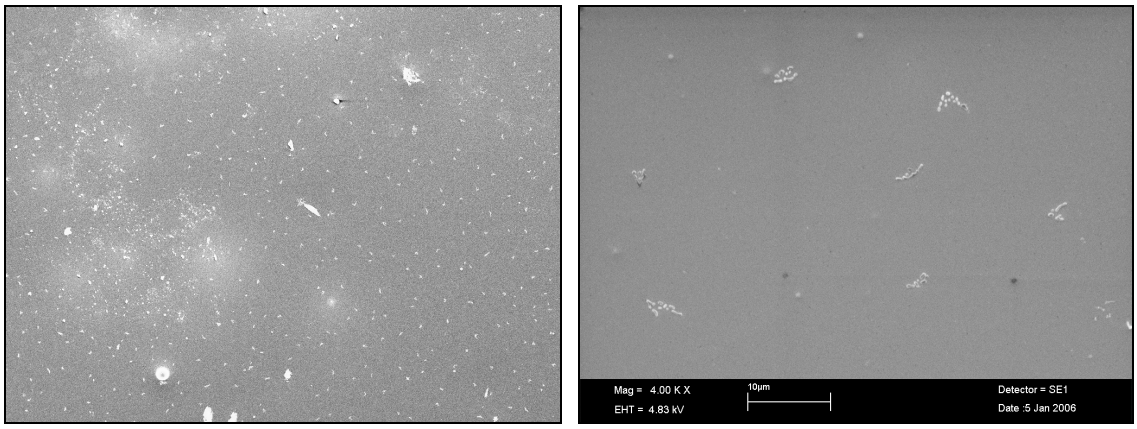

A **B**

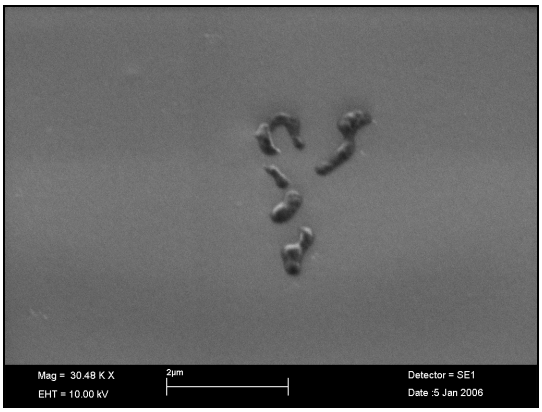

C

Figure 126. SEM photograph of sample 16BN27B heated up to 150°C, at a magnification of (A) 400x, (B) 4000x and (C) 30480x .

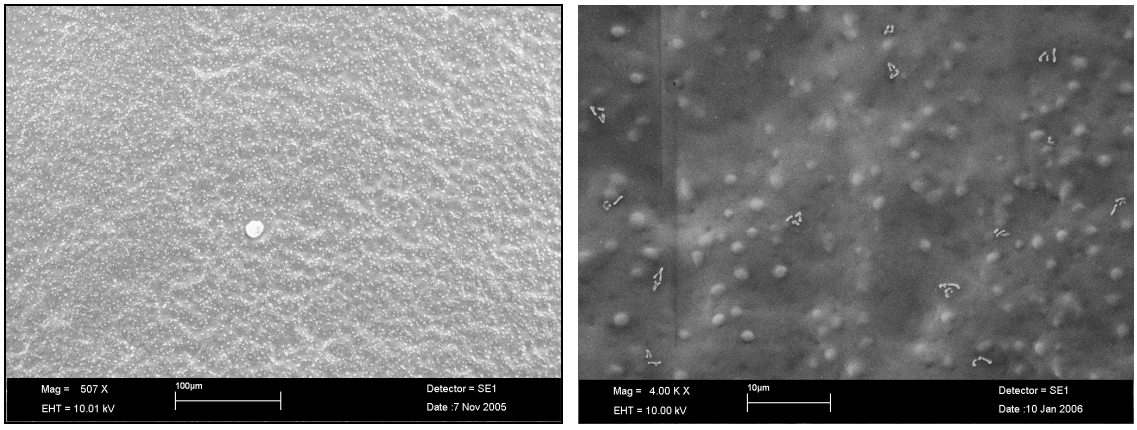

A **B**

Figure 127. SEM photograph of sample 16CN27B heated up to and 240°C, at a magnification of (A) 400x and (B) 4000x.

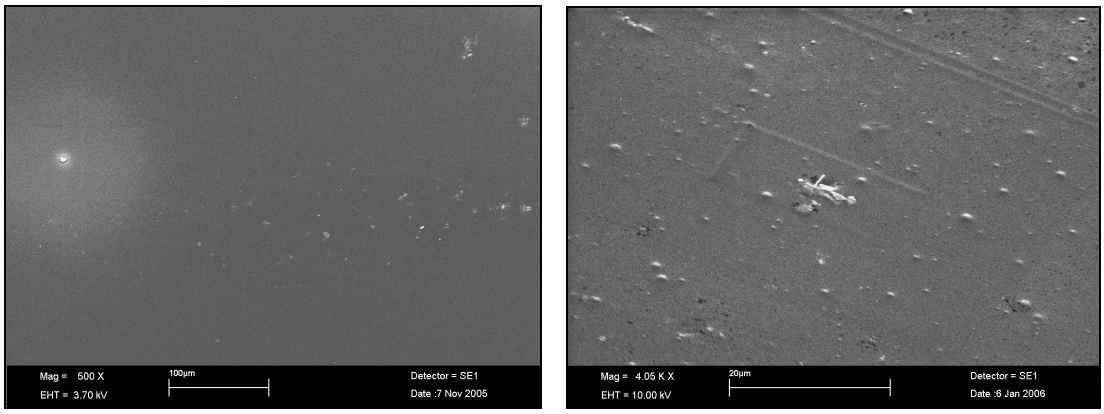

A **B**

Figure 128. SEM photograph of sample 19AN27B heated up to 100°C, at a magnification of (A) 400x and (B) 4000x.

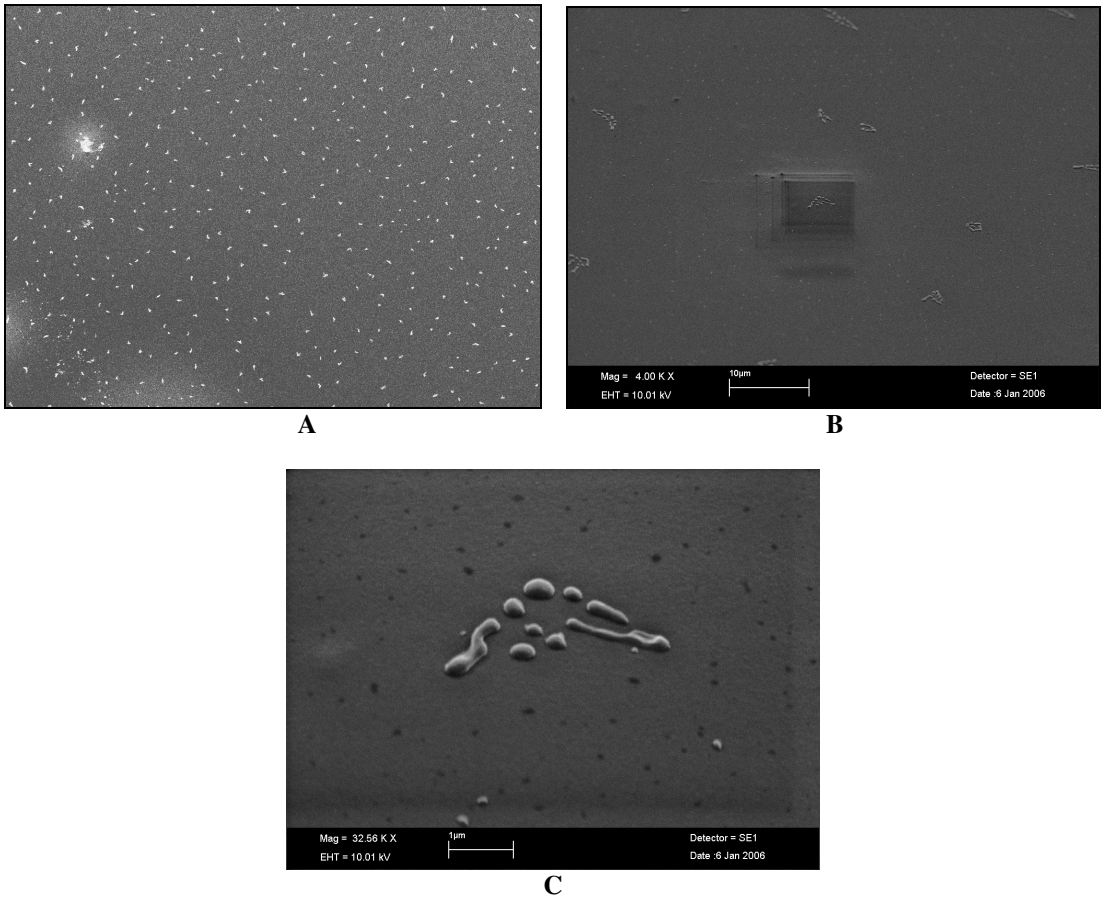

A **B**

C

Figure 129. SEM photograph of sample 19BN27B heated up to 150°C, at a magnification of (A) 400x, (B) 4000x and (C) 32000x.

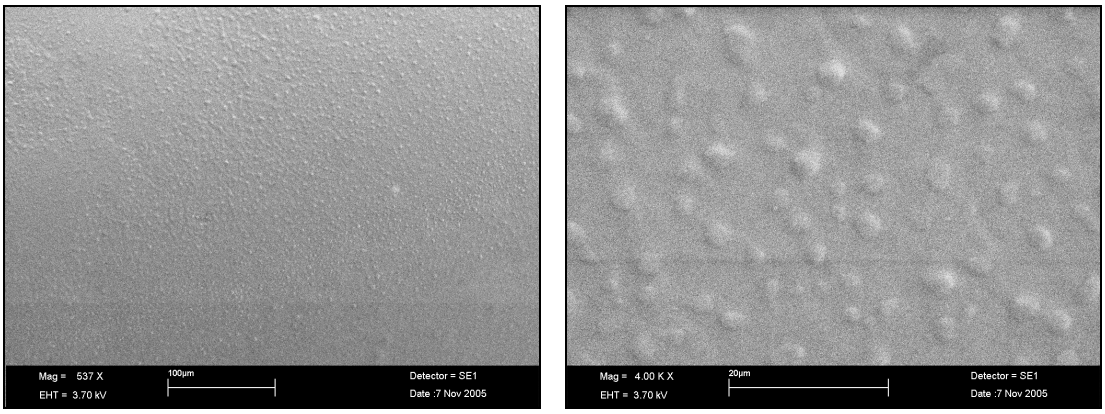

A **B**

Figure 130. SEM photograph of sample 19CN27B heated up to 240°C, at a magnification of (A) 400x and (B) 4000x.

As can be seen from Figure 125, when sample 16AN27B with a NCO/OH equivalence ratio of 1.0, is heated up to 100°C, its surface looks smooth and without irregularities. However at 150°C a consistent pattern of irregular shapes appears on the surface, as can be seen in Figure 126A. In fact, as can be better appreciated in Figure 126B and C, they are a group of small emergent domes, possibly liquid droplets, some of them linked together and some isolated and having a slightly bigger diameter. The diameter of these little domes was found to be between 0.18 to 0.36 μm and they have a regular distribution as a group, while the isolated domes have a diameter of around 1.0 μm.

Despite the domes, the sample surface still looks relatively flat. As the temperature increases up to 240°C the sample surface is more affected in terms of roughness. As can be seen from Figure 127, the high surface roughness is now evident; valleys and hills can be seen all around the observed area and emergent droplets in the form of domes can be seen clearly. Some circular black spots, which look like small holes, also can be seen. Instead of the group of emergent little domes, the surface is now full of small semi- spherical droplets attached to the valleys and hills, with a diameter between 1.0 to 2.0 μm. The high surface roughness suggests that mass has been lost and also that liquid phase material is migrating to the surface, possibly non-cured pre-polymer or products from chain scission passing through the network or through some previously formed cavities that cannot be seen clearly.

Sample 19AN27B, NCO/OH equivalence ratio of 0.7, heated up to 100°C shows similar behaviour to sample 16AN27B but at 100°C some emergent domes can be seen on the surface (Figure 128) which were not seen in sample 16AN27B at the same temperature. These have a diameter between 0.50 to 1.0 μm. Its surface looks smooth and without irregularities. As in sample 16BN27B, at 150°C a consistent pattern of irregular shapes appears on the sample surface, as can be seen in Figure 129A and B. These are a group of small emergent domes, possibly liquid droplets, some of them linked together. The diameter of these little domes was found to be between 0.25 and 0.5 μm and they have a regular distribution pattern as a group.

Also some isolated small domes were observed and they have a diameter of around 0.125 μm. Despite the domes the sample surface still looks relatively flat, although a rectangular shape can be seen in the centre of Figure 129B. It was noticed that this shape was produced by the electron beam applied over that sector when the SEM photograph in Figure 129C was taken. This was also verified by surface profile analysis as discussed in Section 3.4.3.4. Black spots with a diameter between 0.062 and 0.125 μm also can be seen, however it is not clear if they are small cavities or some interference. As the temperature increases up to 240°C, the sample surface still looks flat in comparison with that of sample 19CN27B, as can be seen from Figure 130A.

The surface roughness is not evident but a well-defined pattern of flat semi-spheres or domes can be seen on the surface instead of the group of little domes. The domes attached to the surface have a measured diameter between 1.9 and 3.8 μm, this being bigger than the radius found for the droplets on sample 19CN27B. As stated previously, this could be an indication that liquid phase material is migrating to the surface, possibly non-cured pre-polymer or product from the chain scission passing through the binder network. For sample 19CN27B the bigger droplet diameter compared to sample 16CN27B can be understood assuming there is more of non-cured pre-polymer in sample 19CN27B due to the lower NCO/OH equivalence ratio, i.e. 0.7 compared to 1.0 in sample 16CN27B.

3.4.4.3 HTPE gumstock SEM photographs, analysis and discussion of results

Figure 131 A, B and Figure 132, show SEM photographs of the HTPE gumstock sample 5G27B heated up to a temperature 100°C. This sample has an NCO/OH equivalence ratio of 0.88.

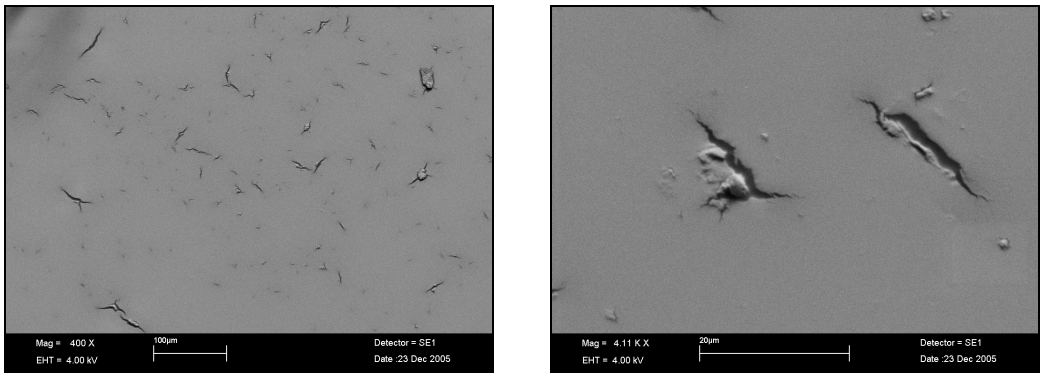

A **B**

Figure 131. SEM photograph of HTPE sample 5G27B heated up to 100°C, at a magnification of (A) 400x and (B) 4000x.

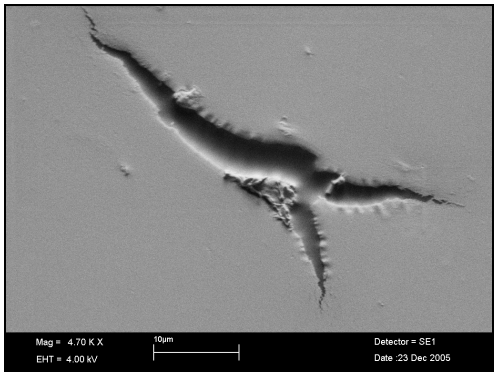

Figure 132. SEM photograph of HTPE sample 5G27B heated up to 100°C, at a magnification 4700x.

As can be seen from Figure 131, when sample 5G27B is heated up to 100°C, its surface looks similar to the surfaces of the binder network samples heated up to 150°C, as shown in Figure 126 and Figure 129, but it has not got a consistent pattern of irregular shapes over all the sample surface. In fact, as can be better appreciated in Figure 131B and Figure 132, they appear to be cracks of irregular shape instead of a group of little domes. The length of these cracks was found to be between 5.0 and 40.0 µm with a thickness of 5µm approximately. These cracks were not appreciated when techniques such as the surface profiler or optical microscope were used, possibly an indication that they can be produced during the conductive material coating and/or during SEM

analysis. It was observed while a new SEM analysis was being developed, that some of the cracks were moving and increasing their size and new lateral cracks also appeared at same the time. From the SEM results it can be concluded that the electron beam was affecting the gumstock surface, possibly by reacting with the plasticizer and pre-polymer and producing a lack of material where the electron beam was focused. The observed movement during SEM analysis was possibly due to the generation of gases that were coming out of the specimen and producing the cracks. Despite these cracks, the sample surface still looks relatively flat. As stated previously, the same sample heated up to 150^{o}C became liquid, so it was not possible to analyse its surface.

The formation of cracks when conducting SEM analysis on HTPE gumstock samples is an indication that the SEM electron beam is causing decomposition of the gumstock and that this decomposition reaction is generating gases which are cracking the surface of the gumstock. Because of this the SEM technique does not look like a reliable technique to be used in the analysis of HTPE propellants, at least if not refined.

3.4.4.4 HTPB binder network SEM photographs, analysis and discussion of results

Figure 133 to Figure 136 show SEM photographs from the HTPB binder network samples 1N2 to 1N5 heated at a temperature ramp rate of 6^{o}C per h. These have an NCO/OH equivalence ratio of 0.87.

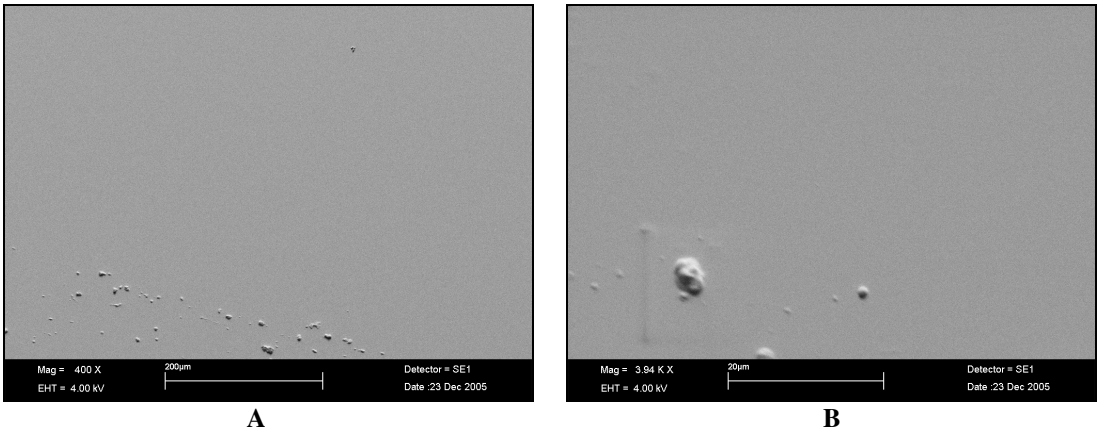

A **B**

Figure 133. SEM photograph of HTPB sample1N2 heated up to 150^{o}C, at a magnification of (A) 400x and (B) 4000x.

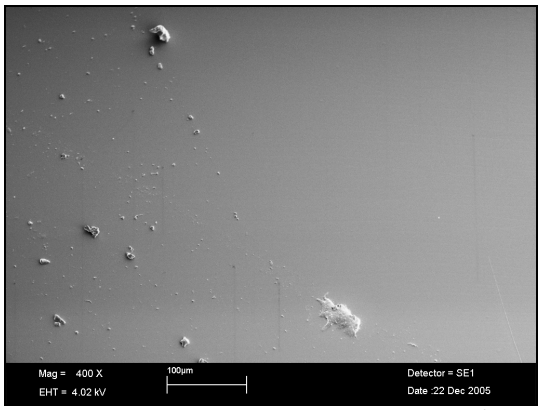

Figure 134. SEM photograph of HTPB sample1N3 heated up to 200°C, at a magnification of 400x.

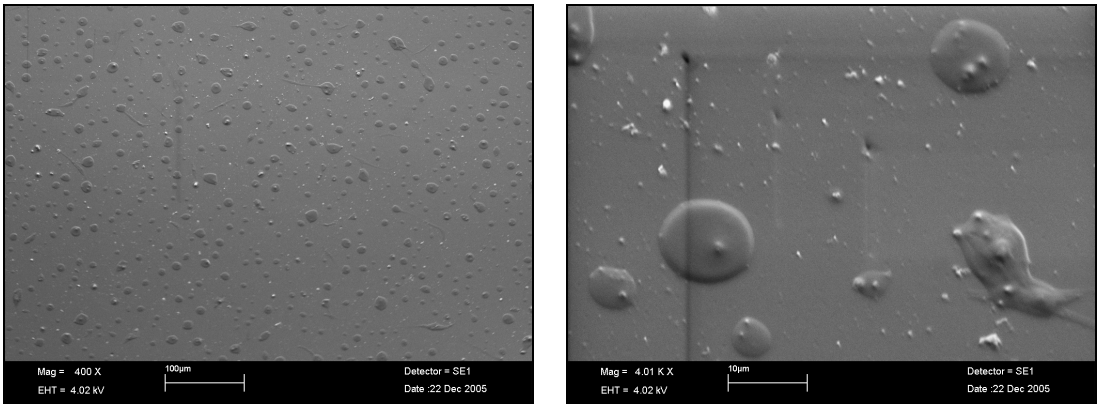

A **B**

Figure 135. SEM photograph of HTPB sample1N4 heated up to 240°C, at a magnification of (A) 400x and (B) 4000x.

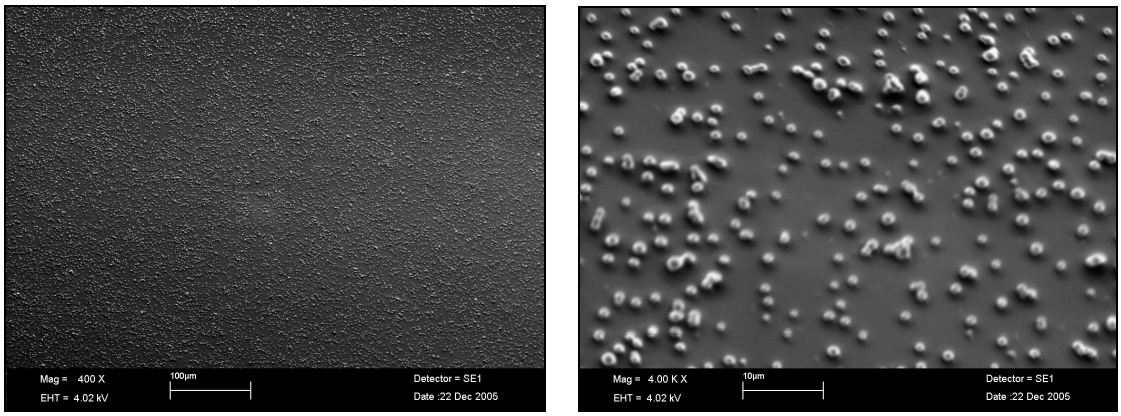

A **B**

Figure 136. SEM photograph of HTPB sample1N5 heated up to 295°C, at a magnification of (A) 400x and (B) 4000x.

As can be seen from Figure 133 and Figure 134, when HTPB binder network sample 1NHTPB with an NCO/OH equivalence ratio of 0.86, is heated up to 150°C and 200°C respectively, the surface looks smooth and without irregularities or cracks, indicating it

was not affected by the slow heating process observed in the case of HTPE samples. However, at 240°C, as can be seen from Figure 135, a consistent pattern of flat hemi-spheres or domes appears on the surface. Despite these domes, the sample surface stills look flat, although some black cavities can be seen, but not in a regular pattern.

The hemi-spherical droplets attached to the surface have a measured diameter between 4.0 and 10.0 μm, being bigger than the diameter found for the droplets of sample 16N27B and sample 19N27B at the same temperature. At 295°C the number of domes or droplets increases dramatically, as can be seen in Figure 136 Their diameter drops to between 1.0 and 1.5 μm and the surface has small valleys and hills. As in the case of HTPE binder network samples, this could be an indication that liquid phase material is migrating to the surface, possibly non-cured pre-polymer or products from chain scission, passing out through the previously formed cracks or diffusing through the binder network . Cracks were not observed at 200°C, suggesting that they should appear in the temperature range 200 to 240°C co-inciding with the droplet formation.

3.4.4.5 HTPB gumstock SEM photograph, analysis and discussion of results

Figure 137 to Figure 139 show SEM photographs from HTPB gumstock samples 3G3-3G4 heated at a temperature ramp rate of 6°C per h. These have an NCO/OH equivalence ratio of 0.86.

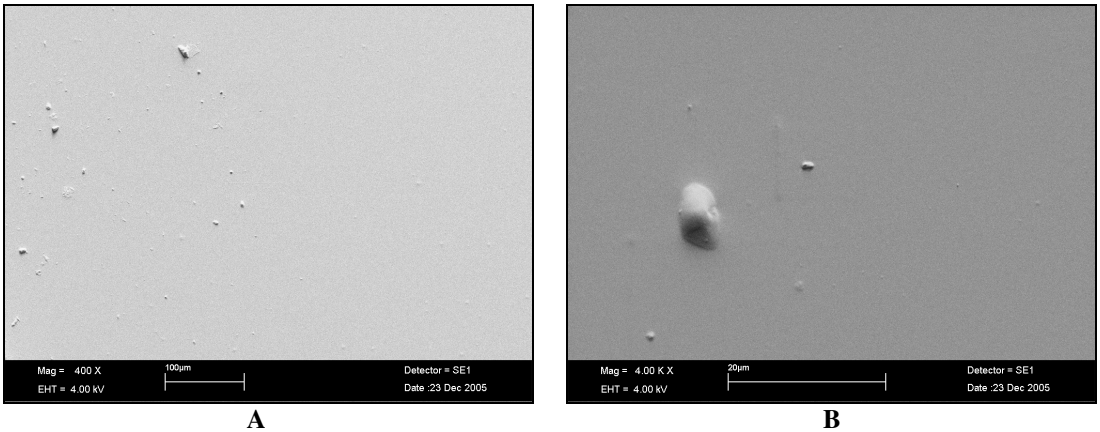

A **B**

Figure 137. SEM photograph of HTPB sample 3G2 heated up to 150°C, at a magnification of (A) 400x and (B) 4000x.

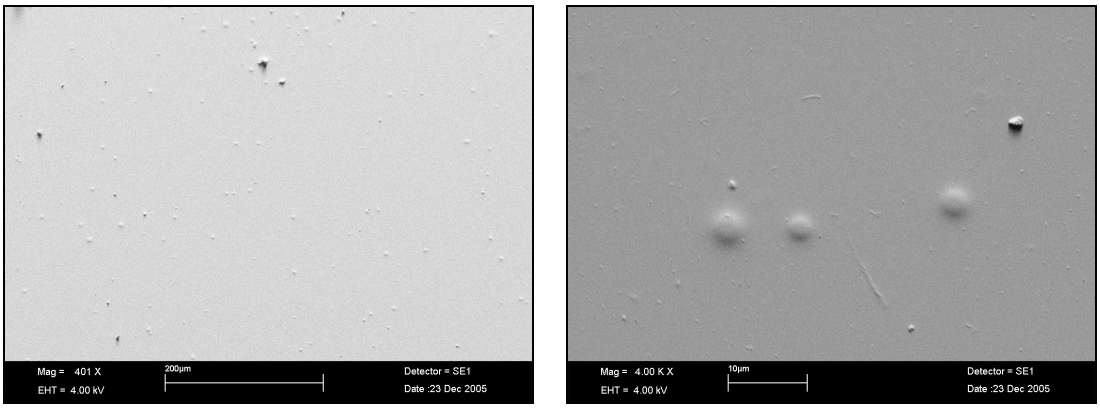

A **B**

Figure 138. SEM photograph of HTPB sample 3G3 heated up to 200°C, at a magnification of (A) 400x and (B) 4000x.

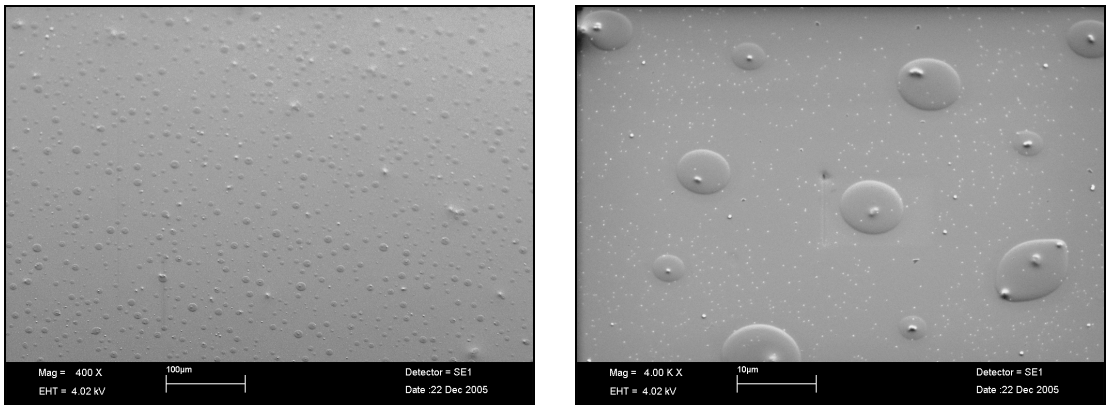

A **B**

Figure 139. SEM photograph of HTPB sample 3G4 heated up to 240°C, at a magnification of (A) 400x and (B) 4000x.

HTPB gumstock sample 3GHTPB with an NCO/OH equivalence ratio of 0.87, shows similar behaviour to the HTPB binder network. When heated up to 150°C the surface does not show changes and looks smooth and without irregularities or cracks. It was not affected by the slow heating process, as can be seen in Figure 137. However, at 200°C, as can be seen in Figure 138, flat hemi-spheres or droplets having different sizes appear on the surface, similar to the ones found in the HTPB binder network samples at 240°C but less densely distributed. Despite these droplets, the sample surface still looks flat. At 240°C, as can be seen from Figure 139, the surface looks very similar to the binder network in Figure 135, and flat hemi-spheres or droplets are distributed in a well-defined pattern on the surface. The surface still looks flat although some cavities can be seen. The hemi-spherical droplets attached to the surface have a measured diameter between 4.0 and 8.0 µm, being similar in diameter to the droplets of sample 1NHTPB at

the same temperature, but a larger number of them is present on the surface. As suggested for HTPB binder network samples, this could be an indication that liquid phase material is migrating to the surface, possibly the plasticizer, the non-cured pre-polymer or products from the chain scission, possibly passing through previously formed cracks or diffusing through the binder network. As in the HTPB binder network samples, cracks were not observed below a temperature of 200°C, suggesting that the liquid phase appears on the surface between 150 and 200°C, co-inciding with the droplet formation. On the other hand, the droplets appear earlier than in HTPB binder network samples i.e. at 200 instead 240°C, indicating the influence of the plasticizer on the thermal behaviour.

3.4.4.6 SEM conclusions

The decrease in surface roughness observed during surface profile analysis can be understand in terms of liquid phase migration to the surface, as was observed when analyzing the SEM photographs from HTPE and HTPB binder network or gumstock samples .

The surface roughness in the SEM photographs is not evident but a well defined pattern of flat hemi-spheres or little domes can be observed on the surface of the binder and gumstock samples. The domes attached to the surface have a measured radius between 0.12 and 3.8 μm. This is an indication that liquid phase material is migrating to the surface during the slow heating process. This liquid is possibly non-cured pre-polymer, plasticizer or products from the chain scission migrating through the binder network or gumstock.

Because when performing SEM analysis on the HTPE gumstock, cracks were created, it is believed that the SEM electron beam is affecting the thermal decomposition of the gumstock and that this decomposition reaction is generating gases which are breaking the surface of the gumstock. Therefore, the SEM technique needs to be refined if it is to be used for the investigation of these samples.

3.5 Aged Binder Network and Gumstock Analyses

To try to understand the changes observed when HTPE binder network and gumstock samples are slowly heated, FTIR, GC-MS and SEC analyses were performed. The samples were taken from the slow heating test and had been heated from ambient temperature up to 150 and 240^{o}C as presented in Section 3.4.2. They were analysed and compared with a fresh sample without slow heating treatment.

3.5.1 HTPE binder network and gumstock FTIR analysis results

A thin layer of the HTPE binder network or gumstock sample obtained from the slow heating test was placed between two plates of sodium chloride and the FTIR spectrum was obtained. The analyses were performed as described in Section 2.3.5.

3.5.1.1 HTPE binder network and gumstock thermal decomposition IR spectrum

A summary of the main peaks and their suggested assignments from the IR spectra for binder network and gumstock samples shown in Figure 140 to Figure 145 are summarised in Table 85.

Table 85. Main Characteristic Infrared Peaks for Thermal Decomposition Products [Bellamy 1980] and [Nakanishi, 1964]

Wave Number cm^{-1}	Assignment	
3476	Primary alcohol, OH stretching	$-CH_2OH$
3342	Urethane groups, NH stretching	-NH-CO-O-R-
2850	Alkane groups, CH stretching	$-CH_2CH_2-$
1722	Urethane groups, CO stretching	-NH-CO-O-R-
1698	Biuret, CO stretching	-HN-CONH-CO-NH-
1639	Urea, CO stretching, Di substituted amide, CO stretching; Asymmetric Stretching of nitrates	N-CO-N; $-CO-N-R_2$; ONO_2
1616	Primary Amine, Amide, covalent nitrite	$-CH_2NH_2$; $-CONH_2$; R-O-NO
1587	Primary amine, Amide, covalent nitrite	$-CH_2NH_2$; $-CONH_2$; R-O-NO
1524	Mono substituted Amide, NH bend;	-CO-NH-R-
1515	Monosubstituted Amide, NH bend; Nitramine	-CO-NH-R ; $=N-NO_2$

Figure 140, Figure 141 and Figure 142 show the FTIR spectra of sample 19N27B heated up to 150 and 240°C and of sample 16N27B heated up to 240°C, as described in Section 3.4. All the binder network samples were made from HTPE pre-polymer 27B, with NCO/OH equivalence ratios of 0.7, 0.7 and 1.0.

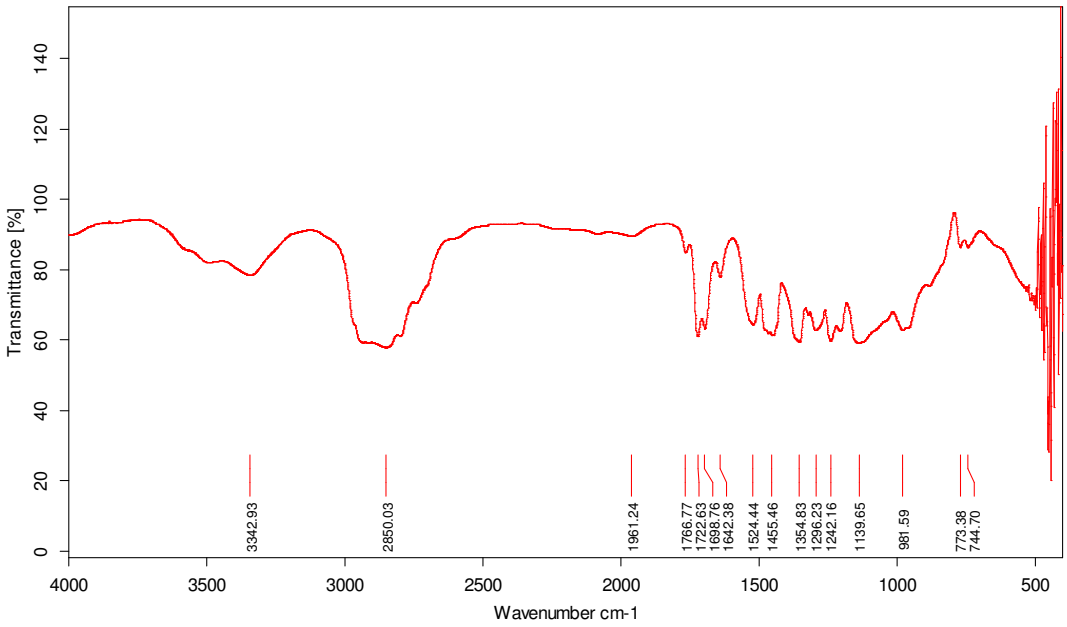

Figure 140. FTIR spectrum of sample HTPE 19N 27B heated up to 150°C

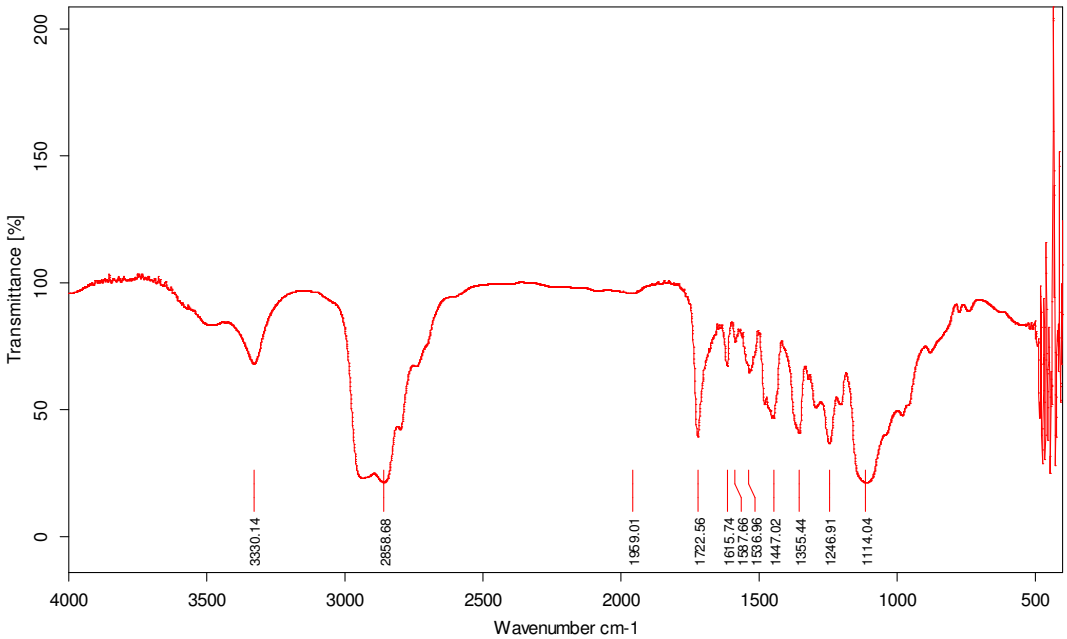

Figure 141. FTIR spectrum of sample HTPE 19N 27B heated up to 240°C

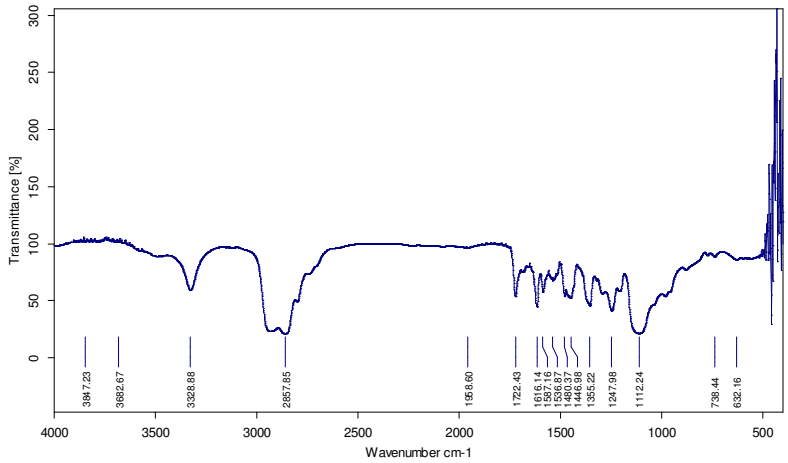

Figure 142. FTIR spectrum for sample HTPE 16N27B heated up to 240°C

Figure 143 to Figure 145 show the FTIR spectra of sample 5G27B, from the slow heating test described in Section 3.4, heated up to 150, 200 and 240°C.

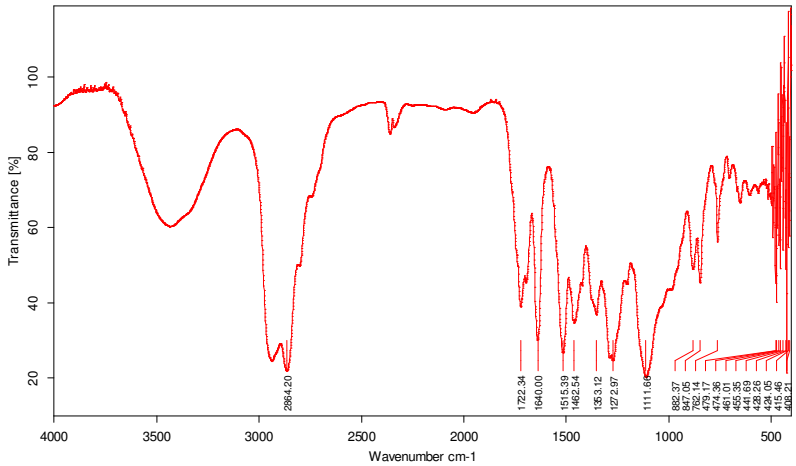

Figure 143. FTIR spectrum of sample HTPE 5G gumstock heated up to 150°C

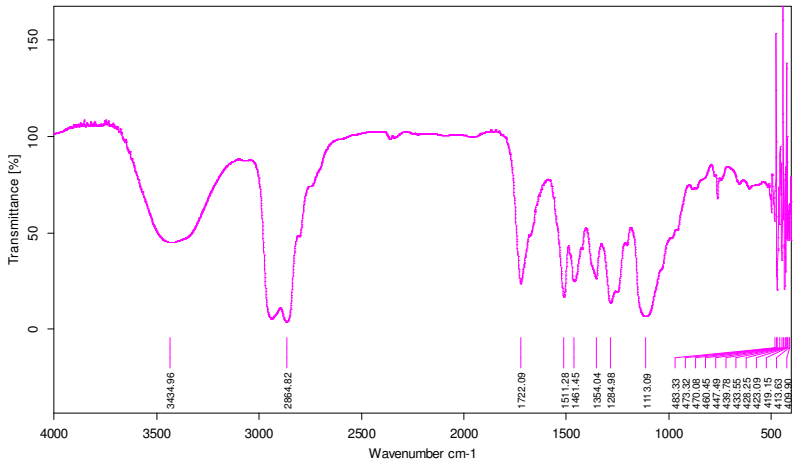

Figure 144. FTIR spectrum of sample HTPE 5G gumstock heated up to 200°C

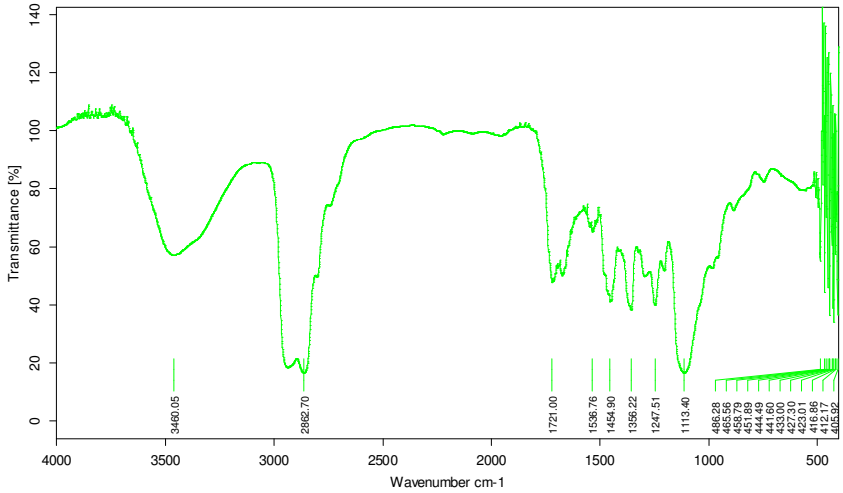

Figure 145. FTIR spectrum of sample HTPE 5G gumstock heated up to 240°C

3.5.1.2 Discussion of FTIR results from binder network and gumstock thermal decomposition

During the slow heating process, samples made from HTPE became soft and liquid. FTIR analyses were performed on these samples and the spectra compared with those of non-heated samples. The groups formed as a result of the curing process, as presented in Section 3.2.2, can be seen in the IR spectra in the bands at 3342 cm^{-1} and between 1743 and 1455 cm^{-1}.

The IR spectra for the slowly heated HTPE 19N27B samples heated up to 150 and 240°C, presented in Figure 140 and Figure 141, are overlayed in one chart in Figure 146. The sample heated up to 150°C is shown in blue and the one heated up to 240°C is shown in red. The IR spectrum for a freshly cured sample is shown in green. The IR spectrum for the slowly heated HTPE gumstock samples, presented in Figure 143 to Figure 145, are overlayed in one chart in Figure 147. In light blue is the gumstock sample before the test, in red the sample heated up to 150°C, in purple the sample heated up to 200°C and in blue the sample heated up to 240°C.

As can be seen in Figure 147, from the light blue IR spectrum, the addition of the energetic plasticizer n-BuNENA does not have a strong effect on the infra red spectrum in comparison with that of the binder network (Figure 146, green IR spectra), probably because almost all the groups from n-BuNENA are absorbing in the same region as the

cured pre-polymer. However, the peaks at around 1639, 1515 and 1460 cm^{-1} are magnified due to the absorption of the n-BuNENA groups in the same region as the main groups of the cured pre-polymer.

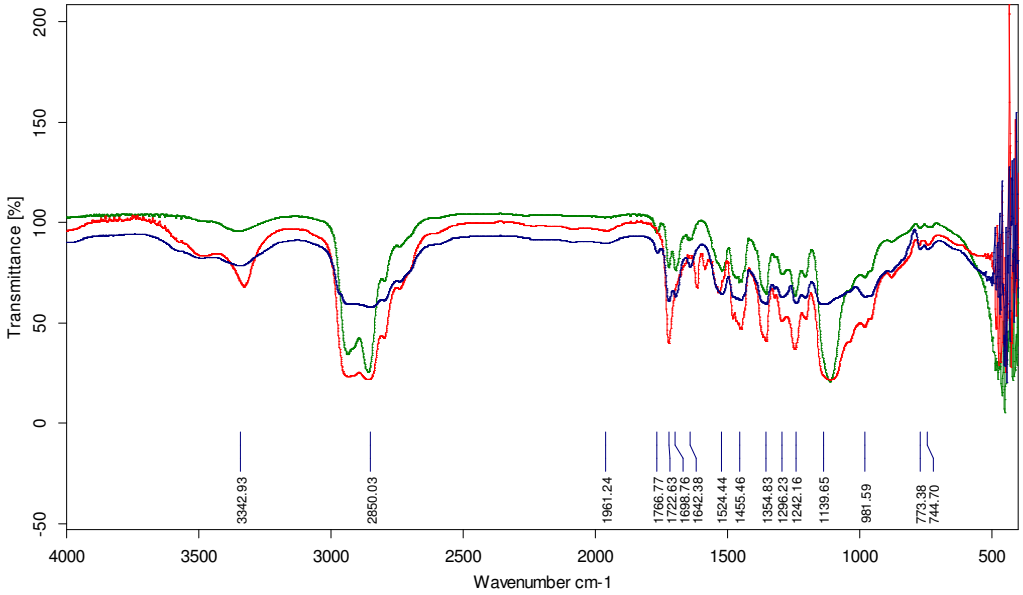

Figure 146. Overlayed FTIR spectra of sample HTPE 19N27B binder network, before heating (green), heated up to 150°C (blue) and heated up to 240°C (red).

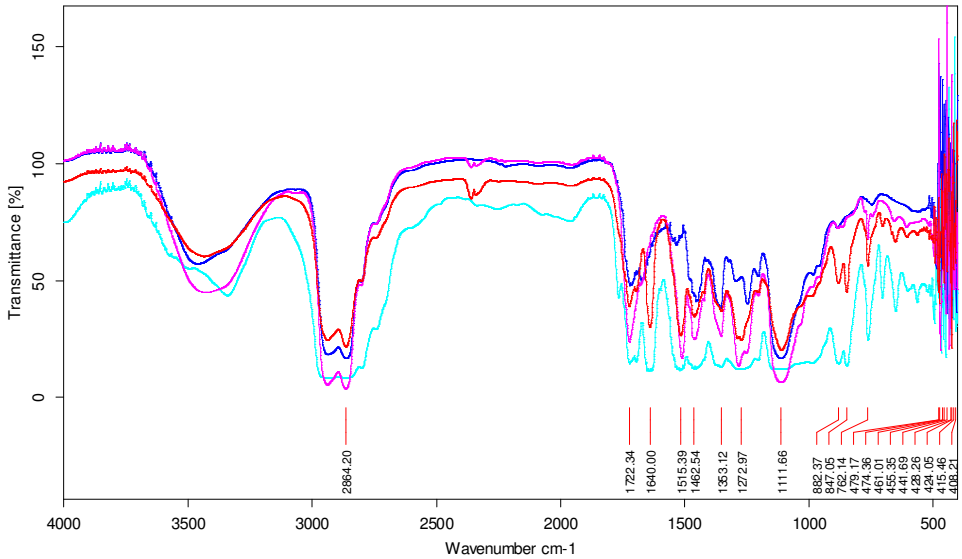

Figure 147. Overlayed FTIR spectra of sample HTPE 5G27BH gumstock, before heating (light blue), heated up to 150°C (red), heated up to 200°C (purple) and heated up to 240°C (blue).

As can be seen from Figure 146, the FTIR spectrum for the sample heated up to 150°C (blue) is very similar to that of the freshly cured sample (green), the only slight difference being in the intensity of the peak at 3342 cm^{-1}. However, when the binder

network sample was heated up to 240°C (red) the peak at 1722 cm^{-1}, assigned to the urethane group, is the only one that remains in place, suggesting that the urethane links are still present when the HTPE binder network sample becomes soft. The peaks at 1698 and 1642 cm^{-1} disappeared and new peaks appeared at 1616 and 1587 cm^{-1}. The first two peaks can possibly be assigned, respectively, to the hard segment carbonyl biuret group and urea group which are present in the curing agent. The new peaks probably arise from new groups formed by the binder network thermal decomposition. At 240°C, the absence of peaks at 1698 and 1642 cm^{-1} can possibly be attributed to some sort of scission of the biuret and urea groups in the hard section, leading possibly to unidentified species absorbing at 1616 and 1587 cm^{-1}. Similar behaviour can be found in the HTPE gumstock sample in Figure 147, however the energetic plasticizer has an effect at temperatures above 150°C. In fact, the peak at 1640 cm^{-1}, that is assigned to the nitrate (ONO_2) groups from the n-BuNENA, is present at 150°C but not at 200°C. This corresponds to the n-BuNENA decomposition as determined by the DSC analysis (see Section 3.3.3) and as reported by Shen [1996] and by Rao [2004]. At 240°C new peaks appear at 1674, 1536, 1454 and 1247 cm^{-1}, possibly resulting from products formed in the decomposition of the cured pre-polymer and n-BuNENA. As the urethane groups are still present in the samples which have been heated up to 240°C, the changes in the binder network physical characteristics, from solid to liquid, can be understood as some sort of scission of the biuret and urea groups in the hard segment, leading to amide or amine groups or other similar species, rather than scission of the urethane groups. A pre-polymer chain scission would have a similar effect on physical characteristics, but the FTIR spectra show no evidence for this. It is more probable that the biuret and urea groups undergo scission, due to the higher reactivity of the carbonyl sites in these groups. However, SEC analyses, as presented in Section 3.5.2, have shown that also the soft segment is scissioning during slow heating.

3.5.1.3 FTIR aged HTPE samples conclusion

The presence of the energetic plasticizer n-BuNENA appears to have an influence on the thermal decomposition of the gumstock when compared with the binder network

thermal decomposition. In fact the binder network became liquid at around 240°C while the gumstock was liquid at 150°C.

Due to the urethane groups still being present in the samples above 150°C, the change in the binder network and gumstock physical characteristics, from solid to liquid, can possibly be assigned from IR analysis to either some sort of scission on the hard segment, biuret and urea groups, leading to amide or amine groups or other similar compounds with an absorption band at 3460 cm^{-1}, or the polymer decomposition i.e. chain scission, rather than the breaking of the urethane links. It was thought more likely to be a biuret and urea group scission rather than a polymer break, due to the higher reactivity of the carbonyl groups. Therefore, possibly some products from the n-BuNENA decomposition, like NO_2 or some other nitro derivative, can be reacting with the carbonyl groups and causing scission of the hard segment at a lower temperature than in the binder network samples. However, from the SEC analyses presented and discussed in Section 3.5.2, it was concluded that the soft segment is also undergoing scission during thermal decomposition.

3.5.2 SEC aged HTPE gumstock analysis and results

In order to determine if, during the gumstock slow heating, the polymeric matrix is undergoing scission, size exclusion chromatography was performed on gumstock samples 5G27B aged at different temperatures. Each gumstock sample was placed in a vial which was flushed with nitrogen gas and heated at either 100, 150 or 200°C for a period of 60 min. A fresh gumstock sample was also included in the analysis. At the end of the heating period samples heated at 150 and 200°C were in the liquid phase, while samples heated at 100°C were in the solid phase, as was the un-aged sample. After the heating process the liquid phase samples were dissolved in THF and their molecular weight determined. Fresh samples and those aged at 100°C were washed with THF and the resultant solution also analysed.

The analysis was performed, as described in Chapter II Section 2, using a Viscotek GPC pump, model VE 1121, with a Waters 2410 Refractive Index Detector (RID) equipped

with a set of two 5 μm PLgel Mixed-C 300 x 7.5 columns and a 5μm PLgel 100 Å 300 x 7.5 mm column. The GPC was controlled via a PC running Walters Millenium software. THF stabilised with BHT (250 ppm) was used as an eluent and polyethylene glycol standards were used for calibration (supplied by Aldrich and Polymer Laboratories respectively).

3.5.2.1 HTPE gumstock, SEC results

Three injections for each sample were performed and the average gumstock broad band SEC results are presented in Table 86, where Mw is the weight-average molecular weight, Mn the number average molecular weight, MP the main peak average molecular weight and the polydispersity is the ratio between Mw and Mn.

Table 86. HTPE 5G27B Gumstock SEC Results

Aged temperature (^{o}C)	Retention time. (min)	Mn	Mw	MP	Polydispersity
Not aged	27.60	133.54	135.24	136.47	1.01
100	27.76	119.30	120.67	121.46	1.01
150	20.35	8534.48	27028.09	13654.37	3.21
150	26.79	218.82	220.84	226.63	1.01
200	22.46	1076.66	1968.05	1895.41	1.83
200	27.05	194.07	196.26	194.83	1.01

The values presented in Table 86 to study the change in molecular weight, have been taken from the average of three injections. The standard deviation (SD) in Table 87 shows acceptable values for the data obtained at retention time 27 min. Their SD is less than 5% for samples not aged and those aged at 100 and 150^{o}C and around 10% for the sample aged at 200^{o}C. However the main peak related to the polymer scission, at retention times of 20 and 22 min have a larger standard deviation at 150 and 200^{o}C. This behaviour is not unexpected, especially taking into account that the polymeric matrix is breaking in a random way and that the new formed broken polymers have irregular shapes. In fact, as can be seen from Figure 150 and Figure 151 there is not a clear limit between polymers of different molecular weight. However, despite the larger

standard deviation observed in the SEC analysis, the results are considered valid enough to demonstrate that the polymer is breaking at the soft segment.

Table 87. HTPE 5G27B Gumstock SEC Standard Deviation from Results

Aged Temp	Ret. Time min	Standard Deviation				
		Ret Time	Mn	Mw	MP	Polydispersity
Not aged	27.60	0.0400	3.8229	3.8639	3.8086	0.0001
100	27.76	0.0090	1.0978	0.9694	0.8036	0.0015
150	20.35	0.0377	1568.3067	2237.7960	660.1087	0.4198
150	26.79	0.0345	3.9753	4.1030	4.3391	0.0005
200	22.46	0.1745	32.1990	178.2737	232.8291	0.1271
200	27.05	0.1031	11.0137	11.1464	11.9114	0.0004

As a reference, HTPE pre-polymer 27B SEC data are presented in Table 88. Figure 148 to Figure 151 show the chromatograms for the fresh and aged gumstock samples and Figure 152 shows the chromatogram for pre-polymer sample 27B.

Table 88. HTPE 27B Pre-polymer SEC Results

Retention time. (min)	Mn	Mw	MP	Polydispersity
20.63	4339.84	8460.01	9711.17	1.95
25.17	502.04	511.90	487.25	1.02
26.91	140.48	141.12	141.04	0.67
27.55	121.32	124.98	140.81	1.03
20.63	4339.84	8460.01	9711.17	1.95
25.17	502.04	511.90	487.25	1.02

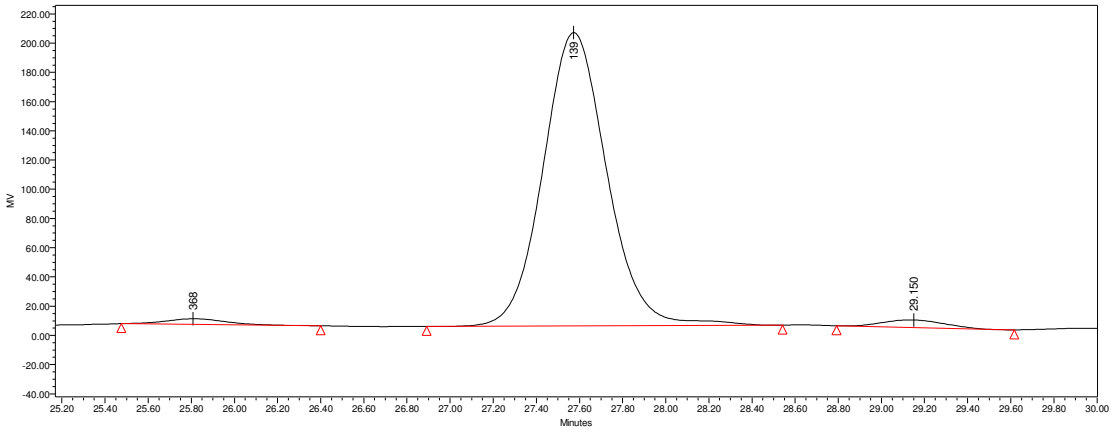

Figure 148. SEC chromatogram for gumstock sample N27B not heated

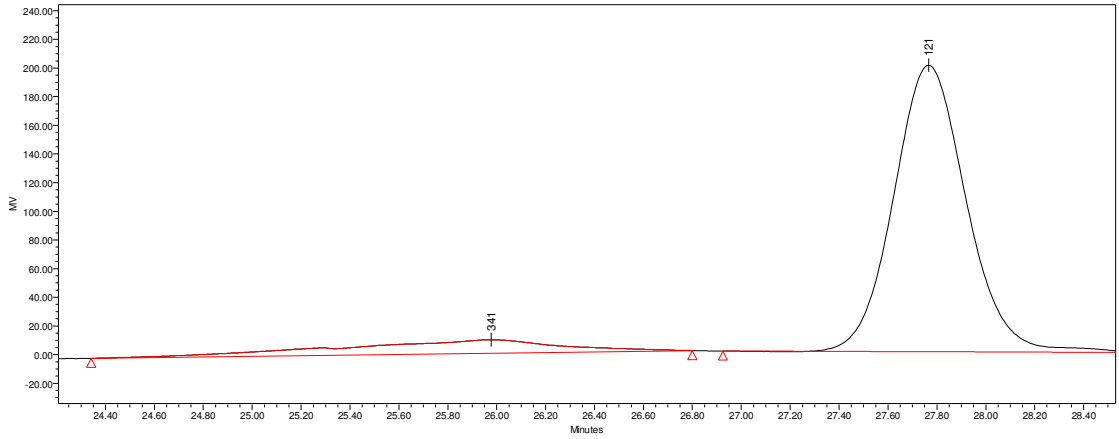

Figure 149. SEC chromatogram for gumstock sample N27B heated at 100°C

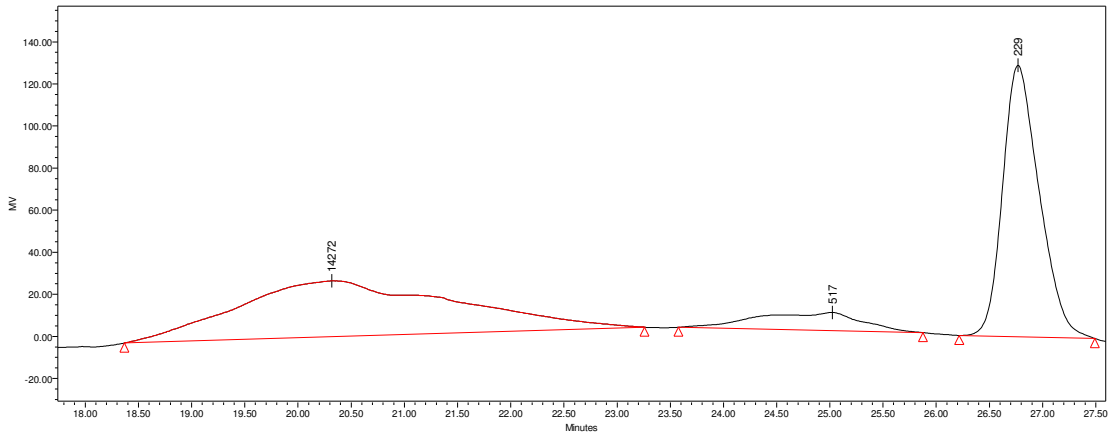

Figure 150. SEC chromatogram for gumstock sample N27B heated at 150°C

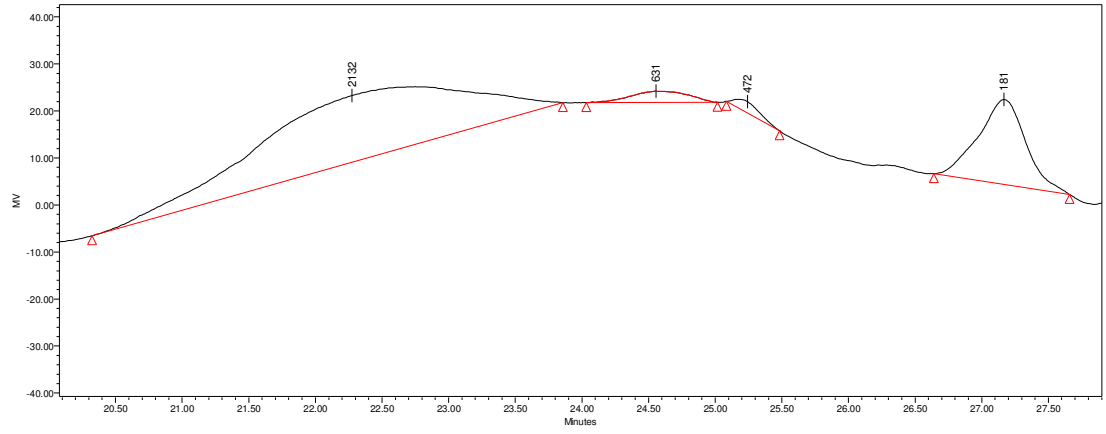

Figure 151. SEC chromatogram for gumstock sample N27B heated at 200°C

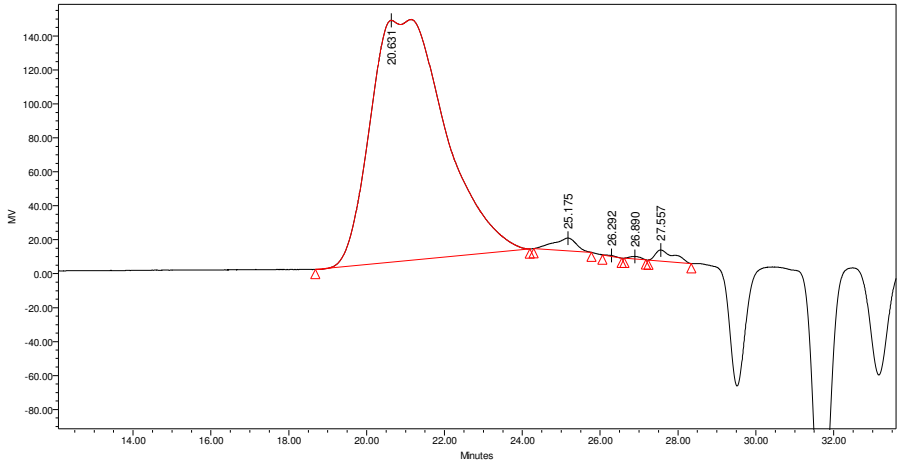

Figure 152. SEC chromatogram for pre-polymer sample 5G27B

3.5.2.2 Discussion of SEC results on aged HTPE gumstock

From the chromatograms for samples heated at 150 and 200°C (Figure 150 and Figure 151), it can be seen that Mn decreases as the heating temperature is increased. In fact, for the sample heated at 150°C two weak peaks, having a wide distribution of molecular weight, can be seen at retention times of 20 and 25 min, corresponding to a Mn of 8500 and 517 g mol^{-1} respectively. The first peak can be correlated to a short polymer chain equivalent to approximately twice the Mn of the pre-polymer i.e. 4339 g mol^{-1}. The peak at retention time 25 min is possibly a short chain material produced by the scission of the main polymeric chain. From the chromatogram in Figure 150, more peaks than in the sample heated at 100°C can be seen (Figure 149). As can be seen from Figure 151, the peaks from the sample heated at 200°C are still wide but the Mn value was decreased to 1070 g mol^{-1}, almost eight times lower than that of the sample heated at 150°C. Also, more peaks can be seen at retention times of 24.5 and 25.2 min, these peaks corresponding to MP values of 631 and 472 g mol^{-1} respectively. This is an indication of polymer chain scission i.e. soft segment scission. These results are in agreement with those presented by Sun [2006], for the thermal decomposition of polyethylene glycol binder and propellant, plasticized with nitrate esters. These authors found that after ageing at 90°C for several hours the molecular weight decreases and the polydispersity increases.

A comparison of the chromatograms of the aged gumstock samples presented in Figure 149 to Figure 151, with a fresh sample of HTPE pre-polymer presented in Figure 152, shows that only the latter has a peak at around Mn 4300 g mol^{-1} with a retention time of 20.6 min. It is suggested that this is because the soft and hard segment of the pre-polymer matrix i.e. pre-polymer segment and curing agent segment, are being scissioned during heating. A more noticeable peak can be seen in all the samples with a retention time of around 27 min, corresponding to an Mn between 119 and 218 g mol^{-1}. They are assigned to fragments of the main chain i.e. EO_3 and THF_1EO_3 segments, as discussed in Chapter II Section 2.4.6, or possibly to n-BuNENA, which has an Mn of 165 g mol^{-1}.

The chromatogram of the sample heated at 100°C, Figure 149, looks very similar to that of the fresh sample presented in Figure 148. In fact, both samples show a peak at a retention time of around 27.6 min, corresponding to an Mn of 119 to 133 g mol^{-1}. Also, a minor peak can be seen at a retention time of 25.8 min, with an MP of 341 and 368 g mol^{-1}. Mn was not able to be obtained. A sample heated at 100°C was not fully liquefied and retained its physical form. This is taken as an indication that decomposition is not happening at that temperature.

3.5.2.3 SEC aged gumstock conclusions

The results obtained from the SEC analysis show that the polymeric chain is scissioning after ageing at different temperatures. Polymers having lower Mn and higher polydispersity than the initial pre-polymer are being produced during the heating process. These low molecular weight segments are produced as a result of the scissioning of the hard segment, as concluded from FTIR analysis in Section 3.5.1, but also from soft segment scissioning.

3.5.3 Binder and gumstock thermal decomposition analysis by GC-MS

In order to determine gases generated during the heating process of binder and gumstock samples, gas chromatography-mass spectrometry (GC-MS) was performed as

explained in Section 2.3.6. A Chrompak DB5 column of 25 metres length, 0.25 mm internal diameter and 0.25 µm film thickness was used. In order to perform the analysis, small amounts of different samples, i.e. pre-polymer HTPE 27B, energetic plasticizer n-BuNENA, binder 16N27B and gumstock 5G27B, were each placed in a headspace vial. The loaded vials were placed in the headspace analyser and kept at 100, 150, or 200˚C for 30 min before being sampled. Gumstock samples were heated at the same temperatures but for 60 min before being sampled.

3.5.3.1 GC-MS results

Characteristic Total Ion Chromatograms (TIC) of samples and components aged at 150°C are presented in Figure 153 to Figure 156. Further chromatograms are presented in Appendix G.

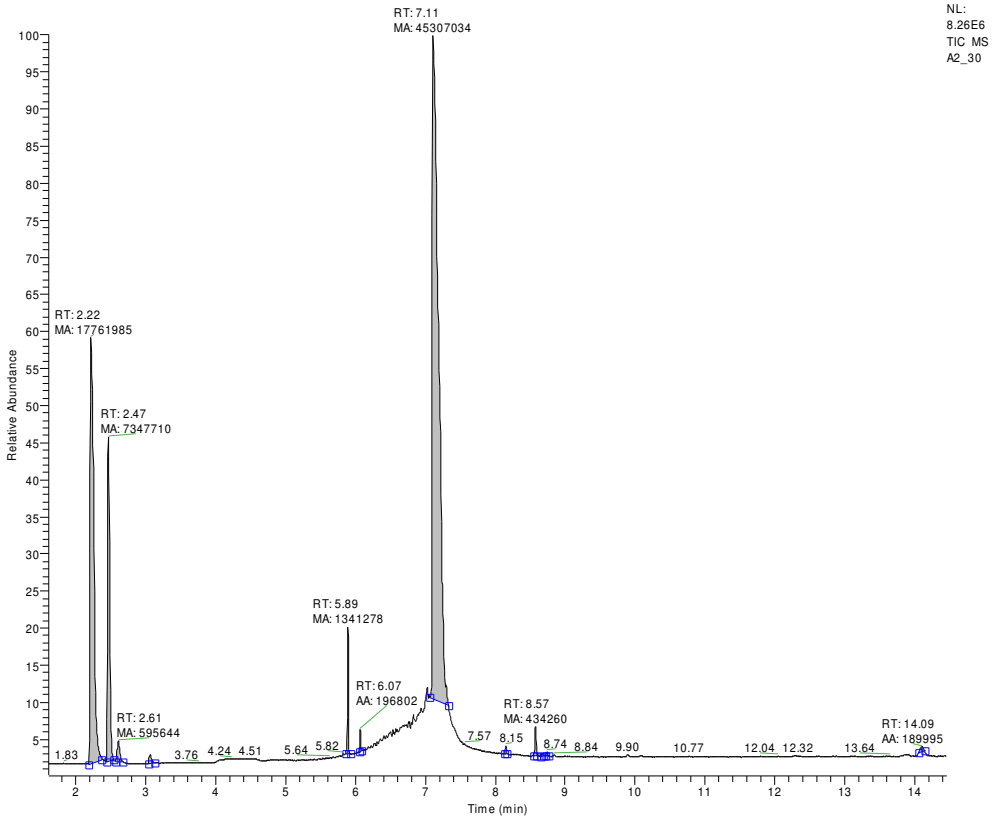

Figure 153. TIC of volatile components from n-BuNENA aged at 150°C for 60 min

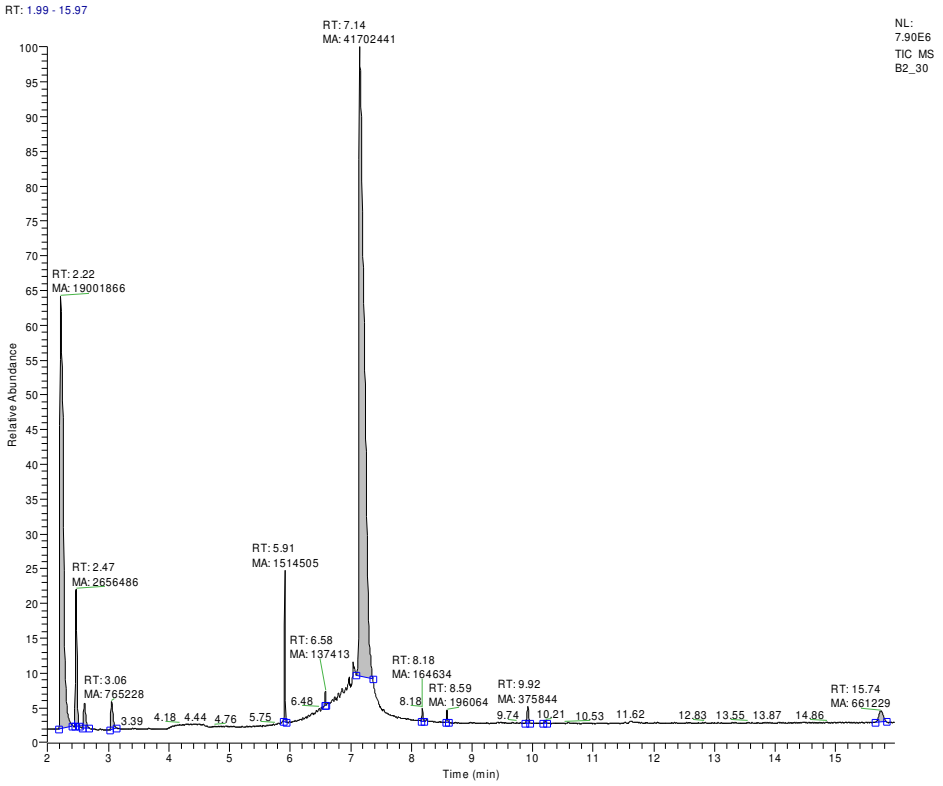

Figure 154. TIC of volatile components from HTPE pre-polymer 27B aged at 150°C

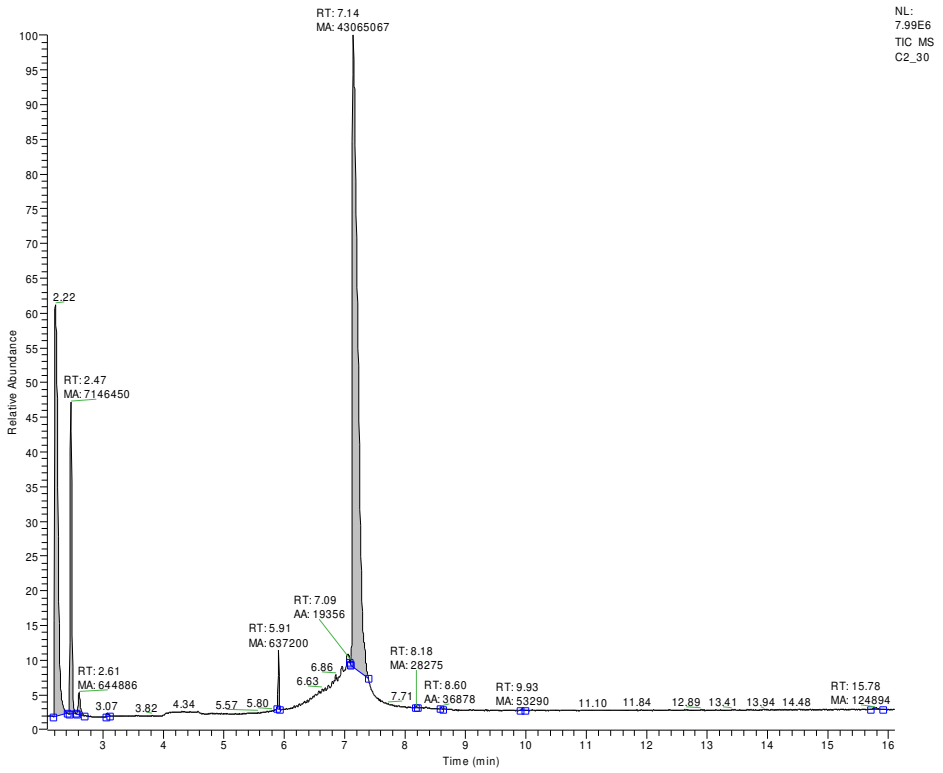

Figure 155. TIC of volatile components from binder network 16N27B aged at 150°C

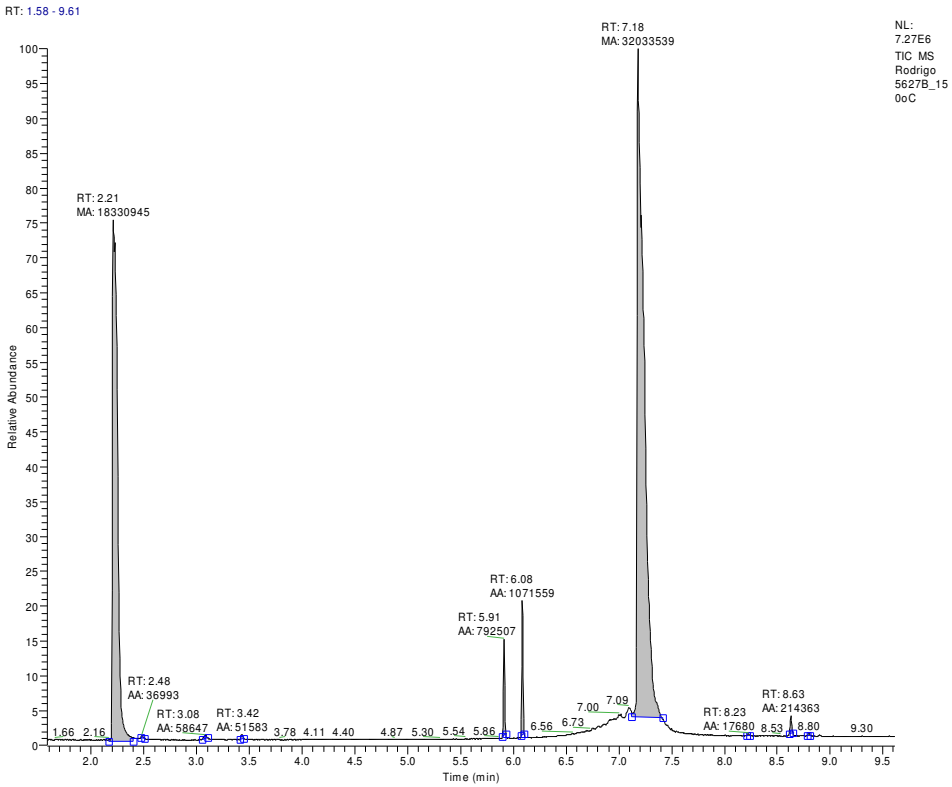

Figure 156. TIC of volatile components from gumstock sample 5G27B aged at 150°C

Table 89 to Table 92 show a summary of the peak retention times and component assignments in the samples. Component identification was based on a NIST Spectral Library Search as explained in Chapter II.

Table 89. Identification of Volatile Components in n-BuNENA from NIST Spectral Library Searches

Peaks in n-BuNENA sample (Retention time, min)	Assignment	SI	RSI	Probability	Hit List Position
2.21	Nitrogen	854	854	74.26	1
2.46	Oxygen	832	837	98.57	1
3.10	Carbon Monoxide	783	901	76.53	1
5.89	Carbon dioxide	893	943	54.08	1
6.10-6.23	Nitrous oxide	870	870	94.41	1
7.08	Water	792	792	96.04	1
8.09	Acetaldehyde	746	91	80.66	1
8.51	2-Butene	843	946	27.80	1
8.68	1-Butene	794	922	27.6	1
13.79	Butanal	732	836	69.05	1
14.01	Chloroform	904	910	92.92	1

Table 90. Identification of Volatile Components in HTPE 27B Pre-polymer Sample from NIST Spectral Library Searches

Peaks in HTPE sample (Retention time, min)	Assignment	SI	RSI	Probability	Hit List Position
2.21	Nitrogen	865	865	75.28	1
2.46	Oxygen	847	852	98.29	1
3.06	Carbon Monoxide	860	862	32.75	2
5.90	Carbon dioxide	933	933	89.73	1
6.58	Ethane	948	949	97.47	1
7.10	Water	912	912	94.36	1
7.57	Propane	869	933	94.04	1
8.18	Acetaldehyde	852	903	84.97	1
8.30	Ethylene oxide	721	899	82.32	1
8.59	Methyl formate	907	917	91.76	1
9.92	Propanal	894	907	90.99	1
10.28	Dichloromethane	717	887	96.75	1
15.74	n-Propyl formate	8.62	888	93.29	1

Table 91. Identification of Volatile Components in Binder Network HTPE 16N27B Sample from NIST Spectral Library Searches

Peaks in HTPE Binder sample (Retention time, min)	Assignment	SI	RSI	Probability	Hit List Position
2.21	Nitrogen	877	877	5845	1
2.46	Oxygen	850	855	98.47	1
3.06	Carbon Monoxide	861	934	83.97	1
5.90	Carbon dioxide	934	934	90.24	1
7.14	Water	937	937	95.09	1
8.18	Ethylene oxide	651	909	66.77	1
8.21	Acetaldehyde	825	862	64.2	1
8.60	Methyl formate	623	813	67.78	1
9.92	Propanal	598	874	72.96	1
15.79	n-propyl formate	613	801	58.93	1

Table 92. Identification of Volatile Components in Gumstock HTPE 5G27B Sample from NIST Spectral Library Searches

Peaks in HTPE Gumstock sample (Retention time, min)	Assignment	SI	RSI	Probability	Hit List Position
2.21	Nitrogen	877	877	5845	1
2.48	Oxygen	771	989	95.86	1
3.09	Carbon Monoxide	782	961	92.90	1
3.44	Nitric oxide	721	859	82.4	1
5.90	Carbon dioxide	934	934	90.24	1
6.08	Nitrous oxide	870	870	94.41	1
7.18	Water	937	937	95.09	1
8.23	Ethylene oxide	584	810	67.62	1
8.63	2-Butene	808	862	64.20	1
8.79	1-Butene	662	863	31.63	1

Table 93 to Table 96 show the integrated area for the main peaks obtained during GC-MS analysis.

3.5.3.2 Binder and gumstock GC-MS thermal decomposition analysis, discussion of results

In order to understand the thermal decomposition behaviour of the binder network and gumstock samples, the results obtained from the GC-MS analyses were normalised. The integration areas from the samples of n-BuNENA, pre-polymer HTPE 27B, Binder Network 16N27B and Gumstock 5G27B presented in Table 93 to Table 96 respectively, were normalized taking into account the presence of Ar as reference and are presented in Table 97 to Table 100.

From the data presented in Table 98 and Table 99, it can be seen that volatile decomposition products from the binder network samples follow a similar trend to the pre-polymer samples. In both cases at 100°C, products such as acetaldehyde, methyl formate, propanal and n-propyl formate are generated as the temperature is increased. These volatile compounds in the binder network samples are possibly generated by the decomposition of the pre-polymer as part of the gel content or by the soft segment of the polymeric matrix. Also, carbon monoxide and carbon dioxide generation increases with temperature while oxygen generation decreases. Slightly different behaviour was observed with water vapour and temperature. While in the pre-polymer samples water generation increases with temperature, in the binder network samples it appears to decrease. This effect can possibly be related to the thermal oxidative decomposition of the binder network. No traces of ethylene oxide were detected in the binder network, in contrast with the pre-polymer aged at 200°C.

Volatile products from the fresh gumstock sample were nitrogen, oxygen, carbon dioxide and water, although some were possibly initially present on the flask or trapped in the sample. Table 100 shows that between 100 and 150°C the generation of carbon dioxide and water vapour increased, while the generation of oxygen decreased. At 150°C nitric and nitrous oxide were generated, which were not present in the binder network decomposition. Also a high amount of carbon dioxide was generated at that temperature. Nitrous oxide on the other hand was present in n-BuNENA decomposition at 100 and at 150°C, but the amount of gas generated in proportion to nitrogen was smaller than in the gumstock sample at 150°C. Also, nitric oxide was generated at

150°C in the gumstock samples but this gas was not observed in n-BuNENA decomposition. At 200°C, an increase in the amount of oxygen generated was observed, while the generation of carbon dioxide, water vapour, nitric oxide and nitrous oxide were reduced. The results suggest that the thermal decomposition of the gumstock arising from the interaction between binder and energetic plasticizer is possibly leading to the decomposition of the hard segment, breaking the urea and biuret links and generating volatile products containing nitric and nitrous oxide. 1-butene and 2-butene compounds were observed at 150°C and these are possible products from the n-BuNENA decomposition. No volatile products that can be related directly to the soft segment, as in binder decomposition, were observed.

3.5.3.3 Binder and gumstock GC-MS thermal decomposition analysis, conclusions

Thermal decomposition of binder network samples at different ageing temperatures is generating volatile compounds that can be related to the scission of the soft segment of the polymeric matrix, i.e. co-polyether chain. On the other hand, the thermal decomposition of the binder when plasticized by n-BuNENA (called the gumstock) is generating volatile products that can be related to the BuNENA decomposition and to the decomposition of the hard segment, i.e. biuret or urea segment.

Table 93. n-BuNENA GC-MS Head Space Integration Peak, 30 min Heating

Tem. °C	Ar	N_2	O_2	CO	CO_2	N_2O	H_2O	CH_3CHO	$CH_3CHCHCH_3$	$CH_3CH_2CHCH_2$	$CH_3CH_2CH_2CHO$	$CHCl_3$	CH_3CN	CH_3CH_2CN
100	612702	18019566	8130556	0	447272	67397	43759177	25733	214446	47178	189938	484035	0	0
150	566768	17762509	7384987	243710	1218551	198369	44649983	96351	442079	37973	147360	521427	0	0
200	1296901	25496662	11766727	0	514573	0	43270923	21638	0	26101	0	0	72514	149599

Table 94. HTPE pre-polymer 27B GC-MS Head Space Integration Peak, 30 min Heating

Tem. °C	Ar	N_2	O_2	CO	CO_2	CH_3CH_3	H_2O	CH_3CHO	EO	CH_3OCHO	CH_3CH_2CHO	CH_2Cl_2	$CH_3CH_2CH_2OCHO$
100	544594	17546819	7863937	0	392108	0	4482009	0	0	0	0	0	0
150	670194	18812346	2707584	757319	1521340	127337	41692769	167549	0	194356	375309	39541	676896
200	716071	18882792	422482	2212659	1997838	279268	47110311	601500	24346	279268	565696	36520	1031142

Table 95. Binder Network 16N27B GC-MS Head Space Integration Peak, 30 min Heating

Tem. °C	Ar	N_2	O_2	CO	CO_2	H_2O	CH_3CHO	EO	CH_3OCHO	CH_3CH_2CHO	CH_2Cl_2	$CH_3CH_2CH_2OCHO$
100	584011	18156902	8316317	0	373767	44332275	0	0	0	0	0	0
150	640146	18192949	7176037	76818	633745	43062621	26886	0	36488	53132	0	166438
200	641262	19077545	5854722	397582	2597111	42086025	109015	0	115427	96189	0	275743

Table 96. Gumstock 5G26E GC-MS Head Space Integration Peak, 60 min Heating

Tem. °C	Ar	N_2	O_2	CO	NO	CO_2	N_2O	H_2O	EO	$CH_3CHCHCH_3$	$CH_3CH_2CHCH_2$
Fresh	4078	20621423	157602	0	0	46669	0	28308390	0	0	0
100	3350	20209847	114480	0	0	51174	0	31030393	0	0	0
150	3370	18238300	56092	94743	77061	855762	1147150	32405846	24629	300575	40435
200	14635	20486289	4406304	0	0	87088	19275	24119357	0	0	41429

Table 97. n-BuNENA GC-MS Head Space Analysis, 30 min Heating

Tem. °C	N_2	O_2	CO	CO_2	N_2O	H_2O	CH_3CHO	$CH_3CHCHCH_3$	$CH_3CH_2CHCH_2$	$CH_3CH_2CH_2CHO$	$CHCl_3$	CH_3CN	CH_3CH_2CN
100	29.41	13.27	0.00	0.73	0.11	71.42	0.042	0.35	0.077	0.31	0.79	0	0
150	31.34	13.03	0.43	2.15	0.35	78.78	0.170	0.78	0.067	0.26	0.92	0	0
200	19.66	9.07	0.00	0.40	0.00	33.36	0.020	0.00	0.020	0.00	0.00	0.06	0.12

Table 98. HTPE 27B GC-MS Head Space Analysis, 30 min Heating

Tem. °C	N_2	O_2	CO	CO_2	CH_3CH_3	H_2O	CH_3CHO	EO	CH_3OCHO	CH_3CH_2CHO	CH_2Cl_2	$CH_3CH_2CH_2OCHO$
100	32.22	14.44	0.00	0.72	0.00	8.23	0.00	0.000	0.00	0.00	0.000	0.00
150	28.07	4.04	1.13	2.27	0.19	62.21	0.25	0.000	0.29	0.56	0.059	1.01
200	26.37	0.59	3.09	2.79	0.39	65.79	0.84	0.034	0.39	0.79	0.051	1.44

Table 99. Binder Network 16N27B GC-MS Head Space Analysis, 30 min Heating

Tem. °C	N_2	O_2	CO	CO_2	H_2O	CH_3CHO	EO	CH_3OCHO	CH_3CH_2CHO	CH_2Cl_2	$CH_3CH_2CH_2OCHO$
100	31.09	14.24	0.00	0.64	75.91	0.000	0	0.000	0.000	0	0.00
150	28.42	11.21	0.12	0.99	67.27	0.042	0	0.057	0.083	0	0.26
200	29.75	9.13	0.62	4.05	65.63	0.170	0	0.180	0.150	0	0.43

Table 100. Gumstock 5G26E GC-MS Head Space Analysis, 60 min Heating

Tem. °C	N_2	O_2	CO	NO	CO_2	N_2O	H_2O	EO	$CH_3CHCHCH_3$	$CH_3CH_2CHCH_2$
Fresh	5056.75	38.65	0.00	0.00	11.44	0.00	6941.73	0.00	0.00	0.00
100	6032.79	34.17	0.00	0.00	15.28	0.00	9262.80	0.00	0.00	0.00
150	5411.96	16.64	28.11	22.87	253.94	340.40	9615.98	7.31	89.19	12.00
200	1399.81	301.08	0.00	0.00	5.95	1.32	1648.06	0.00	0.00	2.83

IV. HTPE PROPELLANT MANUFACTURE AND CHARACTERISATION

4.1 Propellant Manufacture

4.1.1 Introduction

As a preparation for producing hydroxy terminated polyether (HTPE) and hydroxy terminated polybutadiene (HTPB) propellants, initial hand-made batches of HTPE propellants were developed at DCMT. This initial batch preparation helped like a rehearsal for preparing further HTPE batches at Roxel UK rocket motor facilities in a proper propellant mixer. In total, four propellant formulations were prepared for characterisation and testing: two based on HTPE/AP/n-BuNENA, one based on HTPE/AP/PSAN/n-BuNENA and one based on HTPB/AP/DOS. Sample names were similar to those used previously i.e. first in chronological order, the number of the experiment followed by letter P indicating propellant and then the HTPE (or HTPB) pre-polymer sample number. The propellant samples produced at DCMT and at Roxel were designated for HTPE based propellant as: 1P27B, 2P26E and 3P27B and for the HTPB based propellant as 1PHTPB. The reagents and materials used to produced HTPE and HTPB based propellant are listed in Table 101, and the propellant formulation are presented in Table 102.

Table 101. Reagent and Material List for HTPE and HTPB Propellant Manufacture

N°	Reagent	Name	Supplied	Characteristics
1	HTPE pre-polymer	E26E E27B	Cranfield Synthesized	Liquid copolymer from THF and Ethylene Oxide
2	HTPB polymer	R45M	Roxel	Liquid polymer
3	Curing Agent	Desmodur N-3200	Bayer	Pluriisocyanate
4	Curing agent	Isophorone Diisocyanate (IPDI)	Roxel	Diisocyanate
5	Catalyst	Triphenyl Bismuth (TPB)	Roxel	White powder
6	Stabilizer	Nitro Diphenyl Amine (2-NDPA)	Aldrich	Orange crystals
7	Oxidiser	AP	Roxel	Regular, 200µm
8	Oxidiser	AP	Roxel	AP-8000, 7µm
9	Co oxidiser	PSAN	Roxel	ZnO (2.83%) phase stabilized, 160µm
10	Plasticizer	Di Octyl Sebacate (DOS)	Roxel	Transparent liquid
11	Energetic Plasticizer	n-BuNENA	Cranfield Synthesized	Slightly yellow colour liquid

Propellants produced at Roxel were 2P26E and 3P27B and 1PHTPB. Each propellant batch produced at Roxel was used for three small cook off vehicles and one mould specimen for tensile test.

Table 102. HTPE Propellant Formulation Matrix

Propellant Sample	NCO/OH ratio	HTPE (HTPB) g (%)	N-3200 (IPDI) g (%)	n-BuNENA (DOS) g (%)	2NDPA, g (%)	AP Regular g (%)	AP 8000 (%)	PSAN g(%)	TPB mg (%)
1P27B	**0.88**	4.699 (10.39)	0.466 (1.03)	3.619 (8.00)	0.135 (0.29)	25.369 (56.15)	10.873 (24.06)	-.-	0.023 (0.05)
2P26E	**0.85**	54.05 (10.80)	5.49 (1.10)	40.27 (8.05)	0.41 (0.08)	280.04 (55.98)	119.85 (23.96)	-.-	0.14 (0.03)
3P27B	**0.85**	54.47 (10.89)	5.19 (1.04)	40.03 (8.01)	0.41 (0.08)	229.8 (45.96)	119.94 (23.99)	50.0 (10.0)	0.16 (0.03)
1PHTPB	**0.85**	(57.62) (11.51)	(3.92) (0.78)	(17.5) (3.50)	-.-	234.81 (46.91)	186.57 (37.27)	-.-	0.15 (0.03)

4.1.2 HTPE propellant manufacture

4.1.2.1 HTPE hand made propellant manufacture

In order to prepare the first batch of HTPE propellant, HTPE sample 27B together with n-BuNENA, 2-NDPA and TPB were weighed into a round bottomed flask (50 cm^3), degassed by using a 100 cm^3 syringe and then placed into the oven and preheated for 1 h at a temperature of 65^oC. After preheating and degassing the flask, the contents were poured into a polypropylene 50 cm^3 beaker. Because of that, ingredient percentages were recalculated in order to add the appropriate amount of ammonium perchlorate (AP), as presented in Table 102 for sample 1P27B.

In order to add the oxidiser, regular AP was added in two steps, approximately two thirds and one third of the total AP amount. Similarly, milled AP called AP-8000 was added after all the regular AP was mixed with the HTPE-plasticizer mix. This activity was done in three approximately equal additions. After each AP addition, the bulk was manually mixed with a spatula until all the AP particles were coated by liquid phase.

Curing agent was added to the bulk after adding and mixing the last amount of AP. The bulk was stirred manually again for approximately 25 min until the propellant looked

homogenous. The sample was divided and poured into two beakers and placed in an oven at 65°C to proceed with the curing process over a period of 7 days. Figure 157 shows the HTPE propellant sample 1P27B after the curing period of 7 days at 65°C.

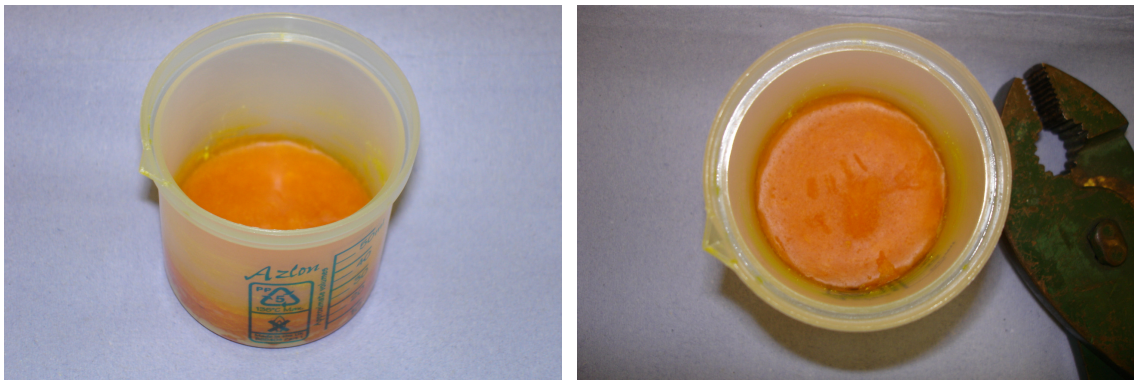

Figure 157. HTPE propellant 1P27B after curing period

4.1.2.2 HTPE and HTPB propellant manufacture in Roxel UK

In order to prepare a bigger batch of HTPE and HTPB propellant, a 1 L mixer HKV 1, model Planetron made by IKA, was used at Roxel UK facilities located in Kidderminster. The mixer allows preparation of up to 1 L of propellant in a vacuum and heated environment. The temperature of the mix is determined via a thermocouple inserted into the mixer blade. A picture of the HKV1 mixer is presented in Figure 158.

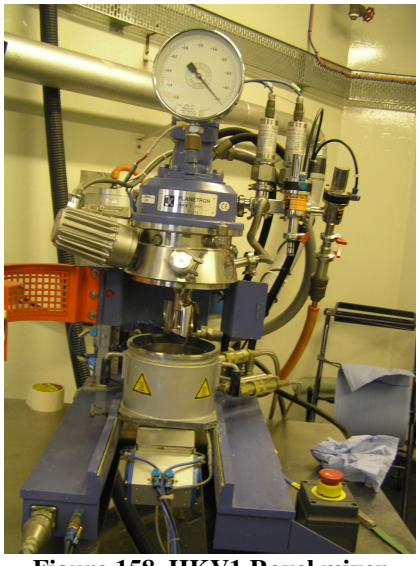

Figure 158. HKV1 Roxel mixer

Two batches of HTPE and one of HTPB propellant were prepared. The first batch of HTPE propellant, called sample 2P26E, contained only AP regular and AP-8000, particle size 200µm and 7µm respectively.

The second batch of HTPE propellant, called 3P27B, contained two oxidisers, AP regular and AP-8000 and PSAN particle size 160µm. Finally, a batch of HTPB AP propellant, called 1PHTPB was also prepared. Details of the formulation for each propellant batch are presented in Table 102.

4.1.2.3 HTPE 2P26E propellant manufacture

HTPE propellant sample 2P26E was prepared according to the following procedure. The regular and milled AP was kept at 60°C overnight in the oven. The moulds and the small cook-off vehicles were placed into the oven at 60°C at the beginning of the activities. The mixer thermo circulator was set to 60°C. HTPE pre-polymer sample 26E (54.05g), n-BuNENA (40.27g) and 2NDPA (0.41g) were placed in the mixer (Figure 159 A). The mixer was closed and ingredients mixed at a blade velocity of 5rpm for 5 min without vacuum. After that, regular AP addition was divided into two steps. In step one 187.05g of AP were added to the bulk (Figure 159 B), the mixer was closed and ingredients mixed at a blade velocity of 15 rpm for 5 min without vacuum. After that (Figure 159 C), a second addition of regular AP was done and 92.99 g were added to the bulk, the mixer closed and the ingredients mixed at a blade velocity of 15 rpm for 5 min without vacuum.

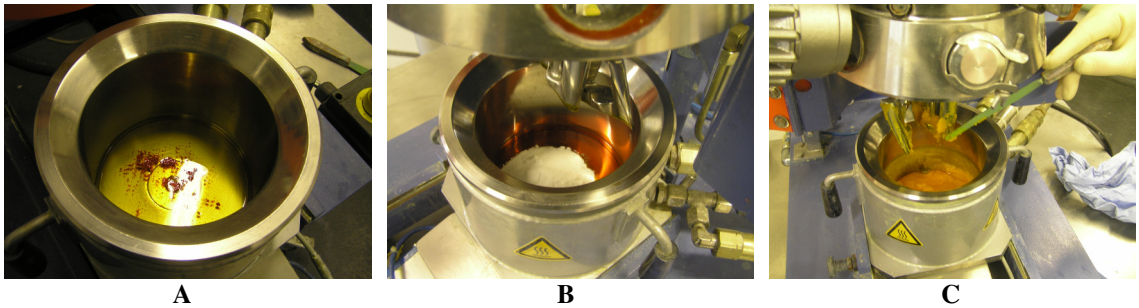

A **B** **C**

Figure 159. Mixing process, (A) HTPE, n-BuNENA and 2NDPA, (B) first AP addition and (C) after mixing of first AP addition.

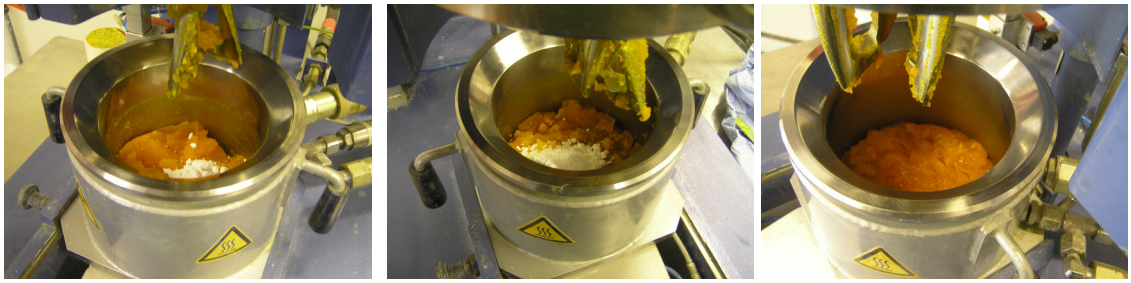

A **B** **C**

Figure 160. Mixing process, (A) after 1st AP-8000 addition, (B) after 2nd AP-8000 addition and (C) 20 min after last AP-8000 addition.

After all regular AP was added, the milled AP (AP-8000) was added in three increments of 40.11, 40.32 (Figure 160A) and 39.42 g (Figure 160B). The mixing was carried on at a speed of 15 rpm for 10 min and vacuum of 2 mbar (200 Pa) was applied after 5 min of mixing. After finishing the AP-8000 addition the propellant mixture was mixed in three periods at a speed of 30 rpm and vacuum, to give a total mixing time of 70 min. During the first 20 min of mixing a vacuum of 28 mbar (2800 Pa) was reached. The propellant appeared homogeneous but the fluidity was not as expected (Figure 160C). At the second period of 20 min, 2 mbar of vacuum was reached and an increase in the samples fluidity was noted. A final period of 30 min mixing was carried out and a vacuum of 2 mbar was reached. After this period the sample became more fluid, having a wet and transparent aspect (Figure 161A).

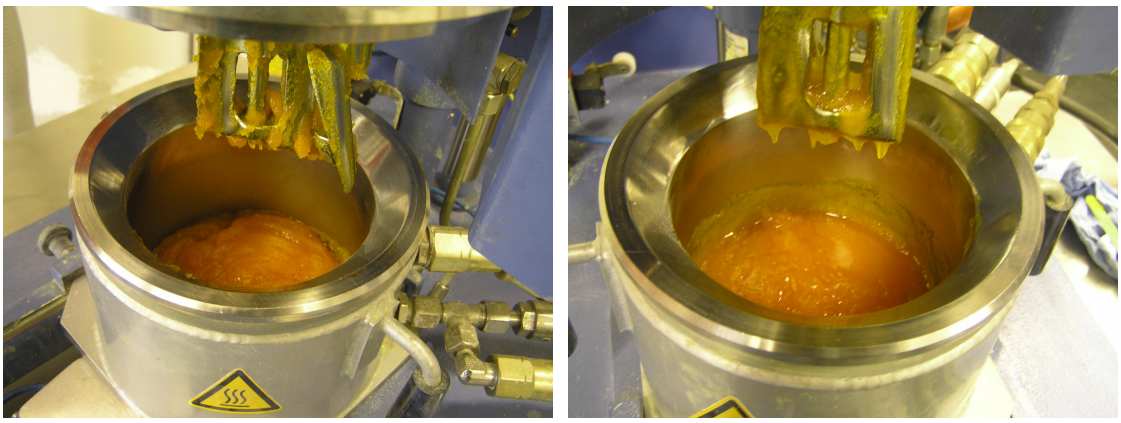

A **B**

Figure 161. Mixing process, (A) 70 min after last AP-8000 addition and (B) 20 min after curing agent addition.

Before addition of the curing agent the sample was left to rest at 60°C and at a vacuum of 500 mbar for 60 min in order to reach a better fluidity. After this period, 0.41 g of

TPB was added to the bulk and mixed for 5 min at 30 rpm. 5.49 g of Desmodur N-3200 was then added to the bulk and mixed for 20 min at 30 rpm and 2 mbar of vacuum. The fluidity of the propellant improved and it appeared wet, transparent and homogeneous. It was decided that the mixture was ready to be poured (Figure 161B).

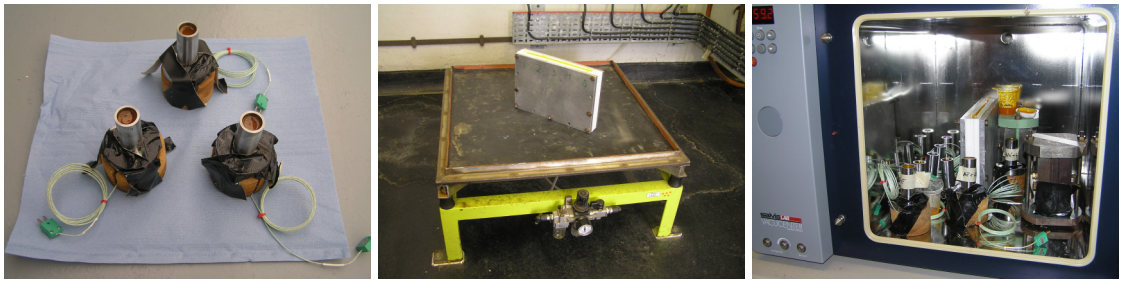

A **B** **C**

Figure 162. (A) Degassing by vibration in the shaker, (B) small cook-off vehicles after shaking and vacuum process and (C) samples in the curing oven.

Once the mixing process was finished the propellant was poured into the small cook-off vehicles (Figure 162A) and the moulds using a spatula. This process was complicated and introduced air into the propellant (during the filling process). In order to try to remove the bubbles, the small cook-off vehicles and the moulds were shaken in a vibrator for 20 min (Figure 162B) and degassed in a vacuum oven until no more bubbles appeared on the surface. Once this process was finished the samples were placed in an oven for 7 days at a temperature of 60ºC (Figure 162C). Table 103 shows the mixing process parameters for the HTPE propellant 2P26E.

Table 103. HTPE2P26E Mixing Parameters

Activity	Mixing time (min)	Mixing speed (rpm)	Vacuum reached (mbar)	Relative bulk viscosity (kW)	Torque (%)	Bulk Temperature (ºC)	Mixer Temperature (ºC)
HTPE, n-BuNENA and 2-NDPA addition	5	5	-	-	-	40	60
AP regular 1st addition	5	15	-	0.12	19	42	60
AP regular 2nd addition	5	15	2	0.12	19	43	60
AP-8000 1st addition	10	15	2	0.12	20	45	60
AP-8000 2nd addition	10	15	2	0.12	22	47	60
AP-8000 3rd addition	5	15	-	0.12	19-20	44	60
Mixing	15	30	17	0.29-0.23	30-29	52	60
Mixing	20	30	2	0.22-0.25	29-30	51	60
Mixing	30	30	2	0.22	22	51	60
TPB addition	5	30	-	0.21-0.22	28	48	60
Curing agent addition	20	30	2	0.21-0.22	28	52	60

After 7 days at a temperature of 60°C the propellant samples were taken out of the oven. As can be seen from Figure 163, propellant HTPE 2P26E looks homogeneous and it has the same orange colour as before the curing process. The propellant surface is smooth and dry and looks well cured. Although the propellant is relatively flexible as can be seen in Figure 163 B, when cut by using a dumbbell shaped cutter it was possible to notice that it is also relatively brittle. Also it was possible to see some small particles of agglomerated AP 8000.

A **B** **C**

Figure 163. HTPE 2P26E propellant samples after curing process.

4.1.2.4 HTPE 3P27B propellant manufacture

HTPE propellant sample 3P27B was prepared according to the following procedure. The regular and milled AP and the PSAN were kept at 60°C overnight in an oven. The moulds and the small cook-off vehicles were placed in the oven at 60°C at the beginning of the activities. The mixer thermo circulator was set to 60°C. HTPE pre-polymer sample 27B (54.47 g), n-BuNENA (40.03 g) and 2NDPA (0.41 g) were placed into the mixer. The mixer was closed and the ingredients mixed at a blade velocity of 5 rpm for 5 min without vacuum.

Regular AP was added in two steps. During step one 130.10 g of AP was added to the bulk, the mixer closed and the ingredients mixed at a blade velocity of 15 rpm for 5 min without vacuum. After that, a second addition of regular AP was done and 99.97 g added to the bulk, the mixer closed and the ingredients mixed at a blade velocity of 15 rpm for 5 min without vacuum. After the AP addition was finished, 50 g of PSAN was added to the bulk and the mixing was performed at 15 rpm for 11 min (Figure 164A).

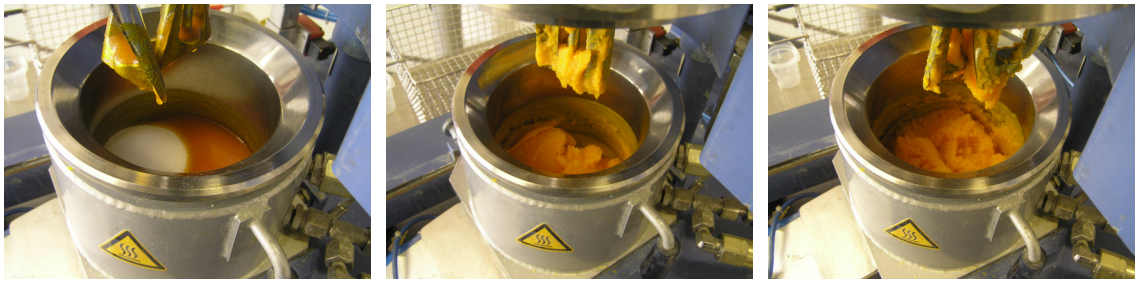

A **B** **C**

Figure 164. Mixing process: (A) PSAN addition after mixing the 2nd regular AP addition, (B) after PSAN addition and mixing and (C) after 1st AP 8000 addition and mixing.

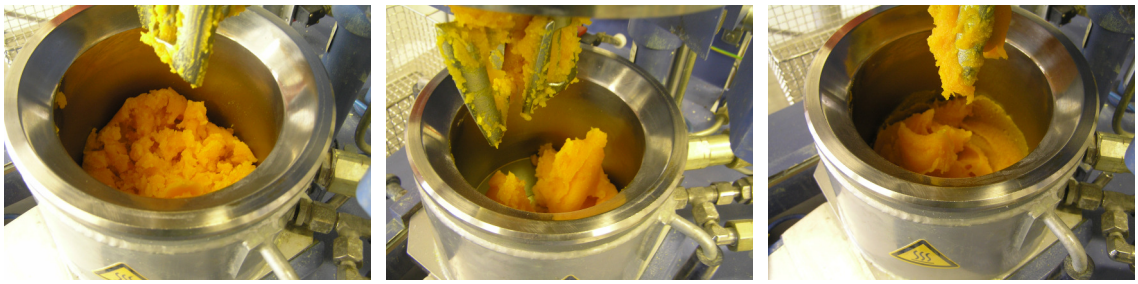

A **B** **C**

Figure 165. Mixing process, (A) after 2nd AP-8000 addition and mixing, (B) 20 min after last AP-8000 addition and (C) after resting by 60 min and mixing second step of 20 min after last AP-8000 addition.

After the PSAN was mixed into the bulk (Figure 164B), the AP-8000 was added in three increments of 40.20, 40.24 and 39.50 g. They were mixed at a speed of 15 rpm for 10 min and a vacuum of 2mbar was applied after 5 min of mixing. At the end of the 1st and 2nd AP-8000 mixing periods (Figure 164C and Figure 165A respectively), the sample looked homogeneous but dry and it was sticking to the mixer blades. After finishing the last AP-8000 addition, the propellant mixture was mixed in three time periods at a speed of 30 rpm and vacuum for a total mixing period of 70 min. The first 20 min of mixing a vacuum of 2 mbar was reached. The propellant looked homogeneous but with a wax-like consistency in terms of flow characteristics (Figure 165B).

Before the second addition of AP-8000 the sample was left to rest at 60ºC at a vacuum of 500 mbar for 60 min in order to reach a better fluidity. After this period, the sample had a more favourable appearance, relatively wet, but still not as expected. During the second period of 20 min, 2 mbar of vacuum was reached and at the end of the mixing process the sample still looked waxy although an increase in its fluidity and wetness was

noted (Figure 165C). A final period of 30 min mixing was done and a vacuum of 2 mbar was reached. At the end of this period the sample had a wetter appearance than previously and its fluidity was greater but still not as expected i.e. at least similar to the previous propellant batch with only AP as oxidiser in the formulation.

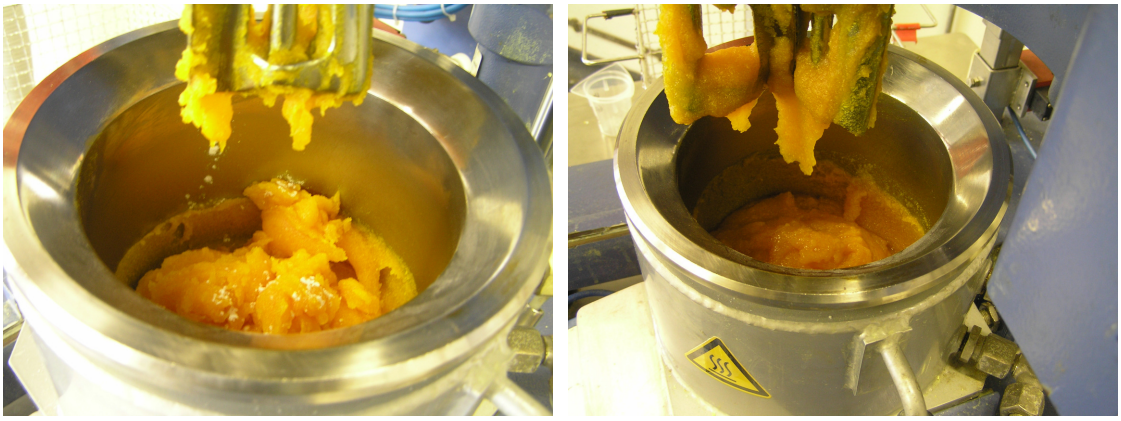

A **B**

Figure 166. Mixing process, (A) addition of TPB after last period of 30 min mixing at the end of the last AP-8000 addition and (B) 20 min after curing agent addition.

After finishing the last addition of AP-8000, 0.41 g of TPB was added to the bulk (Figure 166A) and mixed for 5 min at 30 rpm applying vacuum after 1 min of mixing. 5.19 g of Desmodur N-3200 was then added to the bulk and mixed for 20 min at 30 rpm and 2 mbar of vacuum. At the end of this final mixing period (Figure 166B), the fluidity of the propellant improved after the addition of the curing agent and mixing. It was considered acceptable to be transferred to the small cook-off vehicles and moulds, although its fluidity was not as good as the previous batch at this stage.

Once the mixing process was finished the propellant was poured into the small cook-off vehicles and the moulds using a spatula. As for the previous batch, this process was complicated and introduced air into the propellant. To remove the bubbles from the propellant bulk, the small cook-off vehicles and the moulds were shaken in a vibrator for 20 min and degassed in a vacuum oven until no more bubbles appeared on the surface. Once this process was finished the samples were placed in an oven for 7 days at a temperature of 60^{o}C. Table 104 shows the mixing process parameters for the HTPE propellant 3P27B.

Table 104. HTPE 3P27B Mixing Parameters

Activity	Mixing time (min)	Mixing speed (rpm)	Vacuum reached (mbar)	Relative bulk viscosity (kW)	Torque (%	Bulk Temperature (ºC)	Mixer Temperature (ºC)
HTPE, n-BuNENA and 2-NDPA addition	5	5	-	-	-	37	60
AP regular 1st addition	5	15	2	0.12	19	38	60
AP regular 2nd addition	5	15	2	0.12	19	38	60
PSAN addition	11	15	2	0.12	19	40	60
AP-8000 1st addition	10	15	2	0.12	19	50	60
AP-8000 2nd addition	10	15	3	0.12	20	51	60
AP-8000 3rd addition	5	15	-	0.22	28	47	60
Mixing	15	30	2	0.22	28	53	60
Mixing	20	30	2	0.22	28	54	60
Mixing	30	30	2	0.20-0.21	24-26	55	60
TPB addition	5	30	2	0.21	24-26	55	60
Curing agent addition	20	30	1	0.21	25	56	60

After 7 days at a temperature of 60°C the propellant samples were taken out of the oven. As can be seen from Figure 167 A and C, propellant HTPE 3P27B looks homogeneous and it has the same orange colour as before the curing process. The propellant surface is smooth and relatively sticky, appearing as though it was not fully cured. The propellant is very flexible as can be seen in Figure 167 B; when cut by using a dumbbell shaped cutter it was noticed that it is was not as brittle as propellant sample 2P26E. Also, as for the previous propellant sample, it was possible to see some small particles of agglomerated AP 8000.

A **B** **C**

Figure 167. HTPE 3P27B propellant samples after curing process.

4.1.3 HTPB propellant manufacture

HTPB propellant sample 1PHTPB was prepared according to the following procedures. The regular and milled AP and the PSAN were kept at 60ºC overnight in the oven. The

moulds and the small cook-off vehicles were placed in the oven at 60ºC at the beginning of the activities. The mixer thermo circulator was set to 60ºC. HTPB R45M pre-polymer (57.62 g), DOS (17.5 g) and TPB (0.15 g) were then placed in the mixer. The mixer was closed and the ingredients mixed at a blade velocity of 5 rpm for 10 min without vacuum. After that, regular AP addition was divided into two steps. In step one 155.24 g of AP was added to the bulk, the mixer closed and the ingredients mixed at a blade velocity of 15 rpm for 10 min without vacuum. After that, a second addition of regular AP was done and 79.57 g was added to the bulk, the mixer closed and the ingredients mixed at a blade velocity of 15 rpm for 10 min without vacuum.

After the regular AP was added, the AP-8000 was added in three increments of 61.88, 62.17 and 62.52 g. They were mixed at a speed of 5 rpm for 7 min and vacuum of 2 mbar was applied after 5 min of mixing. After finishing the last AP-8000 addition, the propellant mixture looked very dry and not as wet as expected. It was decided to proceed by mixing periods of 20 min in order to reach a good propellant mix and consistency suitable for pouring into the moulds. A vacuum of 2 mbar was reached during mixing. At the end of the mixing process the propellant still looked dry and did not stick to the mixer blades.

To increase the percentage of liquid and help to improve the mixing conditions, it was decided to incorporate the IPDI. After adding the IPDI to the bulk, different mixing blade speeds were used i.e. 10, 20 and 25 rpm in periods of time of 5, 15 and 5 min respectively. At the end of those periods the bulk looked better in terms of fluidity and started becoming more transparent, like a wet sample. After that, a 30 min period of mixing at 30 rpm was performed. At the end of this period the characteristics of the bulk improved radically and the propellant mixture looked very fluid, wet and transparent aspect. Another two periods of 10 min at 30 rpm allowed the propellant to reach a good fluidity, acceptable to be poured into the small cook-off vehicles and moulds.

Once the mixing process was finished the propellant was poured into the small cook-off vehicles and the moulds using a spatula. As with the previous batches, this process was complicated and introduced air into the propellant. To remove the bubbles from the

propellant bulk, the small cook-off vehicles and the moulds were shaken in a vibrator for 20 min and degassed in a vacuum oven until no more bubbles appeared on the surface. Once this process was finished the samples were placed into an oven for 7 days at a temperature of 60°C. Table 105 shows the mixing process parameters for the HTPB propellant 1PHTPB.

Table 105. HTPB 1PHTPB Mixing Parameters

Activity	Mixing time (min)	Mixing speed (rpm)	Vacuum reached (mbar)	Relative bulk viscosity (kW)	Torque (%)	Bulk Temperature (°C)	Mixer Temperature (°C)
HTPB, DOS and TPB	10	5	-	-	-	39	60
AP regular 1st addition	10	5	2	0.12	19	40	60
AP regular 2nd addition	10	5	2	0.12	19	42	60
AP-8000 1st addition	7	5	2	0.05	17	40	60
AP-8000 2nd addition	7	5	2	0.05	17	42	60
AP-8000 3rd addition	20	10	2	0.05	17	42	60
Curing agent addition	5	10	2	0.21	25	48	60
Mixing	15	20	2	0.22	26	49	60
Mixing	5	25	2	0.24	28	54	60
Mixing	30	30	2	0.23	29	55	60
Mixing	10	30	2	0.22	26	55	60
Mixing	10	30	2	0.22	27	55	60

After 7 days in the oven at a temperature of 60°C the propellant samples were taken out of the oven. As expected, propellant made from the HTPB binder was homogeneous and well cured. It was flexible and when cut by the dumbbell shape cutter no brittleness was observed as can be seen in Figure 168.

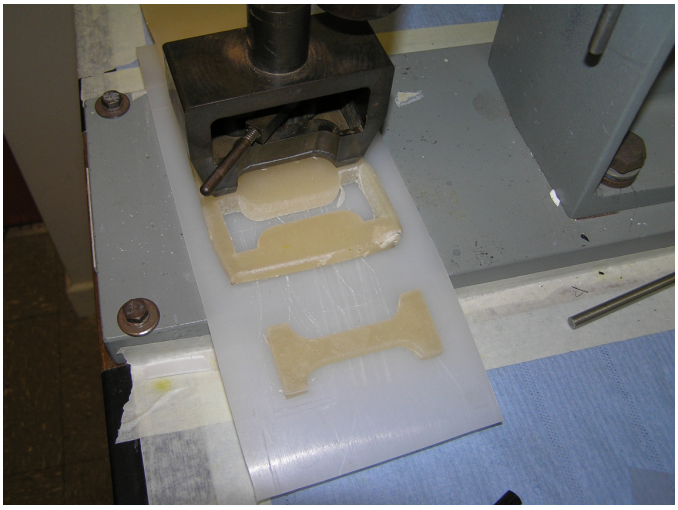

Figure 168. HTPB propellant samples after curing process.

4.1.4 HTPE propellant manufacture conclusions

Two different batches of HTPE and one batch of HTPB propellant were manufactured. Apparently the process conditions in terms of temperature, mixing time and blade speed allowed the production of a homogenous propellant. However, both HTPE propellant batches required different process conditions. In fact, the propellant containing only AP as oxidiser was easier to mix and at the end of the mixing process it look well mixed, wet and with sufficient fluidity to be poured into the mould.

On the other hand, the addition of PSAN to the second HTPE batch changed the mixing conditions in comparison with the previous batch, making it more difficult to reach good fluidity. Also despite the HTPE propellant containing PSAN initially looking to have a lower pot-life than the propellant containing only AP as oxidiser, at the end of the curing process it was not fully cured. Possibly the hygroscopicity of the PSAN or some other of its characteristics have an effect on the interaction between binder and curing agent during the curing process that was only possible to observe when this oxidiser was included in the mix.

4.2 Propellant Characterization

4.2.1 HTPE and HTPB propellant SEM analysis results

In order to study the surface morphology of the HTPE and HTPB propellant samples i.e. 2P26E, 3P27B and 1PHTPB, scanning electron microscopy (SEM) analyses were performed. From each propellant sample a slice was cut from the bulk using a steel blade. Only for HTPE propellant samples a slice was taken from the face that was in contact with the mould.

A JEOL scanning electron microscope model JSM-84AA was used. HTPE and HTPB propellant samples were coated with a thin layer of gold. An accelerating potential of 5kV was used for the analysis. A magnification between the range of 200x and 3300x was used.

4.2.1.1 HTPE 2P26E propellants SEM analysis results

Figure 169 shows the SEM micrograph for a slice of HTPE propellant sample 2P26E, where (A) was taken at a magnification of 200x and (B) is a close up of (A) at a magnification of 900x. Figure 170 shows the SEM micrograph taken of the propellant face that was in contact with the mould, where (A) was taken at a magnification of 300x and (B) is a close up of (A) at a magnification of 3300x.

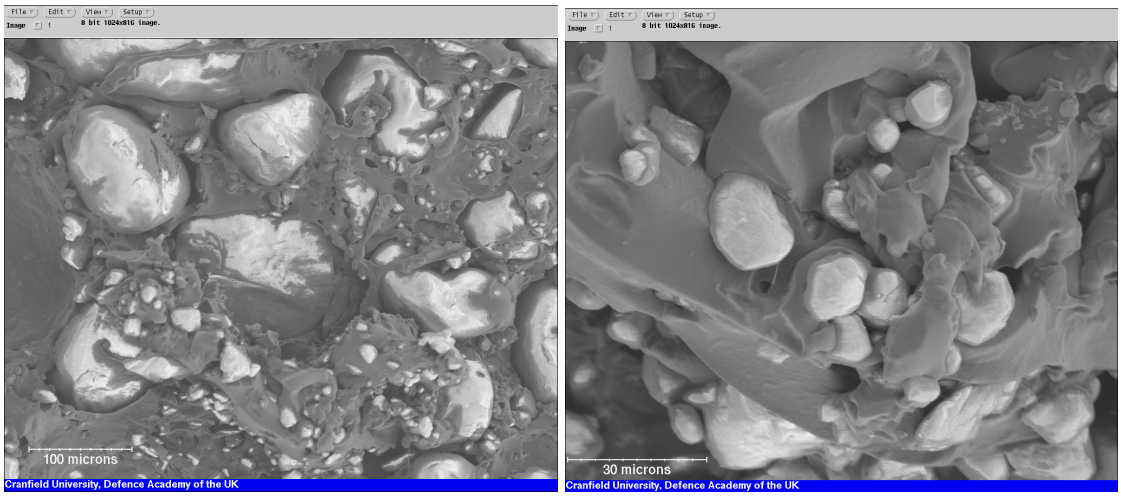

A **B**

Figure 169. HTPE 2P26E SEM micrographs at a magnification of (A) 200x and (B) 900x

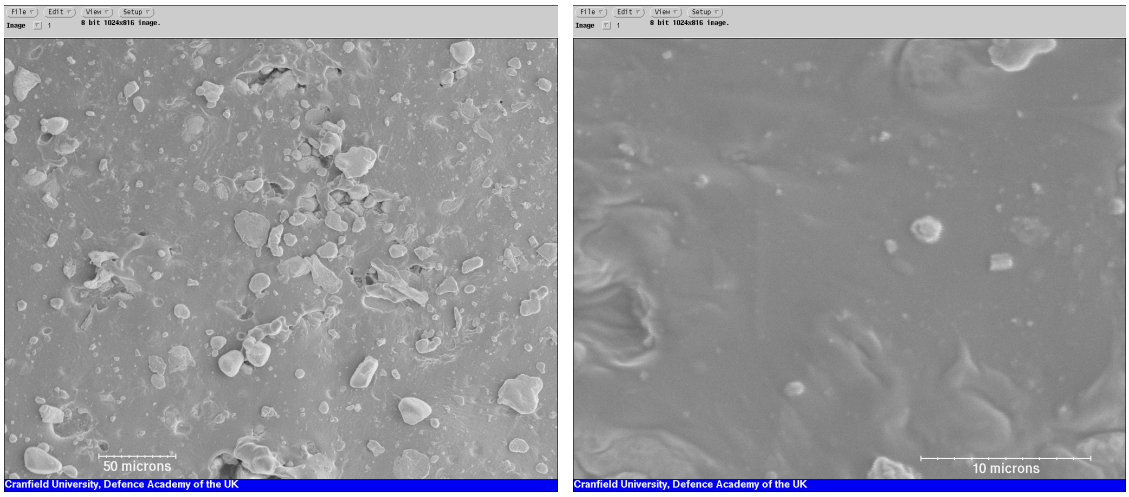

A **B**

Figure 170. HTPE 2P26E SEM micrographs at a magnification of (A) 300x and (B) 3300x.

4.2.1.2 HTPE 3P27B SEM analysis results

Figure 171 shows the SEM micrograph of a slice of HTPE propellant sample 3P27B, where (A) was taken at a magnification of 200x and (B) is a close up of (A) at a magnification of 400x. Figure 172 shows the SEM micrograph of a slice of HTPE propellant sample 3P27B, taken of the propellant face that was in contact with the mould, where (A) was taken at a magnification of 300x and (B) is a close up of (A) at a magnification of 900x.

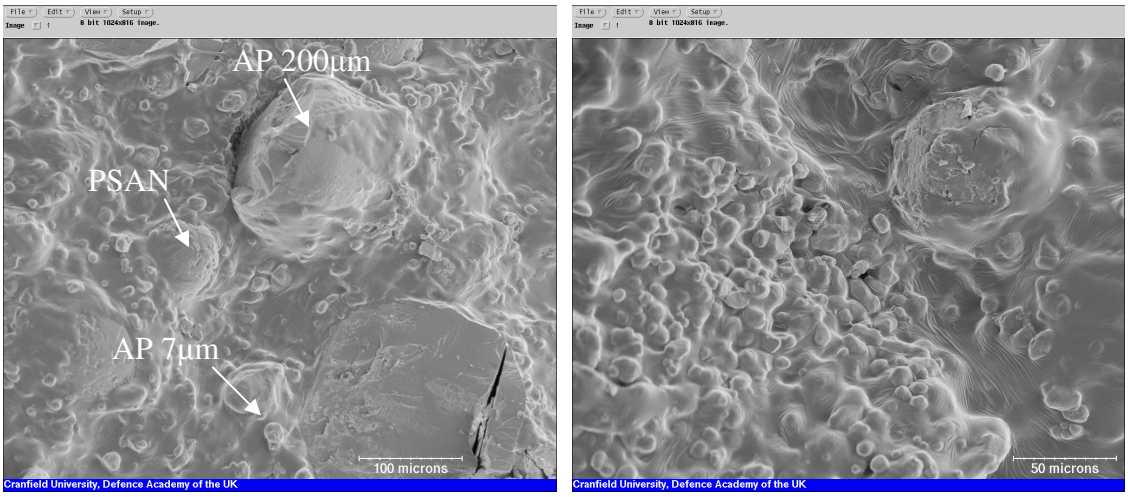

A **B**

Figure 171. HTPE 3P27B SEM micrographs at a magnification of (A) 200x and (B) 400x

Figure 173 shows the energy dispersive X-ray spectroscopy (EDX) spectrum obtained from the propellant sample shown in Figure 171 A, where (A) corresponds to AP of crystal size 200µm, (B) to AP of crystal size 7µm and (C) is PSAN.

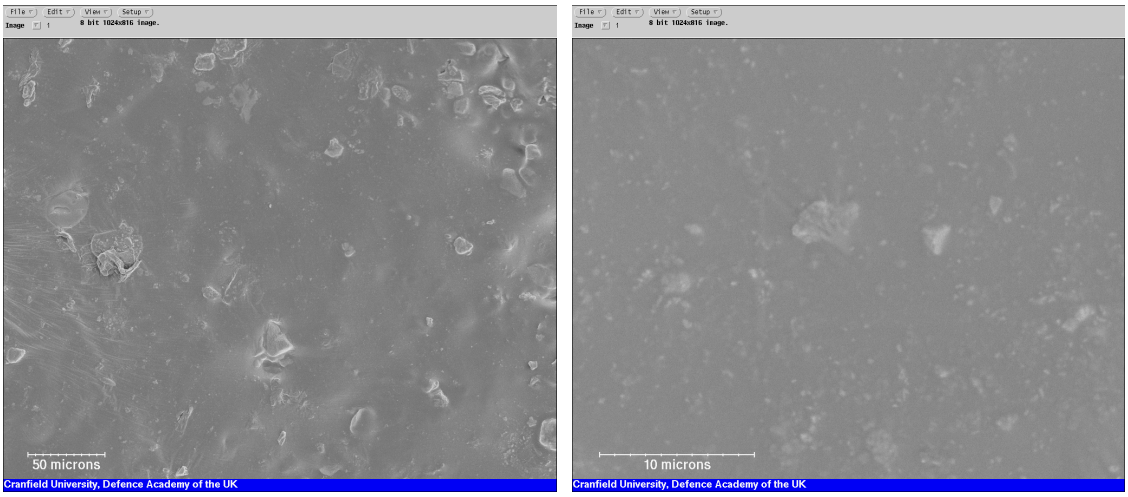

A **B**

Figure 172. HTPE 3P27B SEM micrographs at a magnification of (A) 300x and (B) 900x.

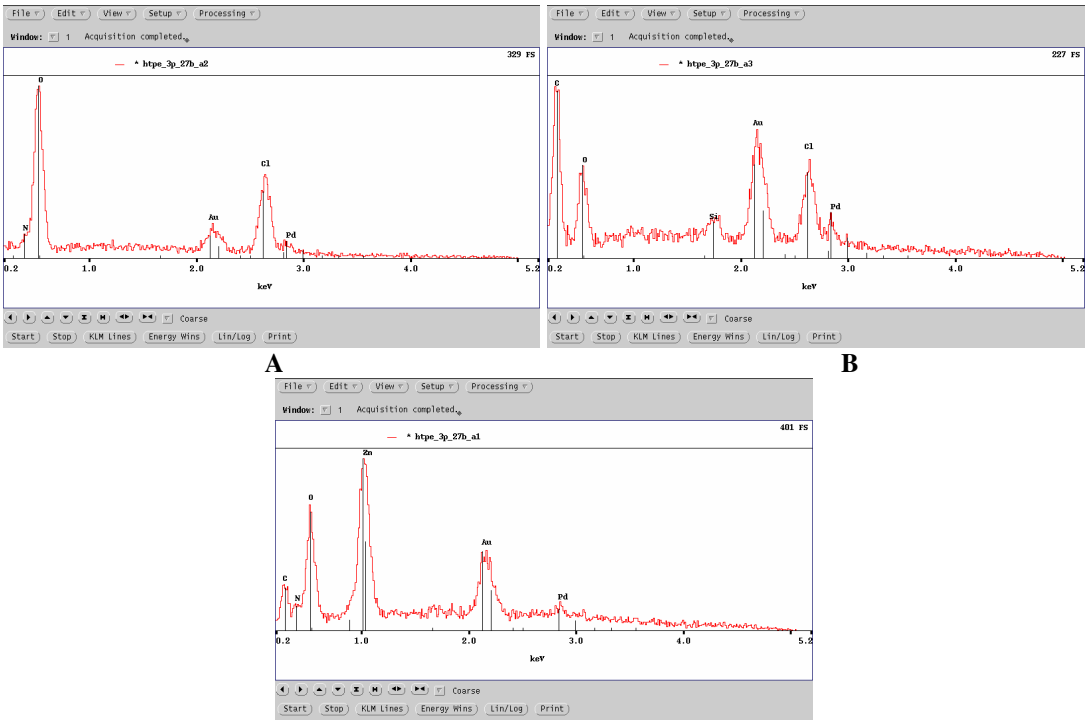

A B C

Figure 173. HTPE 3P27B SEM EDX for a sample of (A) 200µm AP particle and (B) 7µm AP particle and (C) 160µm PSAN particle

4.2.1.3 HTPB 1PHTPB SEM analysis results

Figure 174 shows the scanning electron micrograph for a slice of HTPB propellant sample 1PHTPB, where (A) was taken at a magnification of 200x and (B) is a close up of (A) at a magnification of 900x.

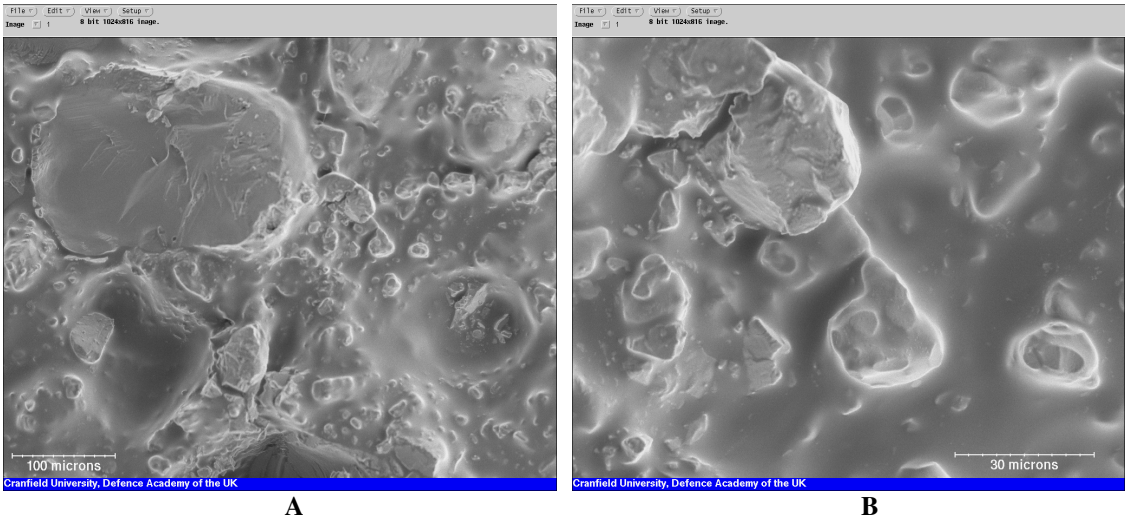

A B

Figure 174. HTPB 1PHTPB SEM micrographs at a magnification of (A) 200x and (B) 900x.

4.2.1.4 Discussion of HTPE and HTPB SEM results

HTPE propellant sample 2P26E contains as oxidiser a bimodal mixture of AP, 200 and 7μm. As can be seen from the SEM micrograph from the transverse section of the propellant in Figure 169, the particle distribution is homogeneous. Although the crystal appears to be coated with a layer of binder, a debond between the crystal and binder can be seen all around the perimeter of the AP crystals. No bonding agent was used in the formulation that might have helped to avoid this separation. In the close up from the same figure this debond can be better appreciated at the 7μm AP crystals. The binder itself looks homogeneous and relatively transparent, though orange in colour. Mechanical properties were not measured but significant qualitative differences in flexibility were found in comparison with PSAN/AP HTPE based propellants. The poor mechanical properties can be partially understood when looking at the bonding between AP crystals and binder. From Figure 170 it can be seen that on the propellant surface that was attached to the curing mould, the crystals appear to be well coated by binder, although some small cavities can be seen.

The situation was different when PSAN was incorporated into the HTPE propellant formulation. In fact, the propellant with PSAN/AP was very flexible although also relatively sticky. Possibly these samples were not fully cured. As can be seen from Figure 171, the three kinds of particles were well distributed. They are AP 200μm, AP 7μm and PSAN 160μm and were identified by using energy dispersive X-ray spectroscopy (EDX) when looking for the Cl and Zn atoms present in AP and in PSAN[1] respectively, as shown in Figure 173. The crack observed on the flat surface of the AP crystal was possibly created by the blade action when cutting the samples for SEM analysis. As can be seen, a good bond between oxidiser crystals and binder was present in this composition and no debonds were observed. However, some wrinkles can be observed on the propellant binder surface. They can be better appreciated on the close up of the surface (Figure 171 B), where the cavities observed on the binder surface can be attributed to the effect of the electron beam on the binder when zooming. As described above, after the curing process during propellant manufacture, samples containing PSAN were very sticky, possibly an indication they were not completely

[1] Zn in the form of ZnO (2.38% weight), is used as phase stabilizer in PSAN.

cured. Perhaps PSAN is introducing water into the mixture due to its hygroscopicity. This water could be interacting with the curing agent, preventing a proper curing process. As explained by Menke [2006], one possibility to avoid introducing water is to have PSAN in spherical particles and coated by a layer of SiO_2. This kind of PSAN has a water content between 0.02 and 0.04%. On the other hand, for HTPE propellant containing only AP as oxidiser (Figure 172), it can be seen that on the propellant surface that was attached to the curing mould, the crystals appear to be well coated by binder.

As can be seen from Figure 174, the HTPB propellant containing a bimodal mixture of AP looks similar to the HTPE 3P27B propellant. However no wrinkles can be observed. There is a good particle distribution and all AP crystals look well coated by the binder. No debonds were observed between the AP crystal surface and binder as in HTPE 2P26E.

4.2.1.5 HTPE and HTPB SEM conclusions

SEM photographs show good oxidiser particle distribution for all the three propellants. The HTPE propellant having only AP as oxidiser appears to have a poor bond between AP particles and binder. This possibly accounts for the observed poor flexibility of the propellant. The HTPE propellant having PSAN and AP as oxidiser shows a better bond between binder and oxidiser. The same was observed for the HTPB/AP propellant. The PSAN propellant looks less cured and the presence of wrinkles on its surface highlights different viscoelastic characteristics in comparison with the HTPE propellant containing only AP as oxidiser. The presence of PSAN in the propellant formulation, possibly due to its hygroscopic properties, appears to be affecting the post-cure properties i.e. mechanical properties.

4.2.2 HTPE and HTPB propellant density measurements

Density determination at 25^{o}C was performed on propellant samples HTPE/AP/n-Bu-NENA (1P27B and 2P26E), HTPE/AP/PSAN/n-Bu-NENA (3P27B) and HTPB/AP/DOS (1PHTPB). In order to do this, an AccuPyc 1330 Pycnometer for 1 cm^3 samples from Micromeritics was used as detailed in Chapter II Section 2.3.7. A

propellant sample weighing between 0.2 and 0.3 g was introduced into the calibrated volume container and then placed in the instrument. Five measurements were taken and the average density was calculated and reported by the instrument, together with the standard deviation. The test was carried on at a helium gas pressure of 20 psi (0.137 MPa). HTPE propellant density data for samples with and without PSAN in its formulation are presented in Table 106. Similarly, HTPB density measurements are presented in Table 107.

Table 106. HTPE Propellant Density Measurements

HTPE propellant Sample	Average density (g cm^{-3})	Sample weight (g)	Average volume (cm^3)	Volume standard deviation (cm^3)	Density standard deviation (g cm^{-3})
1P27B	1.7252	0.3482	0.2018	0.0002	0.0018
2P26E	1.7067	0.2433	0.1426	0.0001	0.0009
3P27B	1.6804	0.1985	0.1181	0.0001	0.0017

Table 107. HTPB Propellant Density Measurements

Sample	Average density (g cm^{-3})	Sample weight (g)	Average volume (cm^3)	Volume standard deviation (cm^3)	Density standard deviation (g cm^{-3})
1PHTPB	1.6368	0.3287	0.2008	0.0001	0.0005

4.2.2.1 *HTPE and HTPB propellant density measurements, discussion of results*

As can be seen from Table 106, for the two HTPE propellant batches containing AP alone as oxidiser, the density is around 1.71 g cm^{-3}. This figure is slightly higher than the density measured for the sample containing PSAN and AP as oxidiser, which was 1.68 g cm^{-3}. This is possibly affected by the PSAN density, which is around 1.64 g cm^{-3}, in comparison with AP density which is around 1.90 g cm^{-3} [Urbanski, 1984]. However in general terms, the measured HTPE propellant density was lower than the figures stated in the literature [Goleniewsky 1998 and Comfort 2000]. The percentage of solid used for this work was around 80% and 20% was liquid with the energetic plasticizer being 8%. This makes it impossible to compare one to one the manufactured propellant density with that of other HTPE propellants, where density figures are between 1.77 and 1.85 g cm^{-3} according to Goleniewsky [1998] and Comfort [2000], possibly because they have a higher solid percentage of between 83 and 88%. Also they have Aluminium

in the formulation and, according to Chan [2005], a higher n-BuNENA content, ranging from 8.5 to 12 %. However, the measured density of the propellant manufactured during this work is not far from these figures.

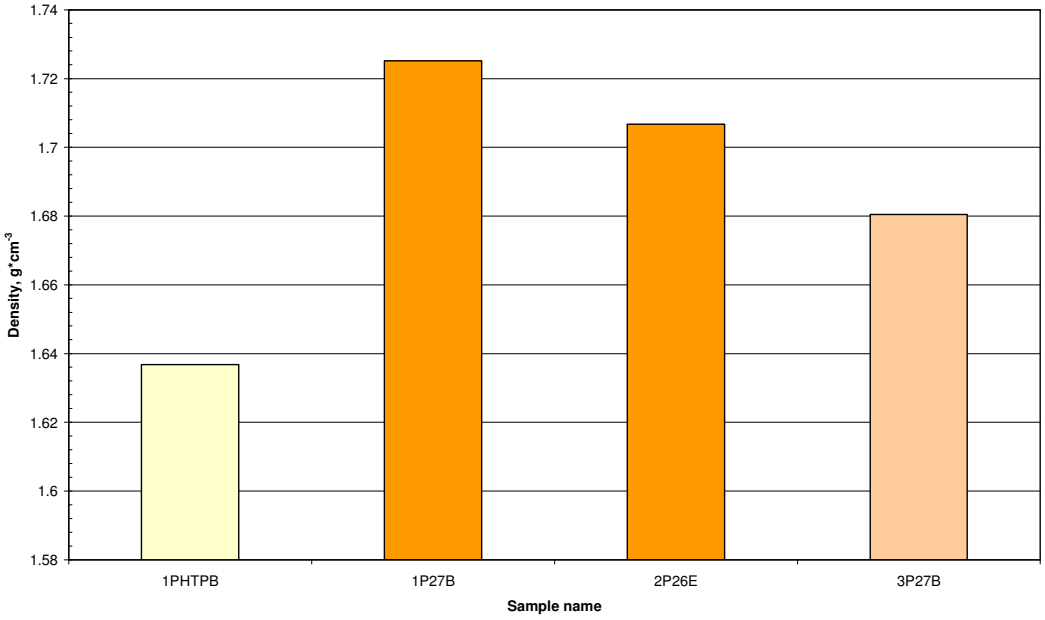

Figure 175. HTPE and HTPB density comparison

When comparing propellant density figures between HTPE and HTPB binder samples, Figure 175, it can be noticed that samples prepared with HTPE had a higher density than HTPB samples, following the same trend as the HTPE binder network and gumstock, as presented in Chapter III Section 3.3.2. As was stated there, the main contribution to density is coming from the presence of the energetic plasticizer i.e. samples made from HTPE were prepared using 42.64% of n-BuNENA (density 1.22 g cm^{-3}) relative to the pre-polymer, and the HTPB sample was prepared using 24.46% of DOS plasticizer (density 0.91 g cm^{-3}) relative to the pre-polymer.

4.2.2.2 HTPE and HTPB propellant density measurements, conclusions

In general terms samples based on HTPE/n-BuNENA plus oxidiser have a higher density than propellant samples based on HTPB. Among HTPE propellant, samples

containing PSAN and AP as oxidiser show the lowest density, this behaviour being due to the lower density of PSAN in comparison with AP.

4.2.3 HTPE propellant DSC and TGA analysis results

In order to analyse the thermal behaviour of HTPE based propellant, differential scanning calorimeter (DSC) analysis was performed to determine glass transition temperature (Tg) and thermal decomposition (TA). Thermogravimetric analyses (TGA) were also carried out. The thermal analyses were performed using the same equipment and procedures stated in Chapter II Section 2.3.4. An inert environment was maintained during all the analyses by using a flow of nitrogen of 40 cm^3 per min. Analyses were performed at a heating rate of 10^oC per min in the temperature range -100 to +30^oC for Tg, 30 to 500^oC for TA analysis and 30 to 550^oC for TGA. Also a thermal decomposition analysis was performed on samples of AP, PSAN and mixtures of both oxidisers with the energetic plasticizer n-BuNENA.

4.2.3.1 HTPE and HTPB Propellants Tg determination and thermal analysis results

Figure 176 shows the DSC Tg thermogram of HTPE propellant samples (A) 9.8 mg of sample 1P27B and (B) 5.4 mg of sample 2P26E, both formulated on HTPE/AP/n-BuNENA. Figure 177 shows the DSC Tg thermogram of HTPE propellant samples, for (A) 4 mg of sample 3P27B formulated on HTPE/AP/AN/n-BuNENA and (B) 5.5 mg of sample 1PHTPB.

Table 108 shows the summary of DSC Tg thermogram information corresponding to HTPE and HTPB propellant samples presented in Figure 176 and Figure 177.

Table 108. HTPE and HTPB Propellant Data From DSC Tg Analysis

Sample N^o	Tg, Inflection point ($^\circ C$)
1P27B	-75.03
2P26E	-76.28
3P27B	-62.89
1PHTPB	-70.43

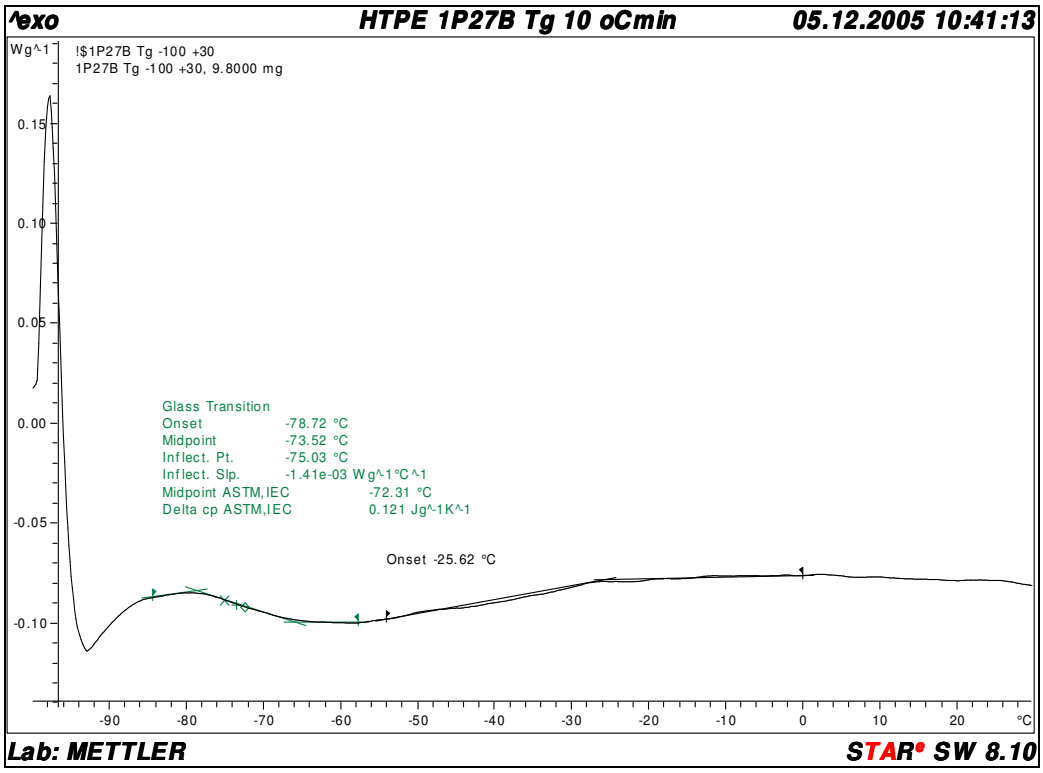

A

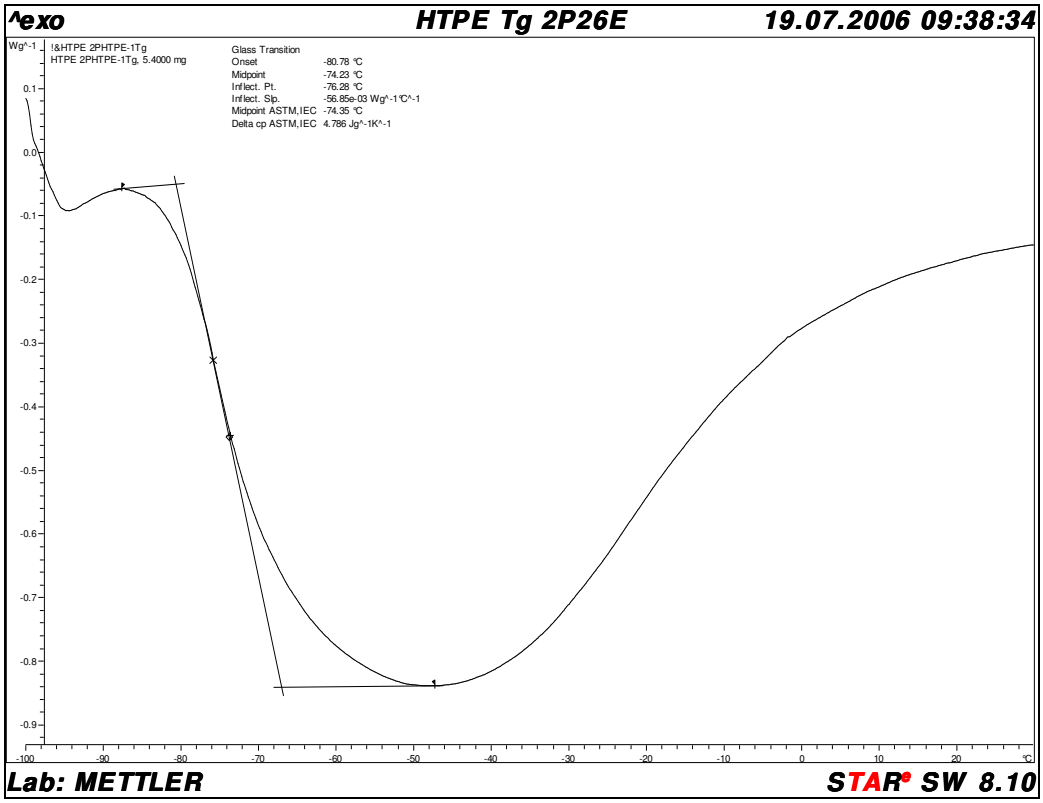

B

Figure 176. DSC Tg thermogram of HTPE propellant samples (A) 1P27B and (B) 2P26E

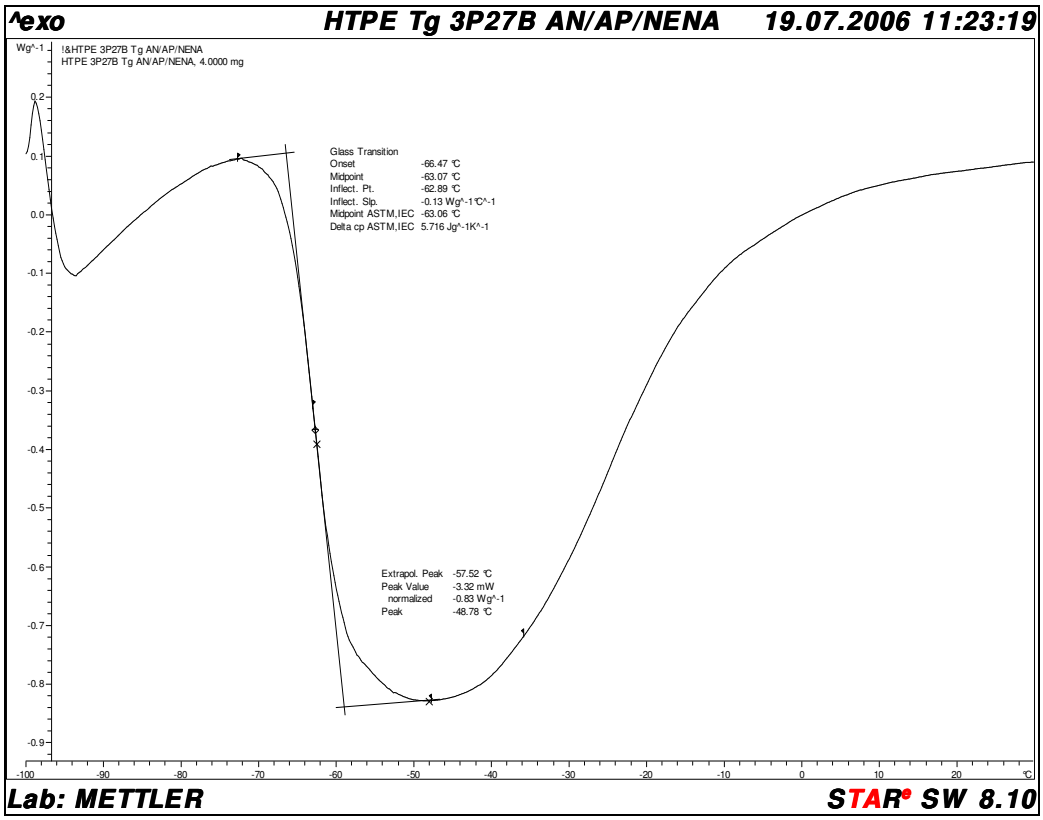

A

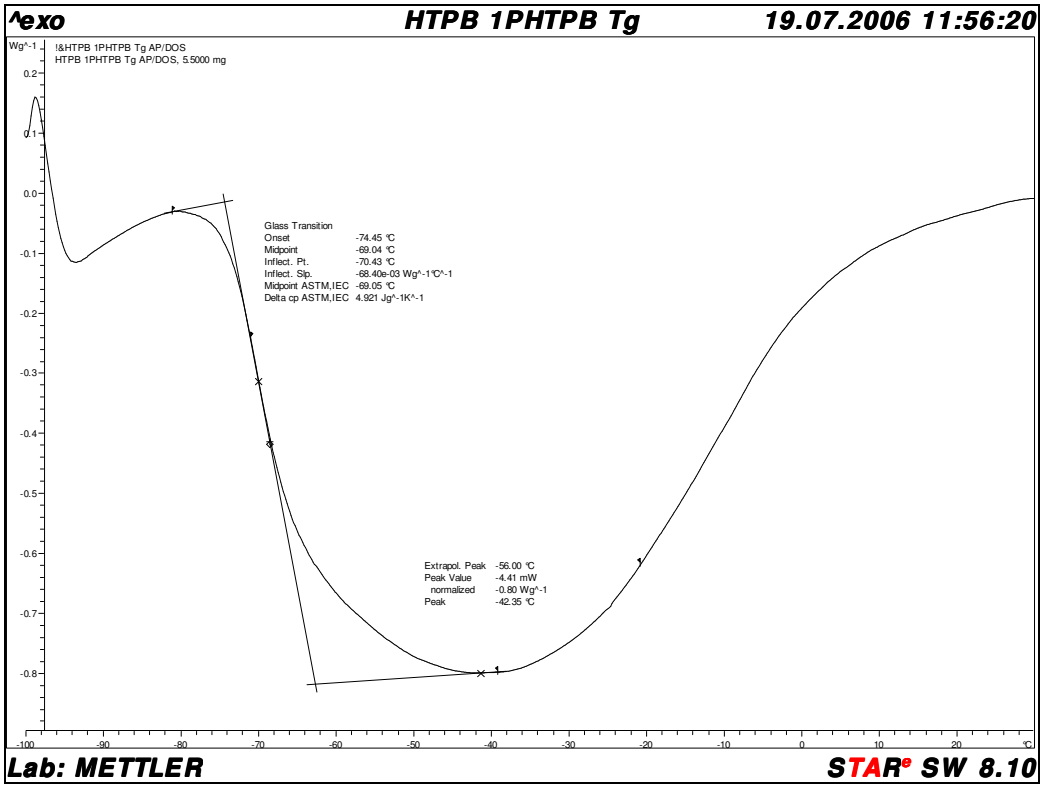

B

Figure 177. DSC Tg thermogram of (A) HTPE propellant samples 3P27B and (B) HTPB propellant sample 1PHTPB.

4.2.3.2 HTPE and HTPB propellants DSC TA analysis and results

Figure 178 shows the DSC TA thermogram for: (A) 0.9mg of sample 1P27B and (B) 5.4 mg of sample 2P26E, both formulated on HTPE/AP/n-BuNENA. Figure 178 shows the DSC TA thermogram for: (A) 4 mg of sample 3P27B formulated on HTPE/AP/PSAN/n-BuNENA and (B) 5.5 mg of sample 1PHTPB formulated on HTPB/AP/DOS.

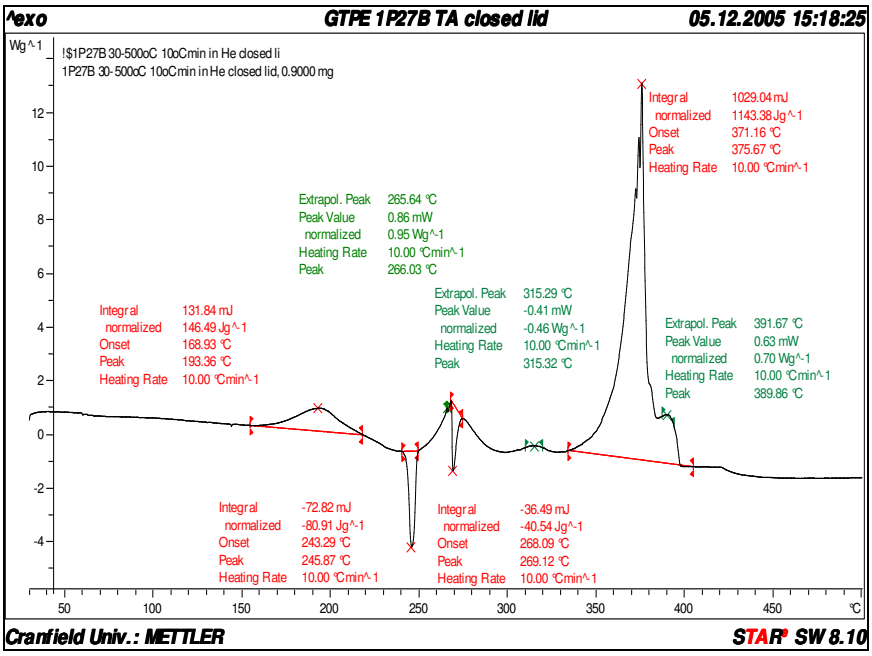

A

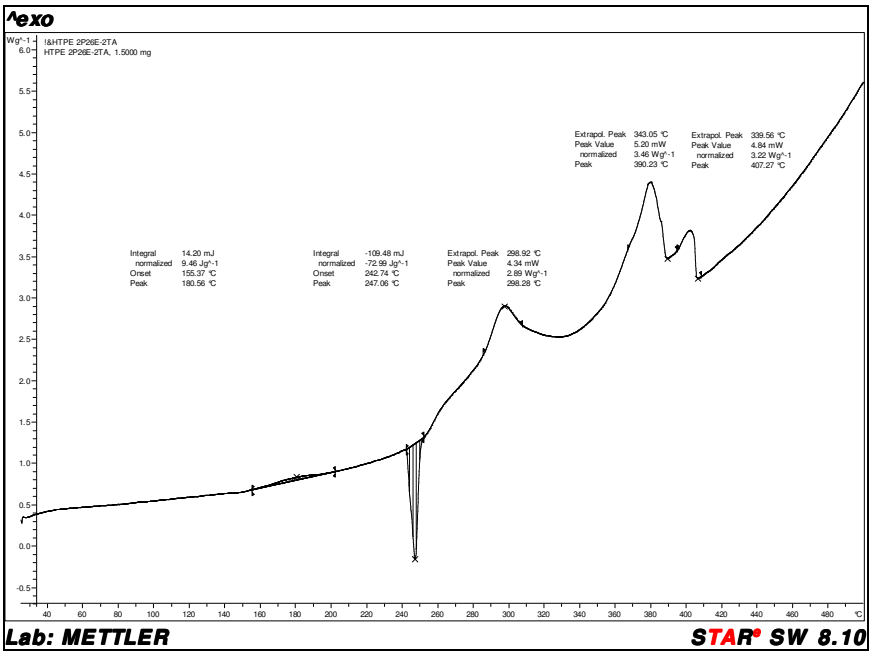

B

Figure 178. DSC TA thermogram of HTPE propellant sample (A) 1P27B and (B) 2P26E.

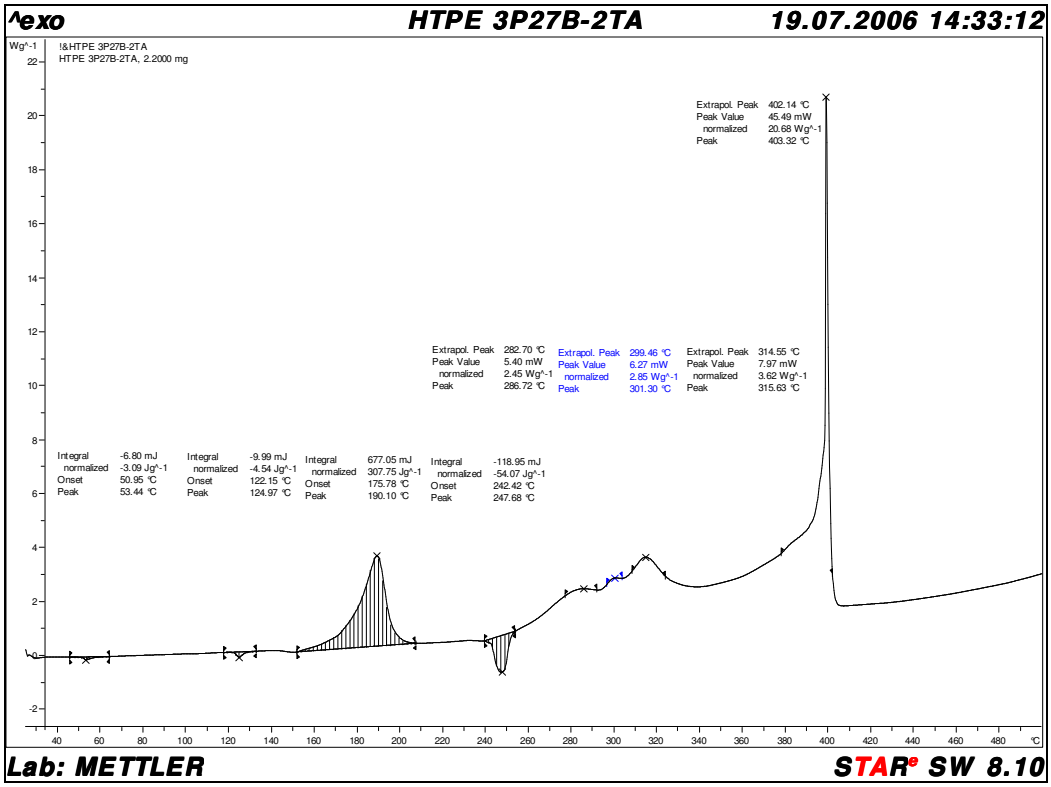

A

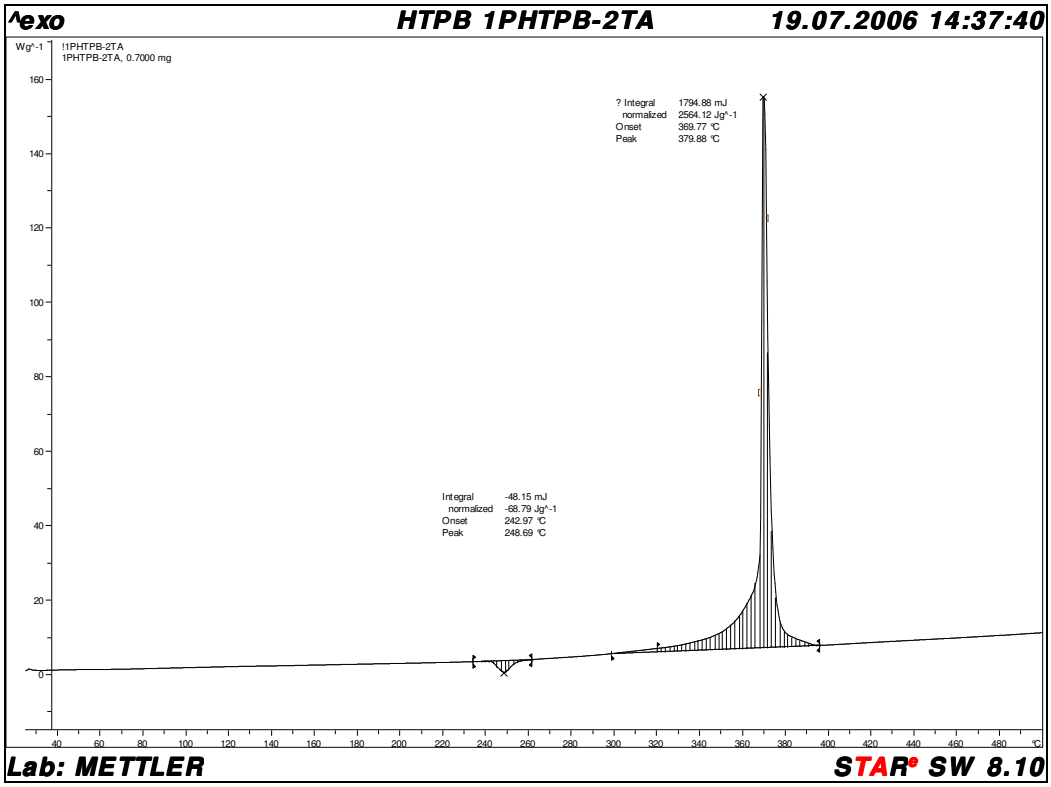

B

Figure 179. DSC TA thermogram of propellant samples (A) HTPE 3P277B and (B) HTPB 1PHTPB.

Table 109 to Table 111 show the summary of DSC thermal decomposition data from the thermograms presented in Figure 178 and Figure 179.

Table 109. HTPE Propellant 2P26E, DSC Thermal Decomposition Data

Nº	Kind of peak	Peak (˚C)	Endothermic Heat (J g^{-1})	Exothermic Heat (J g^{-1})
1	Exothermic	180.56	-.-	9.5
2	Endothermic	247.06	73	-.-
3	Exothermic	298.28	-.-	-.-
4	Exothermic	380.23	-.-	-.-
5	Exothermic	407.27	-.-	-.-

Table 110. HTPE Propellant 3P27B, DSC Thermal Decomposition Data

Nº	Kind of peak	Peak (˚C)	Endothermic Heat (J g^{-1})	Exothermic Heat (J g^{-1})
1	Endothermic	53.44	3.1	-.-
2	Endothermic	124.97	4.5	-.-
3	Exothermic	190.10	-.-	310
4	Endothermic	147.68	54	-.-
5	Exothermic	286.72	-.-	-.-
6	Exothermic	301.30	-.-	-.-
7	Exothermic	315.63	-.-	-.-
8	Exothermic	403.32	-.-	-.-

Table 111. HTPB Propellant 1PHTPB, DSC Thermal Decomposition Data

Nº	Kind of peak	Peak (˚C)	Endothermic Heat (J g^{-1})	Exothermic Heat (J g^{-1})
1	Endothermic	248.69	69	-.-
2	Exothermic	379.88	-.-	2600

4.2.3.3 HTPE and HTPB propellants TGA analysis results

Figure 180 shows the thermo gravimetric thermogram for (A) 4.3 mg of sample 2P26E and (B) 7.3 mg of sample 3P27B respectively and Figure 181 shows the thermo gravimetric thermogram for 2 mg of HTPB sample 1PHTPB.

Table 112 shows the summary of TGA data from the thermogram presented in Figure 180 and Figure 181.

Table 112. HTPE and HTPB Propellant Thermal Gravimetric Data

Sample name	1st Inflect. Pt. Temp. (ºC)	Weight lost (%)	2nd Inflect. Pt. Temp. (ºC)	Weight lost (%)	3rd Inflect. Pt. Temp. (ºC)	Weight lost (%)	4th Inflect. Pt. Temp. (ºC)	Weight lost (%)
2P26E	190.17	9.6	268.33	13.83	313.33	16.4	385.67	61.77
3P27B	192.17	19.32	311.33	29.82	392.83	51.5	-.-	-.-
1PHTPB	352.74	100	-.-	-.-	-.-	-.-	-.-	-.-

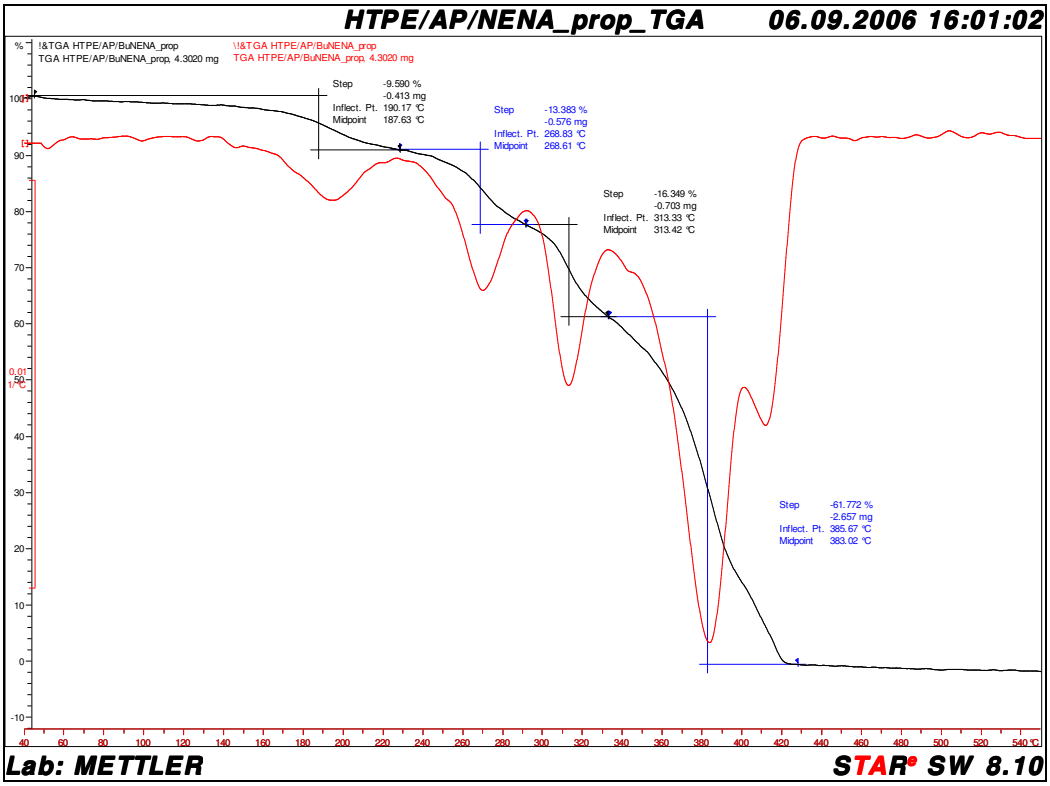

A

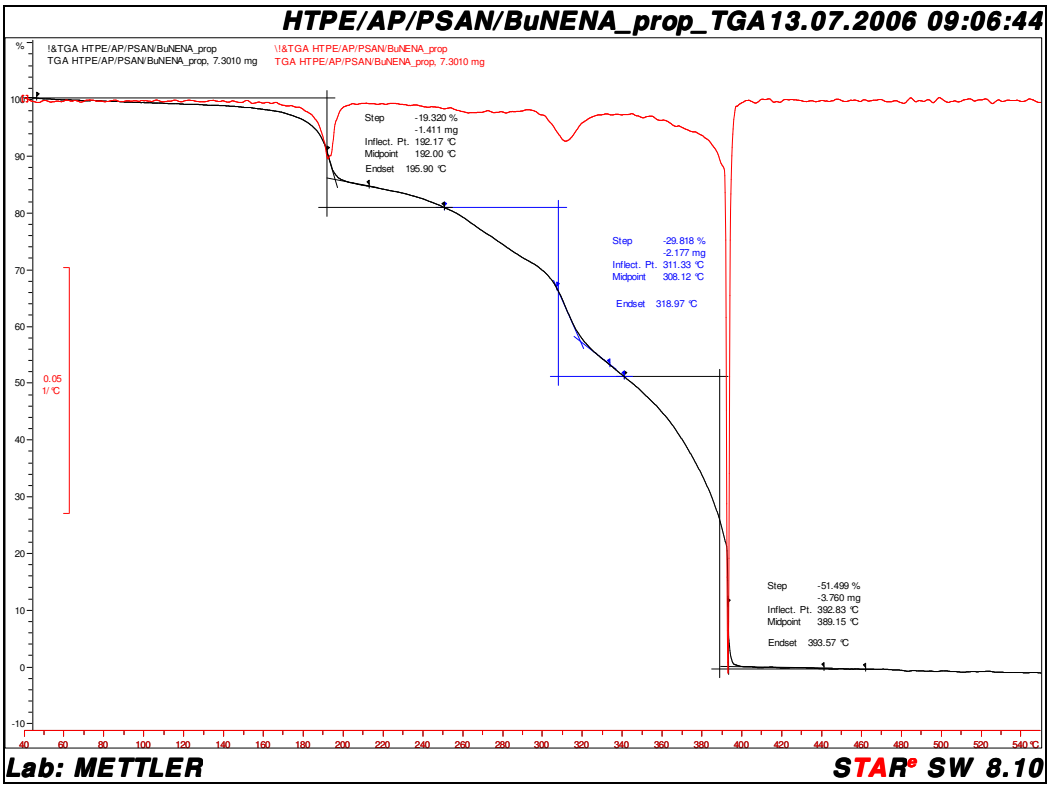

B

Figure 180. TGA thermogram of HTPE propellant samples (A) 2P26E and (B) 3P27B.

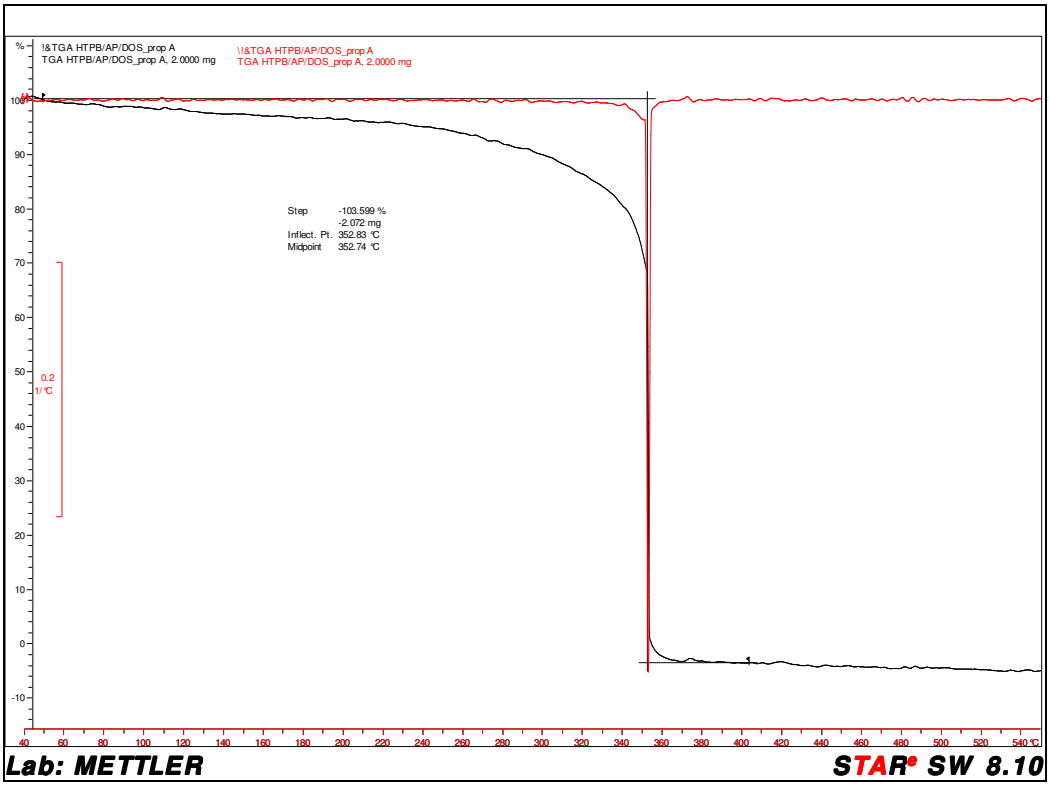

Figure 181. TGA thermogram of HTPB propellant, sample 1PHTPB.

4.2.3.4 Propellant DSC discussion of results

As can be seen from Figure 176, the glass transition temperature for propellant samples 1P27B and 2P26E was similar although they were manufactured in a different way. The Tg for thoses samples was around -75°C, slightly lower than the Tg observed in the binder network for a similar NCO/OH equivalence ratio of 0.8 and 0.9. At that NCO/OH ratio, in samples 17N27B and 18N27B, the Tg was -80.5 and -79.3°C, respectively (as presented in Table 113). This is an indication of the effect of AP on the propellant Tg. On the other hand, the Tg for propellant sample 3P27B, containing PSAN and AP as oxidiser, shows a higher Tg than the propellants containing only AP as oxidiser. There is a difference of almost 15°C, as can be seen from Table 113. Therefore, the increase in Tg in comparison with the propellant containing only AP as oxidiser can be assigned to the presence of PSAN in the formulation.

For HTPB samples the Tg also was increased from -81°C (as presented in Section 2.3.4), corresponding to the pre-polymer R45M, to -70°C in the propellant. There is no

available information in the literature that enables one to compare the Tg properties of the propellant manufactured in this work and that of other authors.

Despite the fact that propellant sample 1P27B and 2P26E NCO/OH equivalence ratio is similar to binder network sample 17N27B i.e. 0.88, 0.85 and 0.88 respectively, the micro crystallisation peak at -37°C and the endothermic peak at -18°C, as in the gumstock formulations, are not present in the propellant samples. This behaviour is related to the presence of the plasticizer, as discussed in Section 3.3.3.

Table 113. HTPE Pre-polymer, Binder Network, Gumstock and Propellant Results From DSC Analysis

Exp. No	NCO/OH Eq. ratio	Glass Transition Temperature (°C)	Micro Crystallization Point (°C)	Melting Heat ($J\ g^{-1}$)	Melting Point (°C)	Melting Heat ($J\ g^{-1}$)
27B	-.-	-81.60	-56.00	29	-7	38
16N27B	1.0	-79.30	0.00	0	0.00	0
19N27B	0.7	-81.66	-42.61	30	-13.29	29
5G27B	0.87	-77.47	-.-	-.-	-.-	-.-
1P27B	0.88	-75.03	-.-	-.-	-.-	-.-
2P26E	0.85	-76.28	-.-	-.-	-.-	-.-
3P27B	0.85	-62.89	-.-	-.-	-.-	-.-
1PHTPB	0.85	-70.43	-.-	-.-	-.-	-.-

In order to have a complete picture of the effect of the different ingredients on the glass transition temperature when HTPE is used as binder, Figure 182 shows the Tg for: binder network sample 16N27B (purple), binder network sample 19N27B (green), gumstock sample 5G27B (black), HTPE propellant sample 3P27B (red), HTPE propellant sample 2P26E (blue) and HTPB propellant sample 1PHTPB (brown).

As can be seen from Figure 182 the microcrystallisation and melting point peaks, that are present in the pre-polymer and in the binder network with an NCO/OH lower than 1 (green curve), disappear (black curve) when the energetic plasticizer is included. At the same time, Tg is increased by around 4°C, as discussed in Section 3.3.3. However, the bigger effect on Tg is when oxidisers are included. In fact, Tg is increased again and this effect is bigger in samples containing a percentage of PSAN, as discussed above.

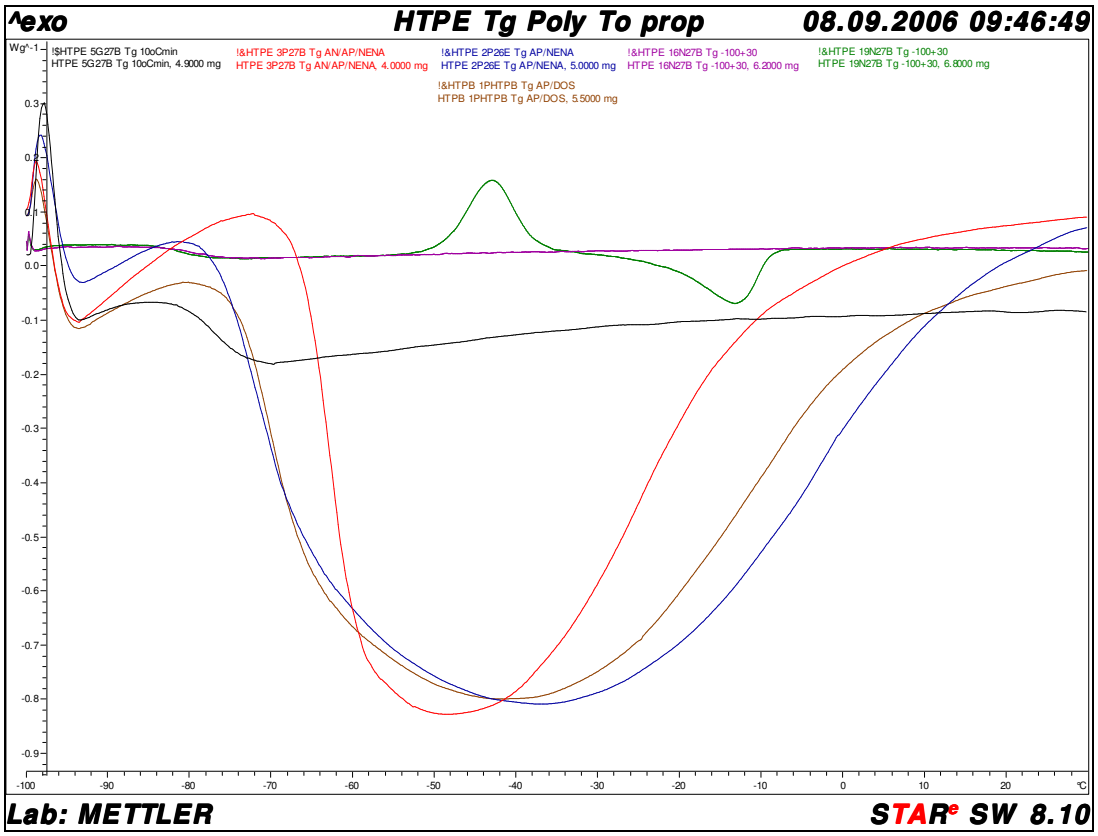

Figure 182. Tg thermogram of HTPE binder network, gumstock and propellant and HTPB propellant.

4.2.3.5 Thermal decomposition discussion of results

As can be seen from Figure 178 A and B and from Figure 179 A, several peaks, either exothermic or endothermic, are present during propellant thermal decomposition. Three endothermic peaks can be seen before 150°C from sample 3P27B in Figure 179 A. They are thought to be due to the presence of the PSAN. The peak at around 53°C corresponds to the phase change from rhombic bipyramids to rhombic. This phase change should be suppressed by the phase stabiliser ZnO, present in the PSAN [Jemmet, 2001]. However, it can be seen that the effect was not completely annulled in this case. From the DSC analysis of a HTPE propellant, similar endothermic peaks to those observed in Figure 178 and Figure 179, due to the presence of PSAN in HTPE at 125 and 150°C, were reported by Atwood [2005]. They correspond to the PSAN phase change from tetragonal to cubic and to the melting of the cubic PSAN crystals respectively.

The exothermic peaks at around 188 and 193°C, with an onset around 160°C, can be assigned to the energetic plasticizer n-BuNENA. In fact as presented in Appendix H, n-BuNENA thermal decomposition onset starts at 160°C and the main peak is at 210°C. Also, according to the gumstock thermal decomposition for samples 1G26E3 and 2G26E3 presented in Section 3.3.3, a n-BuNENA decomposition peak was observed at around 200°C. On the other hand, Atwood [2005] and Chan [2005], assigned the n-BuNENA decomposition peak to that at 175°C. This is at lower temperature than observed in this work, however the onset was at almost the same temperature i.e. 160°C. In propellant 3P27B this peak can be seen at 199°C and it looks more intense than in the other propellant 2P26E, as can be seen in Figure 183. In fact, in 3P27B the heat of decomposition was 307 J g^{-1} and in 2P26E it was 9.6 J g^{-1}. The n-BuNENA heat of decomposition peak for the pure product was observed to be 1117 J g^{-1} at 210°C (Appendix H).

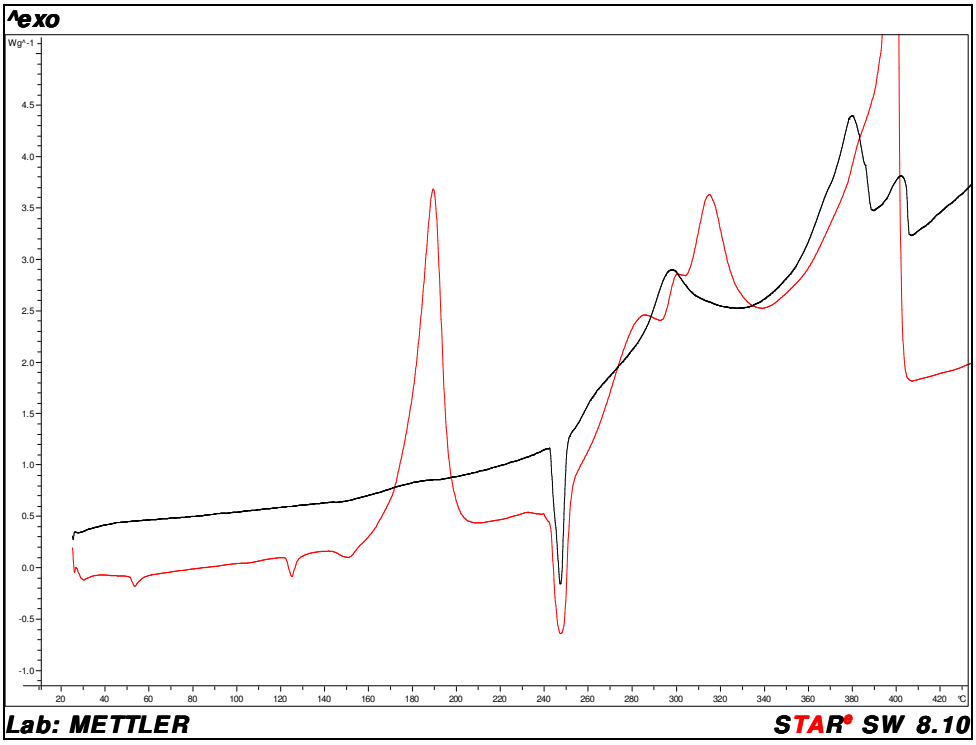

Figure 183. DSC TA thermogram of HTPE propellant sample 2P26E (black) and 3P27B (red).

The endothermic peak at 245°C, which is present in the DSC of the propellant with and without PSAN, can be assigned to the AP. In fact as is presented in Figure 184, the DSC thermogram for pure AP, this endothermic peak is present at 242°C. According to Sadek

[2001], this peak corresponds to the AP solid to solid phase transition from orthorhombic to cubic form.

After the endothermic peak seen in the DSC thermogram of the propellant containing AP and PSAN as oxidiser (Figure 179 A), a series of exothermic and endothermic reactions are occurring at the same time in the temperature range between 250 and 430°C. In fact as can be seen from Figure 184, for samples containing only AP as oxidiser, the decomposition occurs in two stages; an early stage at around 300°C involving decomposition and sublimation [Sadek, 2001] and a final decomposition reaction at around 430°C, where decomposition and more than 98% of sublimation take places [Hussain 1962, Keenan 1969].

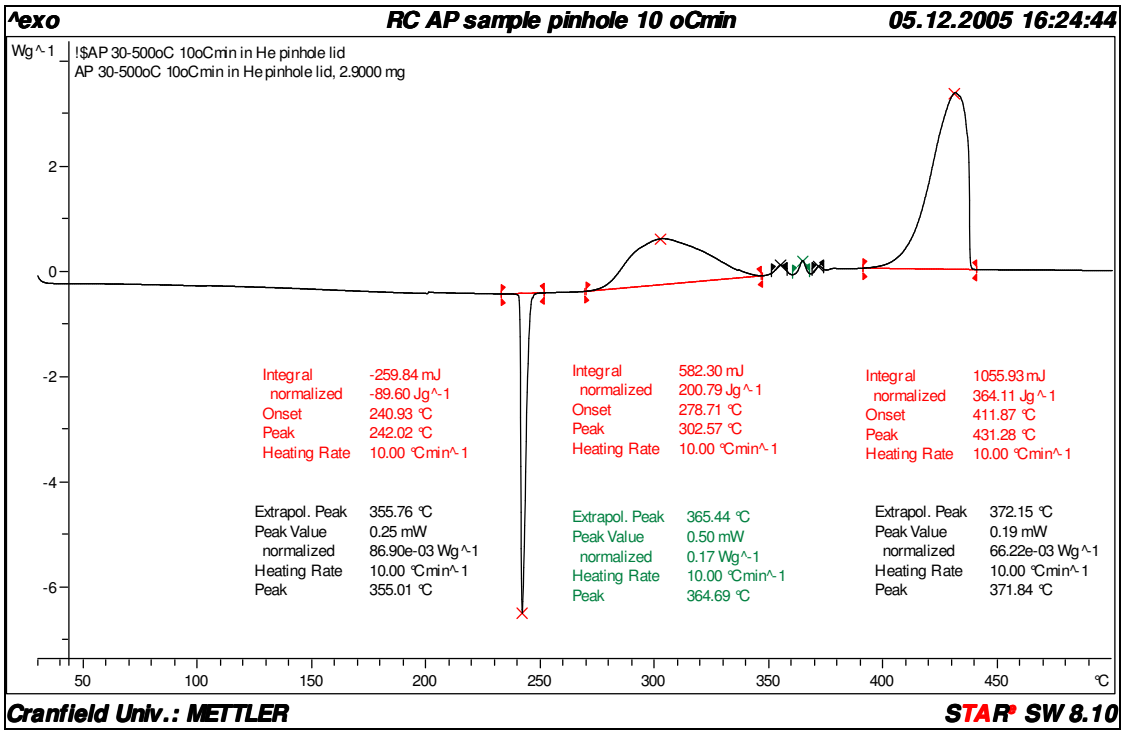

Figure 184. DSC TA thermogram of pure AP 200µm.

Simultaneously PSAN, as can be seen from Figure 185, is decomposing from the liquid phase at 290°C and its decomposition rate, faster or slower, will be a function of the acidic or basic environment respectively [Sinditskii, 2005]. Thus, it appears that both oxidisers are having an influence on the decomposition behaviour of each other over the temperature range of 130°C, and then influencing the full propellant system.

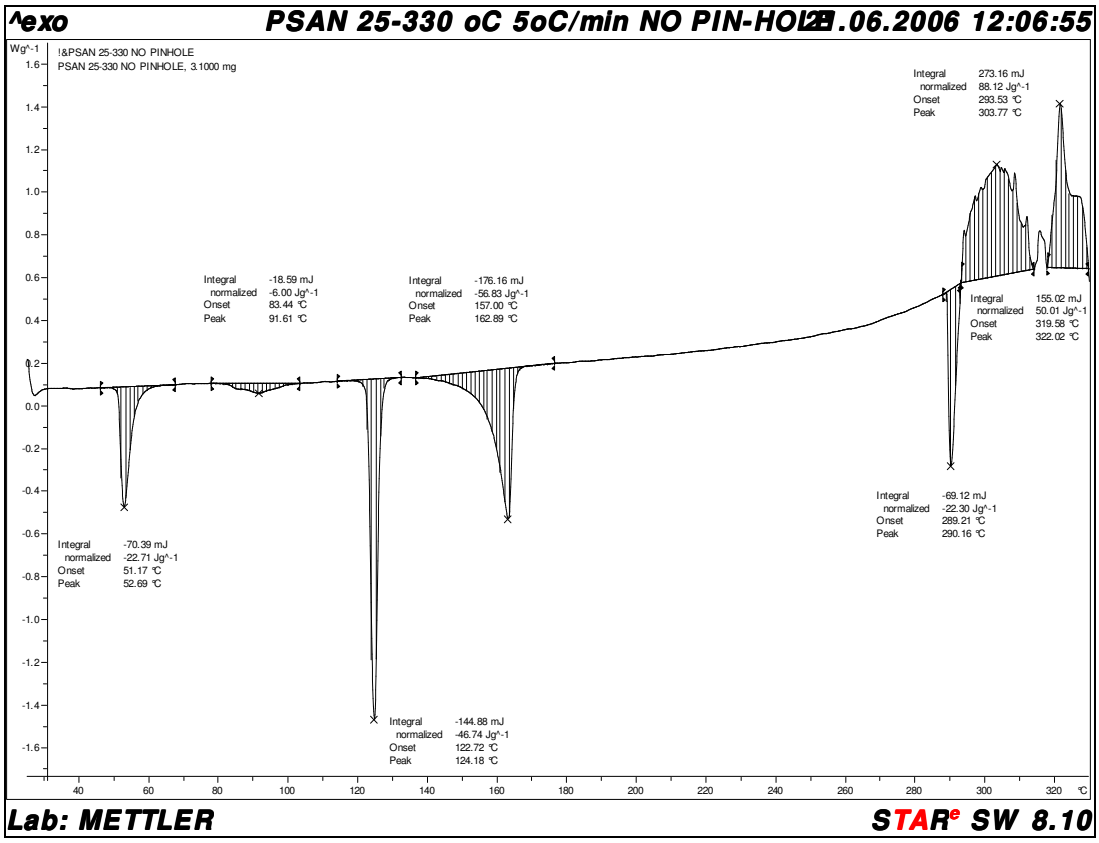

Figure 185. DSC TA thermogram of pure PSAN 70µm.

As can be seen from Figure 186, when comparing pure AP and PSAN oxidisers with a mixture of both in a DSC thermal analysis, some facts can be highlighted: the PSAN melting peak at 124°C has been divided into three small endothermic peaks in the temperature range 142 to 170°C. On the other hand, it appears that the AP solid to solid phase transition from orthorhombic to cubic form has moved to 209°C and the sharp endothermic peak replaced by a wider and smoother peak. It also appears that the PSAN decomposition temperature has been increased from 290 to 315°C.

The presence of the energetic plasticizer n-BuNENA in AP and PSAN mixtures has a slight effect on the behaviour of both oxidisers when they are being thermally decomposed, as can be seen in Figure 187. In fact, PSAN melting has a similar onset to that of pure PSAN and only one endothermic peak between 143 to 170°C can be seen, with the maximum at 157°C, instead of the three peaks observed when PSAN is mixed with pure AP. The exothermic peak at 210°C, due to the n-BuNENA decomposition, can be seen as a weak exothermic peak at around 244°C. This peak is possibly related to

the last part of the endothermic peak that in pure AP appeared at 246°C (Figure 186) and which corresponds to the AP solid to solid phase transition from orthorhombic to cubic form. Finally, the endothermic peak related to the PSAN decomposition that is present in pure PSAN at 290°C and in a AP+PSAN mixture at 310°C is not present, as can be seen in Figure 187. This is possibly due the n-BuNENA exothermic decomposition reaction also decomposing the PSAN.

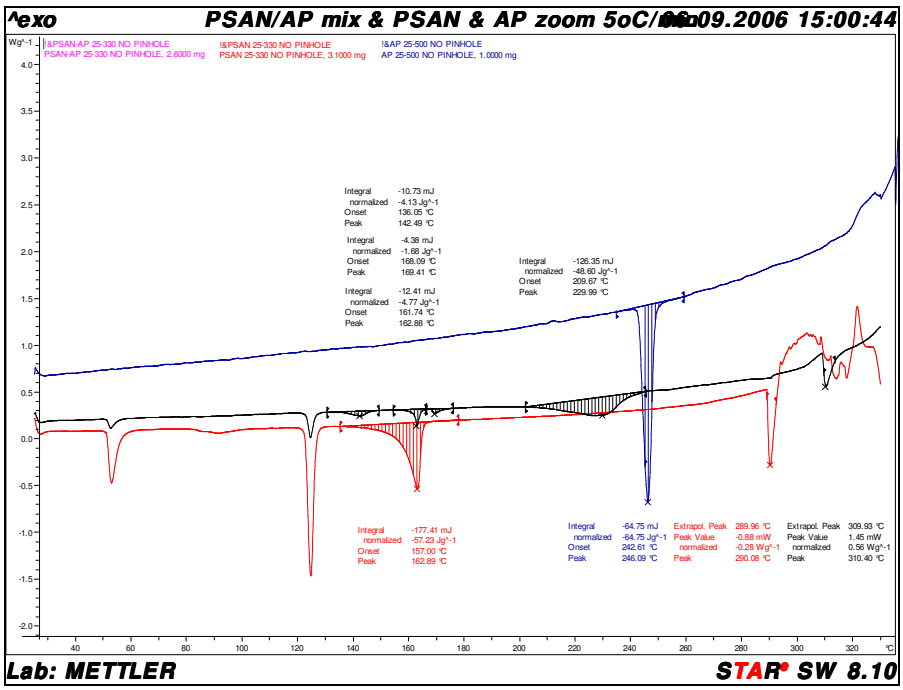

Figure 186. DSC TA thermogram of AP and PSAN mixtures.

A summary of the thermal decomposition behaviour of different samples: HTPE pre-polymer 17B (blue), HTPE binder network 17N27B (green), HTPE gumstock (black) and HTPE propellant sample 3P27B is presented in Figure 188. The influence of the n-BuNENA addition on binder decomposition (black) and on propellant (red) can be appreciated around 190 to 204°C and around 170 to 300°C.

In comparison with HTPB, HTPE propellants start decomposing at lower temperatures and in a more gradual way. In fact as can be seen from Figure 179 B, HTPB propellant decomposition onset was observed at around 320°C and there is only one sharp exothermic peak present during this reaction, while HTPE propellants start the decomposition process first at around 160°C, with an exothermic peak due to the

n-BuNENA decomposition and probably its reaction with the liquid PSAN, a final decomposition with the onset at around 260°C and several exothermic reactions as the temperature increases.

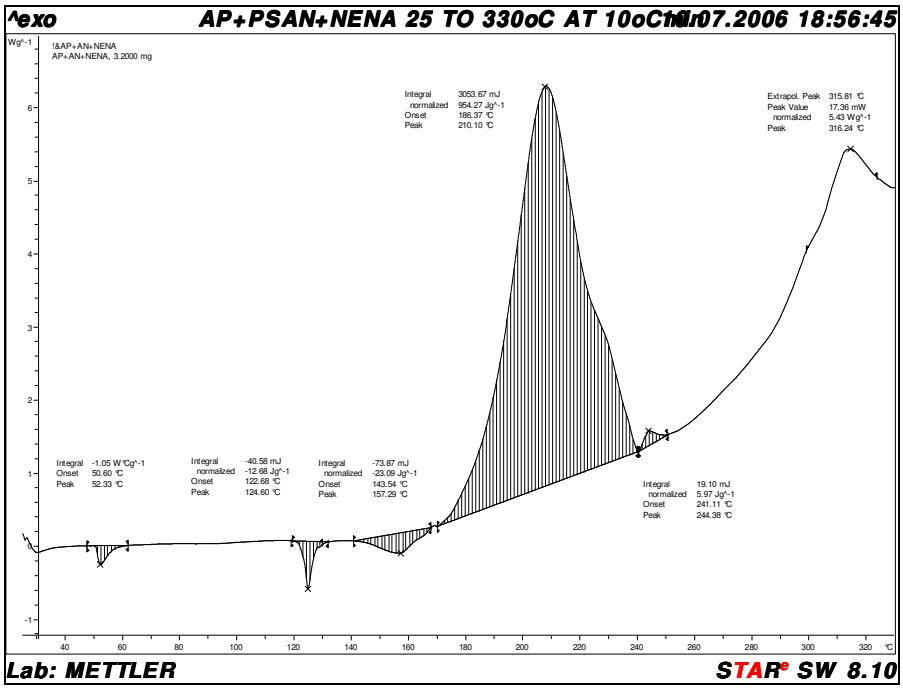

Figure 187. DSC TA thermogram of AP, PSAN and n-BuNENA mixture.

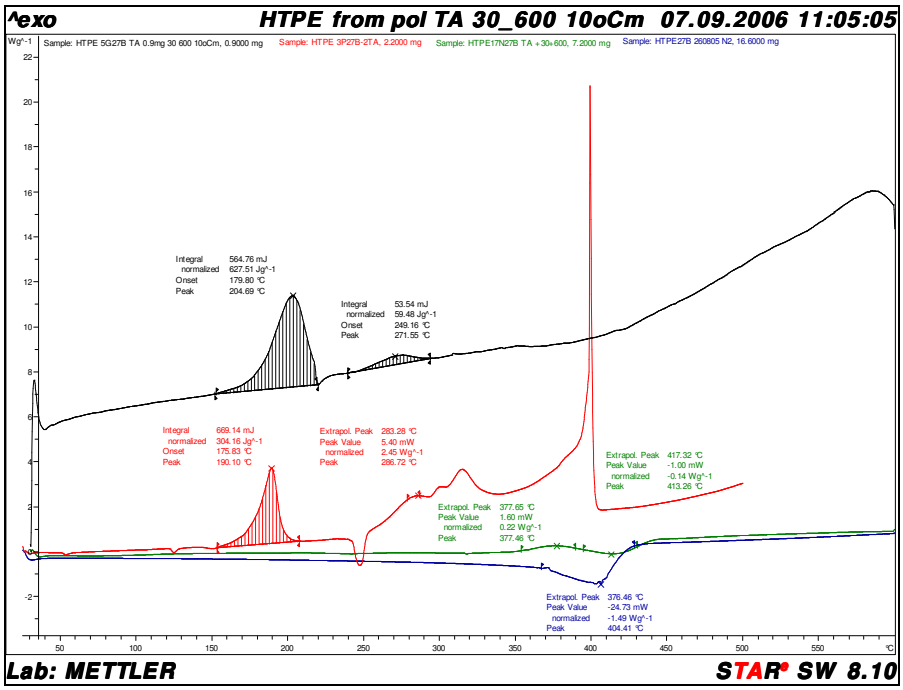

Figure 188. DSC TA thermogram of HTPE pre-polymer, binder network, gumstock and propellant.

4.2.3.6 TGA discussion of results

It is desirable to have a complete picture of the effect of the different ingredients on weight loss when HTPE is used as binder. Figure 189 shows the weight loss curve versus temperature for: pre-polymer sample 27B (light blue), binder network sample 17N27B (brown), gumstock sample 5G27B (red) HTPE propellant sample 3P27B (purple) and HTPB propellant sample 1PHTPB (black).

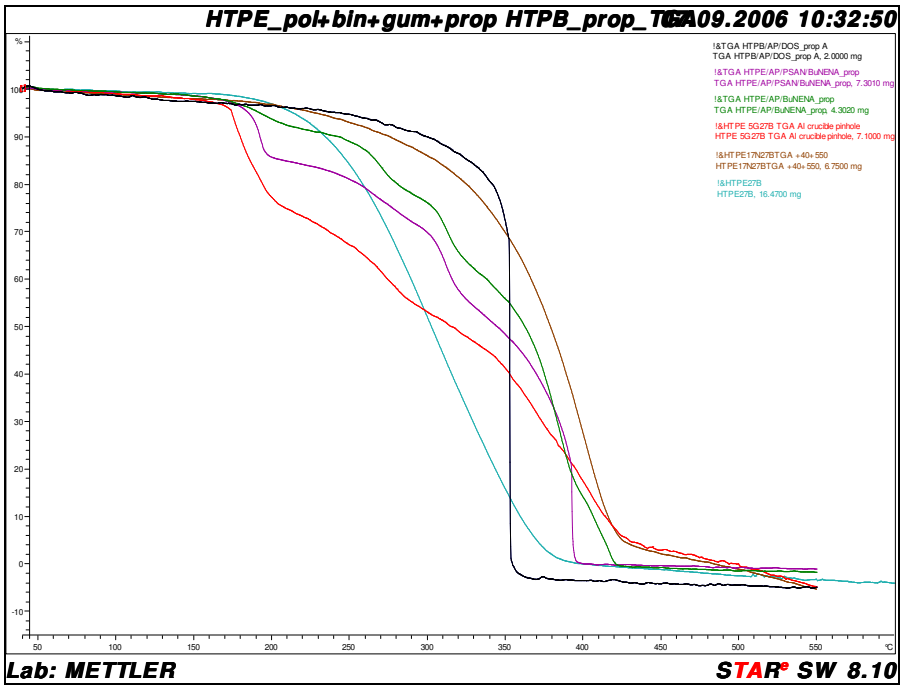

Figure 189. TGA thermograms of HTPE pre-polymer, binder network, gumstock and propellant and HTPB propellant.

As can be seen from Figure 189, the weight loss process is more complex in propellant samples having HTPE as binder than in those with HTPB binder. In fact as can be seen from Figure 181, the DTA curve for HTPB TGA has basically only one phase of weight loss with the inflection point around 352^{o}C. In contrast, propellants made from HTPE binder have several rates of weight loss as can be seen in Figure 180 A and B. The HTPE system is more complex than HTPB due the larger number of components and their interactions.

HTPE propellants show a similar weight loss despite the fact that sample 2P26E, containing only AP as oxidiser, shows one more rate weight loss peak than sample 3P27B in the DTA. In fact, three of the main peaks are present at similar temperatures,

as can be seen in Table 112. The first peak, at around 190°C for both cases, can be assigned to the n-BuNENA decomposition as presented before. However in sample 3P27B the percentage of weight loss was 19% in comparison with 9% for sample 2P26E. Possibly this behaviour is because at that temperature the PSAN present in sample 3P27B is in the liquid phase and part of it is reacting with the n-BuNENA decomposition products and possibly part of the binder.

The second common weight loss for both propellants was at around 311°C. At this point as presented before (Figure 184), the AP first decomposition and sublimation stage is taking place. In fact for pure AP this stage has the onset at around 280°C and the offset at around 340°C. Also PSAN decomposition is taking place around 300°C as presented in Figure 186. Because of that it is also possible that the second phase of weight loss observed in the DTA of sample 2P26E is part of this first decomposition stage. When comparing the weight loss at the end of the second peak in the DTA of sample 3P27B with the equivalent third peak of the DTA from sample 2P26E it can be seen that 49 and 39% of mass was lost respectively. Therefore, it is possible that the 10% difference in weight loss can be attributed to the effect of the PSAN in the propellant system. Coincidently the percentage of PSAN in the propellant composition is around 10%. The last DTA peak for the weight loss is common for both propellants, having an inflection point at around 385 to 392°C. This stage corresponds to the final and complete propellant decomposition that includes the second AP sublimation and decomposition stage discussed before, together with the loss of decomposition products from the binder that did not react with the energetic plasticizer decomposition products.

4.2.3.7 DSC and TGA conclusions

Glass transition temperature increases when oxidisers are included in HTPE propellant formulation in comparison with HTPE alone. This increment is only 1.5% when only AP is used as oxidiser, however when PSAN was included in the propellant, Tg increased around 19%. HTPB propellant has a higher Tg than AP based HTPE propellant but lower than AP+PSAN HTPE propellant.

From the thermal decomposition analysis it appears that in the HTPE propellant containing AP and PSAN as oxidisers, the interaction of both components is having an influence on the decomposition process: the PSAN melting point is divided into three steps and its decomposition point increased while the AP solid-to-solid phase transition peak temperature and intensity decreased. n-BuNENA has an important role in the propellant decomposition process, bringing about the first propellant exothermic reaction due to its decomposition. It was also observed that the decomposition process related to the n-BuNENA is less exothermic in propellant containing only AP as oxidiser. Possibly decomposition products of n-BuNENA are reacting with part or all the liquid phase from the PSAN. On the other hand, most of the exothermic peaks in the propellant containing AP+PSAN as oxidisers are delayed in comparison with the one arising from propellant containing only AP as oxidiser. In comparison with HTPB, HTPE propellants start decomposing at lower temperature and in a more gradual way.

It was observed that propellants containing AP and PSAN as oxidisers lost a bigger percentage of mass at lower temperature than the one containing only AP as oxidiser. The influence of the PSAN appears to be the related to this process as stated in the previous paragraph. On the other hand the lost weight process is more gradual in HTPE based propellant than in HTPB propellants.

4.2.4 HTPE propellant activation energy Ea, analysis results

In order to calculate the activation energy for the decomposition in the HTPE propellant samples 2P26E and 3P27B, Ozawa's method [Ozawa, 1970] used by Matei [2002] was adopted as described in Section 3.3.5. DSC analyses at different heating rates were performed as explained in Section 2.3.4. An aluminium crucible sealed with a lid having a pinhole was used and nitrogen gas was introduced in order to have an inert environment. Ea determination was performed on DSC thermograms recorded at heating rates of 5, 10, 20, 30 and 40^{o}C per min from a temperature range of 25 to 500^{o}C. The decomposition i.e. exothermic, peaks were chosen to fix the temperature range according to Ozawa's method. HTPE activation energy results were compared among themselves and with HTPB Ea data obtained from the literature.

4.2.4.1 HTPE propellant sample 2P26E, Ea analysis results

Figure 190 shows the overlayed DSC thermograms for several HTPE propellant samples 2P26E, at a heating rate of: 5 (red), 10 (blue), 20 (black), 30 (green) and 40°Cmin^{-1} (purple).

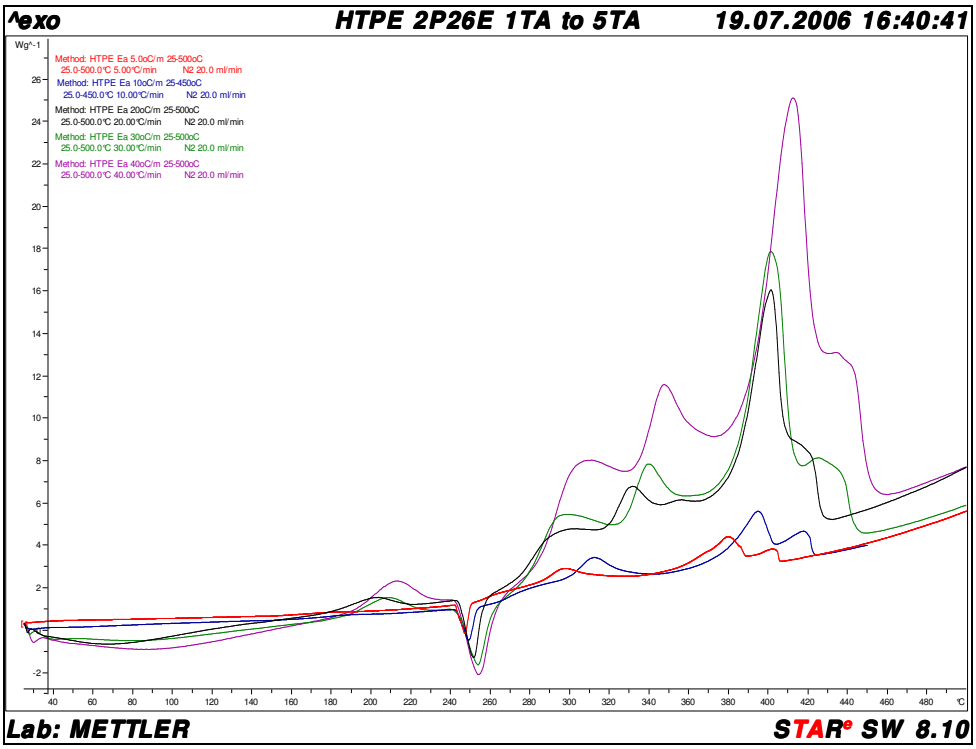

Figure 190. DSC Ea thermogram of HTPE propellant, sample 2P26E.

Table 114 shows the summary of information from DSC thermograms obtained from Figure 190 for the 1st, 2nd and 3rd exothermic peaks and the parameters used to plot the logarithm of the heating rate versus the reciprocal peak temperature. This information was used to obtain the slope Ea/R and the pre-exponential factor A, as presented in Figure 191 and discussed in Chapter III, Section 3.3.5.

Table 114. HTPE Propellant Sample 2P26E Results From DSC Ea Analysis

Heating rate, β (°C min^{-1})	Sample weight, (mg)	1st Exo. peak , Tp_1 (°C)	2nd Exo. peak , Tp_2 (°C)	3rd Exo. peak , Tp_3 (°C)	Ln(β), (K min^{-1})	$1/Tp_1$ (K^{-1})	$1/Tp_2$ (K^{-1})	$1/Tp_3$ (K^{-1})
5	1.5	180.56	298.28	380.61	1.6094	0.0022	0.0017	0.0015
10	1.7	187.33	313.08	395.54	2.3026	0.0022	0.0017	0.0015
20	1.3	201.17	332.20	403.23	2.9957	0.0021	0.0017	0.0015
30	1.7	208.29	340.79	404.26	3.4012	0.0021	0.0016	0.0015
40	1.5	212.05	349.04	415.72	3.6889	0.0021	0.0016	0.0015

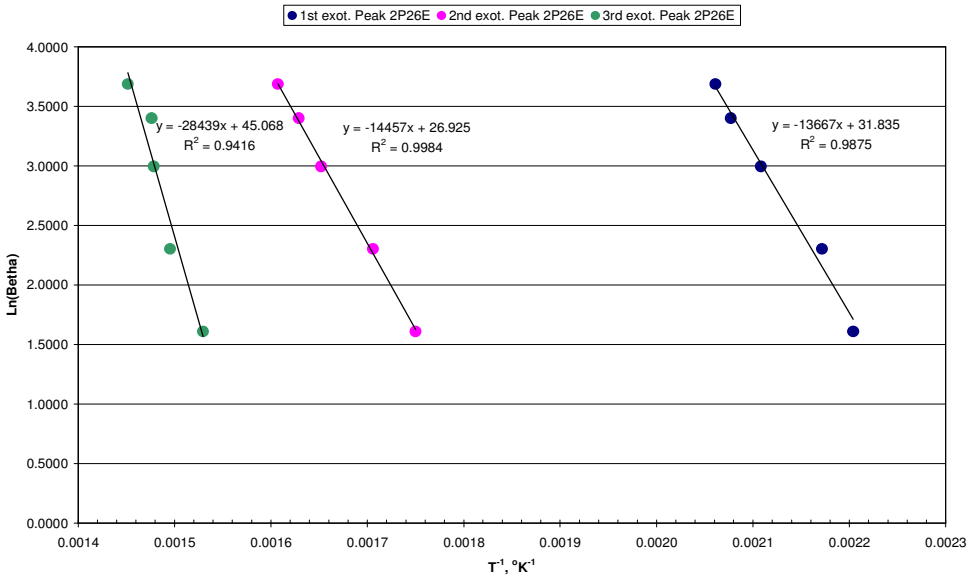

Figure 191. Arrhenius plot of Ln(β) versus $1/Tp_1$, $1/Tp_2$ and $1/Tp_3$ for HTPE propellant sample 2P26E.

In order to calculate the first exothermic peak activation energy Ea_1, from the Arrhenius equation presented in Section 3.3.5, assuming a first order reaction, the slope on the curve in Figure 191 is represented by Ea/R= 13667. Thus, taking the gas constant R as 8.3143 J K^{-1} mol^{-1}, the Ea_1 is equal to 113.631 kJ mol^{-1}, and from Ln*A* the pre-exponential factor *A* will be $1.1x10^{12}s^{-1}$. Similarly the activation energy for the second exothermic peak Ea_2 is 120.199 kJ mol^{-1} and the pre-exponential factor *A* is $8.2x10^{9}s^{-1}$. The activation energy for the third exothermic peak Ea_3 is 236.450 kJ mol^{-1} and the pre-exponential factor *A* is $6.2x10^{17}s^{-1}$.

4.2.4.2 HTPE propellant sample 3P27B Ea analysis and results

Figure 192 shows the overlayed DSC thermograms for HTPE propellant sample 3P27B, at a heating rate of: 5 (purple), 10 (green), 20 (blue), 30 (red) and 40^{o}Cmin^{-1} (black).

Table 115 shows the summary of information from DSC thermograms obtained from Figure 192 for the 1st, 2nd and 3rd exothermic peaks and the parameters used to plot the logarithm of the heating rate versus the reciprocal peak temperature in order to obtain the slope Ea/R and the pre-exponential factor A, as presented in Figure 193.

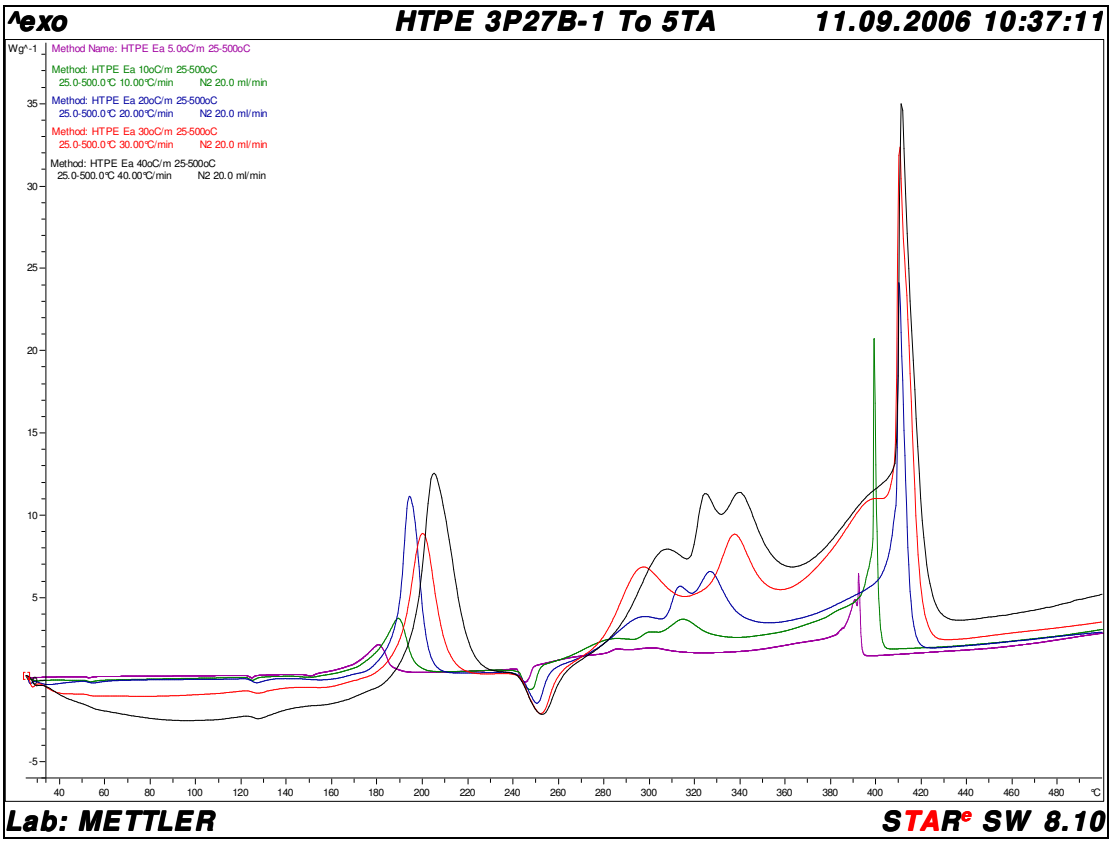

Figure 192. DSC Ea thermogram of HTPE propellant sample 3P27B.

Table 115. HTPE Sample 3P27B DSC Ea Analysis

Heating rate, β (°Cmin^{-1})	Sample weight, (mg)	1st Exo. peak , Tp_1 (°C)	2nd Exo. peak , Tp_2 (°C)	3rd Exo. peak , Tp_3 (°C)	Ln(β) (K min^{-1})	$1/Tp_1$ (K^{-1})	$1/Tp_2$ (K^{-1})	$1/Tp_3$ (K^{-1})
5	2.3	180.89	301.02	393.52	1.6094	0.0022	0.0017	0.0015
10	2.2	190.10	315.63	403.32	2.3026	0.0022	0.0017	0.0015
20	2.6	197.63	328.34	415.65	2.9957	0.0021	0.0017	0.0015
30	2.5	202.51	339.65	417.78	3.4012	0.0021	0.0016	0.0014
40	2.3	208.24	342.56	418.24	3.6889	0.0021	0.0016	0.0014

As shown previously, the Ea_1 is equal to 142.989 kJ mol^{-1} and from Ln*A* the pre-exponential factor *A* is 2.3x10^{15}s^{-1}. Similarly the activation energy for the second exothermic peak Ea_2 is 143.466 kJ mol^{-1} and the pre-exponential factor *A* is 9.2x10^{11}s^{-1}. The activation energy for the third exothermic peak Ea_3 is 290.410 kJ mol^{-1} and the pre-exponential factor *A* is 4.5x10^{21}s^{-1}.

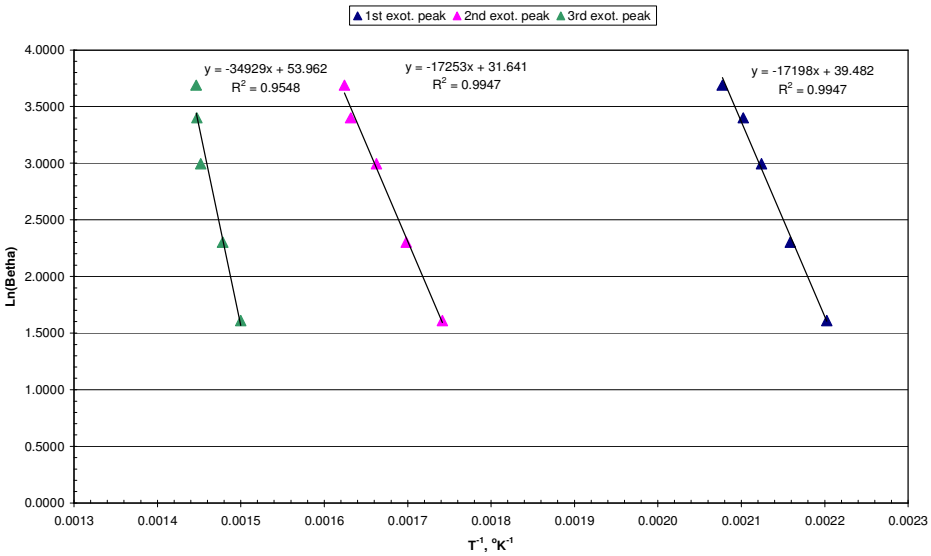

Figure 193. Arrhenius plot of Ln(β) versus $1/Tp_1$ $1/Tp_2$ and $1/Tp_3$ for HTPE propellant sample 3P27B.

4.2.4.3 HTPE propellant, discussion of Ea results

As stated previously, Ozawa's method was used for estimating the activation energy **E**a and the pre-exponential factor **A** from the propellant thermal decomposition. As such, the method is based on the linear relation between peak temperature and heating rate and is also called the isoconversional method [Rocco, 2004]. Although several peak temperatures versus rate of heating from the HTPE propellant were plotted in order to compare the activation energy related to the decomposition of the propellant itself, the first exothermic reactions i.e. first exothermic peaks, were used to compare the HTPE propellant thermal decomposition with that of HTPB. HTPB Ea data were obtained from Sell [1999] and Gore [2004]. Sell [1999] and Gore [2004] found that during HTPB TGA analysis two exothermic peaks can be found, the first was assigned to the inert plasticizer (DOA) decomposition and the second to the AP decomposition and its interaction with the HTPB binder. The second exothermic peak and its associated Ea in HTPB propellant can therefore be used for comparison purposes. Similarly, and because the thermal decomposition is driven by the first exothermic peak in HTPE propellants, this information was used to compare the Ea with that for HTPB propellants.

A summary of the activation energy data obtained from the plots presented in Figure 191 and Figure 193 are shown in Table 116 together with HTPB Ea data obtained from

the literature. Figure 194 shows the Arrhenius overplot of Ln(β) versus $1/Tp_1$, $1/Tp_2$ and $1/Tp_3$ for the different peaks of HTPE propellant samples.

Table 116. HTPE and HTPB Ea Summary

Ea for sample	1st Exo. peak Ea_1 (kJ mol^{-1})	2nd Exo. peak Ea_2 (kJ mol^{-1})	3rd Exo. peak Ea_3 (kJ mol^{-1})
HTPE 2P26E	114	120	237
HTPE 3P27B	143	144	290
HTPB [Sell, 1999]	100	230	-.-
HTPB [Gore, 2004]	188	251	-.-

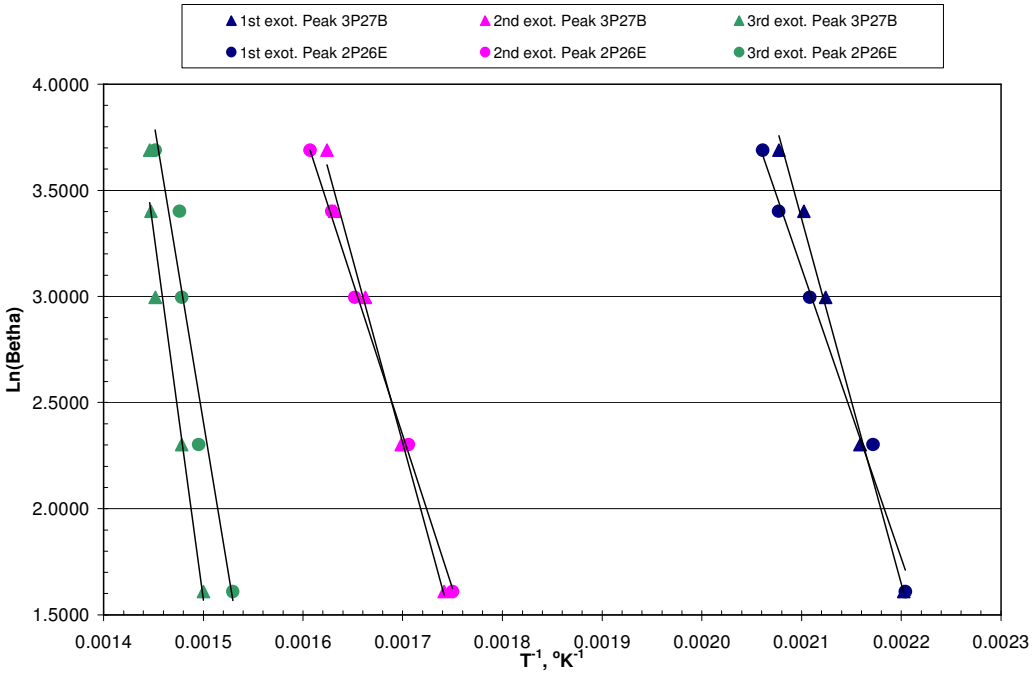

Figure 194. DSC Ea of HTPE propellant samples.

From Table 116 it can be seen that HTPE propellant 2P26E, containing only AP as oxidiser, has a lower activation energy than HTPE propellant 3P27B that contains AP and PSAN as oxidiser i.e. 114 versus 143 kJ mol^{-1} respectively. These Ea values are lower than the Ea found for gumstock and binder network samples presented in Section 3.3.5. As presented there, the Ea values were 179 kJ mol^{-1}, assigned to the n-BuNENA, and 216 kJ mol^{-1}, assigned to the polymer decomposition. The first exothermic decomposition peak, as discussed before, is related to the decomposition of the energetic plasticizer n-BuNENA, and it appears that in the presence of AP its activation

energy is decreased but when PSAN was added to the propellant formulation 3P27B, the energy required to start its decomposition becomes higher, although still lower than in the pure energetic plasticizer. Possibly the low PSAN melting point and also its decomposition together with the plasticizer, are playing a role in this behaviour. As discussed in connection with TGA analysis the weight loss after the first exothermic peak in sample 3P27B was around 19%, which is similar to the combined percentage of n-BuNENA and PSAN in the propellant composition (8 and 10% respectively). The second and third exothermic peaks also follow a similar trend to that discussed previously. Therefore it is believed that the PSAN is affecting the propellant thermal decomposition by delaying the exothermic decomposition reactions.

The second and third exothermic peaks in the DSC of the HTPE propellants are related mainly to the PSAN and AP thermal decomposition together with the binder. In fact, the average Ea_2 derived from the second exothermic peak in the HTPE propellants i.e. 2P26E and 3P27B, is higher than the Ea of pure PSAN i.e. 120 kJ mol^{-1} [Zhao, 2000] and AP i.e. 80 [Brown, 2000] to 92 kJ mol^{-1} [Andreev, 2006]. Similarly, the average Ea_3 derived from the third exothermic peak is also higher than the Ea from pure AP i.e. 120 [Brown, 2000] to 129 kJ mol^{-1} [Andreev, 2006]. Therefore the propellant decomposition appears to be driven by the reaction between the HTPE binder and AP or the HTPE binder and the AP and PSAN decomposition products.

When comparing Ea values of HTPE and HTPB propellants, from Table 116 it can be seen that HTPE propellants have a lower Ea_1 than HTPB propellants. In fact, from the first exothermic peak for HTPE samples 2P26E and 3P27B the Ea_1 values are 114 and 143 kJ mol^{-1} respectively and according to Sell [1999] and Gore [2004] the activation energy derived from second HTPB exothermic peak, Ea_2, is between 230 and 251 kJ mol^{-1}. As discussed above, for the Ea in HTPE propellants, the presence of the energetic plasticizer, n-BuNENA, is driving the overall kinetics and hence the difference in decomposition behaviour between HTPB and HTPE propellants. On the other hand, when comparing the Ea_3 derived from the third exothermic peak in HTPE propellants, it

can be seen that for HTPE/AP propellant the Ea_3 value is similar to that reported by Sell [1999] and Gore [2004] for HTPB propellants. However, in the HTPE propellant containing AP and PSAN, the Ea_3 value appears to be slightly higher than in HTPB propellants. Therefore, the presence of PSAN is affecting the decomposition of the AP and its reaction with the binder.

4.2.4.4 HTPE propellant, Ea conclusions

HTPE propellants containing only AP as oxidiser have lower activation energies than those containing AP and PSAN as oxidiser. On the other hand the Ea of HTPE propellants is lower than the Ea found for HTPE gumstock and binder network samples. It was observed that the presence of the energetic plasticizer n-BuNENA is driving the overall kinetics of the decomposition. However, when PSAN is added as a co-oxidiser, the HTPE Ea is increased in comparison with the propellant with only AP as oxidiser. Therefore, it is believed that the presence of PSAN is affecting the propellant thermal decomposition by delaying the exothermic decomposition reactions. It was also found that HTPE propellants have lower activation energies than HTPB propellants, mainly due to the presence of the energetic plasticizer n-BuNENA and the PSAN and their interaction with the binder.

V. SLOW COOK-OFF TESTS

5.1 Introduction

In order to compare cook-off behaviour between propellants prepared from HTPE and HTPB pre-polymers, several small scale cook-off test vehicles (SCTV) were prepared and tested. SCTV were used because they have been shown to be good for comparing explosives in their response to cook-off, especially slow cook-off. A comprehensive study of cook-off, related with different theories, methodologies, hardware and tests has been undertaken by Frota [2003] and by Matei [2000]. Although these works were mainly orientated to high explosives and tests using rocket propellants have not been done, they were found suitable to be used for composite rocket propellant, either based on HTPE or HTPB binder systems. The SCTV used in this present study are based on those used by Frota's work [Frota, 2003], with improved hardware and methodologies developed by Cartwright [2006]. The design of the SCTV actually in use for testing high explosives was modified to match the rocket motor case burst pressure characteristics.

Following the idea of Komai [2006] for the design of a small cook-off vehicle when comparing GAP and HTPB based rocket propellant, a bursting disk was included in the design of the SCTV. According to Chase [1996] rocket motor tube cases are designed to burst at a pressure between 2 and 25 MPa. However, because of the development of new composite case materials, higher pressures (up to 55 MPa) can be used, that according to Chan [2005], could be useful to avoid pressure break slopes. It was decided to take the higher pressure limit for the SCTV bursting disk design. Two kinds of bursting disk were designed: a 1.2 mm thickness bursting disk was made from aluminium 1050A and designed to work at 25 MPa and a 0.89 mm low carbon content steel CR4 bursting disk, designed to work at 48 MPa. The thickness of the bursting disk was calculated according to the following equation [Chase, 1996]:

$$t = \frac{d * P}{4 * \sigma} \tag{5.1}$$

Where ***t*** is the bursting disk thickness, ***d*** the diameter of the bursting disk, ***P*** the burst at static pressure and σ the aluminium tensile strength.

5.2 Experimental

5.2.1 Small scale cook-off test vehicle

The characteristics of the cook-off vehicle to be used during the slow cook-off test for the rocket propellant samples based on HTPE/AP/PSAN/n-BuNENA and HTPB/AP/DOS systems are presented in Figure 195 and in Table 117.

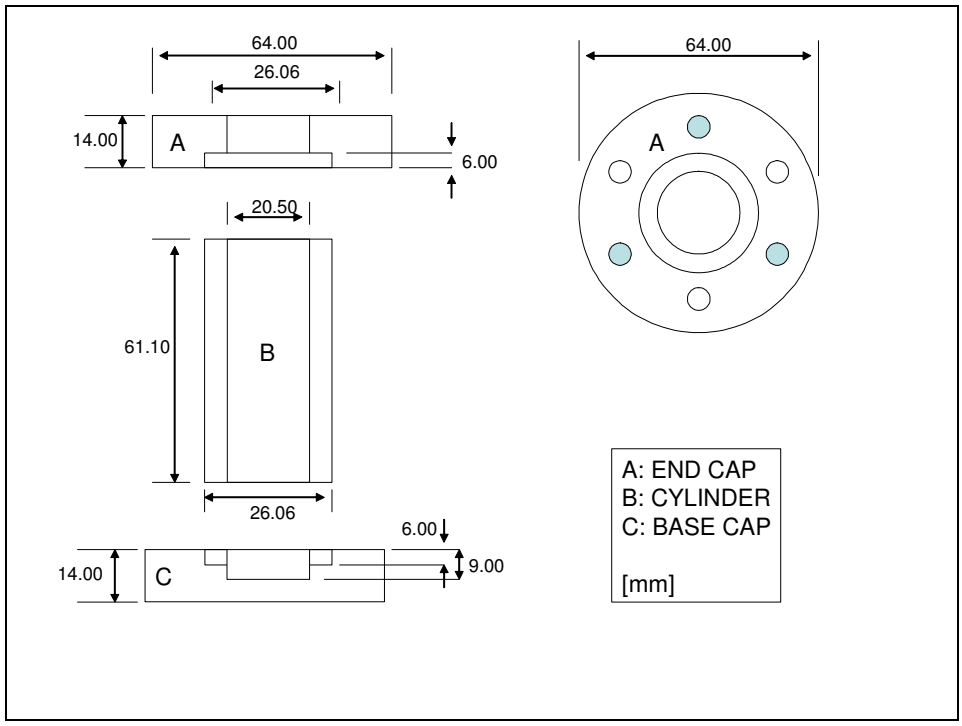

Figure 195. Small cook–off vehicle body drawing

Figure 196 shows the different components used in the small scale cook-off test vehicle. The main body consists of two plates and a cylinder. The plates are called base and end cap. Both have six alternated holes for 8 mm bolts; three of them are normal and the other three have screw bores. Also they have a 6 mm deep groove to contain each side of the cylinder, keeping a sealed unit by the use of a 1 mm thick copper washer. The end cap unit has a central screw bore to contain the 1/16" short male nut. Table 117 present the main characteristics of each component and their suppliers.

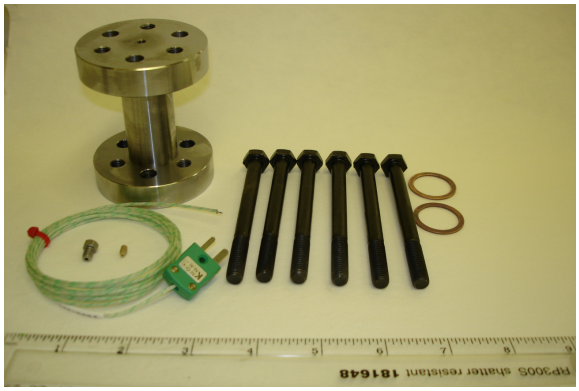

Figure 196. Small cook –off vehicle components

Table 117. Small Scale Cook-Off Test Vehicle Parts and Tools

Component Name	Amount	Supplier	Material	Characteristics	Other
Small scale vehicle body	1	DCMT workshop	Stainless steel EN3, O55M15	Mould steel low carbon content	According to BS 970 1991/83: C (0.25-max), Si (0.05-0.35), Mn (1.0-max), S (0.06-max), P (0.06-max)
Burst disk	1	DCMT workshop	Aluminium 1050A or Steel CR4	Al with high content Aluminium. Steel with Low content carbon	Al: Tensile strength 100-135 N/mm^2 Steel: Tensile strength 270-410 N/mm^2
Bolts	6	DCMT workshop	Steel	DYI 8.8	-.-
Steel Washers	6	Commercial off the shelf	Steel	8 millimetres	-.-
Copper Washers	2	DCMT workshop	Copper	-.-	-.-
Thermocouple	1	RS components Ltd	Nickel Aluminium	K Glass mini fitted plug	Part No: 363-0294
PTFE Ferrules	1	Jones Chromatography Ltd.	PTFE	PF1, 1/166 size (inch)	-.-
Short male nut	1	ANACHEM Ltd.	Stainless steel	Nut 1/16”; 10/32	Part No: U310X
Adhesive	1	RS components Ltd	Epoxy Resin	Fast dried epoxy resin	Part No: 850-956
Torque range	1	BRITOOL	-.-	Torque range up to 30 Nm	-.-
spanner	1	-.-	-.-	13mm	-.-

5.2.2 Small scale cook-off test vehicle assembly

Before assembling the cook-off test vehicle, all the units were cleaned with acetone to take out traces of lubricant oil used during manufacture at the work shop. After washing the samples they were placed in an oven to remove all traces of solvent. In order to measure the internal temperature of the sample during cook-off experiments, a K-type thermocouple was placed in the cook-off vehicle before the propellant was pored into the cylinder. The thermocouple was inserted through the end cap central screw bore and, in order to seal it and avoid gases coming out of the vehicle, a seal of PTFE ferrule, epoxy resin and stainless steel nut was used as explained by Frota [Frota, 2002]. Figure

197A and B show the stainless steel nut and PTFE pack, Figure 197 **C** the sealed end cap units when an aluminium bursting disk was used and Figure 197 D when a steel bursting disk was used where a cooper washer was included in the configuration.

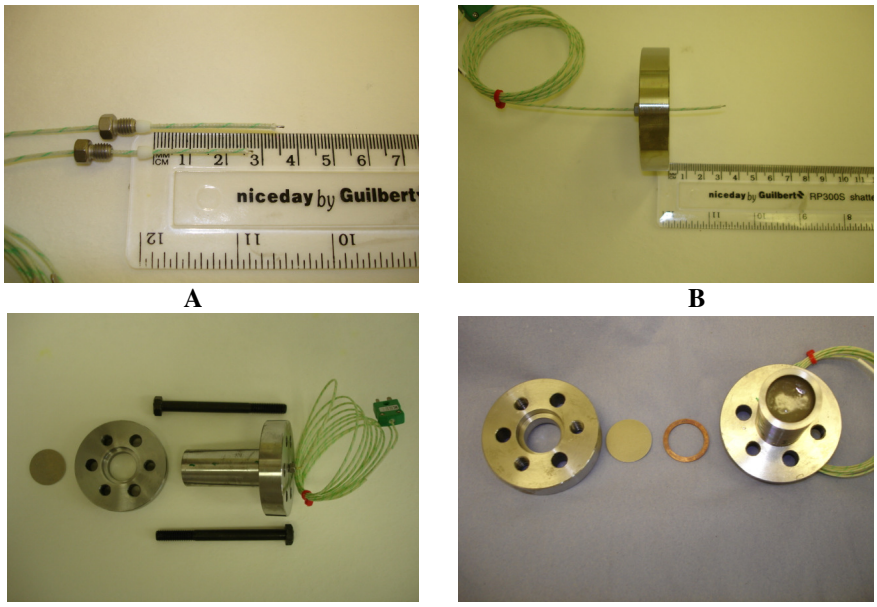

Figure 197. Thermocouple assembly

After assembling the thermocouple, the 1 mm copper washer was placed into the end cap 6 mm deep groove and the cylinder was placed over the 1 mm copper washer into the end cap groove. The cylinder's length was measured from the surface of the base cap to the surface of the end cap to verify it was correctly placed. The SVTC was filled with propellant as explained in the HTPE propellant manufacture Section 4.1.2 and the end cap containing the burst disk was located in place. When a steel bursting disk was used, a 1 mm cooper washer was placed between the bursting disk and the cylinder. Once the end cup with the bursting disk was in placed, the length of the tube between the two caps was measured in order to confirm its correct assembly and the bolts were screwed on, 1 mm washers were used (Figure 198A). The two caps were locked by using six bolts screwed up to reach a torque of 24 Nm as presented in Figure 198B. Special care was taken to clean off the propellant residue added to the SCTV tube wall during the filling process. The distance between propellant surface and bursting disk surface was measured, being around 7 mm, which gives a free volume of 2.2 cm^3.

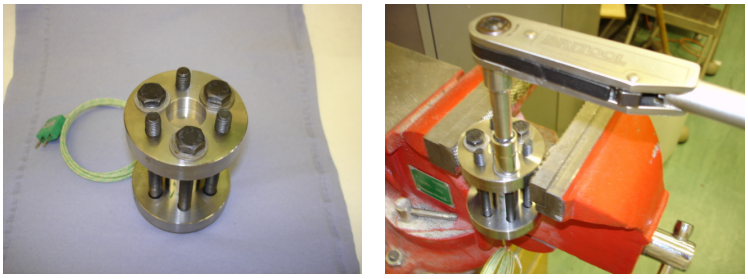

A **B**

Figure 198. SCTV final assembly

The SCTV were designated as SCTV1, SCTV2 and SCTV3 for the HTPE/AP/PSAN based propellant, SCTV4, SCTV5 and SCTV6 for the HTPE/AP based propellant, and SCTV7, SCTV8 and SCTV9 for the HTPB propellant. Each SCTV contained approximately 26 g of propellant. The SCTVs were photographed before and after the slow cook-off test. Figure 199 shows the assembled SCTV with a view from (A) the bursting disk side, (B) base cap side and (C) an SCTV with a configuration without thermocouple.

A **B** **C**

Figure 199. HTPE SCTV, before the slow cook-off test

Table 118. SCTV Configuration for Slow Cook-Off Test

SCTV Nº	Bursting Disk	Internal Thermocouple	Solid Nut	Cooper washer in top end cup
1	Aluminium, 1.2mm thickness	Yes	No	No
2	Steel, 0.89mm thickness	No	Yes	Yes
3	Steel, 0.89mm thickness	No	Yes	Yes
4	Aluminium, 1.2mm thickness	Yes	No	No
5	Steel, 0.89mm thickness	No	Yes	Yes
6	Steel, 0.89mm thickness	No	Yes	Yes
7	Aluminium, 1.2mm thickness	Yes	No	No
8	Steel, 0.89mm thickness	Yes	No	Yes
9	Steel, 0.89mm thickness	Yes	No	Yes

The SCTV configuration was changed, especially for the HTPE based propellant, during the development of the cook-off trials, as explained in Section 5.3.2.2 SCTV5.

Table 118 shows the different SCTV configurations used during the development of the slow cook-off tests.

5.2.3 Preparation of equipment

The general layout for the slow cook-off experiment is displayed in Figure 200 with details in Figure 201A to D.

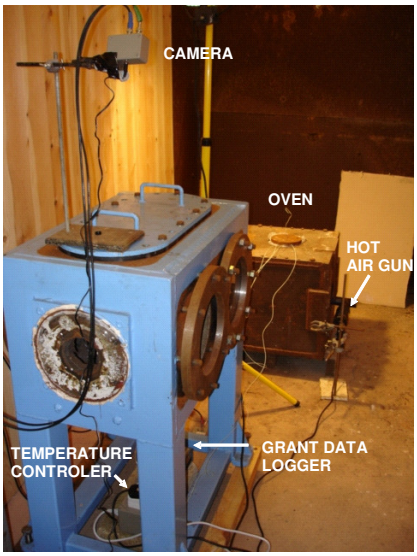

Figure 200. Slow cook-off experiment layout

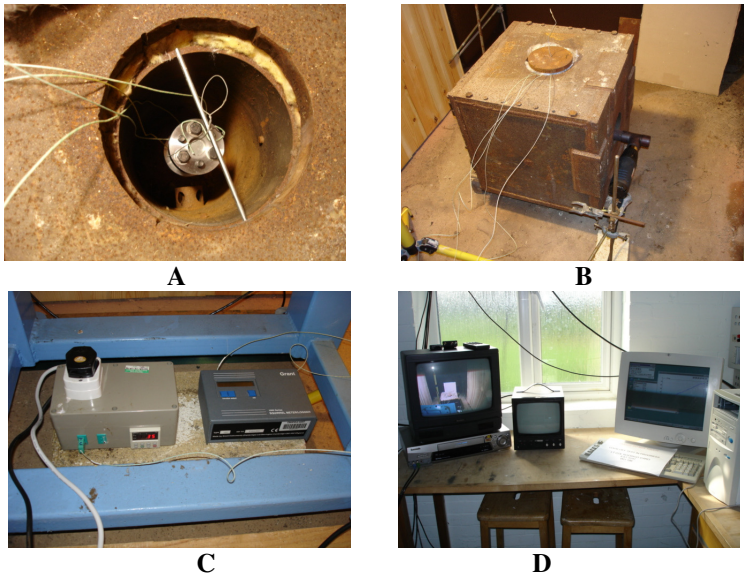

Figure 201. Slow cook-off experiment layout details

The slow cook-off tests were performed in a suitable remote location. The material list to carry out the test is presented in Table 119. The electrical flow sheet is presented in Figure 202.

Table 119. Material List Used in the Slow Cook-Off Test

Component Name	Number	Supplier or manufacturer	Material	Characteristics	Other
SCTV	9	DCMT workshop	Stainless steel	EN3, O055M15. According to Table 117	According to Table 117
Small cook-off oven container	1	DEOS building 82	Carbon Steel	Double tube Isolated with mineral wool	Carbon steel circular cap
Hot Air Gun	1	HomeBase	-.-	Performance Power model Pp1600HAG	1600 Watts, two temperature settings up top 250ºC and 450ºC
Copper T fitting	1	DCMT workshop	Copper	Hot flow driver and blast load dissipater	Brass sheet incorporated as high pressure relief devise
Thermocouple for oven temperature control	1	RS components Ltd	Nickel Aluminium	K Glass mini fitted plug	Part No: 363-0294
Temperature Controller	1	Coulton Instrumentation	-.-	Fuji-electric model PXZ4.	Four ram and soaks.
Data Logger	1	Grant	-.-	Grant 1000 Series model Squirrel meter/Logger	Type 1005
Digital camera	1	RS components Ltd	-.-	Colour PCB spy camera	-.-
Video Monitor	1	ACICA	-.-	model HM223	B&W
Video Recorder	1	Sony	-.-	VHS recorder	-.-
Coaxial Cable	2	RS components Ltd	-.-	25m x 2 video signal	-.-
Extension electrical cable	1	RS components Ltd	-.-	20m extension	2 female plug
Multiple connector	1	RS components Ltd	-.-	6 female plug connector	-.-
Electrical Tungsten lamp	2	-.-	-.-	Halogen 500W lamp with tripod	-.-
SCTV metal stick	1	DCMT Workshop	steel	8mm diameter	To hold in place the SCTV
Cap Isolator	1	DEOS	Mineral wool	-.-	-.-

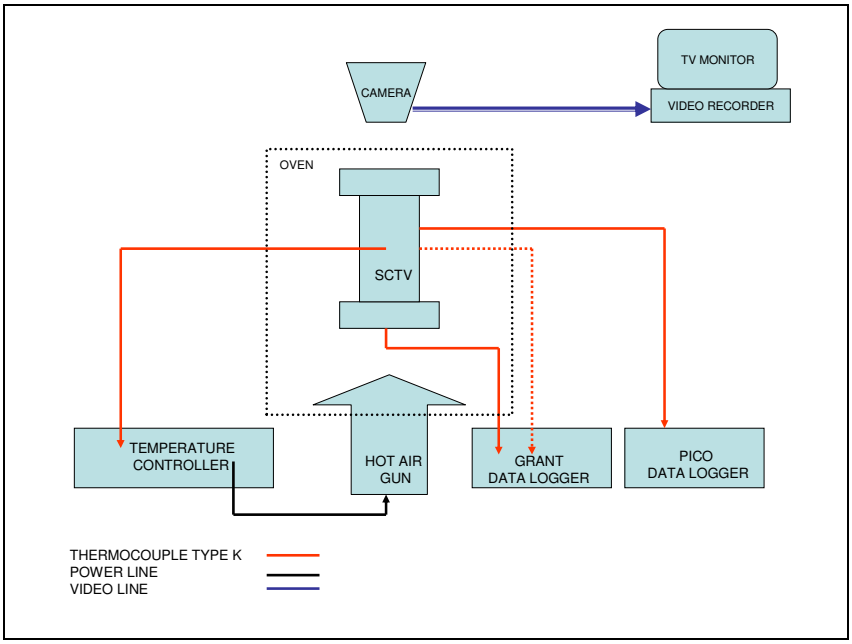

Figure 202. Slow cook-off electrical flow sheet

The temperature cycle for the slow cook-off test was selected taking into account the requirement of STANAG 4382 [1996] and the procedure used by Atwood [2005] for small scale cook-off validation experiments. The expected cook-off ignition temperature was initially estimated by taking into account the information reported by Chan [2005] and Atwood [2005] when doing slow cook-off tests using a small scale cook-off vehicle, being around 133 and 238ºC for HTPE and HTPB based propellants respectively. As can be seen from Figure 203 and Figure 204 there are two ramp temperatures. The first was chosen to reach a temperature 50ºC below the estimated cook-off ignition, and a rate of 5ºC per min was selected as suggested in STANAG 4382 [1996]. During the development of the trials a second ignition temperature of 186ºC was selected for samples based on HTPE, then a second temperature cycle presented as temperature cycle B in Figure 203. This temperature rate was reduced to 2.8ºC for the HTPB based SCTV after the first cook-off trial with the HTPB sample, in order to improve the cycle. After the first temperature ramp, a soak time of 30 min was chosen. However, it was increased to 60 min for the HTPB based SCTV. Finally, a second temperature ramp of 6ºC per min was chosen following Atwood [2005], this being consistent with the temperature rate used for the slow heating test described in Chapter III, Section 3.4.

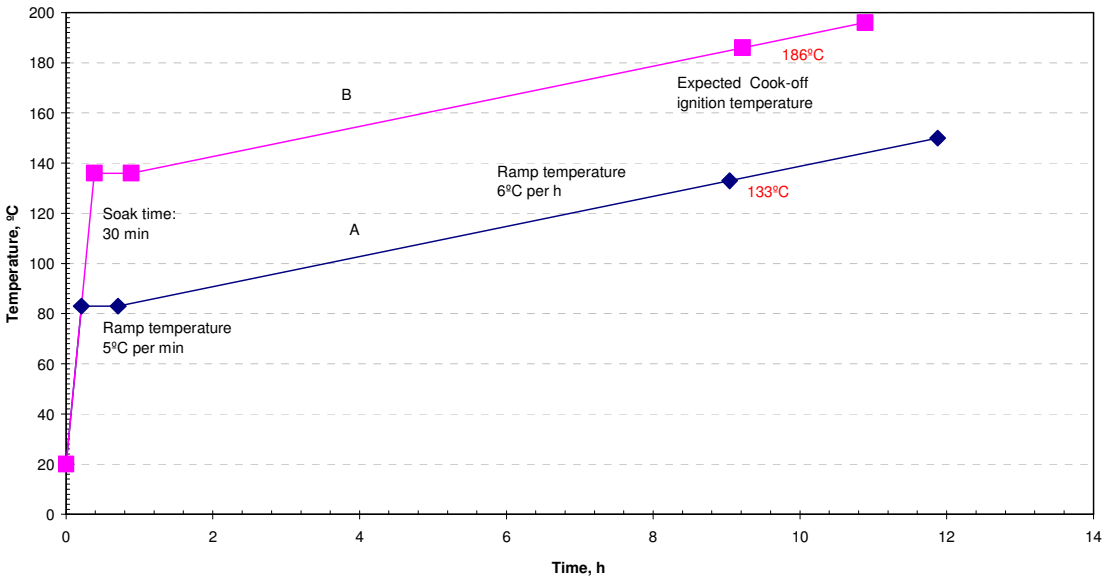

Figure 203. HTPE slow cook-off temperature cycle

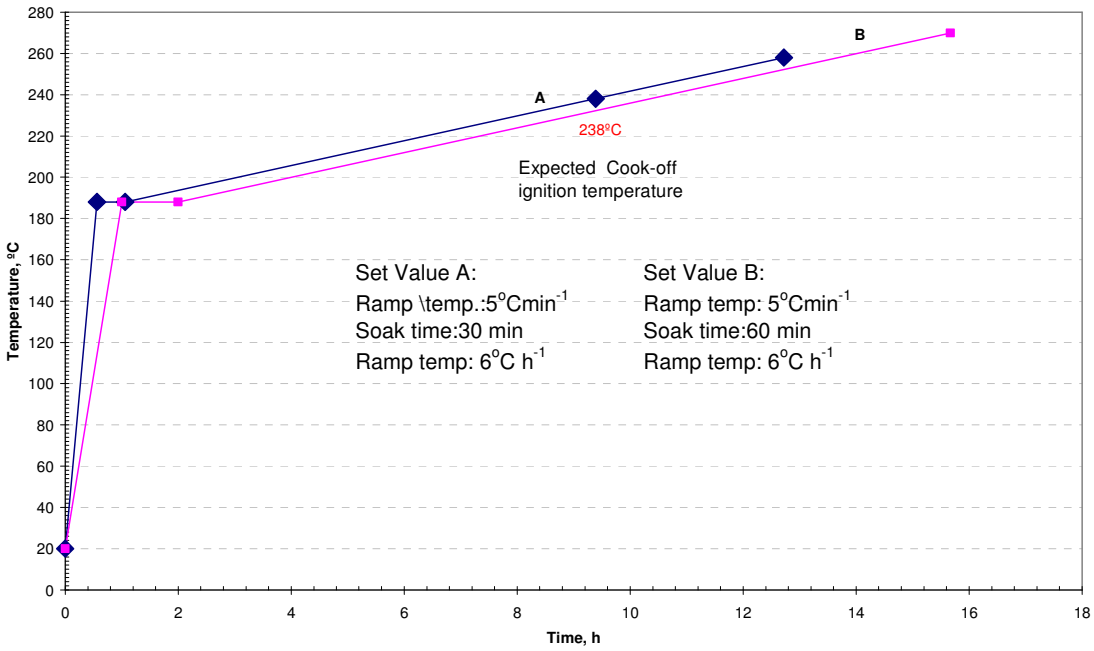

Figure 204. HTPB slow cook-off temperature cycles

5.3 Slow Cook-off Trial Results

The results from the slow cook-off tests presented in this section are grouped according to the kind of propellant used in the SCTV. However, the order of testing was as follow: HTPE/PSAN/AP/n-BuNENA propellant in SCTV1, HTPE/AP/n-BuNENA propellant in SCTV4, HTPB/AP/DOS propellant in SCTV7, HTPB/AP/DOS propellant in SCTV8, HTPE/AP/n-BuNENA propellant in SCTV4 and SCTV5, and then HTPE/PSAN/AP/n-BuNENA propellant in SCTV2 and finally SCTV3.

5.3.1 HTPE/PSAN/AP/n-BuNENA propellants

5.3.1.1 SCTV1

The SCTV1 internal K-type thermocouple was connected to a Grant data logger. Two extra K-type thermocouples were used. One was placed on the lower part of the SCTV1 near the base cap, between the cylinder and the nuts, and was connected to the temperature controller. The other thermocouple was placed at the bursting disk end cap and connected to a PICO data logger running via a 486 personal computer. SCTV1 was

placed in the oven and the test was started, following the heating sequence presented in Figure 203A. The measured heating profile is presented in Figure 205.

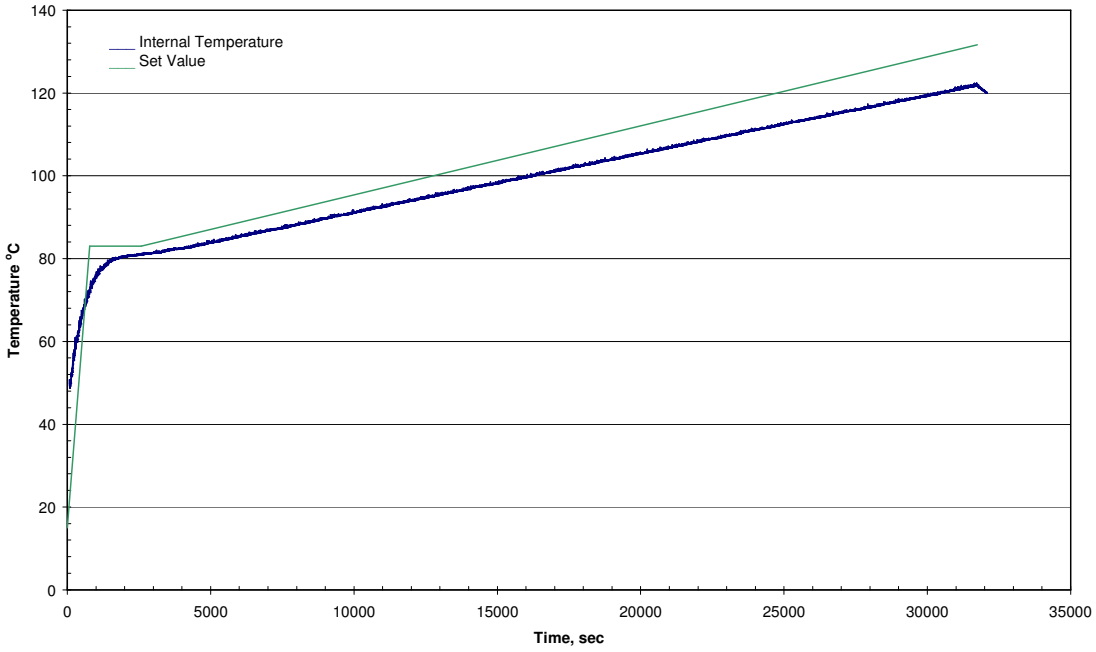

Figure 205. SCTV1 slow cook-off temperature cycle

When the temperature reached 121°C (measured by the internal thermocouple) after 529 min, an event was detected. A soft noise was heard and smoke was noticed coming out of the oven. The SCTV1 was not damaged, as can be seen in Figure 206, but the thermocouple connected through the short male nut and the PTFE ferrule was gone. Also the bursting disk was a little bit bent but no signs of damage due to shear stress could be seen.

A **B** **C**

Figure 206. SCTV1, after the slow cook-off trial

At the bottom of the heating oven the rest of the propellant could be seen. The propellant was liquid, even several hours after the event, and it was not easy to

distinguish the PSAN and AP crystals as before the test. Also the colour of the propellant was dark red instead of orange, as it was before starting the slow cook-off test.

The SCTV1 was disassembled and the propellant was taken out of the vehicle. Like the propellant found on the bottom of the oven, the remaining propellant inside the vehicle looked like relatively dry particles covered by a thin layer of liquid that preventing them from sticking to each other. It did not have any plastic characteristic, as can be seen in Figure 207. In Figure 207C, the sample that looks lighter colour was located close to the thermocouple nut and the darker colour close to the burst disk.

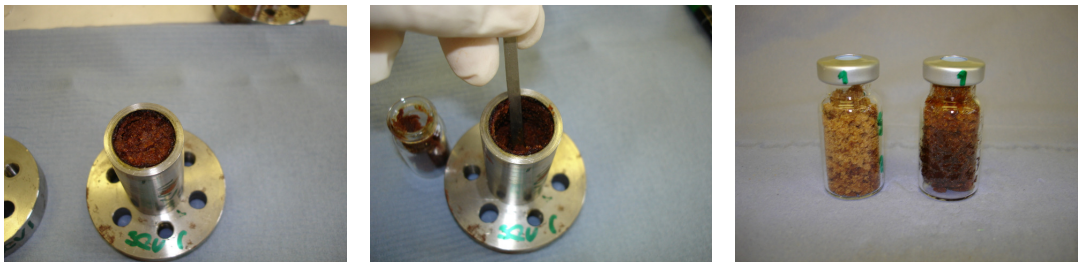

A **B** **C**

Figure 207. SCTV1, propellant residues after the slow cook-off trial

5.3.1.2 SCTV2

After the experience with SCTV5 and SCTV6, as described in the next section, the same temperature profile was used for SCTV2: ramp from ambient temperature up to 50°C below the cook-off temperature (i.e. 136°C) at a rate of 5°C per min, soak for 30 min and then start heating at a rate of 6°C per h. As for SCTV6, the internal K-type thermocouple was disconnected and cut and a solid bolt was put in its place. Three K-type thermocouples were placed at the top surface of the base cap, between the cylinder and the nuts, one connected to the temperature controller, one to the Grant data logger and the last one connected to a PICO data logger running via a 486 personal computer. SCTV2 was placed in the oven and the test started following the heating sequence presented before. As in SCTV6, a bursting disk made from steel, 0.88 mm thickness, designed to burst between a pressure range of 49 and 75 MPa was used. The settled and measured heating profiles are presented in Figure 208.

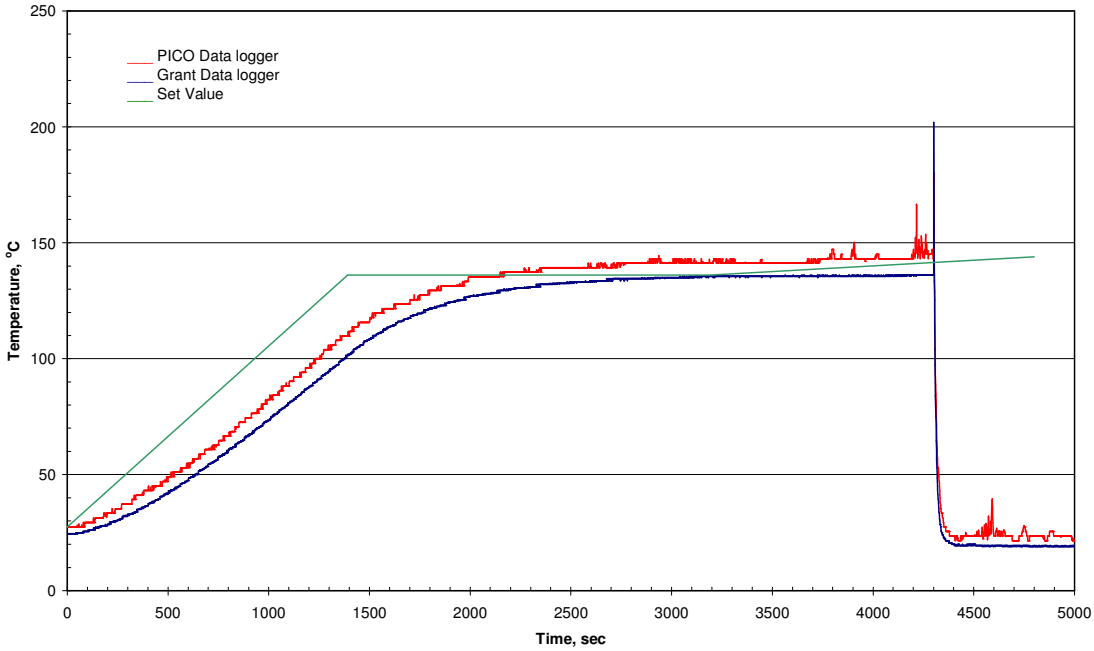

Figure 208. SCTV2 slow cook-off temperature cycle

As can be seen from Figure 208 the event happened before the expected time, at 136°C (Grant data logger measurement) instead of 186°C, and it was at approximately 72 min after starting the cook-off test.

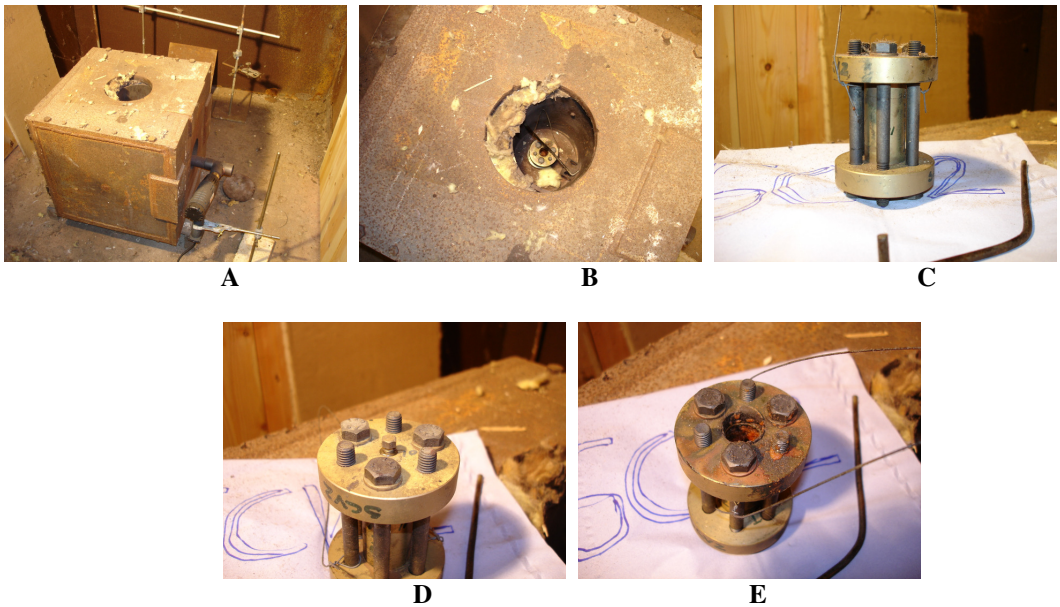

A **B** **C**

D **E**

Figure 209. SCTV2, after the slow cook-off trial

From the video recording it was noticed that just one event happened. A considerable deflagration occurred and because of that the oven lid was blown up to the roof, falling

down next to the oven on the floor. The oven itself was off centre and all the lid insulation was spread around the room (Figure 209A and B). Also the metal baffle for directing the hot air into the oven was blown away and stuck on the wooden wall as it did with the SCTV8 cook-off test. The maximum temperature measured by the external thermocouple connected to the Grant data logger was 202^{o}C. The SCTV2 was not damaged; the cylinder was intact as was the solid bolt seal as can be seen in Figure 209C and D. The bursting disk was cut all around the cylinder diameter and was not recovered. The internal thermocouple was still in place inside the cylinder and some propellant remains were attached to the cylinder bottom and walls and on the surface of the end cap, as can be seen in Figure 209 E.

5.3.1.3 SCTV3

After the experience with SCTV2, it was decided to use the initial temperature cycle "A" stated in Figure 203 i.e. ramp from ambient temperature up to 83^{o}C at a rate of 5^{o}C per min, soak for 30 min and then start heating at a rate of 6^{o}C per h. As for SCTV2, the internal K-type thermocouple was disconnected and cut and a solid bolt was put in its place.

Three K-type thermocouples were placed at the top surface of the base cap between the cylinder and the nuts, one connected to the temperature controller, one to the Grant data logger and the last one connected to a PICO data logger running in a 486 personal computer. SCTV3 was placed in the oven and the test was started following the heating sequence presented before.

The measured heating profile is presented in Figure 210. Due to data logger memory capacity, the temperature at the event time was not measured and no records were saved. Despite this, from the temperature profile, the last recorded temperature and time, it was estimated that the event happened between 211 and 227^{o}C. As previously, a bursting disk made from steel, 0.88 mm thickness, designed to burst in a pressure range of 49 to 75 MPa was used.

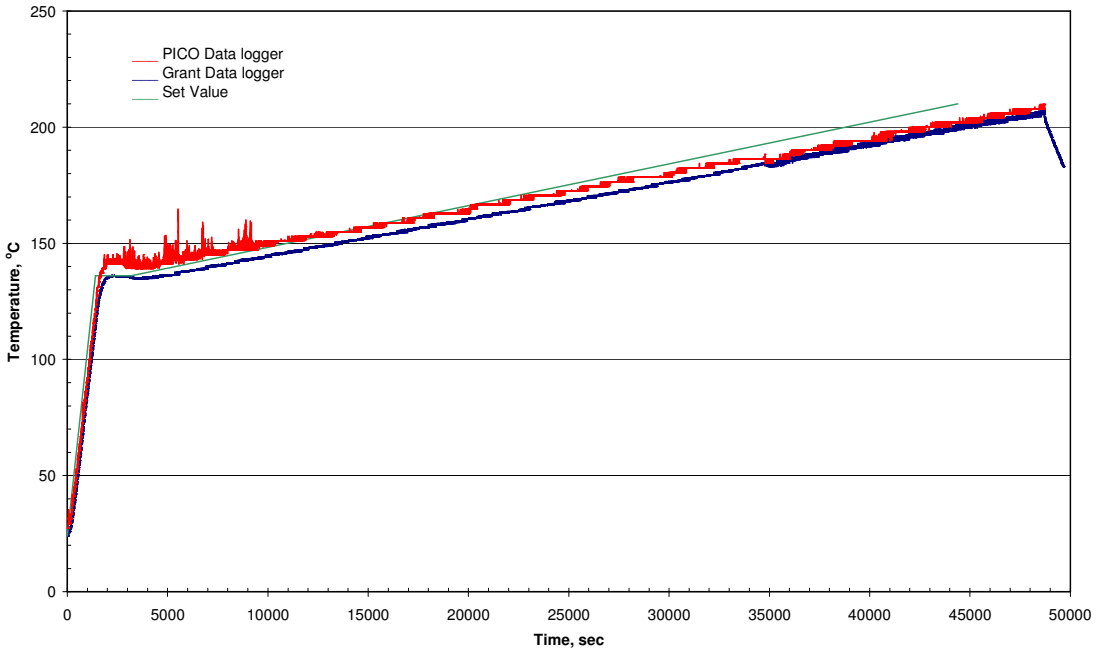

Figure 210. SCTV3 slow cook-off temperature cycle

As can be seen from Figure 211 the SCTV3 was almost completely destroyed. A considerable explosion occurred and because of that the oven lid was blown up to the roof, falling down next to the oven on the floor. The oven itself was still centred and all the lid insulation was distributed around the room (Figure 211A and B).

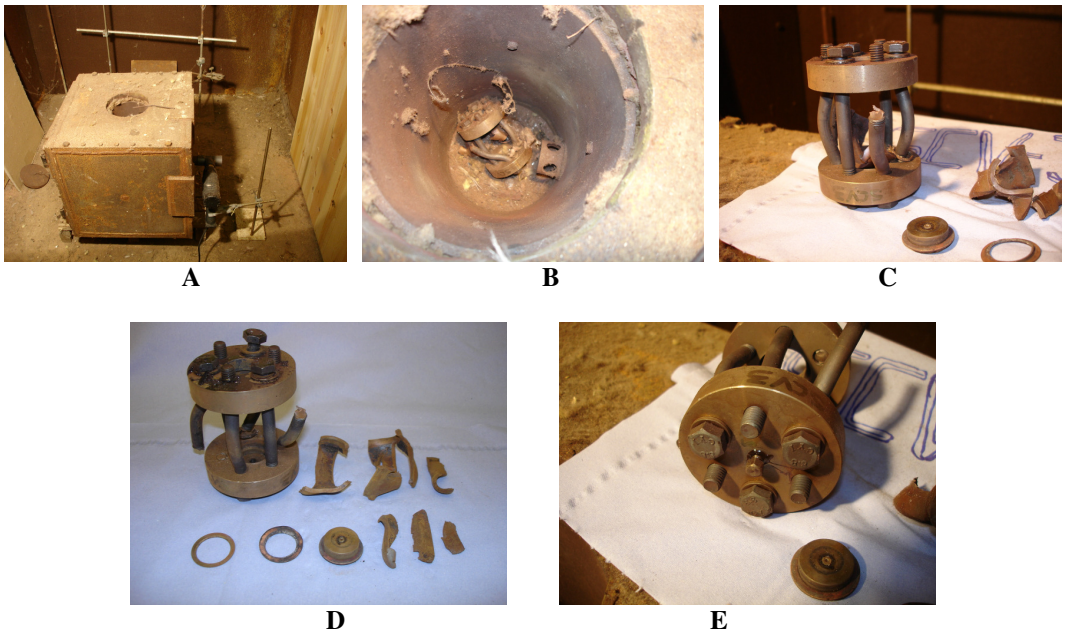

A **B** **C**

D **E**

Figure 211. SCTV3, after the slow cook-off trial

Also the metal baffle for directing the hot air into the oven was blown away and was stuck on the wooden wall, as it was in the SCTV8 and SCTV2 cook-off tests. The SCTV3 was completely destroyed; the cylinder was shattered into several pieces and they were found on the bottom of the oven. Three nuts were cut; the solid nut seal can be seen in Figure 211C and D. The bursting disk was cut all around the cylinder diameter and it was not found. The copper washer and a bursting disk ring were found in the oven too. The seal for the thermocouple was still in place and no signs of leaking were evident as can be seen in Figure 211E. The three thermocouples used to measure the external temperature for the data loggers and temperature controller were completely destroyed.

5.3.2 HTPE/AP/n-BuNENA propellants

5.3.2.1 SCTV4

The SCTV4 internal K-type thermocouple was connected to the Grant data logger. Two extra K-type thermocouples were placed at the top surface of the thermocouple base cap, between the cylinder and the nuts, one connected to the temperature controller and the other connected to a PICO data logger running from a 486 personal computer. SCTV4 was placed in the oven and the test started, following the heating sequence presented in Figure 203. The measured heating temperature profile is presented in Figure 212. When the temperature reached approximately 129^{o}C (measured by the internal thermocouple) after 502 min, an event was detected. A soft noise like a jet was heard and smoke coming out the oven was noticed.

The SCTV4 was not damaged, as can be seen in Figure 213 and, as in the SCTV1 test, the thermocouple connected through the short male nut and the PTFE ferrule was gone. The bursting disk was not bent and no signs of damage due to shear stress could be seen. In Figure 213 at the bottom of the heating oven, the rest of propellant that went through the male short nut can be seen. The propellant recovered from the bottom of the oven was very soft but not a liquid like in the SCTV1 test, even several hours after the event, and it was easy to distinguish the AP crystals in this case. Also the colour of the propellant was dark red instead of orange as it was before the test.

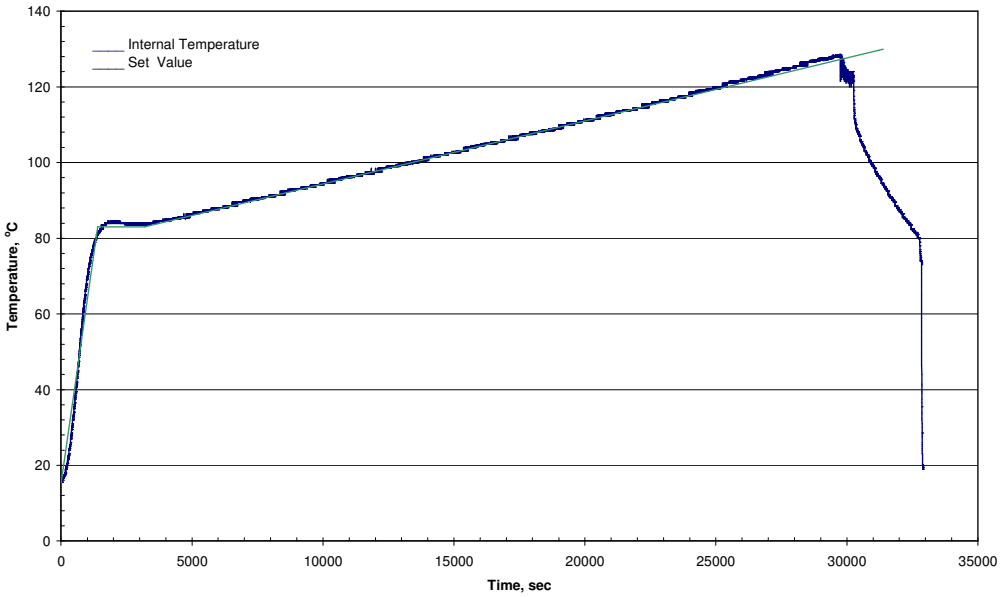

Figure 212. SCTV4 slow cook-off temperature cycle

The SCTV4 was disassembled and the propellant was taken out of the vehicle. Like the propellant found on the bottom of the oven, the remaining propellant inside the vehicle looked like wet crystals only, still having a little bit of consistency, but not having any plastic characteristic as in the SCTV1 test, as can be seen in Figure 213D and E. However they looked like a homogeneous mix. The amount of propellant found inside the tube was small because almost all was expelled, as can be seen in Figure 213D.

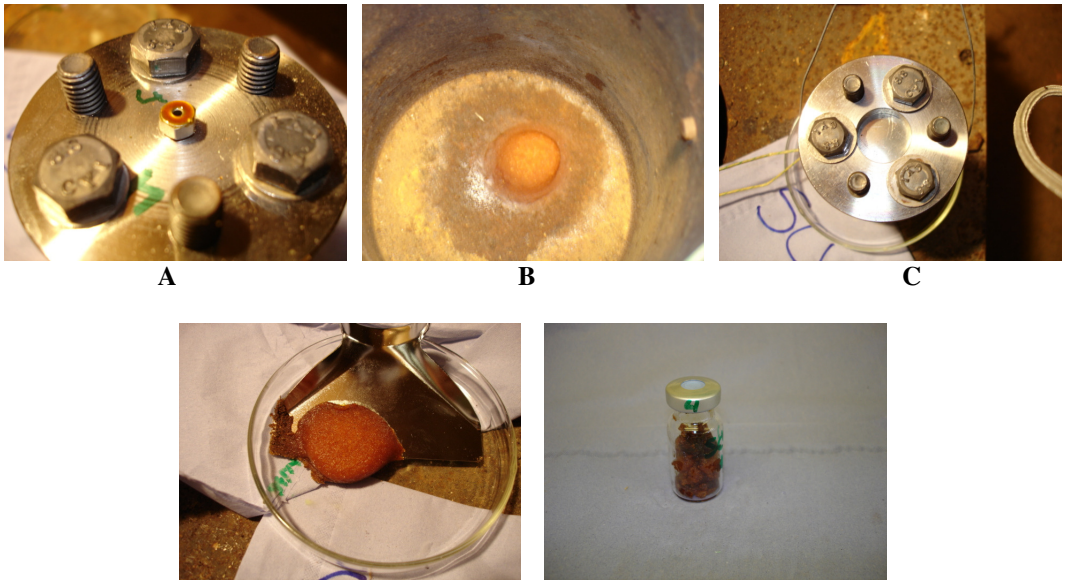

A **B** **C**

D **E**

Figure 213. SCTV4, after the slow cook-off trial

5.3.2.2 SCTV5

Because of the propellant leaking problems during the SCTV1 and SCTV4 tests using HTPE based propellants, it was decided to modify the SCTV containing HTPE based propellant configuration. The internal K-type thermocouple was disconnected and cut and a solid bolt was put in its place. Three K-type thermocouples were placed on the top surface of the base cap, between the cylinder and the nuts, one connected to the temperature controller, one to the Grant data logger and the last one connected to a PICO data logger running via a 486 personal computer. The SCTV5 was placed in the oven and the test was started, following the heating sequence "A" presented in Figure 203. The measured heating profile is presented in Figure 214.

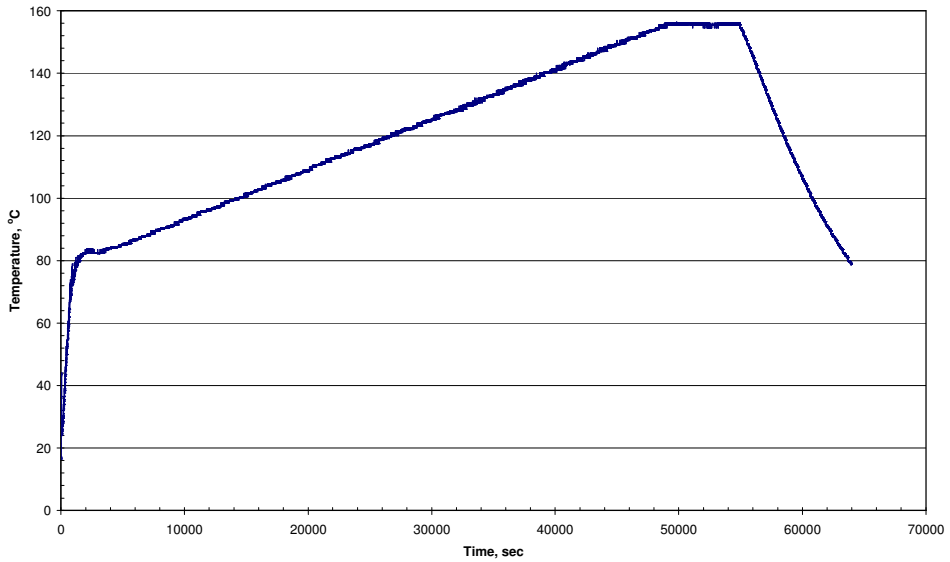

Figure 214. SCTV5 slow cook-off 1st temperature cycle, external temperature

The sample was heated from 83°C up to aproximately160°C (measured by the external thermocouple) and after that was soaked for approximately 60 min. No event was detected. It was decided to stop the test in order to review the hardware. No leaking problems were detected and the SCTV5 appeared to be well sealed. Then it was decided to do a second heating cycle. This time the SCTV was heated up to 156°C at 5°C per min, then soaked for 30 min and after that heated at a heating rate of 6°C per h (Figure 215).

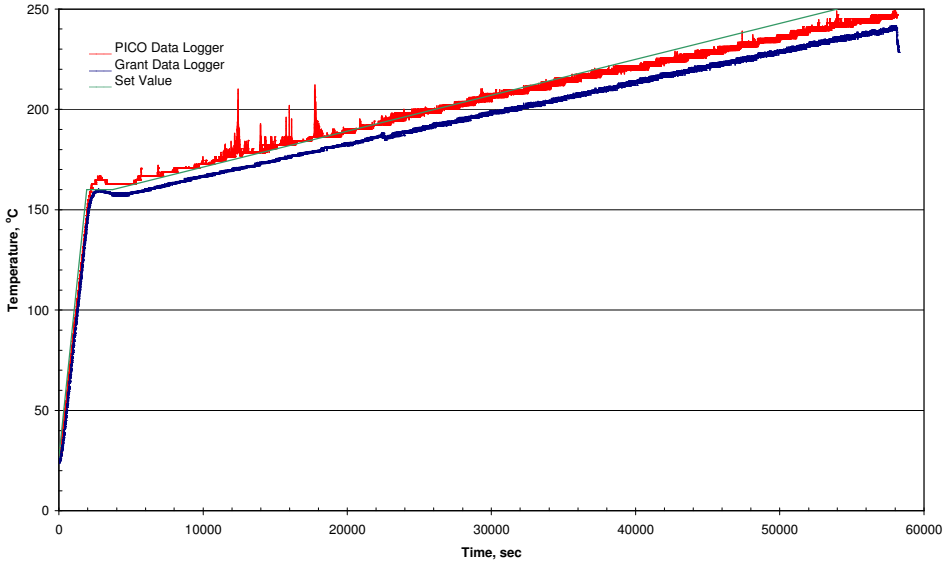

Figure 215. SCTV5 slow cook-off 2nd temperature cycle, eternal temperature

From the video and from the data logger information it was estimated that the event occurred at around 183°C. A mild event in comparison with the SCTV8 test was observed and the reaction was able to lift the steel cover of the oven about 30 cm over its normal location. According to the Grant data logger temperature record, a change in temperature was observed at 186°C. In fact the SCTV5 was found at the bottom of the oven instead of hanging in the middle of the oven. Then the small difference in temperature can be appreciated as a temperature drop.

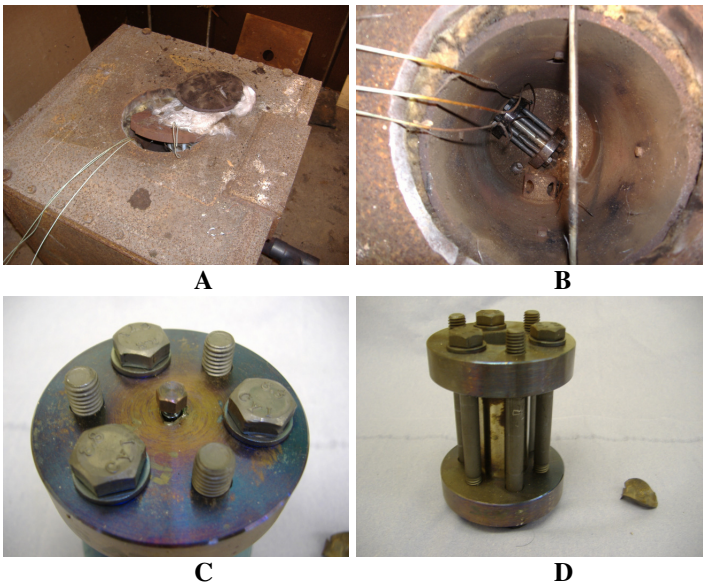

A **B**

C **D**

Figure 216. SCTV5, after the slow cook-off trial

The SCTV5 was not damaged, as can be seen in Figure 216, and the propellant was completely burned, no debris or remains being found. The seal appeared to work perfectly and no signs of leaking were found, as can be seen in Figure 216 C. On the other hand, part of the thermocouple was still on place. Also the bursting disk was bent and cut around the diameter of the cylinder.

5.3.2.3 SCTV6

From the experience obtained with the SCTV5 it was decided to modify the temperature cycle, taking the cook-off temperature as 186°C. Then the slow heating cycle used was as follows: ramp from ambient temperature up to 50°C below the cook-off temperature (i.e. 136°C) at a temperature ramp rate of 5°C per min, soak for 30 min and then start heating at a temperature ramp rate of 6°C per h. As in SCTV5, the internal K-type thermocouple was disconnected and cut and a solid bolt was put in its place. Three K-type thermocouples were placed at the top surface of the base cap, between the cylinder and the nuts, one connected to the temperature controller, one to the Grant data logger and the last one connected to a PICO data logger running via a 486 personal computer. SCTV6 was placed in the oven and the test was started, following the heating sequence presented before. The measured heating profile is presented in Figure 217.

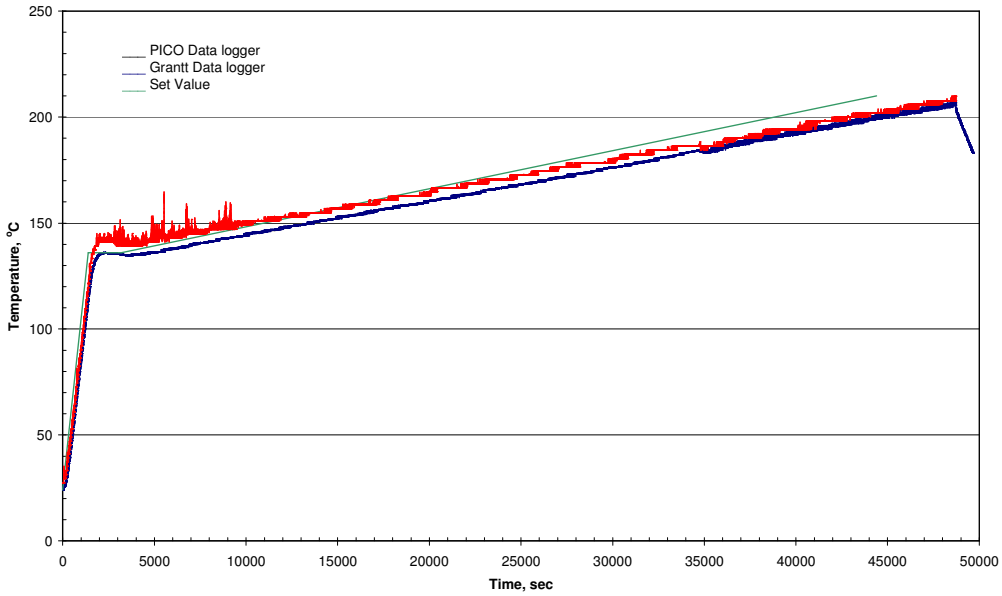

Figure 217. SCTV6 slow cook-off temperature cycle, external temperature

From the video analysis and from the data logger information it was estimated that an event occurred at around 184°C. A mild event in comparison with that for the SCTV8 test and very similar to the SCTV5 test was observed and the reaction was able to lift the steel cover of the oven about 20cm over its normal location. As for the SCTV5 test, and according to the Grant data logger temperature record, at 184°C a change in temperature was observed. In fact the SCTV5 was found in a different position in comparison with the initial position. Possibly this position change also affected the temperature recorded by the thermocouples. Then the small difference in temperature can be seen as a temperature drop at around 184°C according to Grant data logger and around 186°C according to Pico data logger. The SCTV6 was not damaged, as can be seen in Figure 218 and the propellant was completely burned, no debris or remains being found. The seal appeared to work perfectly and no signs of leaking were found, as can be seen in Figure 218. On the other hand part of the thermocouple was still in place. Also the bursting disk was bent and cut around the diameter of the cylinder.

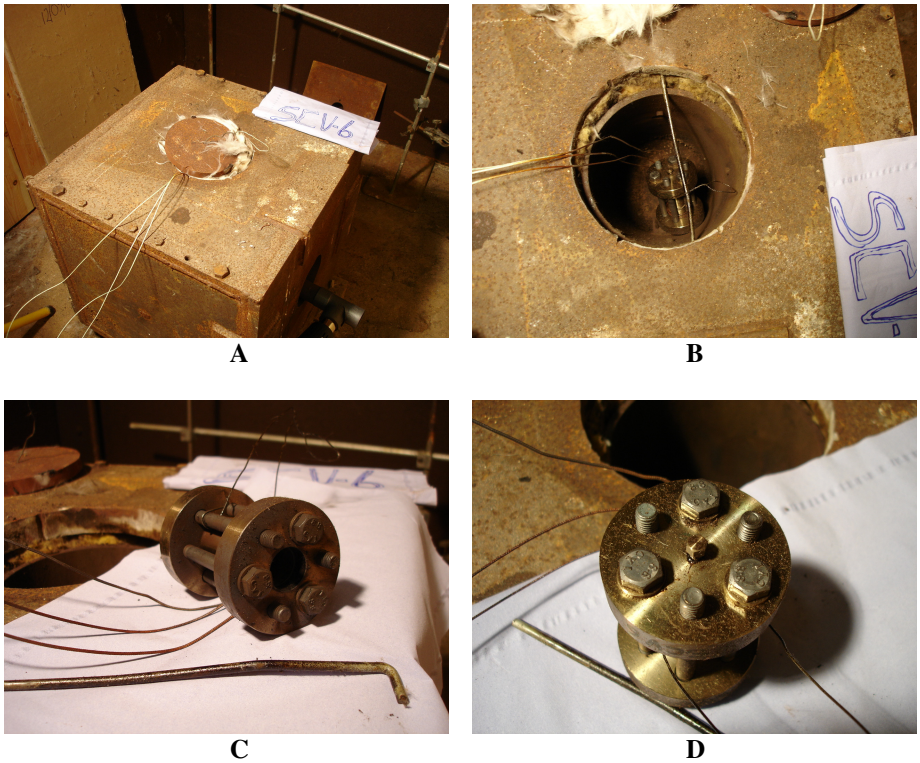

A **B**

C **D**

Figure 218. SCTV6, after the slow cook-off trial

5.3.3 HTPB/AP/DOS propellant

5.3.3.1 SCTV7

The SCTV7 internal K-type thermocouple was connected to the Grant data logger. Two extra K-type thermocouples were placed at the top surface of the base cap, between the cylinder and the nuts, one connected to the temperature controller and the other connected to a PICO data logger running via a 486 personal computer. SCTV7 was placed in the oven and the test was started, following the heating sequence presented in Figure 204. The measured heating profile is presented in Figure 219.

The temperature profile used to raise the temperature from ambient to the soak temperature was not reached, as can be seen in Figure 219. In fact the ramp temperature was 2.47^{o}C per min instead of 5^{o}C per min as was expected. Despite this, after the soak time the temperature increased as expected. When the temperature reached approximately 243^{o}C (measured by the internal thermocouple) after 736 min, a first event was detected. A noise like a small explosion was heard, the oven lid was taken out of it normal place (Figure 221 A) and smoke coming out of the oven was noticed on the monitor.

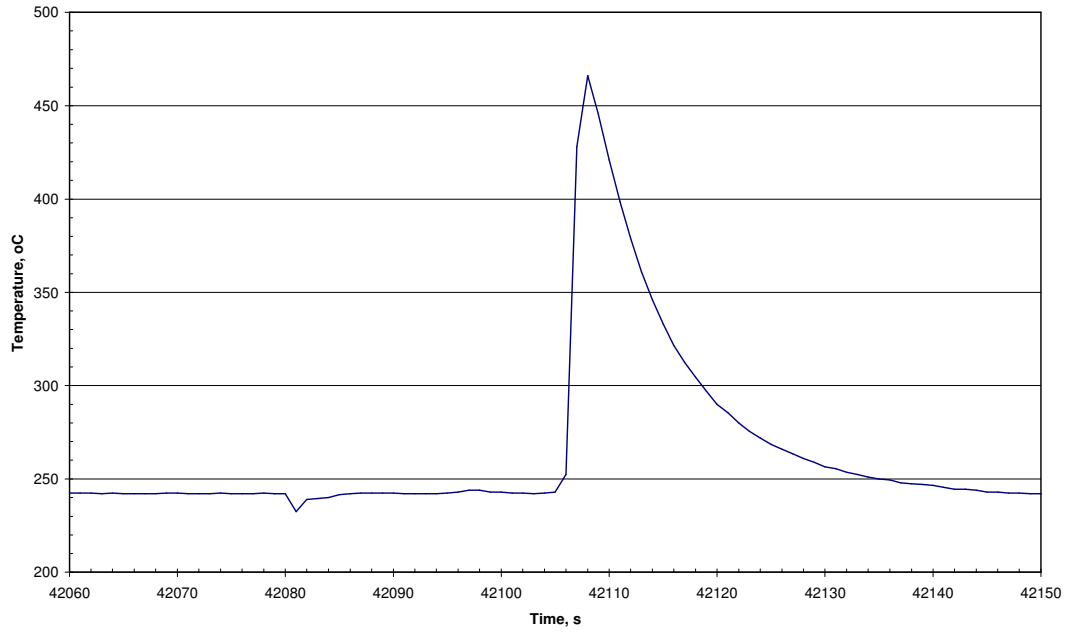

Figure 219. SCTV7 slow cook-off temperature cycle

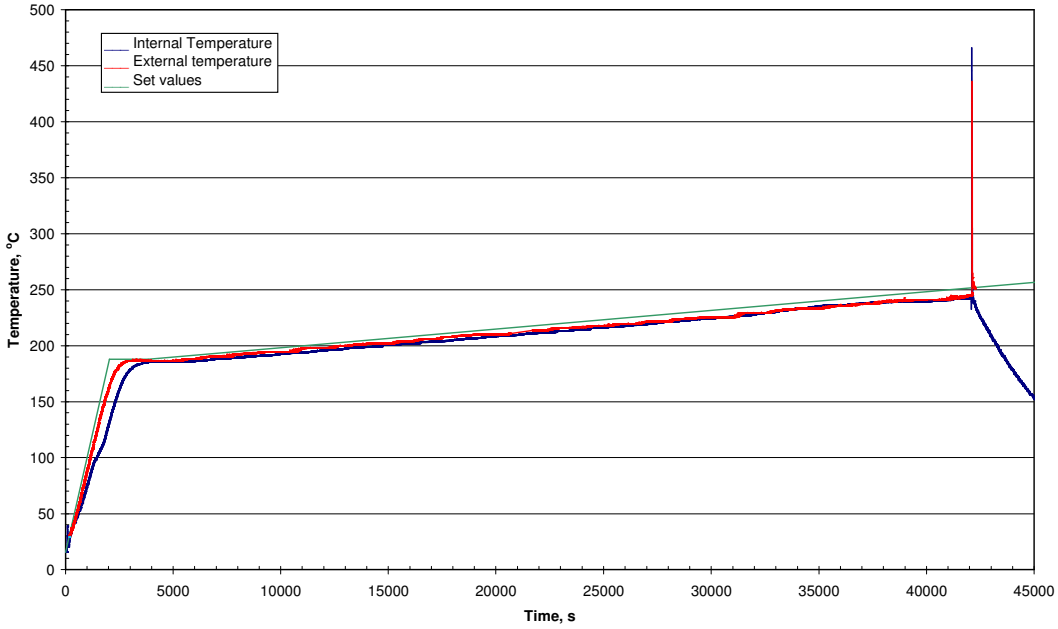

Figure 220. SCTV7 slow cook-off, last period of the temperature cycle

After 21 s of this event, the propellant self ignited and a red flash together with a strong noise was observed. The maximum temperature measured by the internal thermocouple was 466 and 435°C recorded by the external thermocouple connected to the PICO data logger.

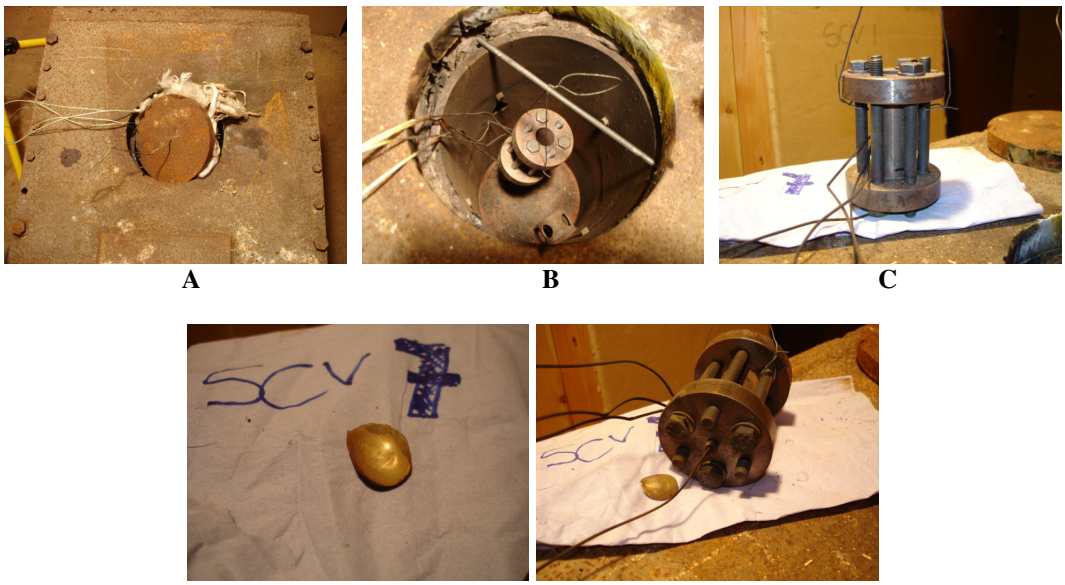

A **B** **C**

D **E**

Figure 221. SCTV7, after the slow cook-off trial

The SCTV7 was not damaged, as can be seen in Figure 221 B, but the bursting disk was bent and found to be out of place (Figure 221 B and D). This time the internal thermocouple connected through the short male nut and the PTFE ferrule was intact and still measuring temperature. No damage to the cylinder body was observed.

5.3.3.2 SCTV8

The configuration was changed for SCTV8. This time a bursting disk made from steel, 0.88 mm thickness, designed to burst between a pressure 49 MPa and 75 MPa was used. The SCTV8 internal K-type thermocouple was connected to the Grant data logger series 1000 and two extra K-type thermocouples were placed at the top surface of the base cap, between the cylinder and the nuts, one connected to the temperature controller and the other connected to a PICO data logger running via a 486 personal computer. The SCTV8 was placed in the oven and the test was started, following the heating sequence presented in Figure 204 B. The measured heating profile is presented in Figure 222, and an expansion of the last part of the curve, just prior to the event, is shown in Figure 223.

The HTPB temperature cycle "B" was used for this test. This time the soak temperature was closer to the set value than in the SCV7 trial, as can be seen in Figure 222. In fact the temperature ramp rate was 2.8 instead of $5^{o}C\ min^{-1}$ as was expected. However, because of the extra 30 min for the soak temperature, after the soak time the temperature increases at a rate of $5.66^{o}C$ per h, slightly lower than expected. When the external temperature reached approximately $252^{o}C$ (measured by the external thermocouple) after 907 min, the internal temperature was $259^{o}C$ and a first event was detected. As in the SCTV7, a noise like a small explosion was first heard and smoke coming out of the oven was noticed through the monitor.

After 25 s of this event the propellant self-ignited and an event like an explosion was produced. The oven lid blew out and up to the roof, falling down next to the oven on the floor, and all the lid insulation was spread throughout the room (Figure 224 A and B). Also the metal baffle for directing the hot air into the oven was blown out and was stuck on the wooden wall as can be seen in Figure 224 B. The maximum temperature

measured by the internal thermocouple was 338°C. No external temperature was recorded due the external thermocouple being damaged during this event.

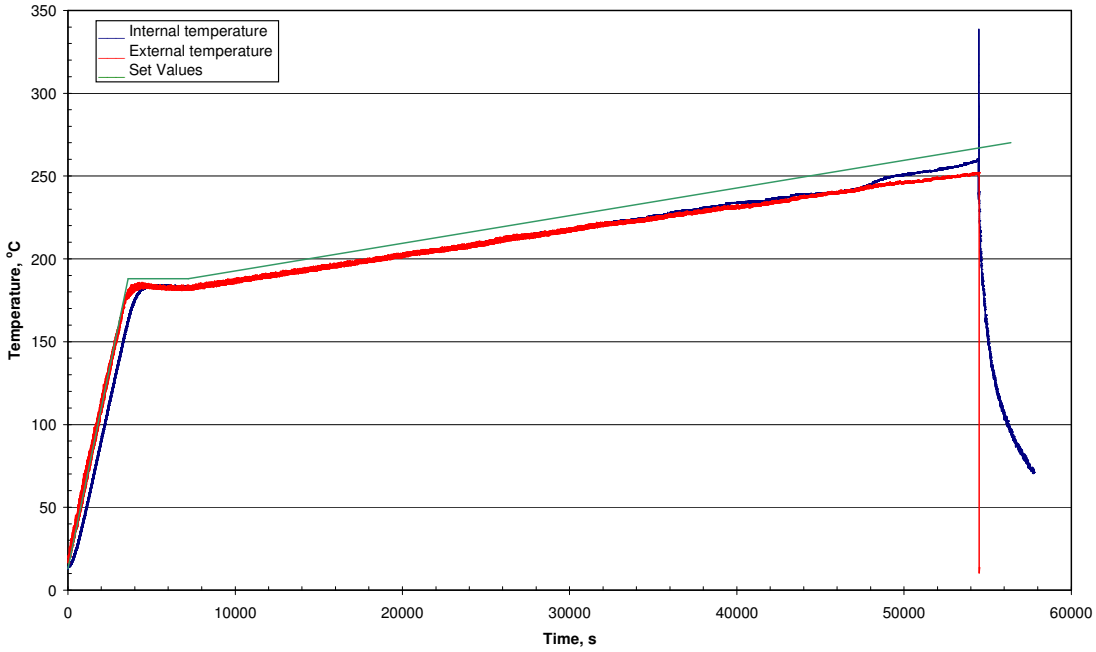

Figure 222. SCTV8 slow cook-off temperature cycle

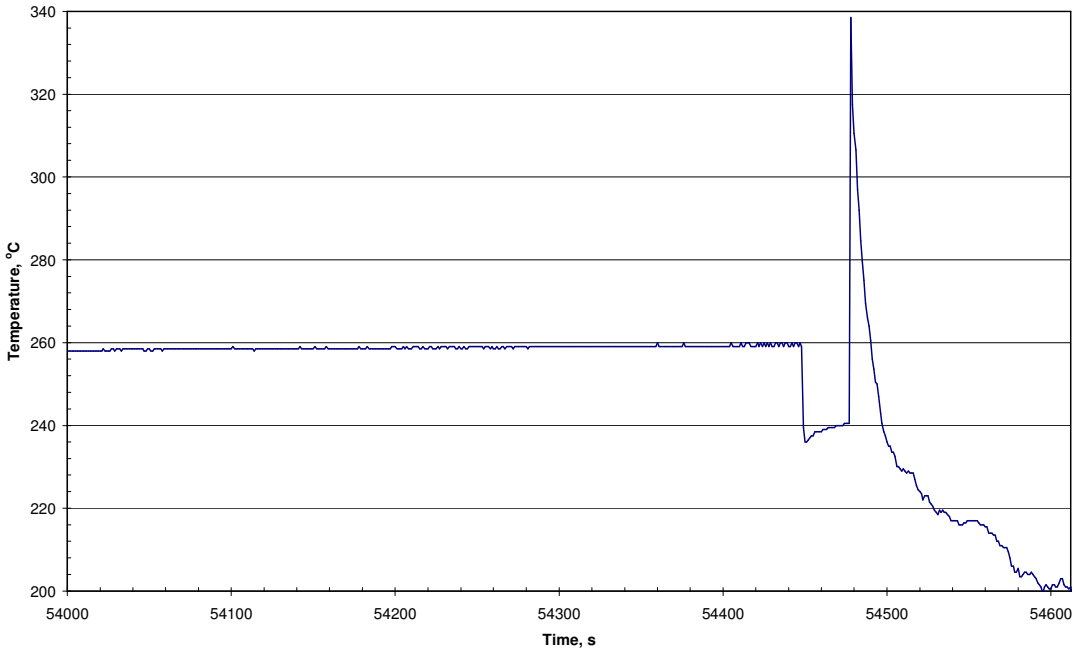

Figure 223. SCTV8 slow cook-off, last period of the temperature cycle

The SCTV8 was damaged; the cylinder bursting and some bolts were bent, as can be seen in Figure 224 C and D. The burst disk was damaged although part of it remained attached to the cylinder (Figure 224 E). This time the internal thermocouple connected through the short male nut and the PTFE ferrule was also in place, intact and still measuring temperature after the explosion. The external thermocouples were damaged.

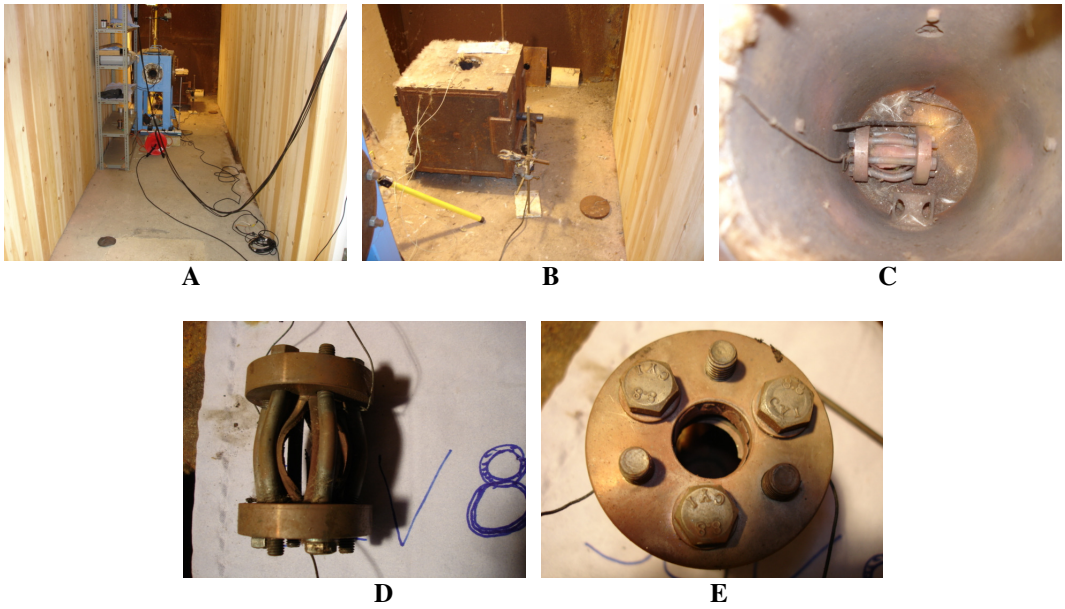

A **B** **C**

D **E**

Figure 224. SCTV8, after the slow cook-off trial

5.4 Discussion of Results

5.4.1 Hardware and equipment

In general terms, the hardware works well for HTPB propellants. However, this was not the case for the HTPE propellants. In fact, for HTPE propellants the thermocouple short male nut seal failed, allowing release of internal pressure and propellant through the nut hole. The HTPE propellant becomes liquid during slow heating and the total internal pressure generated by the decomposition process pushed the thermocouple out of its place. The case was different for HTPB; because the propellant becomes even harder and more brittle than initially it acts like a block seal and the pressure over the thermocouple and short male nut seal is lower. The problem was resolved by cutting the thermocouple wire and replacing the short male nut by a solid short male nut. Of course this action eliminated the possibility of having internal temperature records. A possible

solution for this problem can be to use other kinds of thermocouple instead of the K-type fibre glass protected. The SCTV and its modification to include a bursting disk was shown to be a good vehicle for the comparison of propellant slow-cook of behaviour. This allowed simulation of a closed rocket tube hardware environment (they are normally designed to burst between 2 and 55 MPa). The aluminium bursting disk, designed to burst at 25 Mpa, did not allow enough time to reach the conditions in order to have a proper cook-off reaction to compare propellant behaviour. However, the use of the low content carbon steel, designed to burst at 48 MPa of static pressure, appeared to be a suitable choice for this purpose.

The data logger acquisition systems are a weakness when recording data in long term trials. This was evident during the development of the trial with SCTV3.

5.4.2 HTPB/AP/DOS propellants

Slow cook-off tests for HTPB propellants performed as expected and ignition temperatures for the events in SCTV7 and SCTV8 were 243 and 259^{o}C respectively. These temperatures are in close agreement, although slightly higher, with those reported by Atwood [2005], 238.1^{o}C for a HTPB/AP/Al based composition, and by Komai [2006], 233.1^{o}C for a HTPB/AP based composition.

During the development of the trial with SCTV7 the event did not damage the SCTV as with SCTV8. This was because the bursting disk was designed to burst at a static pressure of 25 MPa, which was not enough to trigger a higher decomposition rate and only a mild event was seen. The expected event happened when the bursting disk was designed to burst at 48 MPa of static pressure in SCTV8. A large explosion was produced this time and the SCTV was damaged. In both cases there was a gap between the time when the bursting disk was broken and the deflagration or explosion; 21 and 25 s for SCTV7 and SCTV8 respectively, as can be seen from Figure 225.

It is believed that the delay is related to the depressurisation which is happening at the moment when the bursting disk is bursting; the self ignition of the propellant starts

again some seconds later. Because the propellant is becoming harder and more brittle due to the oxidative cross linking, the gases generated during this process have possibly cracked the propellant and also cavities have been produced by the migration of some components, as explained in the discussion on the slow heating test, in Chapter III, Section 3.4.

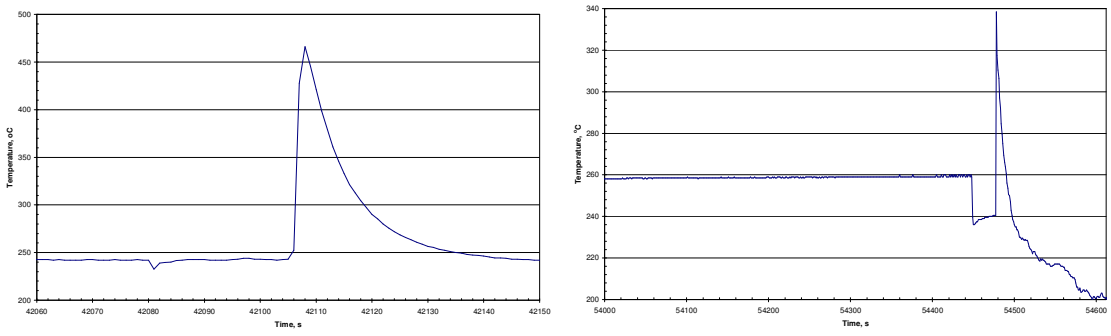

A **B**

Figure 225. SCTV7 (A) and SCTV8 (B) ignition time and temperature

Therefore, at the moment of the re-ignition there is a large surface area and the combination of pressure and burning rate very quickly generates a high volume of gas in a short period of time, finishing in a deflagration as observed in SCTV8. Table 120 presents a summary of the cook-off ignition temperatures and the kinds of event for the various SCTV.

Table 120. Slow Cook-Off Ignition Temperatures

SCTV	Ignition Temperature, ^{o}C	Measured by	Kind of event	Formulation
1	121	Internal thermocouple	Leaking through thermocouple nut, no propellant ignition observed	HTPE/PSAN/AP/n-BuNENA
2	136	External thermocouple	Bursting disk burst and immediately propellant deflagration occurred. No damaged was observed.	HTPE/PSAN/AP/n-BuNENA
3	211-227	Estimated	Explosion, cylinder broken in several pieces, three nuts cuts.	HTPE/PSAN/AP/n-BuNENA
4	129	Internal thermocouple	Leaking through thermocouple nut. No propellant ignition observed	HTPE/AP/n-BuNENA
5	183	External thermocouple	Bursting disk burst and immediately propellant burned mildly.	HTPE/AP/n-BuNENA
6	184	External thermocouple	Bursting disk burst and immediately propellant burned mildly	HTPE/AP/n-BuNENA
7	243	Internal thermocouple	Bursting disk burst. Burn after 21 s	HTPB/AP/DOS
8	259	Internal thermocouple	Bursting disk burst, deflagration after 25 s. Cylinder broken, nuts bent	HTPB/AP/DOS

5.4.3 HTPE/n-BuNENA + PSAN/AP or AP propellants

HTPE/AP/n-BuNENA propellant, either with or without PSAN in its composition, behaved in a different way to that which was expected and in comparison with what has been stated in several papers. First of all, the ignition temperature was expected to range around 133 to 140^{o}C, as reported by Atwood [2005], by Comfort [1994 and 1996], by Hartman [2000] and by Watt [NIMIC, 2004 a]. However, in SCTV5 and SCTV6 propellant based on HTPE/AP/n-BuNENA ignited at around 183^{o}C, which is almost 40^{o}C higher than the reported ignition temperature. It is important to highlight that the information reported by the above researchers is based only on samples containing AP+PSAN in the propellant formulations and not AP alone as oxidiser. No information was found about HTPE based composition using only AP as oxidiser.

5.4.3.1 HTPE/AP/n-BuNENA propellants

There was consistency in the behaviour of SCTV5 and SCTV6 in the ignition temperature and also in the kind of response at the event, despite the fact that SCTV5 was submitted to two temperatures cycles due the unexpected behaviour after the first heating period. In both cases, the SCTV were not damaged and just one event was detected. In other words, no delay from the burst of the disk and the ignition of the propellant was observed. The fast propellant burn suggests a smooth burning rate without a huge increase in pressure as in the HTPB based propellant. Possibly, the fact that the propellant at this temperature and time is liquid, or at least jelly, has an influence on the mechanical properties and burning surface. Being liquid, no cracks or cavities are formed, allowing less surface to be exposed to the burning process and less gas generated.

The observation that the propellant based on AP alone as oxidiser becomes a liquid is in disagreement with the findings of Parr [1999]. They stated that samples containing AP become hard, brittle and crumbly at high temperatures, however they did not say anything about the temperature cycle and other aspects such as the kind of HTPE pre-polymer characteristics or curing agent used. What is described by them does not match with what has been observed in the present study during binder and gumstock thermal

analysis and with that observed during the failed slow cook-off test with SCTV4 when the propellant leaking was evident. One point of agreement with Parr [1999] is that samples containing AP alone decompose at higher temperatures than those containing PSAN/AP. However they do not report any figures.

5.4.3.2 HTPE/ PSAN/AP/n-BuNENA propellants

The slow cook-off behaviour of HTPE samples containing PSAN and AP was different to that for samples containing AP alone. As explained before, for SCTV2 it was decided to start the slow heating at 136^{o}C, assuming that the behaviour would be similar to the HTPE/AP/n-BuNENA propellants used in SCTV5 and SCTV6 i.e. ignition at 183^{o}C. However, the behaviour was completely different, and it was almost at the end of the 30 min soaking period that a deflagration occurred. The event was closer to a fast cook-off test because of the heating rate of 5^{o}C per min plus the soaking period. The SCTV was not damaged, the burst disk was cut smoothly around the cylinder diameter and the tube was intact. However, the rest of the solid propellant was found on the tube wall and bottom and also outside the SCTV in the oven, this being an indication that no liquefaction process happened before the ignition. The reaction most probably started at a point inside the propellant charge (hot spot) and the flame and pressure front were spread through the SCTV, burning most of the propellant and forcing some to be expelled out of the vehicle. Possibly the propellant softened slightly when the ignition started and hence the reaction was not as violent as in SCTV8 where the vehicle was damaged. A DSC analysis using the same temperature cycle as that used in the SCTV2 test was performed on a sample of 0.8 mg of propellant 2P26E. The sample was placed in a sealed aluminium crucible. The same was done with a sample of 3P27B propellant. Figure 226 shows the DSC thermogram.

As can be seen from the curve labelled “A” corresponding to the propellant used for SCTV2 in Figure 226, after the second endothermic peak, corresponding to the PSAN phase change from rhombic to tetragonal cubic phase as explained in propellant DSC analysis in Chapter IV Section 4.2.3, a new endothermic peak can be seen which appears to be the onset of the exothermic peak at around 141^{o}C. So this exothermic peak

should be related to the cook-off ignition observed in SCTV2 during the initial phase. However further thermal analysis should be done in order to better understand the decomposition process that has been occurring during the development of the slow cook-off trials. The DSC thermogram in the curve labelled "B", for the propellant used in SCTV5 and SCTV6, does not show any reaction at all during the heating process, in particular at the temperature of the exothermic peak seen for the propellant containing PSAN+AP. This difference in behaviour suggests that the presence of PSAN in the HTPE propellant formulation is responsible for this earlier exothermic reaction.

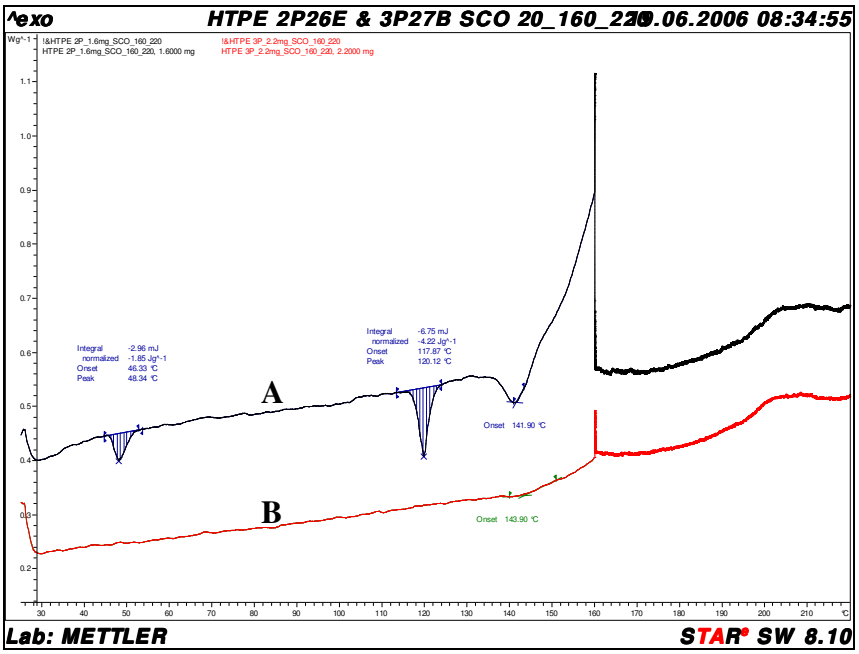

Figure 226. SCTV2 DSC analysis reproducing slow cook-off temperature cycle

The nature of the reaction in SCTV3 was completely different and unexpected again. Because of the early ignition in SCTV2 in comparison with SCTV5 and SCTV6, it was decided to go back to the initial temperature cycle i.e. ramp from ambient to 86°C then soak for 30 min and then ramp again at 6°C per h until the event happened at around 136°C. However, no event happened until 211 to 220°C (exact data were not recorded). The event was a deflagration even more violent than that with HTPB in SCTV8, as can be seen in Figure 227.

From Figure 227 A the violence of the reaction can be clearly appreciated when compared with Figure 227 B. From the shape and size of the fragments shown in Figure

227A and the tube in Figure 227B, it can be stated that in both cases the reaction was a deflagration. A detonation would produce many more very small pieces of metal (random shape and size), rather than the longer and thinner pieces of tube displayed in Figure 227A. By analysing physically the propellant left inside SCTV1 and SCTV4 after the leaking event, the suggestion of the surface area related to the violence of the reaction in a slow cook-off scenario can be applied.

A **B**

Figure 227. SCTV3 containing HTPE/PSAN/AP/ n-BuNENA propellant (A) in comparison with SCTV8 containing HTPB/AP/DOS propellant (B) after slow cook-off test

After physically analysing the residual propellant from SCTV1 and SCTV4, a difference can be noticed between the samples containing AP and those containing AP/PSAN as oxidisers.

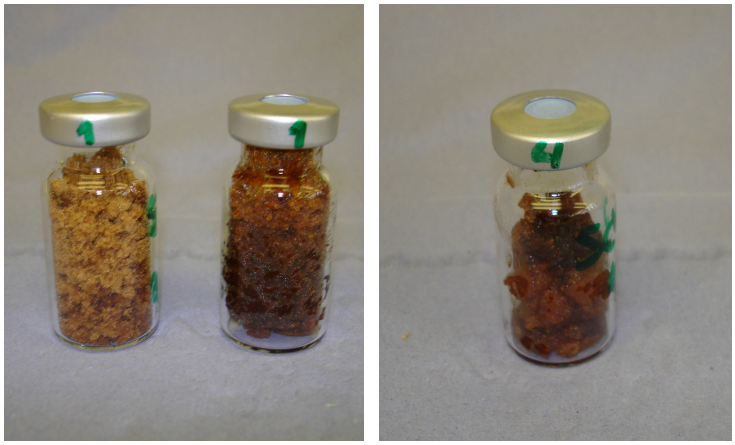

A **B**

Figure 228. (A) HTPE/PSAN/AP/ n-BuNENA propellant sample from SCTV1 and (B) HTPE/AP/n-BuNENA propellant sample from SCTV4

Samples that only contain AP as oxidiser (Figure 228 B) are, or appear to be, wet and, despite the fact it is not a solid sample, it behaves like a very viscous and homogeneous gel, having good consistency and clear shape. Therefore, the surface area that is exposed is not large. On the other hand, propellant samples obtained from SCTV1 (Figure 228 A) appear to be dry particles that do not stick together. From Figure 228 A the darker brown colour sample, which is on the right, was taken from the top of the cylinder and the light brown colour sample was taken from the bottom. The difference in colour is due to the lighter particles being apparently less covered with the organic phase than the darker particles.

The volume of sample found inside SCTV1 is almost twice the volume of that found inside SCTV4. This observation suggests that most of what went out of the SCTV1 was liquid rather than propellant itself. With this consideration, it can be stated that when propellant samples based on HTPE/PSAN/AP/n-BuNENA are slowly heated they behave in a different way to the samples based on HTPE/AP/n-BuNENA and that the one having PSAN in its composition liquefies to a higher degree than the one containing only AP. The liquid organic phase, because of gravity and also because of the internal pressure generated by the decomposition gases, tends to move down to the bottom of the cylinder leaving an empty space between crystals or particles and hence a new large surface area is generated. The same event is thought to have happened in SCTV3. Therefore, if the organic phase of the propellant became liquid and flowed downwards, two different regions were created, the bottom rich in liquid organic phase and the top rich in inorganic phase with particles or crystals covered by a film of organic phase and having a large surface area. Into this context, when the ignition point is reached the surface area allows, almost instantaneously, a huge amount of gas to be generated, increasing very quickly the internal pressure and creating a deflagration event.

5.5 Conclusion

It appears that the liquefaction of the organic phase in HTPE propellants has an important influence on the slow cook-off response, especially if the surface area at the ignition time is taken into account as an important aspect of the violent response to

cook-off. Therefore, this is one of the main differences in behaviour between HTPE and HTPB propellants that will possibly have an influence on the violence of the cook-off response. While HTPB propellants become harder and more brittle during slow heating, HTPE propellants become soft, reaching some degree of liquefaction and thus avoiding the production of cracks and the incremental increase in surface area as in HTPB. However the degree of organic phase decomposition also might be contributing to a violent response if a significant liquefaction of the organic phase occurred, as was the case for the samples containing PSAN in their composition. Because of that it appears that PSAN, at least in the formulation used for this research, is playing an important role in influencing the organic phase decomposition and the propellant ignition temperature in slow cook-off. On the other hand, it was observed that the HTPE propellant containing only AP as oxidiser becomes insufficiently soft to avoid liquefaction but also to avoid the formation of cracks or cavities that can create a large surface area leading to a deflagration. Thus when the ignition point is reached the slow cook-off response is moderated.

It should be taken into account that chain scission is occurring in both kinds of HTPE propellant as was presented and discussed in Chapter III, Section 3.5, and this is causing the polymeric matrix of the propellant to soften during thermal decomposition. If the degree of softening is neglected for the moment, the real fact is that a chain scission is occurring in the hard and soft segments of the polymeric matrix that contains the oxidisers. However, the degree of scissioning appears to be related to the violence of the response, as discussed previously. Therefore by controlling this process, control of the violence of response can possibly be achieved. Additives such as an antioxidant i.e. BHT, was not used during the pre-polymer or propellant manufacture. Therefore, although the antioxidant will probably not eliminate the degradation process in the soft segment chain, it will at least reduce the speed of the reaction until all the antioxidant is consumed. On the other hand, the inclusion of a more suitable nitrate ester stabiliser than 2NDPA, possibly MNA, will also reduce the effect of the n-BuNENA decomposition products on the soft and hard segment, especially in the biuret and urea links when polyisocyanates such as Desmodur N-3200 or N-100 are used. Thus a suitable combination of antioxidants and stabilisers will possibly allow the design of a

binder that will soften enough to avoid extreme liquefaction and, at the other extreme, the creation of cracks or cavities. This will achieve control of the violent response when the propellant is submitted to thermal threat.

VI. CONCLUSIONS AND RECOMMENDATIONS

6.1 Conclusions

A method for the synthesis of a random hydroxyl terminated copolyether (HTPE) from the reaction between tetrahydrofuran and ethylene oxide was designed and implemented. Several samples having different molecular weights and THF/EO ratios were produced and characterised. A synthesis temperature of -20^{o}C was found to be suitable to obtain a copolymer with a molecular weight of around 4000 g mol^{-1} when 3% weight of EG (related to THF) was used.

The HTPE pre-polymers were characterised using a range of techniques to identify the properties and characteristics of different pre-polymer materials. Similar analyses were performed on a sample of an HTPB pre-polymer and the results were compared with those obtained for the HTPE pre-polymers. The comparisons suggest that there are differences in thermal decomposition behaviour and thermal properties. A comparison was then made between various HTPE pre-polymers. The comparisons suggested that there are slight differences in thermal decomposition behaviour. However, further differences in the thermal properties such as glass transition temperature and melting point as a function of the molecular weight and microstructure were observed.

Several HTPE binder network samples were prepared with and without plasticizer and cured using different NCO/OH equivalence ratios. Desmodur N-3200 was used as curing agent and n-BuNENA as an energetic plasticizer. The binder and gumstock HTPE and HTPB samples were characterised by several techniques in order to obtain physical and thermal properties and to study and compare their behaviour under thermal decomposition. It was observed that Tg for the HTPE binder network samples does not change significantly when cured with Desmodur N-3200 at different NCO/OH equivalence ratios. However, peaks for the microcrystallisation process and melting point disappear when the NCO/OH equivalence ratio is equal to one. On the other hand the energetic plasticizer affects the gumstock by increasing slightly the glass transition temperature but at the same time eliminating the micro crystallization effect. It was also

found that the Tg of the HTPB gumstock is lower than that of HTPE gumstock. TGA analysis suggests that there is similarity between binder network and gumstock weight loss processes. However, the energetic plasticizer is playing an important role in the thermal decomposition. From DTA it can be concluded that there are three stages of weight loss, related to: the presence of the n-BuNENA decomposition, hard segment decomposition and finally soft segment decomposition. When the HTPE binder network and gumstock TGA behaviour was compared with that of HTPB two relevant differences were found: the weight loss in HTPE binder and gumstock begins 233^{o}C before that in HTPB, and the weight loss gradient is higher in HTPB than in HTPE, losing almost all the mass in a quarter of the HTPE ΔT gradient.

The thermal behaviour of HTPE and HTPB binder network and gumstock samples is different when they are slowly heated. While HTPB samples retained their shape throughout the heating process, HTPE samples lost their shape and became soft and liquid. This effect was shown to be more severe in gumstock than in binder network samples. It is suggested that the softening process is a result of the breaking of the soft and hard segment links of the HTPE copolymer chains. In contrast, HTPB samples become harder and more brittle during the slow heating process, due to the formation of a secondary network produced by oxidative cross linking between polymeric chains.

From FTIR analysis it was determined that the breaking of the polymeric matrix can possibly be assigned to the scission of the hard segment, biuret and urea groups, leading to amide or amine groups (or similar) due to the polymer decomposition i.e. soft segment chain scission, rather than the breaking of the urethane links. The results from the SEC analysis showed that the polymeric chain is scissioning after ageing at different temperatures and producing polymers having lower Mn and higher polydispersity than the initial pre-polymer.

On the physical analysis of the surface binder network and gumstock samples it was noticed that during slow heating, a migration process is occurring. The migration process suggests that either a non-cured polymer and plasticizer or a combination of both plus fragmented polymer or pre-polymer are migrating from the sample bulk to the

surface. A similar migration process was also observed in HTPB samples. If that is happening, it is likely that some nano or micro cavities are being left during the migration process in the sample bulk. These microcavities potentially can have an influence on the slow-cook off performance when the propellant is ignited. From SEM analysis a well defined pattern of flat semi-spheres or little domes was observed on the surface of the HTPE binder and gusmtock samples.

Two different HTPE propellant batches and one kind of HTPB propellant batch were manufactured, characterised and submitted to slow cook-off tests. SEM photographs show good oxidiser particle distribution for all the three propellants. However, both HTPE propellant batches required different manufacturing process conditions. The addition of PSAN to the HTPE batch changed the processability, and therefore the mixing conditions, in comparison with the HTPE batch containing only AP as oxidiser, it being difficult to reach a good fluidity. At the end of the curing process the HTPE propellant containing PSAN was not apparently as well cured as that containing only AP as oxidiser. It was observed that the HTPE propellant containing only AP as oxidiser was less flexible than the one containing PSAN and AP. SEM analysis showed that the HTPE propellant having only AP as oxidiser appears to have poor bond between AP particles and binder. This possibly accounts for the observed poor flexibility of the propellant.

Following the binder network and gumstock density trend, HTPE propellant samples based on HTPE/n-BuNENA plus oxidisers have a higher density than propellant samples based on HTPB. Among HTPE propellants, samples containing PSAN and AP as oxidiser show the lowest density, this behaviour being due to the lower density of PSAN in comparison with AP. The glass transition temperature increases when oxidisers are included in HTPE propellant formulations in comparison with the HTPE binder network and gumstock. This increase is 3^{o}C when only AP is used as oxidiser, however when PSAN was included as oxidiser in the propellant, Tg increased by around 16^{o}C. HTPB propellant has a higher Tg than AP based HTPE propellant but lower than AP+PSAN HTPE propellant.

From the propellant DSC analysis, it appears that in the HTPE propellant containing AP+PSAN as oxidisers the interaction of the components is having an influence on the decomposition process: the PSAN melting point is divided into three steps and its decomposition point increased while the temperature and intensity of the AP solid to solid phase transition peak decreased. n-BuNENA has an important role in the propellant decomposition process, being responsible for the first propellant exothermic reaction due to its decomposition. It was also observed that the decomposition process related to the n-BuNENA is less exothermic in propellant containing only AP as oxidiser. Possibly decomposition products of n-BuNENA are reacting with part or all the liquid phase from the PSAN. On the other hand, most of the exothermic peaks in the DSC thermogram of AP+PSAN HTPE propellants are delayed in comparison with the peaks in that of the propellant containing only AP.

It was observed from TGA that propellant containing AP and PSAN as oxidiser lost a bigger percentage of mass at lower temperature than that containing only AP as oxidiser. The influence of the PSAN appears to be the related to the process as stated above. In comparison with HTPB, HTPE propellants start decomposing at lower temperature and in a more gradual way. The same behaviour occurs with the weight loss process.

HTPE propellant containing only AP as oxidiser, has a lower decomposition activation energy (Ea) than AP+PSAN HTPE propellant. On the other hand HTPE propellants Ea are lower than the Ea found for HTPE gumstock and binder network samples. It was observed that the presence of the energetic plasticizer n-BuNENA is driving the overall decomposition. However, when PSAN is added as a cooxidiser, the HTPE Ea is increased in comparison with that of propellant having only AP as oxidiser. Therefore it is believed that the presence of PSAN is affecting the propellant thermal decomposition by delaying the exothermic decomposition reactions. It was also seen that HTPE propellants have lower activation energies than the HTPB propellant, mainly due to the presence of the energetic plasticizer n-BuNENA and the PSAN, and their interaction with the binder.

It appears that the liquefaction of the organic phase in HTPE propellants has an important influence on the slow cook-off response, especially if the surface area at the ignition time is taken into account as an important aspect of the violent response to cook-off. This is one of the main differences in behaviour between HTPE and HTPB propellants that will possibly have an influence on the violence of the cook-off response. It is believed that while HTPB propellants become harder and more brittle during slow heating, HTPE propellants become soft, reaching some degree of liquefaction and thus avoiding the production of cracks and the incremental increase in surface area as in HTPB propellants. Therefore, the degree of organic phase decomposition might also be contributing to the violent response if a significant liquefaction of the organic phase occurred. Because of that, it appears that PSAN, at least in the formulation used for this research, is playing an important role in the organic phase decomposition and in the propellant ignition temperature in slow cook-off. On the other hand, it was observed that the HTPE propellant containing AP alone becomes insufficiently soft to avoid liquefaction but also to avoid the formation of cracks or cavities that can create a large surface area leading to a deflagration. Therefore when the ignition point is reached the slow cook-off response is moderated.

The degree of scissioning appears to be related to the violence of the response. Nevertheless, it is believed that by controlling this process by the use of antioxidants and different stabilisers, possibly control of the violence response can be achieved. Antioxidants were not used in this research and it is believed that although they will probably not eliminate the degradation process in the soft segment chain, they will at least reduce the speed of the reaction until all the antioxidant is consumed. A different stabiliser to 2NDPA, possibly MNA, might also reduce the effect of the n-BuNENA decomposition products on the soft and hard segment. Thus a suitable combination of antioxidants and stabilisers might make it possible to design a binder to soften enough to avoid extreme liquefaction and, at the other extreme, the creation of cracks or cavities. This will enable control of the violence response when the propellant is submitted to thermal threat.

It is probable that the inconsistencies reported by different researchers regarding HTPE propellant performance in slow cook-off or ageing trials, can be understood because of the different ingredients and their proportions when an HTPE propellant is formulated and manufactured. However, it is believed that, because of the softening of the polymeric matrix in HTPE propellants in contrast with the hardening in HTPB propellants, HTPE propellants can offer a suitable way to control the violence of the response in slow cook-off tests.

6.2 Recommendations for Future Works

Several recommendations can be made in order to better understand and verify some of the concepts and ideas originating from this work.

- Although a synthesis process was developed and suitable HTPE pre-polymers were obtained, further research should be undertaken to scale the size of the production batch and to define the appropriate chemical reactor to perform the cationic copolymerisation between THF and EO.

- Different HTPE pre-polymers are mentioned as binders in the literature. Possibly a theoretical study looking for ideal HTPE binder properties can be done. Also, because different kinds of HTPE pre-polymers are potentially being offered today on the market, a good understanding of their performance can be achieved if the possibility of testing them exists.

- Compatibility tests should be done for all the possible ingredients to be included in the HTPE propellant formulations especially antioxidants, stabilisers, phase stabilisers, energetic plasticizers and bonding agents.

- HTPE gumstock and propellant samples having different proportions and kinds of stabiliser and antioxidants should be manufactured and tested mechanically, chemically and thermally, in order to determine any correlation between softening properties and thermal threat. Then some tests should be done in order to find a

correlation between HTPE polymeric chain softening and violence of the response in slow cook-off. Also a bonding agent could be added to the formulation matrix. Having that information, possibly an indirect relation between surface area (degree of softening and violence response) at the cook-off ignition point could be investigated

- The solubility of AP and the microstructure of the HTPE pre-polymer should also be assessed, not only to check the mixtures processability but also to verify insensitiveness, mechanical properties and thermal behaviour.

- The reaction mechanism for soft and hard segment scissioning should also be investigated in order to better understand the thermal decomposition process. These mechanisms could be included in a model used to predict violence of response in cook-off.

- The effect of PSAN and AP and their interaction with the thermal decomposition of the energetic plasticizer should be further investigated. Also different kinds of phase stabilised AN and anticaking agents should be taken into account.

- Improved formulations for manufacturing HTPE propellants with good thermal and mechanical properties should also be investigated. The use of bonding agents and PSAN with different particle sizes should be considered. Also other curing agents or mixtures of them should be investigated.

- When performing SEM analysis on HTPE gumstock cracks were created. It is believed that the SEM electron beam is affecting the thermal decomposition of the gumstock and generating gases which are breaking the surface. Therefore, the SEM technique for examining these materials should be refined.

REFERENCES

AGARD (1990), "Hazard Studies for Solid Propellant Rocket Motors," Advisory Group for Aerospace Research & Development. AGARD-AG-316, NATO. September.

AGARD (1997), "Structural Assessment of Solid Propellant Grains," Advisory Group for Aerospace Research & Development. AGARD-AR-350, NATO. December.

Ahlblad G. (1999), Reitberger, T., Terselius, B. and Stenberg, B., "Thermal Oxidation of Hydroxyl-Terminated Polybutadiene Rubber I. Chemiluminescence Studies," Polymer Degradation and Stability Journal. Vol 65. pp 179-184.

Andreev, K. K. (1967), and Sung, Ts'uan-Ts'ai., "Thermal Decomposition of Ammonium Perchlorate and Some of its Mixtures," Trudy Instituta - Moskovskii Khimiko-Tekhnologicheskii Institut Imeni D. I. Mendeleeva. N^{o} 53. pp 99-119. Chemical Abstracts 69:90183.

Arendale, W. F. (1969), "Chemical of Propellants Based on Chemically Crosslinked Binders," Boyars, C. and Klager, K. (ed). Advances in Chemistry Series, Vol. 88. American Chemical Society. Washington, D. C. pp 67-83.

ATK (2004). Alliant Techsystem Inc. URL:http://www.atk.com/aerospace/descriptions/tactical-propulsion/essm.htm.

Atwood A. I. (2005), Rattanapote M. K., and Curran P. O., "Feasibility for Development of an Alternate Test Protocol to the Full-Scale External Fire Test Used in Hazards Classification," 6th ISICP, International Symposium on Special Topics in Chemical Propulsion. Santiago, Chile. 8th-11th March.

Bayer (1960), Farbenfabriken aktiengesellschaft, "Copolymerising Mono-Epoxides with Tetrahydrofuran," GB Patent N^{o} 859,958.

Bayer AG. (2001), Desmodur N-100 product information. 9th November.

Bayer AG. (2004), Desmodur N-3200 product information. Product code D120. 1st January.

Bednarek, M. (1998) and Kubisa, P. "Copolyethers with Controlled Structure. Mechanism of Formation and Microstructure," Macromolecular Symposia Journal. Vol 132. pp 349-358. ISSN: 1022-1360.

Bednarek, M. (1999a) and Kubisa, P. "Cationic Copolymerization of Tetrahydrofuran with Ethylene Oxide in the Presence of Diol: Composition, Microstructure, and Properties of Copolymers," Journal of Polymer Science. Part A: Polymer Chemistry. Vol 37. pp 3455-3463.

Bednarek, M. (1999b), Kubisa, P. and Penczek, S. "Coexistence of Activated Monomer and Active Chain End Mechanism in Cationic Copolymerization of Tetrahydrofuran with Ethylene," Macromolecules Journal. Vol 32 N^{o} 16. pp 5257-5263.

Bednarek, M. (1999c) and Kubisa, P. "Mechanism of Cyclic Formation in the Cationic Copolymerization of Tetrahydrofuran with Ethylene Oxide in the Presence of Diol," Journal of Macromol. Chem. Phys. Vol 200 N^{o} 11. pp 2443-2447.

Bellamy L. J. (1980), "The Infrared Spectra of Complex Molecules," pp 184. (2nd ed). Chapman and Hall Ltd. ISBN: 0-412-22350-3.

British Standard (2001), BS ISO 14900:2001 "Plastics-Polyols for use in the production of polyurethane- determination of hydroxyl number," ISBN: 0-580-37394-0.

Brown, M.E. (2000), Maciejewski, M, Vyazovkin, S., Nomen, R., Sempere, J., Burnham, A., Opfermann, J., Strey R., Anderson, H.L., Kemmler, A., Keuleers, R., Janssens, J., Desseyn, H.O., Chao-Rui Li, Tong B. Tang, Roduit, B., Malek, J. and, Mitsuhashi, T., "Computational Aspects of Kinetic Analysis Part A: The ICTAC kinetics project-data, methods and results," Thermodinamica Acta. Vol 355. pp 125-143.

Carey F. A. (1993) and Sunderberg R. J., "Advanced Organic Chemistry, Part A: Structure and Mechanisms," Chapter 8, Section 8.6, pp 470-473. (3nd ed). Plenum Press New York. ISBN: 0-306-43440-7.

Catton, D. (2005). Personal communications. Roxel UK.

Cartwright M. (2006). Shrivenham, Cranfield University, Department of Environmental and Ordnance Systems. Personal communications.

Chan, M. L. (2000), Russ R. Jr. and Ciaramitaro, D. A., "Advances in Solid Propellants Formulations," Yang, V., Brill, T. and Ren, W. (ed). Progress in Astronautics and Aeronautics, Vol 185. pp 185-206. AIAA, Inc. ISBN: 1-56347-442-5.

Chan, M. L. (2002) and Turner A. D. "Insensitive High Energy Booster Propellant," US Patent Application N^{o} 20,020,166,612.

Chan, M. L. (2005a) and Turner A. D., "Insensitive High Energy Booster Propellant Suitable for High Pressure Operation," 6th ISICP, International Symposium on Special Topics in Chemical Propulsion. Santiago, Chile. 8th-11th March.

Chan, M. L. (2005b). Personal communications. July.

Chase, M. (1996) and Thorp, G. P., "Solid Rocket Case Design," Yang, V., Brill, T. and Ren, W. (ed). Progress in Astronautics and Aeronautics, Vol 170. pp 189-233. AIAA, Inc. ISBN 1-56347-118-3.

Coleno, R. (2003), Nugeyre, J. C., and Longevialle, Y., "Demostrateurs Techonologiques de Moteurs Muratises," Proceeding of the EUROPYRO 2003 Symposium. Saint Malo, France. pp 785-794.

Comfort, T. F. (1994), Dillman, L. G., Hartman, K. O., Magnum, M. G. and Steckman, "Insensitive HTPE Propellants," Proceeding of the ADPA 1994 Insensitive Munitions Technology Symposium. Williamsburg, Virginia. 6th -9th June.

Comfort, T. F. (1996), Dillman, L. G., Hartman, K. O., Magnum, M. G. and Steckman, R. M., "Insensitive HTPE Propellants," Proceeding of the ADPA Meeting, Insensitive Munitions Technology. San Diego, California, US. 18th-21st March.

Comfort, T. F. (2000), "Solid Rocket Propellant," US Patent N° 6,066,214.

Comfort, T. F. (2000) and Hartman, K. O., "High Density HTPE Propellants," Insensitive Munitions and Energetic Materials Technology Symposium, NDIA. San Antonio, Texas, US. 27th -30th November.

Comfort, T. (2004), Shanholtz, C. and Fletcher, G., "Progress in HTPE Propellants," NDIA 39th Annual Gun & Ammunition/Missiles & Rocket Conference. Baltimore, MD, US. 13th-16th April.

Davenas A. (1993), "Solid Rocket Propulsion Technology," Chapter 10. Pergamon Press Ltd. ISBN: 0-08-040999-7.

Davenas, A. (2002) and Rat, R., "Sensitivity of Solid Rocket Motors to Electrostatic Discharge: History and Future," Journal of Propulsion and Power. Vol 18 N° 4. July-August.

Davenas, A. (2003), "Development of Modern Solid Propellants," Journal of Propulsion and Power. Vol 19 N° 6. November-December.

Demay, S. C. (1996), Kong, J. A., Chun, P. A. and Thelen, C. J., "Insensitive Munitions Hazard Test of a Pulsed Rocket Motor," Proceeding of the Insensitive Munition Technology Symposium. San Diego, California, US. 18th-21st March.

Demay, S. C. (1997), and Thelen, C. J., "Insensitive Munitions Propulsion Progress," Kuo, K. K (ed). Proceeding of the 4th International Symposium on Special Topics in Chemical Propulsion. Stockholm. 27th-31st May. pp 337-344. Begell House, N. Y.

Desai, S. (2000), Thakore, I. M., Sarawade, B. D. and Devi, S., "Effects of Polyols and Diisocyanates on Thermo-mechanical and Morphological Properties of Polyurethanes," European Polymer Journal. Vol 36. pp 711-725.

Desilets, S. (2000) and Cote, S., "Chemical Bond Between Stabilizers and HTPB Binders in Propellants," Propellants, Explosives and Pyrotechnics. Vol 25. pp 186-190.

DOS (1994), REOMOL DOS, FMC, MSDS supplied by ROXEL

Elf atochem (1996). HTPB Product Quality Report, Poly BD® Resin R-45-M. Elf atochem, ATO. Loc number 601035. 30th May.

Eroglu, M. S. (1998), "Characterization of the Network Structure of Hydroxyl Terminated Poly(butadiene) Elastomers Prepared by Different Reactive Systems," Journal of Applied Polymer Science. Vol 70, Issue 6. pp 1129-1135.

Fletcher, W. G. (2006) and Comfort, T. S., "Updates on HTPE Propellants Service Life," Insensitive Munitions and Energetic Materials Symposium (IMEMTS). Bristol, UK. 24th-28th April.

Frota, O. (2003), "Development of a Low Cost Cook-Off Test for Assessing the Hazard of Explosives," PhD thesis. Shrivenham, Cranfield University.

Gupta, T. (2003) and Adhikari, B., "Thermal Degradation and Stability of HTPB-Based Polyurethane and Polyurethaneureas," Thermochimica Acta. Vol 402. pp 169-181.

Goleniewski, J. R. (1994) and Roberts, J. A., "Solid Rocket Propellant with non Crystalline Polyether/Inert Plasticizer Binder," US Patent N° 5,348,596.

Goleniewski, J. R. (1998) and Roberts, J. A., "Solid Rocket Propellant with non Crystalline Polyether/Energetic Plasticizer Binder," US Patent N° 5,783,769.

Gore, G. M.(2004), Nazare, A. N., Divekar, C. N., Hait, S. K. and Asthana, S. N., "Studies on Nonaluminized High Burning Rate AP-Composite Propellants," Journal of Energetic Materials. Vol 22. pp 151-169.

Groll P. (1991), "New PolyTHF developments," Polyurethanes World Congress. 24th-26th September. pp 858-862. Chemical Abstracts: 119:96847.

Gupta, T. (2003) and Adhikari, B. "Thermal Degradation and Stability of HTPB-based Polyurethane and Polyurethaneureas," Thermochimica Acta. Vol 402. pp 169-181.

Hartman, K.O. (2000),"Insensitive Munitions Technology for Small Rocket Motors," Proceeding of the RTO Meeting, 23 RTA. Neully sur Seine, France. pp 12/1-12/7.

Huimin Tan (2000), Yingquan Duo and Futai Chen, "Molecular Structure Tailoring of Binders in Solid Propellants," Yang, V., Brill, T. and Ren, W. (ed). Progress in Astronautics and Aeronautics, Vol 185. pp 129-140. AIAA, Inc. ISBN: 1-56347-442-5.

Hussain, G (1992) and Rees, G.J., "Combustion of Ammonium Perchlorate Based Mixture With and Without Black Powder, Studied by DSC and TG/DTG," Fuel. Vol 71. pp 471-473. April.

ICI Explosives (RXL 647). Technical Data, ButylNENA, PB NO.211.

Jain, S. R. (1993), Sekkar, V. and Krishnamurthy, V. N, "Mechanical And Swelling Properties of HTPB Based Copolyurethane Networks," Journal of Applied Polymer Science. Vol 48 Issue 9. pp 1515-1523.

Jemmett, P. (2001), "Investigation of Ammonium Nitrate Propellant Systems," MSc Thesis. Shrivenham, Cranfield University.

Keenan, A. G. (1969) and Siegmund R. F., "Thermal Decomposition of Ammonium Perchlorate," The Chemical Society London, Quarterly Review. Vol 23 N^{o}3. pp 430-452.

KIRK-OTHMER (1994), "Encyclopedia of Chemical technology," (4th ed). John Wiley &Sons. Vol 11. pp 309-311.

Klager, K. (1984), "Polyurethanes, The Most Versatile Binder for Solid Composite Propellants," AIAA Paper 84-1239. June.

Komai, I. (2006) and Sato, W., "Reaction Mechanism in Slow Cook-off Tests of GAP/AP Propellants," Insensitive Munitions and Energetic Materials Symposium (IMEMTS). Bristol, UK. 24th-28th April.

Kudva, G. N. (2000) and Litzinger, T. A., "Low-Pressure Laser and Pressure-Driven Response Measurements on AP/HTPE and AP+AN/HTPE Propellants," JANNAF 37th Combustion Subcommittee Meeting. Vol 1. pp 627-640.

Luo Shanguo (1999), Chen Futai, Luo Yunjun, Tan Huimin, Man Guanglei and Guo Yanwen, "Effect of Propellant Components on Degradation of a Polyether-Urethane Binder. I – Effect of Nitrate Esters," Journal of Propulsion Technology. Vol 20 N^{o} 2. pp 88-94. April.

Luo Guangliang (2003), Cheng Genwang, Shan Jianmin and Guoxia L. I., "Analysis of HTPB Propellant Network," Proceeding of the 2003 International Autumn Seminar in Propellants, Explosives and Pyrotechnics. Guiling, China. 15th-18th October. pp 241-245.

Matei, M. V. (2002), "Study of Cook-Off in One Dimensional Time to Explosion Apparatus," PhD thesis. Shrivenham, Cranfield University.

Menke, K. (2006), Bohn, M and Kempa, P. B., "AN/PolyGLYN Propellants-Minimum Smoke Propellants with Reduced Sensitivity," proceeding of the 37th International Annual Conference of ICT. Karlsruhe, Germany. 27th-29th June. pp 14-1 to 14-14.

Meulenbrugge, J. J. (1988) and Sabel, H. W. R., "Castable Plastic-Bonded Explosives," 37 Examples of Research. The Netherlands: TNO Prints Maurits Laboratory. pp 144-154.

Mohring, E. (1978), Wagner, K. and Muller, H., P., "Process for the Preparation of Polyisocyanates Having Biuret groups," US Patent N^{o} 4,127,599.

Mullay, J. (1994), Johnson, R. and Norman, J.V., "Thermal Stability of Stabilized NENA/AP Mixtures," Proceeding of the ADPA, International Symposium on Energetic Materials Technology. Orlando FL, US. 21st-24th March. pp 405-411.

Mullay, J. J. (1996), Johnson, R. A., and Van Norman, J. F., "Stabilized Munition Containing a NENA Compound," US Patent N° 5,507,893.

Nakanishi, K. (1964), "Infrared Absorption Spectroscopy, Practical," Nankodo Company Limited 1962. Tokio. Tokio, Japan. Second printing. January.

NATO (2002), "Accident Response Descriptors (AOP-39)," OME SMS OP No 1.5.3. Version 1.1. January.

NIMIC (2002), NEWSLETTER, "Solid Rocket Propellant for Improved IM Response-Recent Activities in the NIMIC Nations," 4th Quarter. p 2.

NIMIC (2003) NEWSLETTER, "Solid Rocket Propellant for Improved IM Response-Part 2 IM Propellant Examples," 1st Quarter. pp 2-4.

NIMIC (2004a), FAX dated 02 April 2004. Dr Duncan Watt. Personal communications.

NIMIC (2004b), FAX dated 27 February 2004. Dr Duncan Watt. Personal communications.

Oberth, A. E. (1969), and Bruenner, R. S., "Polyurethane Based Propellants," Boyars, C. and Klager K. (ed). Advances in Chemistry Series, Vol 88. pp 84-121. American Chemical Society. Washington D. C.

Osswald, T. A. (2003) and Menges, G., "Materials Science of Polymers for Engineers," Chapter 9. pp 381. (2nd ed). Hanser Gardner Publications, Inc. ISBN: 3-446-22464-5.

Ozawa, T. (1970), "Kinetic Analysis of Derivative Curves in Thermal Analysis," Journal of Thermal Analysis and Calorimetry. Vol 2 N° 3. pp 301-324.

Panaitov, I. (1980), "On Complex-Forming Properties of Some High Molecular Polyethers," Chimika Chronika. Vol 9 N° 4. pp 305-324.

Parr, T. P. (1999), and Hanson-Parr, D. M., "Flame Structure Studies of AP/HTPE and AP + AN/HTPE Propellants," 18th JANNAF. Propulsion Systems Hazards Subcommittee Meeting. Vol 1. pp. 81-88.

Provatas, A. (2000), "Energetic Polymers and Plasticizers for Explosive Formulations – A Review of Recent Advances," DSTO-TR0966. Department of Defense. DSTO. Australia. April.

Pruckmayr, G. (1979), "Method for Preparing Copolyether Glycols," US Patent N° 4,139,567.

Rao, K. P. C. (2004), Sikder A. K., Kukarni M. A., Bhalerao M. M. and Gandhe, B. R., "Studies on n-Butyl Nitroxyethylnitramine (n-BuNENA): Synthesis, Characterisation and Propellant Evaluations," Propellants, Explosives and Pyrotechnics. Vol 29. pp 93-98.

Rice, J. R. (2005) and Neidert, J. B., "Mechanical and Accelerated Aging Characteristics of an HTPE Propellant," SIAC Conference. Helsinki, Finland. May.

Rocco, J. A. F. (2004), Lima, J. E. S., Frutuoso, A. G., Iha, K., Ionashiro, M., Matos, J. R. and Suarez-Iha, M. E. V., "Thermal Degradation of a Composite Solid Propellant Examined by DSC," Journal of Thermal Analysis and Calorimetry. Vol 75. pp 551-557.

Royal Ordnance (2000), Rocket Motor Division, "Material Specification for Hydroxy Terminated Polybutadiene (HTPB)," 300 763-PD/1/RAYO. Issue N^{o}1. 12th December.

Roxel (2000), "Material Specification for Hydroxyl Terminated Polybutadiene (HTPB)," Determination of Hydroxyl Content, N^{o} 300 763-PD/1/RAYO. Issue N^{o} 1. 12th October.

Sadek, M. A. (2001), Moeen, M. H., Radwan, M. A. and Ameen, H. H., "Effect of Aging on Thermal Decomposition of Ammonium Perchlorate," Proceeding of the 32nd International Annual Conference of ICT. Karlsruhe, Germany. 3rd -7th July. pp 129-1 to 129-12.

Sell, T. (1999), Vyazovkin, S. and Wight, C., "Thermal Decomposition Kinetics of PBAN-Binder Composite Rocket Propellant," Combustion and Flame Journal. Vol 119. pp 174-181.

Serkan Burak (1997), Haska Erdal Bayramli, Fikret Pekel, and Saim Ozkar, "Mechanical Properties of HTPB-IPDI- Based Elastomers," Journal of Applied Polymer Science. Vol 64 N^{o} 12. pp 2347-2354.

Shen Q. H. (1996), Bao G. L, Zhang Y.X and Lu A.F, "Synthetic Study of BuNENA," Proceeding of the 27th International Annual Conference of ICT. Karlsruhe, Germany. 25th-28th June. pp 133-1 to 133-7.

Sinditskii, V. P. (2005), Egorshev, V. Yu., Levshenkov A. I. and Serushkin V. V., "The Role of additives in Combustion of Ammonium Nitrate," 6th ISICP, International Symposium on Special Topics in Chemical Propulsion. Santiago, Chile. 8th-11th March.

Sloan, M. (2004). Personal communications. Roxel UK.

Smith, M. D. (2000), Moser, M. D. and Frederick, R. A., "Temperature Sensitivities of Energetic Binder Propellants," AIAA/ASME/SAE/ASEE. 36th Joint Propulsion Conference and Exhibit. Huntsville, AL. 16th-19th July.

Sparks, J. F. (1990), and Friedlander III, M. L., "Fifty Years of Solid Propellant Technical Achievements at Atlantic Research Corporation," AIAA Paper 99-2932. June.

Stacer, R. G. (1991) and Husband, D. M., "Molecular Structure of the Ideal Solid Propellant Binder," Propellants, Explosives and Pyrotechnics. Vol 4 N^{o} 16. pp 167-176.

STANAG 4382 (1996), "Slow Heating Tests for Munitions" Edition 1. North Atlantic Treaty Organization.

STANAG 4439 (1998), "Policy for Introduction, Assessment and Testing for Insensitive Munitions (MURAT)," Edition 1. North Atlantic Treaty Organization.

Stewart, M. (1993), "Process for the Production of Polyethers Derived from Oxetanes," US Patent N^{o} 5,210,179.

Stewart, M. (1994), "Polymerisation of Cyclic Ethers," US Patent N^{o} 5,313,000.

Steyn, G. J. J. (1998) and Van Zyl, G. J., "Improving the Elongation Capability of HTPB-Based Composite Propellant," Proceeding of the 29th International Annual Conference of ICT. Karlsruhe, Germany. 30th June to 3rd July. pp 92-1 to 92-14.

Sun Xiang-yu (2006), Li Yan Li and Zhao Hai-quan, "The Effect on Aging of Main Components of NEPE Propellants," Proceeding of the 37th International Annual Conference of ICT. Karlsruhe, Germany. 27th-29th June. pp 76-1 to 76-8.

Takaya Takei (1999), Kazuki Kageshima, Megumi Tomita, Yoshinori Sugitani, Kyon Hun Min and Kiyoshi Matsumoto, "State Analysis of Water in Polyether-Polyol by High Frequency Spectroscopy," Analytical Science. The Japan Society for Analytical Chemistry. Vol 15. pp 1083-1086.

Takaya Takei (2002), Kasuo Kurosaki, Yuko Nishimoto and Yoshinori Sugitani, "Behaviour of Bound Water in Polyethylene Oxide Studies by DSC and High Frequency Spectroscopy," Analytical Science. The Japan Society for Analytical Chemistry. Vol 18. pp 681-684.

Tatcher, J. (1991) and Wetherell, R. "Solid Rocket History at Hercules," AIAA/SAE/ASME/ASEE. Proceeding of the 27th Joint Propulsion Conference. AIAA Paper 91-2188. Sacramento, US. 24th-26th June.

Tingfa, D. (1989), "Thermal Decomposition Studies of Solid Propellant Binder HTPB," Thermochimica Acta. Vol 138. pp 189-197.

Tokui, H. (1991) and Iwama, A., "Pot Life Problem and Its Measure with a Reduced Smoke Propellant Production," Propellants, Explosives and Pyrotechnics. Vol 16. pp 105-109.

Tzeng, D. D. (1998) and Jones, M. L. "Low Cost Binder for IM Applications," CPIA publication. JANNAF propulsion meeting. Vol 1. pp 97-99.

Urbanski, T. (1984), Chemistry and Technology of Explosives. Vol. 4 pp 437-461. Pergamon Press. ISBN: 0-08-026206-0.

Victor, A. C. (1996), "Insensitive Munitions Technology for Tactical Rocket Motors," Jensen, G. and Netzer, D. (ed). Progress in Astronautics and Aeronautics, Vol 170. pp 273-347. AIAA, Inc. ISBN: 1-56347-118-3.

Xiao-Bin Zhao (2000), Lin-Fa Hou and Xiao-Ping Zhang, "Thermal decomposition and Combustion of GAP/AN/Nitrate Ester Propellants," Yang, V. Brill, T. and Ren, W. (ed). Progress in Astronautics and Aeronautics, Vol 185. pp 413-424. ISBN: 1-56347-442-5.

Yanagida, S., (1978), Takahashi, K. and Okahara, M., "Metal-Ion Complication of Noncyclic Poly (oxyethylene) Derivatives, II. Proton NMR studies on the Complexation with Alkali and Alkaline Earth Metal Cations," Bulletin of the Chemical Society of Japan. Vol 51 N^{o} 5. pp 1294-1299. ISSN: 0009-2673.

Zhang Jianguo (1994), Pei Feng-Kui, Wu Yi-Jie, Jing Feng-Ying and Zhang Xi-Tian, "Studies of EO/THF Random Copolyether. (I) NMR Analysis of the Liquid Hydroxy Terminated TEO," Gaodeng Xuexiao Huaxue Xuebao. Vol 15 Issue 2. pp. 290-294. ISSN: 0251:0790.

Zhao Fengqi (1999), Yang Dong, Dang Zhimin, Li Shangwen and Li Li, "Study on the Thermal Decomposition of NEPE Propellant and its Oxidisers," Proceedings of the 26th International Pyrotechnics Seminar. pp 634-638. ISSN: 0270-1898.

Zhiping Huang (1997), Sun Zhongxiang, Wu Zhenhai, "Synthesis and Characterization of Hydroxy-Terminated EO-THF Copolyether," 42nd Institute of the Fourth Academy of CASC. Xiangfan, Hubei, People Republic of China. Vol 20 N^{o} 3. pp 53-58. ISSN: 1006-2793.

Zhiping Huang (1999) and Qingwei Cao "Comment on Synthesis and Characterisation of Ethylene Oxide and Tetrahydrofuran copolyether," Proceedings of the 3rd International Autumn Seminar on Propellant, Explosives and Pyrotechnics. Chengdu, China. 5th-8th October. pp 26-32.

Zimmerman, G. A. (1982), Kispersky, J. P., Nahlovsky, B.D. and Newey, S. L., "Embrittlement of Propellant Containing Nitrate Ester Plasticizers," AIAA, SAE, and ASME. 18th Joint Propulsion Conference. Cleveland, OH, US. 21st-23rd June.